ANNEX: INDIVIDUAL REPORTS

Published on the CD-ROM and attached to the hard copy

TOPIC 2: RESARCH REACTOR BASED NEUTRON BEAM FACILITIES

2.1. COLD AND THERMAL NEUTRON BEAMS

Author	Affiliation	Title of the paper
Belgya, T.	Nuclear Analysis and Radiography Department, Hungary	Nuclear data measurements at the PGAA-NIPS facilities of the Budapest research reactor
Révay, Z.	Centre for Energy Research of the Hungarian Academy of Sciences, Hungary	Determination of partial gamma ray production cross-sections in cold neutron beams
Köster, U.	Institut Laue Langevin, France	Precision Nuclear Data Measurements at Institut Laue Langevin
Furutaka, K.	Nuclear Science and Engineering Directorate, Japan	Prompt gamma ray measurement facilities at Japan Research Reactor-3 (JRR-3)
Shibata, M.	Radioisotope Research Center, Japan	Measurements of decay data of fission products using Isotope Separator on-Line

2.2. FILTERED NEUTRON BEAMS

Gritzay, O.	Neutron Physics Department & Ukrainian Nuclear Data Center, Ukraine	Development of the Neutron Filtered Beam Technique for High Precision Nuclear Data Measurements
Anh T.	Nuclear Research Institute, Vietnam	The quasi-monoenergetic neutron spectra for nuclear data measurements on filtered neutron beams at DALAT research reactor
Hossain, S.	Institute of Nuclear Science and Technology, Bangladesh	Uses of monochromized thermal neutron beams for nuclear data measurements

TOPIC: 3. ACCELERATOR BASED NEUTRON BEAM FACILITIES

3.1. MONOENERGETIC AND MAXWELL SPECTRUM NEUTRON BEAMS (< 5 MEV)

Oberstedt, S.	European Commission, Belgium	Nuclear Research with Mono-Energetic NEUTRONS AT the JRC MONNET Facility
Nolte, R.	Physikalisch-Technische Bundesanstalt, Germany	Neutron beams and neutron metrology at the PTB ion accelerator facility PIAF and at the IThemba LABS neutron beam facility
Vlastou, R.	National Technical University of Athens, Greece	The neutron facility at the Athens Tandem Accelerator NCSR “Demokritos” and NTUA Research Activities

Murata, I.	Osaka University, Japan	Intense 14 MeV Neutron Source Facility (OKTAVIAN) at Osaka University
Konno, C.	Japan Atomic Energy Agency, Japan	Fusion Neutronics Source (FNS) Facility at Japan Atomic Energy Agency
Nishio, K.	Japan Atomic Energy Agency, Japan	Surrogate Reaction Study at the JAEA tandem facility
Tanimura Y.	Japan Atomic Energy Agency, Japan	Mono-energetic Neutron Fields Using 4 MV Pelletron Accelerator at FRS / JAEA
Khryachkov, V.	Institute for Physics and Power Engineering, Russian Federation	Neutron experimental facilities for nuclear data measurements at IPPE
Vanhoy, J.	Department of Physics, USA	Measurements with Monoenergetic Fast Neutrons at the University of Kentucky Accelerator Laboratory
Lilley, S.	EURATOM, U.K.	Nuclear Data Capabilities at the ASP Neutron Generator

3.2. ION-INDUCED QUASI-MONOENERGETIC AND WHITE NEUTRON BEAMS

Katabuchi,T.	Research Laboratory for Nuclear Reactors, Japan	Neutron capture cross section measurements in the keV energy region at the Tokyo institute of technology
Iwamoto, Y.	Japan Atomic Energy Agency, Japan	Quasi-monoenergetic Neutron Beam and Its Application at the RCNP Cyclotron Facility
Prokofiev, A.	Uppsala University, Sweden	High-energy Neutron Beam Facilities and Nuclear Data Measurements at The Svedberg Laboratory
Majerle, M.	Nuclear Physics Institute of ASCR PRI, Czech Republic	Fast neutron generators at Nuclear Physics Institute Řež
Ledoux, X.	Grand Accélérateur National d'Ions Lourds, France	The Neutrons for Science Facility at SPIRAL-2
Sakemi Y.	Cyclotron and Radioisotope Center, Japan	High Intensity Fast Neutron Beam Facility at CYRIC
Lantz, J.	Department of Physics and Astronomy, Sweden	Design of a High Intensity Neutron Source for Neutron-Induced Fission Yield Studies

3.3. ELECTRON-INDUCED WHITE SPECTRUM NEUTRON BEAMS

Mondelaers, W.	European Commission, Belgium	Nuclear Data Measurements at GELINA
Junghans, A. R.	Institute of Radiation Physics, Germany	The NELBE Neutron Time-of-Flight Facility
Kim, G.	Department of Physics, Republic of Korea	Activities for Nuclear Data Measurements using Pohang Neutron Facility
Hori J.	Research Reactor Institute, Japan	Nuclear data measurement at KURRI-LINAC

3.4. SPALLATION PROTON-INDUCED (> 200 MEV) WHITE SPECTRUM NEUTRON BEAMS

Ruan, X.	China Institute of Atomic Energy, Peoples republic of China	Study of back-streaming white neutrons at CSNS for nuclear data measurement
Guerrero, C.	CERN Physics Department, Switzerland	Nuclear Data experimental program at CERN for reactor physics
Chiaveri, E.	CERN Physics department Switzerland	The N_TOF Facility at CERN: Status and Perspectives
Shcherbakov,O.	Petersburg Nuclear Physics Institute, Russia	Spallation neutron source of the TOF-facility GNEIS in Gatchina
Katabuchi, T.	Research Laboratory for Nuclear Reactors, Japan	Nuclear Data Measurement Using the Accurate Neutron-Nucleus Reaction Measurement Instrument (ANNRI) in the Japan Proton Accelerator Research Complex (J-PARC)

3.5. NEUTRON BEAMS FROM INVERSE KINEMATIC REACTIONS

Oberstedt, S.	European Commission, Belgium	Nuclear Research with Quasi Mono-Energetic Neutrons at the IPNO LICORNE Facility

2. RESEARCH REACTOR BASED NEUTRON BEAM FACILITIES

2.1 COLD AND THERMAL NEUTRON BEAMS

NUCLEAR DATA MEASUREMENTS AT THE PGAA-NIPS FACILITIES OF THE BUDAPEST RESEARCH REACTOR

T. BELGYA[*], Z. KIS[*], L. SZENTMIKLÓSI[*], ZS. RÉVAY[*, **], F. GUNSING[***], R.B. FIRESTONE[+], A. WALLNER[++]

[*] Nuclear Analysis and Radiography Department, Centre for Energy Research, Hungarian Academy of Sciences, 29-33 Konkoly-Thege M. street, P.O. Box 49
H-1525 Budapest, Hungary
[**] Technische Universität München, Forschungsneutronenquelle Heinz Maier-Leibnitz, Garching, Germany
[***] CEA Saclay, DSM/DAPNIA/SPhN, F-91191 Gif-sur-Yvette, France
[+] Lawrence Berkeley National Laboratory, Nuclear Science Division, Berkeley, CA 94720
[++] Dept. of Nuclear Physics, The Australian National University, Canberra ACT 0200, Australia

Email: belgya.tamas@energia.mta.hu

Abstract

Description of the current status of our PGAA-NIPS experimental setup is presented. Methods, for calculations of thermal capture cross section from partial gamma ray production cross sections are described. High precision radiative capture cross section determination with AMS measurements and methods based on partial gamma ray production cross sections are given for $^{54}Fe(n,\gamma)^{55}Fe$ reaction.

1. INTRODUCTION

Thermal-neutron radiative-capture cross sections (briefly cross section) are important in many fields of applications, including nuclear waste transmutation, reactor design, dosimetry, nuclear medicine, and nuclear astrophysics. In the past few years we worked out a well-established methodology for high-precision measurement of cross sections at the PGAA-NIPS facilities of the Centre for Energy Research [1-4]. Our experimental facility has already been described many times [5, 6], however we will provide here an extended and updated description especially formulated for nuclear-data experiments. This detailed description will be followed by selected examples of international collaborations for nuclear-data–related experiments.

2. THE PGAA-NIPS EXPERIMENTAL FACILITY

The neutron source for the PGAA-NIPS facility is the Budapest Research Reactor (BRR). The VVR-SM type BRR is a 10-MW, water cooled and water moderated research reactor, which has 10 horizontal channels (8 radial and two tangential) for experimental purposes. The conversion from highly enriched (36%) uranium has recently been finished and it will be operated with 19.9% enriched uranium in the future. In the year 2000 a liquid-hydrogen based cold plug was installed close to the beryllium reflector in its 10^{th} tangential channel that serves three neutron guides [7]. The first guide has been upgraded with 2-theta supermirrors, and serves three experimental stations. The PGAA-NIPS facility is situated at the end of the 35 m long curved guide, which reduces the direct view to the core. The highest thermal neutron flux measured in the flux trap is 2.5×10^{14} n·cm^{-2}·s^{-1} and about 10^{14} n·cm^{-2}·s^{-1} fast neutron flux in the fast channel. The initial flux in the first guide tube close to the reactor wall was measured to be 1.18×10^{9} n·cm^{-2}·s^{-1}.

The cross section of guide No. 1 is a 10 cm high and 2.5 cm wide rectangle. The height of the guide center is 100 cm from the ground. The guide ends about 0.5 m from the shielding wall of the PGAA-NIPS cabin. Using a neutron collimator the beam is divided into two 2×2 cm^2 sub-beams. The middles of the upper and lower beams are 6 cm apart. The beam

2.1. Cold and thermal neutron beams

divider is followed by the main beam shutter and downstream an automated upper and lower beam shutters. These can be operated independently and can also be used to chop the beam with programmable cycle time that must be longer than the closing or opening time (about 0.35 s) [5]. The beam chopper system is followed by a neutron monitor and the modular aluminum flight tubes. The first section ends already in the cabin and a rotating disc beam-chopper is attached to its end. This and the beginning of the next flight tube section are shielded by 10 cm thick lead brick box (see Fig. 1.). The aluminum flight tubes are lined with neutron absorbing, enriched ^{6}LiF loaded polymer to shield against the neutrons that are scattered out of the flight path. The flight tubes can be evacuated to decrease the neutron absorption in the air.

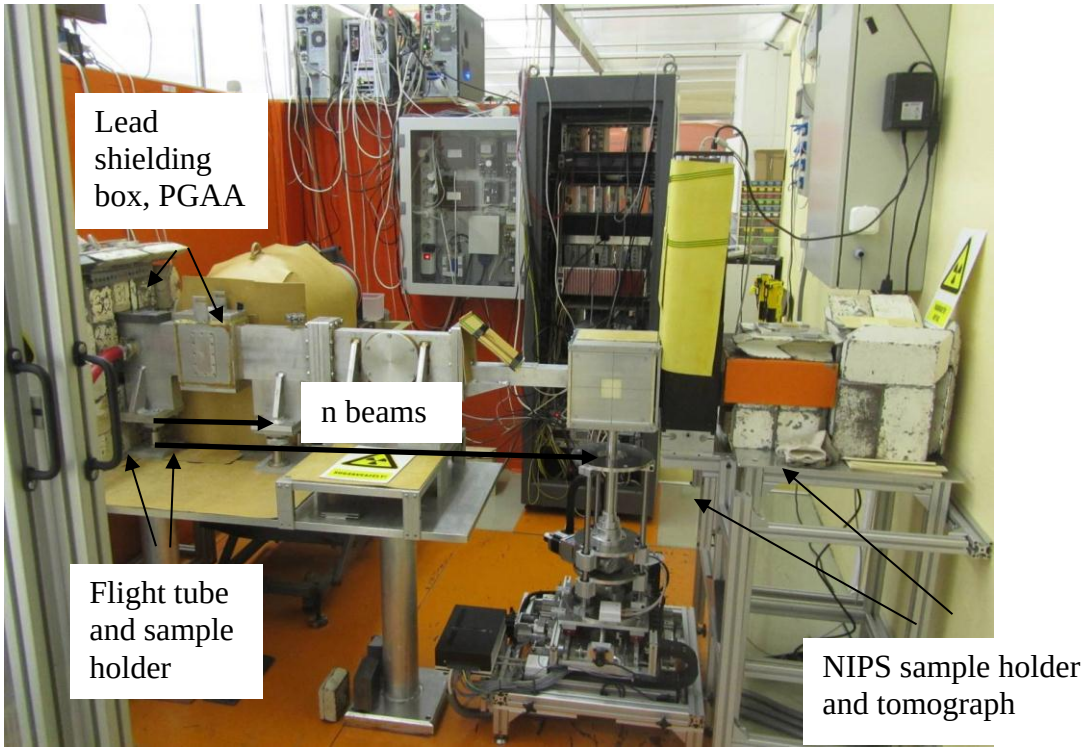

FIG. 1. The photograph of the PGAA-NIPS experimental station. The lead box and the PGAA sample holder are on the left.

The middle of the PGAA sample holder is 60 cm from the wall, and perpendicular to the neutron beam there is a heavily shielded, 27% efficient Compton-suppressed HPGe gamma detector. The upper beam (see Fig. 1.) serves the PGAA station and is stopped 50 cm from the sample, while the lower beam passes through to the NIPS sample holder. The PGAA sample holder can accommodate solid, liquid or gas samples of maximum 4 cm diameter. The most often analysed samples are in powder form and packed in low neutron cross section FEP (Fluorinated ethylene propylene) foil of 25 μm thickness. Radioactive materials can also be irradiated to study their decay properties, but the hazard must be minimized using appropriate sealing. The samples are usually placed in a thin aluminum frame and fixed with FEP strings in their position. The thermal neutron equivalent flux was measured to be 1.2×10^{8} n·cm^{-2}·s^{-1} when evacuated and about 7.75×10^{7} n·cm^{-2}·s^{-1} under normal pressure.

2.1. Cold and thermal neutron beams

At the NIPS station the bottom of the sample chamber is open to the air to host a xyzω sample stage that moves the sample in the 20×20×20 cm^3 box. This station is also equipped with a lead shielded Compton-suppressed 23% HPGe detector, which is not present in Fig. 1 (but shown in Fig. 2) as it would cover the view to the sample stage. Downstream the beam the neutron radiograph can be seen. It contains a neutron-to-light converter scintillation screen and a 45 degree thin aluminum mirror that reflects the converted light to the optics. The optics depicts the 5×5 cm^2 field of view onto the 1.3×1.3 cm^2 CCD chip of Andor iKon-M 934 camera. The setup can also be used to produce neutron tomography pictures that represent the volume absorption in the sample. Selecting interesting points in the sample one can make a PGA analysis of the volume with the collimated HPGe detector. This analysis was named Prompt-Gamma Activation Imaging (PGAI); in combination with neutron tomography we abbreviate it as PGAI–NR/NT [8, 9]. The new tomography system is called NORMA (see Fig. 2.). The currently available thermal equivalent neutron flux is about 2.5×107 n·cm-2·s-1.

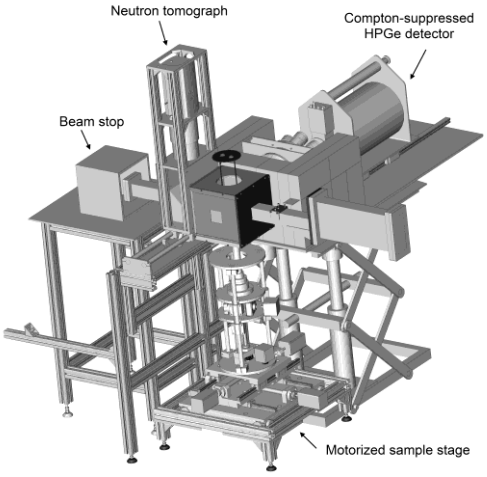

FIG. 2. The CAD drawing of NORMA tomography system and the PGAI detector.The first tomography picture that was made with NORMA is shown in Fig.3.

FIG. 3. Tomography picture of two springs clearly shows the internal small spring placed inside the bigger one.

2.1. Cold and thermal neutron beams

3. THERMAL CAPTURE CROSS SECTION MEASUREMENTS

The measured γ ray-peak count rate R can be described using the following improved equation

$$R_{X\gamma} = P_{X\gamma}\int_V d\underline{r}^3 \varepsilon(E_\gamma,\underline{r}) n_X(\underline{r}) g(E_\gamma,\underline{r}) \int_0^\infty d\nu \int_\Omega d\Omega \cdot \sigma_X(\nu)\Phi(\nu,\underline{\Omega},\underline{r},t)\,, \tag{1}$$

where P_γ is the absolute emission probability (for one neutron capture) of the de-exciting γ ray, $\varepsilon(E\varepsilon,\underline{r})$ is the detector efficiency at gamma energy E_γ, t is the irradiation and measurement time, V is the volume of the target, ν is the neutron velocity, $\underline{\Omega}$ is the unit length direction vector at point $\underline{r}$ in the sample through which the neutron is propagating, $n_X(\underline{r})$ is the number of atoms of type X at point $\underline{r}$ in the unit volume, $\sigma_X(\nu)$ is the capture cross section of atom type X, $\Phi(\nu,\underline{\Omega},\underline{r},t)$ is the scalar neutron flux density, dΩ is the differential solid angle around $\underline{\Omega}$ and $g(E_\gamma,\underline{r})$ is the gamma absorption in the target.

To arrive an analytical solution is rather difficult for a general sample. In practice Monte Carlo simulation is used instead. With the following assumptions we can avoid all of these complications that are posed by the need to solve the neutron transport inside the sample.

1. The cross section of the sample materials are of $1/\nu$ behavior. This means that the cross section can be expressed with the thermal (*th*) values
$$\sigma(\nu) = \sigma(\nu_{th})\frac{\nu_{th}}{\nu} \tag{2}$$
2. The number density of atoms does not depend on the position in the sample (homogeneous sample). Thus $n_X(\underline{r}) = n_X/V$ so the constant can be moved out from the integral.
3. The flux does not change in time.
4. Gamma and neutron absorption of the target is negligible i.e. $g = 1$.
5. The variation of the detection efficiency is small throughout the target volume

With the above assumptions Eq. (1) can be written as

$$R_{X\gamma} = P_{X\gamma}\varepsilon(E_\gamma) n_X \sigma_X(\nu_{th})\nu_{th}\frac{1}{V}\int_V d\underline{r}^3 \int_\Omega d\Omega \int_0^\infty d\nu N(\nu,\underline{\Omega},\underline{r})\,. \tag{3}$$

In this equation the neutron density $N(\nu,\underline{\Omega},\underline{r})$ (= $\Phi(\nu,\underline{\Omega},\underline{r}) / \nu$) in phase in phase space is introduced. The triple integral over the phase space provides the number of neutrons N in the target volume V. The final equation using $\sigma_{X\gamma} = P_{X\gamma}\sigma_X(\nu_{th})$ and $\phi_{th} = \frac{\nu_{th} N}{V}$ notations is

$$R_{X\gamma} = \varepsilon(E_{X\gamma}) n_X \sigma_{X\gamma}\phi_{th}\,. \tag{4}$$

The above assumptions correspond to a very thin, homogeneous sample. If the cross section is low and if the sample contains a homogeneous mixture of an unknown X and a well known comparator C, then dividing Eq. (4) with a similar equation for the comparator we arrive to the equation from which the cross section of the unknown can be determined.

$$\sigma_{X\gamma} = \sigma_{C\gamma}\frac{R_{X\gamma}}{R_{C\gamma}}\frac{n_C}{n_X}\frac{\varepsilon(E_{C\gamma})}{\varepsilon(E_{X\gamma})}\frac{f(E_{C\gamma})}{f(E_{X\gamma})}\,. \tag{5}$$

2.1. Cold and thermal neutron beams

Here we have relaxed assumption 4. and let γ ray and neutron absorptions be taken into account with the appropriate correction factors $f(E_\gamma)$. We call any experiment, which uses Eq. (5) a comparison or standardization experiment. It can be used such a way that the comparator is used to determine the flux ϕ_{th}, which can be used to calculate the partial cross section $\sigma_{X\gamma}$ from Eq. (4). Partial cross sections do not give directly the total capture cross section. We identified the ways to calculate this that are summarized in Table 1.

TABLE. 1. METHODS FOR CALCULATION OF TOTAL CAPTURE CROSS SECTION FROM MEASURED PARTIAL CROSS SECTIONS. METHOD 4, THE CROSSING INTENSITY SUM (CIS) IS EXPLAINED IN DETAIL IN REFS. [12, 13]

Method	Equation	Notes
1	$\sigma_{th} = \frac{\sigma_\gamma}{\theta P_\gamma}$	P_γ must be known, for example from beta decay if the captured nucleus is unstable.
2	$\sigma_{th} = \sum_{f=1}^{n-1} \sigma_{\gamma C \to f}(1+\alpha_f)(1+PCC_f)$	The sum of all primary transitions from the capture state can be used for nuclei with relatively simple decay scheme.
3	$\sigma_{th} = \sum_{i=2}^{n} \sigma_{\gamma i \to g.s.}(1+\alpha_i)(1+PCC_i)$	The sum of all ground state transitions can be used for nuclei with relatively simple decay scheme. Conversion coefficients α must be known.
4	Average of CISs: $Q = \min\left(\sum_{\substack{1\le f\le n-1 \\ 1\le s\le n-1}} (T_f - \sigma_{th}) w_{f,s} (T_s - \sigma_{th}) \right)$	Well balanced and relatively simple decay scheme. Conversion coefficients α must be known.
5	$\sigma_{th} = \sum_i E_i \sigma_{\gamma i}(1+\alpha_i)(1+PCC_i)/B_n$	The energy weighted sum can be used for any nuclei with resolved gamma-transitions. E_i is the energy of the transition, B_n is the binding energy and *PCC* is the pair conversion.

Method 5 is applicable for unfolded spectrums as well if the conversion coefficients are negligible. This and method 1 requires the less knowledge of the decay scheme. The precision of method 1 depends on a priori knowledge of the absolute decay probability P_γ. Precision of method 5 depends on the accurate identification of gamma rays and on the magnitude of the conversion coefficients. If this latter is not negligible then knowledge of the level scheme is vital. All other method requires the knowledge of the decay-scheme. From this point of view method 5 is equivalent to the weighting function technique used for C_6D_6 detectors.

4. AN EXAMPLES FOR HIGH PRECISION CROSS SECTION APPLICATION

Ironically, the uncertainty of thermal neutron radiative capture cross section (briefly cross section) of iron, the basic construction material of reactors is known for 1% only for the element, but not for its isotopic contributors (see TAB 2) [14]. Its cross section is not only important for reactor physics, but also for nuclear astrophysics.

Recently, we have performed two sets of experiments within the EFNUDAT project, which aimed to improve the situation. The first set of experiments was proposed by Anton Wallner from TU Vienna and performed in collaboration. Two samples were used in the

experiments, one natural iron powder mixed with gold powder and pressed to a pellet, and another iron pellet sandwiched in between gold foils to measure the neutron fluence. The activation of the 0.5 cm diameter thin iron samples were performed in the NIPS sample holder. The masses of iron were about 45 mg with about 22 mg gold. Similar samples were also irradiated at the thermal irradiation position of the Atominstitut of the Vienna University of Technology. The amount of activation product in the $^{54}Fe(n,\gamma)^{55}Fe$ reaction was measured at the accelerator mass spectrometry (AMS) laboratory VERA of TU Vienna. Since the 2.73 y half-life ^{55}Fe decays almost exclusively to stable ^{55}Mn ground state without observable gamma radiation, the AMS is the only way to determine the number of activated ^{55}Fe atoms. The obtained 2.32 ± 0.10 b cross section has smaller uncertainty and it is in agreement with the evaluated value of Mughabghab [15].

TABLE. 2. THERMAL NEUTRON CAPTURE CROSS SECTION FOR NATURAL IRON AND IRON ISOTOPES

Isotope	Abundance %	Thermal Xsection (b)	Uncertainty
Fe-nat.		2.56±0.03	1%
Fe-54	5.845	2.25±0.18	8%
Fe-56	91.754	2.59±0.14	5%
Fe-57	2.119	2.48±0.3	12%
Fe-58	0.282	1.28±0.05	4%

Recently, we have performed two sets of experiments within the EFNUDAT project, which aimed to improve the situation. The first set of experiments was proposed by Anton Wallner from TU Vienna and performed in collaboration. Two samples were used in the experiments, one natural iron powder mixed with gold powder and pressed to a pellet, and another iron pellet sandwiched in between gold foils to measure the neutron fluence. The activation of the 0.5 cm diameter thin iron samples were performed in the NIPS sample holder. The masses of iron were about 45 mg with about 22 mg gold. Similar samples were also irradiated at the thermal irradiation position of the Atominstitut of the Vienna University of Technology. The amount of activation product in the $^{54}Fe(n,\gamma)^{55}Fe$ reaction was measured at the accelerator mass spectrometry (AMS) laboratory VERA of TU Vienna. Since the 2.73 γ half-life ^{55}Fe decays almost exclusively to stable ^{55}Mn ground state without observable gamma radiation, the AMS is the only way to determine the number of activated ^{55}Fe atoms. The obtained 2.32 ± 0.10 b cross section has smaller uncertainty and it is in agreement with the evaluated value of Mughabghab [15].

The second set of experiments were proposed by Frank Gunsing (CERN) to measure the purity of highly enriched $^{54,56,57}Fe$ samples. The results were presented at the Final Scientific workshop of EFNUDAT [16]. The measured data is also useful for the determination of high precision cross sections. Here we concentrated on the $^{54}Fe(n,\gamma)^{55}Fe$ reaction. To be able to improve the accuracy of the partial gamma ray cross sections σ_γ-s for

the ^{54}Fe capture, a new standardization experiment was performed on a pyrite (FeS_2) sample. It yielded a more accurate 0.0282(3) b value for the 411.6 keV transition of ^{55}Fe. It was reported to be 0.022(5) b in the PGAA handbook [17]. Using this value in the internal calibration (renormalization) of the gamma ray intensities of the ^{54}Fe enriched sample measurement we obtained accurate σ_γ values.

In collaboration with R.B. Firestone, a new decay scheme of ^{55}Fe was created from the capture data. The new decay scheme contains 58 levels and 234 gamma ray transitions, which 8 times as much that is shown in the ENSDF (see Fig. 4).

Applying methods 2-5 the following thermal total capture cross sections can be obtained:

Sum of primaries	2.26(5) b
Sum of ground state transitions	2.32(5) b
Energy weighted sum	2.26(4) b
Mughabghab (compilation)	2.25(18) b

Method 4 (CIS) and the corresponding in-out balance can be represented in Fig. 5.

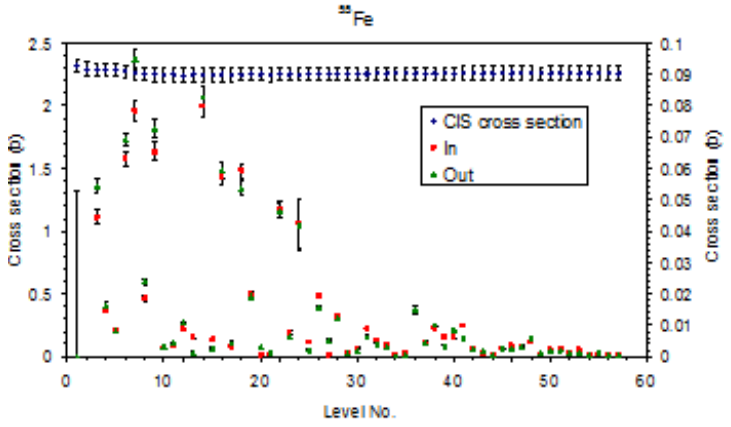

FIG. 5. CIS cross sections (blue), in and out intensities (red and green symbols and right scale). Both of them are in the function of level number.

All of the new cross sections are in agreement with Mughabghab's compilation but they have significantly lower uncertainties.

5. SUMMARY

Description of the current status of our PGAA-NIPS experimental setup is presented. Methods, identified for calculations of thermal capture cross section from partial gamma ray production cross sections are described in detail. Finally, novel method based on AMS measurements and demonstration of methods using partial gamma ray production cross sections are given for ^{54}Fe(n,γ)^{55}Fe reaction. The latter methods utilized the new decay scheme of ^{55}Fe built in collaboration with R. Firestone.

2.1. Cold and thermal neutron beams

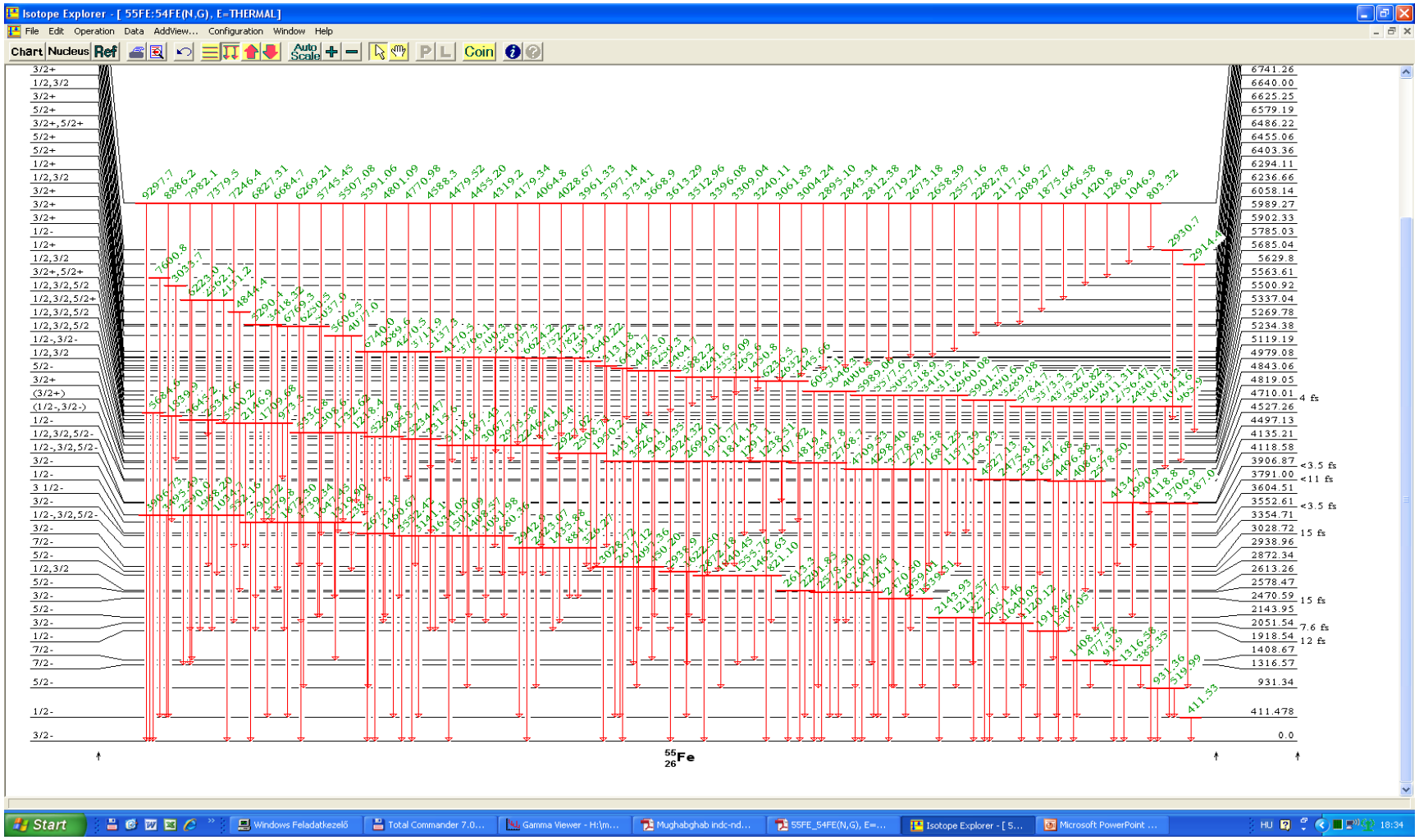

FIG. 4. The new $^{54}Fe(n,\gamma)^{55}Fe$ decay scheme as shown by Isotope Explorer.

ACKNOWLEDGEMENT

Thanks for the support of OMFB 0018/2006 NAP VENEUS05, Baross Gábor project (REG_KM_INFRA_09) NORMA10, EFNUDAT (EURATOM contract no. 036434) and ERINDA no. 269499 projects.

REFERENCES

[1] BELGYA, T., SZENTMIKLÓSI, L., KIS, Z., NAGY, N.M., AND J. KÓNYA, IAEA: Vienna. INDC(HUN)-0037 1-10 (2012)

[2] BELGYA, T., Prompt Gamma Activation Analysis at the Budapest Research Reactor Physics Procedia, 31 99-109 (2012)

[3] BELGYA, T., Determination of thermal radiative capture cross section in: EFNUDAT Slow and Resonance Neutrons, a Scientific Workshop on Nuclear Data Measurements, Theory and Applications, 23-25 September 2009 Budapest, Hungary: II-HAS eds. T. Belgya, 115-120 (2010)

[4] BELGYA, T., REVAY, Z., AND SZENTMIKLOSI, L., Determination of Thermal Neutron Capture Cross Sections Using Cold Neutron Beams at the Budapest PGAA and NIPS Facilities in: ^{12}th International Symposium on Capture Gamma ray Spectroscopy and Related Topics, September 4-9, 2005 University of Notre Dame, Indiana, USA: AIP Melville, New York eds. A.A. Andreas Woehr, 300-306 (2006)

[5] SZENTMIKLÓSI, L., BELGYA, T., RÉVAY, Z., AND KIS, Z., Upgrade of the Prompt-Gamma Activation Analysis (PGAA) and the Neutron Induced Prompt-gamma Spectroscopy (NIPS) facilities at the Budapest Research Reactor, J. Radioanal. Nucl. Chem., 286 501-505 (2010)

[6] RÉVAY, Z., et al., Cold neutron PGAA facility at Budapest, Nucl. Instrum. & Methods B 213 385-388 (2004)

[7] ROSTA, L., L. CSER, and Z. RÉVAY: Gain factors with the new supermirror guide system at the Budapest Neutron Centre, Appl. Phys. A 74 S292-S294 (2002)

[8] BELGYA, T., et al., First elemental imaging experiments on a combined PGAI and NT setup at the Budapest Research Reactor, J. Nucl. Radioanal. Chem., 278(3) 751-754 (2008)

[9] BELGYA, T. AND LAZAR K., First experiments on a new in-beam Mossbauer spectroscopy station at the Budapest Research Reactor, J. Nucl. Radioanal. Chem., 276(1) 269-272 (2008)

[10] KIS, Z., et al., Determination of the total neutron capture cross section for ^{58}Ni(n,γ)^{59}Ni reaction in: EFNUDAT Slow and Resonance Neutrons, a Scientific Workshop on Nuclear Data Measurements, Theory and Applications, 23-25 September 2009 Budapest, Hungary: II-HAS eds. T. Belgya, 121-126 (2010)

[11] BELGYA, T., Target preparation for in-beam thermal neutron capture experiments in: EFNUDAT Fast Neutrons, Scientific Workshop on Neutron Measurements, Theory and Applications Nuclear Data for Sustainable Nuclear Energy, Geel, Belgium, 28 – 30 April, 2009: European Commission eds. F.-J. Hambsch, 21-26 (2010)

[12] BELGYA, T., New gamma ray intensities for the N-14(n,gamma)N-15 high energy standard and its influence on PGAA and on nuclear quantities, J. Nucl. Radioanal. Chem., 276(3) 609-614 (2008)

[13] BELGYA, T., Improved accuracy of gamma ray intensities from basic principles for the calibration reaction ^{14}N(n,γ)^{15}N, Physical Review C, 74 024603-1-8 (2006)

2.1. Cold and thermal neutron beams

[14] Mughabghab, S.F., Thermal Neutron Capture Cross Cections, Resonance Integrals and G-Factors, International Atomic Energy Agency INDC(NDS)-440, Vienna, (2003)

[15] WALLNER, A., et al., Precise Measurement of the Neutron Capture Reaction $^{54}Fe(n,\gamma)^{55}Fe$ via AMS in: Nuclear Physics in Astrophysics IV, Lab. Nazionali di Frascati with Lab. Nazionali del Gran Sasso, June 8th to 12th 2009: Journal of Physics Conference Series 202 eds. 012020 (2010)

[16] BELGYA, T. AND KIS, Z., PGAA analysis of isotopically enriched samples in: Proceedings of the Final Scientific EFNUDAT Workshop, CERN, Geneva, Switzerland, 30 Aug – 2 Sept 2010: European Laboratory for Particle Physics (CERN) eds. E. Chiaveri, 1-7 (2011)

[17] RÉVAY, Z., et al., Handbook of Prompt Gamma Activation Analysis with Neutron Beams, G.L. Molnár, Editor. Kluwer Academic Publishers, Dordrecht, Boston, London 173-366 (2004)

DETERMINATION OF PARTIAL GAMMA RAY PRODUCTION CROSS-SECTIONS IN COLD NEUTRON BEAMS

ZSOLT RÉVAY [*, **]

[*]Technische Universität München, Forscgungsneutronenquelle Heinz Maier-Leibnitz, Garching, Germany
[**]Center for Energy Research, Laboratory for Nuclear Analytical Chemistry and Radiography, Budapest, Hungary
Email:zsolt.revay@frm2.tum.de

1. INTRODUCTION

Cold neutron beam facilities have been used in material science with a great success for a few decades. At the same time, prompt gamma activation analysis (PGAA) using cold neutron beams also started propagating, and these days, most of the large neutron centers operate PGAA facilities, too. In-beam activation is a proper technique for determining nuclear data related to neutron capture, too. A spectroscopy database for PGAA suitable for accurate chemical analysis was not available until the end the 1990s.

The first almost complete series of measurements of prompt gamma spectra for 75 elements was performed at Massachusetts Institute of Technology (MIT) [1, 2]. The most ambitious effort to establish a comprehensive library from these measurements was the Chalk River compilation [3]. The "Lone table" and its electronic version distributed with an IAEA Technical Report [4] has been the only source of spectroscopic data for scientists working in the field of PGAA for twenty years.

After the start-up of the PGAA facility at Budapest in 1996, our goal was to establish a catalog for the neutron capture data that can be reliably used at any laboratories for chemical analysis. The measurements took place from 1997 to 2000. This database has been used in Budapest, Garching and partly at other facilities for analysis, and its different compilations have been published in two books [5, 6]. The revision of the database is continuous.

2. SPECTROSCOPY DATABASE FOR PGAA

Three sets of measurements were performed in the frame of the "library" measurements:

Elemental spectra. Whenever it was possible, the pure element was irradiated in the thermal neutron beam at Budapest [8]. When the elemental form was not available, other simple compound, mainly oxides, sometimes hydroxides, or carbonates were measured. The spectra were evaluated with Hypermet-PC [9]. In these measurements, the relative intensities and the relative positions of the gamma ray peaks were obtained.

Energy calibration. The element of interest was irradiated together with chlorine, either in the form of a chloride containing compound, or together with a PVC foil. A low-energy and a high-energy peak were selected from the elemental spectrum, and their energies were accurately determined based on the energy-difference method using the accurately known energies of close-lying, strong chlorine peaks [10]. In case of heavier elements, sometimes two measurements with different chlorine contributions were performed, so that the peak areas of the selected peaks were similar to those of the calibrating chlorine peaks. The two lines then were used to calibrate the elemental spectrum.

2.1. Cold and thermal neutron beams

Standardization. The partial gamma ray production cross section of the best-statistics line was determined in a relative measurement of a stoichiometric compound, or a homogeneous mixture (e.g. water solution) using the following equation:

$$\frac{A_1/\varepsilon_1}{A_2/\varepsilon_2} = \frac{n_1}{n_2}\frac{\sigma_{\gamma,1}}{\sigma_{\gamma,2}}$$

Where A is the peak area, ε is the counting efficiency, n is the stoichiometric coefficient and σ_γ is the partial gamma ray production cross section, while indices 1 and 2 stand for the two different nuclides, one is the unknown the other is the comparator. Once the cross section of the comparator is known, the detector is calibrated (i.e. the efficiency ratio is determined), the molar ratio is also known, the peak areas have been evaluated carefully, the cross section of the unknown can also be derived from the above equation. As the ultimate comparator, hydrogen was used and everything was standardized directly or indirectly relative to its only line at 2223 keV with the cross section of 0.3326 barn ± 0.2%. Intermediate comparators were Cl, C, N.

The data library has been verified in a large number of chemical analyses in Budapest and in Garching. The data were revised a couple of times during the last 12 years. Besides chemical analysis, it has been used for nuclear model calculations, too [11].

3. PGAA FACILITIES

3.1. THERMAL PGAA FACILITY AT BUDAPEST

The first neutron guide, serving the PGAA facility, was 35 m long, curved and was coated with natural nickel. The flux of the thermal neutrons was 2.5×10^6 cm^{-2} s^{-1}. This flux was enough for the library measurements and for plenty of different applications. In 2001, the cold neutron source started its operation at the Budapest Research Reactor, at the same time the old neutron guides were replace with new 2*m* supermirror-coated ones. As a result of this, the flux is about 10^8 cm^{-2} s^{-1}. The sample chamber can be evacuated. The sample-to-detector distance is 235 mm. The detector system is the same: the main detector is a high-purity germanium detector with a relative efficiency of 25%. It is coaxially surrounded by a bismuth germanate (BGO) scintillator annulus to suppress the Compton-scattered photons. The whole detector system is covered with a lead shielding with a thickness of 10 cm. The Compton-suppression is very efficient; the baseline is reduced with more than an order of magnitude. The room and the beam background count rates were 0.6 and 2.5 counts per second, respectively.

More details on the current status of this facility are given in a separate contribution to this report.

3.2. FOCUSED COLD PGAA FACILITY AT GARCHING

The PGAA facility at Garching is located at the end of a curved supermirror neutron guide with the length of 55m. The last 7 m is elliptically tapered, whose last 110cm can be removed from the beam, and replaced with a series of collimators (see Fig. 1).

2.1. Cold and thermal neutron beams

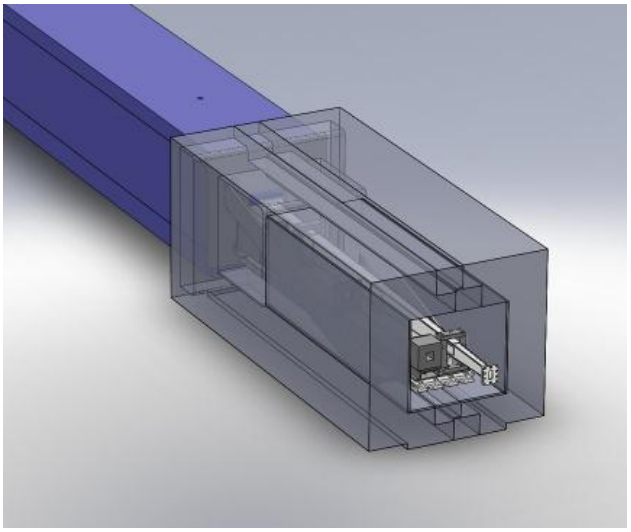

FIG. 1. The last section of the neutron guide at the Garching PGAA facility with the interchangeable elliptical guide-collimator system.

The focused beam has a maximum flux of 6×1010 cm–2 s–1, while the collimated beam 2×10^{9} cm–2 s–1 with a uniform flux distribution. The sample chamber can be evacuated, and contains an automatic sample changer. The sample-to-detector distance is 33 cm. The 60%-efficiency HPGe detector is surrounded by a BGO Compton suppressor and 15–20 cm of lead (see Fig. 2).

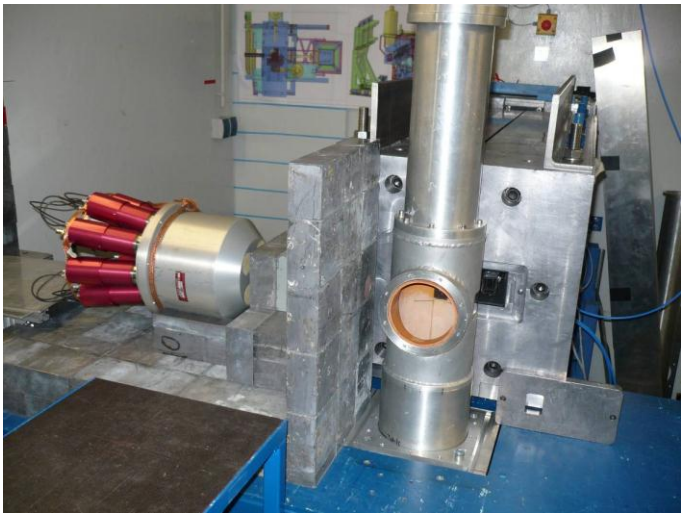

FIG. 2. The PGAA facility at Garching without the lead shielding. To the left: the BGO with the collimator and the frontal lead shielding, in the middle: the sample chamber (lined with 6Li-containing polymer), behind it the end of the neutron guide and its shielding.

The room background is 4 cps. The beam backgrounds are 20 cps and 400 cps for the collimated and for the high flux, respectively. A series of attenuators help to adjust the neutron flux to control the optimum count rate in the spectrometer, they have the transmissions of 50%, 20% and 6%.

REFERENCES

[1] ORPHAN, V.J., et al. Line and Continuum Gamma ray Yields from Thermal Neutron Capture in 75 Elements, Report DASA 2570 (GA 10278), Gulf General Atomic, 1970.

[2] RASMUSSEN, N. C., Yet al., Thermal Neutron Capture Gamma ray Spectra of the Elements, Massachusettes Institute of Technology Report, MITNE-85, Cambridge, MS, 1969.

[3] LONE, M. A., et al., Atomic Data and Nuclear Data Tables, 26 (1981) 511.

[4] Handbook on Nuclear Data for Borehole Logging and Mineral Analysis (Tr-357) International Atomic Energy Agency, Vienna (1993).

[5] CHOI, H.D., et al., Database of prompt gamma rays from slow neutron capture for elemental analysis, International Atomic Energy Agency, Vienna, 2007.

[6] RÉVAY, Zs.,eta al., Catalog and Atlas of Prompt Gamma Rays in Handbook of Prompt Gamma Activation Analysis with Neutron Beams, (G.L. Molnár ed.), Kluwer Academic Publishers, Dordrecht/Boston/New York, 2004, pp. 173–364.

[7] RÉVAY, Zs., et al., New prompt k_0 and partial cross section values measured in the cold neutron beam of Budapest Research Reactor, J. Radioanal. Nucl. Chem., 265 (2005) 2.

[8] BELGYA, T., et al.,The new Budapest capture gamma ray facility, in Proc. 9th International Symposium on Capture Gamma ray Spectroscopy and Related Topics, Budapest, Hungary, October 8-12, (G. Molnár, T. Belgya, Zs. Révay Eds.), Springer Verlag Budapest, Berlin, Heidelberg, 1997, pp. 826–837.

[9] FAZEKAS, B., et al.,The new features of Hypermet-PC, in: Proc. 9th International Symposium on Capture Gamma ray Spectroscopy and Related Topics, Budapest, Hungary, October 8-12, (G. Molnár, T. Belgya, Zs. Révay Eds.) Springer Verlag, Budapest/Berlin/Heidelberg, 1997, p. 774.

[10] KRUSCHE, B., et al., Nucl. Phys. A 386 (1982) 245.

[11] KRTICKA, M., et al., Thermal neutron capture cross sections of the palladium isotopes, Phys. Rev. C, 77 (2008) 054615

PRECISION NUCLEAR DATA MEASUREMENTS AT INSTITUT LAUE LANGEVIN

U. KÖSTER

Institut Laue Langevin, 6 rue Jules Horowitz
38042 Grenoble Cedex 9, France

Email:koester@ill.eu

Abstract

The Institut Laue Langevin in Grenoble hosts about forty instruments that are served with neutrons by a 58 MW high flux reactor. Most instruments use extracted neutron beams with neutron energies ranging from few neV to about 1 eV, reaching capture fluxes up to 2×10^{10} $cm^{-2}s^{-1}$. Optionally these neutron beams can be spin polarized to >99%, rendered monochromatic by crystal diffraction or velocity selectors or chopped for time-of-flight measurements. While the majority of these instruments serves usually for neutron scattering experiments in condensed matter physics, chemistry, biology and materials science, some instruments are entirely dedicated to nuclear physics and others can be shared for nuclear physics applications. Recent campaigns combining an intense cold neutron beam with powerful arrays of gamma ray detectors (Ge and $LaBr_3$ detectors respectively) are providing a wealth of new nuclear data with (n,γ) and (n,f) reactions. In addition in-pile positions with neutron fluxes up to 1.5×10^{15} $cm^{-2}s^{-1}$ are available. These serve for sample activation or on-line studies of fission, of (n,γ), (n,p) and (n,α) reactions respectively.

1. INTRODUCTION

The 58 MW high flux reactor of the Institut Laue Langevin in Grenoble provides slow neutrons for about 40 different instruments. Most of these instruments use extracted neutron beams for neutron scattering applications, but some of them can be used for nuclear data measurements. This covers nuclear data in a wide sense: cross-sections, branching ratios, half-lives, fission yields, fission product properties, gamma ray energies, binding energies, scattering lengths, etc.

Reviews of such applications of ILL instruments were given recently in references [1,2]. In the present contribution we summarize typical applications, show new applications, e.g. those profiting of a unique combination of intense neutron beams and powerful gamma ray detection arrays and give an outlook to future applications of ILL instruments that could contribute in providing precision nuclear data.

2. DIFFERENT NEUTRON ENERGIES

2.1. THERMAL NEUTRONS

Most beam tubes ending in the heavy water tank of ILL's high flux reactor extract thermal neutrons. Bragg diffraction at various crystals (Cu, Ge, HOPG) provides monochromatic neutron beams at fluxes up to 10^8 $cm^{-2}s^{-1}$ over areas of several cm^2 surface. Some monochromators focus the neutron beam horizontally and/or vertically onto the sample to increase the flux.

2.2. HOT NEUTRONS

Some beam tubes are pointing at the "hot neutron source" of the ILL reactor, thermally insulated graphite placed at about 20 cm from the fuel element, which is heated by gamma radiation from the reactor core to about 2000°C. Thus, the neutron spectrum is shifted towards higher energies and shorter wavelengths compared to thermal neutrons. After crystal

diffraction monochromatic "hot" neutrons are available for experiments. At 0.1 eV neutron energy a flux of 4×10^7 $cm^{-2}s^{-1}$ is available, dropping to 10^6 $cm^{-2}s^{-1}$ at 1 eV.

2.3. COLD NEUTRONS

The thermal neutron energy spectrum of the reactor can also be shifted to lower energies and longer wavelengths by down-moderation in one of ILL's two cold sources. These are in-pile vessels filled with 25 K cold liquid deuterium. Neutron guides pointing at a cold source will extract a spectrum of cold neutrons. Several instruments are served by these neutron guides, thereof one instrument that is dedicated to applications in nuclear and neutron physics: PF1B.

2.4. VERY COLD AND ULTRACOLD NEUTRONS

Still lower neutron energies compared are available at the PF2 beam lines. A vertical beam tube extracts neutrons from the vertical cold source. The progressive curvature of the neutron guide eliminates all neutrons but those with the lowest energies. This results in a beam of very cold neutrons with a flux of 4×10^6 $cm^{-2}s^{-1}$ at 8 μeV over an area of 7×3.4 cm^2. Very cold neutrons (VCNs) can be "cooled" even further by collisions with a neutron turbine [4]. The produced ultracold neutrons (UCNs) with energies between 0 and 250 neV are totally reflected under all angles from suitable surfaces (e.g. nickel, diamond-like-carbon, beryllium, etc.) and can thus be stored for several minutes in so-called neutron bottles.

A flux of 3×10^4 $cm^{-2}s^{-1}$ UCNs is available over an area up to 14×10 cm^2. Due to the 1/v behaviour the cross-sections for VCNs and UCNs are huge, making it possible to achieve significant absorption even for very thin samples, e.g. made from rare enriched or highly radioactive isotopes.

Meanwhile three additional UCN sources are operating at ILL. These so-called superthermal sources are based on down-scattering of cold neutrons (E≈1 meV) in pure superfluid ^{4}He [5].

3. DEDICATED NUCLEAR PHYSICS INSTRUMENTS

Most instruments at ILL are devoted to neutron scattering. They can be classified as [3]:

a) two-axis diffractometers with one- or two-dimensional neutron detectors,
b) three-axis spectrometers with an energy analyzing crystal between sample and neutron detector to study inelastic processes,
c) time-of-flight spectrometers with a chopped neutron beam.

However, there are also instruments dedicated or shared for nuclear physics applications.

3.1. THE PF1B INTENSE COLD NEUTRON BEAM WITH POLARIZATION OPTION

PF1B is a multipurpose beam port where an intense beam of cold neutrons with a capture flux of 2×10^{10} $cm^{-2}s^{-1}$ on a 20×6 cm^2 area is available. The cold neutrons are transported from the cold source by a ballistic supermirror neutron guide [6] to the experimental area which eliminates background of gamma rays or fast neutrons from the reactor completely. Remaining background of fast neutrons and gamma rays is mainly

generated locally by the neutron beam collimation system. The average neutron energy of the PF1B beam is 5.4 meV corresponding to a Maxwellian spectrum at 62 K. With the use of super-mirror polarizers, the PF1B neutron beam can be polarized up to 99.7%. For a fully polarized beam the capture flux is still 3×10^{9} $cm^{-2}s^{-1}$.

While many experiments use the entire spectrum of the white neutron beam, it is also possible to select individual energies. A Dornier/Astrium velocity selector rotating at up to 28300 rpm allows selecting neutron energies up to 13 meV with a transmission above 80% and a velocity resolution of about 10% FWHM [7].

The polarized PF1B beam is frequently applied for experiments in "neutron particle physics", i.e. detailed studies of the free neutron decay. Various standard model parameters can be extracted from a precise measurement of angular distributions and correlations of the electrons and protons emitted in neutron decay, see ref. [8] for a review. Parity violating asymmetry was also observed in neutron-induced reactions, namely for the tritons emitted in ^{6}Li(n,α)t and the gamma rays emitted in ^{10}B(n,αγ)^{7}Li reactions induced by polarized cold neutrons [9]. Even the angular distribution of ternary particles emitted in fission induced by polarized neutrons was found to be correlated with the neutron spin [10].

Unpolarized, the intense cold neutron beam can serve for cross-section measurements. Due to the high flux even very rare or radioactive targets can be studied, such as the ^{39}Ar(n,α) reaction [11]. Measurements of fission cross-sections and of yields and energy distributions of ternary fission fragments [12] at PF1B are reviewed in ref. [13].

The large area experimental zone ($3\times10\times3$ m^{3}) permits the installation of complex setups. Fission targets can be surrounded by an array of Ge detectors for spectroscopy of prompt and delayed gamma transitions. The spectroscopy of nanosecond-isomers in fission fragments with such a setup is discussed in ref. [14].

The PF1B neutron beam can also be collimated to a halo-free pencil beam of 1 cm diameter with a capture flux of about 10^{8} $cm^{-2}s^{-1}$. This enables clean gamma ray spectroscopy after (n,γ) or (n,f) reactions. In 2010 and 2011 the first two experimental campaigns with this beam used an array of 8 coaxial Ge detectors arranged in a ring around the target [15]. Thus, detailed angular correlation measurements can be performed to assign unambiguously multipolarities of transitions in a (n,γγ') cascade [16].

In 2012 and 2013, the so-called EXILL campaign uses a powerful Ge detector array consisting of part of the EXOGAM array from GANIL Caen, complemented by ILL clover detectors and GASP coaxial detectors from LNL Legnaro and $LaBr_3$:Ce fast timing detectors of the FATIMA collaboration respectively. The combination of nearly 50 individual Compton suppressed detectors provides high overall efficiency and high granularity. This enables very detailed nuclear spectroscopy, exploiting also higher-fold γγγ or γγγγ coincidences to find and clearly assign weak transitions, assign transition multipolarities by angular correlations, study gamma ray polarization by Compton polarimetry, etc. Now, in addition to (n,γ) reactions on rare targets also fissile targets are employed for precision measurements of prompt gamma rays in fission and detailed nuclear spectroscopy of excited states in neutron-rich nuclei far from stability.

3.2. THE S18 NEUTRON INTERFEROMETER

S18 is a thermal neutron interferometer using perfect Si crystals for beam splitting and merging [18,19]. The incident neutron's wavefunction is split into a transmitted and diffracted component by a first Si lamella protruding out from a Si single crystal. Both beams pass one or two different samples before being diffracted by a second Si lamella onto a third Si lamella where they are recombined. Downstream of the third Si lamella the interference count rates are monitored as function of phase difference between both beams. A turnable Si crystal placed between the second and third Si fin acts as phase shifter. In addition to a multitude of quantum mechanics experiments with neutrons, neutron interferometry allows to measure the coherent scattering length with precision. When a sample is placed in one interferometer arm, the neutron path length in the sample induces an additional phase shift that can be measured by scanning the interference pattern with the phase shifter. The coherent scattering length of the sample material can be precisely deduced from the measured phase shift. When the total scattering differential cross-section is measured, e.g. by diffraction of hot neutrons, also the incoherent scattering length can be deduced [20].

3.3. THE GAMS CRYSTAL SPECTROMETERS

Using perfect Si or Ge crystals for diffraction of gamma rays instead of neutrons allows allows performing precision spectroscopy of gamma rays. This is exploited in the "GAMS" crystal spectrometers. Two such spectrometers are placed at the tangential through-going beam tube H6/H7, see Fig. 1.

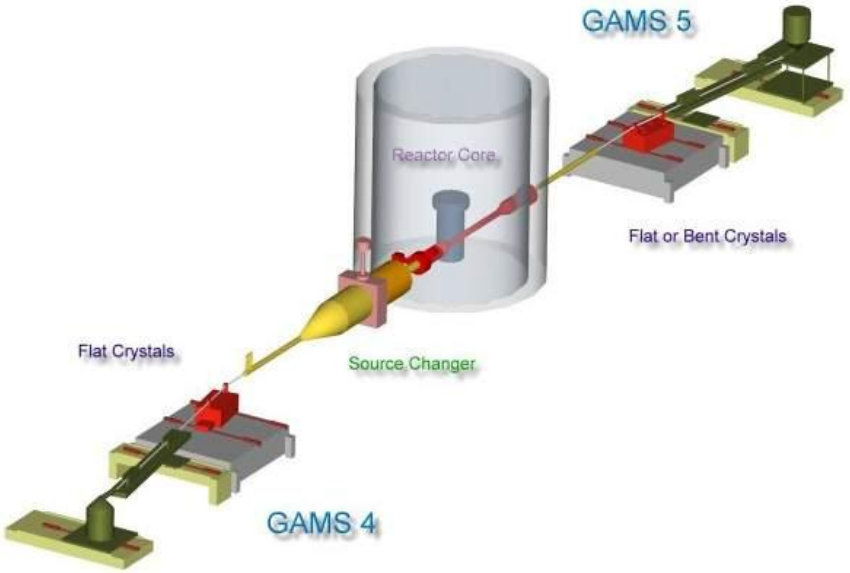

FIG.1. Set-up of the GAMS crystal spectrometers for high resolution spectroscopy of capture and decay gamma rays.

Samples are placed in a thermal neutron flux of 5×10^{14} $cm^{-2}s^{-1}$. Emitted prompt or delayed capture gamma rays are tightly collimated onto the spectrometers. After Bragg diffraction on one or two "perfect" flat Si or Ge crystals, the gamma ray intensity is monitored with a Ge detector. The gamma ray energy is measured by scanning the angle of the well-known diffracting crystals across the rocking curve and simultaneously monitoring the absolute diffraction angles by laser interferometers [21]. Thus gamma ray energies can be derived with sub-ppm accuracy and most reference energies that are today commonly used in

gamma ray spectroscopy are based on such measurements at GAMS. Summing all measured energies of a gamma ray cascade after thermal neutron capture allows deriving the neutron binding energy [22], complementary to Penning trap mass measurements [23]. The very high angular resolution of the spectrometer was recently used to study refraction of MeV gamma rays in silicon, indicating a higher than expected index of refraction [24].

In addition to centre of a measured gamma ray energy distribution also its width can be exploited in the so-called GRID (Gamma Ray Induced Doppler broadening) method [25]. The Doppler broadening of the energy distribution of secondary gamma rays allows deducing the lifetime of intermediate nuclear levels in the range of femtoseconds to picoseconds, thus giving direct access to transition strengths [26]. Even the neutrino-induced Doppler-broadening in electron capture decays is observable [27].

The angular acceptance of flat crystals is intrinsically small therefore flat crystal spectrometers have a tiny solid angle acceptance and require high source strength. Therefore only relatively strong gamma transitions of massive samples can be exploited. Bent crystal spectrometers in DuMond geometry have lower resolution but provide three to four orders of magnitude higher angular acceptance [28, 29]. Thus few milligrams of rare, highly enriched samples are often sufficient for nuclear spectroscopy. For bent crystal spectrometers the resolution power drops with rising gamma ray energy but the “wrong” energies are diffracted under a different angle and thus do not reach the detector. This assures an excellent peak to background ratio and a dynamic range of up to five orders of magnitude, far superior to Compton suppressed Ge detectors. This opens applications that require unambiguous identification of very weak transitions [30].

The bent crystal spectrometer can also serve as a monochromatic gamma ray source with tunable energy, enabling e.g. the detailed study of pair creation close to the threshold [31].

3.4. THE FISSION FRAGMENT SEPARATOR LOHENGRIN

LOHENGRIN is the second instrument at ILL that does not use extracted neutron beams but that exploits an in-pile position at a high thermal neutron, see Fig. 2. A fissile or fertile actinide target is placed in a neutron flux of 5.5×10^{14} $cm^{-2}s^{-1}$, leading to a high fission rate. When the fission fragments leave the thin fission target with kinetic energies of typically 0.3 to 1.3 MeV per nucleon, several electrons are stripped off and the ions acquire an average equilibrium charge state between 18+ and 25+. Ions that happen to be emitted into the small solid angle towards the spectrometer fly through an evacuated beam tube are then separated by a horizontal magnetic deflection according to their momentum over ionic charge ratio and subsequently separated by a vertical deflecting cylindrical condensator according to their kinetic energy over ionic charge ratio. The combination is a parabola mass spectrometer providing beams of mass- and energy-separated fission fragments [32].

Fission yields and kinetic energy distributions of fission fragments are determined by scanning mass by mass the distributions in ionic charge state and kinetic energy and counting the ions in the focal plane. The mass yields are readily obtained by integrating over ionic charge and kinetic energy. For light elements ($Z<40$) an ionization chamber with split anode allows identifying isobars by their specific energy loss.

2.1. Cold and thermal neutron beams

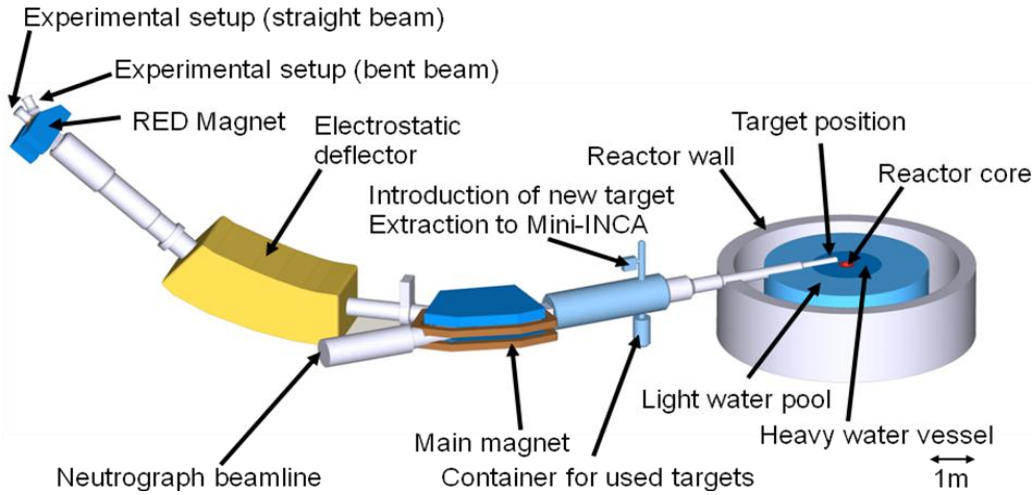

FIG.2. Set-up of the LOHENGRIN recoil separator at the H9 beam tube.

Thus, isotopic yields of light binary and of ternary fission fragments are directly measured by ion counting. LOHENGRIN provides excellent selectivity, thus even very exotic ternary fission fragments like the halo nuclei ^{11}Li and ^{14}Be could be clearly identified with yields as low as 10^{-10} per fission [33].

The so-called RED (reverse energy dispersion) magnet [33] focuses up to 40 cm of the energy dispersed beam (i.e. $\Delta E/E$=5.5%) from the focal plane onto a few cm length. This area can be surrounded by an efficient array of radiation detectors. Usually two fourfold clover Ge detectors or coaxial Ge detectors are used for gamma ray detection. This setup can be used for fission studies where isobaric identification of heavier elements (Z>40) is achieved by gamma ray spectrometry, allowing to measure isotopic and isomeric fission yields of heavy fragments [34,35].

The mass-separated radioactive ion beams can also be used for decay spectroscopy of fission products. The setup is particularly efficient for the study of microsecond isomers ($T_{1/2}$>0.5 µs). Often the Ge detectors are complemented by cooled Si detectors for detection of conversion electrons and X rays. Thus detailed decay spectroscopy of dozens of microsecond isomers could be performed at LOHENGRIN, see e.g. refs. [36-39].

Complementary $LaBr_3$:Ce detectors enable direct lifetime measurements in the ps range via the ultrafast timing method [40].

An electrostatic beam chopper allows modulating the continuous fission fragment beam to beam-on/beam-off periods from few milli-seconds to hours. Thus longer-lived isomers and isotopes can be identified by following the grow-in and decay of the respective gamma rays. A tape system serves for removal of long-lived activity.

Combination of the chopped beam with plastic scintillators for beta detection and an array of 18 ^{3}He tubes embedded in a polyethylene matrix for detection of beta-delayed neutrons enables precise measurements of the beta-delayed neutron emission probability P_n [41]. In certain cases the Pn value is also accessible via gamma ray spectroscopy [42].

2.1. Cold and thermal neutron beams

3.5. THE V4 HIGH FLUX IRRADIATION POSITION

The vertical beam tube V4 (see Fig. 3) provides an even higher neutron flux compared to the GAMS and LOHENGRIN in-pile positions: up to 1.5×10^{15} $cm^{-2}s^{-1}$ thermal neutrons plus some epithermal and fast neutrons. Samples enclosed in quartz ampoules, Al capsules and an irradiation shuttle can be activated for days to many weeks. After decay for some days the irradiation shuttle is opened in a hot cell and the samples can be retrieved for nuclear spectroscopy or other investigations. Also on-line measurements are possible with miniature fission ionization chambers [43]. Ref. [44] discussed in detail transmutation experiments with actinide samples performed in V4.

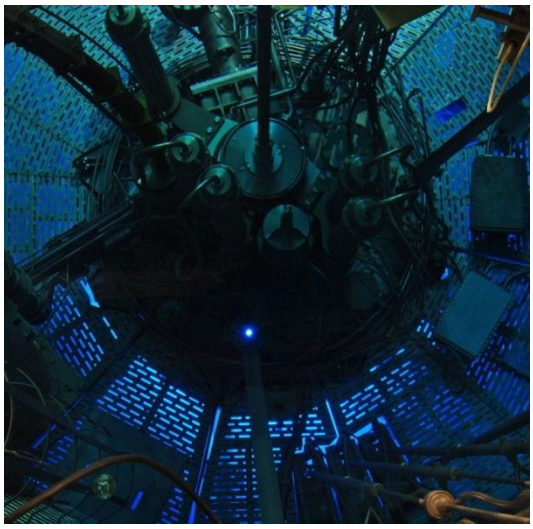

FIG. 3. Top view of the central part of ILL's high flux reactor. The bright blue point below the center of the image shows the Cherenkov light in the V4 beam tube.

4. CONCLUSION AND OUTLOOK

The high flux reactor of ILL is equipped with several unique instruments for nuclear data measurements. LOHENGRIN is the world-leading spectrometer for precise studies of thermal neutron induced fission and competes well for nuclear spectroscopy of isomers and isotopes with lifetimes ranging from microseconds to seconds.

The GAMS crystal spectrometers provide on one hand excellent resolution and accuracy for the determination of absolute gamma ray energies; on the other hand they can be used to perform general nuclear spectroscopy, to measure capture cross-sections of in-situ bred isotopes or to use the monochromatic gamma rays for precision studies of gamma ray refraction or pair creation.

Another strong point of ILL is the availability of a multitude of external neutron beams with neutron energies ranging from few neV up to about 1 eV. Even after monochromatization by Bragg diffraction on crystals or velocity selectors, the neutron fluxes are sufficiently high for most types of cross-section measurements. There is large potential to use such neutron beams of different energies for solving discrepancies of previous cross-section measurements that might be caused by low-lying resonances or measurements in an imperfect Maxwellian neutron spectrum.

2.1. Cold and thermal neutron beams

Various applications of ILL instruments have been presented above without aiming for exhaustive coverage. Since ILL is a user facility, the science performed on these instruments depends directly on the experiments proposed by the user community. You are welcome to propose experiments similar to those presented above or even completely different ones, provided they can profit of the ILL instruments' characteristics. ILL provides not only neutron beams to the users, but also the corresponding instruments, detectors, control and data acquisition systems and, often unique, so-called "sample environment" such as cryostats, ovens, high pressure cells, high field magnets, polarizers, analyzers, etc.

In principle such equipment could also be combined in different, unusual ways, enabling new types of experiments. For instance an (enriched) sample could be placed in a dilution refrigerator reaching low temperatures of tens of millikelvin, inserted into a split pole superconducting magnet (up to 15 T field) for "brute force" low temperature nuclear orientation. If a polarized neutron beam is sent onto such an oriented sample, the spin orientation of the educts (neutron and target) is fully defined. Observing the anisotropic emission of capture gamma rays with detectors under different directions with respect to the neutron- and target orientation respectively allows the unambiguous spin assignment of the capture state in the compound nucleus (I-1/2 or I+1/2) and of the levels populated by primary gamma ray transitions [45]. Then such a setup could be used for a campaign addressing different cases of interest where conventional methods did so far not allow unambiguous spin assignments.

REFERENCES

[1] KÖSTER, U., Proc. of the EFNUDAT Workshop on Nuclear Data Measurements, Theory and Applications, Budapest, 23-25 September 2009, p. 65.
[2] KÖSTER, U., and JENTSCHEL, M., in: IAEA Technical Meeting in collaboration with NEA on Specific Applications of Research Reactors: Provision of Nuclear Data, Vienna, Austria 2009-10-16, IAEA.
[3] The Yellow Book, Guide to Neutron Research Facilities, see: http://www.ill.eu/
[4] STEYERL, A., et al., Phys. Lett. A116 (1986) 347.
[5] ZIMMER, O., et al., Phys. Rev. Lett. 107 (2011) 134801.
[6] ABELE, H., et al., Nucl. Instr. Meth. A562 (2006) 407.
[7] WAGNER V., et al., Physica B180/181 (1992) 938.
[8] DUBBERS D., and Schmidt, M.G., Rev. Mod. Phys. 83 (2011) 1111.
[9] VESNA, V., et al., Hyp. Int. 201 (2011) 31.
[10] GÖNNENWEIN, F., et al., Phys. Lett. B652 (2007) 13.
[11] GOEMINNE, G., et al., Nucl. Instr. Meth. A489 (2002) 577.
[12] VERMOTE, S., et al., Nucl. Phys. A837 (2010) 176.
[13] SEROT, O., Proc. of the IAEA Technical Meeting on Specific Applications of Research Reactors: Provision of Nuclear Data, Vienna, 2009.
[14] SIMPSON, G., et al., Rev. C82 (2010) 024302.
[15] URBAN, W., et al., J. Instr., submitted.
[16] BERNARDS, C., et al., Phys. Rev. C84 (2011) 047304.
[17] SIMPSON, J., et al., Acta Phys. Hung. NS-H 11 (2000) 159.
[18] ZAWISKY, M., et al., Nucl. Instr. Meth. A612 (2010) 338.
[19] SPRINGER, J., et al., Nucl. Instr. Meth. A615 (2010) 307.
[20] FISCHER, H., et al., J. Phys. Condens. Matter. 20 (2008) 045221.

2.1. Cold and thermal neutron beams

[21] KESSLER, E., et al., Nucl. Instr. Meth. A457 (2001) 187.
[22] DEWEY, M., et al., Phys. Rev. C73 (2006) 044303.
[23] RAINVILLE, S., et al., Nature 438 (2005) 1096.
[24] HABS, D., et al., Phys. Rev. Lett. 108 (2012) 184802.
[25] Börner H., and Jolie, J., J. Phys. G19 (1993) 217.
[26] BÖRNER, H., et al., Phys. Rev. Lett. 66 (1991) 691.
[27] STRITT, N., et al., Phys. Rev. Lett. (1997) 2592.
[28] KOCH, H., et al., Nucl. Instr. Meth. 175 (1980) 401.
[29] DOLL, C., et al., J. Res. Natl. Inst. Stand. Technol. 105 (2000) 167.
[30] JENTSCHEL, M., et al., Phys. Rev. Lett. 104 (2010) 222502
[31] JENTSCHEL, M., et al., Phys. Rev. C84 (2011) 052501.
[32] ARMBRUSTER, P., et al., Nucl. Instr. Meth.139 (1976) 213.
[33] KÖSTER, U., et al., Nucl. Phys. A652 (1999) 371.
[34] BAIL, A., et al., Phys. Rev. C84 (2011) 034605.
[35] FAUST, H., et al., J. Korean Phys. Soc. 59 (2011) 879.
[36] SIMPSON, G., et al., Phys. Rev. C76 (2007) 041303(R).
[37] SIMPSON, G., et al., Phys. Rev. C80 (2009) 024304.
[38] SIMPSON, G., et al., Phys. Rev. C81 (2010) 024313.
[39] MALKIEWICZ, T., et al., Phys. Rev. C85 (2012) 044314.
[40] BETTERMANN, L., et al., Phys. Rev. C82 (2010) 044310.
[41] MATHIEU, L., et al., J. Instrum. 7 (2012) P08029.
[42] KURPETA, J., et al., Phys. Rev. C85 (2012) 027302.
[43] CHABOD, S., et al., Nucl. Instr. Meth. A566 (2006) 633.
[44] LETOURNEAU, A., et al., Proc. of the IAEA Technical Meeting on Specific Applications of Research Reactors: Provision of Nuclear Data, Vienna, 2009.
[45] POSMAN, J., and POSTMA, H., Nucl. Instr. Meth. 148 (1978) 331.

PROMPT GAMMA RAY MEASUREMENT FACILITIES AT JAPAN RESEARCH REACTOR-3 (JRR-3)

K. FURUTAKA[*], Y. TOH[*], H. MATSUE[**]

[*] Nuclear Science and Engineering Directorate, Japan Atomic Energy Agency (JAEA),
2-4 Shirakata-Shirane, Tokai-mura, Ibaraki 319-1195, Japan
[**]JRR-3 Users Office, Japan Atomic Energy Agency (JAEA), 2-4 Shirakata-Shirane,
Tokai-mura, Ibaraki 319-1195, Japan
Email:furutaka.kazuyoshi@jaea.go.jp

Abstract

This paper briefly describes the present status of the two prompt gamma ray measurement facilities, PGA and MPGA, installed on neutron beam lines attached to Japan Research Reactor-3 (JRR-3). The description includes those on the configuration of the beam line as well as the supporting system of the irradiation sample, neutron intensity at the irradiation position, and detectors used for the prompt gamma ray measurement, for each of the facilities.

1. INTRODUCTION

Japan Atomic Energy Agency (JAEA) has a few research reactors for scientific research and industrial uses. One of these is Japan Research Reactor-3 (JRR-3) [1] which is the first research reactor constructed with homegrown technologies in Japan. After achieving its first criticality in 1962, the reactor was serving as a high performance multipurpose research reactor. Then, after its upgrading completed in 1990, the reactor is being operated with its maximum thermal power of 20 MW.

JRR-3 has 7 neutron beam lines, five for cold neutron beams and two for thermal, to utilize the neutrons to experimental research performed in an experimental hall outside the reactor vessel. On two of these neutron beam lines, there are two prompt gamma ray measurement facilities; one is "PGA" which is on one of the thermal neutron beam line, and the other is "MPGA" which is on a cold neutron beam line. The two facilities are briefly described in the following sections.

2. PGA FACILITY

The PGA facility has already been described elsewhere a few times [1]-[5], and therefore the description in ref.[5] will merely be excerpted here; for details, the readers should refer to the papers. (The readers should note that, in spite of the description that the PGA facility "can be located either at the end of a thermal, or a cold beam guide" in the following (and therefore ref. [5]) as well as in ref. [1], the end of the cold beam guide (C2-3-2) is now occupied by the MPGA facility which will be described in the following section, and the PGA facility is practically fixed on the thermal beam line (T1-4-1) on which it is on at present.)

"The PGA facility at JAERI can be located either at the end of a thermal, or a cold beam guide. The beam shutter is made of sintered boron carbide with the thickness of 10mm, which is surrounded by 15 cm of lead. The neutron beam is collimated to 2×2 cm^2 by a LiF tile. The airtight sample chamber is made of Teflon PTFE, and can be filled with helium. The windows of the sample chamber at the inlet and at the outlet of the beam are made of PTFE films with the thickness of 0.5 mm. The whole unit is placed inside a large chamber made of 5 to 10 cm thick lead covered with natural LiF tiles from inside. The beam stop is

made of sintered boron carbide and is surrounded by 20 cm of lead. The detector is shielded from the scattered neutron using a 95% enriched ^{6}LiF tile with the thickness of 5mm. The 23.5% relative efficiency, 111 cm^3 HPGe detector is located coaxially in the BGO annulus, on the narrow tubing of the cold finger two sections of catchers made of BGO are also placed to suppress the forward scattered photons. The sample-to-detector distance is 29.5 cm at the cold beam and is 24.5 cm at the thermal. The thermal equivalent neutron fluxes are 1.8×10^{8} $cm^{-2}s^{-1}$ and 2.5×10^{7} $cm^{-2}s^{-1}$ in the thermal and in the cold beams, respectively."

3. MPGA

The other prompt gamma ray measurement facility is installed on one of the cold beam lines (C2-3-2) and is called MPGA (Multiple Prompt Gamma ray Analyzer).

MPGA is being developed for the following two fields of research:

- high-sensitivity trace element analysis with multiple prompt gamma ray analysis method, and
- neutron capture cross section measurement and the development of a method for it by summing the intensity of gamma transitions to the ground state.

At present, to increase the figure of merit for the latter research field with existing gamma ray detectors, the gamma ray detectors are set as close to the sample irradiation position as possible so as to maximize the efficiency of observing all the gamma rays emitted in the decay of excited nuclei produced in the neutron capture reaction at the cost of the crosstalk between detectors. For the details on the design of the detector configuration, the readers should refer to ref. [6]. We are planning an upgrade of the detector setup to attain high signal-to-noise ratios.

The present configuration of the beam line and detectors is described below.The facility consists of the beam line, an automatic irradiation sample exchanger, and detectors and its accompanying data acquisition system (see Fig. 1 below).

The part of the neutron transmission tube made of ^{6}LiF tiles around the irradiation position is surrounded by an aluminum tube ($1mm^{t}$) to efficiently transmit the gamma rays from the irradiated sample. The part of the tube with natural-LiF is covered by lead ($5cm^{t}$) and iron ($1.5\ cm^{t}$). Three collimators (made of ^{6}Li-enriched LiF) are placed between the short supermirror guide tube and the irradiation position to confine the neutron beam to $2\times3\ cm^2$ rectangular shape. The neutrons after passing through the irradiation region are transmitted again through the tube made of natural-LiF (covered by $5\ cm^{t}$ lead) to the beam stop. The beam stop is made of sintered B_4C and placed inside a block made of lead ($40\times40\times30\ cm^3$). The beam stop is surrounded by sheets of silicone rubber in which boron powder is mixed. Although the neutron transmission tube has no inlet/outlet windows and not airtight, the air inside the tube can be purged with continuous flow of a gas such as helium or CO_2 to reduce the influence of the capture gamma rays from the nuclei inside the air.

The holder of irradiation samples is in rectangular shape (inside: $3\times3.5\ cm^2$) made of high-purity Teflon. With the automatic sample-changing system, samples can be irradiated and the prompt gamma rays can be measured at any predefined length of time in an arbitrary order; the maximum number of samples that can be set to the sample-changing system is 180.

2.1. Cold and thermal neutron beams

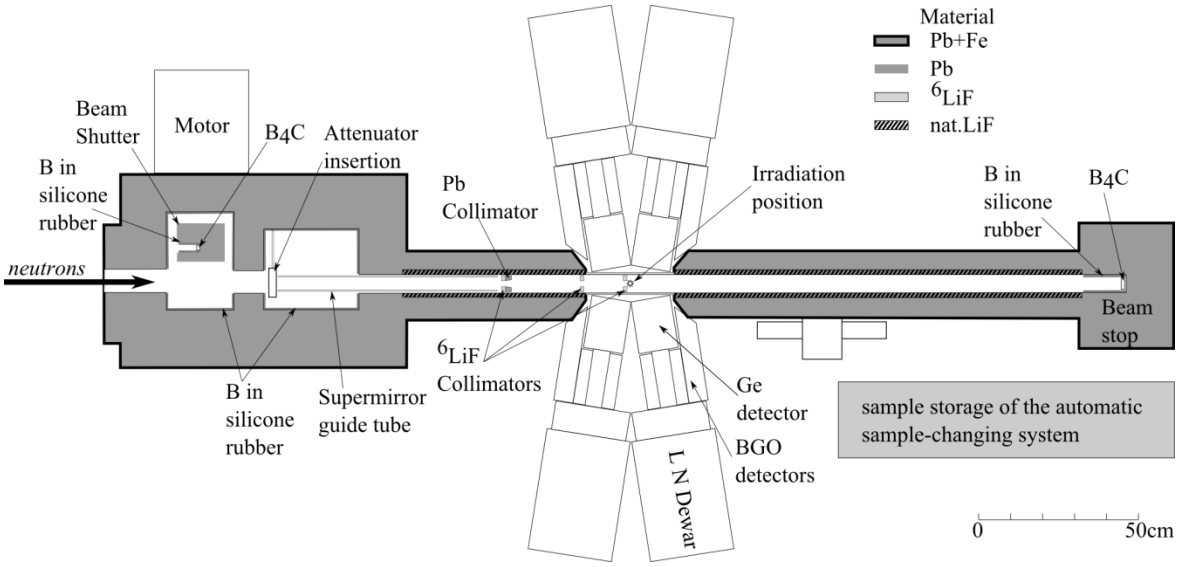

FIG. 1. Layout of the JRR-3 MPGA system at the cold neutron guide beam line C2-3-2.

For gamma ray detection, eight units of so-called clover-type HPGe detector are used (Fig. 2), in which four Ge crystals are placed inside a common endcap; the signals from the crystals are read independently. Of these units, seven are so-called backcatcher type, and backcatcher scintillation detectors are attached to them which utilize the bismuth-germanate ($Bi_4Ge_3O_{12}$, BGO) scintillator. The clover detectors are placed around the irradiation position in four pairs of two detectors; the two detectors in each pair are placed so that they make a Λ-character shape towards the irradiation position (the polar angle of the detector axis with respect to the direction of the neutron beam is 90±9 deg.), and that the axes of the two detectors and the beam axis are coplanar. The planes are either horizontal or vertical. The sum of the peak efficiency over all Ge crystals amounts to 4.41% for 1.33MeV gamma rays. Each clover detector has a sidecatcher BGO detector attached to its far side of the endcap with respect to another detector in the pair. The signals from all the 32 Ge crystals are read, processed, and stored separately using the accompanying data taking system [7]. The trigger condition for the system can be set fairly arbitrarily. With the system, one can monitor energy as well as timing spectrum for each of the crystals on-line. Data can be recorded on event-by-event basis. For the details of the MPGA, please refer to the paper that is in preparation [8].

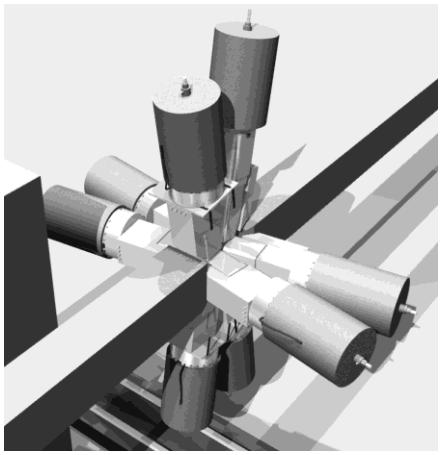

FIG. 2. A schematic drawing (C.G.) of the MPGA detectors. The neutron beam goes through the tube from upper-right to lower-left.

2.1. Cold and thermal neutron beams

4. FINAL REMARKS

The operation of the JRR-3 reactor is stopped due to the Great East Japan Earthquake occurred on 11th of March, 2011. JAEA is aiming at resuming the operation of the reactor within 2014 Japanese fiscal year or later.

REFERENCES

[1] JRR-3 USERS OFFICE http://jrr3uo.jaea.go.jp/jrr3uoe/about/index.htm.

[2] YONEZAWA, C., et al., "The characteristics of the prompt gamma ray analyzing system at the neutron beam guides of JRR-3M", Nucl. Instrum. Meth. A, **329** (1993) 207-216.

[3] MATSUE, H., YONEZAWA, C., "Measurement and evaluation of k_0 factors for PGA at JAERI", J. Radioanal. Nucl. Chem., **257** (2003) 565-571.

[4] MATSUE, H., YONEZAWA, C., "The recommended k_0-factors for neutron-induced prompt gamma ray analysis and the prompt gamma ray emission probabilities", J. Radioanal. Nucl. Chem., **262** (2004) 49-55.

[5] MOLNÁR, G. (Ed.), Handbook of Prompt Gamma Activation Analysis with Neutron Beams, Kluwer Academic Publishers, Dordrecht, 2004.

[6] FURUTAKA, K., et al., "The design and construction of a spectrometer to efficiently identify nuclear levels", Nuclear Data for Science and Technology (Proc. Symp. Nice, 2007), Vol. 1 (BERSILLON, O., et al., Eds.), EDP Sciences, Paris (2008), 517-520.

[7] KIMURA, A., et al., "Performance of a high speed and high density data acquisition system for multiple gamma ray detection", IEEE Nuclear Science Symposium 2008 (Conf. Record Symp. Orlando, 2008), 2107-2111.

[8] KIN, T., et al., (in preparation).

MEASUREMENTS OF DECAY DATA OF FISSION PRODUCTS USING ISOTOPE SEPARATOR ON-LINE

M. SHIBATA[*], Y. KOJIMA[**], H. HAYASHI[**], Y. SHIMA[***], A. TANIGUCHI[+], M.ASAI[++], A. OSA[++]

[*]Radioisotope Research Center, Nagoya University, Chikusa-ku, Nagoya, 464-8602, Japan
[**]Institute of Health Biosciences, The University of Tokushima Graduate School, Kuramoto-cho, Tokushima, 770-8509, Japan
[***]Graduate School of Engineering, Nagoya University, Chikusa-ku, Nagoya 464-8603, Japan
[+]Research Reactor Institute, Kyoto University, Kumatori 590-0494, Japan
[++]Japan Atomic Energy Agency, Tokai 319-1195, Japan
Email: i45329a@nucc.cc.nagoya-u.ac.jp (M. Shibata)

Abstract

Decay data of fission products are measured using an isotope separator on-line installed at research reactor in Kyoto University, Japan. Especially for measurements of Q_β of fission products around A=150, three type total absorption type detector were developed. These detectors can determine Q_βs without decay scheme information. We successfully measured the Q_β of fission products including some new isotopes. The other decay data measurements are also described.

1. INTRODUCTION

Both β-decay energy (Q_β) and half-life determinations are important quantities in decay spectroscopy for the nuclei far from the stability line. For most new isotopes, the half-lives of are proposed, nevertheless, the Q are not still proposed. For nuclear physics or astrophysical interests, also decay heat evaluations on nuclear engineering, the Q_β are more essential quantities in decay spectroscopy of unstable nuclei. In determining Q_β by means of a conventional β-γ coincidence method, a well-constructed or reliable decay scheme is needed. However, decay schemes information of nuclei far off the stability is usually scarce and sometimes γ rays are miss-assigned. In case the gated γ ray is misplaced in the decay scheme, the Q_β result in an incorrect value. With respect to theoretical studies such as atomic mass predictions, experimental values of Q_β for neutron-rich nuclei are important even if they have uncertainties of 0.5 MeV. So we aim to develop total absorption detectors having high efficiency and measure the Q_β of new or rare radioisotopes with the uncertainty below 100 keV using them installed at on-line mass separator facilities. The total absorption detectors have a following advantage. Owing to its high full-energy absorption efficiency, both β ray to the ground state and β rays to excited states which has subsequent γ rays show the same end-point energy in a decay spectrum, then, the end point correspond Q_β directly. It means the detectors can determine Q_β independently on decay schemes, and they are applicable to new isotopes with scarce information of their decay schemes. For the above purpose, three type total absorption detectors have been developed and installed at on-line mass separators. The Q_β of fission products including new isotopes were successfully measured and some of them have been proposed for the first time. In this report, the performances of three detectors are introduced as well as recent results of Q_β measurements of fission products at two ISOL facilities.

2. EXPERIMENTS

2.1. ISOTOPE SEPARATOR ON-LINE (ISOL)

The unstable nuclei are produced with the fission reaction ^{235}U with thermal neutrons using an on-line mass separator (KUR-ISOL) (Fig. 1) [1]. The 50 mg UF_4 target is irradiated with a through hole facility at the Kyoto University Reactor (KUR) where thermal neutron flux is 3×10^{12} n cm^{-2}·s^{-1}. The nuclei of interests are transported into a thermal-ionization type

ion source with the He-N_2 gas jet system, including a small amount of O_2 gas if needed. The ions are extracted with 30 kV and separated with two dipole analyzing magnets with mass resolution of ~800 at BL-1, ~500 of BL-2, respectively. The BL-1 is the decay spectroscopy line. The separated radioactive beams are implanted into aluminized Mylar tape in a tape collector. The KUR-ISOL can provide the fission products up to A~156 and half-life of ~1 s. The collection tape mounted on tape station moved by computer control to reduce the background of daughter nuclei. On the other hand, at the BL-2, a post-accelerator are installed. This line is used for implantation of radioactivity for material sciences such as on-line perturbed angular correlation. The other ISOL (Tokai-ISOL, JAEA, Japan) are also used for Q_β measurements. This ISOL is a gas-jet type and is installed at a Tandem accelerator. It adopts the ^{238}U(p,*f*) reaction and can provide heavier neutron-rich isotopes to A~166 than those of KUR-ISOL.

2.2. TOTAL ABSORPTION DETECTOR FOR Q_β MEASUREMENTS

For Q_β measurements, three type total absorption detectors have been developed.[2] One is a BGO total absorption detector, composed of the large volume twin BGO scintillators (12.7 cm$^\phi$ x 10.2 cm^t) (Fig. *2* (left)). The nuclei of interests which are collected on the Mylar tape by ISOL are sandwiched with two BGO scintillation detectors, and energy sum spectra are obtained. The distance between two scintillators is 3 mm to cover almost 4π solid angle. By sandwiching radioactivities, not only backscattering electrons and γ rays but also bremsstrahlung photons caused by high-energy β particles are not allowed to escape from the detector. For mono-energetic electrons and γ rays at the energy of 8 MeV, the full energy peak efficiencies were evaluated to be 90% and 75%, respectively.

The emitted radiations are almost absorbed with two detectors with high efficiency, as the consequence, the end point of the measured energy sum spectra directly indicates the Q_β. It is enough to deduce the Q_β with uncertainty below 100 keV. Thus the efficiency of the system as a Q_β determination detector is expected more than two orders of magnitude larger than that of plastic scintillation, Ge or Si detectors.

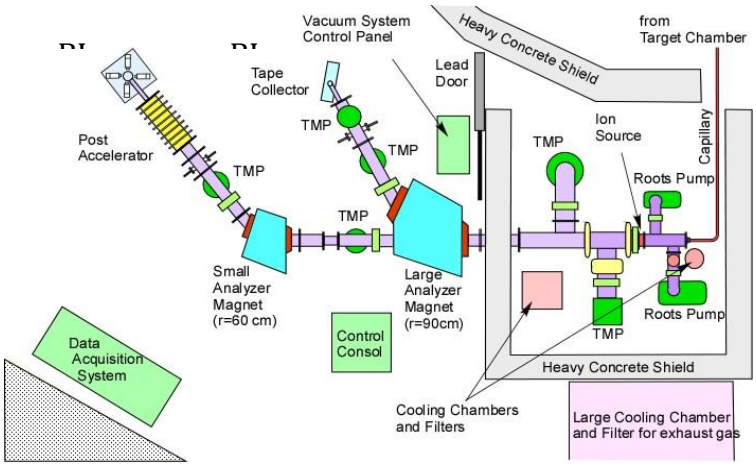

FIG. 1 Schematic view of KUR-ISOL.

2.1. Cold and thermal neutron beams

The next is the through-hole type Ge detector coupled with a BGO Compton suppressor (total absorption through-hole Ge detector). [3] As shown in Fig. 2 (right), the detector is composed of two detectors. One is a custom-made Ge detector in which the large-volume single crystal (84 mm^{ϕ} x 90 mm^{t}) has a through-hole (20 mm^{ϕ}) in the center. This allows radiation to be measured with an almost 4π solid angle and to be measured as energy sum of β ray and γ ray following the β-decay. The diameter of housing is 15 mm and the thickness of the well is 0.4 mm in order to reduce the energy loss and absorption as low as possible. The Ge detector is surrounded by the other detector, a 25 mm thick anti-Compton BGO detector. Singles spectra with the Ge detector and a coincidence spectrum with the BGO detector are measured simultaneously. The coincidence events correspond to incomplete energy absorption in the Ge detector, namely Compton components of γ rays or bremsstrahlung photons associated with β-particles. By subtracting the coincidence spectrum from the singles spectrum, total absorption events are extracted. As the results, the deduced spectrum principally corresponds to the superimposed spectrum of a fully absorbed β ray, and the end-point of the spectrum corresponds to the Q_{β}. In practice, β ray spectra are distorted by the energy distribution resulting from energy straggling by the Al housing, a dead layer including some materials on the surface of the crystals.

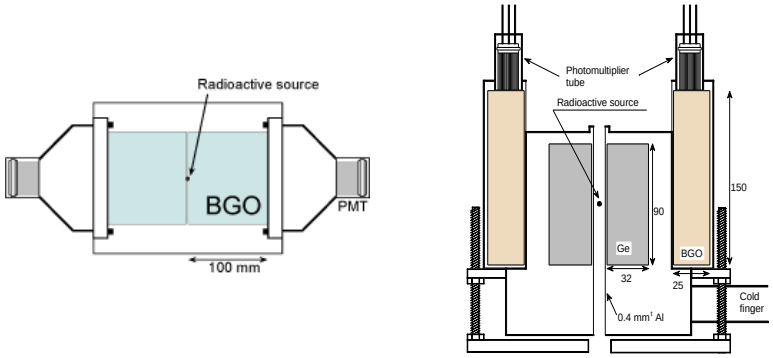

FIG. 2. total absorption BGO detector (left) and total absorption through-hole Ge detector (right)

The third is improved type of the second detector, a through-hole type clover (80 mm^{ϕ} x 90 mm^{t} x 4) detector is adopted in place of through-hole type Ge detector and the clover detector is covered with 30 mm thick BGO Compton suppressors to cover with 4π solid angle, with five parts: top×2, side×2, and bottom×1. (Fig. 3). [4] Crystals in the clover detector is electrically isolated each other, then, each crystal work independently. In addition to the singles spectrum, an add-back spectrum can be also produced by the off-line sorting after experiments. The efficiency is up to 10 times larger than the previous type detector at higher energy region.

In the ISOL experiment, the mass-separated radioactive beams were implanted into a thin Mylar tape, and the sources on the tape were moved periodically with predetermined time interval from the collecting port in a vacuum chamber to the measuring position in the air using differential pumping. The tape was computer-controlled and the reproducibility of the source position was within 1mm. The detector was shielded with lead blocks and borated paraffin blocks from the backgrounds. The counting rates need to be kept below 2 kcps to reduce pile-up.

2.1. Cold and thermal neutron beams

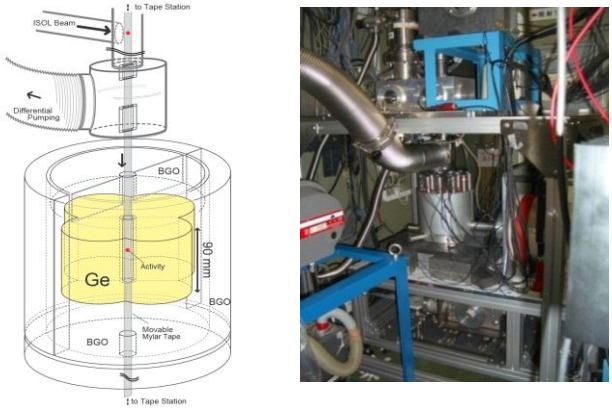

FIG. 3. Schematic view of total absorption clover detector and experimental set-up at Tokai-ISOL

In practice, for energy calibration of the BGO total absorption detector, while for evaluation of the effective energy loss of the detector housing of the through-hole and clover total absorption detector experimentally, many fission products having well-determined Q_β's such as $^{91-94}$Rb, ^{93,95}Sr and $^{139-142}$Cs are measured, and evaluated the end-point energies. On the analysis of the end-point, Monte-Carlo simulation code GEANT4 was also used.

3. RECENT RESULTS

Figure 4 (left) is the typical total absorption spectrum for the decay of ^{91}Rb measured with the BGO detector for calibration measurements, and Fig. 4 (right) is for the decay of ^{164}Eu, one of the new isotopes, measured with the clover detector. As described above, the total absorption BGO detector has high efficiency, while not better energy resolution. By measuring many nuclei for calibration, and application of practical analyzing method based on the Fermi-Kurie plot, the Q_β's were successfully determined with systematic uncertainty of 60 keV. Fission products of ^{235}U and ^{238}U were measured at KUR-ISOL and Tokai-ISOL, respectively[2,5-8] On the other hand, with total absorption through-hole Ge detector which have better energy resolution than the BGO detector, Q_β's can be determined with systematic uncertainty of 20 keV. Those of $^{147, 148}$La were proposed for the first time as demonstration of the detector performance. [3] On the basis of the through-hole detectors' results, the Q_β's of europium isotopes which had been measured with BGO detector were re-determined with good accuracy with the last developed clover total absorption detector. Preliminary results were proposed in ref. [4].

Figure 5 shows the measured nuclei with a series of experiments. At KUR-ISOL, the BGO detector and through-hole Ge detector were adopted, while, the BGO and clover type detector were adopted at Tokai-ISOL. The comparisons between atomic masses deduced from the measured Q_β's of Eu isotopes with BGO detector and some predictions by systematics are shown in Fig. 6. It shows the predictive abilities in the region with no experimental values are not necessary well. The experimental values are important for the theoretical studies.

2.1. Cold and thermal neutron beams

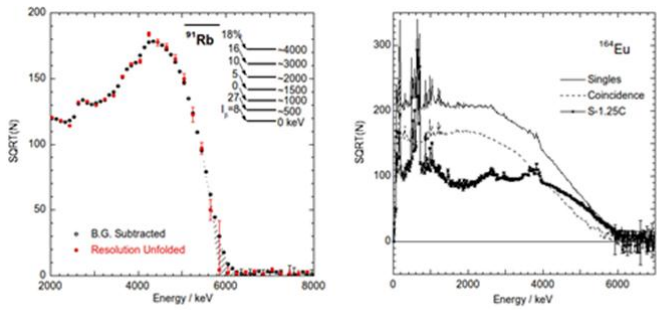

FIG. 4. Typical measured spectra with total absorption BGO (left) and clover (right) detector.

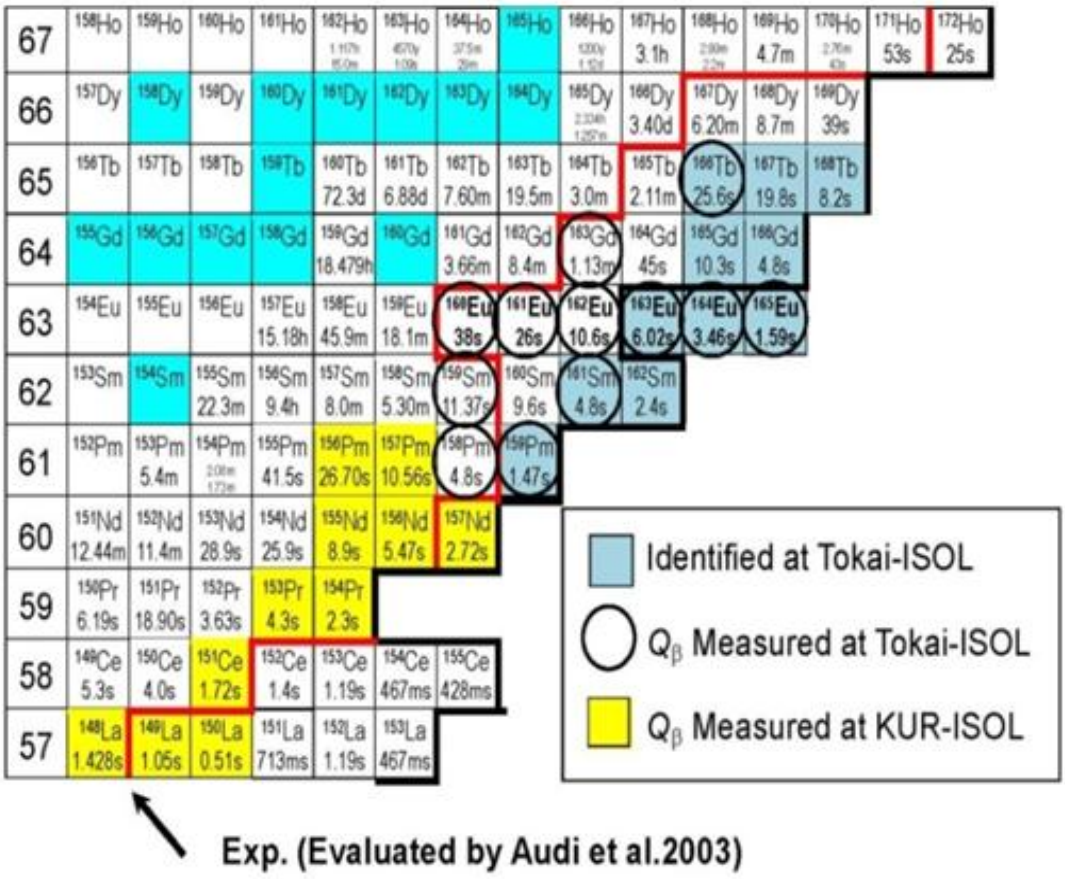

FIG.5. Measured nuclei produced with ^{235}U(n,f) reaction at KUR-ISOL and with ^{238}U(p,f) reaction at Tokai-ISOL.

4. OTHER EXPERIMENTS AND FUTURE PLAN

In the region near A=150, there are some nuclei in which the maximum energy of the observed excited state are quite lower the Q_β's. There are probably missing excited levels in high energy region having β-feedings. For such nuclei, the β-branching ratio I_β to the ground state probably over-estimated. The clover detector has high efficiency and can measure both singles and add-back spectrum simultaneously. From the singles spectra, γ ray intensities can be determined with proper correction of coincidence summing. On the other hand, the add-back spectra show the excited states intensively, because the energies of γ rays with cascade relations are summed up owing to its high detection efficiency. Coincidence relation of γ rays

between 4 Ge detectors can be also analyzed. By using this feature, high energy excited states up to 3.5 MeV of ^{147}Ce have been identified through the β-decay of ^{147}La.[9] The detailed analysis is in progress. Finally, the I_βs will be re-evaluated. In addition, there are some nuclei which emit β-delayed neutrons such as ^{147,148}La in this region. Delayed neutron measurements are also expected.

In research for nuclear structure, transition probabilities are sensitive to the properties of excited stats. The time resolution of $LaBr_3$ scintillation detector is not better than that of a BaF_2 scintillator. Nevertheless, Energy resolution is better than that of BaF_2 scintillator, and detection efficiency is larger than that of Ge detector. Lifetime measurements of excited states around sub-nanosecond are in progress by means of β-γ delayed coincidence technique with the combination of $LaBr_3$, plastic scintillation and Ge detectors. [10]

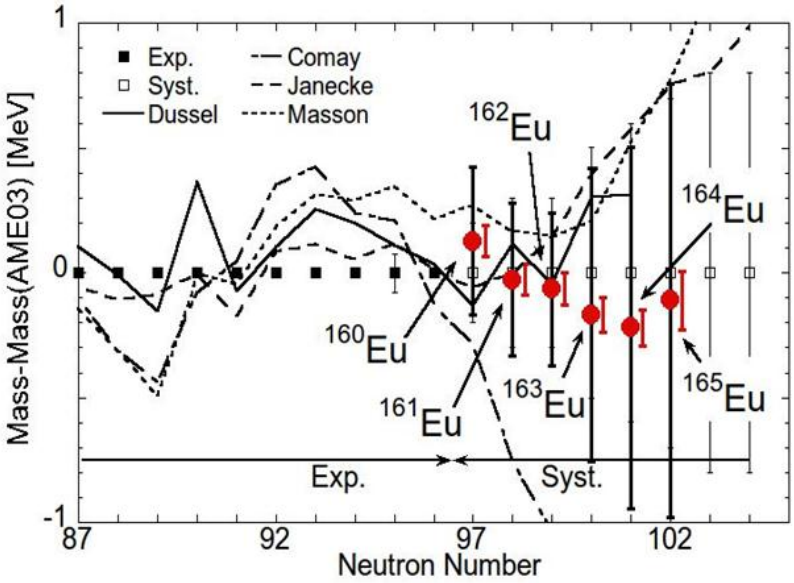

FIG.6. Comparison of atomic masses of Eu isotopes between the experimentally deduced value and some predictions by systematics.

REFERENCES

[1] TANIGUCHI, A., et al., ”Characteristics of a mixed-gas jet system in KUR-ISOL”, Nucl. Instr. and Meth. in Phys. Res. A351 (1994) 378.

[2] SHIBATA, M., et al., “Application of a total absorption detector to Q_β determination without the knowledge of the decay scheme”, Nucl. Instr. and Meth in Phys. Res. A 459 (2001) 581.

[3] HAYASHI, H., et al., “Q_β-measurements with a total absorption detector composed of through-hole HPGe detector and anti-Compton BGO detector” Nucl. Instr. and Meth. in Phys. Res. A 606 (2009) 484.

[4] HAYASHI, H., et al., Abstract Book of the Int. Conf. Nucl. Data for Sci. and Technol. (ND2010), (2010), Jeju Island, Korea, 232.

[5] SHIBATA, M., et al., “Q_β Determination of Neutron-Rich Isotope ^{144}La with a Total Absorption Detector”, J. Phys. Soc. Japan 71 (2002) 1401.

[6] SHIBATA, M., et al., “Q_β determination of fission products with a total absorption detector without information of the decay scheme” Proc. of the Third Int. Conf. on Atomic masses and Exotic nuclei, (2001), Hämeenlinna, Finland, 479.

[7] HAYASHI, H., et al., "Q_β measurements of ^{158,159}Pm, ^{159,161}Sm, $^{160–165}$Eu, ^{163}Gd and ^{166}Tb using a total absorption BGO detector", Eur. Phys. J. A 34 (2007) 363.

[8] HAYASHI, H., et al., "Practical Q_β analysis method based on the Fermi–Kurie plot for spectra measured with total absorption BGO detector", Nucl. Instr. and Meth. in Phys. Res. A 613 (2010) 79.

[9] SHIMA, Y., et al., "Identification of High-Energy Levels with a Total Absorption Clover Detector" Proc. The 2011 Symposium on Nucl. Data. JAEA-Conf 2012-001, INPC (JPN)-197.141-146.

[10] KOJIMA, et al., "A spectrometer for lifetime determination by β-γ-γ delayed coincidence technique at KUR-ISOL", Nucl. Instr. and Meth. in Phys. Res. A 659 (2011) 193.

2. RESEARCH REACTOR BASED NEUTRON BEAM FACILITIES

2.2 FILTERD NEUTRON BEAMS

2.2. Filtered neutron beams

DEVELOPMENT OF THE NEUTRON FILTERED BEAM TECHNIQUE FOR HIGH PRECISION NUCLEAR DATA MEASUREMENTS

O. GRITZAY, A. GRYMALO, V. LIBMAN, S. VOLKOVETSKYI

Institute for Nuclear Research of NAS of Ukraine,
47 Prospect Nauky, Kyiv
Ukraine, 03680
Email: ogritzay@kinr.kiev.ua

Abstract

A neutron filtered beam technique (NFBT) was launched at the Kyiv Research Reactor (KRR) for more than 30 years. The most significant advantage of this method is its suitability to produce high-intensity neutron lines in the keV energy region. More than ten quasi- mono-energetic neutron beams were designed in the energy range from thermal energy to several hundred kilo-electron-volts at the KRR. These beams were used and continue to use in fundamental scientific, namely for determination of the average value of neutron cross sections with high accuracy. As a rule, only one filtered neutron line is created by the used composite neutron filter, so in the traditional NFBT. So, only one average cross section value may be determined in the proper energy region. To get a set of the average values, two new approaches were developed at the KRR. The first experimental results are presented in this paper. Both methods are in progress and further measurements are planned in the future.

1. INTRODUCTION

The idea of filtering reactor neutrons possessing a continuous spectrum by means of materials whose total neutron cross sections possess deep interference was first suggested by O.D. Simpson and L.G. Miller in 1968. Basing on this idea, the neutron filtered beams were created in many laboratories and were used for measurements of the averaged neutron cross sections. At the Kyiv Research Reactor (KRR) the neutron filtered beam technique was developed, too. More than ten quasi- mono-energetic neutron beams were designed in the energy range from thermal energy to several hundred kilo-electron-volts at the KRR during more than 30 years. The beam intensity may reach 10^6-10^8 n/(cm^2 ·s), it allows determination of the average value of total neutron cross sections with accuracy 1% and better, neutron scattering and capture cross sections with 3-6% accuracy. There is definite advantage of the neutron filtered beam technique (NFBT), however only one filtered neutron line is created in the traditional NFBT. So, only one average cross section value may be determined in the proper energy region, and energy-dependent cross section behaviour cannot be extracted. A set of the average values is necessary in the investigated energy interval to provide information for the cross section behaviour. Two new approaches were developed at the KRR for solving of this problem.

One of them, named as method of the modified filtered beams (MMFB), is that the primary neutron line after traditional filter is divided into the narrower lines by addition of the different modifying component. A set of 10 values of the averaged total neutron cross-sections of natural carbon was measured in the energy region 90-60 keV using the modified filters.

The second method, named as average energy shift method (AESM), is that the primary neutron line after traditional filter is shifted using the neutron energy dependence on scattering angle. A set of 3 values of the averaged total neutron cross sections of ^{52}Cr were measured in the energy region 48.4-58.6 keV using the scattering samples carbon and polyethylene.

2. MEASUREMENTS USING A METHOD OF THE MODIFIED FILTERED BEAMS

2.1. RATIONALE FOR MEASURING TOTAL CROSS SECTION OF CARBON

The measurements of the total neutron cross-section of carbon were done in our department in 2006 [1]. A strong dependence on the sample thickness of the effective cross-section of natural carbon was observed by us at the energy region 119-57 keV. The total cross-section of natural carbon, obtained by extrapolation of the observed cross-sections to zero sample thickness, was determined as equal to 4.63 barns. This value is much more than the EXFOR and ENDF/B library values as shown in Fig. 1a. The majority of the presented in EXFOR measurements were carried out with one carbon sample, so the cross-section dependence on the sample thickness could not be detected in these works. Our measurements [1] were done with ten samples of natural carbon. The observed dependence may be due to the fact that the strong resonance exists in this energy region. Really, in compliance with [2] a p-wave resonance is present at the energy 152.4 keV for ^{13}C+n reaction. But the natural abundance of the ^{13}C isotope is 1.1%, so the observed dependence cannot be explained by presence of this resonance (Fig. 1b). Simultaneously with release of our work [1], the theoretical work [3] was published. The strong resonance for ^{12}C+n reaction was predicted by these authors near 0.1 MeV. Therefore, an experimental investigation of the total cross-section of natural carbon in this region was continued [4 - 5] and is continued now. The main purpose of these researches is to identify this resonance in experiment and determine its parameters (if it exists).

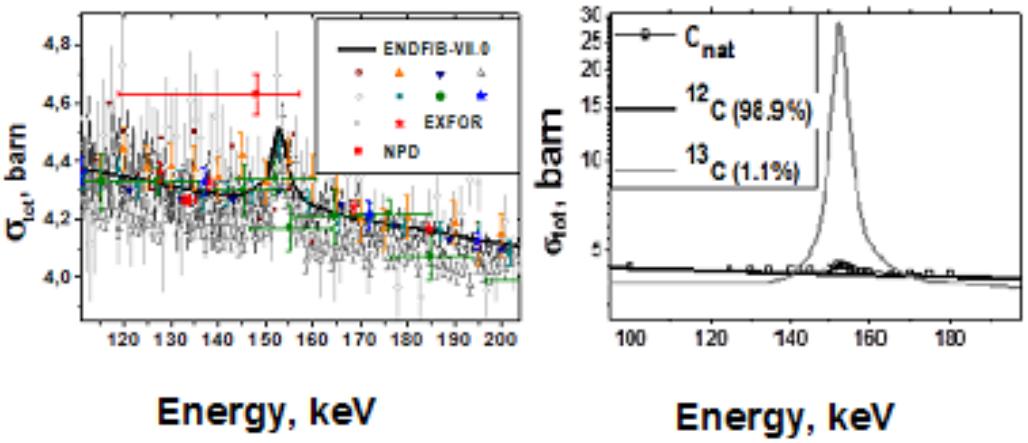

a) b)

FIG. 1. a) The ENDF/B and EXFOR data for the total neutron cross-section of natural carbon. b) The total neutron cross-section of natural carbon, ^{12}C and ^{13}C isotopes from the ENDF/B library.

2.2. THE METHOD'S IDEA OF THE MODIFIED FILTERED BEAMS

Identification of the resonance is not possible if only one value of the average total cross section of carbon is obtained in the energy region near 150 keV. A set of the average values is necessary in the investigated energy interval to provide information for a resonance. Traditional method of the filtered neutron beams does not allow implementation of this task using a standard set of the filters. Therefore, this technique has been improved by means of development of the method of the modified filtered beams (MMFB).

2.2. Filtered neutron beams

The main idea of the MMFB is to divide the primary neutron line after the silicon filter (average energy of 144 keV) into the narrower lines by addition of a modifying component. The modifying components are chosen from the materials, the total neutron cross sections of which have the minimums and maximums in the energy range of this primary neutron line. For example, the total neutron cross sections of the main component (silicon) and ^{54}Fe (modifying component) are presented in Fig. 2a. As it is seen in Fig. 2a, three minimums in $\sigma_{tot}^{54Fe}(E)$ are located in the energy region of the interference minimum of the basic component. By means of an optimization of the modifying component thickness, we can obtain three neutron lines after this modified filter. The result of this modification is shown in Fig. 2b.

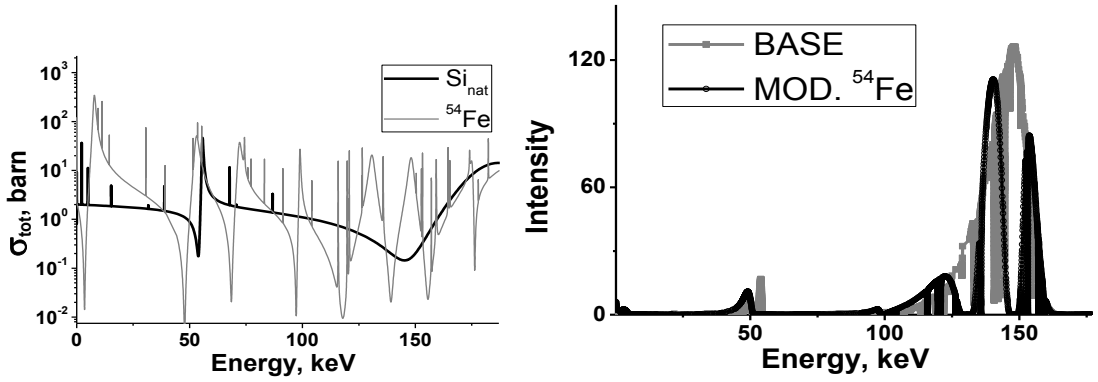

a) b)

FIG.2. a) The total neutron cross-section of Si and ^{54}Fe. b) Calculated neutron spectra after the base and modified by ^{54}Fe filters.

[1] 2.3. THE EXPERIMENTAL SET-UP AND MEASURING

Measurements were carried out on the horizontal experimental channel HEC-9 at the Kyiv Research Reactor using the MMFB. The experimental installation is shown in Fig. 3. A composition of the filter assemblies used in this experiment is presented in Table 1.

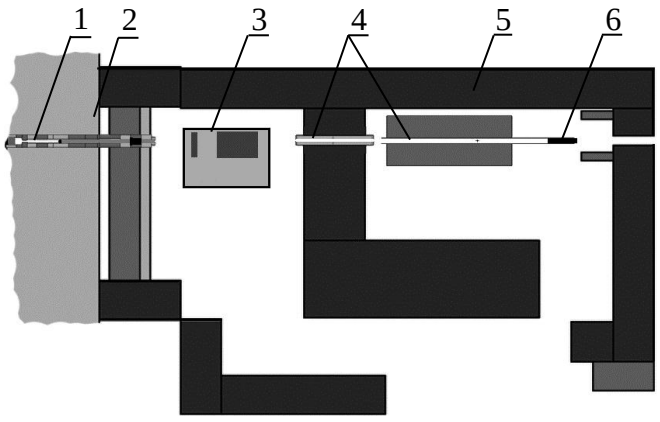

FIG. 3. Scheme of the experimental installation mounted on the HEC-9. 1 – filter assembly; 2 – biological protection of reactor; 3 – system of the sample movement; 4 – collimators; 5 – protection of the channel; 6 – neutron detector.

2.2. Filtered neutron beams

TABLE 1. A COMPOSITION OF THE USED FILTERED ASSEMBLIES

Name of filter	Number of lines	Components (g/cm^2)						
		^{10}B	Si_{nat}	Ti_{nat}	V_{nat}	^{58}Ni	^{54}Fe	Al
Base	1	0.2	213.43	11.49	-	-	-	-
Mod. V	3	0.2	184.07	7.66	24.44	-	-	-
Mod. Ni	2	0.2	184.07	7.66	-	20.49	-	-
Mod. Fe	3	0.2	184.07	-	-	-	77.45	-
Mod. Al	1	0.2	213.43	-	-	-	-	10.00

Two types of the carbon samples were used in these measurements: 1) solid samples from a reactor graphite (C 99.9%); 2) carbon discs, each of them has thickness 1 mm (C 99.997%). The characteristics of the used samples are presented in Table 2. The measurements were carried out using at least 3 samples for each filter modification.

TABLE 2. CHARACTERISTICS OF THE USED CARBON SAMPLES

Mod. Fe-54, Mod. Al				
Massa, g	Diameter, mm	Thickness		
		mm	10^{-3} nuclear/barn	Type
1.2800	30.40	1.00	8.842±0.029	1
2.5620	30.40	2.00	17.697±0.058	1
3.8495	30.40	3.00	26.591±0.088	1
5.0650	29.95	4.16	36.047±0.120	2
8.1635	29.90	6.76	58.293±0.195	2
13.2350	29.90	10.94	94.506±0.316	2
15.3650	29.90	12.91	109.716±0.367	2
21.2325	29.90	17.74	151.614±0.507	2
25.6870	29.95	21.27	182.810±0.610	2
Base, Mod. V, Mod. Ni-58				
Massa, g	Diameter, mm	Thickness		
		mm	10^{-3} nuclear/barn	Type
1.2870	30.04	1.00	8.898±0.006	1
2.5657	30.04	2.00	11.774±0.012	1
3.8494	30.04	3.00	26.614±0.018	1
5.0720	29.90	4.16	36.024±0.024	2
6.2886	29.90	5.15	46.646±0.030	2

2.2. Filtered neutron beams

2.3. ALGORITHM FOR TREATMENT OF EXPERIMENTAL SPECTRA

Algorithm for treatment of experimental spectra is divided into two stages:

- Initial processing of the proton recoil spectra and reconstruction of the neutron spectra;
- Getting the parameters of the neutron lines, determination of the total neutron cross-section.

The first stage contains of the following procedures: dead time correction, background corrections, summation of the similar spectra, smoothing the summed spectra, differentiation of the smoothed proton recoil spectra to obtain the non-adjusted neutron spectra. These procedures were described in [5]. It was assumed that this differentiation could recover the neutron spectrum. However, the subsequent analysis showed that this recovery is not complete, and the differentiated spectra have to be adjusted.

So, a new approach is being developed to do this adjustment. It consists of the following steps. Output results after each step are presented in Fig. 4.

- Calculation of a neutron spectrum after the given modified filter (1 in Fig. 4). This calculation is performed by the FILTER-7.1 code [6] using the ENDF/B libraries. A thickness of the filter components are taken just the same as in reality.
- Reconstruction of the proton recoil spectrum from the calculated neutron spectrum (2 in Fig. 4). It is performed by formula:

$$Q_i = \sum_{j=i}^{N-1} \frac{\left(I_{j+1} + I_j\right) \cdot \left(E_{j+1} - E_j\right)}{\left(E_{j+1} + E_j\right)}, \quad (1)$$

where Q_i – number of counts in i-th channel (energy of this channel is E_i) in the proton recoil spectrum; I_{j+1}, I_j – number of counts (j+1)-th and j-th channels in the calculated neutron spectrum at the relevant energies E_{j+1} and E_j.

- Blurring the reconstructed spectrum to take into account the energy resolution of the detector system (3 in Fig. 4). It is performed by formula:

$$R_i = \sum_{j=1}^{N} Q_j \cdot \frac{\exp\left(-\frac{\left(E_i + E_j\right)^2}{2\sigma^2}\right)}{\sigma\sqrt{2\pi}}, \quad (2)$$

where R_i – number of counts in i-th channel (energy of this channel E_i) in the blurred proton recoil spectrum; Q_j – number of counts in i-th channel (energy of this channel E_j) in the reconstructed proton recoil spectrum; σ – an energy-dependent resolution parameter. It was estimated from experiment and was taken $\sigma = 0.075 \cdot E$.

- Differentiation of the blurred spectrum (4 in Fig. 4).

2.2. Filtered neutron beams

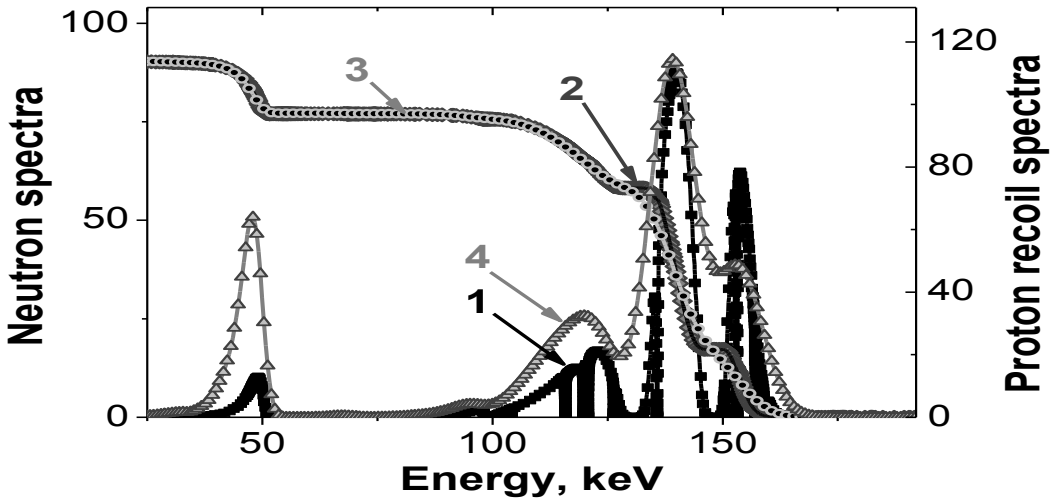

FIG. 4. Output calculated spectra. 1 – neutron spectrum; 2 – reconstructed proton recoil spectrum; 3 – blurred proton recoil spectrum; 4 – differentiated proton recoil spectrum, i.e. reconstructed neutron spectrum.

Then, this reconstructed neutron spectrum 4 was fitted by the function

$$F(x) = \sum_{i=1}^{M} A_i \frac{1}{1+e^{-\frac{x-Xc_i+\frac{W_{1i}}{2}}{W_{2i}}}}\left(1 - \frac{1}{1+e^{-\frac{x-Xc_i-W_{1i}/2}{W_{3i}}}}\right) + \sum_{j=1}^{N} \frac{A_j}{W_j\sqrt{\frac{\pi}{2}}} e^{-2\frac{\left(x-Xc_j\right)^2}{W_j^2}} \quad , \quad (3)$$

where the first sum describes non-symmetrical lines, the second one describes symmetrical lines (A_i, A_j – amplitudes, Xc_i, Xc_j – energy parameters, which correspond to coordinate position of maximum for i-th and j-th lines, W_{1i}, W_{2i}, W_{3i} , W_j – width parameters, M – number of non-symmetrical lines, N – number of symmetrical lines). This fitting was carried out using the OriginPro ver.8 software. A result of this procedure is presented in Fig. 5a. Similar procedure was performed with the non-adjusted neutron spectrum (see description of the treatment of experimental spectra in the beginning of this paragraph). The output results after the last two procedures are compared and the corresponding energy calibration corrections are brought in the non-adjusted neutron spectrum (see Fig. 5b). These corrections are also introduced in the obtained spectra, when the carbon samples are on the beam. All spectra ("direct beam" and after samples) are fitted by the same chosen function with keeping energies and widths of the lines. The areas under the approximated lines are used for calculation of the sample transmission.

2.4. THE OBTAINED RESULTS

The modified filters allowed determination of 10 values of the averaged total neutron cross-sections of natural carbon in the energy region 90-60 keV. The cross-section dependence on the sample thickness was not observed in these measurements, so the final total neutron cross-sections were determined as mean values of the data obtained for the different samples. These final values are presented in Table 3. A visual comparison of these values with the ENDF/B data is shown in Fig. 6a.

2.2. Filtered neutron beams

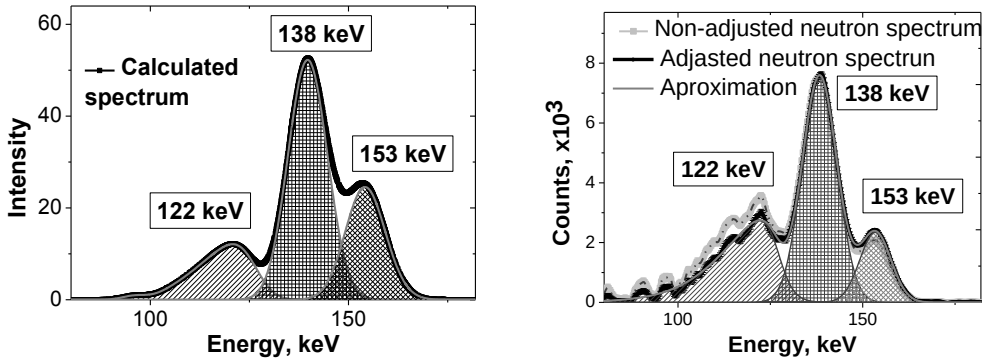

a) b)

FIG. 5. Fragments of the differentiated spectra and the separate line approximations: a) for the calculated spectrum; b) for the experimental spectrum.

Simultaneously with creation of the neutron lines in the energy region 90-160 keV, the filters, modified by ^{58}Ni, V and Al, create in the filtered neutron spectra a line with the average energy close to 54 keV. The averaged total neutron cross-sections of natural carbon were also determined at this energy, using this new processing approach. As the total neutron cross section of natural carbon is very well known in the energy region near 54 keV, the determined values may be used as the reference data. These determined values are presented in Fig. 6b. As it can see in Fig. 6b, a good agreement is observed between the ENDF/B data and our results. It is a good confirmation test of the chosen processing approach.

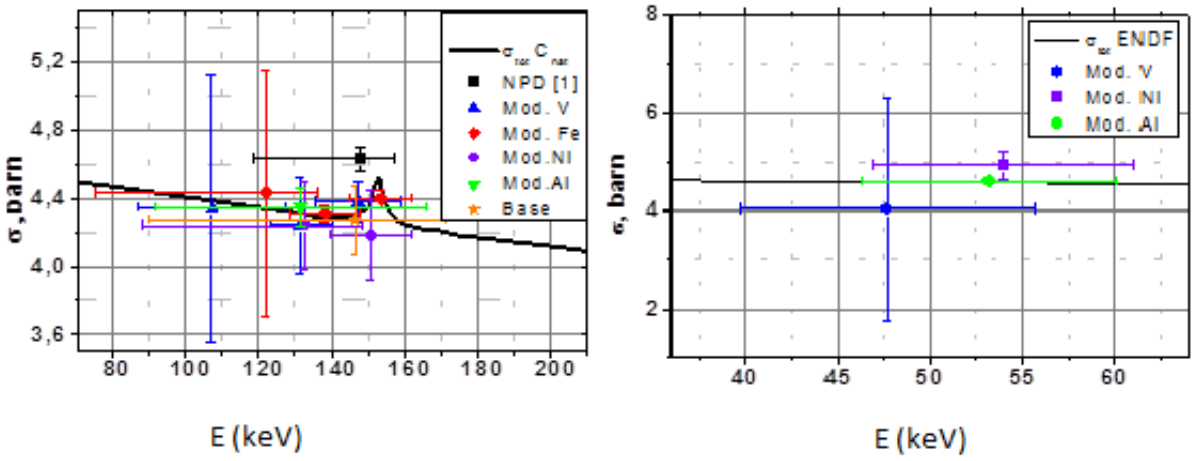

a) b)

FIG. 6. Comparison of the experimental σ_{tot} of carbon with the ENDF/B data.

Now we are developing algorithm to recover the energy dependence of the neutron cross-section in the energy region 90-160 keV, using the measured average values. To do the recovery in this region, we also plan to carry out additional measurement to get better accuracy. Analysis of these measured average total neutron cross-section of natural carbon gives grounds to assume that a strong resonance for ^{12}C+n reaction, predicted in [3], is absent in energy region 130-160 keV.

2.2. Filtered neutron beams

TABLE 3. THE MEASURED AVERAGED TOTAL NEUTRON CROSS-SECTION OF NATURAL CARBON

Filter name	E_c, keV	E_{min}, keV	E_{max}, keV	σ, barn	Δσ, barn	Δσ/σ,%
Base	146.5	90.9	171.2	4.27	0.21	4.9
Mod. V	107.3	87.0	127.5	4.34	0.79	18.2
	131.6	123.2	140.1	4.24	0.29	6.7
	147.5	135.7	159.2	4.38	0.12	2.7
Mod. Ni	132.7	88.1	148.8	4.24	0.26	6.1
	150.9	139.6	162.2	4.18	0.26	6.3
Mod. Fe	122.1	75.3	136.2	4.43	0.73	16.4
	138.3	128.8	147.8	4.30	0.05	1.2
	153.5	145.0	161.9	4.40	0.05	1.1
Mod. Al	131.8	91.7	166.2	4.35	0.11	2.5

3. MEASUREMENTS USING A METHOD OF THE AVERAGE ENERGY SHIFT

3.1. RATIONALE FOR MEASURING TOTAL CROSS SECTION OF CROMIUM-52 ISOTOPE

The ^{52}Cr isotope was used as an object of our experimental investigation. The averaged total neutron cross section of this isotope was measured by us in the energy region 50.7-60.4 keV in 2004 [7], and the obtained result shown a good agreement with the ENDF libraries, except BROND-2 and CENDL-2. One wide s-wave resonance at the energy near 50 keV and two narrow p-wave resonances at the energies near 48 keV and 58 keV are presented for the ^{52}Cr total neutron cross section in all ENDF libraries (see, for example, Fig. 7), but parameters of these resonances are different.

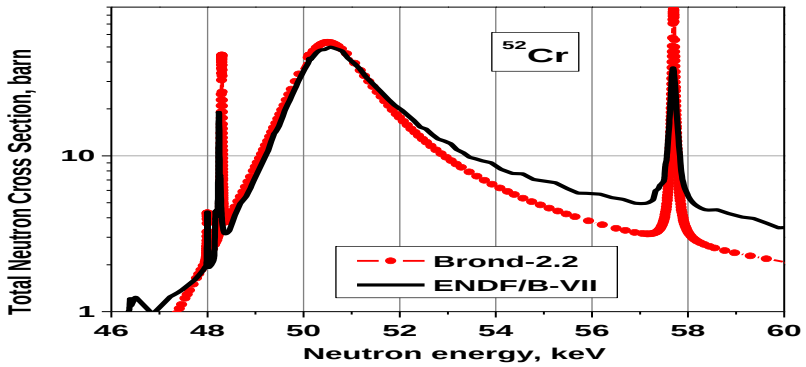

FIG. 7. Total neutron cross section of the ^{52}Cr from libraries BROND-2.2 ma ENDF/B-VII.

2.2. Filtered neutron beams

Determination of the resonance parameters is not possible if the average neutron cross section is measured only in one energy region. A set of these values, measured in the shifted energy regions, makes it possible to determine the parameters of resonance in the energy range of coverage. The measurement of the total neutron cross section of ^{52}Cr at the neutron energies 48.4, 52, 55, 58, 58.3 and 58.6 keV is the first step to solve this task.

3.2. EXPERIMENTAL DETAILS: SET-UP, FILTER, SCATTERING SAMPLE, INVESTIGATED SAMPLE

The experimental investigations of the total neutron cross sections for ^{52}Cr were carried out at the 8-th horizontal experimental channel (HEC-8) at the Kyiv Research Reactor WWR-M10. The composite neutron filter with the average energy 59 keV was used. The components of the filter take place in the first three disks of shutter and in the outside collimator. A scheme of the experimental installation on the HEC-8 is shown in Fig. 8.

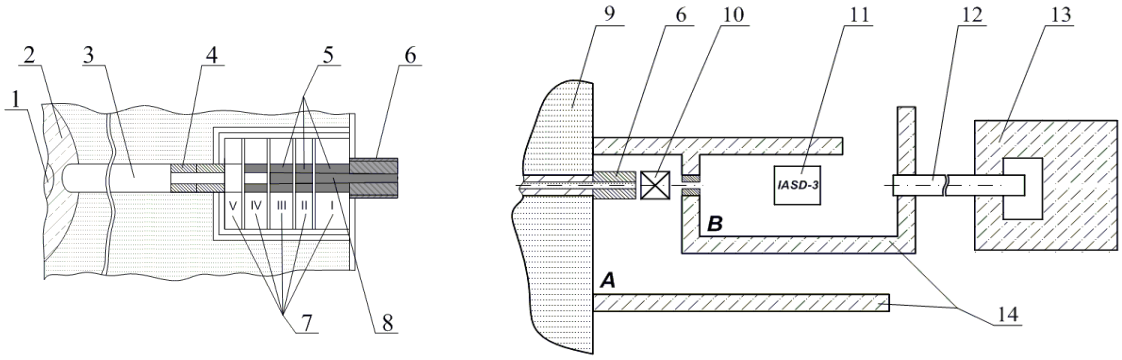

FIG. 8. A scheme of the experimental installation on the HEC-8. 1 – reactor core; 2 – beryllium reflector; 3 – horizontal channel; 4 – preliminary collimators; 5 – elements for forming of the beam; 6 – outside collimator; 7 – shutter disks; 8 – filter components; 9 – biological shielding; 10 – device for sample removing; 11 – Installation for Angle Scattering Distribution (IASD-3); 12 – tube to conduct of beam to neutron catching; 13 – neutron beam catching; 14 – radiation shielding of installation.

The multipurpose automatized IASD-3 was used to receive a set of the total neutron cross sections for the energies 48.4, 52, 55, 58, 58.3 and 58.6 keV. The detailed description of this installation was published in [8]. A scheme of the IASD-3 is shown in Fig. 9.

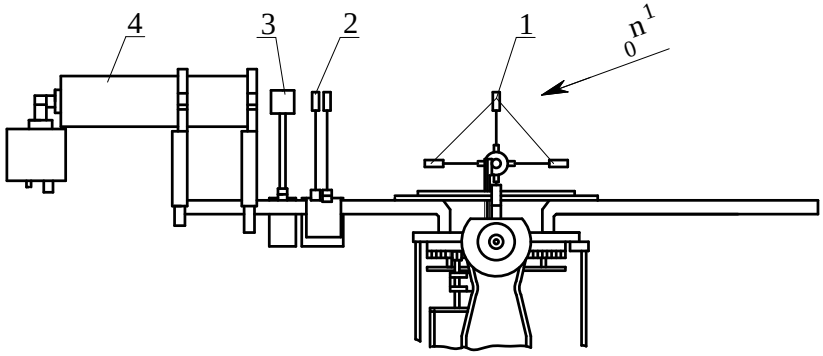

FIG. 9. Version of the IASD-3 configuration for measurements of the total neutron cross sections using the shift average energy method. 1 – scattering-samples; 2 – investigated sample, 3 – device to overlap a neutron beam by polyethylene (background measurement); 4 – detector.

2.2. Filtered neutron beams

The proton recoil detector LND-281 (Gas Filling $H+CH^4+N_2$, diameter – 38.1 mm, length – 254.0 mm, gas pressure – 3240 torr), electronic blocks: preamplifier, CAMAC blocks, personal computer and communication lines were used for neutron registration.

The filter with the average neutron energy 59 keV was used in the experimental investigations [1, 7 - 9]. Now this filter was recalculated and complemented by the new components. These calculations were done by the Filter-7 code using the CENDL-2 and JENDL-3.3 libraries. The components of this filter are presented in Table. 4. The calculated neutron spectrum after this filter is presented in Fig. 10.

TABLE 4. THE 59 KEV FILTER COMPONENTS

Elements	S	^{58}Ni	V	Al	^{10}B
Thickness, g/cm^2	116.53	81.42	24.44	5.4	0.5

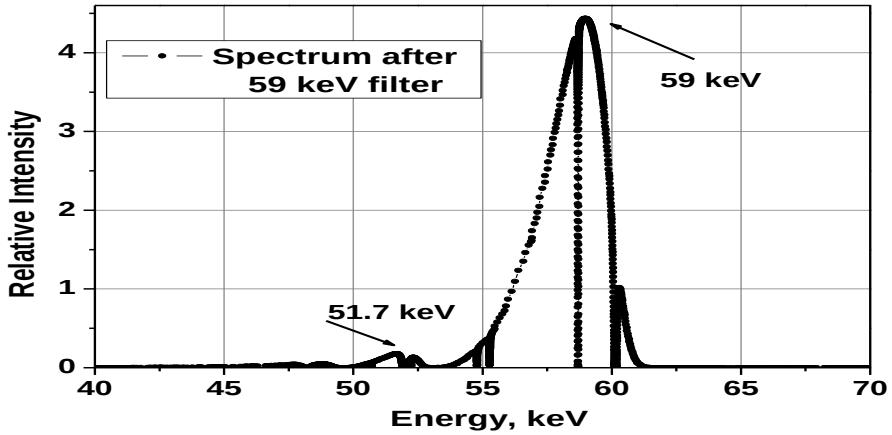

FIG. 10. Calculated neutron spectrum after the 59 keV filter.

The purity of the filter was about 99.7%. Other additions to the main neutron line were negligible: a line with the energy 36.1 keV was about 0.1%, two groups of the energy lines 230-280 keV and 325-368 keV were about 0.15% and 0.62%, respectively. The contribution of the lines above 540 keV was 0.4%. The calculated energy and width of the neutron line (95% response function) after this filter are: $59 \pm^{1.2}_{6.7}$ keV.

To provide appreciable shift of the initial average energy 59 keV, a number of elements and compounds were considered by us as a scattering-sample. More detailed information about choosing of the scattering-samples is presented in [8]. As it is well known, the largest shift of the initial energy is provided by scattering on hydrogen. As hydrogen cannot be used as a sample (because it is gas), polyethylene sample was decided to apply as a scatter. As the scattered neutron spectrum after the CH_2 scattering-sample consists of two energy lines – neutrons scattered on H and neutrons scattered on C, the measurements with the scattering-

sample C were carried out to make correction on a contribution of the neutrons scattered on carbon. The initial neutron line with the average energy 59 at keV produces at the scattering angles 15^0, 20^0 and 25^0 the scattered neutron lines with the average energies 55, 52, 48.4 keV and 58.6, 58.3, 58 keV if neutrons are scattered by hydrogen and carbon, respectively (see Fig. 11). Thickness of the used scattering-samples C and CH_2 was 10.02±0.01 and 4.52±0.01 mm. An investigated ^{52}Cr sample was made of a metal powder, loaded into aluminum container. A thickness of the ^{52}Cr sample was 0.0173±0.0002 nucl/barn.

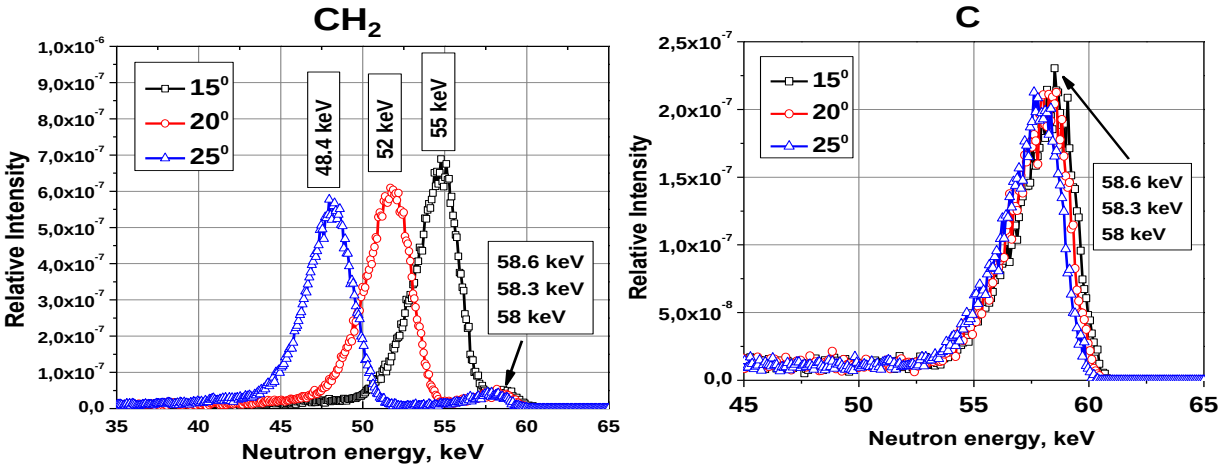

FIG. 11. The calculated scattered neutron spectra at the angles 15^0, 20^0 and 25^0 on the scattering-samples CH_2 and C.

[2] 3.3. THE EXPERIMENTAL AND CALCULATED RESULTS

Two series of measurements were carried out. Eight types of measurements (four for the scattering-sample C and four for the scattering-sample CH_2) were done in each run: 1) the investigated ^{52}Cr sample on the scattered neutron beam (position 2 in Fig. 9); 2) the ^{52}Cr sample on the beam with the polyethylene sample (position 3 in Fig. 9); 3) aluminum container on the scattered neutron beam (position 3 in Fig. 3, so called “direct” beam); 4) aluminum container on the beam with the polyethylene sample (position 2 in Fig. 9).

Duration of one measurement run was 2-4 hours. To remove the influence of instability factors, the samples at the neutron beam were replaced every minute. The total measured time in the first series amounts to 15, 26, 22 hours at the scattering angles 15^0, 20^0 and 25^0, this time in the second series was about 23, 20, 22 hours. After careful examination, the measured spectra of the same type were summed for each series of measurements. A transmission of the ^{52}Cr sample was calculated with using the formula:

$$T = \frac{\sum_{i=I1}^{I2} N_{iSMP} - \sum_{i=I1}^{I2} N_{iSMP+PE}}{\sum_{i=I1}^{I2} N_{iDB} - \sum_{i=I1}^{I2} N_{iDB+PE}}, \qquad (4)$$

2.2. Filtered neutron beams

where N_{iSMP} – the number of counts in the i-th channel of the spectrum beam after sample; $N_{iSMP+PE}$ – the same, but after sample + polyethylene; N_{iDB} – the number of counts in the i-th channel of the "direct" beam spectrum; N_{iDB+PE} – the same, but "direct" beam + polyethylene. The channel numbers I1 and I2 have been chosen in the region of the proton-recoil plateau. The spectra after polyethylene were corrected on gamma-attenuation in the used polyethylene sample. The transmission values T_γ were calculated by the MCNP 4C code. They are a little different for each angle and equal to 0.81±0.08, 0.81±0.07 and 0.80±0.07 for the angles 15^0, 20^0 and 25^0, respectively.

To determine the total neutron cross section ^{52}Cr for the average energies 55, 52 and 48.4 keV, the observed total neutron cross section was corrected. This correction is connected with existence in the neutron scattered spectrum on CH_2 neutrons scattered on carbon. It was introduced by a design-experimental approach. The ^{52}Cr total cross section at the neutron energies 58, 58.3, 58.6 keV was given from this experiment. On account of these energies are very near in value, it is assumed that these cross sections are equal in value, too. So, the experimental spectra, measured with the carbon-scatter at the angles 15^0, 20^0 and 25^0, were respectively summed. Its value was determined equal to 2.97 ± 1.22 barn. The proportions of the scattered neutron lines were given from the calculated scattered spectra (see Fig. 11) obtained by the MCNP 4C code.

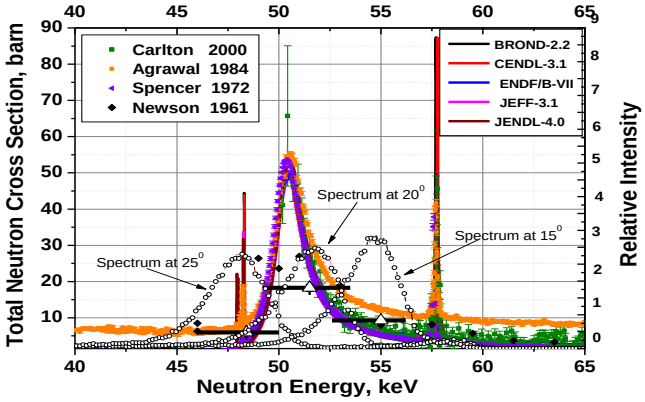

FIG. 12. The measured total cross sections (solid black horizontal lines) and data from the EXFOR and ENDF/B libraries.

The measured total cross sections are presented in Fig. 12 together with the data from the EXFOR and ENDF/B libraries. For compare our experimental results with the evaluated data, the point-wise total neutron cross section of ^{52}Cr from the ENDF/B libraries was averaged on the calculated spectrum of the scattered neutrons. In this procedure the next energy limits were taken: 48.4-57.6 keV, 45.9-55.1 keV and 42.0-52.0 keV at the scattering angles 15^0, 20^0 and 25^0, respectively. The obtained values are presented in Table 5.

In Table 5 it is seen, the changes of our experimental results with changes of the angles reproduce a trend of changes of the cross sections from the ENDF/B libraries. Unfortunately, for today we cannot say which library provides more reliable results, because at present time just one sample of ^{52}Cr was used in our experiment, so a correction on the self-shielded effect was not be done for the measured values of the total cross sections of ^{52}Cr.

2.2. Filtered neutron beams

TABLE 5. OUR RESULTS AND THE AVERAGED TOTAL CROSS SECTIONS OF ^{52}CR FROM THE ENDF/B LIBRARIES

Angle	Average energy, keV	ENDF/B-VII	JEFF-3.1 ROSFOND	JENDL-4.0	CENDL-3.1	BROND-2	Our results n=0.0173nucl/b
Scatter-sample H							
5^0	55	10.51	10.05	9.62	8.22	8.62	9.27 ± 0. 51 (6%)
0^0	52	23.21	23.36	23.10	20.87	22.91	18.29 ± 0.89(5%)
5^0	48.4	6.57	5.75	6.06	6.62	6.99	5.94 ± 0.49 (8%)

The rough estimation, done by the MCNP 4C code calculations, shown that the difference between the total cross sections at these energies and these observed self-shielded cross sections may rich 2-6%. The measurements of the different ^{52}Cr samples are planned in the future.

REFERENCES

[1] GRITZAY, O.O., et al., ”The Total Neutron Cross Section for Natural Carbon in the Energy Range 2 to 148 keV”, Proceedings of the ND2007, April 22 - 27, Nice, France, pp. 543-546.

[2] MUGHABGHAB, S.F., ”Atlas of Neutron Resonances, Resonance Parameters and Thermal Cross Sections”, 5-th Edition, NNDC BNL Upton, USA.

[3] CANTON, L., et al., ”Particle-unstable light nuclei with a Sturmian approach that preserves the Pauli principle”, Nucl. Phys. (2007), Vol.A790, pp. 251-256.

[4] GRITZAY, O.O., et al.,”Analysis possibility of using of neutron filtered beam technique at reactor for determination of carbon resonance parameters in the 150 keV region”, Nuclear Physics and Atomic Energy (2009), Vol. 10, No. 4, pp. 418 - 423.

[5] GRITZAY, O.O., et al., ”Using of neutron filtered beam technique at reactor for determination of carbon resonance parameters in the 150 keV region”, Proceedings of the NPAE-2010, June 7 – 12, 2010, Kyiv, Ukraine, pp. 468-472.

[6] http://ukrndc.kinr.kiev.ua/FILTER-7.html

[7] GRITZAY, O.O., et al.,” Total Cross Section and Self-Shielding Effects of Cr-52 Isotope Measured at Kyiv Research Reactor Neutron Filtered Beams”, Proc. of the ND2004, Santa Fe, USA, 2004.

[8] GRITZAY, O.O., et al., ”Research of Isolated Resonances Using the Average Energy Shift Method for Filtered Neutron Beam”, Proceedings of the NPAE-2010, June 7 – 12, 2010, Kyiv, Ukraine, pp. 483-486.

[9] LIBMAN V.A., et al.,”Average Resonant Capture Cross Section of 181Ta at 59 keV Filtered Neutron Beam”, Proceedings of the NPAE-2008, June 9 - 15, 2008, Kyiv, Ukraine, pp. 548-552.

THE QUASI-MONOENERGETIC NEUTRON SPECTRA FOR NUCLEAR DATA MEASUREMENTS ON FILTERED NEUTRON BEAMS AT DALAT RESEARCH REACTOR

T. T. ANH[*], P. N. SON[*], V. H. TAN[**], P. D. KHANG[**]

[*]Research Institute, 01 Nguyen Tu Luc, Dalat, Vietnam
[**]Vietnam Atomic Energy Institute, 59 Ly Thuong Kiet, Hanoi, Vietnam
Email: ttanhfr@yahoo.com

Abstract

Neutron filter technique was applied for extracting quasi-monoenergetic neutrons from the horizontal neutron channel No. 4 of the Dalat Nuclear Research Reactor. Neutron spectra of 24 keV, 54 keV, 59 keV, 133 keV and 148 keV have been simulated by MCNP code and measured based a gas-filled proton-recoil spectrometer. The total neutron cross sections for ^{12}C and ^{238}U and capture cross sections for ^{185}Re and ^{187}Re have been measured on those filtered neutron beams. The obtained results are in good agreement with the evaluated data of ENDF/BVII.0 and previous measurement values.

1. INTRODUCTION

Neutron induced reaction cross sections are the most important data needed in calculations and safety designs of nuclear power systems, and in many other applications of nuclear science and technologies. In many laboratories around the world, research works on nuclear data have been developed for many years with a lot of significant achievements. However, until now, for many nuclear isotopes or neutron energy regions, the experimental nuclear data are deficiency or inconsistent, and in many cases the measured nuclear data often show large differences among each other laboratories. Accordingly, with the aim to have a contribution to the high precise measurements of cross section data for neutron-induced reactions, the present research topic of investigation of neutron total and capture cross sections using filtered neutron beams at the Dalat Nuclear Research Reactor (DNRR) is proposed.

Neutron beams from nuclear research reactors are ideal facilities for experimental researches on nuclear reaction data. In recent years, at the DNRR, the filtered neutron beams and high resolution nuclear spectroscopes for nuclear reaction data measurements have been developed. At the horizontal channel No. 4 of DNRR, based on the application of filtered neutron beams of 24keV, 54keV, 133keV and 148keV with neutron flux about 10^5 - 10^7 n/cm^2/s; energy purity > 85%, and based on a high efficient (58%) HPGe spectrometers and/or LND-281 proton recoil counter, the precise measurements for neutron total and radiactive capture cross sections can be performed. The experimental results would be obtained with uncertainty within 1-2% for total neutron cross section values and 5-7% for radiactive capture cross sections.

2. SIMULATION OF NEUTRON ENERGY SPECTRA

The phenomenon of neutron filtration is conditioned by existence in the total neutron cross sections for some atomic nuclei of deep interference minimums which are the result of interference between the coherent waves of resonance and potential neutron scattering in these nuclei. Therefore, the white neutron spectrum from reactor (Fig. 2) transmitted such filter components becomes mono- energetic neutrons [1].

2.2. Filtered neutron beams

The model for neutron spectrum calculations is described by following expressions:

$$\phi_o(E) = \phi_i(E) * \mathrm{e}^{-\sum_k \rho_k d_k \sigma_t(E)} \quad (1)$$

$$I = \frac{\int_{E_l}^{E^h} \phi_o(E) dE}{\int_{10^{-5}eV}^{20MeV} \phi_o(E) dE} \quad (2)$$

where $\phi_i(E)$, $\phi_o(E)$ are the neutron reactor and filtered neutron spectra; ρ_k, d_k, $\sigma_t(E)$ are the density, length and total cross section of *k*-th filter component ; *I* is the relative intensity of the filtered neutron, *E* is the neutron energy [2].

A computer code named CFNB (Calculation for Filtered Neutron Beams) was developed to simulate neutron spectra after filter components. The characteristic parameters of monoenergetic filtered neutron beams are neutron spectra, relative intensity, energy resolution, dimension of filters, and suitable composition of materials are given in TABLE I. These parameters have been calculated to create the new filtered neutron beams with monoenergies of 24 keV, 54 keV, 133 keV and 148 keV at the horizontal channel No.4 of the DNRR. Calculated data by this code were in good agreement with ones by MCNP4C2. The compared results were shown in Fig. 2-6.

TABLE 1. THE PROPERTIES OF THE FILTERED NEUTRON BEAMS

En (keV)	Φ x 10^5 ($n.cm^{-2}.s^{-1}$) MCNP	I (%)	Φ x 10^5 ($n.cm^{-2}.s^{-1}$) CFNB	I (%)	Filter components
24 ± 1.8	2.7	98.3	2.6	96.72	0.2g/cm^2 ^{10}B + 20cm Fe + 30cm Al + 35g/cm^2 S
54 ± 1.5	1.9	76.9	1.7	78.05	0.2g/cm^2 ^{10}B + 98cm Si + 35g/cm^2 S
59 ± 2.7	0.83	93.02	1.1	92.28	0.2g/cm^2 ^{10}B + 10cm Ni + 15cm V + 5cm Al + 100g/cm^2 S
133 ± 3.0	0.41	92.74	0.5	92.89	0.2g/cm^2 ^{10}B + 50g/cm^2 Cr + 10cm Ni + 60cm Si
148 ± 14.8	7.4	91.4	7.2	95.78	0.2g/cm^2 ^{10}B + 98cm Si + 2cm Ti

2.2. The filtered neutron beam technique

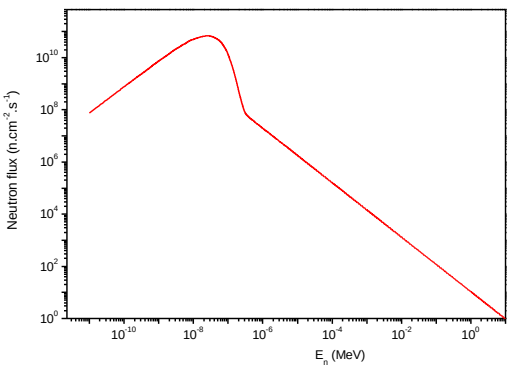

FIG. 1. White neutron spectrum.

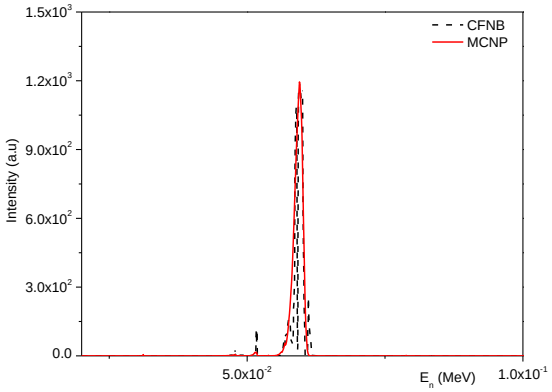

FIG. 4. 59keV neutron spectrum.

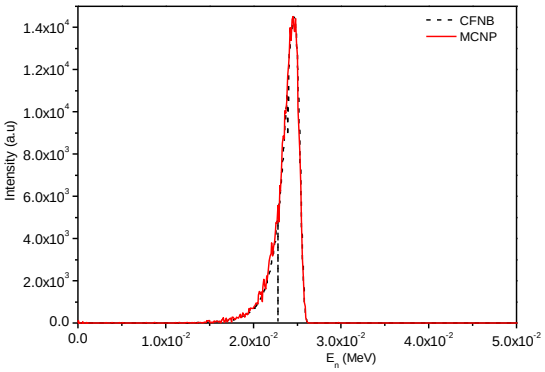

FIG. 2. 24 keV neutron spectrum.

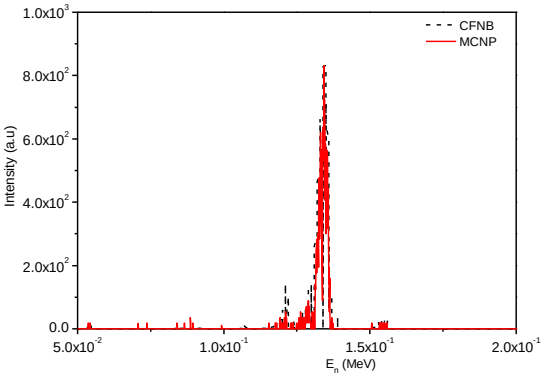

FIG. 5. 133 keV neutron spectrum.

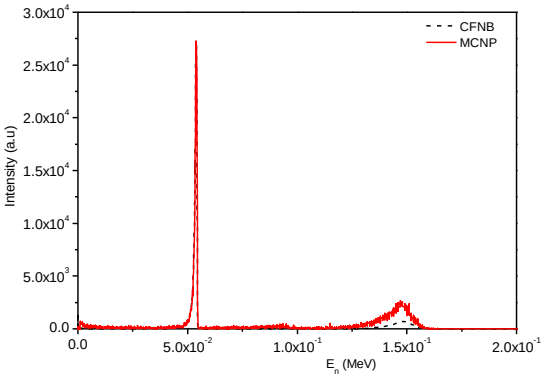

FIG. 3. 54keV neutron spectrum.

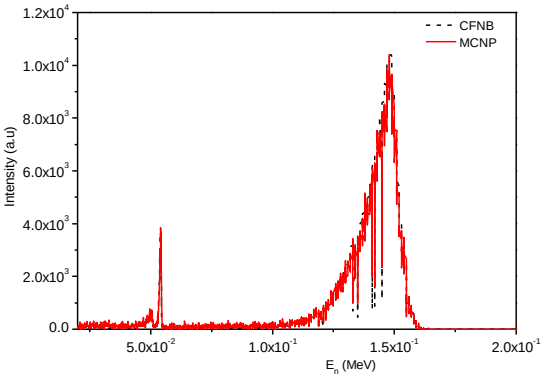

FIG. 6. 148keV neutron spectrum.

3. MEASUREMENTS OF FILTERED NEUTRON SPECTRA

For monoenergetic neutrons of energy, E_n < 10MeV, recoil-proton has a uniform energy distribution. The probability that a recoil-proton will have energy between E_p and $E_p + dE_p$ is:

$$f(E_p)dE_p = \begin{cases} \dfrac{dE_p}{E} & 0 \le E_p \le E \\ 0 & E_p > E \end{cases} \qquad (3)$$

2.2. The filtered neutron beam technique

Therefore, the response of a proton-recoil counter has a rectangular shape. Such a simple response-function will subsequently produce, by ionization, a pulse-height distribution of the same shape. This simple shape makes it relatively easy to determine the neutron-energy using the slope of the distribution, which increases in definitely at a pulse height corresponding to the neutron energy.

The proton-recoil distribution $f(E_p)$ is related in a simple way to the neutron spectrum $\phi(E)$:

$$\phi(E) = -\frac{1}{NT}\frac{E}{\sigma(E)}\left|\frac{df(E_p)}{dE_p}\right|_{E_p=E} \tag{4}$$

where $\sigma(E)$ is the neutron-proton scattering cross section and NT is the product of the hydrogen atom number in the effective counter volume by the time. Thus, the neutron spectrum $\phi(E)$ would be obtained by differentiation of $f(E_p)$from measured data [3].

The filtered neutron beams of 24 keV, 54 keV, 59 keV, 133 keV and 148 keV were measured at the horizontal beam port by using the LND-281 neutron spectrometer. The obtained proton- recoil spectrum was then subtracted background determined by intercepting the neutron beam with a 10 cm long polyethylene absorber. This spectrum will be corrected the wall effect which was calculated by Monte Carlo method. The corrected proton-recoil spectrum was carried out by Eq. 4. From the differential spectrum, the intensity and resolution of the beam can be determined. The proton-recoil distribution spectrum and the intensity of filtered neutron beam of 54 keV were shown in Figs. 7 and 8.

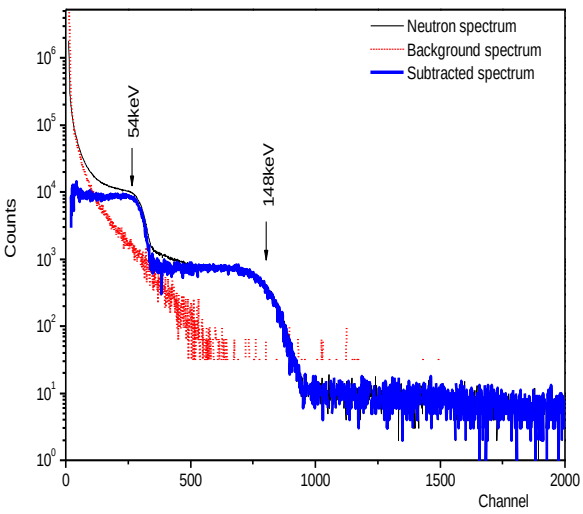

FIG. 7. Proton-recoil distribution of 54 keV.

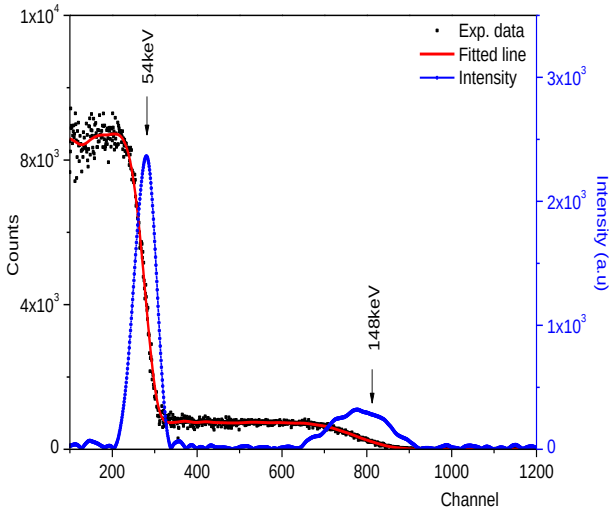

FIG. 8. Measured neutron spectrum of 54 keV.

2.2. Filtered neutron beam technique

4. RADIATIVE CAPTURE CROSS SECTION MEASUREMENTS

4.1. EXPERIMENTAL ARRANGEMENTS

The measurements for neutron capture cross sections for ^{185}Re and ^{187}Re were performed on the filtered neutron beams of 24 keV, 54 keV, 59 keV, 133 keV and 148 keV. The neutron beams were collimated to 3cm in diameter by using the usual materials of LiF, Cd, B_4C, Pb and borated paraffin. The physical properties of these beams are given in Table 1. The samples were prepared from the high purity metal foils of Au (99.99%, 1.3 cm x 1.3 cm, 0.05 mm in thickness) as a standard for neutron flux monitor, and Re (99.98%, 1.3 cm x 1.3 cm, 0.125 mm in thickness). Each sample was sandwiched between two gold plates, and the sample groups were wrapped in Cd-covers (0.5 mm in thickness) with aim to reject most of thermal neutron background. The irradiation time was 48 hours for every sample group. The specific activities of the targets and the gold disks were measured by using a DSP-base gamma ray spectrometer with HPGe detector (58% efficiency, 1.9 keV energy resolution at 1.332 MeV of ^{60}Co). The detector efficiency was calibrated by using a set of standard radioisotope sources: ^{241}Am, ^{57}Co, ^{113}Sn, ^{137}Cs, ^{60}Co, ^{88}Y and ^{152}Eu. [3]

4.2. DATA PROCESSING [4]

During irradiation in the neutron beam with energy spectrum $\phi(E)$, the reaction rate, R, of samples is defined as follows:

$$R = N\int \phi(E)\sigma_a(E)dE \tag{5}$$

where N is the number of nuclei in sample, and $\sigma_a(E)$ is the neutron capture cross section at energy E. The average capture cross section, $<\sigma_a>$, and neutron flux, $<\phi>$, are defined as following:

$$<\sigma_a>=\int \sigma_a(E)\phi(E)dE / \int \phi(E)dE$$

$$<\phi>=\int \phi(E)dE$$

Applying these average quantities, the integrating Eq. (1) can be rewritten as follows:

$$R = N.<\sigma_a>.<\phi> \tag{6}$$

The radioactivity, A, of the sample at the end of neutron irradiation has related with the reaction rate as well as the number of count, C, obtained from the measurement of the decay gamma rays, by the following expressions:

$$A = R(1-e^{-\lambda t_i}) \tag{7}$$

2.2. Filtered neutron beam technique

$$A = \frac{C f_c \lambda}{\varepsilon_\gamma I_\gamma e^{-\lambda t_d}(1-e^{-\lambda t_c})} \tag{8}$$

where t_i, t_d and t_c are irradiating, cooling and measuring times, respectively, λ is the decay constant of activated nucleus, ε_γ is the detection efficiency of detector, I_γ is the intensity of interesting γ ray and f_c is the correction factor for self-shielding, multiple scattering and background resonance capture in sample. Finally, from Eqs. (6), (7) and (8), the average capture cross sections, $<\sigma_a>^x$, for the samples at energy E can be obtained relative to that of ^{197}Au standard by the following relations:

$$<\sigma_a>^{=} \frac{C^x f(\lambda,t)^x f_c^{\,x} I_\gamma^{Au} \varepsilon_\gamma^{Au} N^{Au}}{C^{Au} f(\lambda,t)^{Au} f_c^{\,Au} I_\gamma^{x} \varepsilon_\gamma^{x} N^{x}} <\sigma_a>^{Au} \tag{9}$$

$$f(\lambda,t) = \frac{\lambda}{(1-e^{-\lambda t_i})e^{-\lambda t_d}(1-e^{-\lambda t_c})} \tag{10}$$

where the superscript 'x' means the nucleus of sample, and as above-mentioned the correction factors, f_c, for samples and gold plates were calculated by Monte Carlo method [4].

4.3. RESULTS AND DISCUSSION

The neutron capture cross sections of ^{185}Re and ^{187}Re were derived at average neutron energies of 24 keV, 54 keV, 59 keV, 133 keV and 148 keV, as given in Table 2. The present results are compared with previous measurements and the evaluated data of ENDF/B VII.0 [4], as shown in Fig. 9 and Fig. 10. In the present works, the errors of the measured cross sections are about 6.3 – 8.5%. The uncertainties are mainly due to the statistical errors (0.1-1.0%), the uncertainties of γ ray detector efficiency (2.7%), the reference cross section (3%) and the correction factors for self-shielding, multiple scattering and background resonance capture effects (3%).

In comparisons with the other measurements and the evaluated data for the case of ^{185}Re, the present results are in good agreement with the previous measurements of M. Lindner [6], and it is about 0.1 - 14.2% lower than the evaluated data of ENDF/BVII.0. In case of ^{187}Re, the present measured values of capture cross section are 1-20% lower than the evaluated data of ENDF/BVII.0, and about 50% lower than the previous measured values of M. Lindner [6] and S. J. Friesenhahn [7]. However, at 24 keV neutrons, the present result is consistent with the measured values of R. L. Macklin [8] and R. P. Anand [9] within the uncertainties.

5. TOTAL CROSS SECTION MEASUREMENTS

5.1. EXPERIMENTAL ARRANGEMENTS

The neutron beams were collimated to 1 cm in diameter by using the usual materials of LiF, Cd, B_4C, Pb and borated paraffin. The LND-281 counter was properly shielded with borated paraffin and led against scattered neutrons and prompt gamma rays. ^{12}C and ^{238}U were choosen as targets. The target samples were prepared from nuclear grade graphite and

metallic depleted uranium pellets with 2.54 cm in diameter and 0.5 cm in thickness. The experimental set-up for neutron transmission measurements is shown in fig. 11.

TABLE 2. NEUTRON CAPTURE CROSS SECTIONS OF ^{185}RE AND ^{187}RE

Average neutron energy [keV]	Capture cross section [barn]	
	^{185}Re(n, γ)^{186}Re	^{187}Re(n, γ)^{188}Re
24	1.080 ± 0.073	0.802 ± 0.048
54	0.655 ± 0.047	0.464 ± 0.035
59	0.609 ± 0.042	0.425 ± 0.027
133	0.418 ± 0.032	0.396 ± 0.033
148	0.509 ± 0.043	0.356 ± 0.024

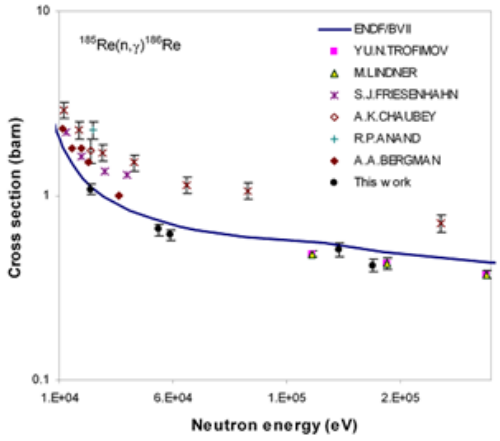

FIG. 9. Neutron capture cross section of ^{185}Re

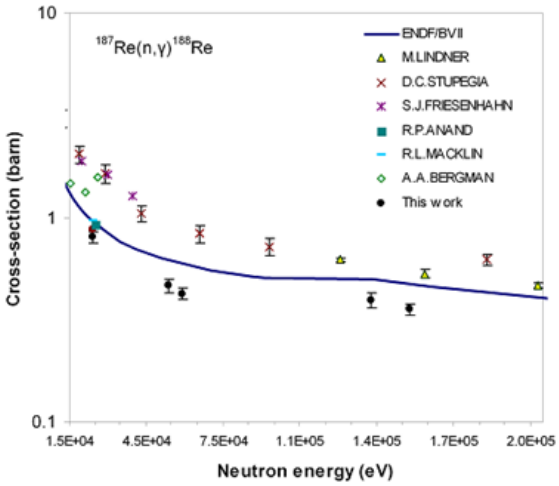

FIG. 10. Neutron capture cross section of ^{187}Re

2.2. Filtered neutron beam technique

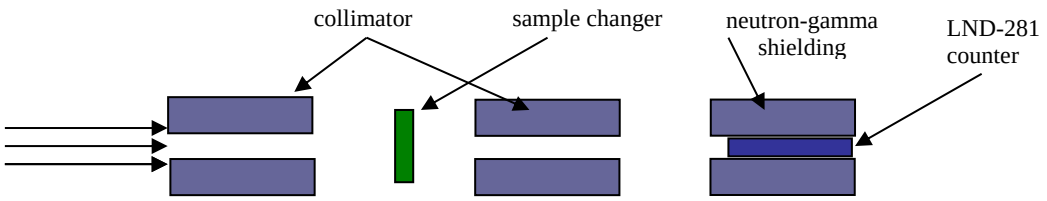

FIG. 11. Neutron transmission system at piercing beam port of DNRR

5.2. DATA PROCESSING

The total neutron cross sections were measured by neutron transmission technique. For a target of thickness *x*, the experimental total neutron cross section is determined by the formula:

$$\sigma_t = \frac{1}{\rho x} \ln \frac{1}{T} \tag{11}$$

where ρ is the concentration of the target nuclei and T is the neutron transmission ratio defined experimentally as:

$$T = \frac{a - a^b}{a_0 - a_0^b} \tag{12}$$

where a_0 and a are the neutron count rates of the incident and transmitted beams, a_0^b and a^b are the corresponding backgrounds.

Mathematically, the neutron transmission T is given by the formula:

$$T = \frac{\int e^{-\rho x \sigma_t(E)} f(E) dE}{\int f(E) dE} \tag{13}$$

with $\sigma_t(E)$ is total neutron cross section at energy E and $f(E)$ is energy distribution function of incident neutrons.

In case of infinitely thin target ($x \to 0$), we have:

$$\sigma_t \to \frac{\int \sigma_t f(E) dE}{\int f(E) dE} \tag{14}$$

As $f(E)$ varies more slowly with E than $\sigma_t(E)$, the averaging in Eq. (14) can be further simplified as:

$$\sigma_t \to \frac{1}{\Delta E} \int_{\Delta E} \sigma_t(E) dE \tag{15}$$

when $x \rightarrow 0$ the experimental value σ_t will approach the averaged total neutron cross section, $\sigma_t \rightarrow <\sigma_t>$.

5.3. RESULTS AND DISCUSSION

For the given target thickness the incident and transmitted neutron fluxes were measured alternatively in many cycles in order to minimize the influence of the reactor neutron flux fluctuation.

Due to self shielding effect, the experimental cross sections of ^{12}C and ^{238}U slightly vary with the thickness of the target and can be expressed by a linear function [10]:

$$\sigma_t = <\sigma_t> - ax \quad (16)$$

The averaged total neutron cross sections $<\sigma_t>$ can be obtained by extrapolating the experimental cross sections to zero target thickness.

The total neutron cross sections of ^{12}C and ^{238}U have been measured on filtered neutron beams of 54 keV and 148 keV, as given in Table 3 and Table 4. The present results are in good agreement with the results obtained in the previous measurements [10, 11, 12] and evaluated data ENDF/B VII.0 (Fig. 12 - 13). The experimental errors are about 1-2% and could be further reduced by increasing the number of measuring cycles. The main uncertainties are due to statistics (2%), reference cross section (0.3%), the corrections for scattering and attenuation (0.5%), background (<1%) and the error of sample weight (<0.05%).

TABLE 3. TOTAL NEUTRON CROSS SECTIONS OF ^{12}C IN KEV REGION

Average neutron energy [keV]	ENDF/B VII.0	C.T.Hibdon et al	W.P.Poenitz et al	P. D Hien et al	Present
54	4.57	4.85 ± 0.24	4.53 ± 0.045	4.37 ± 0.15	4.38 ± 0.18
148	4.31	4.2 ± 0.21	4.31 ± 0.043	4.28 ± 0.01	4.21 ± 0.08

TABLE 4. TOTAL NEUTRON CROSS SECTIONS OF ^{238}U IN KEV REGION

Average neutron energy [keV]	ENDF/B VII.0	L. L. Litvinski et al	V. V. Filipov et al	P. D Hien et al	Present
54	12.97	13.343 ± 0.051	12.95 ± 0.2	13.31 ± 0.11	12.74 ± 0.13
148	11.34	11.55 ± 0.022	11.7 ± 0.15	11.52 ± 0.10	11.44 ± 0.18

2.2. Filtered neutron beam technique

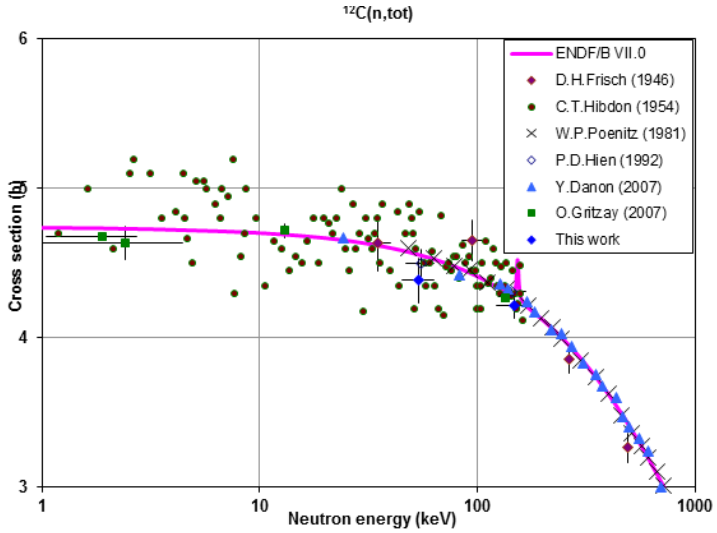

FIG. 12. Total neutron cross section of ^{12}C in keV region.

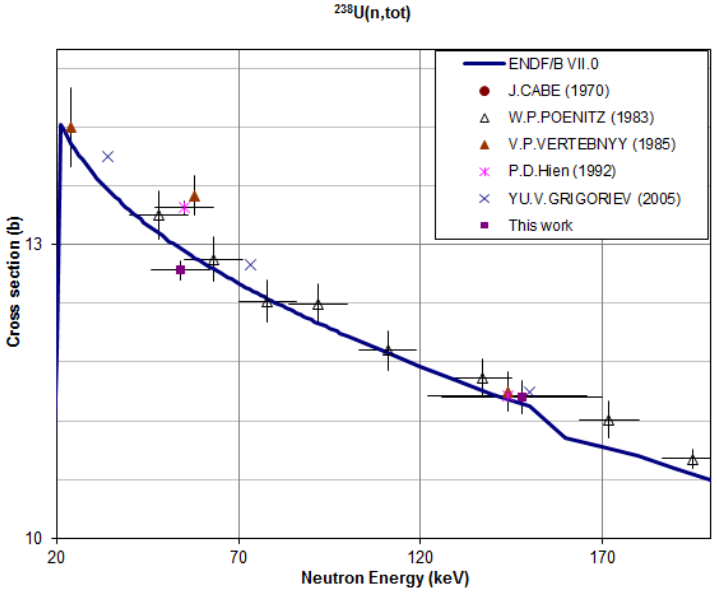

FIG. 13. Total neutron cross section of ^{238}U in keV region.

6. CONCLUSION

The neutron beams of 24 keV, 54 keV, 59 keV, 133 keV and 148 keV have been developed by using neutron filter technique. The experimental measurements of neutron capture cross sections of ^{185}Re and ^{187}Re and total neutron cross sections of ^{12}C and ^{238}U at those neutron energies have been performed by means of activation method and neutron transmission technique.

Results of research on nuclear reactions data at the DNRR will contribute a significantly sense into the development of nuclear database in Vietnam. In addition, the present researches make it possible to still open an important service for personal training and education on nuclear physics.

ACKNOWLEDGMENTS

The authors would like to express their sincere thanks to the operation staffs of DNRR for their cooperation concerning to neutron irradiations. This research is funded by Vietnam National Foundation for Science and Technology Development (NAFOSTED) under grant number “103.04-2012.59”. The expense for participating in the Technical Meeting was supported from IAEA.

REFERENCES

[1] SIMPSON, O. D., and MILLER, L. G., A technique to measure neutron cross sections in the low kev energy region, Nucl. Instr. and Meth. 61 (1968), pp. 245-250.
[2] GRITZAY, O. O., et al, Neutron filters at Kyiv research reactor, Preprint KINR-01-6 (2001).
[3] VERBINSKI, V.V., and GIOVANNI, R., Proportional counter characteristics and applications to reactor neutron spectrometry, Nucl. Instr. and Meth. 144(1974), pp. 205-231.
[4] RSICC Computer Code Collection MCNP4C2, Monte Carlo N-Particle Transport Code System, Los Alamos National Laboratory, Los Alamos, New Mexico.
[5] Java-based Nuclear Data Display Program, JANIS 3.3, www.nea.fr/lists/janis.html.
[6] LINDNER, M., NAGLE, R. J., and LANDRUM, J. H., Nucl. Sci. Eng. 59, 381 (1976).
[7] FRIESENHAHN, S. J., et al., J. Nucl. Energy 22, 191 (1968).
[8] MACKLIN, R. L., LAZAR, N. H., and LYON, W. S., Phys. Rev.107, 504 (1957).
[9] ANAND, R. P., et al., Nuovo Cimento A 50, 274 (1979).
[10] HIEN P.Z., et al, Total neutron cross-section of U-238 as measured with filtered neutrons of 55 keV and 144 keV, INDC(NDS)-0256, Vienna, 1992.
[11] LITVINSKI, L. L., et al, Preprint, Kiev, Inst. of Nucl. Phys., 85-35, 1985.
[12] FILIPOV, V. V., in INDC (CCP)-335, p.45, IAEA, August 1991.

USES OF MONOCHROMIZED THERMAL NEUTRON BEAMS FOR NUCLEAR DATA MEASUREMENTS

S.M. HOSSAIN[*], M.S. UDDIN[*], N. AFROZE[*], M.A. SALAM[**], K. NAHER[*], M. A. ISLAM[*], A.K.M. ZAKARIA[*], T.K. DATTA[*], I. KAMAL[*], S.M. YUNUS[*]

[*]Institute of Nuclear Science & Technology, Atomic Energy Research Establishment, G.P.O. Box No.-3787, Savar, Dhaka-1000, Bangladesh
[**]Reactor Operation and Maintenance Unit (ROMU), Atomic Energy Research Establishment, G.P.O. Box No.-3787, Savar, Dhaka-1000, Bangladesh
Email: syed9495@yahoo.com

Abstract

The aims of the present paper are two folds: to explore the newly installed a high resolution neutron powder diffactometer (namely SAND) facility in the radial beam port-2 of 3 MW TRIGA Mark-II research reactor of Bangladesh Atomic Energy Commission (BAEC) and to assess the possibility of measuring neutron capture cross sections for various targets using the reflected monochromized neutron beam of energy 0.03339 eV from this newly installed facility. Several irradiations of Sm_2O_3 with pure Au-foils were performed to optimize the experimental conditions for the measurements of neutron capture cross section data at 0.03339 eV from SAND. The neutron flux was found to be ~1.0×10^5 n/cm^2/sec in SAND at 3 MW. Results revealed that SAND is an excellent facility to perform neutron capture cross section data measurements.

1. INTRODUCTION

Uses of cadmium cut-off technique for the measurements of neutron capture cross sections at average thermal energy 0.025 eV in the reactor environment is a common practice. The technique is quite complex and possibility of inclusion large uncertainties. Uses of guided/monochromized neutron beam might be the solution to address this problem. The experimental determination of neutron capture cross sections for various targets using the reflected monochromized (Cu 200 plane) beam (0.0536 eV) from the Triple axis spectrometer (TAS) installed in the radial piercing beam port of BAEC 3 MW TRIGA Mark-II research reactor is well established [1-5]. Recently, a high performance neutron powder diffactometer (SAND) facility has been installed in the radial beam port-2 of the 3 MW TRIGA Mark-II research reactor for neutron scattering experiments. In SAND neutrons beam are monochromized by (511) plane of Si single crystals with wavelength λ = 1.5656 Å, which corresponds to 0.03339 eV neutron energy. The neutrons coming from SAND facilities (0.03339 eV) are quite effective compared to TAS facilities (0.0536 eV) because the energy of reflected neutrons of SAND are lower, as a consequence neutron capture cross sections for many targets will be higher. The monochromized neutron beam coming from this new SAND facility will be utilized for high precision nuclear data measurements. The scope of this article is to explore the newly installed SAND facility and to assess the possibility of measuring neutron capture cross sections for various targets using the reflected monochromized beam at 0.03339 eV from this new facility.

2. EXPERIMENTAL

2.1 NEUTRON SOURCE

The TRIGA is a research reactor having a maximum continuous thermal power output of 3 MW. The TRIGA Mark II reactor installed at the campus of Atomic Energy Research Establishment, Savar, Dhaka has several irradiation facilities including four external neutron beam tubes namely tangential, radial piercing, radial-1 and radial-2 beam ports. The technical details of this reactor can be seen in Hossain et al. [6] and Zulquarnain et al. [7]. Neutrons

2.2. Filtered neutron beam technique

coming out of the reactor are of various wavelengths. At the radial beam port-2 of TRIGA reactor neutrons are monochromatized before reaching the target for irradiation. A high performance neutron powder diffractometer namely SAND (Savar Neutron Diffractometer) has been installed at the radial beam port-2 of TRIGA reactor. Here an appropriate monochromatic neutron beam can be obtained by Bragg reflection from a Si(511) monochromator. A schematic diagram of the arrangement for monochromatization of reactor neutrons and experimental setup is shown in Fig. 1.

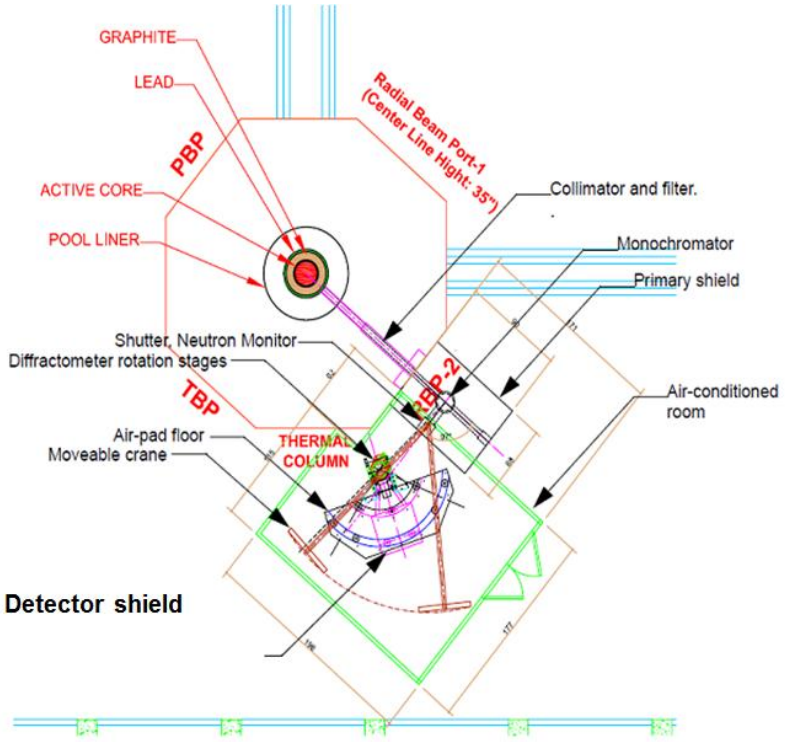

FIG.1. SAND instrument layout at RBP-2 showing some of the principal instrument components.

The reactor neutrons (mixed energies) from the radial beam port-2 (RBP-2) pass through a primary collimator and neutron filter with adequate shielding to the monochromator, which is also surrounded with appropriate shielding as shown in Fig. 1. The primary collimator consists of 20.3 cm (8″) OD outer aluminum tube which is welded to a 14 cm (5.5″) OD inner tube. The space between the outer and inner tubes is filled with neutron absorbing grout. A 12.7 cm (5″) diameter and 15.2 cm (6″) long single crystal (sapphire crystal) is mounted in the tapered section at the front (upstream) end of the collimator as a fast neutron filter. Monochromatization can very effectively be done by Bragg reflection from a Si(511) monochromator using a suitable single crystal. The monochromator is fabricated from 9 single crystal silicon slabs 1.4×0.5×19.1 cm^3 (0.570×0.210×7.5 in^3) that have been cut from the same 6 mm thick wafer of silicon. The monochromator is positioned with the bending screw at the top, appropriate for use of the Si(511) reflection. The thickness, offset angle and bending radius of silicon slabs have been selected to optimize the intensity and diffractometer resolution for the Si(511) reflection of the monochromator at 97^o take-off angle and a sample – monochromator distance of 1.90 m yielding a wave length of λ = 1.5656 Å, which corresponds to 0.03339 eV neutron energy. The difractometer has been installed at the 1.90 m position appropriate for the (511) reflection.

2.2. Filtered neutron beam technique

2.2. SAMPLE PREPARATION

A powder sample of samarium oxide (Sm_2O_3; 99.99% purity) was used as a samarium target of natural isotopic composition. In nature, samarium occurs as seven isotopes, three of which are radioactive with extremely long half-lives. The isotopes and their natural occurrences are ^{144}Sm (3.1%), ^{147}Sm (15%), ^{148}Sm (11%), ^{149}Sm (14%), ^{150}Sm (7.4%), ^{152}Sm (27%) and ^{154}Sm (23%). The three naturally occurring radioactive isotopes and their half-lives are ^{147}Sm (110 billion years), ^{148}Sm (8000 trillion years) and ^{149}Sm (10,000 trillion years). Their extremely long half-lives make these three radioactive isotopes essentially indistinguishable from the stable (nonradioactive) isotopes. The Sm_2O_3 powder was pressed with a pressure of 5 ton/cm^2 using a hydraulic press to prepare a pellet. The pellet was sandwiched with two pure gold foils for irradiation. Gold foils were used to measure the effective neutron flux using the ^{197}Au(n,γ)^{198}Au monitor reaction. Two gold foils of approximately same size and weight were attached at the front and back of the pellet to determine the neutron beam attenuation along the target.

2.3. SAMPLE IRRADIATION

The Sm_2O_3 pellet sandwiched with pure Au-foils (>99.99%) were irradiated with monochromatic neutrons of energy of 0.03339 eV. The irradiation was performed at reactor power of 1.5 MW. The irradiation time of 9.5 h was selected by considering the sufficient activity of the radionuclide ^{153}Sm in samarium oxide and ^{198}Au induced in gold foils at the present experimental conditions.

2.4. GAMMA RAY MEASUREMENT AND DATA ANALYSIS

The activities of the radioactive products of the target and monitor were measured nondestructively using high-purity germanium (HPGe) gamma ray spectroscopy (Canberra, 25% relative efficiency, 1.8 keV resolution at 1332.5 keV of ^{60}Co) coupled with a digital gamma spectrometry system and Maestro data acquisition software (ORTEC). The activity measurement was done after sufficient cooling time (>24 h) to complete the decay of most of the undesired short-lived activities to identify and separate complex gamma lines. Spectrum analysis was done using the Hypermet PC version 5.12 software and GammaVision software.

For the counting distance the efficiency versus energy curve of the HPGe gamma ray detector was determined using the standard point sources, ^{133}Ba, ^{22}Na, ^{60}Co, ^{57}Co, ^{54}Mn and ^{137}Cs. Using the ^{197}Au(n,γ)^{198}Au monitor reaction the neutron beam intensity was determined from the measured activities induced in gold monitor foils. The monitor foils were irradiated simultaneously and measured with the same detector and in a comparable geometry as the pellet.

By correcting for the gamma ray intensities and the efficiency of the detector the gamma ray count rates were converted to decay rates using the following formula:

Reaction rate, $$R = \frac{\lambda C}{N \varepsilon I_\gamma \; e^{-\lambda t_c} \; (1 - e^{-\lambda t_m}) \cdot (1 - e^{-\lambda t_i})} \qquad (1)$$

where,

λ = decay constant, s^{-1}

2.2. Filtered neutron beam technique

C = total counts of gamma ray peak area
N = number of target atoms, atom
ε = peak efficiency
I_γ = branching ratio of gamma ray
t_c = cooling time, s
t_m = counting time, s
t_i = irradiation time, s

Neutron having pure mono-energetic spectrum and the cross-section at the peak neutron energy is known. Therefore, neutron flux can simply be obtained as:

$$\phi(E_{peak}) = \frac{R}{\sigma(E_{peak})} \quad (2)$$

where, $\phi(E)$ = neutron flux, n cm^{-2} s^{-1}

From the NUDAT database (National Nuclear Data Center, information extracted from the NuDat database, http://www.nndc.bnl.gov/nudat2) the radioactive products decay data were taken.

3. RESULTS AND DISCUSSION

Several irradiations of Sm_2O_3 sandwiched with pure Au-foils (12 mm diameter) were carried out to optimize the experimental conditions for assessing the possibility of measuring neutron capture cross sections for various targets using recently installed high resolution neutron powder diffactometer facility in the radial beam port-II of the 3 MW TRIGA Mark-II research reactor. The target Sm_2O_3 has selected for the optimization because the same target has been used for the former experiments using TAS facilities at 0.0536 eV neutron energy [5]. The fist irradiation was performed for 2.5 hours at 2.4 MW reactor power selecting the slit size aperture of neutron beam of 5 mm diameter and 50 mm length. The activity of the expected product nuclides from Sm and Au were checked using the high-purity germanium (HPGe) gamma ray spectroscopy (Canberra, 25% relative efficiency, 1.8 keV resolution at 1332.5 keV of ^{60}Co) coupled with a digital gamma spectrometry system and Maestro data acquisition software (ORTEC). Unfortunately, none of the Sm and Au was activated with the mentioned irradiation conditions. The second irradiation was performed for 9.5 hours with reactor power of 1.5 MW and selecting the slit size aperture of neutron beam of 15 mm diameter and 95 mm length that ensuring the exposed of entire sample and the Au foils. The irradiated sample and Au foils were then counted using the same detector and same counting conditions. Fortunately, from second irradiation, excellent peaks were found in all the expected product nuclides of Sm and Au, as shown in Figs 2-3.

As seen, the peak of ^{153}Sm [via $^{152}Sm(n,\gamma)^{153}Sm$ reaction] at 103.3 keV in Fig. 2 and of ^{198}Au [via $^{197}Au(n,\gamma)^{198}Au$ reaction] at 411.8 keV in Fig. 3 were clearly identified, which ensures the possibility of measuring neutron capture cross section of various targets at 0.03339 eV neutron energy reflected from Si(511) crystals.

2.2. Filtered neutron beam technique

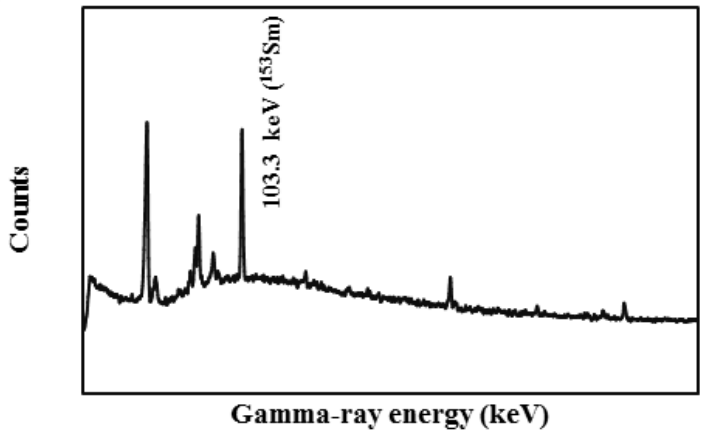

FIG.2. Gamma ray spectrum of an irradiated Sm_2O_3 at the slit aperture of the SAND facility.

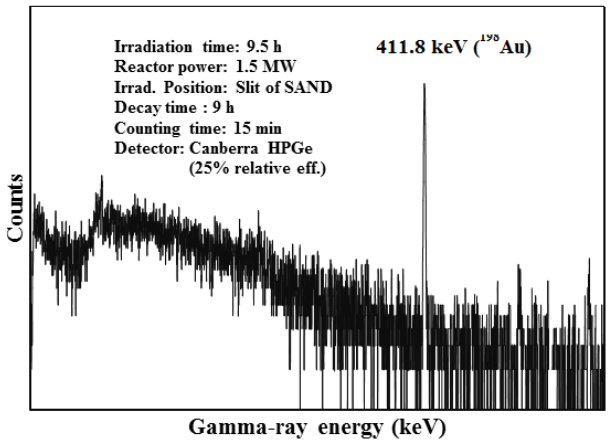

FIG.3. Gamma ray spectrum of an irradiated gold foil at the slit aperture of the SAND facility.

4. CONCLUSION

The neutron flux as well as the possibility of measuring neutron capture cross sections for $^{152}Sm(n,\gamma)^{153}Sm$ reaction were assessed at 0.03339 eV neutron energy reflected by Si crystal with (511) plane of SAND facility installed in the radial beam port-2 of BAEC TRIGA Mark-II research reactor. The quantitative determination of neutron capture cross section of the above mentioned reaction is in progress. Only the qualitative assessment of the reaction was performed in the present study by measuring the peak of its gamma spectrum. This finding ensures the possibility of measuring neutron capture cross sections for other targets using the reflected beam of SAND facility.

ACKNOWLEDGEMENT

Authors are grateful to all the members of Reactor operation and Maintenance Unit (ROMU) for ten hours continuous operation of the reactor. Thanks are deserved to all the members of Neutron Scattering (NS) Group to allow and help us for operating SAND facilities.

2.2. Filtered neutron beam technique

REFERENCES

[1] HOSSAIN, S.M., and UDDIN, M.S., "Experimental determination of neutron capture cross sections at a rare thermal energy using the BAEC TRIGA reactor", INDC (NDS)-0574, IAEA Nuclear Data Section (July 2010) 55-66.

[2] UDDIN, M. S., et al.,"Experimental cross-section measurement for the $^{139}La(n,\gamma)^{140}La$ reaction at 0.0536 eV energy", Radiochim Acta, 98 (2010) 1-6.

[3] UDDIN, M. S., et al., "Neutron capture cross-section measurement for the $^{186}W(n,\gamma)^{187}W$ reaction at 0.0536 eV energy", Applied Radiation and Isotopes, 66 (2008) 1235-1239.

[4] UDDIN, M. S., et al., "Measurement of neutron capture cross section of the $^{171}Ga(n,\gamma)^{172}Ga$ reaction at 0.0536 eV energy", Nuclear Inst. and Methods in Physics Research B , 266 (2008) 3341-3345.

[5] UDDIN, M. S., M. H. Chowdhury, S.M. Hossain, Sk. A. Latif, M.A. Hafiz, M. A. Islam, S. H. Mubin, A. K. M. Zakaria, S. M. Yunus and S. M. Azharul Islam, "Thermal neutron cross sections for the $^{152}Sm(n,\gamma)^{153}Sm$ and $^{154}Sm(n,\gamma)^{155}Sm$ reactions at 0.0536 eV energy", Nuclear Inst. and Methods in Physics Research B , 266 (2008) 4855-4861.

[6] HOSSAIN, S. M., et al., "Current status and perspectives of nuclear reactor based research in Bangladesh", IAEA TECDOC 1659 (2011), proceedings of IAEA Technical meeting (TM-34779), Research Reactor Application for Materials under High Neutron Fluence.

[7] ZULQUARNAIN, M.A., et al., "Experience with operation, maintenance and utilization of the 3 MW TRIGA Mark-II research reactor of Bangladesh", Int. J. Nuclear Energy Science & Technology, Vol 4, No.4 (2009) 299-312.

3. ACCELERATOR BASED NEUTRON BEAM FACILITIES

3.1. MONOENERGETIC AND MAXWELL SPECTRUM NEUTRON BEAMS (<5 MEV)

NUCLEAR RESEARCH WITH MONO-ENERGETIC NEUTRONS AT THE JRC MONNET FACILITY

S. OBERSTEDT[*], A. AL-ADILI[*] R. BILLNERT[*,**], G. GIORGINIS[*], F.-J. HAMBSCH[*], A. KRASA[*], A. OBERSTEDT[**], A. PLOMPEN[*], P. S. CASTIÑEIRA[*,**]

[*]European Commission, DG Joint Research Centre IRMM, Retieseweg 111, B-2440 Geel
[**]Fundamental Fysik, Chalmers Tekniska Högskola, S-41296 Göteborg
[***]Dept. de Física i Enginyeria Nuclea, Institut de Tècniques Energètiques,
Escola Tècnica Superior d'Enginyeria Industrial de Barcelona (ETSEIB), E-08028 Barcelona
Email: stephan.oberstedt@ec.europa.eu

Abstract

The MONNET (MONo energetic NEutron Tower) facility is used for research on neutron-induced reactions with mono-energetic neutrons. MONNET is based on a 7 MV Van-de-Graaff-accelerator, where the accelerated ions, mainly protons and deuterons, are used to produce the neutrons by means of reactions on ^{7}Li, tritium and deuterium-containing targets. Neutrons with energies between practically 0 keV up 10 MeV and between 12.5 and 24 MeV can be produced. However, between E_n = 7 and 10 MeV and above 19 MeV secondary neutron-producing reactions have to be taken care of. The measurement program focuses on fission research and neutron-induced reaction cross-sections. The MONNET facility also contributes to the nuclear science education and hosts PhD students and post-doc fellows on a regular basis.

1. INTRODUCTION

The MONNET (MONo energetic NEutron Tower) neutron source in Geel is based on a Van-de-Graaff (VdG) 7 MV electrostatic accelerator for the production of proton-, deuteron- and helium ion beams. The accelerator is equipped with a klystron bunching system for optional generation of pulsed beams. Presently, four beam lines and experimental set-ups are installed in the upper experimental hall (level 4.6) and a fifth beam line for high intensity ion beams is available in the lower hall (level 0). The accelerator is today exclusively used for the production of high-energy quasi-mono-energetic neutrons.

The accelerator is a single stage, belt charged, vertical Van-de-Graaff hitherto operated with a radio-frequency (RF) ion source producing proton-, deuteron- or helium ions. The ion beam is guided through one of the two installed 90° analysing magnets, installed in series, to the neutron producing targets and experimental set-ups located in the two experimental halls. Either DC or pulsed ion beams can be produced with a current of up to 60 μA on target in DC mode and up to 1 μA in pulsed mode, with a pulse repetition rate of 2.5, 1.25 or 0.625 MHz and ion pulses of 2.50 -1.25 ns FWHM depending on the ion energy. The accelerator may be operated in unattended mode, on demand even during the weekend.

Since about one year an ECR (Electron Cyclotron Resonance) source is replacing the RF ion source. This unique combination with a single-stage VdG accelerator, operating at terminal voltage of up to 7 MV, led to a considerable increase of operation time. The ECR source allows producing higher ion currents and also facilitates the generation of higher charged and heavier ions.

3.1. Monoenergetic and maxwell spectrum neutron beams (<5 MeV)

TABLE 1. LIST OF NEUTRON PRODUCTION REACTIONS AND THE CORRESPONDING NEUTRON ENERGY RANGE; THE RIGHT COLUMN LISTS THE REGIME, WHERE THE BEAM IS QUASI MONOENERGETIC

reaction	neutron energy (MeV)	mono-energetic neutron range (MeV)
$^{7}Li(p,n)^{7}Be$	0 – 5.3	0.3 – 0.65
$T(p,n)^{3}He$	0 – 6.2	0.3 – 6.2
$D(d,n)^{3}He$	1.8 – 10.1	4.0 – 7.5
$T(d,n)^{4}He$	12.5 – 24.1	12.5 – 24

Quasi mono-energetic neutrons in the energy regions 0-10 MeV and 12.5-24 MeV are produced by using lithium-fluoride (^{7}LiF), and deuterium or tritium deposited in a titanium matrix (D/Ti = T/Ti = 1.4) as target materials. Also a deuterium gas-cell is available. Depending on the neutron energy and ion intensity at target the neutron flux may reach 10^{9} neutrons/s/sterad. Tables I and II summarize the characteristic neutron energies, which may be delivered, and the neutron beam characteristics, respectively. However, it has to be noted that secondary reaction enter with increasing proton and deuteron energies, which have to be carefully monitored and taken into account during data reduction.

TABLE 2. LIST OF NEUTRON PRODUCTION REACTIONS AND THE CORRESPONDING NEUTRON BEAM PARAMETERS

reaction	target	Weight (mg/cm^2)	E_{ion} (MeV)	E_n (MeV)	Neutron (10^6/s/sr/μC) yield	σ_{En}/E_n (%)
$^{7}Li(p,n)^{7}Be$	LiF	0.5	2.1	0.3	1.8	7
		2.0	3.6	1.8	12	3
$T(p,n)^{3}He$	TiT	2	1.3	0.3	10	50
		2	7.0	6.2	2	0.3
$D(d,n)^{3}He$	D_2	4 cm, 200 kPa	1.4	4.0	10	18
			4.4	7.5	30	3
	TiD	2	1.1	4.0	5	15
			4.4	7.5	20	3
$T(d,n)^{4}He$	TiT	2	0.9	15.7	10	8
	TiT	2	3.5	20.0	4	2

Neutron fluxes and energy spectra are monitored and characterised using proton recoil telescope counters, proportional counters, BF_3 long-counters, Bonner multiple sphere systems, fission chambers and activation foils.

2. MEASUREMENT PROGRAM AT THE MONNET FACILITY

The experiment program consists of neutron-induced cross-section measurements by either directly measuring the reaction products with particle telescopes or by the activation technique using subsequently high-resolution γ ray spectrometry, fission-fragment emission yields and prompt neutron emission [1]. In a complementary approach quasi mono-energetic Neutron beams are used to measure cross-section and reaction-product angular distribution from reactions belonging to the nuclear data standards, e.g. ^{10}B(n,α) [2-4] and ^{6}Li(n,α) [5], in the incident neutron energy regime beyond 0.5 MeV, which provide an energy overlap with the GELINA neutron TOF facility [6] at IRMM for consistency check. With the implementation of a slow beam chopping device, NEPTUNE [7], investigation of isomeric decay with half lives as long as milliseconds has become feasible [8].

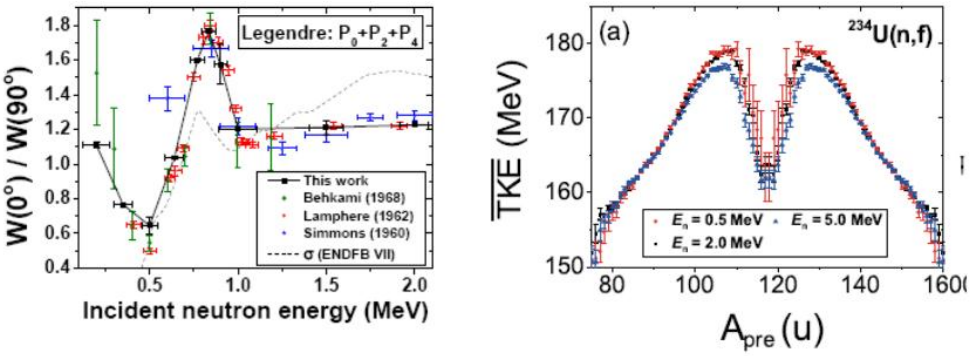

FIG.1. Angular anisotropy as a function of incident neutron energy around the vibrational resonance at E_n = 0.9 MeV (left part); Average total kinetic energy (TKE) as a function of the pre-neutron mass, Apre, for three different incident neutron energies E_n = 0.5 MeV, 2 MeV and 5 MeV [20].

The neutron beams are also offered within a trans-national access scheme to external scientific groups [9,10], and are used for detector development, testing and calibration (see e.g. Ref. [11]) as well as neutron beam profiling e.g. for astrophysics applications [12]. Within the work program MONNET contributes to the nuclear science education through hosting a number of PhD students and post-doc fellows.

Progressively, data acquisition is being based on wave-form digitization allowing for a refined data processing and analysis offline. This opens the possibility to measure highly radioactive isotopes, where up to now signal pile-up limited final data quality [13].

2.1. FISSION FRAGMENT YIELD MEASUREMENTS

Fission-fragment yield distributions are measured from neutron-induced fission on non-fissile actinide isotopes, e.g. ^{234,238}U[14-16] and ^{237}Np[17]. Measurements are performed employing the double-energy method by using a twin Frisch-grid ionization chamber (TFGIC, [18]) filled with a mixture of 90% argon and 10% methane (P10) at about 5 kPa above atmospheric pressure. The detector is radiation hard and allows measuring simultaneously pulse height and angular distribution of both fission fragments. The actinide sample is deposited on an ultra-thin polyimide backing in the centre of the cathode, so that both fission fragments may leave the target without major energy loss.

3.1. Monoenergetic and maxwell spectrum neutron beams (<5 MeV)

In recent years the focus of the measurements were put on the incident neutron energy region which corresponds to the threshold region of the fission cross-section and the vibrational resonances present. As it is depicted in the left part of Fig. 1 the energy region around the vibrational resonance in ^{234}U(n,f) is associated with strong changes in the angular anisotropy. A thorough investigation of a correlation with fission-fragment mass and total kinetic energy (TKE) is under way [19, 20].

2.2. NEUTRON-INDUCED FISSION CROSS-SECTIONS

Within the context of modern nuclear applications, either based on the thorium-uranium fuel cycle or of GenIV type, OECD/NEA [21] had formulated several high-priority fission cross-section data requests with the goal to considerably reduce uncertainties or to eliminate existing discrepancy between different data sets.

Some years ago, an extended measurement program on the reaction ^{231,233}Pa(n,f) [22-25] was carried out. Where as for ^{231}Pa discrepant cross-section data around 14 MeV had to be removed [23], for ^{233}Pa the first ever direct neutron-induced fission cross-section measurements have been carried out between E_n = 1 MeV and 8.5 MeV [24,25]. As cross-section reference ^{237}Np was used. Again, we used the TFGIC with the measured and the reference sample mounted in back-to-back geometry in the centre of the cathode. Details on the set-up may be found in Refs. [22-25]. Experimental results are depicted in the upper part of Fig. 2. Based on the new fission cross-section data existing inconsistencies could unambiguously be removed.

Very recently IRMM responded to the OECD/NEA high priority data request H37 and H39, where new data in the incident neutron energy between 500 keV (200 keV) and 5 MeV (20 MeV) are requested for ^{240}Pu (^{242}Pu). In addition, the measurement against another reference than ^{235}U was recommended. Therefore, IRMM is being undertaking a measurement program measuring against ^{238}U [26] and ^{237}Np [27], again with the TFGIC and in back-to-back geometry. Preliminary results are shown in the lower part of Fig. 2 [28]. Left, the new cross-section for the reaction ^{240}Pu(n,f) is shown and compared to existing evaluated data. The corresponding data for the reaction ^{242}Pu(n,f) is shown in the lower right of Fig. 2. The resonance structure at $E_n \approx 1.1$ MeV is much less pronounced in the new data, if existing all, and will be subject of forthcoming measurements.

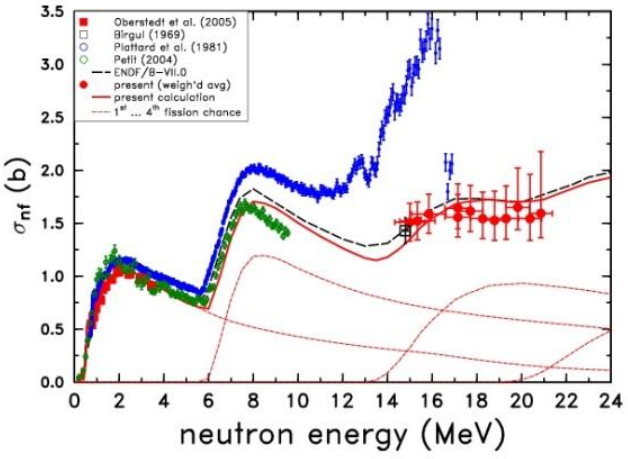

3.1. Monoenergetic and maxwell spectrum neutron beams (<5 MeV)

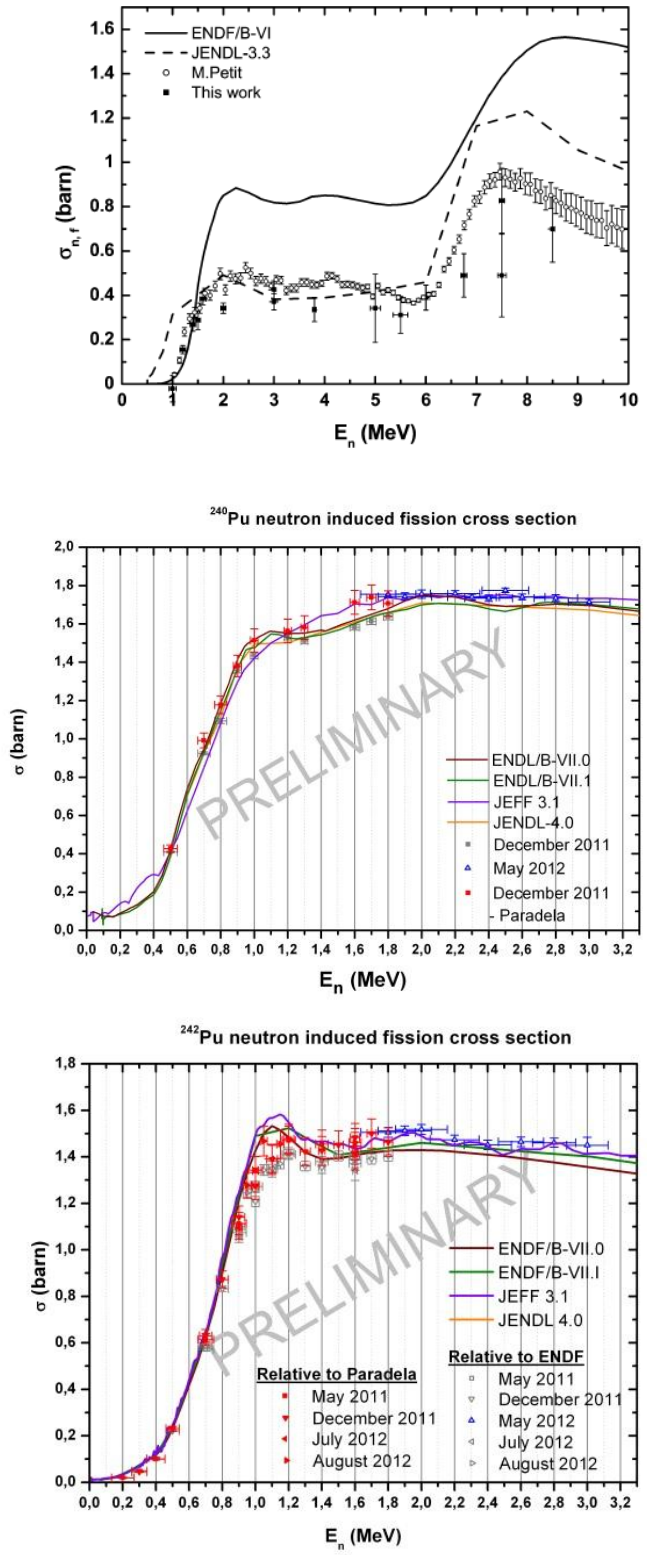

FIG.2. Neutron-induced fission cross-section for ^{231}Pa (1st top) and ^{233}Pa (2nd top) as a function of incident neutron energy compared to data from literature (figures taken from Refs. [23,25];3rd and 4th: preliminary data on neutron induced fission cross-sections of ^{240,242}Pu, which are presently under investigation at the MONNET facility [28].

3.1. Monoenergetic and maxwell spectrum neutron beams (<5 MeV)

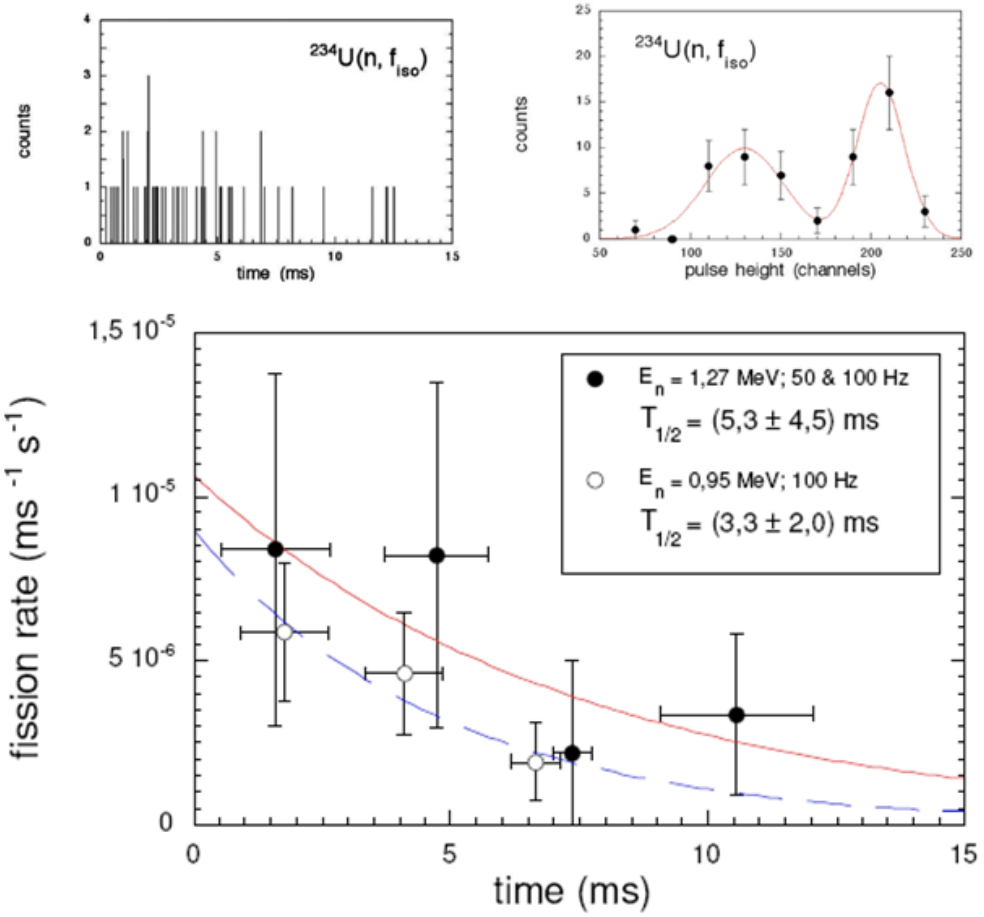

FIG. 3. Time distribution of shape isomeric fission events from $^{235}U^{*}$ prior to any background subtraction (upper left) and shape isomeric (delayed) fission fragment pulse-height distribution corrected for angular dependent energy loss prior to any background subtraction (upper right); shape isomeric fission decay of ^{235f}U: events are summed in time bins of 3 ms and background corrected as outlined in Ref. [8]. The average half-life is $T_{1/2}$ = (3.6 ± 1.8) ms (figures taken from Ref.[8]).

2.3. THE ISOMER SPECTROMETER NEPTUNE

Parameters of the double-humped fission barrier in the nuclear energy landscape are important input for fission models attempting to describe cross-sections as well as mass and kinetic energy distributions. Investigations of fission isomers, i.e. the decay of a meta-stable state in the outer, super-deformed minimum of the fission barrier may contribute to providing this information. The puzzling situation that no shape isomer for odd mass uranium isotopes had been discovered yet triggered the installation of the slow beam chopper NEPTUNE (NEutron beam Pulsed and TUNEable) at the MONNET facility. NEPTUNE switches the proton (or deuteron) beam away from the neutron production target allowing for detecting a possible decay of an isomeric state [7]. Neutron pulse length and repetition frequency may be selected in a range of 200 μs and 1 s (5 kHz – 1 Hz) and a duty cycle of 1-75%.The result of our successful search for the fission decay of the shape isomer in ^{235}U is shown in Fig. 3. The spectra have been taken from Ref. [8]. NEPTUNE allows detecting neutron-induced isomeric decay processes at cross-sections as low as 10 μb. Further experiments on the shape isomer in ^{237}U and ^{239}U are on-going.

3.1. Monoenergetic and maxwell spectrum neutron beams (<5 MeV)

Recently, we have started using the ^{7}Li(p,n) reaction with incident proton energy close to reaction threshold to produce a neutron beam collimated in a forward cone of about ±60 degrees. In conjunction with an appropriate shielding against the gamma-flash from the neutron source high-resolution γ ray detectors, high-purity germanium and $LaBr_3$ detectors, are used to measure γ rays from neutron-induced reaction in the target. The forward collimated beam allows placing sample and detectors relatively close to the neutron source. This maximizes the neutron flux on the sample whilst minimizing radiation damage to the detector.

2.5. ACTIVATION MEASUREMENTS

Neutron-induced reactions on structural materials are basic data for evaluating processes occurring on materials under irradiation in nuclear reactors. Many reaction channels open in the energy range above 14 MeV, including complex multiple particle emission reactions. The predictive power of nuclear model codes can be validated and improved by comparison with good quality experimental data. High-resolution γ ray spectrometry in combination with the use of enriched samples provides an excellent means to disentangle the different reaction channels. At IRMM mainly two lead-shielded high-purity germanium detectors are used. Details about the mode of operation, the analysis software and calibration procedure may be found elsewhere [29-32].

We present in the following only results from two recent measurement campaigns. The first one is about zirconium, because it is used in structural materials of present and in most of the innovative reactor concepts [33, 34]. Several reaction channels lead to the production of hydrogen, deuterium or helium gas. As example we show in the left part of Fig. 4 our recent results on (n,α) reactions in zirconium isotopes, which provide strong arguments for removing apparent discrepancy between different model calculations and different experimental data (see Ref. [35] for details).

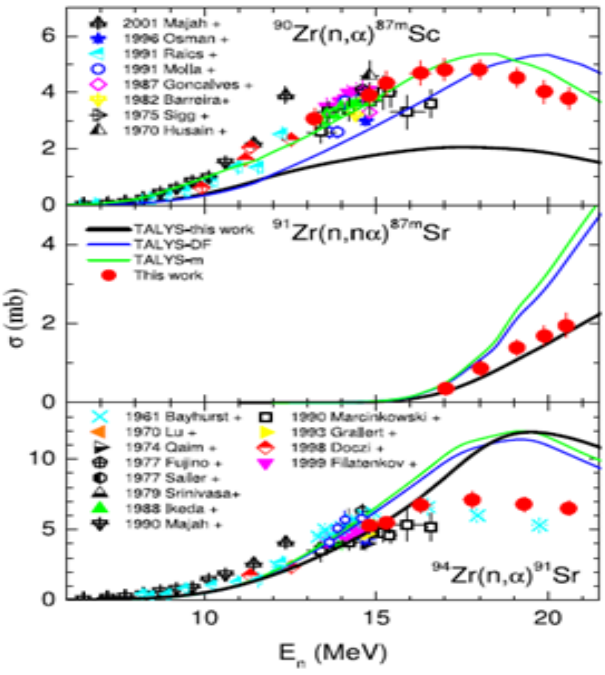

3.1. Monoenergetic and maxwell spectrum neutron beams (<5 MeV)

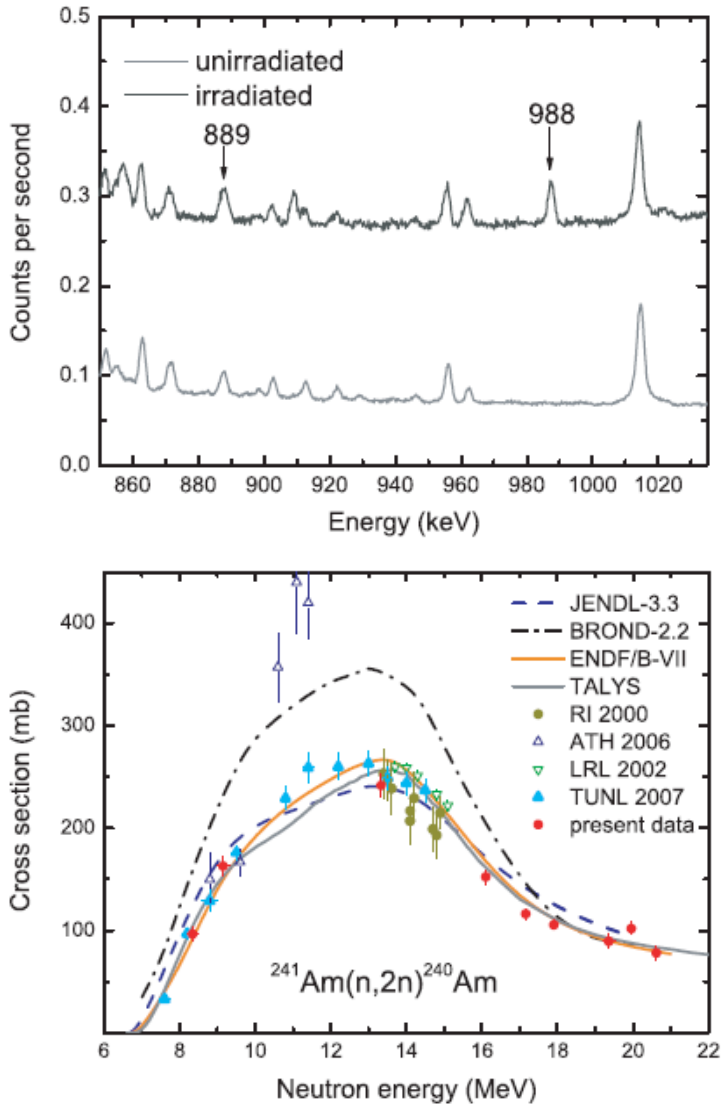

FIG. 4. Experimental results and model calculations for the $^{90}Zr(n,\alpha)^{87m}Sr$, $^{91}Zr(n,n\alpha)^{87m}Sr$, and $^{94}Zr(n,\alpha)^{91}Sr$ reactions (top, from Ref. [35]); High-energy part of the measured spectra for an irradiated and non-irradiated 241Am samples (middle up, from Ref. [36]) and new (n,2n) cross-section values (red bullets) compared to literature data and different evaluations (bottom, from [36].

The other example deals with the reaction ^{241}Am(n,2n) [36], which is extremely difficult to measure otherwise than with the activation technique due to the strong fission neutron component in the prompt-neutron emission spectrum. Prompt γ ray measurements instead would lead to an underestimation of the cross-section due to internal conversion, which makes it impossible to observe the direct population of the ground state in ^{240}Am. The activation technique offers in contrast, provided that the sample material is of sufficient purity and reasonable natural activity, the possibility to measure the decay of the reaction product. This is the case for ^{240}Am, which offers a high-energy γ ray (E_γ = 988 keV) with a high probability after β decay and with a half life of 50.8 h. A typical γ spectrum is shown in the upper right part of Fig. 4. The obtained cross-section data are shown in the lower part of Fig. 4 as red bullets in comparison with data from literature and different evaluations (see Ref. [36] for details).

3. OUTLOOK

The MONNET quasi mono-energetic neutron source provides neutrons in the energy range between 0 – 10 MeV and 12 – 24 MeV with high fluxes and at long-term beam stability. The facility allows measuring neutron-induced reaction cross-sections with high accuracy. The present program covers fission cross-section and emission yield measurements, investigation of neutron reactions in structural materials with one focus on gas production in nuclear fuel and cladding material under radiation as well as basic research relevant for nuclear reaction modeling.

The MONNET infrastructure offers experiment areas for detector development and test of state-of-the-art instrumentation prior to in-beam measurements. Digital data acquisition is progressively being implemented to the different types of experiments enhancing measurement capability and data quality.

REFERENCES

[1] KORNILOV, N., et al., Nucl. Sci. Eng. 165, 117 – 127 (2010)
[2] CARLSON, A. D., et al., Nucl. Data Sheets 110 (2009) 3215 – 3324
[3] GÖPFERT, A., et al. , Nucl. Inst. Meth. A441 (2000) 438 – 451
[4] GIORGINIS, G., and KHRYACHKOV, V., Nucl. Inst. Meth. A562 (2006) 737 – 740
[5] GIORGINIS, G., and BENCARDINO R., et al., AIP Conf. Proceedings 1412 (2011) 169 – 176
[6] OBERSTEDT, S., et al., "Nuclear data measurements at GELINA", this Technical Report
[7] OBERSTEDT, S., et al., AIP Conference Proceedings, Vol. 798, p. 273-276
[8] OBERSTEDT, A., N. Kornilov and S. Oberstedt, Phys. Rev. Lett. 99, 042502 (2007)
[9] NUDAME, *"NeUtron DAta MEeasurements at IRMM"*, FP6 EURATOM Management of Radioactive waste programme
[10] EUFRAT, *"EUropean Facility for innovative ReActor and Transmutation data"*, FP7 EURATOM Nuclear Research and Training Activities programme,
[11] PILLON, M., et al., Nucl. Phys. Meth. A640 (2011) 185 – 191
[12] FEINBERG, G., et al., Phys. Rev. C85, 055810 (2012)
[13] AL-ADILI, A., et al., Nucl. Inst. Meth. A624 (2010) 684 – 690
[14] AL-ADILI, A., et al., Phys. Rev. C86, 054601 (2012)
[15] VIVÈS, F., et al., Nucl. Phys. A662 (2000) 63 – 92
[16] BIRGERSSON, E., et al., Nucl. Phys. A817 (2009) 1 – 34
[17] HAMBSCH, F.-J., et al., Nucl. Phys. A679 (2000) 3 – 24
[18] GÖÖK, A., et al., Nucl. Inst. Meth. A621 (2010) 401 – 405
[19] AL-ADILI, A., et al., manuscript submitted
[20] AL-ADILI, A., PhD thesis, Uppsala Universitet, ISBN 978-91-554-8554-2 (2013)
[21] http://www.oecd-nea.org/dbdata/hprl/
[22] OBERSTEDT, S., et al., Ann. Nucl. Energy 32 (2005) 1867 – 1874
[23] OBERSTEDT, S., et al., Ann. Nucl. Energy 43 (2012) 26 – 30
[24] TOVESSON, F., et al., Phys. Rev. Lett. 88, 062502 (2002)
[25] TOVESSON, F., et al., Nucl. Phys. A733 (2004) 3 – 19
[26] ENDF-B/VII.1, U238, MAT = 9237, MF = 1, MT = 451
[27] PARADELA, C., et al., Phys. Rev. C82, 034601 (2010)

[28] SALVADOR, P., Castiñeira, private communication (2013)
[29] REIMER, P., et al., Phys. Rev. C71, 044617 (2005)
[30] SEMKOVA, V., et al., Nucl. Phys. A730 (2004) 255 – 284
[31] REIMER, P., et al., Nucl. Phys. A705 (2002) 265 – 278
[32] REIMER, P.,et al. , Phys. Rev. C65, 014604 (2001)
[33] FORREST, R. A., *"Data requirements for neutron activation, part I: Cross sections"*, Fusion Eng. Design 81 (2006) 2143
[34] ALBERTI, G., et al., Ann. Nucl. Energy 33 (2006) 700
[35] SEMKOVA, V., et al., Nucl. Phys. A832 (2010) 149 – 169
[36] SAGE, C., et al., Phys. Rev. C81, 064604 (2010)

NEUTRON BEAMS AND NEUTRON METROLOGY AT THE PTB ION ACCELERATOR FACILITY PIAF AND AT THE ITHEMBA LABS NEUTRON BEAM FACILITY

R. NOLTE[*], R. BÖTTGER[*], A. BUFFLER[**], D. GEDULD[**], U. GIESEN[*], M. ERHARD[*], R. NCHODU[***], E. PÖNITZ[A], S. RÖTTGER[*], F.D. SMIT[***], F. WISSMANN[*]

[*]Physikalisch-Technische Bundesanstalt, Bundesallee 100, 38116 Braunschweig, Germany
[**]Physics Department, University of Cape Town, Rondebosch, 7700, South Africa
[***]iThemba Laboratory for Accelerator Based Sciences, Somerset West, 7129, South Africa
[A]present address: Institute for Nuclear and Particle Physics, Technische Universität Dresden, Zellescher Weg 19, 01069 Dresden, Germany
Email:ralf.nolte@ptb.de

Abstract

Well-characterised neutron fields are a prerequisite for the investigation of neutron detectors. Partly in collaboration with external partners, the PTB neutron metrology group offers neutron reference fields covering the full energy range from 10 keV to 200 MeV. The specification of the neutron fluence in these beams is traceable to primary reference instruments which are based on the evaluated n-p scattering cross sections.

1. INTRODUCTION

The precise measurement of cross sections for nuclear reactions with neutrons in the entrance or exit channels requires well-characterised neutron detectors, since only a few self-normalising techniques are available [1]. In addition to the detection efficiency, other detector properties such as the light yield of organic scintillation detectors or the pulse-height response of inorganic scintillation detectors or diamond detectors have to be determined. Although Monte Carlo based methods of detector characterisations have become more and more powerful and popular in recent years, these data have, to a large extent, still to be determined experimentally.

The monoenergetic and quasi-monoenergetic neutron beams and fields available at the PTB Ion Accelerator Facility (PIAF) of the Physikalisch-Technische Bundesanstalt (PTB) and at the iThemba Laboratory for Accelerator Based Sciences (iThemba LABS) are well suited for this purpose. They cover the energy range from about 10 keV to 200 MeV almost continuously. In addition to their use for the detector calibrations, the neutron beams available at PIAF and iThemba LABS are also used directly for nuclear data measurements. In particular, the time-of-flight (TOF) spectrometer at PIAF is dedicated to this work.

Monoenergetic or quasi-monoenergetic reference fields are produced by bombarding low-Z targets (D, T, ^{7}Li) with light ions (p, d). At PTB, a 3.7 MV single-ended Van-de-Graaff (VdG) accelerator and an isochronous CV28 cyclotron [2] are used to produce proton, deuteron and alpha particle beams, while the proton beams used at iThemba LABS are accelerated by the $K = 200$ Separated Sector Cyclotron (SSC) [3]. All beams are available with a nanosecond pulse structure which is a prerequisite for time-of-flight (TOF) spectrometry. Important features of all accelerators are the pulse selector systems which can be employed to adjust the beam repetition frequency to the needs of TOF measurements. Fig. 1 shows the overall layout of PIAF and the neutron beam facility at iThemba LABS.

3.1. Monoenergetic and maxwell spectrum neutron beams (<5 MeV)

Under ideal conditions, the reactions mentioned above provide monoenergetic neutrons. In reality, however, the effects of finite target thickness, neutron scattering in the target assembly, parasitic reactions in the backing and target material as well as the finite detector size, modify the spectral distribution. At higher projectile energies, break-up reactions cause deviations from the monoenergetic distributions, i.e. the fields are only quasi-monoenergetic with a high-energy peak of finite width and a low-energy continuum down to zero energy.

Neutron beams with continuous ('white') distributions are produced using stopping-length targets. They are an important addendum to quasi-monoenergetic fields and beams. These beams are particularly useful for studying detector properties when neutron energy selection can be performed using the TOF method [4], or for the investigation of detector properties at elevated fluence rates.

Part of this contribution is an updated and extended version of an earlier overview [5]. It discusses the techniques used for the specification of the PIAF and TLAB fields as well as their beams and most important properties. In addition, some examples of nuclear data measurements at PIAF and iThemba LABS are reported.

2. NEUTRON BEAMS AND FIELDS

2.1. MONOENERGETIC LOW-ENERGY FIELDS AT THE PIAF LOW-SCATTER FACILITY

The monoenergetic reference fields with peak energies between 24 keV and 19 MeV are generated at the PTB accelerator facility PIAF. They are produced in a low-scatter experimental hall in open geometry using the ^{7}Li(p,n), D(d,n), T(p,n) and the T(d,n) reactions. These reactions are used at neutron emission angles $\Theta = 0°$ to produce the reference fields defined in the ISO 8592 standard (neutron energies of 144 keV, 250 keV, 565 keV, 1.2 MeV, 2.5 MeV, 5 MeV, 8 MeV, 14.8 MeV, 19 MeV). However, almost any intermediate energy between 144 keV and 20 MeV can be realised as well. At neutron emission angles $\Theta > 0°$ monoenergetic fields of lower energies can be produced. For example, the ^{7}Li(p,n) reaction with a proton energy $E_p = 1.95$ MeV is used to produce the 144 keV field at $\Theta = 0°$ and the 24 keV field at $\Theta = 75°$. To limit the relative width of the spectral distribution to 5% at maximum, rather thin targets have to be used. Hence, the 0° neutron yields per unit beam charge, (Y/Q), are low, ranging from to 1×10^{6} sr^{-1}μC^{-1} to 2×10^{7} sr^{-1}μC^{-1}. The relative contribution of neutrons scattered in the target assembly ranges between 1% and 4% of the fluence of neutrons leaving the target without further interaction. Shadow cones are used to subtract the room-return neutrons. Blank targets are available to separately measure parasitic neutrons from reactions with target and backing materials. This is of particular importance for the production of neutrons with energies above 16 MeV using the T(d,n) reactions and Ti(T) targets.

A quality management system according to ISO 17025 is effective for the ISO reference fields at PTB. In a key comparison organised by the Comité Consultatif pour les Rayonnements Ionisants (CCRI), it could be demonstrated that the neutron fluence determination in these fields is consistent with the results obtained by other national metrology institutes (NMIs).

3.1. Monoenergetic and maxwell spectrum neutron beams (<5 MeV)

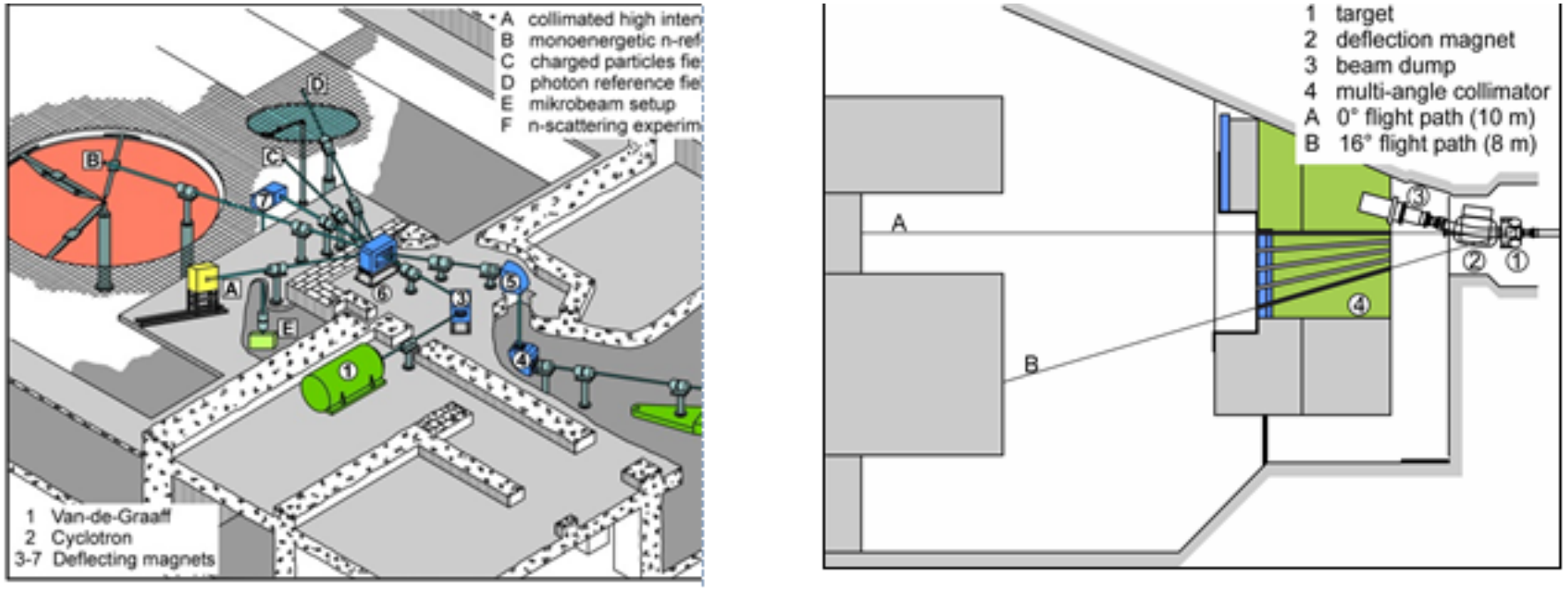

FIG. 1. Layout of the PIAF facility at PTB in Braunschweig (left panel) and the neutron beam facility at iThemba LABS in Cape Town (right panel).

3.1. Monoenergetic and maxwell spectrum neutron beams (<5 MeV)

2.2. NEUTRON BEAMS AT THE PIAF TOF SPECTROMETER

The layout of the PTB TOF spectrometer is shown in Fig. 2. In addition to its use for the measurement of differential neutron scattering cross sections in the energy range between 6 MeV and 14 MeV [6], the spectrometer can also be employed as a neutron source for other measurements. In this mode, the moveable cyclotron and the short beam tube with the neutron production target attached to its end is positioned in line with collimator channel 3. At this channel flight distances of up to 30 m are available when detector D3 is removed from the flight path.

The neutron production reactions used at the TOF spectrometer are $D(d,n)^3He$ and $^{15}N(p,n)^{15}O$, both using a gas target. The D(d,n) reaction produces quasi-monoenergetic neutrons in the energy range from about 6 MeV to 15 MeV while the $^{15}N(p,n)$ reaction can be employed to produce monoenergetic neutrons at selected energies between 2 MeV and 5 MeV. In addition, white beams are produced using the reactions $^9Be(p,nx)$ and $^9Be(d,nx)$ with a stopping-length beryllium target [4]. The continuous spectral distributions proved to be very useful for the characterisation of detectors which allow the TOF method to be used for selection of neutron energies [7].

2.3. INTERMEDIATE-ENERGY REFERENCE BEAMS AT ITHEMBA LABS

At the iThemba LABS neutron beam facilities [8], collimated quasi-monoenergetic neutron beams are produced using the $^7Li(p,nx)$ reaction. The spectral distribution exhibits a high-energy peak resulting from transitions populating the ground state and the first excited state (E_x = 0.429 MeV) of ^7Be and a continuum, which is caused by break-up reactions. Fig. 3 shows the relative spectral fluence (Φ_E/Φ) of the neutrons beams. The spectral distributions with peak neutron energies below 60 MeV were measured earlier at the cyclotron of the Université Catholique de Louvain (UCL) [9] in Louvain-la-Neuve (Belgium), but similar beams can be produced at iThemba LABS. The lowest and highest neutron energies available at the iThemba LABS facility are 30 MeV and 200 MeV, respectively. For neutron energies above 30 MeV, the 0° target yield per unit beam charge (Y/Q) is about 10^9 $sr^{-1}\mu C^{-1}$ for a lithium target 1 mm in thickness. The ratio (Φ_{peak}/Φ) of the fluence in the high-energy peak to the total fluence increases from 0.4 at 33 MeV to 0.7 at 200 MeV. The experimental width of the high-energy peak is determined by the time-resolution of the scintillation detector used for the TOF measurements; the intrinsic width resulting from the proton energy loss in the targets is smaller than the experimental width and indicatedby the horizontal error bars.

3.1. Monoenergetic and maxwell spectrum neutron beams (<5 MeV)

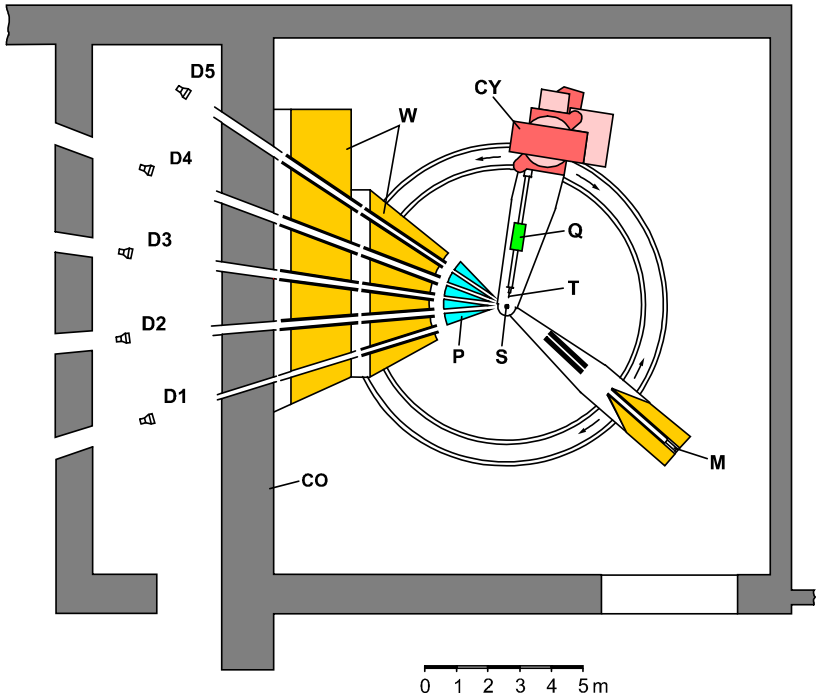

FIG. 2. Layout of the PTB TOF Spectrometer with the moveable cyclotron (CY), collimators (P, W), monitor detector (M), gas target (T) and NE213 detector (D1 – D5). The cyclotron can also be positioned in line with the collimator channel directed at detector D3. In this position flight paths of up to 30 m are possible.

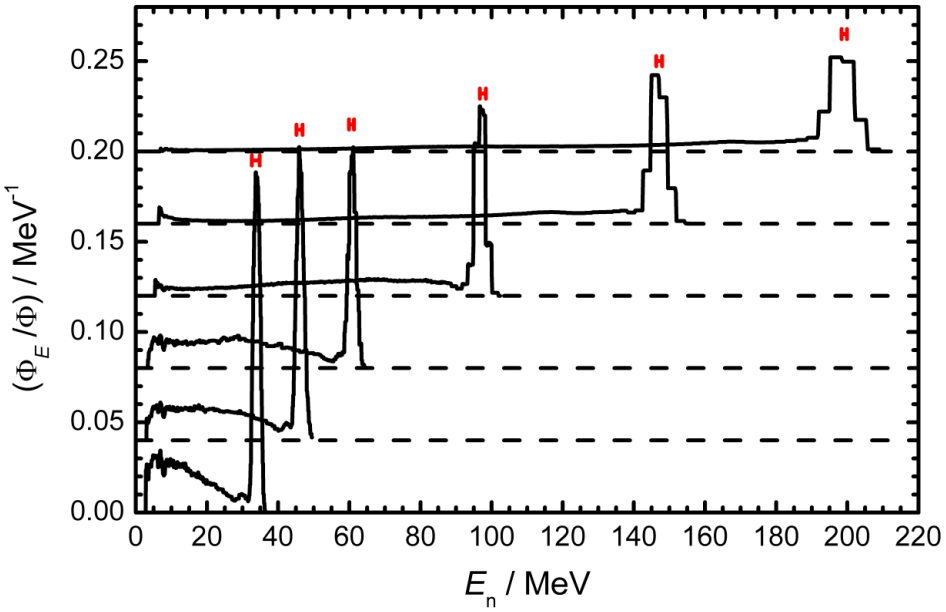

FIG. 3. Relative spectral fluence Φ_E/Φ of the medium-energy beams produced with the ^{7}Li(p,n) reaction at UCL (Louvain-la-Neuve) and iThemba LABS (Cape Town). The spectra are offset for better visualisation. The target thickness ranged between 1.6 g cm^{-2} and 4.3 g cm^{-2}. The spectra were measured using the TOF method with an BC501A scintillation detector. The widths of the high-energy peaks are dominated by the time resolution of the detector and of the proton beam; the intrinsic width calculated from the energy loss of the protons in the Li-target is indicated by the error bars. The spectral distributions realised earlier at UCL (maximum neutron energies below 65 MeV) can also be produced at the iThemba LABS neutron beam facility with almost identical properties.

3.1. Monoenergetic and maxwell spectrum neutron beams (<5 MeV)

At the iThemba LABS facility a multi-angle collimator is available with openings at angles of 0°, 4°, 8°, 12° and 16°. This makes it possible to take advantage of the fact that the neutrons resulting from transitions to the groundstate and the first excited state in ^{7}Be are strongly forward-peaked, whereas the break-up neutrons are much more isotropic. Hence, the high energy peak is strongly suppressed at 16° while the background is not affected very much. Therefore, irradiations with virtually monoenergetic neutrons can be carried out by performing a 0° - 16° difference measurement [10]. This procedure is illustrated in Fig. 4 which shows the spectral distributions obtained with 100 MeV (left panel) and 40 MeV protons (right panel) on a ^{nat}Li target at 0° and 16° together with the difference distribution $\Phi_E(0°)/M - f\cdot\Phi_E(16°)/M$. Here M denotes the reading of one of the beam monitors, e.g. the target charge Q, and f is a factor chosen such that the resulting spectral difference distribution remains positive (f = 0.77 for 100 MeV, f = 0.92 for 40 MeV). The ratio of the fluence of low-energy neutrons to the total neutrons fluence Φ_{cont}/Φ is reduced from 0.6 for the pure 0° distribution to 0.3 for the 100 MeV difference distribution and from 0.55 to 0.35 for the 40 MeV distributions. At lower beam energies, the forward peaking of groundstate transitions is less pronounced and the kinematical reduction of the neutron energy as a function of the emission angle effects a mismatch of the shapes of the high-energy peaks at 0° and 16°. Hence, as demonstrated by the 40 MeV spectra depicted on the right panel of Fig. 4, the subtraction procedure affects the peak shape to a larger extent for peak energies below 50 MeV.

For the measurement of activation cross sections, the factor f can also be made equal to the ratios of the integrals $\int \Phi_{\mathrm{cont},E}\sigma(E)\,\mathrm{d}E$ for 0° and 16° where $\sigma(E)$ is an a priori guess function for the production cross section investigated. In this case, the difference of the activities produced at 0° and 16° is predominantly produced by peak neutrons and the remaining correction for the activity resulting from continuum neutrons becomes very small.

2.4. CHARACTERISATION OF THE NEUTRON FIELDS AND BEAMS

The specification of the quasi-monoenergetic reference beams comprises two main tasks:

i) Measurement of the peak fluence

The peak fluence of all quasi-monoenergetic beams made available by the PTB group is measured relative to the primary standard cross section for neutron measurements, the differential n-p scattering cross section. Depending on the peak energy, a recoil proton proportional counter (RPPC) or recoil proton telescopes (RPT) are used [9, 11, 12, 13]. The uncertainty of the fluence measurements is dominated by the uncertainty of the differential n-p scattering cross section, which varies from 1-2 % at energies below 20 MeV and amounts to 5-10 % at energies between 30 MeV and 200 MeV. At energies below 20 MeV, a de Pangher long counter can be used as a reference instrument as well [14]. The advantage of this instrument is its high energy-independent detection efficiency, excellent stability and photon insensitivity. The main disadvantage is the lack of energy discrimination which makes a detailed characterisation of the spectral neutron distribution mandatory. Fission ionisation chambers with a ^{235}U deposit are very versatile secondary standard reference instruments over the full energy range covered at the iThemba LABS and PIAF facilities. They can be used for TOF measurements as well.

3.1. Monoenergetic and maxwell spectrum neutron beams (<5 MeV)

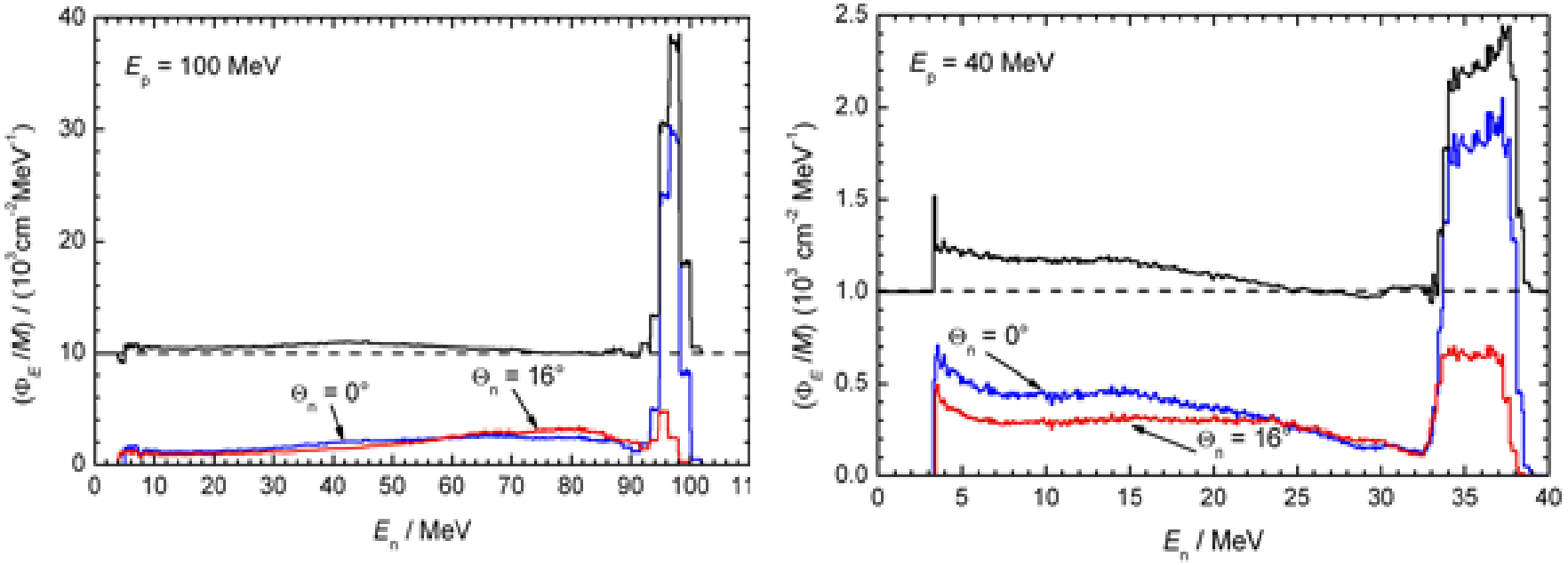

FIG. 4. Spectral fluence Φ_E/M per unit proton beam monitor reading M for 100 MeV (left panel) and 40 MeV (right panel) protons on a natLi target at the iThemba LABS neutron beam facility. Experimental spectral distributions for neutron emission angles of 0° and 16° (thin histograms) are shown together with a difference spectrum $\Phi_E/M = \Phi_E$ (0°)/M – $f \cdot \Phi_E$ (16°)/M (thick histogram) with f = 0.77 (100 MeV) and f = 0.92 (40 MeV). The difference distributions are offset for better visualisation.

ii) Measurement of the spectral fluence

The most important method for the measurement of the relative spectral neutron fluence (Φ_E/Φ) is the TOF method. The time resolution of the neutron sources available at PIAF and iThemba LABS varies from a few nanoseconds (VdG accelerator) to less than one nanosecond (SSC cyclotron). The TOF measurements are carried out using inorganic ^{6}Li-glass scintillators, fast organic scintillators (NE102, NE213) or ^{238}U and ^{235}U fission ionisation chambers. TOF measurements always have a lower threshold energy determined by the repetition frequency of the neutron source and the flight distance. Hence, the neutron spectrum at energies below this 'frame-overlap' threshold has to be measured using other spectrometric methods, e.g. unfolding of Bonner sphere readings [10].

Fluence measurements, TOF measurements and irradiations of detectors or samples are usually carried out at different distances. Hence, the range of neutron emission angles contributing to the reading of these detectors will in general be different. This is why it is more appropriate to relate the measurements to each other by Monte Carlo calculations of the field properties averaged over the sensitive areas of the detectors or samples at their respective positions instead of using a $1/r^2$-extrapolation together with a correction for fluence attenuation in air.

In addition, the contribution of neutrons scattered in the target assembly have to be included in the analysis of fluence measurements. For the PIAF reference fields, the TARGET code [15] is used to model the influence of target properties and neutron scattering in the target assembly on the spectral neutron fluence. This code also models the effects of energy loss as well as energy and angular straggling of the ion beams on the spectral neutron distribution. The left panel of Fig. 5 shows a typical spectral distribution exhibiting the 'monoenergetic' peak resulting from uncollided neutrons and the continuum of low-energy neutrons caused by scattering of neutrons in the target assembly. As mentioned above, the relative contribution of the two components can be calculated using the Monte Carlo method for the particular irradiation geometry used. These calculations are confirmed by TOF measurements.

At present, TARGET is being replaced by the general purpose Monte Carlo code MCNPX with the MCUNED patch [16]. MCUNED provides a very efficient sampling scheme for the neutron production and includes an improved description of low-energy ion transport. The right panel of Fig. 5 shows a comparison of spectral neutron distributions calculated with TARGET and MCNPX+MCUNED for the T(d,n)^{4}He reaction and 150 keV deuterons incident on a stopping-length Ti(T) target. The T(d,n)^{4}He reaction shows so-called 'kinematical focusing' at an emission angle of 97.5°, i.e. the spectral neutron distribution is almost independent of the deuteron energy and mainly determined by the angular straggling of the low-energy deuterons. The MCNPX+MCUNED calculations show a slightly broader peak and the continuum of scattered neutrons is also different. The reasons for these differences are presently investigated.

3.1. Monoenergetic and maxwell spectrum neutron beams (<5 MeV)

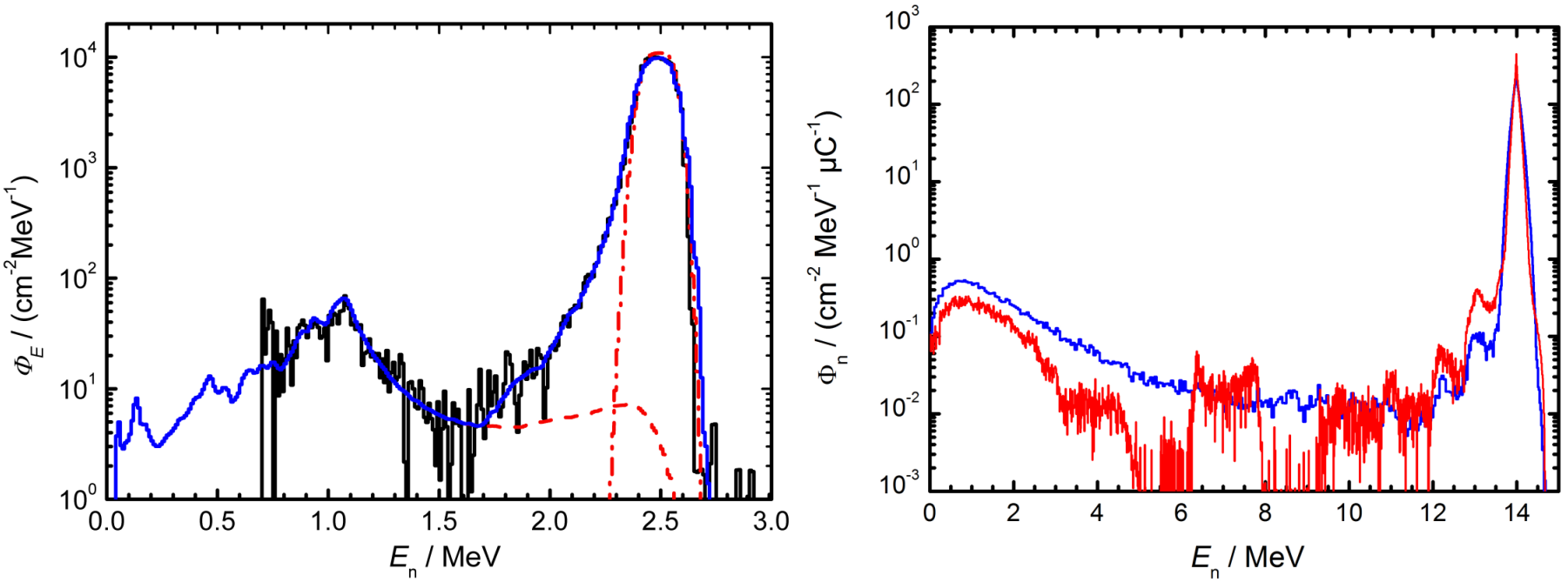

FIG. 5. Left panel: Spectral fluence Φ_E of neutrons produced by the T(p,n) reaction for a proton energy of 3.372 MeV and a neutron emission angle of 0° (histogram). The calculated total (solid line), scattered (dashed line) and uncollided (dash-dotted line) neutron distributions were obtained with the TARGET code [15]. For the total neutron spectrum, the distortion of the TOF measurement by the temporal shape of the proton beam pulses was included in the simulation with the TARGET code. Right panel: Spectral fluence Φ_E of neutrons produced by the T(d,n) reaction by 150 keV deuterons incident on a stopping-length Ti(T) target, as calculated using MCNPX + MCUNED (blue line) and TARGET(red line). The neutron emission angle is 97.5°. At this angle the T(d,n) reaction shows 'kinematical focussing' and the spectral distribution is determined by the angular straggling of the deuterons only.

3.1. Monoenergetic and maxwell spectrum neutron beams (<5 MeV)

In collimated beams the spectral fluence rate varies over the cross section of the bea m. Hence, corrections have to be applied if the sensitive areas of the reference instrument and the sample or detector under investigation cover different solid angles. Several methods are available to measure the spatial distribution, for example scanning a small detector through the beam or using a multiwire chamber with spatial resolution. A simple method employed in the iThemba LABS high-energy beams is the use of an image plate covered with a Lucite radiator, a few millimetres in thickness. Difference measurements with and without radiator allow background subtraction but the main disadvantage is the missing discrimination of the neutron energy.

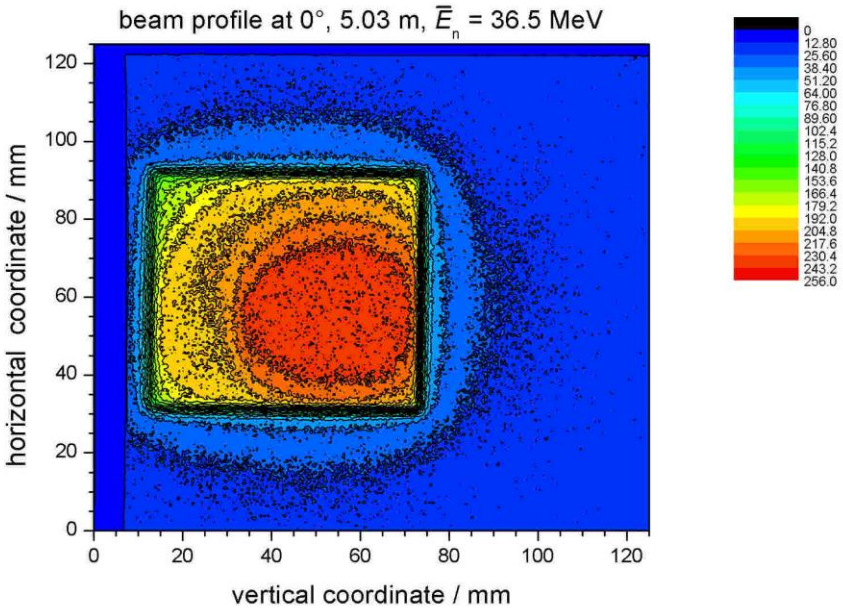

FIG. 6. Profile of an iThemba LABS neutron beam produced by 40.4 MeV protons incident on a 6 mm ^{nat}Li target. The rectangular collimator has a constant cross section over the full length of 4 m. The image plate was positioned about 1 m behind the collimator exit.

Figure 6 shows an image of the intensity distribution in one of the iThemba LABS beams. The inhomogeneous structure of the profile is partly affected by misalignment of the proton beam on the target and partly by inhomogeneous attenuation of the neutron beam. The images of the beam profiles were instrumental in identifying sources of spectrum instabilities and possible remedies.

Neutron yield monitors are required to relate the field characterisation to measurements carried out with other detectors or samples. The main requirements for monitor detectors are excellent stability and a large dynamic range in count rate. The most simple neutron fluence rate monitor is the integrated beam current, but its use depends on proper charge measurements without varying offset currents and, most importantly, on the stability of the target properties and the beam focusing. This is why special neutron detectors are usually used to relate the field or beam specification to the measurements with the sample or detector under investigation.

3.1. Monoenergetic and maxwell spectrum neutron beams (<5 MeV)

At PIAF, long counters positioned at 17° and 92° relative to the ion beam are used for this purpose. In the open geometry at PIAF, corrections for inscattering form the sample into the monitors have to be determined in separate measurements. They can be as large as 10% if massive objects, such as moderator-detector assemblies for the measurement of β-delayed neutrons [17] are positioned close to the neutron production target. In the collimated high-energy beams at iThemba LABS a gain-stabilised NE102 transmission detector a few millimetres in thickness, and a low-mass ^{238}U fission ionisation chamber are used. These two instruments are placed permanently in the beam. The fission chamber monitors the total neutron yield while the NE012 detector is also used in TOF mode for monitoring variations of the spectral distribution induced by beam spot movement on the target.

More details on the production and characterisation of neutron reference fields below and above 20 MeV can be found in a recent series of review publications [18, 19, 20].

3. MORE RECENT EXAMPLES FOR NUCLEAR DATA MEASUREMENTS AT PTB AND ITHEMBA LABS

At the PTB TOF spectrometer, the use of the ^{15}N(p,n)^{15}O reaction for the production of monoenergetic neutrons was studied in the neutron energy range from 2 MeV to 4 MeV using a gas target [21]. Angular distributions were measured for several proton energies around the prominent resonances at E_p = 5.6 MeV, 6.3 MeV and 7.6 MeV. Fig. 7 shows a comparison of measured zero-degree cross sections in the centre of mass system in comparison with other experimental or evaluated data.

A comprehensive overview of the use of the PTB spectrometer for the measurement of differential cross sections for neutron scattering and neutron emission is given in ref. [6]. The most recent measurements of differential neutron scattering cross sections were carried out for the inelastic neutron scattering of ^{206,207}Pb and ^{209}Bi using the ^{15}N(p,n) source. Fig. 8 shows results for the angular integrated cross section for inelastic scattering involving the lowest excited states of ^{206,207}Pb [22].

The low-scatter facility was used recently to carry out measurements of the mean yield $\bar{\nu}_d$ of β-delayed neutrons emitted after neutron induced fission of ^{232}Th [17] and ^{237}Np. The neutrons were detected in a moderator-detector assembly equipped with ^{3}He proportional counters. For these experiments the low neutron background in the low scatter facility and the availability of a fast magnetic steerer were important. The fast beam switch allowed repetitive measurements of β-delayed neutrons after irradiation cycles lasting only a few seconds.

In addition to the measurements of cross sections for neutron-induced reactions of interest for nuclear technology, the PIAF facility is also used to study charged-particle induced reactions of relevance for nuclear astrophysics. Here, the high-energy alpha particle beams available from the CV28 cyclotron at PIAF proved to be very useful for the measurements of (α,n) cross sections [23].

At iThemba LABS fission cross sections for ^{235,238}U, ^{209}Bi and ^{nat} Pb were measured using quasi-monoenergetic neutron beams with peak energies between 100 MeV and 200 MeV [24]. These measurements extended earlier experiments at the UCL cyclotron in Louvain-la-Neuve (Belgium) to higher energies. The error bars indicated in Fig. 9 are mainly due to the uncertainty of the fluence measurements and the instability of the spectral neutron

distribution during the time required for the measurements. New measurements with an improved set-up and hopefully better control of beam parameters are presently being prepared as part of a PhD thesis.

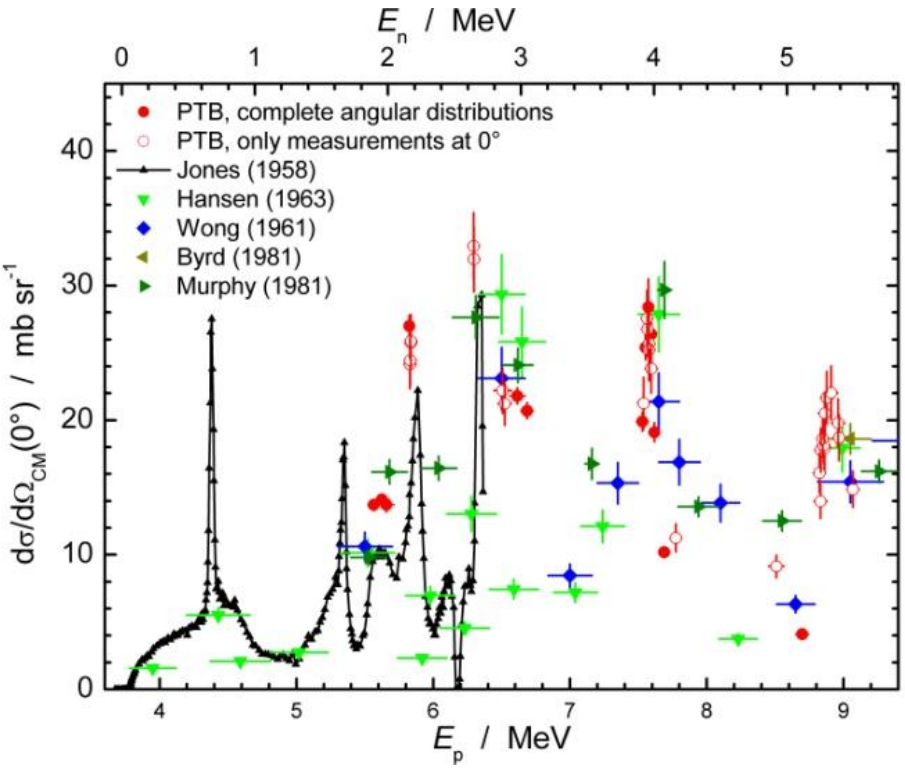

FIG. 7. Differential centre-of-mass cross sections for the reaction $^{15}N(p,n)^{15}O$ at 0° measured at PTB and data taken from the literature for comparison. Red dots show the energies where complete angular distributions were measured. Red circles show the measurements for $\Theta = 0°$ only.

The most recent activities at the iThemba LABS neutron beam facility are measurements of activation cross sections of relevance for the prediction of neutron-induced backgrounds in underground experiments searching for the neutrinoless double beta decay [25].

7. SUMMARY

In collaboration with external partners, the PTB neutron metrology group has extended their ‘traditional’ range of mono-energetic calibration fields between 24 keV and 19 MeV by including medium energy beams up to 200 MeV. The specification of the fields and beams in terms of peak fluence and spectral fluence is traceable to primary standard cross sections. This provides a unique possibility for the measurement of nuclear data in the energy range from 20 keV to 200 MeV.

3.1. Monoenergetic and maxwell spectrum neutron beams (<5 MeV)

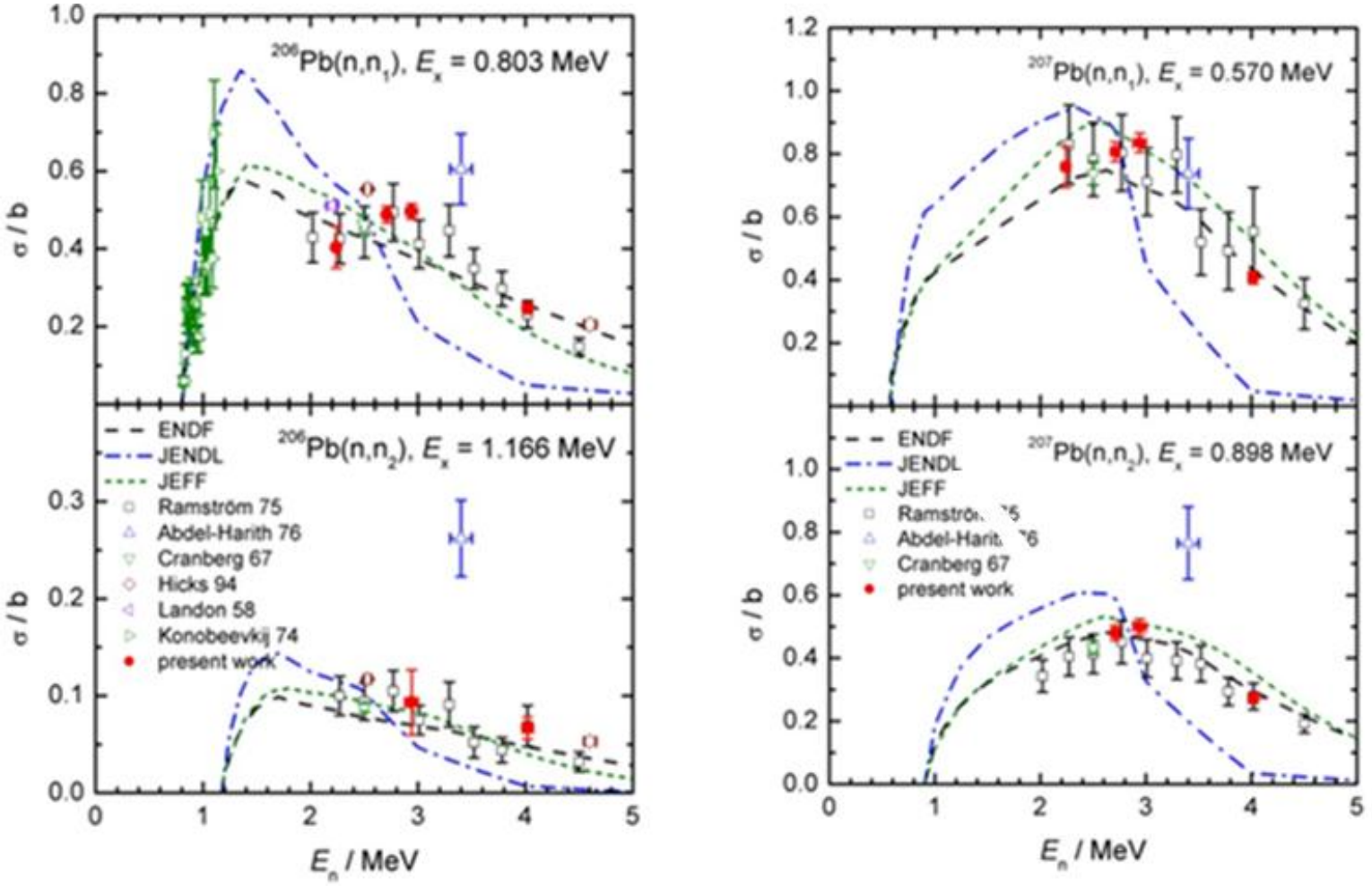

FIG. 8. Cross sections for inelastic scattering involving the two lowest excited states of ^{206,207}Pb. The data marked by the red symbols were measured at the PIAF TOF spectrometer using the ^{15}N(p,n) source [20].

3.1. Monoenergetic and maxwell spectrum neutron beams (<5 MeV)

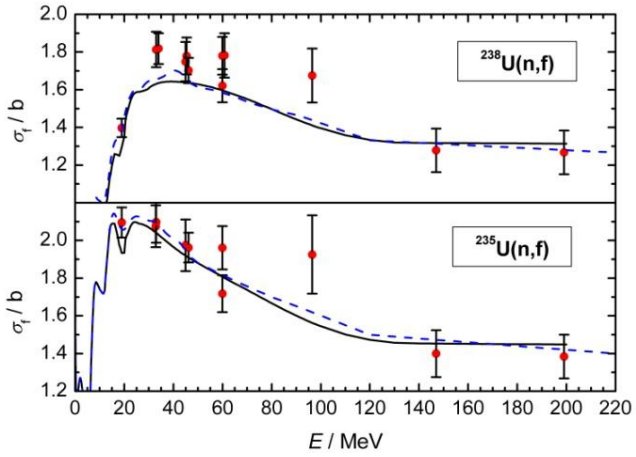

FIG. 9. Cross sections for ^{235,238}U(n,f) measured at the neutron beam facilities of UCL and iThemba LABS [22]. The solid and dashed lines show evaluated cross sections from ENDF/B-VI and INDC(NDS)-368.

ACKNOWLEDGEMENTS

The authors would like to thank the accelerator staffs of PTB and iThemba LABS for their support. The co-operation between PTB, iThemba LABS and the University of Cape Town would not exist without the inspiration of the late Prof F.D. Brooks. The activation measurements at iThemba LABS were carried out in collaboration with A. Domula and K. Zuber of Technische Universität Dresden (TUD), Germany. The measurement of $\bar{\nu}_d$ was a joint project initiated by D. Doré and X. Ledoux of the CEA centres at Saclay and Bruyères-le-Chatel, France. Their collaboration is gratefully acknowledged.

REFERENCES

[1] SCHILLEBEECKX, P., BORELLA, A., DROHE, J.C., EYCKENS, R., KOPECKY, S., MASSIMI, C., MIHAILESCU, L.C., MOENS, A., MOXON, M., WYNANTS, R. "Target requirements for neutron-induced measurements in the resonance region" Nucl. Instrum., and Methods A613 (2010) 378.

[2] BREDE, H.J., COSACK, M., DIETZE, G, GUMPERT, H., GULDBAKKE, S., JAHR, R., KUTSCHERA, M., SCHLEGEL-BICKMANN, D., SCHÖLERMANN, H. "The Braunschweig accelerator facility for fast neutron research 1: Building design and accelerators" Nucl. Instrum. and Methods. 169 (1980) 349.

[3] BOTHA, A.H., JUNGWIRTH, H.N., KRITZINGER, J.J., REITMANN, D., SCHNEIDER,, S., Commissioning of the NAC separated-sector cyclotron, Proc 11th Int. Conf. On Cyclotrons and their Applications, Ionics, Tokyo, (1987) 9.

[4] BREDE, H.J., DIETZE, G., , KUDO, K., SCHREWE, U.J., TANCU, F., WEN, C. "Neutron yields from thick Be targets bombarded with deuterons or protons", Nucl. Instrum. and Methods A274 (1989) 332.

[5] NOLTE, R., ALLIE, M.S., BOETTGER, R., BROOKS, F.D., BUFFLER, A., DANGENDOF, V., FRIEDRICH, H., GULDBAKKE, S., KLEIN, H., MEULDERS, J.P., SCHLEGEL, D., SCHUHMACHER, H., SMIT, F.D.: "Quasi-monoenergetic neutron calibration fields in the energy range from thermal to 200 MeV", Radiat. Prot. Dosim. 110 (2004) 97.

[6] SCHMIDT, D., "Determination of neutron scattering cross sections with high precision at PTB in the energy region 8 to 14 MeV", Nucl. Sci. Eng. 160 (2008) 349.
[7] OEHRN, A., BLOMGREN, J., PARK, H. KHURANA, S., NOLTE, R., SCHMIDT, D., "A Monitor for flux measurements up to 20 MeV", Nucl. Intrum and Methods A592 (2008) 405.
[8] McMURRAY, W.R., ASHMAN, D.G., BARUTH-RAM, K., FEARICK, R.W., "The Faure cyclotron neutron source and a particle spectrometer for neutron induced emission of charged particles at energies between 60 and 200 MeV", Nucl. Instrum. and Methods A329 (1993) 317.
[9] SCHUHMACHER, H., BREDE, H.J., DANGENDOF, V., KUHFUSS, M., MEULDERS, J.P., NEWHAUSER, W.D., NOLTE, R., "Quasi-monoenergetic neutron beams with energies from 25 to 70 MeV", Nucl. Instrum. and Methods. A421 (1999) 284.
[10] NOLTE, R., ALLIE, M.S., BINNS, P.J., BROOKS, F.D., BUFFLER, A., DANGEMDORF, V., MEULDERS, J.P., ROOS, F., SCHUHMACHER, H., WIEGEL, B., "High-energy neutron reference fields for the calibration of detectors used in neutron spectrometry", Nucl. Instrum. and Methods, A476 (2002) 369.
[11] SCHLEGEL, D., GULDBAKKE, S., "Neutron fluence measurements with a recoil proton proportional counter", PTB-Laborbericht PTB-6-41-2002-03, Braunschweig 2002.
[12] SCHLEGEL, D., GULDBAKKE, S., "Neutron fluence measurements with a recoil proton telescope", PTB-Laborbericht PTB-6-41-2002-04, Braunschweig, 2002.
[13] DANGENDOF, V., NOLTE, R., ROOS, F., SCHUHMACHER, H., SIEBERT, B.R.L., WEYRAUCH, M., "Proton recoil telescopes for fluence measurements in neutron beams of 20 - 200 MeV energies", Nuclear Instrum. Meth. A469 (2001) 205.
[14] ROBERTS, N.J., TAGZIRIA, H. and THOMAS, D.J. "Determination of the effective centres of the NPL long counters" NPL Report DQL RN004, Teddington 2004.
[15] SCHLEGEL, D., "TARGET user's manual", PTB-Laborbericht PTB-6.41-98-1, Braunschweig 1998.
[16] SAUVAN, P., SANZ, J., OGANDO, F., "New capabilities for Monte Carlo simulation of deuteron transport and secondary products generation", Nucl. Instrum. and Methods, A614 (2010) 323.
[17] LEDOUX, X., DORE, D. MOSCONI, M., NOLTE, R., ROETTGER, S., "Delayed neutron measurements for ^{232}Th neutron-induced fission", (Proc. EFNUDAT – Measurements and Models of Nuclear Reactions, Paris, France, 25–27 May, 2010) EPJ Web of Conferences 8 (2010), available online at: http://dx.doi.org/10.1051/epjconf/20100807010.
[18] NOLTE, R., THOMAS, D.J., "Monoenergetic fast neutron reference fields: I. Neutron production", Metrologia 48 (2011) S263.
[19] NOLTE, R., THOMAS, D.J., "Monoenergetic fast neutron reference fields: II. Field characterization", Metrologia 48 (2011) S274.
[20] HARANO, H., NOLTE, R. "Quasi-monoenergetic high-energy neutron standards above 20 MeV", Metrologia 48 (2011) S292.
[21] POENITZ, E. "Messung von Wirkungsquerschnitten für die Streuung von Neutronen im Energiebereich von 2 MeV bis 4 MeV mit der ^{15}N(p,n) Reaktion als Neutronenquelle", PhD Thesis, Technical University Dresden, 2010, available online at www.qucosa.de
[22] POENITZ, E., NOLTE, R. SCHMIDT, D., "Elastic and inelastic neutron scattering cross sections for ^{nat}Pb, ^{209}Bi and ^{nat}Ta in the energy range from 2 MeV to 4 MeV", J. Korean Phys. Soc. 59 (2011) 1876.

3.1. Monoenergetic and maxwell spectrum neutron beams (<5 MeV)

[23] SAUERWEIN, A., BECKER, H.-W., DOMBROWSKI, H., ELVERS, M., ENDRES, J., GIESEN, U., HASPER, J., HENNIG, A., NETTERDON, L., RAUSCHER, T., ROGALLA, D., ZELL, K.O. and ZILGES, A., "Determination of ^{141}Pr(α,n)^{144}Pm cross sections at energies of relevance for the astrophysical p process using the γγ coincidence method", Phys. Rev. C 84 (2011) 045808.

[24] NOLTE, R., , ALLIE, M.S., BROOKS, F.D., BUFFLER, A., DANGENDOF, V., MEULDERS, J.P., SCHUHMACHER, H., SMIT, F.D., WEIERGANZ, M.: "Cross sections for neutron induced fission of ^{235}U, ^{238}U, ^{209}Bi and ^{nat}Pb in the energy range from 33 MeV to 200 MeV measured relative to n-p scattering", Nucl. Sci. Eng. 156 (2007) 197.

[25] DOMULA, A., et al, "New nuclear structure and decay results in the 76Ge-76As system", accepted contribution for the conference "Nuclear Data for Science and Technology 2013", New York, 4-8 March 2013.

3.1. Monoenergetic and maxwell spectrum neutron beams (<5 MeV)

THE NEUTRON FACILITY AT THE ATHENS TANDEM ACCELERATOR NCSR "DEMOKRITOS" AND NTUA RESEARCH ACTIVITIES

R.VLASTOU

National Technical University of Athens (NTUA)
Department of Physics, Zografou Campus,
Athens 15780
Greece
Email: vlastou@central.ntua.gr

Abstract

Quasi-monoenergetic neutron beams, in the energy range 4.6 -11.4 MeV, have been used at the 5.5 MV tandem T11/25 Accelerator Laboratory of NCSR "Demokritos", produced via the ^{2}H(d,n) reaction. The latest most important experimental results will be presented in this report. The neutron facility has been characterized by means of Monte Carlo simulations with MCNP5. In addition, an investigation of the energy dependence of the neutron fluence has been carried out with two independent techniques: With a liquid scintillator BC501A detector and deconvolution of its recoil energy spectra, as well as via the multiple foil activation technique. The availability of ^{7}Li(p,n) and ^{3}H(d,n) set-ups will be also presented, as well as future plans for further neutron induced cross section measurements.

INTRODUCTION

The investigation of neutron induced reactions is of considerable interest, not only for their importance to fundamental research in Nuclear Physics and Astrophysics, but also for practical applications in nuclear technology, dosimetry, medicine and industry. These tasks require improved nuclear data and higher precision cross sections for neutron induced reactions. The available compilation databases, based on both experimental and theoretical evaluations, present many differences and discrepancies and they cannot be considered as reliable basis for practical applications and for testing nuclear models. These tasks require improved nuclear data and higher precision cross sections for neutron induced reactions [1].

In the 5.5 MV tandem T11/25 Accelerator Laboratory of NCSR "Demokritos", quasi-monoenergetic neutron beams have been used for cross section measurements of threshold reactions in the energy range 7-11.4 MeV. The neutron beam is produced via the ^{2}H(d,n) reaction, its flux variation is monitored by using a BF_3 detector and its absolute flux is obtained with respect to reference reactions. An investigation of the energy dependence of the neutron fluence will be presented in this report along with a few illustrative examples of experimental results, for neutron energies up to 11.4 MeV. The availability of ^{7}Li(p,n) and ^{3}H(d,n) set-ups will be also presented, as well as future plans for the facility and its implementation to further neutron induced cross section measurements.

EXPERIMENTAL FACILITY

In the 5.5 MV tandem T11/25 Accelerator Laboratory of NCSR "Demokritos" monoenergetic neutron beams can be produced at a maximum flux of the order of 10^{5}-10^{6} n/cm^{2}sec, in the energy ranges 120-650 keV, 4-11.4 MeV and 16-20 MeV by using the ^{7}Li(p,n), ^{2}H(d,n) and ^{3}H(d,n) reactions, which have Q = -1.6, 3.3 and 17.6 MeV, respectively. The corresponding beam energies and ions delivered by the accelerator are 1.92-2.37 MeV protons, 0.8-8.2 MeV deuterons and 0.8-3.7 MeV deuterons, for the three reactions, respectively [2]. The targets are a thin ^{7}LiF on Al backing for the ^{7}Li(p,n) reaction, a 5Ci Ti tritiated on Ag for the ^{3}H(d,n) reaction and a 3.7cm long gas cell filled with deuterium gas at a pressure of ~1300 mbar for the ^{2}H(d,n) reaction [3].

3.1. Monoenergetic and maxwell spectrum neutron beams (<5 MeV)

The flux variation of the neutron beam is monitored by using a BF_3 detector whose spectra are stored at regular time intervals in a separate ADC during the irradiation process. In addition, the beam current on the target is also recorded at the same time intervals in another ADC, in order to test the reliability of the BF_3 counter during long irradiation time. Furthermore, a new BC501A liquid scintillator detector has been recently used for the investigation of the energy distribution of the neutron beam. The absolute flux of the beam can be obtained with respect to reference reactions, such as ^{197}Au(n,2n), ^{27}Al(n,α) and ^{93}Nb(n,2n), whose cross sections are well determined in the literature. Both reference and target samples are exposed to neutron beam and the induced activity of product radionuclides is measured with two HPGe detectors of 56% and 80% properly shielded with lead blocks to reduce the contribution of the natural radioactivity. The efficiency of the detectors at the position of the activity measurements is determined via a calibrated ^{152}Eu source. In most cases the same reference foils are put before and after the target and the mean value of the flux is considered to be the actual flux of the neutron beam and is cross-checked with the simulated results performed with the Monte Carlo code MCNP[4].

In the case of ^{7}Li(p,n) ^{7}Be reaction the neutron flux can be determined by using the ^{7}LiF target as reference foil after the deuteron irradiation, and measuring with a HPGe detector the 477.6keV γ ray from the deexcitation of ^{7}Be to the first excited state of ^{7}Li, with a probability of 10.44% and a $t_{1/2}$ of 53.22 days. Thus, no activated foils are needed, and cross-check can be achieved by accurately measuring the proton charge, just by mounting the target in a reasonably efficient faraday cup.

IMPLEMENTATION

The low energy beam (120-650 keV) has only been used for applications in detector physics and not for cross section measurements. An interesting application has been the study and the determination of the response of ATLAS MDT (Muon Detector Tubes) to relatively low-energy neutron irradiation [5]. The high energy beam (16-20 MeV) has been tested and used for preliminary cross section measurements, but no final results have been published up to now. It has been used for detector applications, as for example to determine the response function and efficiency of a BC501A Liquid Scintillator in comparison with GEANT4 Monte-Carlo simulations [6]. The medium energy neutron beam (4-11.4 MeV) has been extensively used for cross section measurements as will be presented in section 3.

The neutron beam produced by the ^{2}H(d,n) reaction is not purely monoenergetic due to parasitic neutrons mainly coming from deuteron break up reactions : ^{2}H(d,pn)^{2}H above E_d = 4.5 MeV, ^{2}H(d,2n)^{2}He above E_d = 8.9 MeV and reactions with the isotopes of Mo gas cell window, above the Coulomb barrier E_d = ~7 MeV, producing high energy neutrons, which however, are not expected to contribute considerably to the neutron flux due to their low differential cross section. It was thus of importance that the performance of the neutron source is well understood and that the experimental conditions are well characterized. In view of this remark and in absence of time-of-flight capabilities, the ^{2}H(d,n) neutron facility has been studied by means of multiple foil activation unfolding technique and deconvolution of recoil energy spectra taken with the BC501A liquid scintillator detector at various neutron energies as well as by MCNP5 Monte Carlo simulations [7], as will be described below.

3.1. Monoenergetic and maxwell spectrum neutron beams (<5 MeV)

CHARACTERIZATION OF THE NEUTRON FLUX DISTRIBUTION

The energy spectrum of the neutron beam has been investigated by means of the Multiple Foil Activation Analysis technique using the ^{115}In(n,n')^{115m}In, ^{197}Au(n,γ)^{198}Au, ^{58}Ni(n,p)^{58}Co, ^{47}Ti(n,p)^{47}Sc, ^{64}Zn(n,p)^{64}Cu, ^{46}Ti(n,p)$^{46m+gSc}$, ^{56}Fe(n,p)^{56}Mn, ^{27}Al(n,α)^{24}Na, ^{48}Ti(n,p)^{48}Sc, ^{197}Au(n,2n)^{196}Au, ^{93}Nb(n,2n)^{92m}Nb and ^{59}Co(n,α)^{56}Mn reactions with different energy thresholds varying from ~1 to ~9 MeV. From the analysis of the experimental data, the reaction rate was deduced for each reaction *i* and the results were given as input in the unfolding code SULSA [8] to produce the energy dependence of the neutron flux *φ(E)*, from the expression:

$$\int_{E_{th},i}^{\infty} \sigma_i(E)\varphi(\mathrm{E})dE = \frac{\lambda_i N_i(t_B)}{N_{\tau i}[1-\exp(-\lambda_i t_\mathrm{B})]}$$

where t_B is the irradiation time, λ_i is the decay constant, N_i the number of product nuclei, $N_{\tau i}$ the number of target nuclei and $\sigma_i(E)$ the excitation function of the reaction *i* taken from the IRDF-2002 Dosimetry Library along with the covariance matrix.

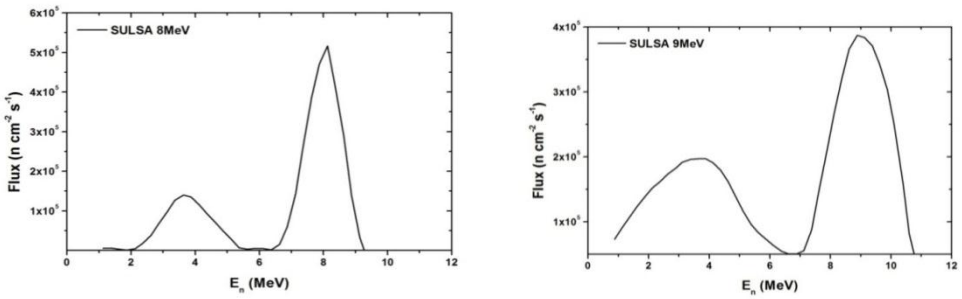

FIG. 1. The neutron flux at 8 and 9 MeV neutron energy, extracted from the SULSA code.

The iterative code used *N*=45 energy bins and the calculated neutron spectra for several neutron irradiation energies were evaluated without the implementation of input spectra. Figure 1 shows the 8 and 9 MeV spectra deduced from the unfolding process. At 8 MeV, the main neutron peak is followed by a weak tail of low energy parasitic neutrons centered at ~3 MeV, while at 9 MeV, the spectrum indicates a significant production of parasitic neutrons around 3-4 MeV, which is expected to become severe with increasing energy.

Furthermore, the energy spectrum of the neutron beam has been studied by using the deconvolution of recoil energy spectra taken with the BC501A liquid scintillator detector at various neutron energies with the DIFBAS code [9]. The algorithm is based on the Bayesian conditional probability assuming normal distributions of the pulse height spectra. The input files are the pulse height spectrum, and an a priori neutron energy spectrum, while the covariance matrix and the neutron response matrix are incorporated in the program for the BC501A detector under study. The results for neutron beam energies 5.4, 6.4, 7.4, 8.4, 9.0 and 10.0 MeV are presented in Fig. 2. The low energy neutron beams seem to be monoenergetic, while above 7 MeV parasitic neutrons start to appear and above E_n = 9 MeV, they contribute considerably to the neutron flux. These results are in consistency with the neutron energy

spectra deduced with SULSA code, within the limitations of the multiple foil activation technique.

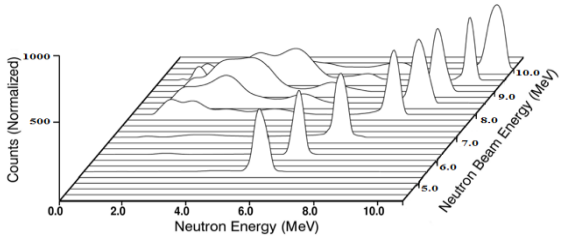

FIG. 2. The energy distribution of the neutron flux at 5.4, 6.4, 7.4, 8.4, 9.0 and 10.0 MeV nominal neutron beam energies, deduced from the DIFBAS code.

The tail of parasitic neutrons is important in the region 2-3 MeV, mainly due to the deuteron break-up process above E_d = 4.5 MeV and/or deuteron induced reactions and multiple scattering of neutrons within the structural materials of the gas-cell. In addition, parasitic neutrons may result from the deuteron beam bombarding the collimators and from neutrons scattered by the surrounding materials and the walls of the experimental room, since the liquid scintillator was placed at a distance of ~3 m from the gas cell to avoid high counting rates.

Finally, MCNP5 [4] calculations have been performed in order to simulate the neutron flux energy distribution of monoenergetic neutron fields around 0^o with respect to the beam line axis. The neutron source used for the simulation has been described as a cylinder corresponding to the gas cell, producing neutrons within 4π, distributed according to the kinematics and the cross section angular distribution of the ^{2}H(d,n) reaction. The simulations contain also the contribution of the neutrons scattered from the various elements in the experimental area but not from the deuteron break-up and reactions with the collimators and the gas cell materials. The results of the simulations at 11.2 MeV neutron energy and at three different distances (10 cm, 1 m, 3 m) from the middle of the cell are presented in Fig. 3.

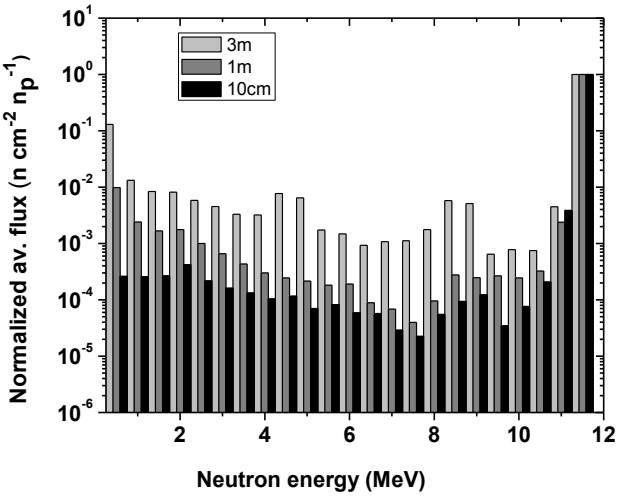

FIG. 3. MCNP5 simulations for the energy distribution of neutrons at three different distances from the gas cell along its axis. The neutron beam energy is 11.2 MeV and the normalized flux is given in neutrons per cm^2 and per primary neutron n_p produced by the source within 4π.

3.1. Monoenergetic and maxwell spectrum neutron beams (<5 MeV)

The MCNP5 simulations indicate that the main beam of the highest energy 11.2 MeV, is followed by a long tail of scattered neutrons with an intensity lower by 3-5 orders of magnitude, depending on their energy. It can also be observed that the contribution of the scattered neutrons increases with distance from the neutron source and at 10 cm it exhibits a minimum value around 5 orders of magnitude compared to the main beam. Thus, all reaction cross section measurements carried out at this distance, are not expected to be significantly affected by the scattered neutrons.

In addition, gas-in and gas-out measurements have been performed at 11.3 MeV using multiple foil activation technique and the parasitic neutrons bearing energies high enough to activate the ^{27}Al reference foil was ~3%. Furthermore, reference foils were put inside and outside a Cd cell and irradiated with 11.0 MeV neutrons. The difference "with and without Cd" was ~5%, indicating that close to the gas cell the presence of low energy neutrons (below ~10keV) is insignificant.

It is thus concluded that in facilities, where the neutron TOF technique is not applied, only low energy neutron beams, produced by the d+d reaction, are mono-energetic (~4-7 MeV). At higher energies, only reactions with a high energy threshold can be safely measured with monoenergetic neutrons, since then, the low energy parasitic neutrons cannot affect the cross section measurements, provided that the reference reaction used for the determination of the absolute neutron flux also has a threshold in the same energy region.

REACTION MEASUREMENTS

Two areas of investigation of threshold reactions have been performed at the tandem Accelerator Laboratory of NCSR "Demokritos". Reactions relevant to nuclear energy applications, ^{232}Th(n,2n), ^{241}Am(n,2n) and ^{237}Np(n,f) as well as (n,2n) and (n,p) reactions on medium and heavy nuclei, such as natural Ge, Ir, Au and Hf, by using the activation method. Systematics on reaction channels are important for the optimization of input parameters in statistical model calculations based on compound and pre-compound mechanisms.

Within the framework of the CERN n-TOF collaboration [10], the ^{232}Th(n,2n) reaction which is important for the Th-U cycle leading to the highly radiotoxic ^{232}U, has been investigated in the energy range from 7.5-11.5MeV. The experimental details about these measurements and the analysis of the data are described in Ref. [11]. In addition, the ^{241}Am(n,2n) reaction has been measured at four energies from 8.8 to 11.4 MeV. ^{241}Am is one of the most abundant isotopes in spent nuclear fuel and one of the most highly radiotoxic among the actinides. The experimental details and problems about this reaction are described in section 3.1. Measurements of fission cross section on ^{237}Np, which is a major component of the spent nuclear fuel in current reactors, were also carried out with a new MicroMegas detector, based on the innovative Microbulk technology, as will be presented below.

Concerning natural Ge and Hf neutron induced reactions, among the possible reaction channels being able to be measured by the activation method, the (n,p) reactions on several Ge isotopes [12] and the ^{174}Hf(n,2n)^{173}Hf [13, 14], were studied both experimentally and theoretically, within the framework of the statistical model, implementing the code EMPIRE [15]. The ^{176}Hf(n,2n)^{175}Hf threshold reaction is contaminated by the ^{174}Hf(n,γ)^{175}Hf, which is open to the parasitic low energy neutrons. A method has been developed to account for this effect as will be described in section 3.3. Furthermore, isomeric cross section ratios are of fundamental interest since they are governed by the spins of the levels involved in the

compound nucleus evaporation process. Within this context, the ^{191}Ir(n,2n)^{190}Ir and ^{197}Au(n,2n)^{196}Au reactions have been investigated both experimentally and theoretically, using the codes EMPIRE [15], STAPRE [16] and TALYS [17], as will be described in section 3.4.

THE ^{241}AM(N,2N)^{240}AM REACTION

Five recent works provide data for ^{241}Am(n,2n)^{240}Am reaction, from threshold to 20 MeV [18-22]. The data by Perdikakis et. al. [20], have been measured at NCSR "Demokritos" from 8.8 to 11.4 MeV, using the activation technique. Below 10 MeV there is good agreement between data of [20], [21] and [22]. However, there is a discrepancy between the data of [20] and [21] in the energy region 10 to 12 MeV, thus further experimental work was required to resolve this discrepancy.

Since in the measurements by Perdikakis et al. [20], the ^{241}Am target consisted of 37 GBq AmO_2 encapsulated in stainless steel, with significant contaminants, mainly ^{154}Eu, new measurements had to be performed with a high purity Am target. For this purpose, two new Am targets have been provided by IRMM, coming from the same batch of targets used by Sage et al. [22]. They consist of ~40 mg Am in the form of AmO_2 pressed into pellets with Al_2O_3 and encapsulated into Al containers. The targets are highly radioactive (~5GBq) and were placed inside a 3mm lead cylindrical box for safety reasons. One of the samples was irradiated with 10.4 MeV neutrons and the other with 10.8 MeV. The irradiation lasted three days and the absolute flux of the beam was obtained with respect to reference reactions. High purity foils of Al were placed at the front and the back of the Am sample along with Au and Nb foils at the back, to monitor the neutron flux and to account for its variation with distance. MCNP simulations were carried out, which reproduced fairly well the experimentally deduced neutron flux at the back foils. Thus, the simulated flux in the middle of the Am pellet was used to deduce the cross section.

Gamma ray spectra were taken at a distance of ~10 cm from the Ge detector, before and after the irradiation, to ensure that there is no contamination in the 987.8 keV photopeak. The efficiency of the detection setup, including the extended geometry of the Am sample and self-absorption effects, was extracted by using two different techniques, an experimental and a simulated one. The experimental technique is based on the activity of the Am target as described in Ref. [20]. The simulated efficiency was deduced via a series of MCNP calculations which helped to fix the various geometry parameters involved, by reproducing the experimental spectra taken for different setups: (a) Ge detector and ^{152}Eu point source to fix the detector, (b) Ge detector and ^{152}Eu point source with the lead cylindrical box in front to fix the shielding, (c) Ge detector and ^{152}Eu point source at the back of the lead cylindrical box with the Al container inside, to fix the container and (d) Ge detector and Am in its shielding before irradiation. All these experimental spectra were reproduced fairly well by the MCNP simulations and the deduced parameters were then used to simulate the efficiency for the 987.8 keV γ ray.

The preliminary results for the cross sections at 10.4MeV and 10.8 MeV, are plotted in Fig. 4 along with the other data from literature and are seen to agree with the data by Tonchev et al. [21] within their experimental errors.

3.1. Monoenergetic and maxwell spectrum neutron beams (<5 MeV)

A possible explanation for the previous data by Perdikakis et al. [20] is that a neutron induced reaction on the contaminants of the target, opens above 10MeV and produces a gamma ray which interferes with the 987.8keV transition.

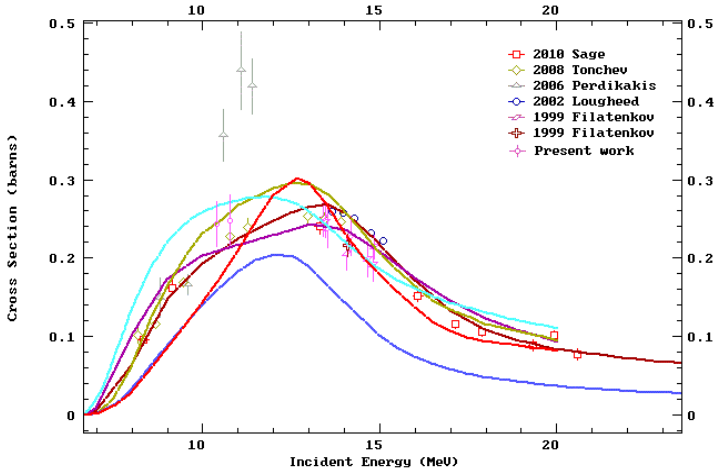

FIG. 4. Status of the ^{241}Am(n,2n) cross section data and evaluations.

THE ^{237}Np(n,f) Measurements At 4.5-5.3 MeV WITH A MICROMEGAS DETECTOR ASSEMBLY.

Previous data for fission cross section on ^{237}Np around 4-6 MeV, present discrepancies of approximately 8 % and the latest evaluations (ENDF/B-VII.1 /JEND-4.0) discrepancies of ~2-3%. Thus, measurements of the ^{237}Np(n,f) cross section were carried out at NCSR "Demokritos", with reference to the standard ^{238}U(n,f) reaction, by using a new MicroMegas detector, based on the innovative Microbulk technology, especially developed at CERN for these measurements, within the framework of the n_TOF collaboration. The actinide targets were thin discs of isotopically pure oxides (NpO_2 and U_3O_5) of 5cm diameter, deposited on 100μm Al backing via the painting technique. They were provided by the Institute of Physics and Power Engineering, Obninsk, and the Joint institute of Nuclear Research, Dubna within the context of the n_TOF collaboration. The target and Micro-Bulk assembly was mounted in the Micromegas chamber and each actinide target served as the detector drift electrode. Each micro-bulk consists of a 5 μm perforated copper foil ("micromesh") on 25 μm or 50 μm thick kapton pillars deposited on 5 μm of a bulk copper foil ("anode"). The electric field in the drift region was kept low, at approximately 0.8 kV/cm, while in the mesh region approximately 70 kV/cm. The detector was filled with a mixture of 80% of Argon and 20% of CO_2 provided with a gas flow of 6-8 l/h.

Neutron beams were used and produced via the d+d reaction, at energies below the deuteron break-up, where the beam is purely monoenergetic. Monte-Carlo simulations were performed with the code MCNP5 implementing the neutron beam setup and the MicroMegas assembly in order to determine the neutron flux at the position of each target and possible parasitic neutrons due to scattering. Additional simulations with FLUKA were performed, studying the energy deposition of the fission fragments in the active area of the detector, in order to accurately estimate the detection efficiency.

3.1. Monoenergetic and maxwell spectrum neutron beams (<5 MeV)

Four measurements were performed at 4.6, 4.9, 5.1 and 5.3 MeV and are presented in Fig. 5 in comparison with the latest data by Paradela et. al. [23] and the ENDF-VII.1 evaluations [24]. They are seen to be in good agreement within their experimental errors.

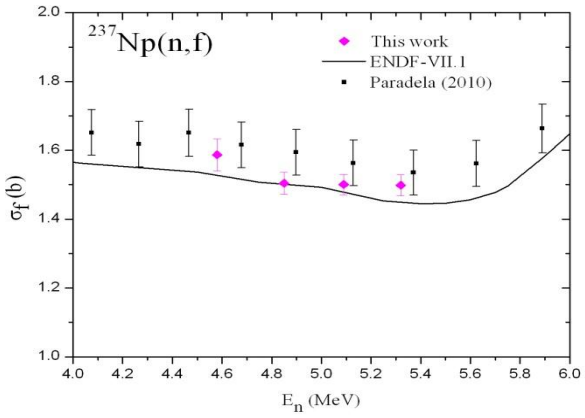

FIG. 5. The ^{237}Np(n,f) cross section data. The error bars correspond to the statistical uncertainties.

METHOD FOR THE CORRECTION OF THE ^{176}HF(N,2N)^{175}HF REACTION CROSS SECTION

The ^{176}Hf(n,2n)^{175}Hf threshold reaction is contaminated by the ^{174}Hf(n,γ)^{175}Hf during the irradiation of natural Hf. The ^{176}Hf(n,2n) reaction has an energy threshold of ~8.2MeV and opens with En >~9MeV, while the contaminant ^{174}Hf(n,γ) reaction has no threshold and is activated by the low energy parasitic neutrons of the beam. In order to account for the contribution of the ^{174}Hf(n,γ)^{175}Hf reaction a method has been developed, based on the investigation of the parasitic neutrons in the case of the (n,2n) and (n,γ) reactions on ^{197}Au [14].

The ^{197}Au(n,2n)^{196}Au and ^{197}Au(n,γ)^{198}Au reactions have well known cross sections and produce different daughter nuclei which are detected by using different γ rays, thus allowing the comparison between the flux of useful neutrons which activate the threshold (n,2n) reaction and the parasitic ones which activate the (n,γ) reaction. Neutron activation measurements on ^{197}Au were performed at several neutron energies and from the ^{197}Au(n,2n)^{196}Au and ^{197}Au(n,γ)^{198}Au data, a correction factor has been produced for ^{197}Au. The behavior of the two (n,γ) reactions on ^{174}Hf and ^{197}Au with respect to the neutron energy is similar, implying that the effect of parasitic neutrons on both reactions is also similar. So it is reasonable to use the same correction factor to account for the contribution of the ^{174}Hf(n,γ) to the production of the ^{176}Hf(n,2n) reaction. The results are presented in Fig. 6 for the cross section measurements at 8.8, 9.0, 10.0, 10.5 and 11.0 MeV. The squares represent the values of the ^{176}Hf(n,2n)^{175}Hf cross section which include the contamination by the ^{174}Hf(n,γ)^{175}Hf reaction, which becomes important above 10 MeV, while the circles represent the corrected values.

3.1. Monoenergetic and maxwell spectrum neutron beams (<5 MeV)

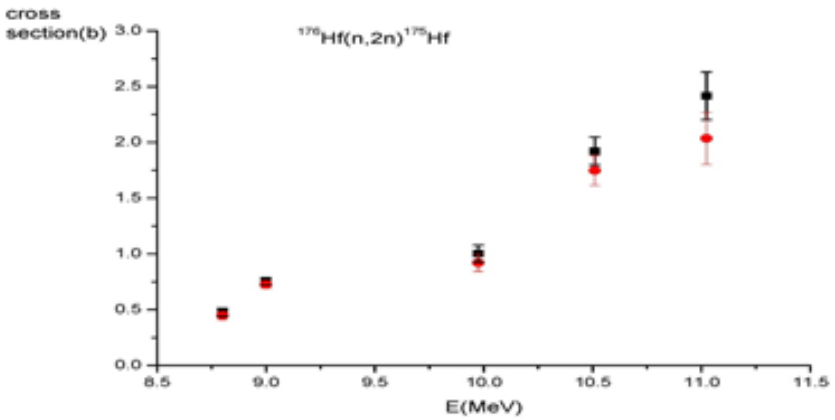

FIG. 6. The squares represent the values of the ^{176}Hf(n,2n)^{175}Hf cross section which include the contamination by the ^{174}Hf(n,γ)^{175}Hf reaction, while the full circles represent the corrected values.

ISOMERIC CROSS SECTION MEASUREMENTS

The presence of a high-spin isomeric state in the residual nucleus of a neutron threshold reaction provides a sensitive test for existing nuclear models. The study of such reactions is a powerful tool for obtaining information on the structure of nuclei since the isomeric cross section ratios are governed by the spins of the levels involved in the compound nucleus evaporation process. Two reactions leading to isomeric states have been studied at incident neutron energies in the range ~ 9.0–10.5 MeV by means of the activation technique. The ^{191}Ir(n,2n)^{190}Ir and ^{197}Au(n,2n)^{196}Au reaction cross sections have been experimentally determined relative to the ^{27}Al(n,α)^{24}Na reaction [25, 26]. The cross sections for the population of the second isomeric states m_2 (11−) of ^{190}Ir and (12−) of ^{196}Au and the sum of the ground (1−) and (2−) and first isomeric states (4−) and (5−) g+$m_1$cross sections for ^{190}Ir and ^{196}Au, respectively, were independently determined and are presented in Fig. 7 and 8. Auxiliary Monte Carlo simulations were performed with the MCNP code.

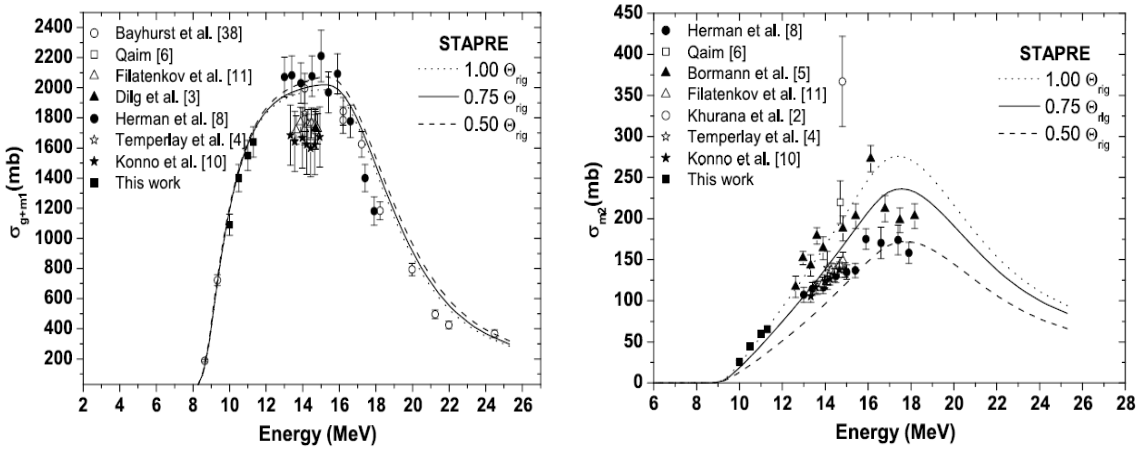

FIG. 7. The ^{191}Ir(n,2n)^{190}Ir reaction cross sections. Experimental values and theoretical calculations for the population of the ground and first isomeric state of ^{190}Ir (g + m_1) and the second isomeric state of ^{190}Ir (m_2).

3.1. Monoenergetic and maxwell spectrum neutron beams (<5 MeV)

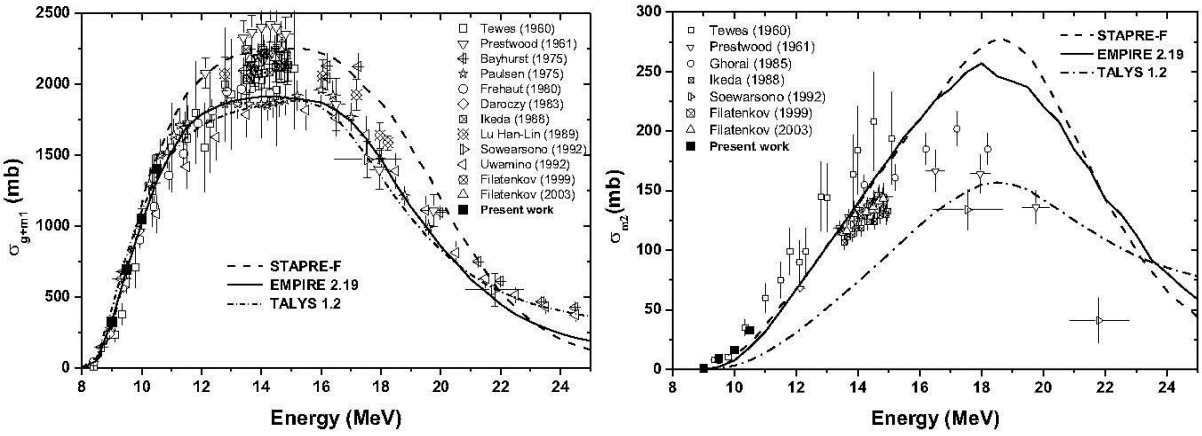

FIG. 8. The ^{197}Au(n,2n)^{196}Au reaction cross sections. Experimental values and theoretical calculations for the population of the ground and first isomeric state of ^{196}Au (g + m_1) and the second isomeric state of ^{196}Au (m_2).

Statistical model calculations with code STAPRE-F have been performed for the ^{191}Ir(n,2n)^{190}Ir reaction in the 8–25 MeV region by using the Generalized Superfluid Model (GSM) for the calculation of nuclear level densities in the continuum to test it in the mass region ~190 and for the isomeric cross section production. Despite the fact that Ir isotopes are transitional nuclei and exhibit very complex structure, the level density calculations using GSM, reproduce fairly well the experimental data. The high spin isomeric state m_2 is fed by a small part of the continuum which depends on the spin cut-off parameter and consequently on the moment of inertia. A reduced value of the rigid body moment of inertia is needed for a better agreement with data.

Theoretical calculations of the ^{197}Au(n,2n)^{196}Au reaction in the 8–25 MeV region were carried out with the use of the STAPRE-F, EMPIRE, and TALYS codes, which were also compared in their implementation of the Generalized Superfluid Model. The σ_{g+m1} cross section was easily reproduced by the calculations, while for σ_{m2}, the theoretical results could only reproduce the general trend of the experimental data, with the distribution shifted at higher energies. Several tests were performed to improve the theoretical predictions which reveal the importance of the level scheme of the residual nucleus and the limitations of the nuclear codes to embed high spin discrete states in the continuum, which would increase the feeding of the isomeric state. Further theoretical investigation [27] revealed that a moment of inertia equal to that of the rigid body for ^{196}Au is adequate to fit the data of the population of the high–spin second isomeric state m_2 for the ^{197}Au(n,2n) reaction.

FUTURE PERSPECTIVES AND RECOMMENDATIONS

Further measurements are planned in the near future around 17 MeV neutron energy, implementing the ^{3}H(d,n) reaction. The ^{241}Am(n,2n)^{240}Am cross section measurement at 17 MeV will be performed since it is essential for the comparison with the data by Sage et al. [22], which are the only ones existing in this energy region. The ^{197}Au(n,2n)^{196}Au measurement at 17 MeV is also planned to resolve discrepancies in experimental points of isomeric (m_2) and (g+m_1) cross sections as well as in the predictions of theoretical models. Fission cross section measurements will be also carried out by using the MicroMegas detector. Supplementary measurements of the ^{237}Np(n,f) cross section will be performed from 5.5-7 MeV, as well as ^{242}Pu(n,f) in the energy range ~4-7 MeV.

3.1. Monoenergetic and maxwell spectrum neutron beams (<5 MeV)

In fact, theoretical investigations of (n,2n) reactions revealed the necessity of accurate high energy data of (n,xn), (n,p) and (n,α) reactions for the understanding of model constraints which are responsible for the calculated cross section variations. Indeed, at neutron energies above 20-30 MeV, where the pre-equilibrium emission (PE) processes become dominating, there is a lack of accurate and consistent experimental data for (n,3n), (n,4n) and (n, charged particle) reactions. Such measurements should be performed at large scale facilities since they may definitely contribute to the increase of the predictability power of phenomenological models [27].

ACKNOWLEGMENTS

This report is based on a collaborative effort of many people. Special thanks are devoted to my colleagues M.Kokkoris, C.T.Papadopoulos, S.Harissopulos, A.Lagoyannis, C.A.Kalfas, P.Demetriou, M.Serris, S.Galanopoulos and N.Patronis, as well as to the post graduate students M.Diakaki, A.Tsinganis, A.Kalamara, M.Lambrou and E.Mara, for their hard work and fruitful physics discussions.

REFERENCES

[1] FESSLER, A., et al., "Neutron activation cross section measurements from 16 to 20 MeV for isotopesof F, Na, Mg, Al, Si, P, Cl, Ti, V, Mn, Fe, Nb, Sn and Ba", Nucl.Sci.Eng. 134 (2000)171.

[2] VLASTOU, R., et al., "The neutron facility at NCSR "Demokritos" – Implementation in the case of the ^{232}Th(n,2n) reaction", Proc. Int. Conf. on the Labyrinth in Nuclear Structure, 2003, edited by A.Bracco and C.A.Kalfas, AIP Conference Proceedings 701, American Institute of Physics, Melville, NY, (2004) 324-328.

[3] VOURVOPOULOS, G., et al., "Utilization of the high current capability of the "Demokritos" tandem", Nucl.Instr. Meth. 220(1984)23.

[4] BRIEMEISTER, J.F., Ed., MCNP-a general Monte Carlo n-particle transport code, version 4C. Report LA-13709 (2000).

[5] ALEXOPOULOS, Th., et al., "Determination of the ATLAS MDT chambers response to 0.5-10 MeV neutrons and development of a simulation model", Nucl.Instr.Meth. A 575 (2007)402.

[6] PATRONIS, N., et al., "Aspects of GEANT4 Monte-Carlo calculations of the BC501A neutron detector", Nucl.Instr.Meth. A578(2007)351.

[7] VLASTOU, R., et al., "Characterization of the neutron flux distribution at the Athens Tandem Accelerator NCSR Demokritos", Nucl.Instr.Meth. B269 (2011)3266.

[8] SUDAR, S., A solution for the neutron spectrum unfolding problem without using an input spectrum INDC(HUN)-0261, IAEA,Vienna,1989.

[9] TICHY, M., PTB Laboratory Report PTB-7.2-1993-1, Braunschweig,1993.

[10] RUBBIA, C., et al., "A high resolution spallation driven facility at the CERN-PS to measure neutron cross sections in the interval from 1eV to 250 MeV, CERN/LHC/98-02(EET).

[11] KARAMANIS, D., et al. , "Neutron cross measurements in the Th-U cycle by the activation method", Nucl.Instr. Meth. Phys.Res. A505(2003)381.

[12] GALANOPOULOS, S., et al. , "Experimental and theoretical studies of (n,p) reactions on Ge isotopes", Nucl. Instr. Meth. Phys.Res. B261(2007)969.

[13] SERRIS, M., et al. , "Study of the (n,2n) cross section measurement of the ^{174}Hf isotope", Nucl. Instr. Meth. Phys.Res. B261(2007)941.

[14] SERRIS, M., et al. , "Experimental and theoretical study of the (n,2n) reaction on ^{174,176}Hf isotopes", Phys.Rev. C86(2012)034602.
[15] HERMAN, M., et al. , EMPIRE-II, Nuclear Reaction Model code, Nuclear Data Sheets 108, 2655 (2007).
[16] UHL, M. and STROHMAIER, B., Tech. Rep. IRK-76/01, 1976 (unpublished).
[17] TALYS-1.0, edited by O. Bersillon, F. Gunsing, E. Bauge, R. Jacqmin, and S. Leray in Proceedings of the International Conference on Nuclear Data for Science and Technology (EDP Sciences, France, 2008).
[18] FILATENKOV, A.A. and CHUVAEV, S.V., "Measurement of cross sections for the reactions ^{241}Am(n,2n) and ^{241}Am(n,3n)", Physics of Atomic Nuclei 63(2000)1504.
[19] LOUGHEED, R.W., et al., Radiochim. Acta 90(2002)833.
[20] PERDIKAKIS, G., et al., "Measurement of the ^{241}Am(n,2n)^{240}Am reaction cross section using the activation method", Phys. Rev. C73(2006)067601.
[21] TONCHEV, A.P., et al., "Measurement of the ^{241}Am(n,2n)^{240}Am reaction cross section from 7.6 to 14.5 MeV", Phys.Rev.C77(2008)054610.
[22] SAGE, C., et al., "High resolution measurements of the ^{241}Am(n,2n) reaction cross section", Phys. Rev. C81(2010)064604.
[23] PARADELA, C., et al., "Neutron-induced fission cross section of ^{234}U and ^{237}Np measured at the CERN Neutron Time-of-Flight (n TOF) facility", Phys.Rev. C82(2010) 034601.
[24] DIAKAKI, M., et al., "Detarmination of the ^{237}Np(n,f) reaction cross section for En=4.5-5.3 MeV, using a Micromegas detector assembly", (2013), Submitted to EPJ.
[25] PATRONIS, N., et al., "Activation cross section and isomeric cross section ratio for the (n,2n) reaction on ^{191}Ir", Phys.Rev.C75(2007)034607.
[26] TSINGANIS. A., et al., "Isomeric cross section of the ^{197}Au(n,2n) reaction", Phys.Rev. C83 (2010)024609.
[27] AVRIGEANU, M., et al., "Isomeric cross sections of fast-neutron induced reactions on ^{197}Au", Phys.Rev. C85 (2012)044618.

3.1. Monoenergetic and maxwell spectrum neutron beams (<5 MeV)

INTENSE 14 MEV NEUTRON SOURCE FACILITY (OKTAVIAN) AT OSAKA UNIVERSITY

I. MURATA

Osaka University, Yamada-oka 2-1, Suita, Osaka 565-0871, Japan
Email: murata@eei.eng.osaka-u.ac.jp

Abstract

The Intense 14 MeV Neutron Source Facility (OKTAVIAN) is a 14 MeV neutron generator by deuteron-triton, DT, reaction. Its operation started in 1981. For more than 30 years were carried out various fusion-reactor related experimental studies, i.e., neutron-nuclear reaction cross section measurements, integral benchmark experiments, tritium breeding ratio (TBR) measurements, and so on. Until 1995, the facility was open to outside scientists in Japan. Since 1996 only internal use was available.

1. INTRODUCTION

In Japan, there are two 14 MeV (deuteron-triton, DT) neutron sources available for fusion reactor researches. One is Fusion Neutronics Source (FNS) facility of JAEA. And the other is Intense 14 MeV Neutron Source Facility (OKTAVIAN) of Osaka University. In this report, details of the OKTAVIAN facility are presented.

2. OKTAVIAN FACILITY

The OKTAVIAN (Intense 14 MeV Neutron Source Facility) was originally implemented in Nuclear Instrumentation Division, Department of Nuclear Engineering, Graduate School of Engineering, Osaka University, in 1981.

THE SPEC OF THE FACILITY IS AS FOLLOWS

Accelerator:	Cockcroft-Walton
Acceleration voltage:	300 kV
Ion source:	Duoplasmatron
DT Neutron intensity:	DC 3×10^{12} n/sec (20mA) (1×10^{11}n/sec currently available because rotating targets are not used now.)
Pulse	1×10^{9} n/sec (20μA)
Repetition frequency:	2 MHz
Pulse width:	2 nsec

The top view of the facility is shown in Fig. 1. The whole building size is 30 m by 30m and the height of the large experimental room is about 10 m, in which the accelerator is positioned. In the figure photos of the accelerator and the control room are also described. Fig. 2 shows inside of the large experimental room and the DC neutron source (older one).

3.1. Monoenergetic and maxwell spectrum neutron beams (<5 MeV)

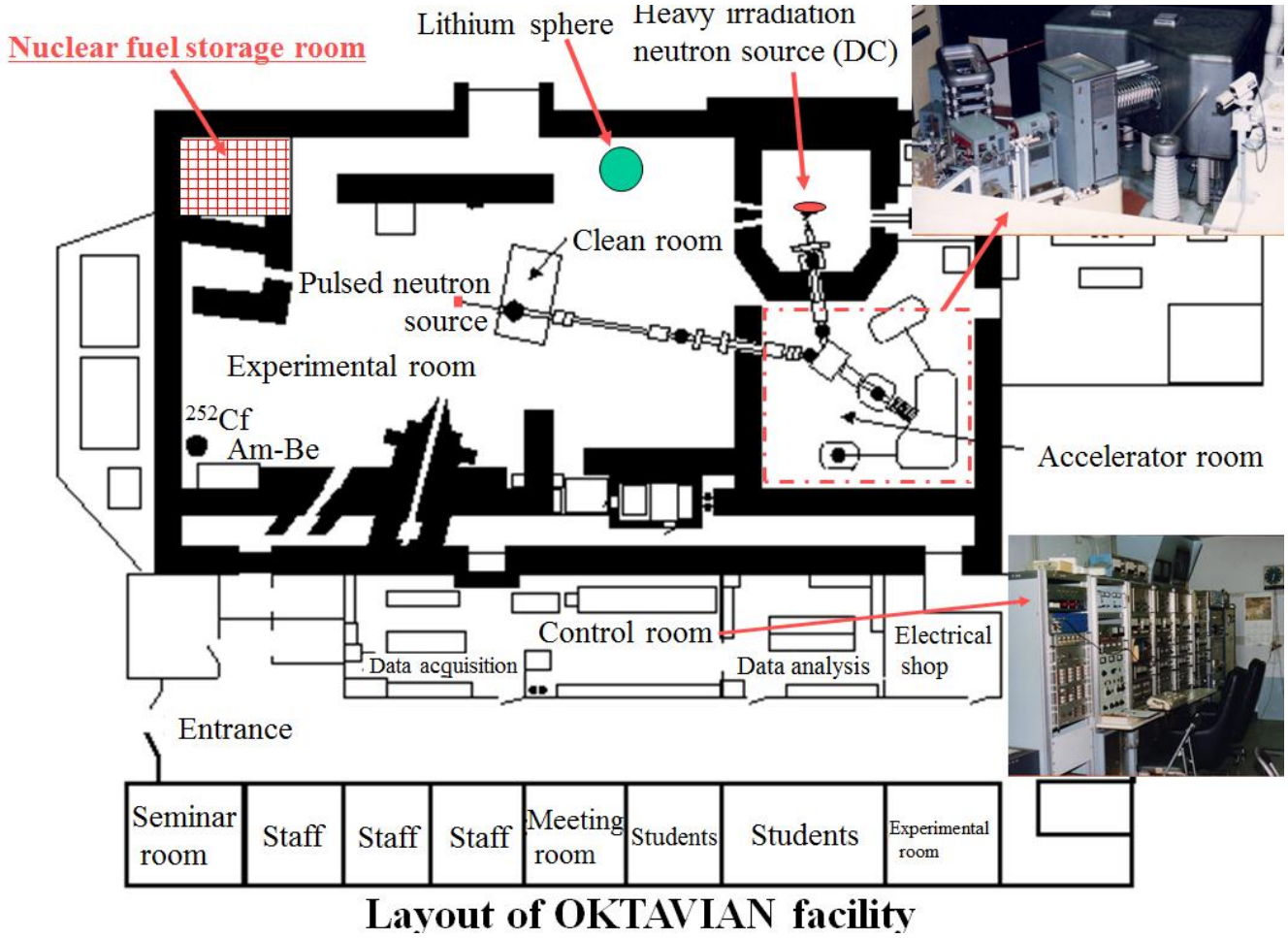

FIG. 1. Layout of OKTAVIAN facility building.

3.1. Monoenergetic and maxwell spectrum neutron beams (<5 MeV)

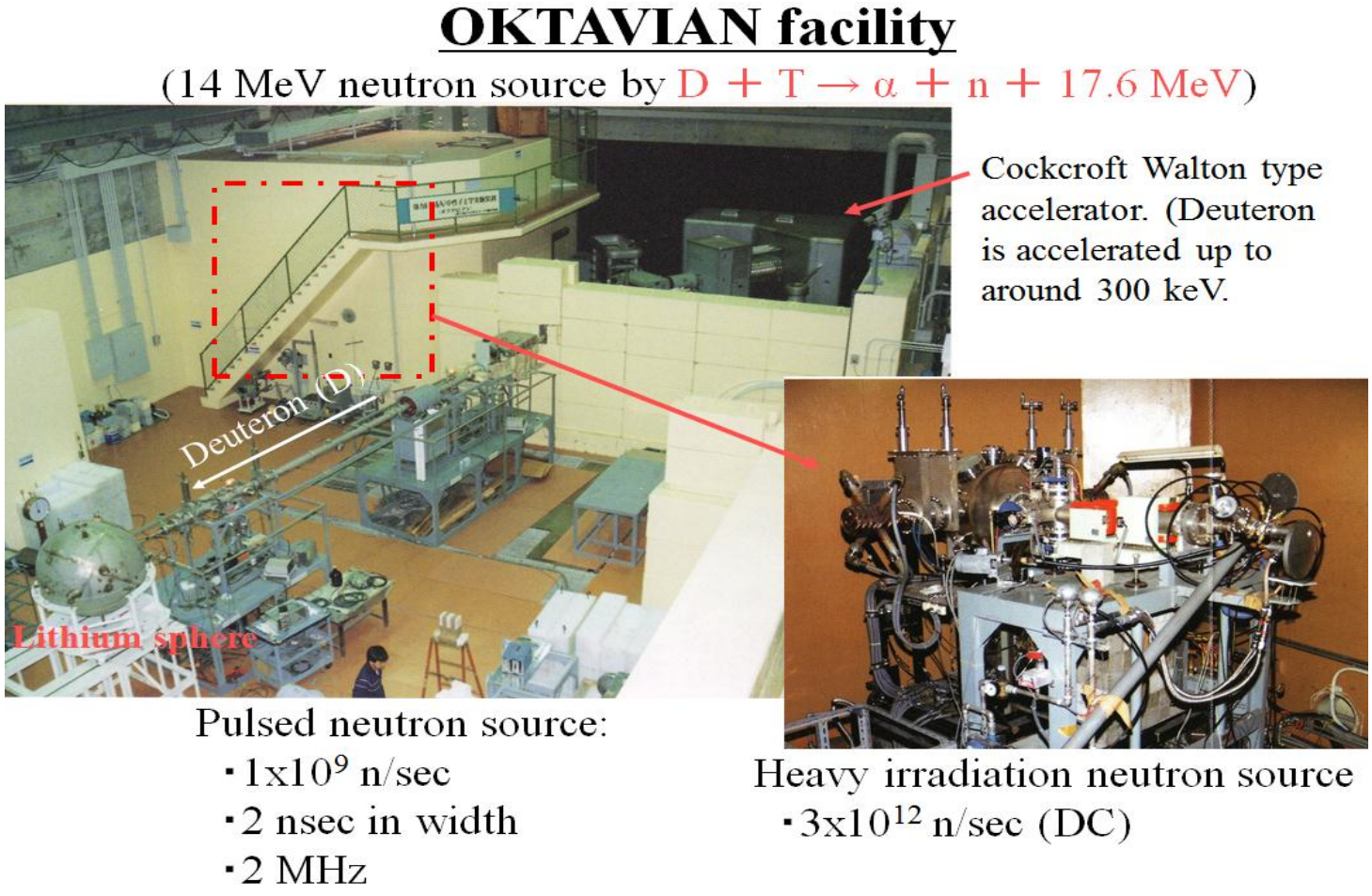

FIG. 2. Large experimental room and heavy irradiation neutron source (currently not available).

3.1. Monoenergetic and maxwell spectrum neutron beams (<5 MeV)

The OKTAVIAN facility was utilized at first as a DT neutron source. Later it was also used for light ion irradiation. Low energy hydrogen isotopes of about mA could be irradiated for material studies. DD neutrons are also available via interaction between self-loading deuterons and incident deuterons. At the moment, four AmBe sources of about ~2×10^6 n/sec for each are also available in this facility, which can be used by outside researchers.

However, the operation rate is very low now because it is difficult to obtain tritium target since the facility maintenance budget decreased and cut after 2001 and the price of the target gets extremely expensive. For these reasons, the cooperation research with outside scientists was stopped reluctantly. However, some experiments aiming at pure research objectives by national research institutes, universities and so on are sometimes accepted even now. Anyway, currently tritium targets (second-hand) are supplied from FNS of JAEA very fortunately. The FNS group can produce tritium target by themselves.

Measuring techniques available are time-of-flight measurement with NIM modules, Rutherford backscattering, liquid scintillation analysis, tritium measurement, foil activation analysis, gamma ray discrimination by pulse shape analysis, and so on. Experimental studies carried out so far including inside and outside research groups are summarized in Table 1.

Details for studies before 1995 in Table Ⅰ were summarized in OKTAVIAN reports as shown in Fig. 3. The OKTAVIAN reports, i.e., Progress Report of OKTAVIAN Utilization, were annually published from 1983 to 1996.

3. ONGOING RESEARCH PROJECT

At present, the following researches concerning nuclear data are being carried out at the OKTAVIAN facility.

3.1 LARGE-ANGLE SCATTERING REACTION CROSS SECTION BENCHMARK

From the result of integral experiment with a slab stainless steel assembly using a beam DT neutron source, it was found that the C/E value of niobium foils is getting large with increase of the distance from the beam position. We started a study to develop a benchmark method to be able to examine the evaluated angular distribution of emitted neutrons via scattering reaction, especially aiming at backward scattering.

As shown in Fig. 4, a slab assembly was arranged in front of the tritium target. On the assembly, a niobium foil was put. A shadow bar is placed between the target and the foil to shield direct contribution from the target. By setting the assembly thickness to be about one mean free path, contribution of back scattering neutrons can be increased artificially.

3.2. OTHER STUDIES BY COMPANIES

It is not possible to describe precisely because of patent problem. However, besides Sec. 3.1, there are some basic studies by companies, i.e., soft error benchmark experiment, collimator development for imaging plate and development of neutron non-destructive inspection method are underway.

3.1. Monoenergetic and maxwell spectrum neutron beams (<5 MeV)

TABLE 1. RESEARCH ACTIVITIES CARRIED OUT AT THE OKTAVIAN FACILITY (OUTSIDE GROUP ACTIVITY IN RED)

Research summary		With maintenance budget												Decreasing				Without maitenance budget								
Research content	Staff in charge	83	84	85	86	87	88	89	90	91	92	93	94	95	96	97	98	99	0	1	2	3	4	5	6	7	8	9
Radiation hormesis	Yoshida																				To tokai-u							
BNCT	Miyamaru, Murata																											
Heavy concrete benchmark	Murata																											
Skyshine (gamma-ray)	Yoshida, Murata																				To Kinki-u, Tokyo-u, JAERI							
Activation cross section	Nagoya-u			○			○			○	○	○	○	○		○			To FNS of JAERI									
Semiconductor damage	Miyamaru													○	○													
Charged particle DDX	Murata									○		○	○	○		○					To FNS of JAERI							
Cold fusion	Takahashi							○				○	○	○	○													
Benchmark (spherical)	Kyoto-u						○						○	○	○													
FP cross section	Murata														○	○												
Gas-production x-sec	Kyushu-u													○		○												
Soft error	Iida									○		○		○														
Seramic luminescence	Tanabe												○	○														
Si-SSD damage	Kyoto-u													○														
TBR (spherical)	Tohoku-u		○	○	○	○					○		○															
γ production x-sec	Murata						○						○															
Neutron DDX	Takahashi	○	○		○	○	○	○			○																	
Streak camera	Yamanaka				○		○	○	○		○																	
Irradiation damage	Iida		○			○	○	○	○	○			○															
Radiation streaming	Tokyo-u					○	○	○																				
TBR (slab)	Takahashi		○					○																				
Nuclear model verification	Kyushu-u						○																					
Back scattering	Kyoto-u						○																					
Al(n,2n) cross section	Tohoku-u				○	○																						
Leakage neutron (spherical)	Yamamoto			○																								
Skyshine (neutron)	Tokyo-u		○	○																								
Leakage neutron (spherical)	Tokyo-u	○	○	○																								
Leakage neutron (slab)	Yamamoto	○																										

3.1. Monoenergetic and maxwell spectrum neutron beams (<5 MeV)

4. UPCOMING RESEARCH PROJECT

Basically we continue a study of large-angle scattering reaction cross section benchmark described in Chap. 3 for next several years. In addition, we plan to carry out the following studies from the next fiscal year, 2013.

4.1. KEV NEUTRON SPECTRUM MEASUREMENT WITH LONG/SHORT-LIVED ACTIVATION FOILS

This is basically for characterization of the neutron field for BNCT. However, the spectrometer to be developed will clearly contribute to neutron-nuclear reaction cross section measurement. It is known that neutron spectrum can be measured if using any currently available technique as well as the foil activation method, that is, multi-foil technique. However, it is still difficult for keV neutrons. We now reconsider activation reactions very carefully. Some of them of course have large cross sections in keV energy region. By mixing these foils, it may become possible to fix the spectrum. Especially very short/long half-lived radioisotopes have a significant ability for this purpose.

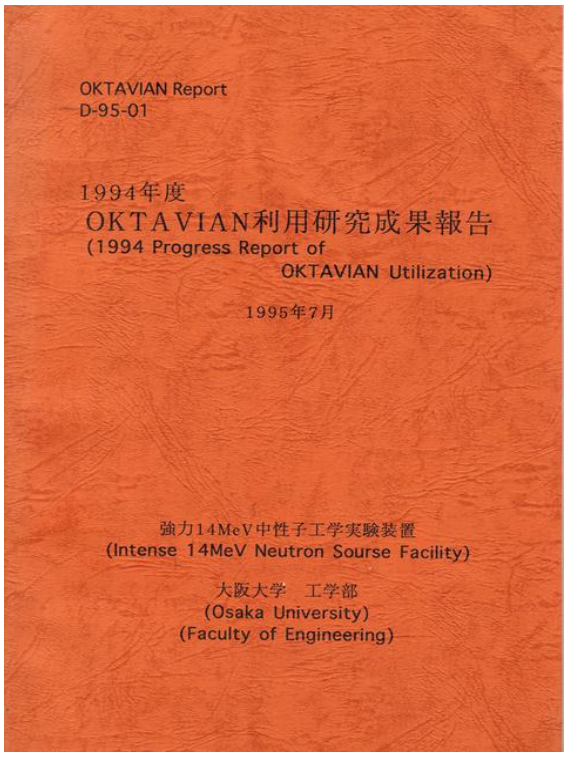

FIG. 3. OKTAVIAN report.

4.2. SPECTROMETER WITH IMAGING PLATE

There are some researches for this purpose with CR39. However, it requires a little troublesome post process to obtain the final result. In this point, imaging plate is more convenient. We will establish a procedure to get spectrum information from an imaging plate for high energy neutron integral experiment in order to benchmark nuclear data.

3.1. Monoenergetic and maxwell spectrum neutron beams (<5 MeV)

5. CONCLUSION

Thirty years have passed since the OKTAVIAN facility started its operation. Now the machine is working for new researches. The critical issue is getting tritium target. Commercial target is too expensive. We have a strong intention to continue the operation until fusion reactor would be realized. For that, supports from outside are indispensable, we believe. Any help would be very welcome!

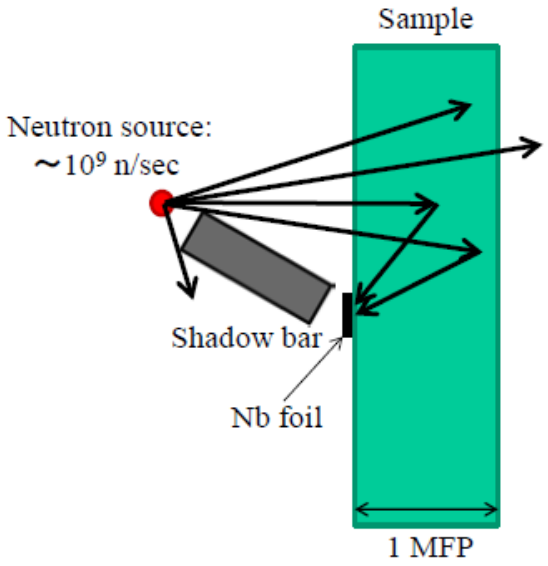

FIG. 4. Schematic of experimental arrangements for large scattering angle scattering reaction cross section benchmarks.

REFERENCES

References in the following include the ones also for researches not described here but only after 1996. Before 1995, OKTAVIAN Reports summarise the details as mentioned in Chap. 2. More information would be given by the corresponding author.

[1] YAMAMOTO, J., et al., “Gamma ray Energy Spectra Emitted from Spheres with 14 MeV Neutron Source”, INDC(NDS)-338 (1996) 205-225.

[2] MURATA, I., et al., "Measurement of DT Neutron Cross Sections of 129I with Foil Activation Method", Proc. Int. Conf. on Nucl. Data for Sci. and Technol., Trieste (1997) 1338-1340.

[3] TAKAHASHI, A., et al., "A Time of flight Spectrometer with Pulse-Shape Discrimination for the Measurement of Double-Differential Charged-Particle Emission Cross Sections", Nucl. Instr. and Meth., A401 (1997) 93-103.

[4] KOKOOO, et al., "Measurements of Double Differential Cross Sections of Charged Particle Emission Reactions by 14.1 MeV Incident Neutrons", Proc. Int. Conf. on Nucl. Data for Sci. and Technol., Trieste (1997) 520-522.

[5] NAKANO, D., et al., "Measurement of Reaction Cross Sections of I-129 Induced by DT Neutrons", Proc. '96 Symposium on Nucl. Data, Tokai, JAERI-Conf 97-005 (1997) 216-221.

[6] KOKOOO, et al., "Double Differential Charged Particle Emission Cross Sections of Vanadium for 14.1 MeV Incident Neutron", Proc. '96 Symposium on Nucl. Data, Tokai, JAERI-Conf 97-005 (1997) 273-278.
[7] NAKANO, D., et al., "Measurement of Reaction Cross Sections of Fission Products Induced by D-T Neutrons", Proc. '97 Symposium on Nucl. Data, Tokai, JAERI-Conf 98-003 (1998) 210-214.
[8] KOKOOO, et al., "Measurements of Double Differential Cross Sections of Charged Particle Emission Reactions For Several Structural Elements of Fusion Power Reactor by 14.1 MeV Incident Neutrons", Nucl. Sci. Eng., 132 (1999) 16-29.
[9] KONDO, T., "Measurement of Secondary Gamma ray Production Cross Sections of Vanadium Induced by D-T Neutrons", Proc. '98 Symposium on Nucl. Data, Tokai, JAERI-Conf 99-002 (1999) 198-203.
[10] TAKAGI, H., et al., "Measurement of Double Differential Cross Sections of Charged Particle Emission Reactions for natZr, 27Al and natTi by Incident DT Neutrons", Proc. '98 Symposium on Nucl. Data, Tokai, JAERI-Conf 99-002 (1999) 204-209.
[11] TAKAGI. H., et al., "Measurement of Double Differential Cross Sections of Charged Particle Emission Reactions by Incident DT Neutrons -Correction for Energy Loss of Charged Particle in Sample Materials-", Proc. '99 Symposium on Nucl. Data, Tokai, JAERI-Conf 2000-005 (2000) 178-183.
[12] KONDO, T., et al., "Measurement of Secondary Gamma ray Production Cross Sections of Structural Materials for Fusion Reactor -Extraction of Discrete and Continuum Components-", Proc. '99 Symposium on Nucl. Data, Tokai, JAERI-Conf 2000-005 (2000) 184-189.
[13] TERADA, Y., et al., "Measurement of Double Differential Cross Section for Proton Emission Reactions of Silicon and Fluorine by Incident DT Neutrons", Proc. 2000 Symposium on Nucl. Data, Tokai, JAERI-Conf 2001-006 (2002) 178-183.
[14] MURATA, I., TAKAHASHI, A., "Recent Measurements of Nuclear Data and Integral Tests for Fusion Reactor Application", J. Nucl. Sci. and Technol., Sup. 2 (2002) 1112-1117.
[15] MITSUDA, M., et al., "Measurements of Secondary Gamma ray Production Cross Sections for natFe, 51V, natMo, natZr, natNi and 181Ta with Hp-Ge Detector Induced by DT Neutrons", J. Nucl. Sci. and Technol., Sup. 2 (2002) 437-440.
[16] TERADA, Y., et al., "Measurements of Double Differential Cross Sections for Charged Particle Emission Reactions by 14.1 MeV Incident Neutrons", J. Nucl. Sci. and Technol., Sup. 2 (2002) 413-416.
[17] MURATA, I., MIYAMARU, H., “Low Energy Neutron Spectrometer Using Position Sensitive Proportional Counter – Feasibility Study Based on Numerical Analysis -”, Nucl. Instrum. Meth. in Phys. Res. A589 (2008) 445-454.
[18] KONDO, K., “Nuclear Data Benchmarking for Lead by LiAlPb Fusion Blanket Mockup Experiment”, Nucl. Technol., 168 (2009) 591-595.
[19] KONDO, K., “Problems of lead nuclear data in fusion blanket design”, Fusion Eng. Des., 84 (2009) 1076-1080.
[20] KANASUGI, H., MURATA, I., “Study on Neutron Spectrometer for Thermal to Epithermal Energy Regions with An Advanced Multi-Activation-Foil Method”, Proc. of the 2011 Annual Symposium on Nucl. Data, Nov. 16-17, 2011, RICOTTI, Tokai-mura, Ibaraki-ken, Japan, JAEA-Conf 2012-001, (2012) pp.153-158.

FUSION NEUTRONICS SOURCE (FNS) FACILITY AT JAPAN ATOMIC ENERGY AGENCY

C. KONNO*, I. MURATA**

*Japan Atomic Energy Agency, Tokai-mura, Naka-gun, Ibaraki-ken 319-1195, Japan
**Osaka University, Suita, Osaka 565-0871, Japan
Email: chikara.konno@jaea.go.jp

Abstract

The Fusion Neutronics Source (FNS) facility is a 14 MeV neutron generator by deuteron-triton, DT, reaction. Its operation started in 1981. For more than 30 years various fusion-reactor related experimental studies especially for ITER project have been carried out. Many scientists have been accepted for years to perform leading edge neutronics studies using high energy neutrons. At present, the facility is back to the original state from Fukushima accident and is again open to outside scientists in Japan as a cooperated fusion research facility.

1. INTRODUCTION

In Japan, there are two 14 MeV (deuteron-triton, DT) neutron sources available for fusion reactor researches. One is Fusion Neutronics Source (FNS) facility of JAEA, and the other is Intense 14 MeV Neutron Source Facility (OKTAVIAN) of Osaka University. In this report, details of the FNS facility are presented.

2. FUSION NEUTRONICS SOURCE FACILITY

The Fusion Neutronics Source (FNS) facility was installed at the current Nuclear Science Research Institute of Japan Atomic Energy Agency in 1981 in order to investigate the neutronics characteristics for candidate materials of fusion reactors including nuclear data measurements and has been successfully operated for 30 years. The FNS is an accelerator-based D-T neutron source. It consists basically of a 400 keV high current electrostatic deuteron accelerator, heavy-duty tritium metal target assemblies, tritium handling and processing devices, experimental equipments and a building which houses the source facility at the same time plays an important role in the experimental arrangement by its shield structure and various ports imbedded in it. Figure 1 shows the bird's eye view of the main part of the early FNS facility. Note that the present facility is slightly different from Fig.1.

The accelerator is made up of the following components:

1. A cascade insulation-transformer type high voltage power supply that is capable of delivering 80 mA at 450 kV.
2. A 25 kVA power supply of the insulated transformer type for the high voltage terminal.
3. A high voltage terminal containing :
   Two multi-cusp ion sources (high current one : ~ 20 mA, and low current one : ~ 2 mA) with a 90-degree analyzing magnet for each, a diverter and a sweeper for the pre-acceleration pulsing, an einzel and a solenoid lenses for the beam focusing, and the associated equipments.
4. A strong field, 7-stage accelerator tube with epoxy insulation bushings.
5. Two drift tubes (0-degree beam line of 15 m in length and 80-degree beam line of 17 m in total length, which is deflected by 80 degrees at the pair of two 40-degree bending magnets.)

6. A vacuum system of four turbo-molecular pumps (TMPs) on the terminal, four TMPs on the drift tubes, a cryo-sorption pump next to the target end of the 0-degree beam line and a Sorb-AC pump at 80-degree beam line end.
7. Three triplet quadruple lenses for the beam transmission in each beam line, sharing the nearest to the acceleration tube in common, and X-Y steerers for fine beam adjustment.
8. Retractable Faraday cups for beam monitoring.
9. A deflector and a buncher for post-acceleration pulsing.
10. A control desk and a dia-grammatical display panel for the operation.

There are two types of the Ti-T metal targets:

a) A large-size rotating target of RTNS-1 type with a special sliding vacuum seal. The size of the target is 310 mm in diameter. The tritium of about 1,000 curies (37 TBq) is absorbed in the target. The target is cooled by high speed water flow.

b) A small-size stationary target of about 30 mm in diameter and about 10 curies (370 GBq) of tritium cooled by high speed water flow.

The beam and neutron source performances for the typical case are summarized in Table 1. The minimum pulse width and repletion time at the 80-degree beam line are 4 nsec and 8 μsec, respectively, and the peak current is 80 mA. The beam spot size is about 15 mm in diameter for each.

TABLE 1. TYPICAL BEAM AND NEUTRON PERFORMANCES

	0-degree beam line DC mode	80-degree beam line DC mode
Deuteron Beam energy	350 keV	350 keV
Max beam current	20 mA	2 mA
Max neutron yield	4×10^{12} n/sec	4×10^{11} n/sec

The vacuum exhaust gas containing tritium released from the Ti-T target is transferred with the purge gas system to the tritium removal device TAP. The gas is once kept in a storage tank and then recirculates in a catalyzing unit for the oxidation and a molecular sieve dryer column where tritium is fixed in the form of water. The TAP can reduce the tritium concentration in the gas down to the tritium concentration at the stack well below Japanese regulation level.

The following experimental equipments are installed at FNS.

a) Time-Of-Flight (TOF) measuring system (see Fig. *2.*)

   This system is mainly used to measure angular leakage neutron spectra from a thick slab assembly.

b) DT neutron beam system (see Fig. *3.*)

3.1. Monoenergetic and maxwell spectrum neutron beams (<5 MeV)

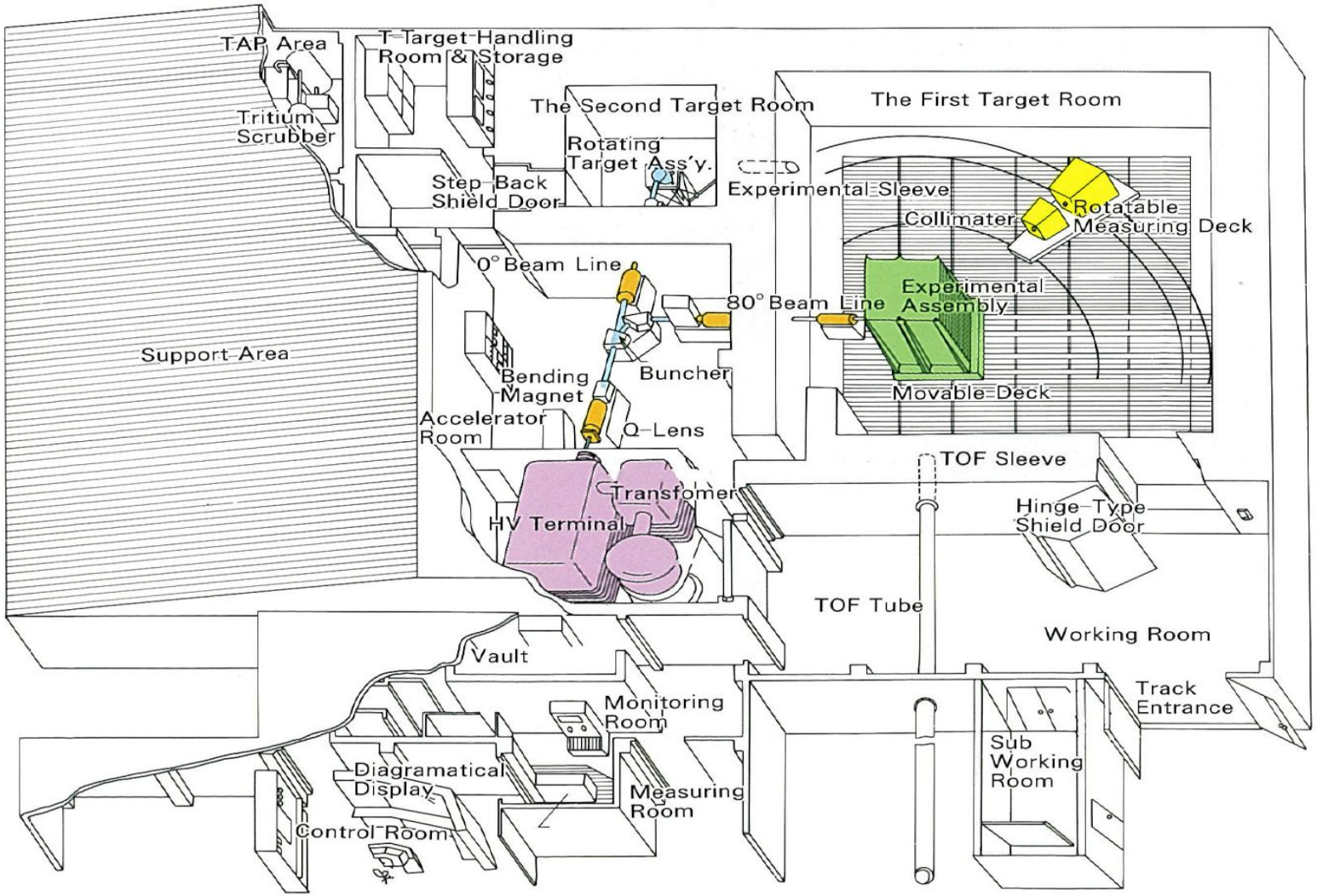

FIG. 1. Bird's eye view of the main part of the early FNS facility.

3.1. Monoenergetic and maxwell spectrum neutron beams (<5 MeV)

This system was installed around 1998 inside the concrete wall between the first and second target rooms. This system produces a high quality DT neutron beam of 20 mm in diameter from the DT neutron source in the second target room with very few background neutrons. The DT neutron beam has very few background neutrons and it is used for charged particle production cross-section measurements, various detector tests, etc.

So far a lot of fusion neutronics experiments were carried out; blanket nuclear property experiment, *in-situ* nuclear data benchmark experiment, Time-Of-Flight (TOF) experiment, activation cross section measurement, direct nuclear heating measurement, induced activity measurement, ITER shielding experiment, and so on. These experimental data have been useful for nuclear data evaluation and benchmark.

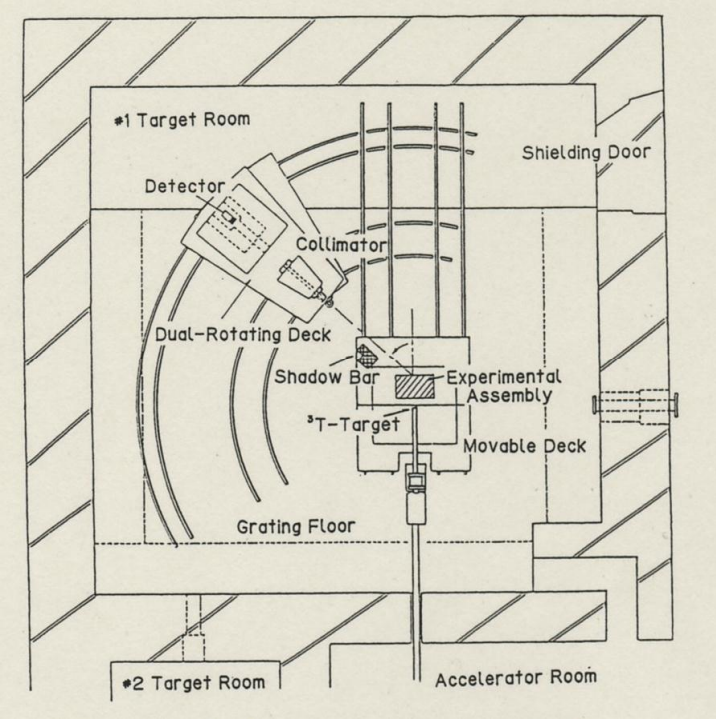

FIG. 2. TOF measuring system.

3. ONGOING RESEARCH PROJECT

At present, the following researches concerning nuclear data are being carried out.

3.1 LARGE-ANGLE SCATTERING REACTION CROSS SECTION BENCHMARK

For nuclear data benchmark for fusion reactor design, development of an experimental procedure to benchmark especially backward angl scattering cross section is being carried out. As shown in Fig. 4., a cylindrical stainless steel assembly was set up just behind a pencil beam neutron source at the 80 degree line of the FNS facility. The beam neutrons are incident to the right-hand side assembly in Fig. 4. to activate niobium foils placed at positions ①~⑥. Especially in offset positions it is expected that backward scattering contribution could be extracted. The experimental results are precisely analysed with PTRAC option of MCNP to find better experimental arrangements to be able to take backward scattering contribution more clearly.

3.1. Monoenergetic and maxwell spectrum neutron beams (<5 MeV)

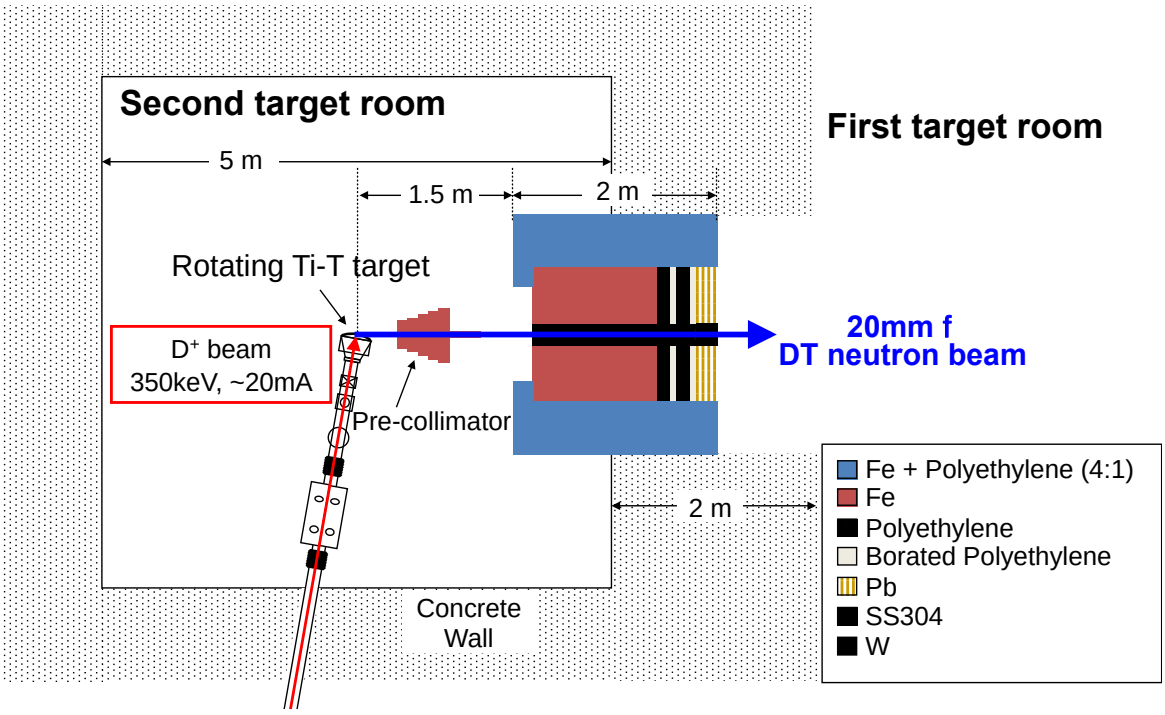

FIG. 3. D-T neutron beam system.

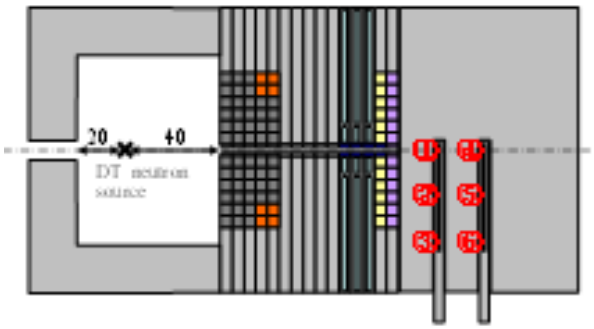

FIG. 4. Experimental arrangement for large-angle scattering reaction cross section benchmark. A large block in right hand side is a stainless steel assembly. In ①~⑥, niobium foils are inserted.

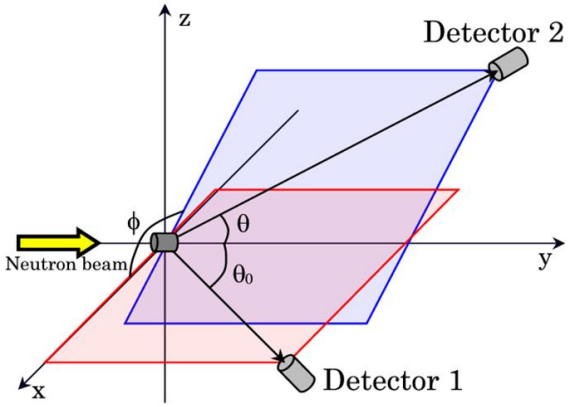

FIG. 5. Sample and detector setup for spectrum measurement. Pencil beam neutrons come from left-hand side.

3.1. Monoenergetic and maxwell spectrum neutron beams (<5 MeV)

3.2 DIFFERENTIAL EXPERIMENTS

a) Spectrum Measurement of Neutrons Emitted from (n,2n) Reaction

(n,2n) reaction is quite important for fusion reactor design because the reaction multiplies the number of neutrons and it occurs at energies around 10 MeV strongly. However, it is difficult to measure cross sections of isotopes which would be transmuted into stable isotopes by (n,2n) reaction. Moreover, especially for light nuclides the precise spectrum measurement becomes crucial because the spectrum is more complicated than normally observed evaporation spectrum.

In the measurement, a beam neutron source at 0 degree line as shown in Fig. *3*. was used. On the beam, a small sample is set. Secondary neutrons emitted from the sample are measured by two NE213 detectors arranged close to the sample as in Fig. *5*. By the coincidence detection technique, only neutrons originating from (n,2n) reaction can be measured. By changing the position of the two detectors within 4π space, triple differential cross section (TDX) is obtained. By integrating the TDX over energy and angle, the total (n,2n) reaction cross section can be deduced. Fig. 6 shows the measured TDX of beryllium.

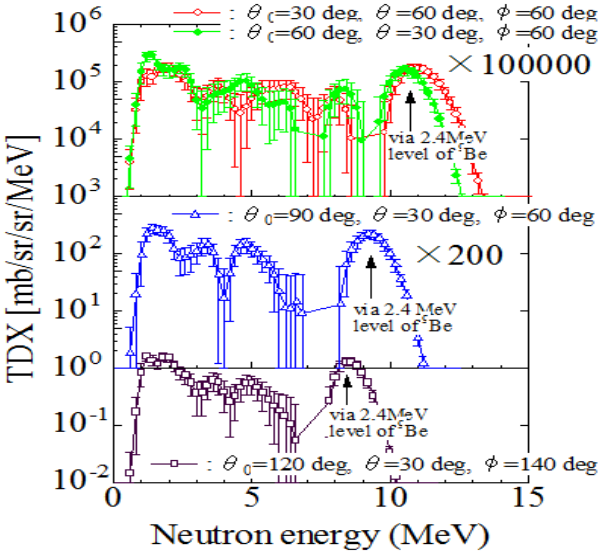

FIG. 6. Measured triple differential cross section (TDX) for beryllium.

b) Charged Particle Emission Double Differential Cross Section Measurement

Charged particle emission reaction is quite crucial for evaluation of nuclear heat and material damage in fusion reactor design. Especially for light nuclides, breakup reactions can occur. And then the spectrum may become complicated. The measurement is thus important also for examination of nuclear model to evaluate nuclear reaction cross sections.

In the measurement, similar to the (n,2n) experiment a beam neutron source at 0 degree line of the FNS facility was used. As shown in Fig. *7*, a very thin sample is positioned on the beam and inside a vacuum chamber. Emitted charged particles are measured by two Si-SSD systems set up very close to the sample.

3.1. Monoenergetic and maxwell spectrum neutron beams (<5 MeV)

Each system consists of two Si-SSD which are a ΔE-E counter telescope. By this, spectrum of charged particles of interest can be extracted. Also, from the difference of the stopping power of charged particles some energy part in the measured spectrum by ΔE detector could be assigned to a part of α particle spectrum. Consequently, the lower measurable energy of α particle could successfully be decreased. Fig. 8 shows the result of beryllium.

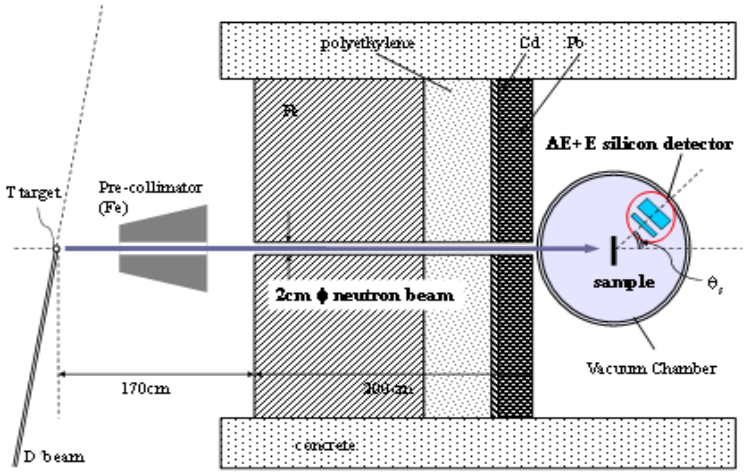

FIG. 7. Experimental arrangement of charged-particle emission DDX measurement.

3.3 INTERMEDIATE-ENERGY NUCLEAR DATA BENCHMARK

a) Benchmark Experiment with Spectrum Shifter

In DT neutron source facilities, nuclear data benchmark experiments have been carried out for years for fusion reactor development. However, for intermediate energies, sufficient benchmark experiments have not been performed so far because appropriate neutron sources did not exist. We thus started a project of intermediate-energy region benchmark experiment by using a special neutron field formed by shifting the neutron spectrum to a lower energy region with an appropriate neutron spectrum shifter at DT neutron source facilities. By Monte Carlo simulations, beryllium is the best shifter to make an appropriate neutron field for intermediate-energy benchmark experiments. We plan to carry out the source term spectrum measurement followed by benchmark experiments with a beryllium spectrum shifter.

b) Benchmark Experiment with Theoretical Benchmark Performance Analysis Result

It is believed that DT neutron benchmark experiments are also for benchmarking nuclear date in intermediate energy region. To make theoretically clear how it is, Monte Carlo simulations were carried out for several years. Now, a special function was derived from the simulation to estimate the performance of benchmark experiments. We will carry out ideal nuclear data benchmark experiments with the developed performance estimation function.

3.1. Monoenergetic and maxwell spectrum neutron beams (<5 MeV)

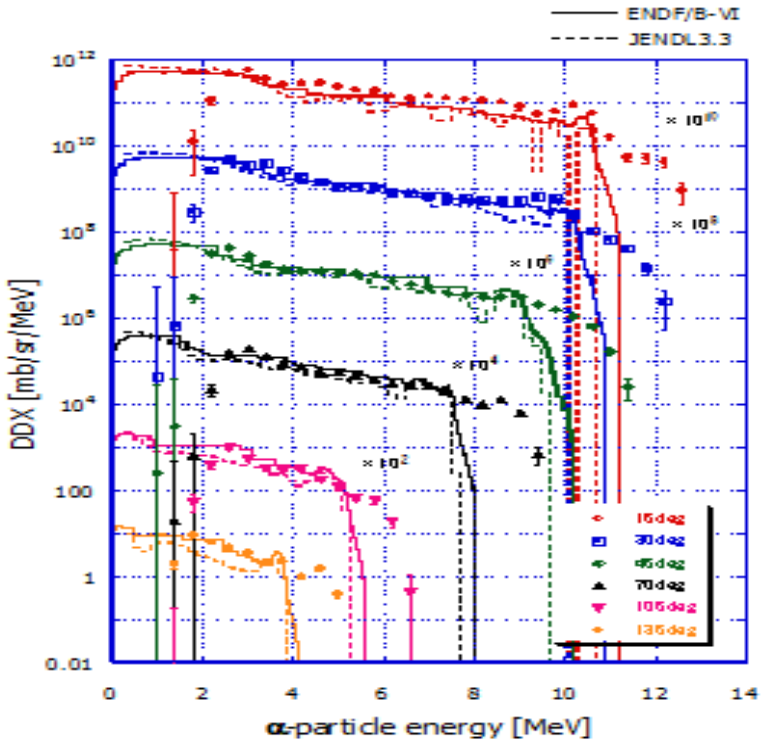

FIG. 8. Measured α particle emission DDX for beryllium.

3.4 *IN-SITU* NUCLEAR DATA BENCHMARK EXPERIMENT

We still continue the *in-situ* nuclear data benchmark experiment because we have obtained the experimental data only for lithium oxide, beryllium, graphite, silicon carbide, titanium, vanadium, iron, type 316 stainless steel (SS316), copper, tungsten, lead, etc. A typical experimental configuration is shown in Fig. 9. Neutron spectra of almost the whole neutron energy, reaction rates for various reactions, gamma heating rates and so on were measured inside the experimental assembly of simple geometry. Size of experimental assemblies is different for each experiment depending on material amounts which we have. These experimental data are very useful for nuclear data validation through simulation with a radiation transport code and nuclear data libraries. A typical result is shown in Fig. 10.

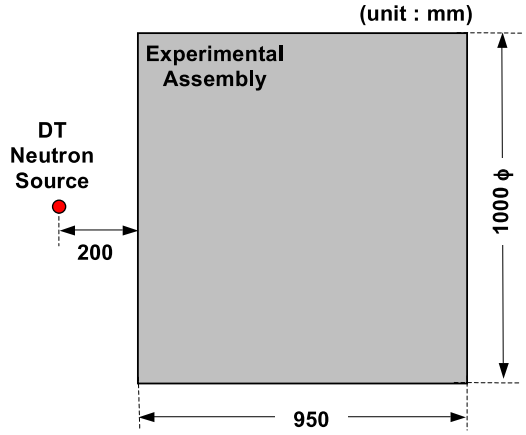

FIG. 9. Experimental configuration for in-situ experiment.

3.1. Monoenergetic and maxwell spectrum neutron beams (<5 MeV)

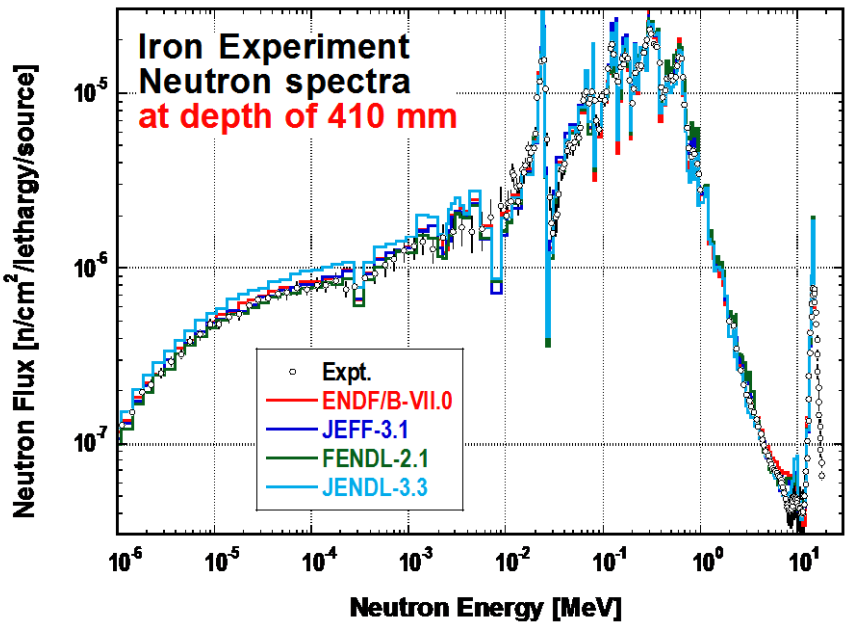

FIG.10. Neutron spectra at 410 mm in iron in-situ experiment.

4. UPCOMING RESEARCH PROJECT

Basically we continue studies described in Chap. 3. In addition, we plan to carry out the following studies from the fiscal year, 2014.

4.1 ANGLE ORIENTED BENCHMARK EXPERIMENT WITH BEAM 14 MEV NEUTRONS

This is an advanced research of large-scattering-angle scattering reaction cross section benchmark with a beam neutron source described in Sec. 3.1. Normally, in neutron benchmark experiments are used an isotropic source in a spherical sample or a broad parallel beam incident to a slab sample. In this experiment, pencil beam neutrons are guided to inside of a spherical or slab assembly. Neutron spectra inside the assembly thus have strong angular dependence. From precise measurements with detectors and foils, angle oriented benchmark can be carried out combined with the benchmark performance function described in Sec. 3.3.

5. CONCLUSION

The FNS facility has been working for more than 30 years to contribute fusion reactor project in Japan. Especially the facility and the staffs are engaged in tasks for ITER project for years as a national fusion neutronics source to realize ITER. After Fukushima accident the machine once stopped operation. However, it was recently back to the original state. The FNS facility is willing to support Japanese fusion reactor related basic studies in the same way as before.

3.1. Monoenergetic and maxwell spectrum neutron beams (<5 MeV)

REFERENCES

References in the following include the ones not only for the researches described in this report but also others carried out at the FNS facility so far.

[1] NAKAMURA, T., et al., Proc. 4th Symp. on Accelerator Science Technol., RIKEN, Saitama, 24-26 Nov, (1982) 155.
[2] OYAMA, Y., et al., JAERI-M 90-092 (1990).
[3] IKEDA, Y., et al., JAERI 1312 (1988).
[4] KONNO, C., et al., JAERI 1329 (1993).
[5] MAEKAWA, F., et al., JAERI-Data/Code 98-021 (1998).
[6] Special issue for JAEA/U.S. DOE collaborative program on fusion neutronics : Fusion Technol., 28, No. 1 and 2, (1995).
[7] KONNO, C., et al., Proc. 20th Symposium on Fusion Technology, Marseille, France, Sept. 7-11, (1998) 1263.
[8] KONNO. C., et al., Proc.20th Symposium on Fusion Technology, Marseille, France, Sept. 7-11, (1998) 1473.
[9] MAEKAWA, F., et al., "Benchmark Experiment on Vanadium with D-T Neutrons and Validation of Evaluated Nuclear Data Libraries by Analysis of the Experiment", J. Nucl. Sci. Technol., 36 (1999) 242-249.
[10] MURATA, I., et al., “Experiment on $LiAlO_2$, Li_2TiO_3 and Li_2ZrO_3 Assemblies with D-T Neutrons -Leakage Neutron Spectrum Measurement-", Fusion Eng. Des., 51-52 (2000) 821-827.
[11] MURATA, I., et al., "Neutron-Nuclear Data Benchmark for Copper and Tungsten by Slab Assembly Transmission Experiments with DT Neutrons", Fusion Eng. Des., 58-59 (2002) 617-621.
[12] MURATA, I., et al., "Fusion Neutronics Benchmark Experiment on Structural and Advanced Blanket Materials -Leakage Neutron Spectrum Measurement-", J. Nucl. Sci. and Technol., Sup. 2 (2002) 978-981.
[13] MURATA, I., et al., "(n,2n) Reaction Cross Section Measurement with A Beam DT Neutron Source", J. Nucl. Sci. and Technol., Sup. 2 (2002) 433-436.
[14] NISHIO, T., et al., "Fusion Neutronics Benchmark Experiment on Structural and Advanced Blanket Materials -Leakage Gamma ray Spectrum Measurement-", J. Nucl. Sci. and Technol., Sup. 2 (2002) 955-958 (2002).
[15] MURATA, I., et al., “Development of Charged-Particle Emission DDX Spectrometer with SSD Telescope and Pencil-Beam DT Neutron Source”, Proceedings of International Conference on Nuclear Data for Science and Technology, Sept. 26 – Oct. 1, 2004, Santa Fe, New Mexico (2004) 769-772.
[16] OCHIAI, K., et al., “Measurement of Energetic Charged Particles Produced in Fusion Materials with 14 MeV Neutron Irradiation”, Fusion Eng. Des., 75-79 (2005) 859-863.
[17] KONDO, K., et al., “Charged-particle spectrometry using a pencil-beam DT neutron source for double-differential cross section measurement”, Nucl. Instrum. Meth., A568 (2006) 723-733.
[18] KONDO, K., et al., “ New approach to measure double-differential charged-particle emission cross sections of several materials for a fusion reactor”, Fusion Eng. Des., 81 (2006) 1527-1533.
[19] KONDO, K., et al., “Verification of nuclear data for DT-neutron induced charged-particle emission reaction of light nuclei”, Fusion Eng. Des., 82 (2007) 2786-2793.

3.1. Monoenergetic and maxwell spectrum neutron beams (<5 MeV)

[20] MURATA, I., et al., "Angle-Correlated Spectrum Measurement for Two Neutrons Emitted from (n,2n) Reaction with the Coincidence Detection Technique Using A Pencil-Beam DT Neutron Source", Nucl. Instrum. Meth. in Phys. Res. A595 (2008) 439-446.

[21] KONDO, K., et al., "Measurement and Analysis of Neutron Induced Alpha-Particle Emission Double-Differential Cross-Section of Carbon at 14.2-MeV", J. Nucl. Sci. Technol., 45 (2008) 103-115.

[22] KONDO, K., et al., "Experimental study on breakup reaction of beryllium and carbon induced with 14-MeV neutrons based on emitted charged-particle measurements", Proc. Int. Conf. Nucl. Data on Sci. and Technol.(ND2007), April 22-27, 2007, Nice (2008) 407-410. Doi : 10.1051/ndata:07579

[23] MURATA, I., et al., "Measurement of Angle-correlated Neutron Spectrum for ^{9}Be(n,2n) Reaction with A Pencil-beam DT Neutron Source", Proc. Int. Conf. Nucl. Data on Sci. and Technol.(ND2007), April 22-27, 2007, Nice (2008) 999-1002. Doi :10.1051/ndata:07596.

[24] KONDO, K., et al., "Verification of KERMA Factor for Beryllium at Neutron Energy of 14.2 MeV Based on Charged-Particle Measurement", Fusion Eng. Des., 83 (2008) 1674-1677.

[25] MURATA, I., et al., "Direct Neutron Spectrum Measurement To Validate ^{nat}Zr(n,2n) Reaction Cross section at 14 MeV", Fusion Eng. Des., 84 (2009) 1376-1379.

[26] Ohta, M., et al., "Preliminary spectrum shifter design for intermediate energy nuclear data benchmark experiments with DT neutrons", Fusion Eng. Des., 84 (2009) 1446-1449.

[27] MURATA, I., "High-precision Measurements of Nuclear Data with Beam DT-Neutrons", Proc. of the 2009 Annual Symposium on Nucl. Data (NDS 2009), Nov. 26-27, 2009, RICOTTI, Tokai-mura, Ibaraki-ken, Japan, JAEA-Conf 2010-005 (2010) 15-20.

[28] MURATA, I., et al., "Performance Analysis of Fusion Nuclear-data Benchmark Experiments for Light to Heavy Materials in MeV Energy Region with A Neutron Spectrum Shifter", J. Nucl. Mater., 417 (2011) 1127-1130.
OHNISHI, S., et al., "Implementation of A DT Neutron Beam at the 1st Target Room of JAEA/FNS for New Integral Benchmark Experiments", J. Korean Phys. Soc., 59[2] (2011) 1949-1952.

SURROGATE REACTION STUDY AT THE JAEA TANDEM FACILITY

K. NISHIO[*], H.MAKII[*], I. NISHINAKA[*], T. ISHII[*], S. MITSUOKA[*], K. TSUKADA[*], M. ASAI[*], K. FURUTAKA[*], H. KOURA[*], Y. UTSUNO[*], S. CHIBA[**], Y. ARITOMO[***], T. OHTSUKI[***]

[*]Japan Atomic Energy Agency, Tokai, Ibaraki 319-1195, Japan
[**]Tokyo Institute of Technology, Tokyo 152-8550, Japan
[***]Research Center for Electron Photon Scinece, Sendai 982-0826, Japan
Email: nishio.katsuhisa@jaea.go.jp

Abstract

Using multi-nucleon transfer reactions, we are promoting surrogate reactions to obtain nuclear data for wide variety of isotopes including short-lived nuclei. The experiments have been carried out at the JAEA tandem Pelletron accelerator 20UR.

1. INTRODUCTION

We have a program to study surrogate reaction [1-4] using heavy ion beams supplied by the JAEA tandem facility at the Tokai campus of Japan Atomic Energy Agency (JAEA). By using transfer reaction populating a specific compound nucleus, we are measuring fission cross sections of actinide nuclei and capture cross sections for medium-mass nuclei. In the fission of excited compound nuclei, measuring the fission fragment mass distributions and number of prompt neutrons in fission is our scope. We are especially investigating reactions using relatively heavy projectile such as oxygen. This allowing us to populate many compound nuclei than using lighter projectiles, and required sensitivity to isolate different transfer channels was established.

2. THE JAEA TANDEM FACILITY AND BOOSTER

Layout of the beam lines in the JAEA tandem facility is shown in Fig. 1. The JAEA tandem is designed to achieve 20 MV in the terminal voltage. At a moment, the available voltage is in the range of 2.5 - 18.0 MV. From the negative ion source, ions are accelerated up to 50 - 350keV and injected to the accelerator tube. Most of the ions from hydrogen to lead can be supplied from the negative ion source. There are five target rooms in the facility. One beam line guided to the 1st heavy ion target room is connected to the superconducting booster accelerator to gain high energy, and the energetically boosted beams are guided to the booster target room. An unique feature of the facility is that the ECR (electron cyclotron resonance) ion source is installed on the top of the tandem terminal to supply positive ions, with which we can extract beams from inert gases such as Ne, Ar, Kr and Xe.

We have unique setup for the nuclear physics experiment. At the light-ion target room, the heavy ion spectrometer called ENMA is installed. In the irradiation room, the isotope separator on-line is available, where neutron-rich nuclei produced by the proton-induced fission of ^{238}U can be extracted. In the booster target room, the recoil mass separator (JAEA-RMS) is installed. Also germanium detector array is available for the nuclear structure study. We are now arranging a new beam line especially to study the surrogate reaction (see Fig. 1)

Advantage of this facility is that radioactive target material can be used for nuclear physics and solid-state physics. In most of the beam lines, target materials of ^{232}Th, ^{233,235,238}U can be used. In the irradiation room, we can use more radioactive target such as Np, Am, Cm, Cf isotopes. The same nuclei will be available also in the surrogate reaction room, so that we can access wide variety of actinide nuclei using these targets.

3.1. Monoenergetic and maxwell spectrum neutron beams (<5 MeV)

At a moment, the surrogate reaction is studied at the beam line L1 in the light ion target room as shown in the next section. Soon, the setup will be moved to the Surrogate reaction room after the new beam line is installed and getting the license to use radioactive material.

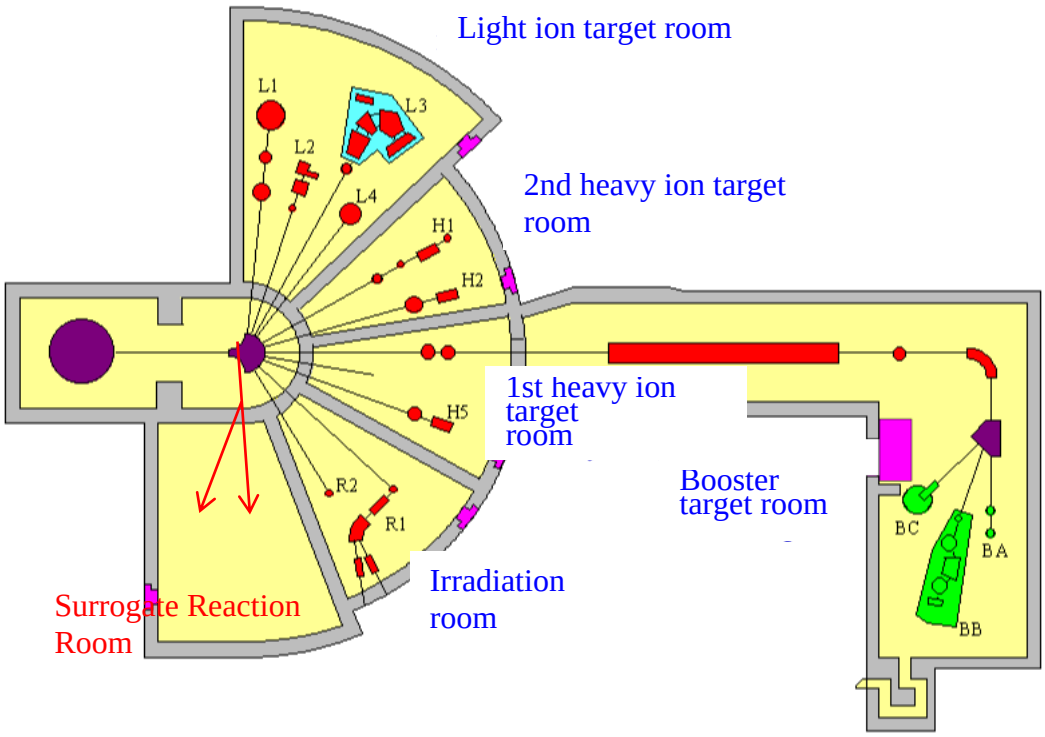

FIG.1. Layout of the tandem facility.

3. SETUP FOR SURROGATE REACTION STUDY

3.1. SILICON DE-E DETECTORS

Program for the surrogate reaction study has started in 2009 at JAEA. Among the several programs of the surrogate reaction study, we are especially studying reactions using heavier ions. This is firstly because nuclei far from the target nucleus itself can be accessed by multi-nucleon transfer reaction, allowing us to populate more exotic nuclei and obtain nuclear data for these nuclei. Also, data for many nuclei can be obtained in a single run compared to the reaction using lighter projectiles such as helium. This, however, requires a sophisticated setup especially to isolate the scattered projectile-like nuclei formed by nucleon-transfer. We developed a silicon *dE-E* detector for reactions using oxygen beams. The dE detector to isolate oxygen isotopes has a typical thickness of about 60-70 μm, and the uniformity of the thickness within 1 μm has been achieved by ion implantation technique. Typical example of the spectra on dE and E are shown in Fig. 3, obtained in the $^{18}O + ^{238}U$ reaction (E_{beam} = 162 MeV). In this figure, isotopes of oxygen, nitrogen and carbon are produced. They can be the surrogate for the neutron-induced fission of uranium, neptunium and plutonium.

3.1. Monoenergetic and maxwell spectrum neutron beams (<5 MeV)

3.2. FISSION FRAGMENT DETECTORS

To measure the fission cross sections, we developed a position-sensitive multi-wire proportional counters (MWPCs) to detect fission fragment. It has active area of 400 mm (H) x 200 mm (V). Taking advantage of the fast rise time properties of the detector, time-of-flight measurement of fission fragments can be possible. Using the kinematic consideration, we can determine the fission fragment mass distribution for each nuclei, for example we obtained the preliminary data of the mass distribution of $^{240}U^{*}$ populated by $^{238}U(^{18}O, ^{16}O)^{240}U^{*}$. Typical mass resolution is 5.0 u (FWHM).

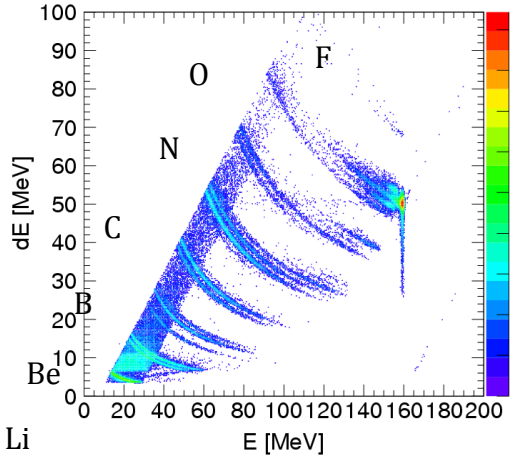

FIG.2. Plot of the projectile-like nuclei on the dE - E plane obtained in the ^{18}O + ^{238}U reaction.

3.2. FISSION FRAGMENT DETECTORS

To measure the fission cross sections, we developed a position-sensitive multi-wire proportional counters (MWPCs) to detect fission fragment. It has active area of 400mm (H) x 200 mm (V). Taking advantage of the fast rise time properties of the detector, time-of-flight measurement of fission fragments can be possible. Using the kinematic consideration, we can determine the fission fragment mass distribution for each nuclei, for example we obtained the preliminary data of the mass distribution of $^{240}U^{*}$ populated by $^{238}U(^{18}O, ^{16}O)^{240}U^{*}$. Typical mass resolution is 5.0 u (FWHM).

3.3. NEUTRON DETECTOR

Measurement of average number of prompt neutron in fission is our scope for the surrogate reaction study. The data is obtained by coincidence measurement of fission fragment and neutron. We have 12 neutron liquid scintillation detectors (12.7 cm diameter × 5.1 cm thickness). Pulse-shape discrimination technique is used to separate neutrons and gamma rays. The experimental program has started.

3.4. GAMMA RAY DETECTOR

In order to measure capture cross sections in the surrogate reaction technique, we developed a large volume $LaBr_3(Ce)$ scintillation detector (10.2 cm diameter x 12.7 cm length) surrounded by Compton suppression BGO detector (thickness = 2.54 cm, length = 25.4 cm). We have two set of $LaBr_3(Ce)$+BGO detector.

3.1. Monoenergetic and maxwell spectrum neutron beams (<5 MeV)

3.5. DATA ACQUISITION

New data acquisition system based on VME standard was developed. We also designed 16 channel PDC (Peak detection), 16 channel QDC (charge detection), and 16 channel TDC (time difference) modules. In the list mode acquisition, a time stamp is recorded in each event with resolution of 5 ns (the time resolution is adjustable). With the time information the coincidence events can be selected in offline analysis.

3.6. TARGET PREPARATION

For the surrogate reaction study, we have two methods to make a thin target layer. For the radioactive material, we use electro-deposition method. Other target using enriched material can be produced by RF sputtering methods.

4. PLANNED EXPERIMENT

4.1. FISSION

The following reactions will be studied until 2016 in order to obtain fission cross section, fission fragment mass distribution and prompt neutrons and their dependence on the excitation energy of compound nucleus produced by transfer reactions.

(1) $^{18}O + ^{238}U$
(2) $^{18}O + ^{232}Th$
(3) $^{18}O + ^{248}Cm$
(4) $^{18}O + ^{237}Np$

4.2. CAPTURE

We have completed experiment of

(1) $^{18}O + ^{155}Gd \rightarrow ^{16}O + ^{157}Gd^{*}$
(2) $^{18}O + ^{157}Gd \rightarrow ^{16}O + ^{159}Gd^{*}$

The neutron induced capture cross section is available for $n + ^{156}Gd$ and $n + ^{156}Gd$. We will verify the applicability of the surrogate ratio methods in the analysis.

5. SUMMARY

We developed an experimental set up to take neutron-induced data by surrogate reaction technique. In this program, measurement of fission cross sections, capture cross sections, fission fragment mass distribution and average number of prompt neutrons will be obtained during several-years plan.

REFERENCES

[1] BURKE, J.T., *et al*., Phys. Rev. **73**, 054604 (2006).
[2] ESCHER, J.E., and Dietrich, F.S., Phys. Rev. C, **74**, 054601 (2006).
[3] CHIBA, S., IWAMOTO, O., ARITOMO, Y., Phys. Rev. C, **84**, 054602 (2011).
[4] ARITOMO, Y., CHIBA, S., NISHIO, K., Phys.Rev.C, **84**, 024602 (2011).

3.1. Monoenergetic and maxwell spectrum neutron beams (<5 MeV)

MONO-ENERGETIC NEUTRON FIELDS USING 4 MV PELLETRON ACCELERATOR AT FRS / JAEA

Y. TANIMURA, M. KOWATARI, H. YOSHITOMI, S. NISHINO AND M. YOSHIZAWA

Japan Atomic Energy Agency (JAEA),
2-4 Shirakata Shirane, Tokai-mura,
Naka-gun, Ibaraki, 319-1195
Japan
Email: tanimura.yoshihiko@jaea.go.jp

Abstract

Mono-energetic neutron calibration fields have been developed in the energy range of 8 keV to 19 MeV using a 4MV Pelletron accelerator at the Facility of Radiation Standards in the Japan Atomic Energy Agency. The neutron fields with the energies of 8, 27, 144, 250, 565 keV and 1.2, 2.5, 5.0, 14.8, 19 MeV are established. Protons or deuterons are accelerated and transported to bombard various targets for neutron production. The targets are prepared by depositing scandium, lithium fluoride or tritiated titanium on the backing disks for $^{45}Sc(p,n)^{45}Ti$, $^{7}Li(p,n)^{7}Be$ and, $^{3}H(p,n)^{3}He$ and $^{3}H(d,n)^{4}He$ reactions, respectively. For $^{2}H(d,n)^{3}He$ reaction, a gas target is prepared by filling a target cell with D_2 gas. A pulsed beam can be derived with the pulsing system installed in the high voltage terminal of the accelerator. The minimum pulse width was evaluated to be 2 ns in FWHM. Neutron fluence rates at the irradiation point were measured with a Bonner sphere, a lithium glass scintillation detector, a silicon semi-conductor detector with a polyethylene radiator and a BC501A organic liquid scintillation detector. Though the maximum fluence rates should not be high enough to obtain the nuclear data using an activation method, they can be available to obtain the nuclear data by using the prompt gamma ray analysis.

1. INTRODUCTION

Mono-energetic neutron fields in the energy range from 8 keV to 19 MeV were developed at the Facility of Radiation Standards (FRS) in the Japan Atomic Energy Agency (JAEA) using a 4 MV Pelletron accelerator [1-3]. The main purpose of these fields is to calibrate neutron detectors for radiation protection. The neutrons energies are shown in Fig. 1 are available for determining energy responses of neutron detectors. The neutron energies in these fields correspond to the energy points specified in the international standard (ISO 8529-1) and Japanese industrial standard (JIS Z4521) [4,5].

This paper describes the features of the accelerator and fields.

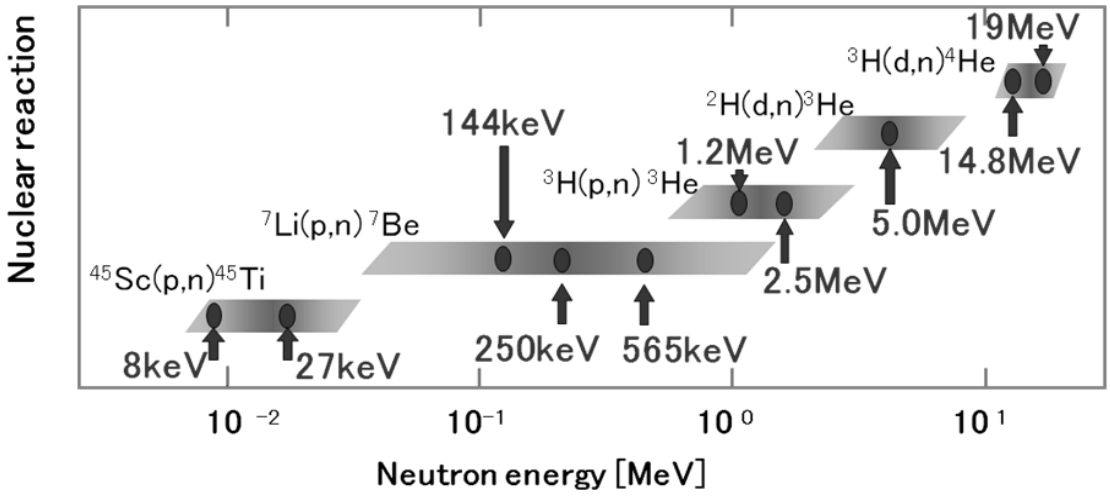

FIG. 1. Available energy points and nuclear reactions employed for neutron production in the mono-energetic neutron fields.

2. OUTLINE OF FACILITY

Figure 2 shows a cut-away view of the mono-energetic neutron fields. Protons or deuterons are accelerated up to 4 MeV with a single-end Pelletron accelerator (National Electrostatic Corporation 4UH-HC) installed in the basement floor. The accelerated particle beam is transported to a neutron beam line with two 90˚ bending magnets and a 6.5˚ bending magnet. Then the beam bombards a target for neutron or photon production which is set at the center of an irradiation room. The energy of the accelerated particles can be precisely determined using the first bending magnet (an analyzing magnet) and a slit in the vertical beam line. A system with a NMR probe is adopted to accurately measure the strength of a magnetic field in the analyzing magnet. Two beam lines were installed in the irradiation room. One is for neutron production and the other is for 6-7 MeV high energy gamma ray production using the $^{19}F(p,\alpha\gamma)^{16}O$ reaction.

A Duoplasmatron ion source was installed in the high-voltage terminal of the accelerator to produce a proton or deuteron beam. The maximum beam current is 50 and 5 μA at the target in a DC and pulse operating mode of the accelerator, respectively.

The photograph of the fields is shown in Fig. 3. The dimensions of the irradiation room are 11.5 m in width, 16.5 m in depth and 12.5 m in height. The room has the low scattering floor with a grating structure made of aluminum. A Long Counter is installed as a neutron yield monitor. The irradiation point is set on the calibration table shown in Fig. 3 except for the 8 and 27 keV fields. A distance from the target to the point centered on the table can be remotely controlled from an accelerator control room and changed from 1 m to 5 m within an accuracy of 1 mm. For the 8 and 27 keV fields, the point was set at 50 cm from the target using another calibration table in order to obtain enough neutron fluence rate. The angle of the point to the proton or deuteron beam direction was determined to be 0˚, except for the 14.8 MeV field, where neutron yield is generally highest and contamination of higher energy neutrons can be neglected. For producing the 14.8 MeV neutron on 0˚ to the beam, it is necessary to lower deuteron energy to about 200 keV. Such low energy causes two problems. One is that stable operation and beam transport is difficult for our accelerator. The other is that loss of the deuteron beam in the tantalum foil, as shown in Fig. 4, becomes significant and then the neutron yield decreases. Therefore, the point for the 14.8 MeV field was determined on the angle of 45˚ to the beam by swinging the calibration table in order to increase the deuteron energy.

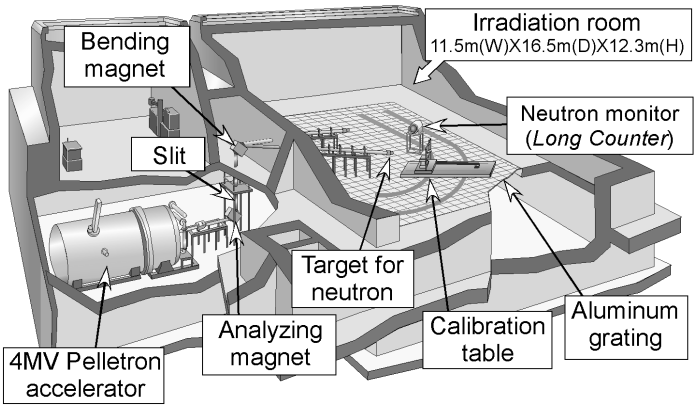

FIG. 2. Cut-away view of the mono-energetic neutron fields.

3.1. Monoenergetic and maxwell spectrum neutron beams (<5 MeV)

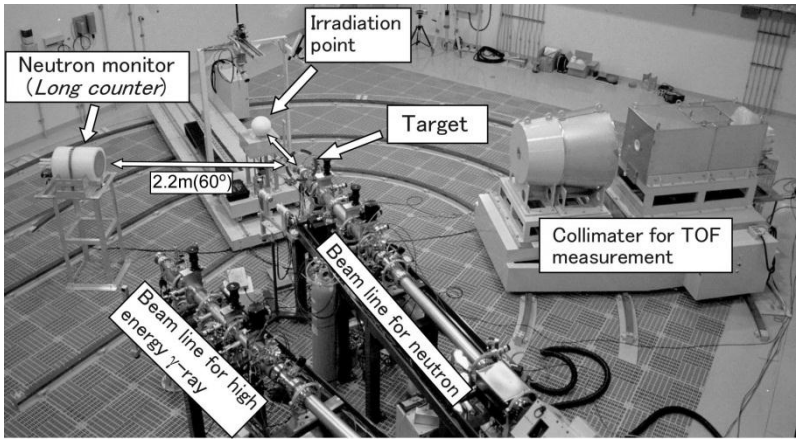

FIG. 3. Photograph of the irradiation room.

3. TARGET STRUCTURE

The neutron source reactions employed in these fields are $^{45}Sc(p,n)^{45}Ti$ for the 8 and 27 keV fields, $^{7}Li(p,n)^{7}Be$ for the 144, 250 and 565 keV, $^{3}H(p,n)^{3}He$ for the 1.2 and 2.5 MeV fields, $^{2}H(d,n)^{3}He$ for the 5.0 MeV field and $^{3}H(d,n)^{4}He$ for the 14.8 and 19 MeV fields. The target structure is shown in Fig. 4. The targets for the $^{45}Sc(p,n)^{45}Ti$, $^{7}Li(p,n)^{7}Be$ and $^{19}F(p,\alpha\gamma)^{16}O$ reactions were prepared by vacuum-evaporating scandium metal, lithium fluoride and calcium fluoride with 17 mm diameters on platinum or molybdenum backing disks with 0.5 mm thicknesses. For the $^{3}H(p,n)^{3}He$ and $^{3}H(d,n)^{4}He$ reactions, the target was prepared by the absorption of tritium in titanium layer which was vacuum-evaporated on a copper disk. Additionally a tantalum foil with 3 μm thickness was set at 2.5 mm before the target in order to prevent the pollution of the beam line by the tritium. For the $^{2}H(d,n)^{3}He$ reaction, a gas target was prepared by filling a gas cell with 0.1 MPa D_2 gas. The cell consists of an entrance window made of a molybdenum foil with 5 μm thickness, a tantalum aperture with a 10 mm hole and a platinum beam stopper with 0.5 mm thickness. The length of the gas cell is 23.5 mm.

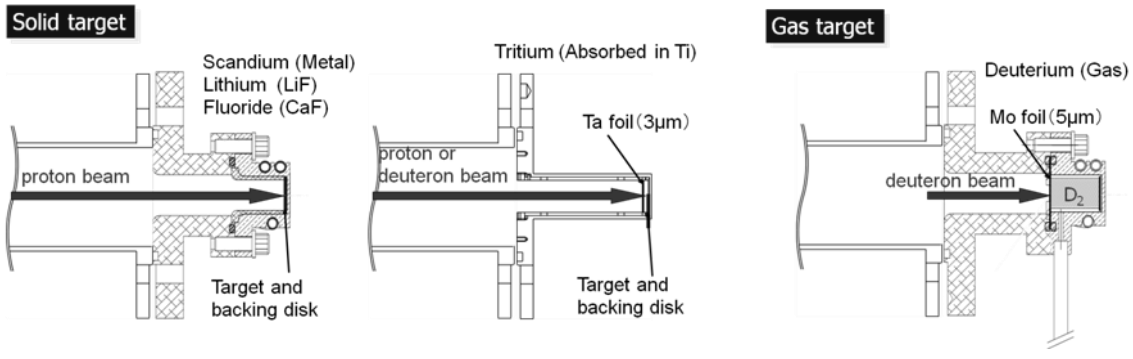

Fig. 4. Target structures.

3.1. Monoenergetic and maxwell spectrum neutron beams (<5 MeV)

4. PULSING SYSTEM

A pulsed beam can be derived by a pulsing system installed in the high-voltage terminal of the accelerator. The pulsing system consists of a sweeper and a klystron buncher. The minimum length of the pulsed beam is about 2 ns in full width at half maximum (FWHM). The repetition frequency of the pulsed beam can be chosen from 0.5, 1, 2 and 4 MHz. A triggering signal of the pulsed beam can be obtained by a capacitive pickup probe with a cylindrical electrode. The probe was installed in the beam line at about 25 cm before the target.

The width of the pulsed beam was measured by a BC501A liquid scintillation detector in the 565 keV field. Figures 5 and 6 show the block diagram of the measuring system and a time spectrum of the flash gamma ray which was produced by bombarding the target with an accelerated proton. The pulse width of the proton beam was evaluated to be 1.95 ns in FWHM.

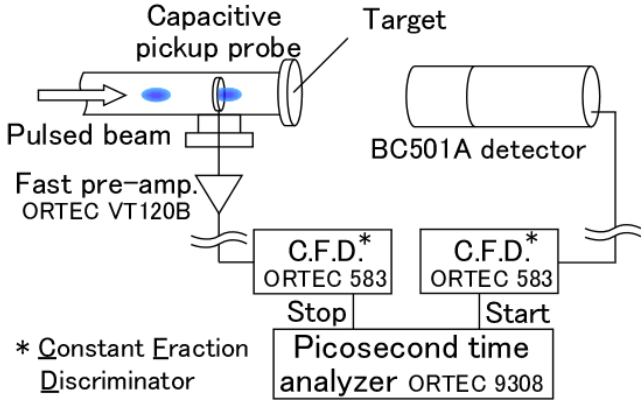

FIG. 5. Block diagram of the pulse width measuring system.

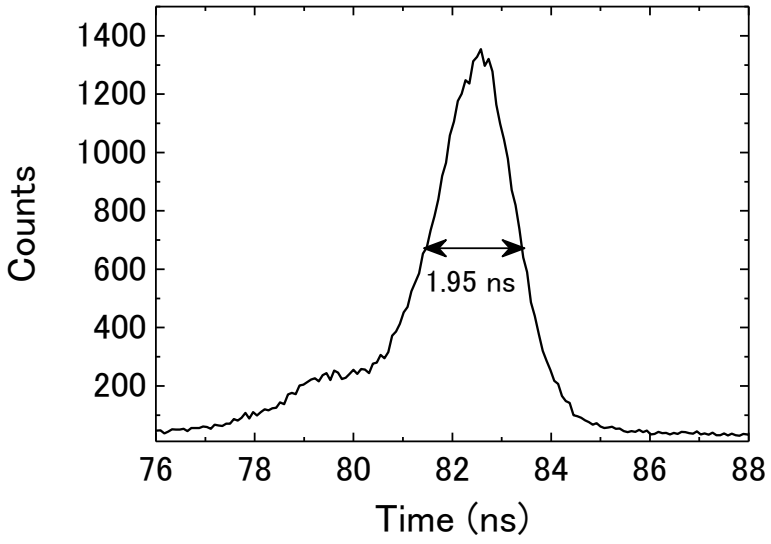

Fig. 6. Time spectrum measured with a BC501A detector in the 565 keV mono-energetic neutron field.

3.1. Monoenergetic and maxwell spectrum neutron beams (<5 MeV)

5. NEUTRON FLUENCE

The neutron fluence at the irradiation point is a key characteristic and should be precisely determined for the development of the mono-energetic neutron fields. The fluences in the 144, 565 keV and 5.0, 14.8 MeV fields were measured using a Bonner sphere, which consists of a spherical moderator made of polyethylene and a BF_3 proportional counter as a thermal neutron detector. The fluence responses of the Bonner sphere were calibrated at the Japanese primary standard fields with the same neutron energies in the National Institute of Advanced Industrial Science and Technology (AIST). For the 8 keV field, a lithium glass scintillation detector was used to measure the neutron fluence. For the 27 and 250 keV fields, the neutron fluences were determined with the Bonner sphere whose responses were calculated through interpolation or extrapolation of the calibrated response at the primary standard with the MCNP-4C code [6]. For the 1.2 MeV and 2.5 MeV fields, a silicon semi-conductor detector with a polyethylene radiator was developed to measure the neutron fluence. For 19 MeV field, the neutron fluence was determined with the BC501A detector whose response was calibrated at the 14.8 MeV field.

Table 1 summarizes the maximum neutron fluence rates and maximum ambient dose equivalent rates. For the fields with neutron energies 144 keV and above, the fluence rates are high enough to calibrate neutron detectors for radiation protection, which is the main purpose of these fields. Though the fluence rates in the 8 and 27 keV fields are low, they are practicable available for the calibration of the detectors with relatively high sensitivity to neutrons. On the other hand, these fluence rates should not be high enough to obtain the nuclear data of the cross-section using an activation method. However, these fields are available to obtain the nuclear data using *in–situ* measurements such as prompt gamma ray analysis [7].

TABLE 1. SUMMARY OF THE MAXIMUM FLUENCE RATES AND AMBIENT DOSE EQUIVALENT RATES OF THE MONO-ENERGETIC NEUTRON FIELDS. THESE VALUES ARE EVALUATED AT 50 CM FROM THE TARGET FOR 8 AND 27 KEV FIELDS AND AT 100CM FROM THE TARGET FOR THE OTHER FIELDS

Neutron Energy	Maximum beam current [□A]	Maximum fluence rate ($cm^{-2}s^{-1}$)	Ambient dose equivalent rate H*(10) [mSv/h]
8 keV	50	70	0.0024
27 keV	50	110	0.0085
144 keV	50	3,000	1.4
250 keV	50	2,000	1.4
565 keV	50	6,000	7
1.2 MeV	6	1,000	1.5
2.5 MeV	6	2,000	3
5.0 MeV	3	7,000	10

6. SUMMARY

The mono-energetic neutron calibration fields are developed using the 4MV Pelletron accelerator for type-test of the energy responses of neutron detectors. The neutron fields with the energies of 8, 27, 144, 250, 565 keV and 1.2, 2.5, 5.0, 14.8, 19 MeV are established and provided to users inside and outside of the JAEA. The maximum fluence rates should not be high enough to measure the nuclear cross-sections using an activation method. However, they are available to obtain the nuclear data by *in-situ* measurement such as the prompt gamma ray analysis.

REFERENCES

[1] TANIMURA, Y., et al., Construction of 144, 565 KeV and 5.0 MeV Monoenergetic Neutron Calibration Fields at JAERI, Radiat. Prot. Dosim., 110 (2004), pp. 85-89.
[2] TANIMURA, Y., et al., Construction of Monoenergetic Neutron Calibration Fields Using 45Sc(p,n)45Ti Reaction at JAEA, Radiat. Prot. Dosim., 126 (2007), pp. 8-12.
[3] SHIKAZE, Y., Development of the Neutron Calibration Fields using Accelerators at FRS and TIARA of JAEA, J. Nucl. Sci. Technol., Suppl. 5 (2008), pp. 209-212.
[4] ISO, Reference meutron radiations – Part 1: Characteristics and methods of production, ISO 8529-1, (2001).
[5] Japanese Industrial Standard, Method of calibration for neutron dose equivalent (rate) meters, JIS Z 4521: 2006 (2006) [in Japanese].
[6] BRIESMEISTER, J. F., "MCNP – A general Monte Carlo N-particle transport code, version 4C", LA-13709-M (2000).
[7] SEGAWA, M., et al., "A facility for measurements of (n,γ) cross-sections of a nucleus in the range $0.008 < E_n < 20$ MeV", Nucl. Instrum. Meth, A618 (2010) 153-159.

3.1. Monoenergetic and maxwell spectrum neutron beams (<5 MeV)

NEUTRON EXPERIMENTAL FACILITIES FOR NUCLEAR DATA MEASUREMENTS AT IPPE

V. KHRYACHKOV, B. ZHURAVLEV

State Scientific Center of Russia
Institute of Physics and Power Engineering,
249033 Obninsk,
Russian Federation
Email: hva@ippe.ru

Abstract

Neutron facilities used for the measurements of nuclear data at Institute of Physics and Power Engineering are presented. These facilities are created on the basis of six accelerators (two cascade generators, two Van-de-Graaff and two tandem Van-de-Graaff accelerators produced the continuous and pulsed beams of protons and deuterons in the energy range from 0.3 MeV to 15 MeV) and allow to obtain neutron sources with energy from 30 keV to 30 MeV. The measurements of neutron - charge particle, differential elastic and inelastic neutron scattering, neutron fission, neutron capture cross-sections, yields of the fission products and delayed neutrons, neutron emission cross-sections in various reactions and neutron leakage spectra from spherical samples for testing of neutron libraries are carried out. The results of the studies carried out are well-known in the leading neutron centers.

1. NEUTRON SOURCES OF IPPE

Neutron facilities used for the measurements of nuclear data at Institute of Physics and Power Engineering (IPPE) are created on the basis of six electrostatic accelerators. Two cascade generators, two Van-de-Graaff and two tandem Van-de-Graaff accelerators produced the continuous and pulsed beams of protons and deuterons in the energy range of 0.3 MeV to 15 MeV allow to obtain neutron sources with energy range of 30 keV to 30 MeV. The main characteristics of the IPPE high-voltage accelerators are presented in the table 1.

Using the pulsed beams of these accelerators in Division of Neutron and Nuclear Physics of IPPE the time-of-flight neutron spectroscopy techniques are developed and on this base during a long time carried out the measurements of differential neutron emission and neutron induced cross-sections for a wide range of nuclear reactions. The statistical properties of high-excited nuclei, the role of different reaction mechanisms, the competition of different nucleus decay channels were studied and a number of requirements in nuclear data were satisfied. In the present time in Division were carried out next studies:

2. DOUBLE-DIFFERENTIAL NEUTRON EMISSION CROSS-SECTIONS MEASUREMENTS

The measurements and analysis of double-differential neutron emission cross-sections in reactions induced by charge particles to obtain the new data on nuclear level density in a wide range of excitation energy and spin [1].

The time-of-flight spectrometers on base of 5 MV and 7.5 MV pulsed tandem Van-de-Graaff accelerators (EGP-10M and EGP-15) producing a beams of protons, deuterons and light ions are used for these measurements.

3.1. Monoenergetic and maxwell spectrum neutron beams (<5 MeV)

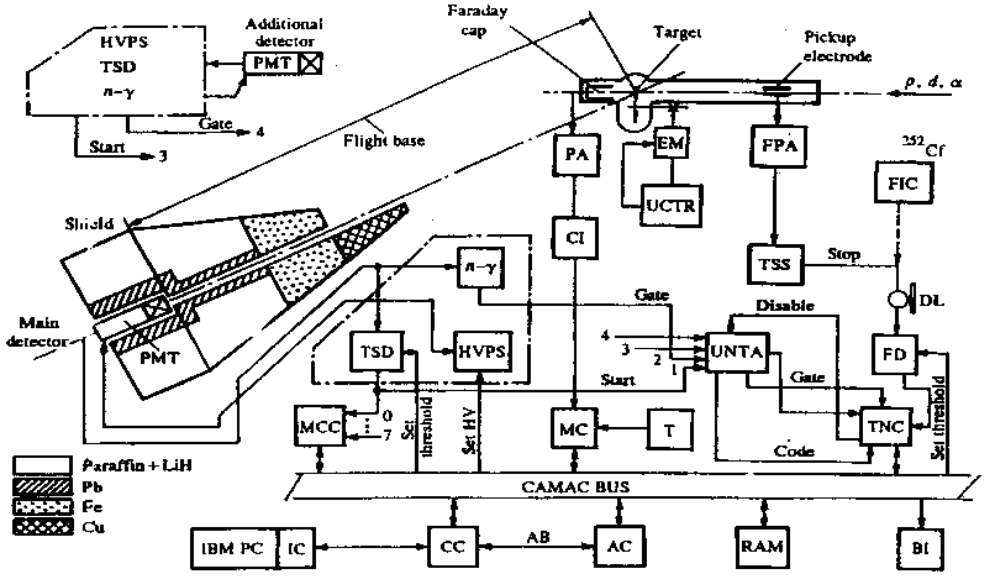

FIG. 1. Block diagram of the spectrometer, its detecting, storing, and data processing circuits; HVPS – high-voltage power supply; TSD) tunable threshold discriminator: n-γ) separation circuit; PA) preamplifier; CI) current integrator; EM) electric motor; UCTP) unit controlling the target position; FPA) fast preamplifier: TSS) time signal shaper; FIC) fission ionization chamber; DL) delay unit; FD) fast discriminator; UMTA) unit of multidetector time analysis; MCC) multichannel counter; MC) monitoring counter; T) timer; TNC) time to number converter; BI) bus indicator; RAM) random-access memory; AC) additional controller; CC) 106A crate controller; IC) interface circuit; AB) additional bus.

The spectrometer [2] has following parameters: pulse width – 1 ns, frequency – 1; 2; 5 MHz, average current – 1 mkA, threshold of neutron detectors on the basis of p-terphenyl and stilben crystals with (n-γ) discrimination – 0.1 MeV, massive shielding of detector may move around the target in the angle range of (0-160) degrees with different steps. For obtaining of monoenergetic neutrons there are deuterium and tritium gas targets allowing to produce incident neutron energies of 2 MeV to 30 MeV. Block diagram of the spectrometer, its detecting, storing, data processing circuits are presented in Fig. 1.

3. INELASTIC NEUTRON SCATTERING MEASUREMENTS

The measurements of inelastic neutron scattering near threshold of low-lying levels to obtain the information about the mechanisms of neutron emission and to satisfy the requirements on these data. The time-of-flight spectrometer on base of 4.5 MV Van-de-Graaff accelerator (EG-1) producing a beams of protons and deuterons is used for these measurements. The spectrometer has following main features: incident neutron energy – 0.2-2 MeV, Li(p,n) and T(p,n) reactions with solid targets are used, energy threshold of neutron scintillation detector – 0.1 MeV, flight path – 1.5-2 m, pulse width – 1 ns, frequency – 1; 2 MHz, average current – 5 mkA, angle range measured – 0-120 degrees. The results of measurements for ^{238}U are presented in works [3,4].

3.1. Monoenergetic and maxwell spectrum neutron beams (<5 MeV)

TABLE 1. THE MAIN CHARACTERISTICS OF THE IPPE HIGH-VOLTAGE ACCELERATORS

Accelerator	Ions energy (MeV)	Ions	Operating mode	Current parameters
EG-2,5 (1961 г.)	0,2 – 2,7	H, D, He, N, Ar, O	DC	0,1 – 30,0 μA 0,01 – 10,0 μA
EG-1 (1958 г.)	0,9 – 4,5	H, D	DC Pulsed	1,0 – 20,0 μA Amplitude 2 -3 mA Pulse duration 1 – 2 ns Frequency 1 – 5 MHz
EGP-10M (1968 г.)	3,5 – 9,0	H, D	DC Pulsed	1,0 – 10,0 μA Amplitude 0,4 mA Pulse duration 1 – 2 ns Frequency 1 – 5 MHz
KG-2,5(1968 г.)	0.3 – 2,2	H, D	DC	0,1 – 2,0 mA
KG-0,3 (1968 г.)	0,05 – 0,3	H, D	DC Pulsed	0,01 – 2,0 mA Amplitude 3 -5 mA Pulse duration 1 – 3 ns Frequency 0,5 – 2,5 MHz
EGP-15(1993)	4,0 – 12,0	H, DF, C, O, Al, Si, Cl, Ni, Fe, Zr	DC Pulsed	0,01 – 5,0 μA Amplitude 0,3 -0,5 mA Pulse duration 1 – 3 ns Frequency 1,0 – 5 MHz 0,01 – 1,0 μA

THE SPECTROSCOPY OF LEAKAGE NEUTRONS FROM THICK SPHERES

The energy spectroscopy of leakage neutrons from thick spheres with 14 MeV and ^{252}Cf neutron sources in the center for testing of transport codes and neutron libraries.

Time-of-flight spectrometer at pulsed neutron generator KG-0.3 producing 280 keV deuterons with 2.5 ns width of pulse, 500 kHz repetition frequency and with solid tritium target is used. Flight path – from 2-7 m, energy threshold of neutron detector – 0.05 MeV. Total number of 14 MeV neutrons are determined by measuring of α - associated particles. This facility we use also for measurements of double-differential inelastic scattering and gamma production cross-sections at incident energy of 14 MeV [5]. The ^{252}Cf neutron source was electrodeposited inside a 1 cm circle of thin stainless-steel backing with an initial decay rate of 350 kHz and situated in a fast ionization chamber for fission fragments registration [6]. Full time resolution of the time-of-flight spectrometer with such source was 2.5-3 ns. Lay-out of experiment for measuring the neutron leakage spectra from thick spheres is presented in Fig. 2. Neutron leakage spectra from lead sphere with 14 MeV neutron source and with ^{252}Cf neutron source are shown in Figs. 3 and 4.

3.1. Monoenergetic and maxwell spectrum neutron beams (<5 MeV)

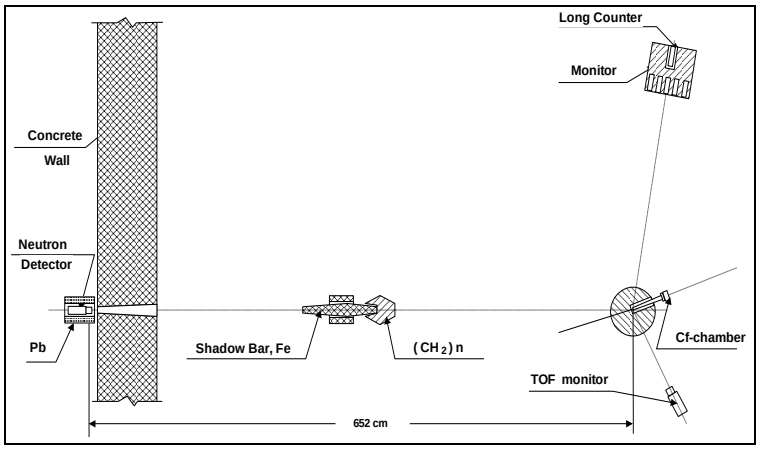

FIG.2. Lay-out of experiment for measuring the neutron leakage spectra from thick spheres

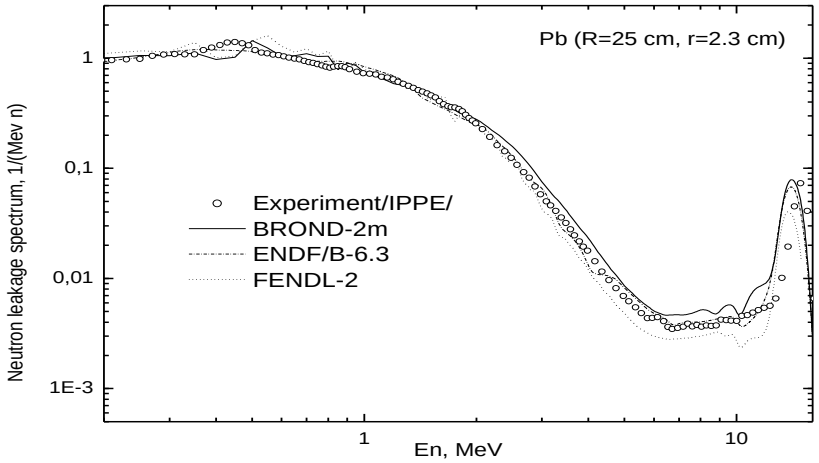

FIG. 3. Neutron leakage spectra from lead sphere with 14 MeV neutron source.

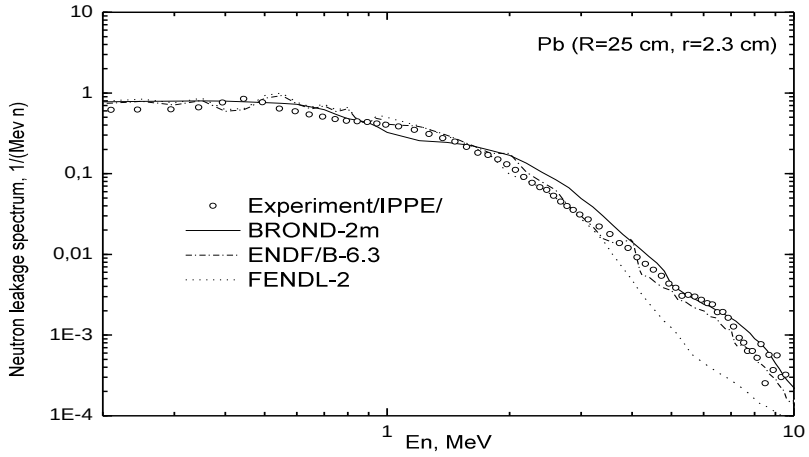

FIG. 4. Neutron leakage spectra from lead sphere with ^{252}Cf neutron source

3.1. Monoenergetic and maxwell spectrum neutron beams (<5 MeV)

Except measuring of leakage spectra such ^{252}Cf sources of prompt fission neutrons we use for determination of detector efficiency in real geometry on all enumerated time-of-flight spectrometers in laboratory, because spectrum of neutrons from spontaneous fission of ^{252}Cf is known in the range of 0.1 MeV to 10 MeV with 3% accuracy.

5. MEASUREMENTS OF CHARGE PARTICLES YIELDS IN NEUTRON INDUCED REACTIONS

The spectrometer on the basis of twin ionization chamber with Frisch grid and the waveform digitizer installed at the cascade generator KG-2.5 and EG-1 is used for measurements mass-energy-angle-charge correlations of fission fragments and partial cross-sections of (n,α), (n, p), (n,t) reactions. Block diagram of the spectrometer is shown in Fig. 5.

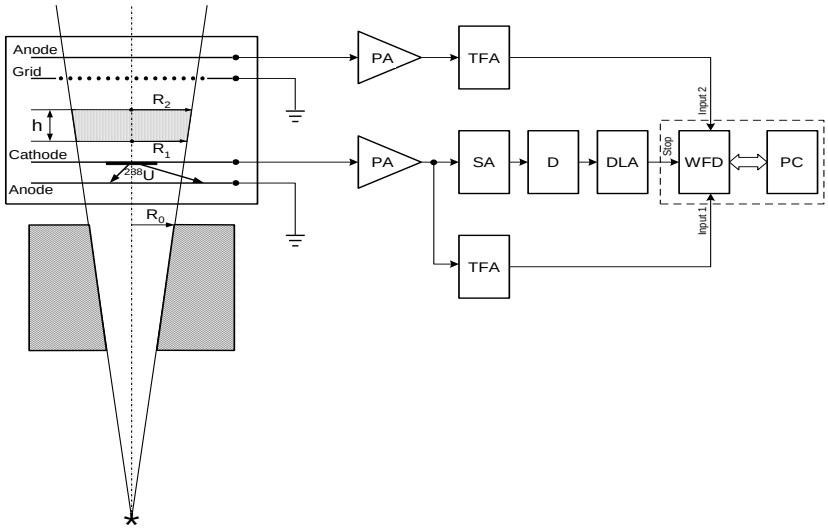

FIG. 5. Block diagram of experimental setup. PA – preamplifier, TFA – timing filter amplifier, D – discriminator, SA – spectroscopy amplifier, DLA – delay line amplifier, WFD – waveform digitizer, PC – personal computer.

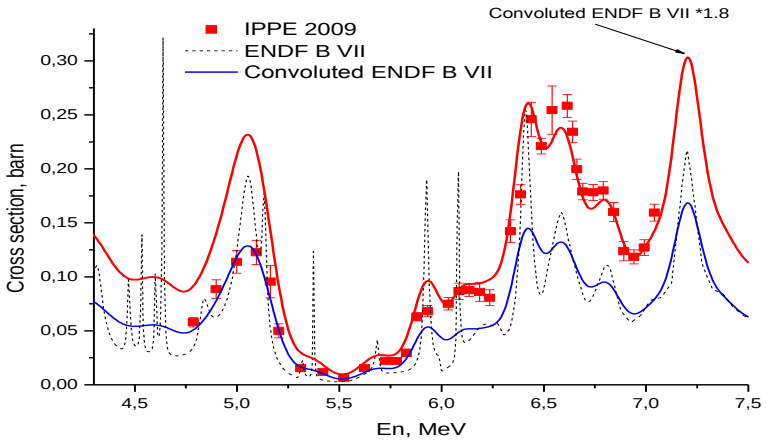

FIG. 6. Energy dependence of ^{16}O (n, α_0) cross section.

3.1. Monoenergetic and maxwell spectrum neutron beams (<5 MeV)

Anode-grid distance is 2 mm, while cathode-grid distance is 40 mm. The working gas is a mixture of 90% of Ar and 10% of CH_4 under pressure of 0.65 atm. High voltage of 3.5 kV is applied to the cathode. Applying the waveform digitizer with this ionization chamber allowed to have much more information on fission fragments properties. Figure 6 shows the energy dependence of $^{16}O(n,\alpha_0)$ cross section obtained with this ionization chamber on accelerators EG-1 with continuous beams of proton and deuterons [7].

6. THE MEASUREMENTS OF FISSION CROSS-SECTIONS

The measurements of fission cross-sections on high-activity Am and Cm – isotopes the fission detector is a low-mass double-ionization chamber. Two parts of fissile samples can be inserted inside the container and two fission cross-section ratios can be measured in one experiment. The time-of-flight technique on the basis of Van-de-Graaff accelerator EG-1 is used in the fission rate measurement to suppress the spontaneous fission.

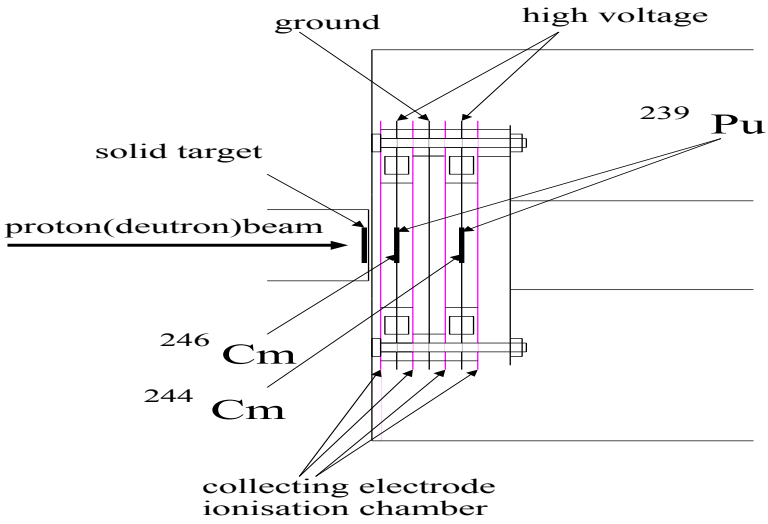

FIG. 7. Lay-out of experiment for measuring fission cross-sections

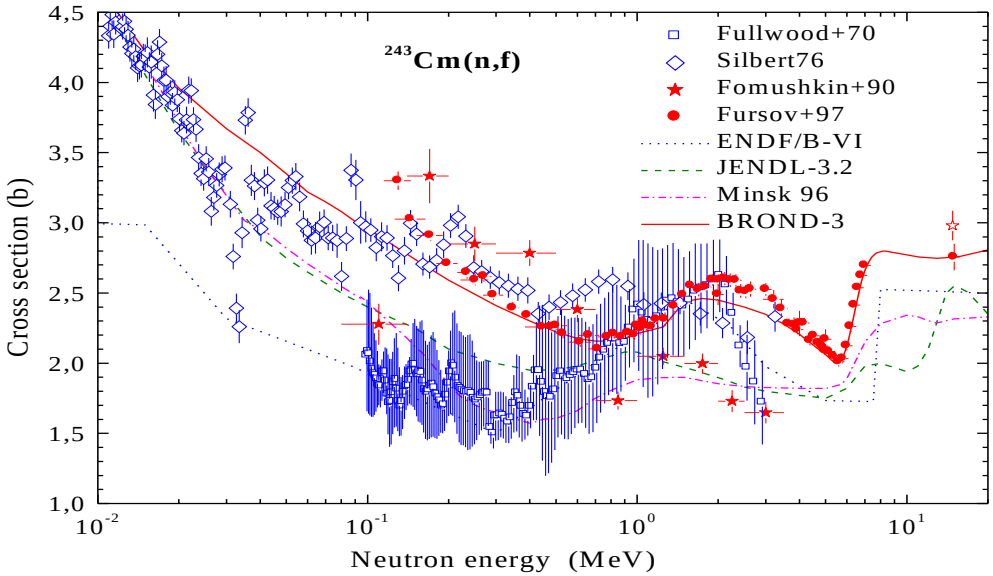

FIG. 8. Energy dependence of ^{243}Cm fission cross section.

3.1. Monoenergetic and maxwell spectrum neutron beams (<5 MeV)

^{239}Pu was used as a reference sample (standard), because half-life and spectrum of α particles for ^{239}Pu are more suitable for α particle counting and mass ratio determination. Figure 7 demonstrates lay-out of experiment for measuring of fission cross-sections and Fig. 8 the measured data for ^{243}Cm in comparison with other measurements and evaluations of ENDF/B-6 and JENDL-3 libraries [8].

7. THE DELAYED NEUTRON MEASUREMENTS

Experimental set-up employed in the delayed neutron measurements was installed on the beam line of electrostatic accelerators CG-2.5 and EG-2.5 (Fig. 9). The measurements of absolute total yields, relative abundances and periods of delayed neutrons in neutron energy range of 0.5 MeV to 15 MeV are based on periodic irradiation of fissionable samples by neutrons from suitable nuclear reaction at the different accelerators and following measurements of the delayed neutron activity. The fast pneumatic transfer system is used for transportation of a sample from irradiation position to the neutron detector. The minimal sample delivery time is about 150 ms. Neutron detector is an assembly of 30 boron counters distributed in polyethylene along three concentric circles [9]. At the present time the measurements of the total yields, relative abundances and periods of delayed neutrons have been made for fast neutron induced fission of ^{232}Th, ^{233}U, ^{235}U, ^{237}Np, ^{239}Pu. Fig. 10 demonstrates the measured data for ^{233}U in comparison with other measurements and evaluations.

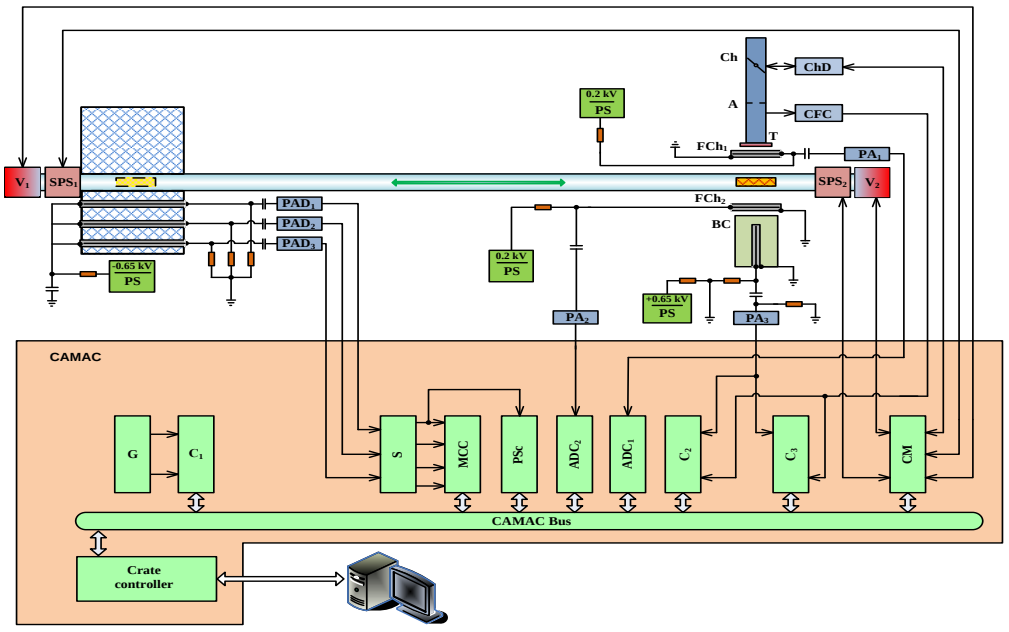

FIG. 9. Block diagram of the experimental setup employed in the delayed neutron measurements: (PAD) preamplifier, amplifier, and discriminator; (S) summator; (PA) preamplifier and amplifier; (V) electromagnetic valve; (SPS) sample position sensor; (CM) controlled unit; (CFC) current-to-frequency converter; (ADC) analog-to-digital converter; (PSc) preset-scaler ; (MCC) multichannel counter; (G) quartz generator of pulses; (PS) power source; (Ch) chopper; (ChD) magnetic chopper drive; (A) ion guide aperture; (T) accelerator target; (FCh) fission chamber; (BC) boron counter of neutrons; (C1) counter with a preset exposure time; (C2) counter of total counts from the CFC and BC; and (C3) counter of the CFC and BC counts within preset time intervals.

3.1. Monoenergetic and maxwell spectrum neutron beams (<5 MeV)

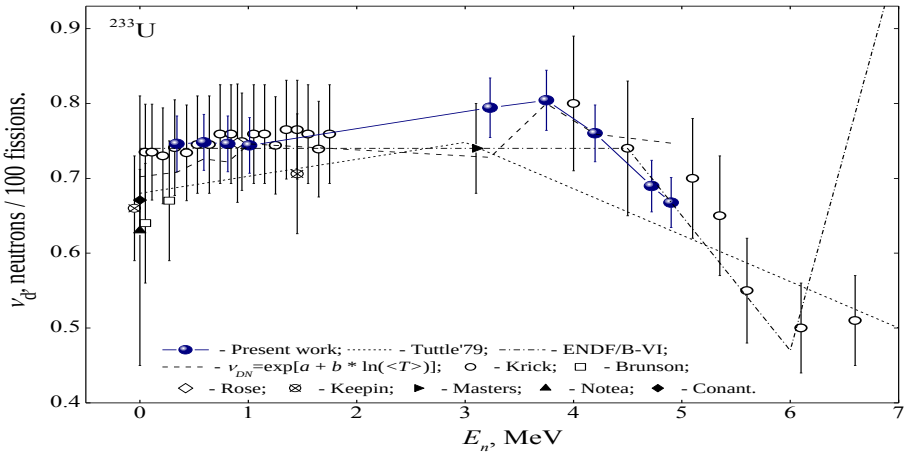

FIG. 10. The energy dependence of the total delayed neutron yield from fission of ^{233}U.

REFERENCES

[1] ZHURAVLEV, B.V., et al., Physics of Atomic Nuclei, 2012, Vol. 75, No. 9, p. 1035-1040.

[2] DEMENKOV, V.G., et al., Instruments and Experimental Techniques, Vol.38, No.3, Part 1, 1995, p. 314.

[3] KORNILOV. N.V., and Kagalenko, A.B., Nuclear Science and Engineering, V.120, p.55, 1995

[4] KORNILOV, N.V., et al., Proc. of 5 Inter. Seminar on Interaction of Neutrons with Nuclei. Dubna, May 14-17,1997. JINR E3-97-213, P. 297-304.

[5] ZHURAVLEV, B.V., et al., Proc. of Inter. Conference on Nuclear Data for Science and Technology, Santa Fe, USA, 26 September-1 October 2004, Part 1, p. 490-493.

[6] ZHURAVLEV, B.V., et al., Proc. of 13 Inter. Seminar on Interaction of Neutrons with Nuclei. Dubna, May 25-28, 2005. JINR E3-2006-7, p. 106-109.

[7] KHRYACHKOV V.A., et al., Workshop proceedings "Nuclear Measurements, Evaluations and Applications – NEMEA – 6, 25 – 28 October 2010, Krakow, Poland, p. 287.

[8] FURSOV, B.I., et al., Proc. of Inter. Conference on Nuclear Data for Science and Technology, Trieste, 19-24 May 1997, Part 1, p. 488-490.

[9] PIKSAIKIN, V.M., et al., Proc. of Inter. Conference on Nuclear Data for Science and Technology, Trieste, 19-24 May 1997, Part 1, p.485-487.

3.1. Monoenergetic and maxwell spectrum neutron beams (<5 MeV)

MEASUREMENTS WITH MONOENERGETIC FAST NEUTRONS AT THE UNIVERSITY OF KENTUCKY ACCELERATOR LABORATORY

J.R. VANHOY[*], S.F. HICKS[**], H.E. BABER[***], B.P. CRIDER[***], E.E. PETERS[***], F.M. PRADOS-ESTÉVEZ[***], M.T. MCELLISTREM[***], S.W. YATES[***], B.R. CHAMPINE[+]

[*]Department of Physics, U.S. Naval Academy, Annapolis, Maryland 21402 USA
[**]Department of Physics, University of Dallas, Irving, Texas 75062 USA
[***]Departments of Chemistry and Physics & Astronomy, University of Kentucky, Lexington, Kentucky 40506 USA
[+]Department of Physics & Nuclear Engineering, U.S. Military Academy, West Point, New York 10996 USA
Email: vanhoy@usna.edu

Abstract

The University of Kentucky Accelerator Laboratory, which is operated entirely hands-on by the internal and external user groups, has served the scientific community continuously for 50 years. Features of the laboratory specific to neutron-induced reactions are presented and techniques for data analysis are discussed.

1. INTRODUCTION

The High Voltage Engineering Corporation single-ended 5.5 MV Model CN Van de Graaff accelerator was purchased with funding from the Governor of Kentucky and the Kentucky Research Foundation [1] and installed at the University of Kentucky in 1963. The original installation featured an rf ion source capable of producing intense beams of all gaseous ions, an in-terminal chopping system, and a Mobley post-acceleration bunching system [2]. From the beginning the facility has served as a factory for pulsed monoenergetic fast neutrons.

Early experiments involved γ ray nuclear spectroscopy with (n,p) and (p,n) reactions. Neutron time-of-flight measurements emerged in the early 1970s and these led to tests of the Hauser-Feshbach (HF) treatments explaining reaction cross sections. These soon evolved into studies of deviations and refinements to HF model theory. The development of high-purity germanium detectors (HPGe) during the 1980s stimulated a rapid growth in the (n,n'γ) program and development of new techniques for extracting spectroscopic information for testing advanced collective and single-particle models of nuclear structure. Electromagnetic transition rate determinations via Doppler-shift attenuation measurements became the hallmark signature of the laboratory.

The laboratory has served other fields with studies of atomic excitation mechanisms, radiation detector development, nuclear astrophysics, radio-pharmaceutical development, and testing neutron active interrogation systems for illicit materials.

In the following sections, we describe features of the accelerator itself and the techniques applied to (n,n) and (n,n'γ) measurements.

2. FACILITY DESCRIPTION

The laboratory underwent a significant upgrade in 1989 with the installation of a completely new terminal ion source pulsing system, Dowlish spiral-inclined field accelerator tubes, new column and tube resistors, and a new rf-cavity post-acceleration bunching system.

The upgrade greatly improved the reliability and stability of the accelerator, extended source maintenance cycles, reduced the radiation environment, and enabled operation up to 7 MV on terminal. The terminal ion pulsing system can deliver several microamperes of protons, deuterons, ^{3}He, or ^{4}He ions on target with ~1 ns bunch widths. Use of the post acceleration buncher can reduce pulse widths to ~250 ps.

The terminal (Fig. *1*) is a modified version of the Studsvik design [3,4]. Ions are generated in an rf bottle and pre-accelerated with an extraction electrode. An Einzel lens focuses the beam onto a chopping aperture. The beam is swept through an elliptical path across the aperture with sweep plates operating at 1.875 MHz. A velocity selector before the aperture provides a clean chopped beam. Immediately following, the beam passes through a double-gap buncher with two possible buncher tube lengths. An additional gap electrode couples with the fringing field of the accelerator tube to provide focusing of the ion beam during acceleration. An Einzel lens was placed just before the entrance of the accelerator tube to enable a beam waist in the middle of the 90-degree analyzing magnet, but its field gradient has proven to be too weak.

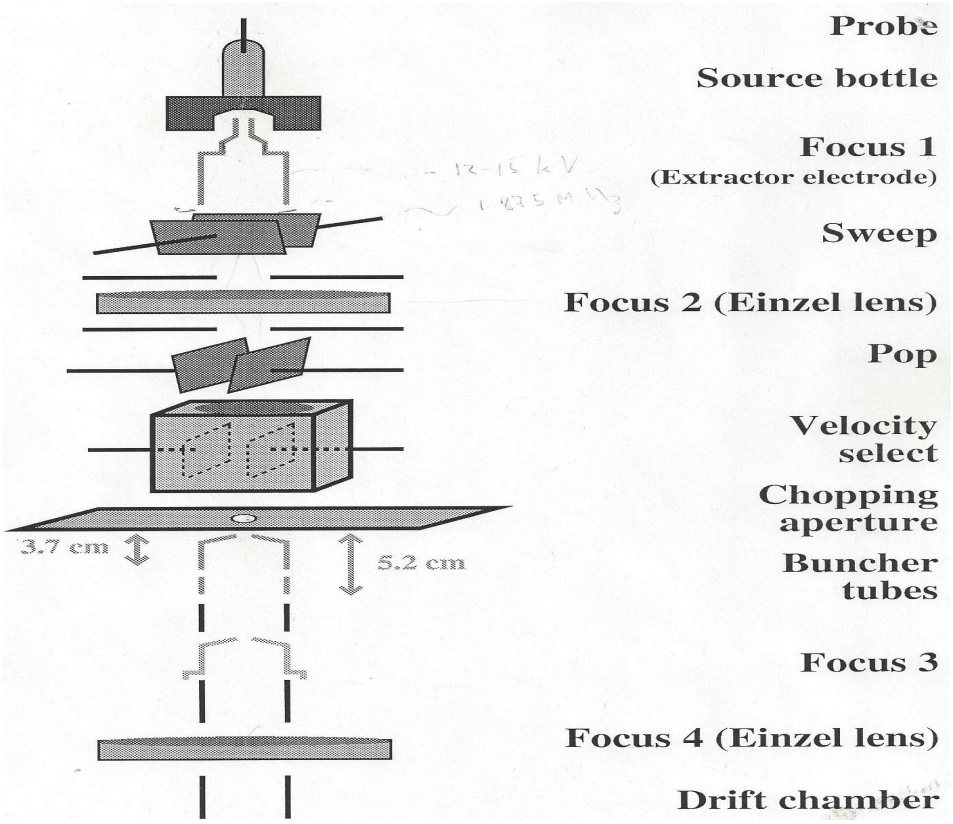

FIG. 1. Ion source and pulsing/bunching system.

3.1. Monoenergetic and maxwell spectrum neutron beams (<5 MeV)

Because the CN is a vertical design, a 90 degree analyzing magnet redirects the beam horizontally. The analyzing magnet is mounted on a turret which rotates to direct the beam into one of seven beam lines in two experimental halls.

The beam lines have served a variety of purposes over the years and have accommodated setups for charged-particle scattering, multi-sample proton-induced x ray and γ ray emission (PIXE, PIGE) measurements, neutron detection with a 4π ball, charged-particle capture measurements, and neutron active-interrogation development, as well as neutron scattering and reaction measurements to be discussed.

One experimental hall and a beam line were specially constructed with a 4-meter flight path for neutron time-of-flight (TOF) measurements. It has a high ceiling and a false floor which covers a 2.8 m deep pit. The primary neutron production reaction is ^{3}H(p,n) in a gas cell constructed of stainless steel and lined with a tantalum foil and beam stopper (Fig. *2*). The entrance foil is 0.13 mil (3.3 μm) molybdenum. The inner gas cell length is 3 cm and a pressure of 1 atmosphere is typically used. Detectors are mounted on a carriage which can be rotated to cover scattering angles up to 155^{o}. The carriage supports a full-length collimation system.

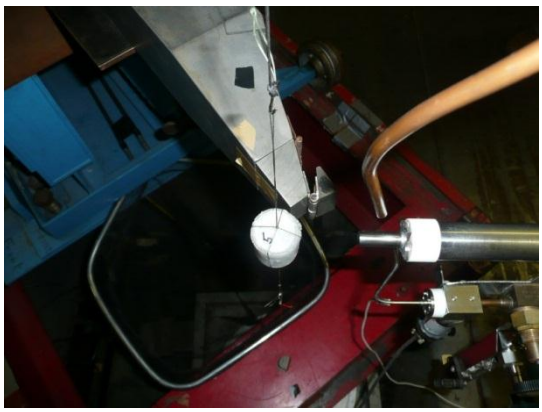

FIG. 2. Top-down view of the end of the neutron TOF beam line. The accelerated charged-particle beam enters from the right and produces neutrons in the 3-cm long gas cell at the end of the beam line. The tungsten shadow bar prevents the detector from directly viewing the gas cell.

Although neutron fluences produced in this fashion are considered monoenergetic, there is some total effective spread in the energy due to straggling in the cell entrance foil, energy loss throughout the ^{3}H gas, and the kinematic neutron energy spread across the scattering sample.

Neutron production rates are recorded with a long counter (LC) [5,6] and a forward monitor (FM) liquid scintillator. The long counter is positioned at ~85^{o} with respect to the beam direction. At this angle, the source-neutron energy is in a relatively smoothly varying region of the long counter efficiency curve, avoiding resonances in the response [7]. The FM is placed at 45^{o} and high on the wall to provide a direct, collimated view of the gas cell. On-pulse source neutrons are identified in the FM by TOF and pulse shape discrimination (PSD).

3.1. Monoenergetic and maxwell spectrum neutron beams (<5 MeV)

For many measurements, the optimum samples for (n,n), (n,n') and (n,n'γ) measurements are solid cylinders of the isotopically enriched single element of interest. For some samples, such as metallic sodium or powdered oxides, the sample is enclosed in a thin metal or polypropylene container. Care must be taken to eliminate effects arising from the container in the neutron or γ ray detector spectrum.

3. (N,N) MEASUREMENTS AND TECHNIQUES

3.1 OVERVIEW

Scattered neutrons are detected and analyzed using TOF techniques. The carriage configuration is shown in Fig. *3*. A 2.5 cm thick × 11 m diameter C_6D_6 liquid scintillator is employed for the 'MAIN' neutron detector. C_6D_6 provides better definition in the pulse amplitude spectrum and the 2.5 cm thick fluid is important for timing resolution. Pulse-shape discrimination (PSD) is used to separate neutron and γ ray events in the detector and remove unwanted γ ray background. An example of a TOF spectrum from recent scattering measurements on ^{23}Na is shown in Fig. 4.

FIG. 3 Neutron time-of-flight end station pictured at $\theta = 0^o$. Copper is an effective shield for both neutrons and γ rays and is visible in the section nearest the gas cell [8]. The remaining red collimation is Li_2CO_3-loaded paraffin with collimation rings. The 'MAIN' detector is housed in the last blue shield which is filled with loaded paraffin containing several Cd and Pb concentric rings to reduce thermal neutrons and photons in the vicinity of the detector.

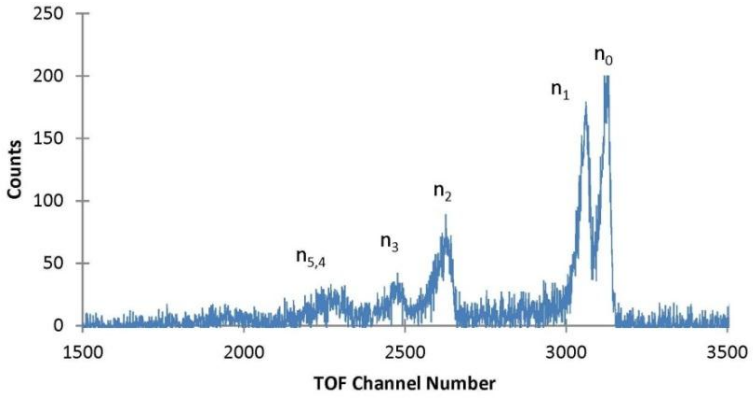

FIG.4. TOF spectrum of 4.0-MeV neutrons scattered at 100^o from ^{23}Na. Flight time increases to the left. Peaks corresponding to scattering to the various final states in ^{23}Na are labeled.

3.1. Monoenergetic and maxwell spectrum neutron beams (<5 MeV)

Peaks in the TOF spectra are fitted with SAN12, an in-house program that fits each neutron peak with two Gaussians plus tails. A specialized fitting code is required (rather than the single Gaussian + tail gamma ray codes) because peaks are relatively broad, have tails, and overlap. SAN12 incorporates kinematic constraints into peak positions and peak shapes.

3.2. NEUTRON DETECTION EFFICIENCY FOR THE MAIN DETECTOR

The general energy dependence of the MAIN detector efficiency, $eff(E_n)$, can be described analytically [9,10]; however, details of the shape of the efficiency curve involve taking into account complications such as impurities, response times, and sub-threshold pulse pileup [9]. Rather than attempting to model the detector efficiency with Monte Carlo or closed-form expressions, we measure it directly for best accuracy. We make use of the T(p,n) angular distribution and kinematic angular variation.

For efficiency measurements, the detector carriage is repositioned to view the gas cell directly. The T(p,n) angular distribution specifies how many neutrons are emitted toward the MAIN detector at angle $\theta_{lab,}$ and the T(p,n) kinematic angular variation specifies the energy of these neutrons. We define the efficiency as the scattered neutron yield per $d\sigma/d\Omega_{Tpn}$ cross section for each measured laboratory detector angle. The detector angle is directly related to the scattered neutron energy. An example of an efficiency curve is shown in Fig. *5*.

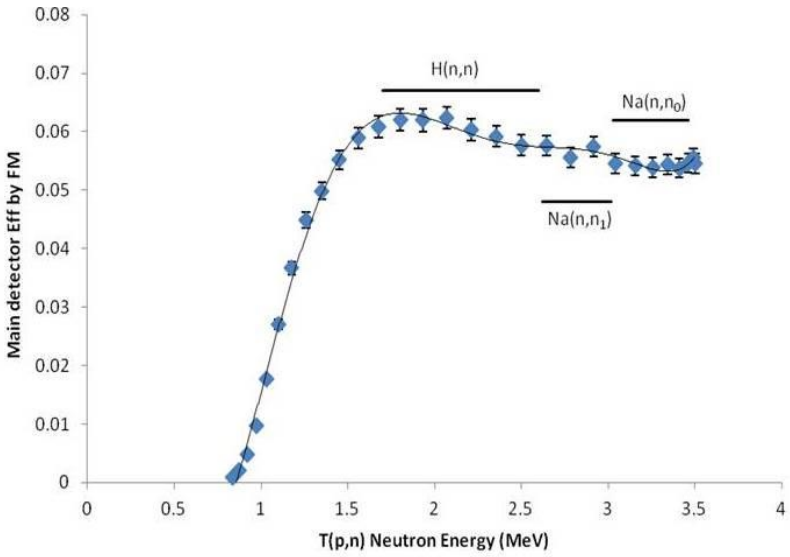

FIG.5. Efficiency curve for E_n = 3.50 MeV used in the ^{23}Na investigation. Uncertainties in the region >1.5 MeV average ±3%. Scattered neutrons for the reaction channels often lie at energies along the 'flat' part of the efficiency curve.

One has choices for the $d\sigma/d\Omega_{Tpn}$ cross section. Recommended values may be taken from:

- Liskien & Paulsen (LP) [11],
- the DROSG-2000 program series [12], or
- the evaluated ENDF/B-VII.1 database [13].

3.1. Monoenergetic and maxwell spectrum neutron beams (<5 MeV)

LP and DROSG values are closely connected to actual ^{3}H(p,n) experimental measurements, where the data exist. Absolute $d\sigma/d\Omega$ uncertainties in LP and DROSG are given as ~3%. LP values are an evaluation of information available as of December 1972. DROSG values contain updated information current as of January 2000. ENDF values are produced through the nuclear data evaluation process on the ^{4}He compound nucleus system, the description of which is constrained by many types of experimental measurements [14-17]. Absolute $d\sigma/d\Omega$ uncertainties in ENDF appear to be <5%. A comparison of cross sections from these references is shown in Fig. 6.

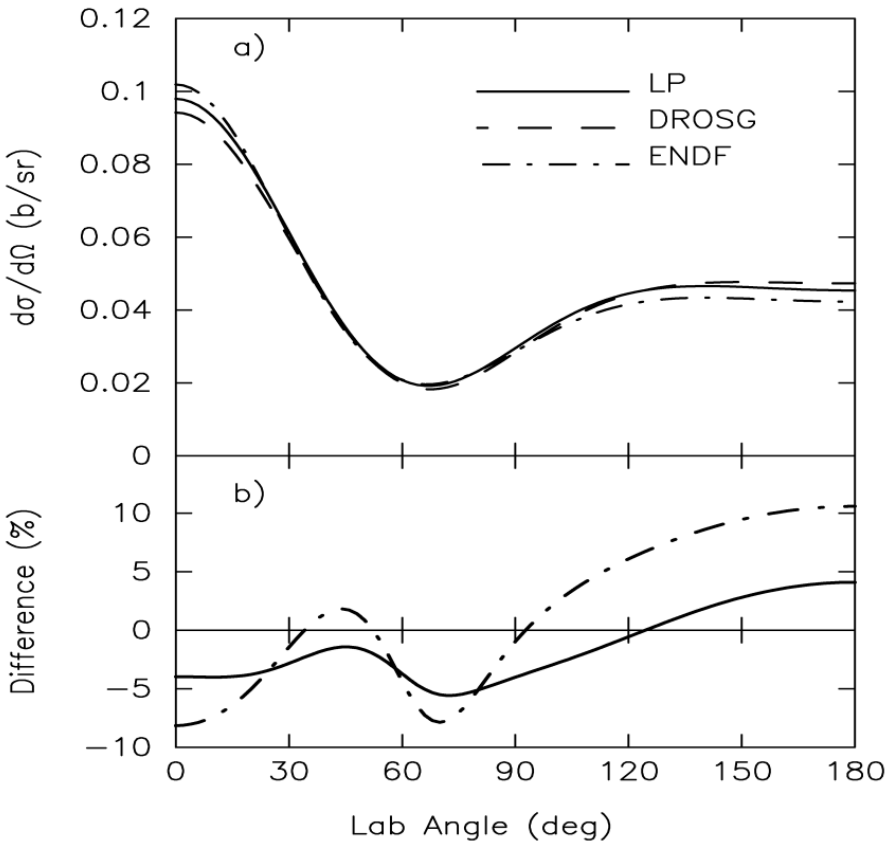

FIG. 6. Comparison of the three reference T(p,n) cross sections at E_p=4 MeV. The lower subfigure displays the percentage difference with respect to the DROSG parameterization. Differences between descriptions can be as much as ±10% and vary with angle.

The uncertainty in the yield is determined by i) counting statistics and ii) the ability to reliably extract the net peak yield from the TOF spectrum. The contribution from counting statistics can be made negligible by taking data for a sufficient time. The best yield extraction methods produce uncertainties of ~1-2%. Interestingly, this effect primarily impacts the absolute scale of *eff(E_n)* in the neutron energy regions of interest to elastic and excited level inelastic scattering and not so much the shape of the efficiency curve. Because our overall data analysis technique employs ratios of efficiencies, slight disagreement in the absolute efficiencies between techniques is not as critical for relative yields within a spectrum.

3.3. CONVERSION OF YIELDS TO DIFFERENTIAL CROSS SECTIONS

Normalization of (n,n_k) angular distributions to absolute (n,n_k) cross sections is performed by comparison to the angular distributions of $^1H(n,n)$, the cross section of which is generally known to 0.50% in the fast region [18,19]. The conversion factor is determined by $^1H(n,n)$ measurements on a polyethylene sample at 3 or 4 lab angles between 30 and 50°. The conversion factor must include corrections for neutron attenuation and multiple scattering in the polyethylene, (CH_2), sample.

Attenuation and multiple scattering corrections are accomplished with the code MULCAT, developed at the University of Kentucky [20,21]. The code performs iterative Monte Carlo calculations, taking as input the normalized experimental angular distribution as determined from the data analysis, first for scattering from hydrogen in the polyethylene sample. The resultant corrected angular distributions are then re-entered iteratively until the process converges to the known values of $^1H(n,n)$. The magnitudes of the corrections are then known. The Kentucky group has years of experience with MULCAT on medium-mass single-element samples [22-28].

To obtain a proper scaling factor the properly normalized, measured $d\sigma/d\Omega$ in this case for H-scattering, must be known. The scaling factor is actually obtained through a manually iterative process, because MULCAT can only treat one element of a sample at a time, as for example in the polyethylene sample. The uncertainty in the choice of technique for handling multiple elements is at most 2%. Usually three iterations are required to converge on the proper value. The total uncertainty in the value of the normalization process is ≤ 6% depending on the completeness of the original dataset.

After the normalization factor is known, the sample angular variations are easily converted to uncorrected cross sections and passed through MULCAT for the final finite sample corrections. Examples of final elastic and inelastic differential cross sections at 3.60 MeV incident neutron energy are shown in Fig. 7.

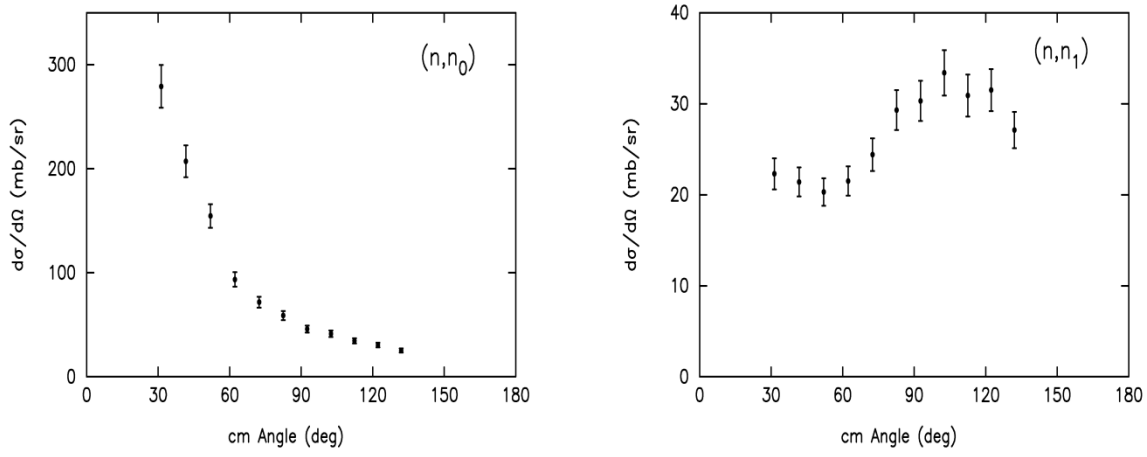

FIG. 7. $^{23}Na(n,n)$ differential cross sections provide detailed guidance for reaction model interpretations. Elastic scattering is largely explained by the optical model description; however, the inelastic channels contain the crucial information on direct mechanisms.

3.1. Monoenergetic and maxwell spectrum neutron beams (<5 MeV)

A project has been initiated at the University of Kentucky to test MULCAT against MCNP [29] calculations and properly estimate the uncertainty in the MULCAT technique. The testing technique begins with ENDF cross sections and uses these to construct an 'experimentally' observed count rate as a function of angle. This distribution should then be converted into an uncorrected differential cross section. MULCAT is then run to re-construct the primitive cross section. If all goes well, the starting and ending cross sections will be the same.

4. (N,N'γ) MEASUREMENTS AND TECHNIQUES

Much of the research program at the University of Kentucky Accelerator Laboratory is focused on nuclear structure investigations with the (n,n'γ). Nuclear spectroscopic information obtained from these measurements includes level schemes, excitation energies, decay branching ratios, spins and parities, multipole mixing ratios, and level lifetimes. Analysis techniques and numerous examples for nuclear structure investigations are described in detail in Ref. [30]. We only briefly mention the techniques employed.

For a single γ ray detector, the carriage in the neutron hall is configured as shown in Fig. *8* where the HPGe detector is inserted into the first two collimation elements. The HPGe detector has a simple cylindrical geometry BGO Compton shield to improve the signal-to-background ratio. Six phototubes service the single crystal and a few are visible in Fig. *8*. Both neutrons and γ rays will create events in the detector, so neutron TOF techniques are used to diminish neutron-induced background in the γ ray spectrum.

FIG. 8. Singles γ ray measurement configuration. The carriage is shown at 90^{o} to the beam direction.

Two types of measurements are performed with the singles configuration: γ ray angular distributions and γ ray neutron-energy-dependent excitation functions. Before extensive analysis, the γ ray yields must be corrected for HPGe detector efficiency and incident neutron and outgoing γ ray attenuation and multiple scattering in the sample. Relative detector efficiency is easily measured using multi-line sources such as ^{56}Co, ^{152}Eu, and ^{226}Ra. Sample-related corrections are performed with an in-house code GAMBIT which is based upon the Engelbrecht treatment for the (n,n'γ) reaction on cylindrical samples [31-33].

3.1. Monoenergetic and maxwell spectrum neutron beams (<5 MeV)

For angular distribution measurements, the incident neutron energy is chosen and spectra are typically taken for detector angles of 40^o–150^o. Because the γ rays are emitted from residual nuclear states of definite parity, the angular variation is expressed as $W_i(\theta_\gamma) = A_0 + A_2 P_2(\theta_\gamma) + A_4 P_4(\theta_\gamma)$, where the P_i are Legendre polynomials. Higher-order terms do not occur for dipole and quadrupole γ ray transitions. The coefficient A_0 is directly proportional to the intensity of the transition and is used to determine the branching ratios of transitions from an excited level. The coefficients $a_2=A_2/A_0$ and $a_4=A_4/A_0$ can be helpful in determining spins of levels and multipolarities of transitions [34].

As an added bonus, angular distribution measurements can provide level lifetimes via the Doppler-shift attenuation method [35]. The energies of γ rays emitted from the recoiling nucleus vary with observation angle as $E_\gamma(\theta_\gamma) = E_o[1 + F\beta_{\max}\cos(\theta_\gamma)]$. The factor $F\beta_{max}$ can be interpreted as the average speed at which the residual nucleus decays, and is related to the lifetime of the state and the stopping power [36].

For γ ray excitation functions, the detector carriage is positioned at $\theta_\gamma = 90^o$ or 125^o and spectra are taken as the incident neutron energy is raised. At 125^o the a_2P_2 term in the angular distribution is identically zero and the a_4P_4 term is typically small, < 7%. An excitation function measurement therefore returns A_o coefficients as a function of bombarding energy. The A_o coefficient is proportional to the production cross section for individual γ rays. The shape of the excitation function is also sensitive to the spin of the parent excited levels. If fidelity in γ ray energy is a concern, measurements can be performed at 90^o where no Doppler shifts are observed.

To convert A_o coefficients to γ ray production cross sections, we compare properly corrected yields to a γ ray cross section standard. Unfortunately high-quality γ ray standards do not exist for few-MeV (n,n'γ) scattering, although several are under development. We frequently choose to make a comparison to the ^{56}Fe(n,n'γ) inelastic cross sections from the ENDF evaluation [37]. Reference ^{56}Fe cross sections must be averaged over the incident neutron energy spread. Our uncertainty in determining the conversion is ~6%.

Figure 9 shows the γ ray coincidence configuration on the detector carriage, which is useful for quickly constructing level schemes of nuclei, resolving near-degenerate level energies, and placing multiple γ rays of the same transition energy.

The initial design considerations for the blue collimator in Fig. 10 are discussed in [38] using an attenuation model for neutrons. It is essentially a 60 cm diameter × 70 cm long Li-loaded paraffin cylinder with a 2 cm diameter central bore hole. Because neutron attenuation is an inherently non-analytic process, the actual mechanism of operation is slightly different from the considerations used in 1974. The collimator functions by scattering all neutrons except those that travel through the bore hole. The Li serves to absorb neutrons which have been thermalized.

Measurements indicate that the neutron flux emerging from the blue collimator/Pb wall arrangement is well defined. The four HPGe detectors do suffer slight neutron damage, with ^{60}Co resolutions changing from about 2.0 keV FHWM to over 2.5 keV FWHM after 1000 hours of exposure. After several months of operation, detectors are re-annealed to repair the damage [39].

3.1. Monoenergetic and maxwell spectrum neutron beams (<5 MeV)

FIG. 9. Two views of the γ–γ coincidence configuration. The left photo shows the arrangement from the beam-line view. The blue collimator is placed over the gas cell and forms a ~2 cm diameter neutron "collimator". A 10 cm thick lead wall just after the collimator attenuates γ rays generated in the collimator. Four HPGe detectors follow and are operated in a γ–γ coincidence arrangement. The right photo shows the arrangement from the detector viewpoint. The sample of interest is placed along the flux in the center of the 4 detectors.

5. DATA ACQUISITION

The electronics and data acquisition systems at the University of Kentucky Accelerator Laboratory are NIM and CAMAC based. These modules are reasonably simple for students and visiting researchers to learn to use, and they are extremely reliable and simple to diagnose. For many years, the laboratory employed home-written software to service the CAMAC crate and modules. A major problem is that in-depth knowledge of the software and its intricacies are rather easy to lose when postdoctoral scholars and graduate students complete their time at the laboratory. We recently completed a transition to the commercial package KMAX^{TM} [40]. With this product, the local programmer does not have to manipulate the low-level routines and it is easier to maintain and develop proficiency with the data acquisition codes. The package is a collection of java subroutines and a graphical user interface that requires far less effort to program and modify.

6. EXPERIMENTAL PROGRAM OUTLOOK

Recent experimental investigations at the laboratory involve nuclear structure measurements of importance to double β-decay (^{76}Ge, ^{76}Se) and neutrino mass measurements, collectivity in transitional nuclei (^{130,132}Xe), and shape coexistence and evolution in nuclei (^{94}Zr, ^{106}Pd). A major theme of the present program is the need for updating and affirming the accuracy of cross sections for ^{23}Na, a possible liquid coolant for ^{232}Th-based nuclear power reactors.

Upcoming experimental investigations will extend the interests above to the neighboring Xe and Zr nuclei and to additional transitional nuclei. New investigations impacting electric dipole moment searches ($^{198\text{-}200}$Hg) and nuclear astrophysics [^{1}H(n,γ) between 50 keV and 400 keV] are planned. In the near future, nuclear data efforts will turn to cross sections for the Fe isotopes ^{54,56}Fe. Another set of needed cross sections are those for

^{204,206,207,208}Pb. The first two were accurately measured by present investigators in this research program [22], but reviewing, updating, and extending these earlier measurements to a wider range of energies is certainly important. The Cr, Ni, and Zr isotopes all need careful attention, with careful measurement of their cross sections over an energy region from 1-9 MeV. A major review of cross section covariances for these materials has recently been released by a group at the National Nuclear Data Center in Brookhaven [41].

The University of Kentucky Accelerator Laboratory maintains collaborations with a variety of universities and facilities: University of Dallas, United States Naval Academy, University of Guelph, Georgia Institute of Technology, IUMF, Radiation Monitoring Devices, Qynergy Corporation, University of Cologne, HIγS at the Triangle Universities Nuclear Laboratory (TUNL), Yale University, iThemba Labs and the University of the Western Cape (South Africa). The Laboratory is a founding member of the Association for Research at University Nuclear Laboratories (ARUNA).
http://aruna.physics.fsu.edu/MemberLabs.html.

ACKNOWLEDGEMENTS

Research at the University of Kentucky Accelerator Laboratory is supported by grants from the U.S. Department of Energy-Nuclear Energy Universities Program, the U.S. National Science Foundation, the USMA Nuclear Science and Engineering Research Center, the USNA James Kinnear Fellowship, and the Cowan Physics Fund at the University of Dallas. The Kentucky collaborations are especially grateful to Tamás Belgya for representing the laboratory at the technical meeting.

REFERENCES

[1] Science Magazine, 142 (1963) 1128.
[2] CRANBERG, L., et al., "Production of High Intensity Ion Pulses of Nanosecond Duration", Nucl. Instrum. Meth. 12 (1961) 335-340.
[3] OLSSON, N., "100 Picosecond Post-Acceleration Bunching System at the Studsvik 6 MV Van de Graaff Accelerator", Nucl. Instrum. Meth. 187 (1981) 341-346.
[4] TYKESSON, P., and WIELDLIND, T., "A Klystron Bunching System for a 6 MV Van de Graaff Accelerator", Nucl. Instrum. Meth. 77 (1970) 277-282.
[5] HANSON, A.O., and MCKIBBEN, J.L., "A Neutron Detector Having Uniform Sensitivity from 10 Kev to 3 Mev ", Phys. Rev. 72 (1947) 673-677.
[6] TAGZIRIA, H., and THOMAS, D.J., "Calibration and Monte Carlo Modeling of Neutron Long Counters", Nucl. Instrum. Meth. A 452 (2000) 470-483 and references therein.
[7] MARION, J.B., and YOUNG, F.C., "Nuclear Reaction Analysis: Graphs and Tables", North Holland Publishing, Amsterdam, 1968.
[8] ATTIX, F.H, THEUS, R.B., and MILLER, G.E., "Attenuation Measurements of a Fast Neutron Radiotherapy Beam", Phys. Med. Biol. 21 (1976) 530-543.
[9] DROSG, M., "Accurate Measurement of the Counting Efficiency of a NE213 Neutron Detector Between 2 and 26 MeV", Nucl. Instrum. Meth. 105 (1972) 573-584.
[10] KELLERMAN, H.J., and LANGKAU, R., "Neutron Detection Efficiency of the Liquid Scintillator NE214 in the MeV Range", Nucl. Instrum. Meth. 94 (1971) 137-140.
[11] LISKIEN, H., and PAULSEN, A., "Neutron Production Cross Sections and Energies for the Reactions T(p,n)^{3}He, D(d,n)^{3}He, and T(d,n)^{4}He", Nuclear Data Tables 11 (1973) 569-619.

3.1. Monoenergetic and maxwell spectrum neutron beams (<5 MeV)

[12] DROSG, M., "DROSG-2000: Neutron Source Reactions", IAEA-NDS-87 rev. 8, and "Codes DROSG-2000 of the IAEA version 2.21", Jan 2003.

[13] HALE, G.M., "ENDF/V-II.1 p-T Reaction Evaluation", Evaluation of Sep 2001, Distribution of Dec 2006. Available at http://www.nndc.bnl.gov/sigma/ .

[14] BRUNE, C.R., et al. "Total Cross Section of the ^{3}H(p,n)^{3}He Reaction from Threshold to 4.5 MeV", arXiv:nucl-ex/9902010v1 22Feb1999.

[15] DROSG, M., "The ^{3}H(p, n)^{3}He Differential Cross Sections Below 5 MeV and the n-^{3}He Cross Sections", LA-8215-MS, UC-34c, July 1980.

[16] HOFFMAN, H.M., and HALE, G.M., "Microscopic Calculation of the ^{4}He System", Nucl. Phys. A 613 (1997) 69-106.

[17] HOFFMAN, H.M., and HALE, G.M., "^{4}He Experiments Can Serve as a Database for Determining the Three-Nucleon Force", Phys. Rev. C77 (2008) 044002

[18] Carlson, A.D., et al., "International Evaluation of Neutron Cross Section Standards", Nucl. Data Sheets 110 (2009) 3215-3324.

[19] HALE, G.M., "ENDF/V-II.1 ^{1}H(n,n) Reaction Evaluation", Evaluation of Oct 2005, Distribution of Dec 2006. Available at http://www.nndc.bnl.gov/sigma/ .

[20] VELKEY, D.E., et al., "Sample-Size Effects in Neutron Scattering Studied with Analytic and Monte Carlo Methods", Nucl. Instrum. Meth. 129 (1975) 231-239.

[21] LILLEY, J.R., "MULCAT-BRC, A Monte Carlo Neutron and Gamma ray Multiple Scattering Correction Program", Internal Service de Physique et Techniques Nucléaire, Centre d'Études de Bruyères-le-Châtel, Report P2N/934/80, (1980).

[22] HICKS, S.F., et al. "Neutron Scattering Cross Sections for ^{204,206}Pb and Neutron and Proton Amplitudes of E2 and E3 Excitations", Phys. Rev. C49 (1994) 103-115.

[23] HICKS, S.F., et al., "Collective Doorway Configurations in ^{49}Ca Through Neutron Scattering on ^{48}Ca", Phys. Rev. C41 (1990) 2560-2570.

[24] HICKS, S.E., et al., "Nuclear Dynamics of ^{192}Os as Probed in Neutron Scattering", Phys.Rev. C40 (1989) 2509-2519.

[25] HICKS, S.E., and McELLISTREM, M.T., "Energy Dependence of the Mean-Field Potential for Neutron Scattering from ^{190,192}Os and ^{194,196}Pt", Phys. Rev. C37 (1988) 1787-1790.

[26] HICKS, S.E., et al., "Influence of Nuclear Dynamics on Neutron Scattering from ^{194}Pt", Phys. Rev. C36 (1987) 73-82.

[27] HICKS, S.E., and McELLISTREM, M.T., "Ground State Reorientation Effects in Elastic Scattering Cross Sections", Nucl. Phys. A 468 (1987) 372-380.

[28] MIRZAA, M.C., et al., "Collective Excitations of ^{194}Pt in Low Energy Neutron Scattering", Phys. Rev. C32, (1985) 1488-1495.

[29] MCNPX, a general-purpose Monte Carlo N-Particle eXtended radiation transport code, Los Alamos.

[30] GARRETT, P.E., WARR, N., and YATES, S.W., "Nuclear Structure Studies with the Inelastic Neutron Scattering Reaction and Gamma ray Detection", J. Res. Natl. Inst. Stand. Technol. 105 (2000) 141-145.

[31] ENGELBRECHT, C.A., "Multiple Scattering Correction for Inelastic Scattering from Cylindrical Targets", Nucl. Instrum. Meth. 80 (1970) 187-191.

[32] ENGELBRECHT, C.A., "Recipes for Multiple Scattering Corrections", Nucl. Instrum. Meth. 93 (1971) 103-107.

[33] PARKER, J.B., et al., "Multiple Scatter Corrections Using the Monte Carlo Program MAGGIE", Nucl. Instrum. Meth. 30 (1964) 77-87.

[34] SHELDON, E., and VAN PATTER, D. M., Rev. Mod. Phys. 38, (1966) 143-186.

3.1. Monoenergetic and maxwell spectrum neutron beams (<5 MeV)

[35] BELGYA, T., MOLNÁR, G., and YATES, S.W., "Analysis of Doppler-Shift Attenuation Measurements Performed with Accelerator-Produced Monoenergetic Neutrons", Nucl. Phys. A 607 (1996) 43-61.

[36] WINTERBON, K.B., "An Analytic Theory of Doppler Shift Attenuation", Nucl. Phys. A 246 (1975) 293-316.

[37] CHADWICK, M.B., YOUNG, P.G., FU, C.Y., "ENDF/V-III.1 ^{56}Fe(n,n) Reaction Evaluation", Evaluation of Sep 1996, Distribution of Dec 2006. Available at http://www.nndc.bnl.gov/sigma/ .

[38] GLASGOW, D.W., et al., "Shielding for Fast Neutron Scattering Experiments of High Sensitivity", Nucl Instrum Meth. **114** (1974) 521-534.

[39] DARKEN, L.S., et al. "Mechanism for Fast Neutron Damage of Ge(HP) Detectors". Nucl. Instrum. Meth. **171** (1980) 49-59.

[40] Sparrow Corporation, www.sparrowcorp.com

[41] HOBLIT, S., et al., "Neutron Cross Section Covariances for Structural Materials and Fission Products", Nucl. Data Sheets **112** (2011) 3075-3097.

3.1. Monoenergetic and maxwell spectrum neutron beams (<5 MeV)

NUCLEAR DATA CAPABILITIES AT THE ASP NEUTRON GENERATOR

S LILLEY*, L PACKER*, S HUGHES**

*EURATOM/Culham Centre for Fusion Energy (CCFE) Fusion Association, Culham Science Centre, Abingdon, OX14 3DB, U.K
**AWE Aldermaston, Reading, Berkshire, RG7 4PR, U.K
Email: Steven.Lilley@ccfe.ac.uk

Abstract
The ASP accelerator is primarily a low energy high current deuteron accelerator which generates neutrons by bombarding targets impregnated with either deuterium or tritium. The accelerated deuterons have sufficient energy to cause either the D-D or D-T fusion reactions to occur and hence generate neutrons of 2 MeV and 14 MeV respectively. The ASP facility is the UK 14 MeV primary neutron standard and is accredited by the National Physical Laboratory.

The main use of the ASP facility is testing of high integrity electronic components for use in aircraft and other safety critical equipment. However over the last 3 years the facility has been increasingly used for nuclear data experiments. The facility now includes a rapid transfer system and low background count station. The neutron spectrum has been characterised using a combination of simulation and experimental data. Recent work by CCFE has shown the potential to use the facility for integral cross section measurements used to validate nuclear reaction cross sections and indeed several reactions without integral cross sections were measured. The next step is to further improve the facility for nuclear data experiments including additional beam diagnostics and characterising additional irradiation positions. This paper describes the ASP facility and the recent nuclear data work performed at the ASP facility.

1. INTRODUCTION

The 14 MeV neutrons generated in the plasma of future fusion reactors will initiate nuclear reactions in the materials of the surrounding first wall and vacuum-vessel components, leading to compositional changes in the constituent materials. Accurate predictions of this transmutation and the resulting activation are vital to inform the engineering design and material choice for fusion reactors.

Neutron transport simulations combined with inventory calculations, with codes such as MCNP and FISPACT, respectively, can produce the necessary quantitative predictions, but the reliability of these is largely dependent on the quality of the nuclear reaction cross section data. In many cases, the data for a particular reaction, in a database such as the European Activation File (EAF) [1], is either largely or entirely based on theoretical calculations because little or no experimental data exists.

In an effort to further improve the quality of data for fusion relevant materials, CCFE has undertaken a series of neutron irradiation experiments at the ASP experimental facility. Here, a deuteron beam is directed onto a tritium target, leading to the DT fusion reaction and the production of 14 MeV neutrons.

The ASP facility is similar to the Frascati Neutron Generator (FNG), Technical University Dresden (TUD) and Fusion Neutron Source (FNS) facilities in Italy, Germany and

Japan respectively, and this allows ASP to perform complimentary experimental work and inter-comparisons

2. THE ASP NEUTRON GENERATOR

The ASP facility is located at Aldermaston on the AWE site and is best classified as a low energy high current accelerator. The ASP accelerator uses a duoplasmatron to extract ions from the supply gas, this uses a combination of electric and magnetic fields to produce a high density plasma. The ASP system can produce up to 15 mA of light ions depending on the supply gas. The ionised gas is the deflected in a magnetic field to create a pure ion beam before entering the main accelerating tube. The accelerating tube, consisting of alternating ceramic insulators and aluminium electrodes can impart up to 300 keV of kinetic energy to the ions. The beam then passes through a series of collimators and steering devices which allow the precise location and incident angle of the beam to be varied. The beam then hits the target, currently three different targets are available, a deuterium impregnated target, a small tritium impregnated target and a large tritium impregnated target.

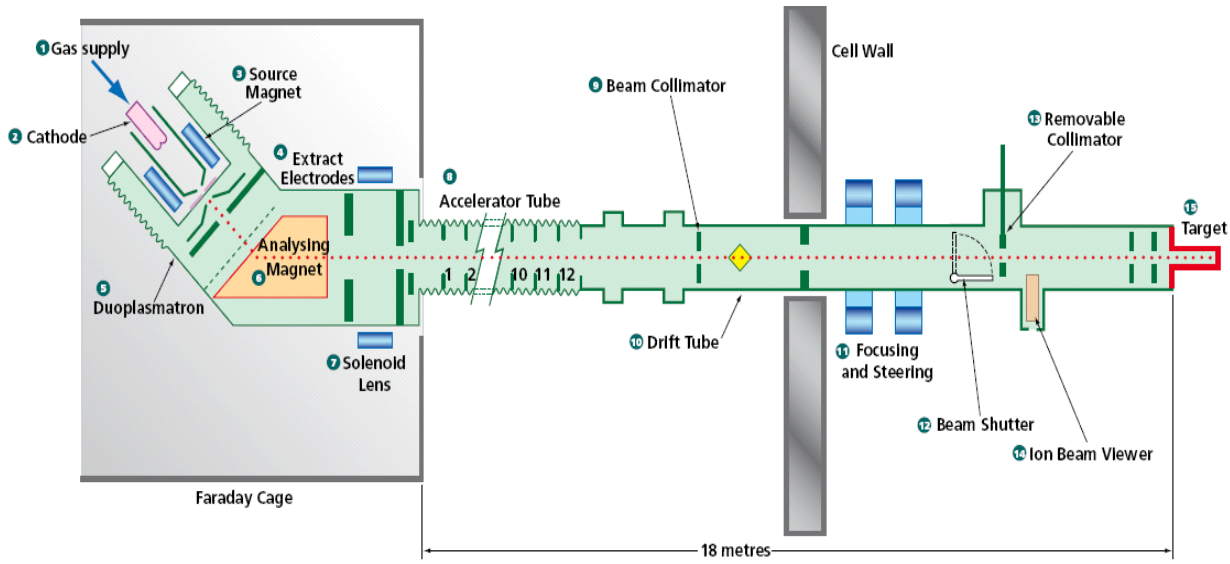

FIG. 1. Schematic of the ASP Accelerator.

The neutron output with a new tritium target can be up to 2.5×10^{11} s^{-1} and is only restricted due to radiological limits rather than machine capability.

The ion beam has the potential to be operated in a pulsed mode up to 0.2 kHz which has not currently been used for any nuclear data applications but may be considered for some future experiments.

ASP is currently the UK 14 MeV neutron primary standard and is accredited by the National Physical Laboratory (NPL). The accreditation is performed using neutron activation of Al and Fe foils which are measured at NPL using the low background beta detector. The primary standard uses a smaller tritium impregnated target which can be used with the alpha arm drift tubes, which are fitted with charged particle detectors at the end. This method is an

absolute count of the associated alpha particle produced in the D-T fusion reaction. Additional details on the ASP accelerator and the primary standard can be found in Bainbridge [2].

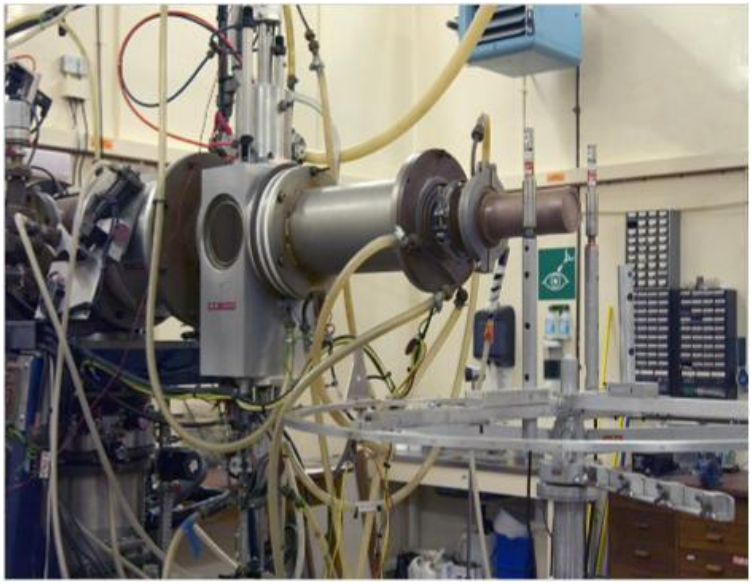

FIG.2. The ASP Neutron Generator target cell.

3. RE-ESTABLISHING THE ASP NUCLEAR DATA CAPABILITY

In 2010 CCFE and AWE started a collaboration to use ASP for nuclear data work specifically neutron activation cross section measurements focused initially on performing integral cross section measurements.

One of the key capabilities re-designed and re-commissioned was a rapid transfer system to send and retrieve samples to the chamber. The rapid transfer system is linked with the control system so accurate irradiation timing information is available. The system has been used to retrieve samples from the irradiation position to the counting station in around 4 seconds; so far the shortest half-life activation product that has been measured is ^{203}Pb with a 6 second half life.

The counting station consists of a HPGe gamma spectroscopy system with digital signal processing equipment and low background lead shielding.

Another very important part of the nuclear data capability is the neutron spectrum characterisation and flux monitoring. Information about the neutron flux and energy has been obtained at the irradiation position using both experimental and computational techniques such as Al and Fe flux monitoring foils in each experiment, using Zr and Nb reactions to establish mean neutron energy as described by Agrawal and Pepelnik [3].

In addition simulations using MCUNED [4] have also been used to gain a detailed understanding of the neutron spectrum changes produced as a result of changes in the deuteron beam. MCUNED is a patch for MCNPX which allows cross section data for ion interactions at low energies to be used. This means it is possible to model changes in the

beam and monitor their effect on the neutron spectrum at the foil position such as if the beam position moves by 10mm as shown.

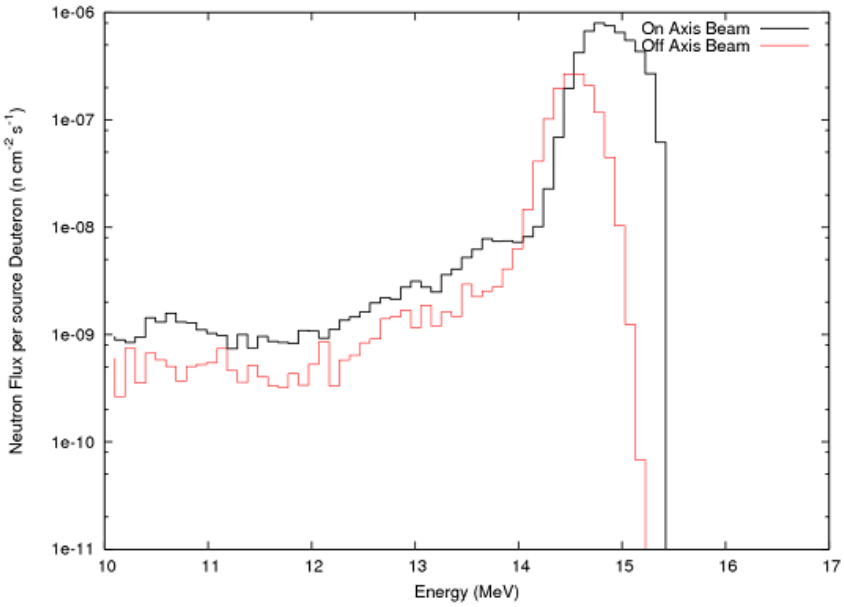

FIG. 3 Comparison of neutron spectra at the foil location for two different deuteron beam position.

The simulations can be combined with the experimental data for known reactions to perform unfolding calculations using MAXED [5]. An example neutron spectrum shown in figure comparing the ASP unfolded neutron spectrum with the FNG neutron spectrum used for previous integral cross section experiments.

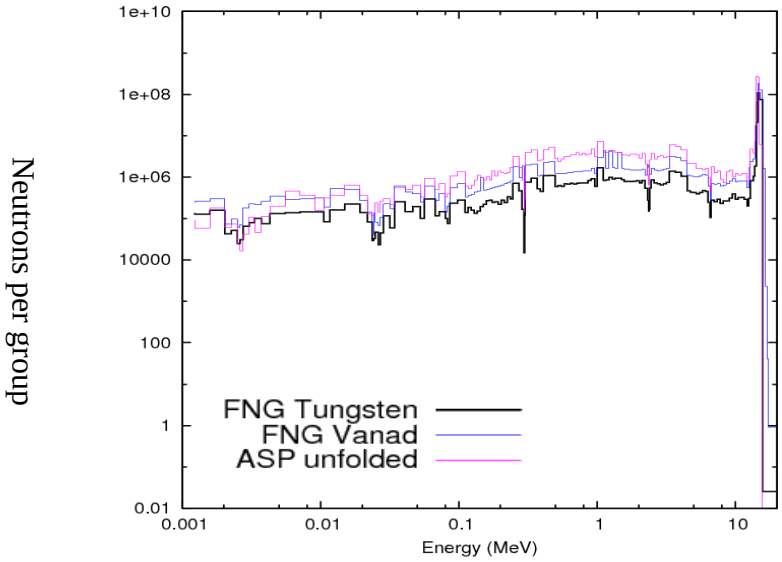

FIG. 4. Comparison of Neutron spectra from ASP and FNG

3.1. Monoenergetic and maxwell spectrum neutron beams (<5 MeV)

4. RECENT NUCLEAR DATA WORK

The CCFE program of work involved 150 irradiations of over 20 different high purity elemental foils for irradiation times between 2 minutes and 1hour in 3 separate irradiation campaigns. The induced gamma spectrum was measured in time bins and analysed using an automated processing system developed at CCFE. The automated system allowed the 10,000 time binned spectra to be quickly analysed to identify peaks, calculate peak area and calculate an experimental integral cross section. The experimental cross section is considered an integral cross section because whilst the 14 MeV neutron peak is more than an order of magnitude greater than any other energy, it is a broad peak due to the tritiated thick target leading to a range of energies around the main peak. In addition as the target ages there is likely to be an increasing 2 MeV peak due deuteron build up in the target leading to more DD fusion reactions. Integral cross section measurements are an important validation method for cross section data [6]. This method has been used to improve and validate the EAF library with integral cross section measurements from several facilities. The EAF database has 470 validated reactions out of over 66000 reactions.

The initial results from the first irradiations are published in Packer et al [7], which demonstrated the feasibility and tested the experimental procedure. One key area that was identified as needing improvement was the neutron flux monitoring, currently for the large tritiated target the main method of determining the neutron flux are two fission chambers mounted approximately 10 cm from the target. When using the rapid transfer system the foil is positioned less than 1 cm from the target, the typical foil dimensions are 12 mm and the deuteron beam diameter is approximately 10 mm. This means that a small change in the deuteron beam position can mean a large change in neutron flux at the foil but only a very small change in the fission chamber count rates. As a result the majority of irradiations included Al and Fe foils as well as the foil of interest in order to estimate the neutron flux based on well known reactions in the Al and Fe.

An example gamma spectrum for a high purity W foil, measured with the Al and Fe flux monitoring foils is shown in Fig. 5. The zoomed in view of the low energy region highlights the ^{185m}W peaks in red which are from the ^{186}W(n,2n)^{186m}W reaction. The peak areas are calculated using the automatic processing tool described earlier and an integral cross section value is derived. The ratio of the calculated integral cross section based on the current cross section and the experimentally derived cross section (C/E) is used to determine if the current cross section matches the results from the experiment. C/E values for this reaction are shown in Fig.1 for several separate irradiations of high purity W foils alongside the values from determined at FNG and FNS. The results show that ASP is capable of performing high quality useful measurements comparable to other facilities.

3.1. Monoenergetic and maxwell spectrum neutron beams (<5 MeV)

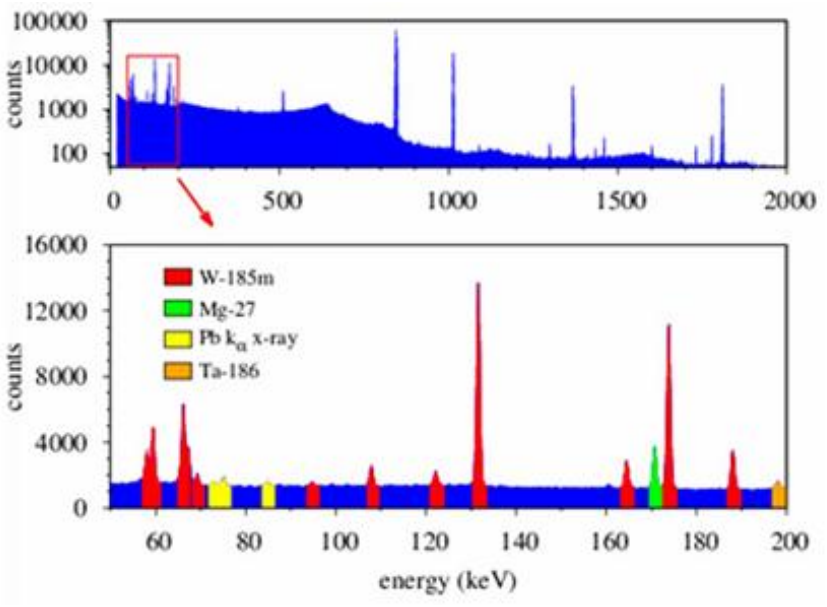

FIG. 5. Example Gamma Spectrum from W foil irradiation.

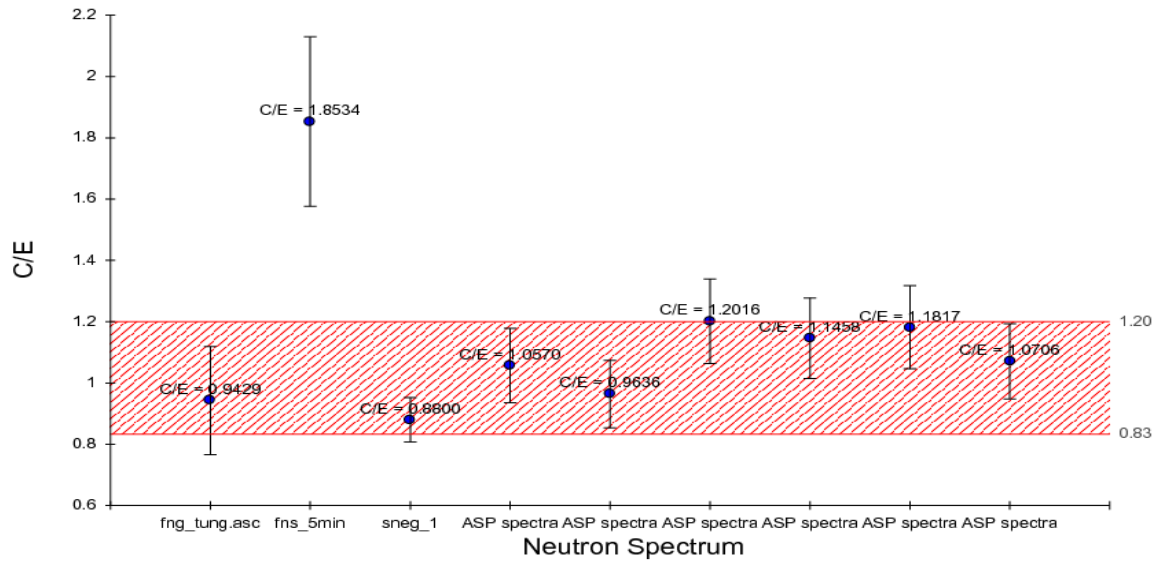

FIG. 1. Integral C/E results for ^{186}W(n,2n) ^{185m} W- for several separate ASP experiments.

The large range of elemental foils irradiated in the 3 experimental campaigns allowed over 38 reactions to be detected including 6 reactions (listed in TABLE 1) which previously had no integral cross section measurements. The large range of foils has enabled the capability to be demonstrated and to establish the limits of the facility. The *C/E* results for a selection of reactions are shown in Fig.2, it shows that some reactions have a wide spread of *C/E* values such as ^{64}Zn(n,2n)^{63}Zn. Other reactions have a small spread and are close to a value of 1 such as ^{186}W(n,2n)^{185m}W and some such as ^{46}Ti (n,p)^{46m}Sc have a small spread but are not that close to a *C/E* value of 1. This Ti reaction is one of the 6 reactions that has no previous integral nuclear data and hence it might be an indication that the calculated cross section is not correct.

3.1. Monoenergetic and maxwell spectrum neutron beams (<5 MeV)

TABLE 1. REACTIONS MEASURED WHICH HAVE NO PREVIOUS INTEGRAL CROSS SECTION RESULTS

Reaction
^{107}Ag (n,n) ^{107M}Ag
^{107}Ag (n,p) ^{107M}Pd
^{109}Ag (n,n) ^{109M}Ag
^{109}Ag (n,p) ^{109M}Pd
^{92}Mo (n,α) ^{89M}Zr
^{46}Ti (n,p) ^{46M}Sc

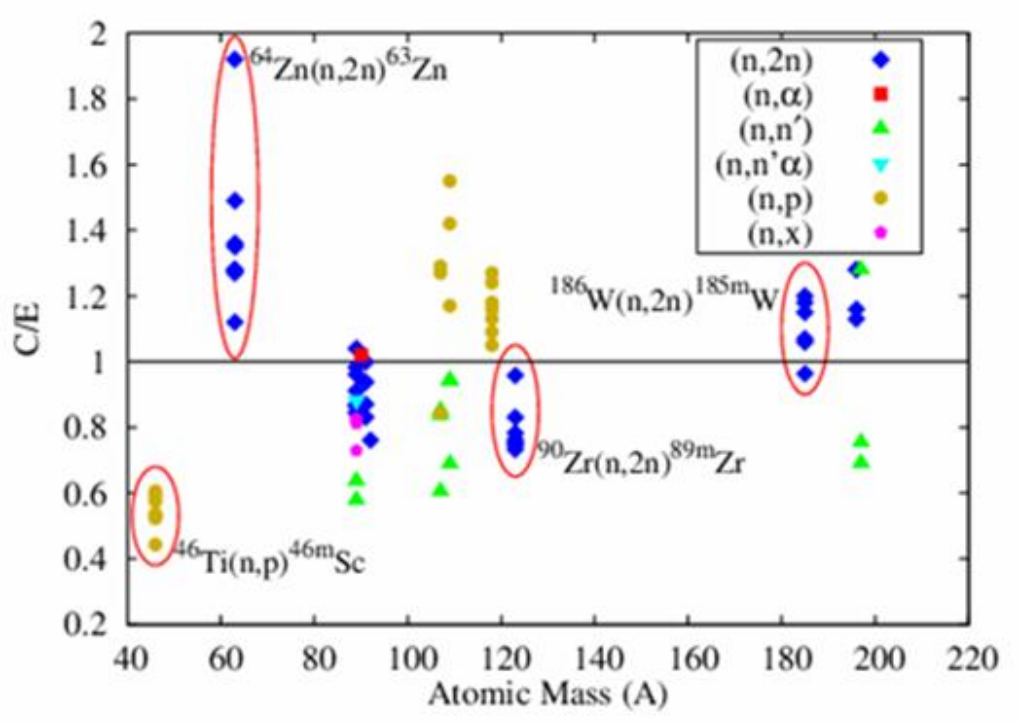

FIG. 2. C/E values for a range of reactions as measured at ASP.

3.1. Monoenergetic and maxwell spectrum neutron beams (<5 MeV)

5. FUTURE NUCLEAR DATA WORK

The next step for the CCFE program of work is to optimise the experimental timings for specific reactions in order to maximise detection efficiency and reduce statistical errors. This may include using isotopically tailored samples for low abundance isotopes such as ^{183}W. Over the next 3 years the plans include further understanding of the uncertainties in the experiments, and targeting several difficult to measure cross sections with relevance to fusion such as those listed by Forrest [8].

Further facility developments include improved beam diagnostics and neutron flux measurements. The longer term aim is to develop the capability to perform differential nuclear cross section measurements at the ASP facility.

6. CONCLUSIONS

The recent work at the ASP facility has demonstrated its capability to perform a range of integral nuclear data measurements including some reactions which have no integral data. The neutron spectrum characterisation at the irradiation position suggests that the spectrum is very similar to the spectrum seen at FNG and this means that the two facilities are complimentary to each other. However more work is required to reduce the uncertainty on the neutron spectrum estimate.

Integral nuclear data measurements are an important part of the validation process for cross section reactions and complement differential measurements.

The future measurements will be optimised to target specific reactions rather than the large range of reactions which have been performed to date, this may include using isotopically tailored samples.

The CCFE and AWE collaboration aims to continue to improve the ASP facility for nuclear data work. The planned improvements will help to reduce the uncertainty such as the neutron flux and deuteron beam parameters.

ACKNOWLEDGEMENTS

The authors wish to thank the ASP facility staff J Hughes, G Davies & B Hymes for all their hard work during the experiments.

This work was funded by the RCUK Energy Programme under grant EP/I501045 and the European Communities under the contract of Association between EURATOM and CCFE. The views and opinions expressed herein do not necessarily reflect those of the European Commission.

REFERENCES

[1] SUBLET, J-Ch., et al., Forrest ‘The European Activation File: EAF-2010 neutron-induced cross-section library’, CCFE-R (10) 05, 2010

[2] BAINBRIDGE, N., ‘ASP particle accelerator’, Discovery Journal, Issue 9, August 2004

3.1. Monoenergetic and maxwell spectrum neutron beams (<5 MeV)

[3] AGRAWAL, H. M., and PEPELNIK, R., Determination of the mean neutron energy using the Zr/Nb and the Ni method, Nucl. Instr. Meth. A 366 (1995) 349-353

[4] SAUVAN, P., et al., New Capabilities for Monte Carlo simulation of deuteron transport and secondary products generation, Nuclear Instruments and Methods in Physics Research Section A: Accelerators, Spectrometers, Detectors and Associated Equipment, vol 614, number 3, 2010

[5] REGINATTO, M., et al., MAXED/GRAVEL U_M_G version 3.3, PTB, March 2004

[6] FORREST, R. A., et al., Validation of EASY-2007 using integral measurements, UKAEA FUS 547 (2008)

[7] PACKER, L.W., et al., UK fusion technology experimental activities at the ASP 14MeV neutron irradiation facility, Fusion Engineering and Design, Volume 87, Issues 5–6, August 2012, Pages 662-666, ISSN 0920-3796

[8] FORREST, R. A., Data requirements for neutron activation Part I: Cross sections, Fus. Eng. Des. 81 (2006) 2143-2156

3. ACCELERATOR BASED NEUTRON BEAM FACILITIES

3.2. ION-INDUCED QUASI-MONOENERGETIC AND WHITE NEUTRON BEAMS

NEUTRON CAPTURE CROSS SECTION MEASUREMENTS IN THE KEV ENERGY REGION AT THE TOKYO INSTITUTE OF TECHNOLOGY

T. KATABUCHI, M. IGASHIRA

Research Laboratory for Nuclear Reactors,
Tokyo Institute of Technology,
2-12-1 Ookayama, Meguro-ku,
Tokyo 152-8550,
Japan

Email: buchi@nr.titech.ac.jp

Abstract

Measurement of neutron capture cross sections in the keV energy region by the time-of-flight method has been continued for 20 years at the Tokyo Institute of Technology. The neutron capture cross sections of more than 70 nuclides have been determined. Neutrons are generated via the ^{7}Li(p,n)^{7}Be reaction using a proton beam from a Pelletron accelerator. Gamma rays from the neutron capture reaction are detected with an NaI(Tl) spectrometer. A pulse height weighting technique is used to deduce neutron capture cross sections from the pulse height spectra. The neutron capture experiment system is explained.

1. INTRODUCTION

Measurements for neutron capture cross sections have been performed at the Tokyo Institute of Technology (Tokyo Tech) for 20 years. A Pelletron accelerator was installed in the Research Laboratory for Nuclear Reactors of Tokyo Tech in 1979. After several upgrades of the accelerator and detectors, a low background measurement system for neutron capture experiments was realized. Combing a pulsed ^{7}Li(p,n)^{7}Be neutron source and an anti-Compton shielded NaI(Tl) spectrometer, reliable measurements have been accomplished. The system was designed to measure neutron capture cross sections by the time-of-flight (TOF) method in the keV neutron energy region. The neutron capture cross sections of more than 70 nuclides have been determined for various scientific and engineering fields such as nuclear engineering, astrophysics and nuclear physics. Experimental cross section data measured with the Tokyo Tech system significantly contributed to evaluated nuclear data libraries. This report overviews the neutron capture experiment system and nuclear data research activities of Tokyo Tech.

2. FACILITY AND INSTRUMENTS

2.1. NEUTRON SOURCE

A 3UH Pelletron accelerator at the Research Laboratory for Nuclear Reactors at the Tokyo Tech is used to generate neutrons. The accelerator has a single-ended terminal, on which an ion source and a beam pulsing system are located. The rated maximum terminal voltage is 3 MV. A proton beam from the ion source can be pulsed with the pulsing system. The repetition rate is 4 MHz or 2 MHz. The beam pulse width is approximately 1.5 ns.

Neutrons are produced via the ^{7}Li(p,n)^{7}Be reaction by bombarding a Li target with the accelerated proton beam. The Li target is metal Li deposited on a Cu plate. The end of the beam duct is closed with the Cu plate. The deposited Li layer is on the vacuum side of the Cu plate. Deposited beam power in the Li target is removed by cooling water on the atmospheric side of the Cu plate. Using this ^{7}Li(p,n)^{7}Be neutron source, we carry out measurements in two neutron energy regions: 15-100 keV and around 550 keV. For the low energy region, the proton energy is set at 1.9 MeV, which is 20 keV above the reaction threshold. At the near-

threshold energy, neutrons are produced in only a kinematically limited forward cone with a maximum emission angle of about 50° with respect to the proton beam direction. The kinematically collimated neutron beam reduces unwanted background caused by neutron-induced reactions in surrounding material around the neutron source, thereby realizing low-background measurement. For experiments in the high energy region around 550 keV, the proton energy is set at around a resonance peak (E_p = 2.6 MeV) of the ^{7}Li(p,n)^{7}Be reaction. At this energy, neutrons are emitted in all directions, inevitably causing large background, but a high neutron flux are obtained. The width of the neutron energy distribution is 100-150 keV in full-width at half-maximum.

The neutron flight-path length to a sample for neutron capture cross section measurement is 12 cm for the low energy experiment and 20 cm for the high energy experiment. The reference signal for TOF measurement is generated with a beam monitor picking off the proton beam pulses. An incident neutron spectrum at the near-threshold proton energy, measured with a ^{6}Li glass scintillator, is shown in Fig. 1. The ^{6}Li glass detector was placed at a distance of 30 cm from the neutron source. The neutron energy was determined by the TOF method. The neutron energy ranges from a few keV to 100 keV. The low energy part of the spectrum was discriminated at around 10 keV. The average neutron energy is about 45 keV.

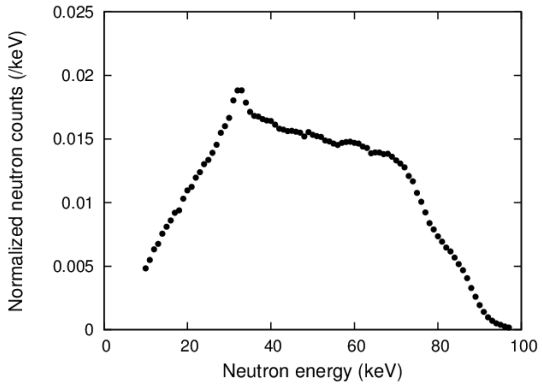

FIG. 1. Incident neutron spectrum from the ^{7}Li(p,n)^{7}Be reaction at a near-threshold energy. Neutrons were detected with a ^{6}Li glass scintillator. The neutron energy was determined by the TOF method. Neutron counts were normalized to the total count.

2.2. Detector

An NaI(Tl) spectrometer with an anti-Compton shield is used to detect γ rays from the neutron capture reaction [1,2]. The detector setup is illustrated in Fig. 2. The NaI(Tl) spectrometer consists of a main NaI(Tl) detector (crystal size: 152 mm diameter x 305 mm length) and an annular NaI(Tl) detector (crystal size: 330 mm outer diameter × 172 mm inner diameter × 356 mm length) surrounding the main detector. Anti-coincidence detection between the main and annular NaI(Tl) detectors suppresses the Compton scattering events in the main detector. The detectors are shielded with borated polyethylene (or paraffin), potassium-free lead and cadmium. In front of the spectrometer, lithium-6 hydride is placed to cut down the number of scattered neutrons coming into the main NaI(Tl) crystal.

3.2. Ion-induced quasi-monoenergetic and white neutron beams

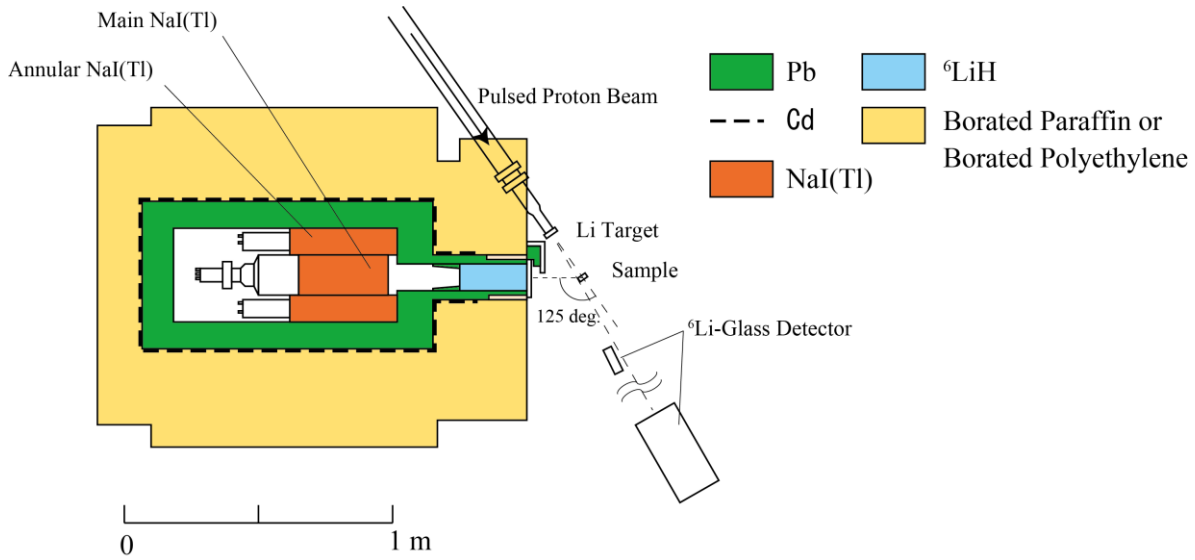

FIG. 2. Tokyo Tech NaI(Tl) spectrometer for neutron capture cross section measurement.

2.3. Data Reduction

The pulse-height (PH) and TOF of the signals from the NaI(Tl) detector are recorded sequentially in a list-data format file. A typical TOF spectrum for the standard sample ^{197}Au in the low energy experiment is shown in Fig. 3. The x-axis is the time difference between the detected events and the TOF reference signals from the beam pulse pick-off monitor. Fast TOF corresponds to large channel since the reference signal fired at 4 MHz (or 2 MHz) was used as the stop trigger for a time-to-amplitude converter instead of the start trigger, to avoid saturation of processing capacity of electronics from the high frequency inputs. A broad bump below 500 ch is induced by neutron capture events in the sample. A prominent peak around 600 ch is the (p,γ) reaction in the Li target of the neutron source. The absolute TOF is calculated from the (p,γ) peak. Typical TOF foreground and background gates are shown in Fig. 3. A set of the four foreground gates (15-25 keV, 25-35 keV, 35-55 keV, 55-100 keV) is often used in our analysis.

Different gate sets are sometimes used when a resonance structure is observed in a TOF spectrum. However an extremely larger number of TOF gates cannot be set due to the low time resolution originating from the short flight path length of this system. After sorting list-data into PH spectra using the foreground and background TOF gates, a net PH spectrum is made by subtracting the background PH spectrum from the foreground PH spectrum. Foreground and background PH spectra for ^{197}Au are shown in Fig. 4. Peaks of background γ rays from ^{40}K and the ^{56}Fe(n,γ)^{57}Fe reaction are observed in the PH spectra. These background γ rays are perfectly removed from the foreground PH spectrum by background subtraction.

3.2. Ion-induced quasi-monoenergetic and white neutron beams

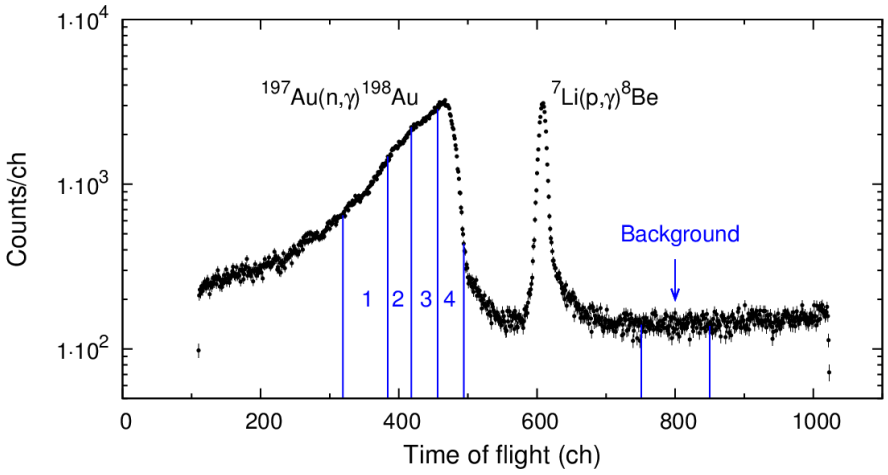

FIG. 3. TOF spectrum for the standard sample ^{197}Au. 1 ch = 0.245 nsec. Fast TOF corresponds to large channel (see the text). Foreground and background TOF gates are shown. Foreground gates are labeled with gate numbers: Gate 1 (15-25 keV), Gate 2 (25-35 keV), Gate 3 (35-55 keV) and Gate 4 (55-100 keV).

The neutron capture cross sections are determined based on the pulse height weighting technique [3]. Neutron capture yields are calculated from a weighted integral of a net PH spectrum. The weighting function is determined from response functions of the detector system calculated by the Monte Carlo method, including attenuation of γ rays in a sample. The neutron capture cross section is determined relative to the cross section of the standard reaction ^{197}Au(n,γ)^{198}Au. Measurements for a nuclide of interest, ^{197}Au and blank are repeated cyclically to reduce systematic uncertainties from fluctuations of experimental conditions such as neutron flux. The evaluated ^{197}Au(n,γ)^{198}Au cross sections of ENDF/B-VII or ENDF/B-VI were used as standard.

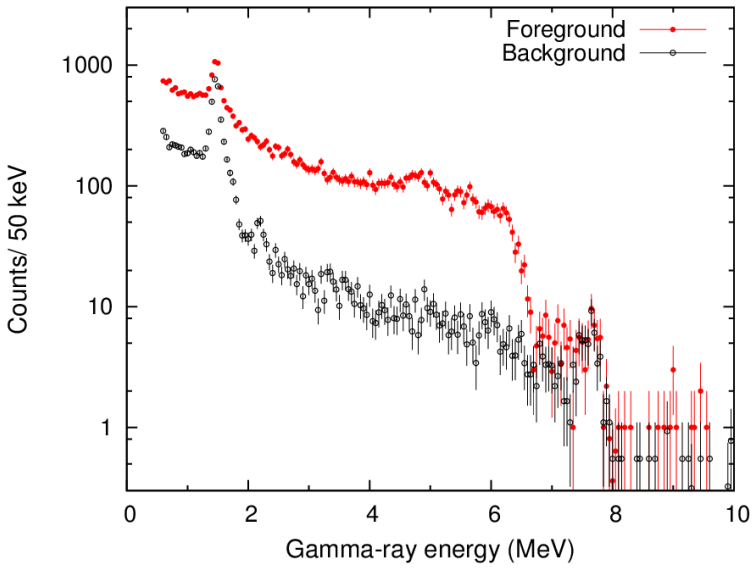

FIG. 4. Foreground and background PH spectra for the standard sample ^{197}Au. The low energy peak below 2 MeV is natural background γ rays from ^{40}K. The high energy peak around 7.6 MeV is background γ rays from the ^{56}Fe(n,γ)^{57}Fe reaction.

3.2. Ion-induced quasi-monoenergetic and white neutron beams

In contrast to the poor time resolution, the detection sensitivity of the Tokyo Tech system is very high. Fig. 5 shows a plot of neutron capture cross sections at 30 keV vs. sample amount in mol, measured in the past experiments. Results with a former NaI(Tl) detector, which was replaced to the current detector about 15 years ago, are also shown. The product of the detectable cross section and the sample amount, $\sigma_{30}M$ gives a measure of the detection sensitivity. The current system reaches a line of $\sigma_{30}M$ = 0.0003 b mol. This means that a cross section of 30 mb can be measured with a sample amount of 0.01 mol, which corresponds to 1 g for a molecular weight of 100. Although a "detectable" cross section depends on acceptable uncertainties and accordingly should be discussed more carefully, only an example of a measurement is given here. The cross section of ^{94}Zr(n,γ)^{95}Zr at E_n = 30 keV has been determined to be 26.5 mb with an uncertainty of 6.5% using an enriched sample of 1g (shown as a star in Fig. 5) [4]. Total beam time for the ^{94}Zr experiment was 4 days.

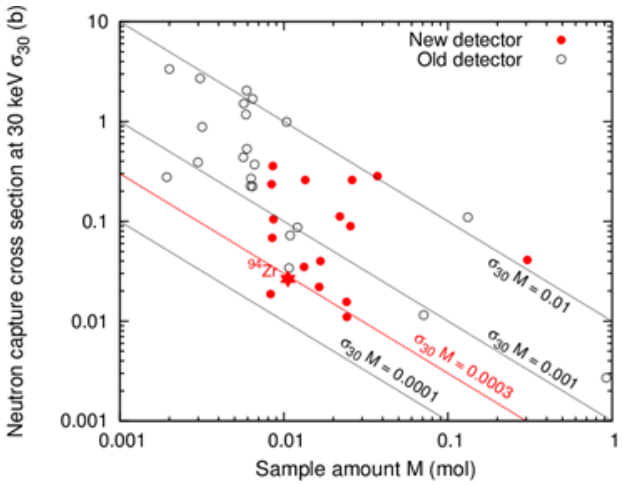

FIG.5. Plot of neutron capture cross sections at 30 keV vs. sample amounts in mol in the past experiments using the Tokyo Tech NaI(Tl) spectrometer. An example point of ^{94}Zr (see the text) is shown as a star.

2.4. Examples of Measurements

Measurements of the neutron capture cross sections of long-lived fission products (LLFPs) and one minor actinide (MA) have been performed at Tokyo Tech. Accurate nuclear data of LLFPs, MAs and their stable isotopes are necessary for the design of nuclear transmutation systems, such as an accelerator-driven system. Using radioactive samples of ^{99}Tc, ^{129}I and ^{237}Np, their keV-neutron capture cross sections were measured [5-7]. Neutron capture cross section measurements for stable isotopes of Se, Zr and Sn have been also completed [4,8-14]. Systematics of the experimental cross section data of the stable isotopes were used to predict the neutron capture cross sections of ^{79}Se, ^{93}Zr and ^{126}Sn. A series of measurements for Pd stable isotopes regarding ^{107}Pd is ongoing [15].

Astrophysics has also motivated us to measure neutron capture cross sections. In the nucleosynthesis scenario, elements heavier than ^{56}Fe were formed by the neutron capture process in the stellar environment. The temperature of the slow process (s-process) nucleosynthesis site corresponds to keV energy range. Thus, neutron capture cross sections in the keV energy region are very important inputs for nucleosynthesis models. In particular, cross sections at neutron magic numbers N=50 and N=82 give constraints to determine the neutron density and the temperature of the s-process site. Measurements of ^{88}Sr, ^{139}La, ^{140}Ce,

^{141}Pr and ^{142}Nd have been done [16-18]. Neutron capture cross section measurement of ^{138}Ba is ongoing.

In addition to the studies described above, many other topics in nuclear engineering, astrophysics and nuclear physics have inspired experiments at Tokyo Tech. Reports on the experiments can be found in Refs. 19-28 or references therein.

3. SUMMARY

The facility and instruments for neutron capture cross section measurement at Tokyo Tech were briefly discussed. The measurement system was designed to measure capture cross section in the keV energy region by the TOF method using a pulsed neutron beam produced via the ^{7}Li(p,n)^{7}Be reaction. Gamma rays from the capture reaction are detected using the NaI(Tl) spectrometer with anti-Compton shielding. Accurate cross section measurements for more than 70 nuclides have been accomplished for the past 20 years. Projects for nuclear engineering and astrophysics are still actively ongoing.

REFERENCES

[1] Mizuno, S., et al., Measurements of keV-Neutron Capture Cross Sections and Capture Gamma ray Spectra of ^{161,162,163}Dy, Journal of Nuclear Science and Technology 36, 493-507 (1999).

[2] Ohsaki, T., et al., An NaI(Tl) Spectrometer System for keV Neutron Radiative-Capture Reactions, Nuclear Instruments and Methods in Physics Research, A425, 302-319 (1999).

[3] Macklin, R. L., and Gibbons, J. H., Capture-Cross-Section Studies for 30-220 keV Neutrons Using a New Technique, Physical Review 159, 1007-1015 (1967).

[4] Ohgama, K., A Systematic Study of keV-Neutron Capture Cross Section and Capture Gamma rays of Zr Isotopes, Doctoral Dissertation, Tokyo Institute of Technology, (2005), [in Japanese].

[5] Matsumoto, T., et al., Measurement of keV-Neutron Capture Cross Sections and Capture Gamma ray Spectra of ^{99}Tc, Journal of Nuclear Science and Technology 40, 61-68 (2003).

[6] Matsumoto, T., A Study of keV-Neutron Capture Cross Section of the Long-Lived Fission Products ^{99}Tc and ^{129}I, Doctoral Dissertation, Tokyo Institute of Technology, (2005), [in Japanese].

[7] Kurokawa, N., A Study of keV-Neutron Capture Cross Section of ^{237}Np, Master Thesis, Tokyo Institute of Technology, (1999), [in Japanese].

[8] Kamada, S., et al., Measurement of keV-Neutron Capture Cross sections and Capture Gamma ray Spectra of ^{77}Se, Journal of Nuclear Science and Technology, 47, 634-641 (2010).

[9] Kamada, S., A Systematic Study of keV-Neutron Capture Cross Section of Se Isotopes, Doctoral Dissertation, Tokyo Institute of Technology, (2010), [in Japanese].

[10] Igashira, M., Systematic Study on keV-Neutron Capture Reaction of Se Isotopes, Journal of the Korean Physical Society 59, 1665-1669 (2011).

[11] Ohgama, K., et al., Measurement of keV-Neutron Capture Cross Sections and Capture Gamma ray Spectra of ^{91,92}Zr, Journal of Nuclear Science and Technology 42, 333-340 (2005).

[12] Katabuchi, T., et al., Measurement of keV-Neutron Capture Cross Section of ^{96}Zr, Journal of Nuclear Science and Technology 48, 744-750 (2011).

[13] Nishiyama, J., et al., Measurements of keV-Neutron Capture Cross Sections and Capture Gamma ray Spectra of ^{117,119}Sn, Journal of Nuclear Science and Technology 45, 352-360 (2008).
[14] Nishiyama, J., A Systematic Study of keV-Neutron Capture Cross Section and Capture Gamma rays of Sn Isotopes, Doctoral Dissertation, Tokyo Institute of Technology, (2007), [in Japanese].
[15] Terada, K., et al., Systematic Measurements of keV-neutron Capture Cross Sections and Capture Gamma ray Spectra of Pd Isotopes, Fourteenth International Symposium on Capture Gamma ray Spectroscopy and Related Topics, University of Guelph, Canada, August 28 - September 2 (2011).
[16] Katabuchi, T., et al., Measurement of Neutron Capture Cross Section and Gamma ray Spectra of ^{88}Sr in keV Energy Region, Journal of the Korean Physical Society 59, 1844-1847 (2011).
[17] Harnoond, S., et al., Measurement of keV-Neutron Capture Cross Sections and Capture Gamma ray Spectra of ^{140}Ce and ^{141}Pr, Journal of Nuclear Science and Technology 45, 740-749 (2000).
[18] Katabuchi, T., et al., Measurement of kev-Neutron Capture Cross Section and Gamma ray Spectra of ^{142}Nd, Fourteenth International Symposium on Capture Gamma ray Spectroscopy and Related Topics, University of Guelph, Canada, August 28 - September 2 (2011).
[19] Igashira, M., et al., Systematics of the Pygmy Resonance in keV Neutron-Capture Gamma ray Spectra of Nuclei with N≈82-126, Nuclear Physics A 457, 301-316 (1986).
[20] Nagai, Y., et al., Measurement of the Neutron-Capture Rate of the ^{12}C(n,γ)^{13}C Reaction at Stellar Energy, Astrophysical Journal 372, 683-687 (1991).
[21] Ohsaki, T., et al., New Measurement of the ^{12}C(n,γ)^{13}C Reaction Cross Section, Astrophysical Journal 422, 912-916 (1994).
[22] Nagai, Y., et al., Measurement of ^{1}H(n,γ)^{2}H Reaction Cross Section at a Comparable M1/E1 Strength, Physical Review C 56, 3173-3179 (1997).
[23] Veerapaspong, T., et al., Measurement of keV-Neutron Capture Cross Sections and Capture Gamma ray Spectra of ^{143,145,146}Nd, Journal of Nuclear Science and Technology 36, 855-864 (1999).
[24] Hori, J., et al., Measurement of Capture Gamma rays from the Broad 53-keV and the Narrow 35-keV Neutron Resonances of ^{23}Na, Journal of Nuclear Science and Technology 36, 91-101 (2001).
[25] Tomyo, A., et al., Neutron Capture Cross Section Measurement of ^{20,22}Ne for Stellar Nucleosynthesis, Nuclear Physics A 718, 527c-529c (2003).
[26] Saito, K., et al., Measurement of keV-Neutron Capture Cross Sections and Capture Gamma ray Spectra of ^{209}Bi, Journal of Nuclear Science and Technology 41, 406-412 (2004).
[27] Segawa, M., et al., Neutron Capture Cross Sections of ^{186}Os, ^{187}Os, and ^{189}Os for the Re-Os Chronology, Physical Review C 76, 022802 (2007).
[28] Wang, T., et al., Measurement of keV-Neutron Capture Cross-Sections and Capture γ ray Spectra of ^{56}Fe and ^{57}Fe, Nuclear Instruments and Methods in Physics Research B 268, 440–449 (2010).

3.2. Ion-induced quasi-monoenergetic and white neutron beams

QUASI-MONOENERGETIC NEUTRON BEAM AND ITS APPLICATION AT THE RCNP CYCLOTRON FACILITY

Y. IWAMOTO[*], H. YASHIMA[**], D. SATOH[*], M. HAGIWARA[***], H. IWASE[***], T. NAKAMURA[+], T. SHIMA[++], A. TAMII[++], K. HATANAKA[++]

[*]Japan Atomic Energy Agency (JAEA), 2-4 Shirane Shirakata, Tokai, Naka, Ibaraki 319- 1195, Japan
[**]Research Reactor Institute, Kyoto University, 2-1010 Asashiro-nishi, Kumatori-cho, Sennan-gun, Osaka 590-0494, Japan
[***]High Energy Accelerator Research Organization (KEK), 1-1 Oho, Tsukuba, Ibaraki 305- 0801, Japan
[+]Shimizu Corporation and Tohoku University, 6-3 Aoba, Aramaki, Aoba-ku, Sendai, 980- 8578, Japan
[++]Research Center for Nuclear Physics (RCNP), 10-1 Mihogaoka, Ibaraki, Osaka 567-0047, Japan
Email: iwamoto.yosuke@jaea.go.jp

Abstract

A quasi-monoenergetic neutron field using ^{7}Li(p,n) reaction for the higher energy range of 100 to 400 MeV has been developed at the RCNP cyclotron facility of Osaka University. The neutron energy spectra at angles from 0° to 30° have been investigated for the proton beams with the energies of 140, 250, 350 and 392 MeV. The highest neutron fluence reaches 1.0×10^{10} n/sr /μC, and the contribution of peak intensity to the total intensity varied between 0.4 and 0.5. Using the quasi-monoenergetic neutron beam, measurement of neutron induced activation cross sections, elastic scattering cross sections for neutron and a shielding benchmark experiment have been performed, successfully. Thus quasi-monoenergetic neutron field at RCNP are suitable for measurement of nuclear data, shielding experiments and the calibration of monitors in the energy region from 100 to 400 MeV.

1. INTRODUCTION

Quasi-monoenergetic neutron reference beams using ^{7}Li(p,n)^{7}Be (g.s. +0.429 MeV, Q = -1.64 and -2.075 MeV) are of special importance for cross-section studies of neutron-induced reactions, shielding benchmark experiments and calibrating the detectors, taking advantage of the narrow energy distribution at the peak. In this report, we describe our studies for the development of neutron fields in energy range from 100 to 400 MeV [1-3] at the Research Center for Nuclear Physics (RCNP) cyclotron facility [4-6] and its application to the measurements of cross sections [7-9] and the neutron shielding experiment [10-12].

2. QUASI-MONOENERGETIC NEUTRON FIELD AT RCNP

The quasi-monoenergetic neutron field developed at the neutron TOF tunnel of the RCNP cyclotron facility is shown in Fig. 1. The layout of the neutron TOF tunnel and the neutron experimental room is schematically illustrated in Fig. 2. Proton beams extracted from the ring cyclotron are transported to the neutron experimental hall and hit a 1.0 cm-thick ^{7}Li placed in the swinger which is in a vacuum chamber. Protons passing through a target are bent to the beam dump using a swinger magnet to measure the proton beam intensity with a Faraday cup. The beam current is kept up to 1 μA. Neutrons produced at 0° from the target are extracted into the 100 m tunnel through a 10 × 12 cm aperture in a 150 cm-thick concrete wall located 4.5 m away from the target. For example, the radius of the neutron beam at 20 m from the target is about 22 cm. The clearing magnet in the movable collimator serves to reduce charged particles contaminating the neutron beam. The movable collimator and the swinger magnet allow neutron emissions to be measured through angles between 0° and 30°.

3.2. Ion-induced quasi-monoenergetic and white neutron beams

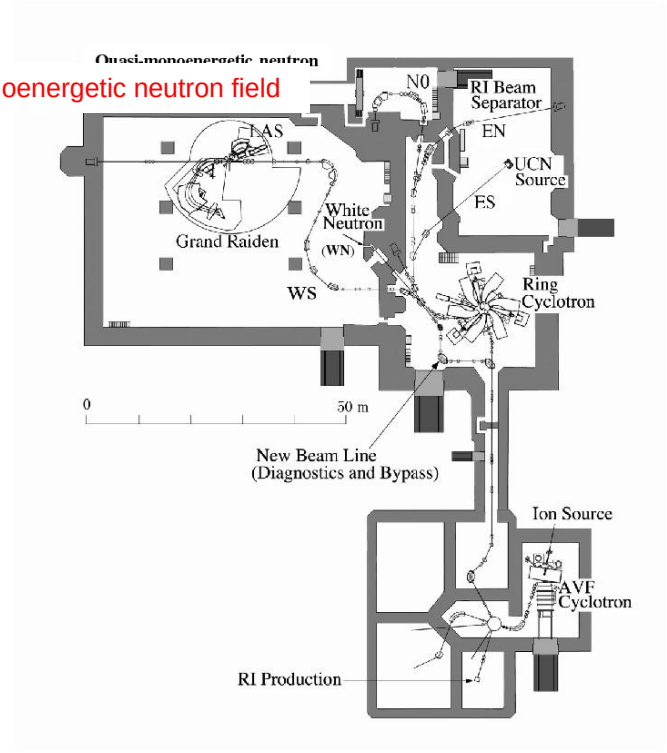

FIG. 1. Schematic layout of the RCNP cyclotron facility.

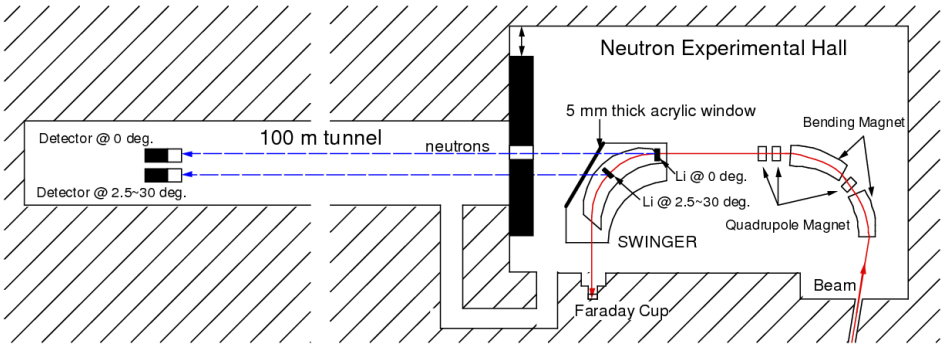

FIG. 2. Illustration of experimental setup in the neutron experimental hall and the 100 m tunnel.

The neutron time-of-flight (TOF) measurements for ^{7}Li(p,n) reaction in the energy above 1 MeV were performed using NE213 organic liquid scintillators [1-3]. The time intervals between successive proton beam pulses can be enlarged from about 500 ns using a beam chopper to avoid contamination with lower energy neutrons. In the TOF measurements, the total and slow components of the light outputs of NE213 were measured with two different timing gates placed on the output signals of NE213 to discriminate neutron events from photon events. Neutron events clearly distinguished from photon events using two-dimensional plots with total and slow components. Neutron flight time was measured as the time difference between the chopper signal and the detector signal. The data were recorded using a conventional computer automated measurement and control system in event-by-event mode using the DAQ system for the CAMAC controller CC/NET [13, 14]. The neutron detection efficiency of NE213 was calculated using the SCINFUL-QMD code [15].

3.2. Ion-induced quasi-monoenergetic and white neutron beams

The interaction of monoenergetic neutrons at 246 and 389 MeV with the collimator, the wall and the floor was investigated using PHITS [16]. It was concluded that the ratio of the continuum to the total in 100 m tunnel ranged from 0.3% to 1.5%, and the contribution to TOF measurement in energy regions above 1 MeV was almost negligible.

Figure 3 shows measured neutron energy spectra at 0°. Peak neutrons covered the range from transitions to the ground state and the first excited state of ^{7}Be and from transitions to the ground state of ^{6}Be. Most of the continuum of data comes directly from the Li(p,xn) reaction because there are 0.3-1.5% room-scattered neutrons to the reaction neutrons. Experimental neutron intensities of the high-energy peak was about 1×10^{10} (n/sr/μC) and was not dependent on incident proton energy. The contribution of peak intensity to the total intensity varied between 0.4 and 0.5 in the incident proton energy range from 137 to 389 MeV.

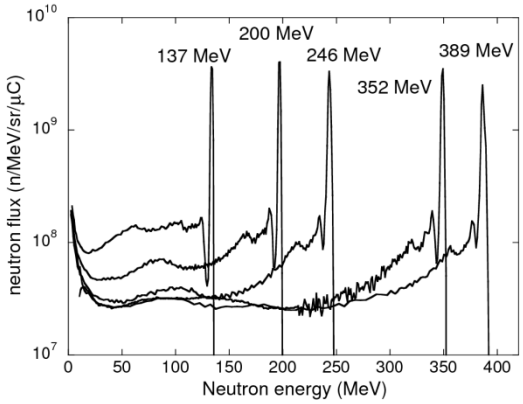

FIG. 3. Measured neutron energy spectra for the 137, 200, 246, 352 and 389 MeV.

Figur 4 shows angular distributions of neutron energy spectra for 137, 200, 246 and 389 MeV Li(p,xn) reactions at angles of 0°, 5°, 10°, 15°, 20° and 25° for 137 and 200 MeV and 30° for 246 and 389 MeV. All neutron energy spectra in the energy region below 50 MeV were comparable, but the shape of the continuum above 100 MeV changed considerably with the angle and incident proton energy. The angular distribution of the high-energy peak neutron production cross section agreed well with calculated results using the Taddeucci formula which was deduced by fitting other experimental data [17].

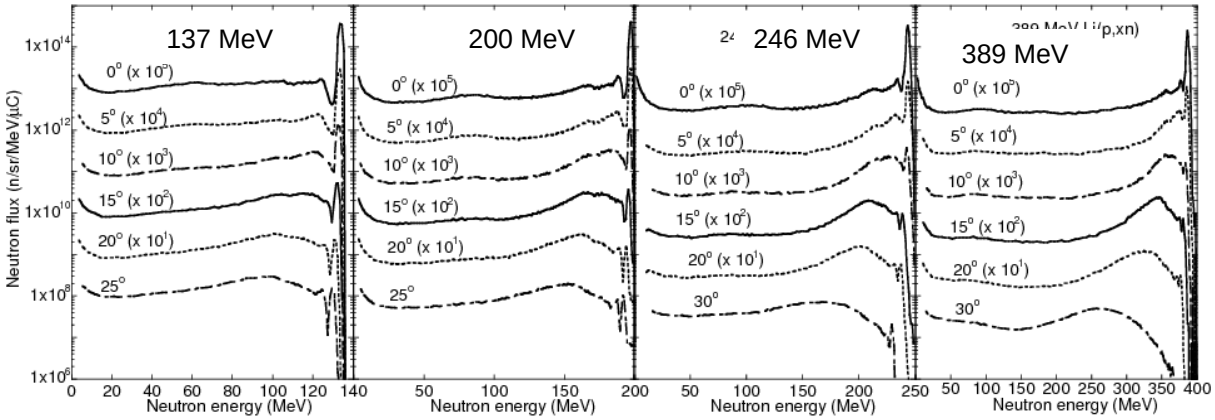

FIG. 4. Experimental results of neutron energy spectra at 0°, 5°, 10°, 15°, 20°, 25° and 30° for 137, 200, 246 and 389 MeV.

3.2. Ion-induced quasi-monoenergetic and white neutron beams

In order to consider the correction required to derive the response in the peak region from the measured total response for neutron-induced activation cross sections and high-energy neutron monitors, we found that subtracting the response at larger angles (20° - 30°) from the 0° data almost eliminates the continuum component [2,3]. This method has potential to eliminate problems associated with continuum correction for measurements of activation cross sections and high-energy neutron monitors.

3. APPLICATION USING QUASI-MONOENERGETIC NEUTRON FIELD

3.1 NEUTRON ACTIVATION CROSS SECTION

Cross sections for neutron-induced activation of Bi at 287 and 370 MeV have been measured [7]. The Bi samples were placed at 0° to measure activities induced by both the peak and continuum components of neutron beam. On the other hands, to measure activities induced by the continuum component, Bi sample was placed at an angle of 30° from the direction of the proton beam. The conditions of the irradiation experiments (distance between Li target and sample) are listed in Table 1. Average proton beam intensity was about 1 μA. During the irradiation time, the proton beam current at the beam dump was recorded with a digital current integrator, connected to a multi-channel scaler (MCS) to monitor the fluctuations of the proton beam currents. After irradiation, the gamma rays emitted from the irradiated samples were measured with a high-purity germanium (HPGe) detector to be connected to 8192 multichannel analyzers. The samples were measured several times in order to identify newly created radio-active nuclides by their half-lives.

TABLE 1. CONDITION OF THE IRRADIATION EXPERIMENTS

proton energy[MeV]		flight path for spectra measurement[m]	distance between Li target and Bi sample[m]	Irradiation time [hours]
300	0˚	17.1	8.05	25.7
	30˚	16.1	7.05	17.9
392	0˚	45.0	8.03	26.7
	30˚	44.0	7.03	22.0

To remove the component of nuclides produced by the continuum part, the 30° spectrum is normalized to the one measured at 0° by equalizing the neutron fluence in low energy region, then the corrected result is obtained by subtracting the normalized 30° spectrum from the 0° spectrum. Thus, the subtraction of the nuclide component produced by a beam angled at 30° from one angled at 0◦ gives a yield produced by high energy peak neutrons only. Other measurements of activation cross sections have also been done and reported in Refs. [18-20].

Figure 5 shows the cross sections obtained for ^{209}Bi(n, xn) ^{201,203,204,205,206}Bi, ^{209}Bi(n, x)^{183g}Os and table 2 summarizes the experimental data of the irradiation experiments. The experimental data measured by Kim et al. [7] gives good agreements with nuclear data below

150 MeV, but there is no data above 150 MeV. Based on *Fig. 5*, the following can be stated: (1) nuclear data file results are less than our measurements, except for nuclides of higher threshold energy. (2) At 370 MeV, our results agree with proton-induced reaction data, but at 287 MeV, proton-induced data differ from our results for some reactions.

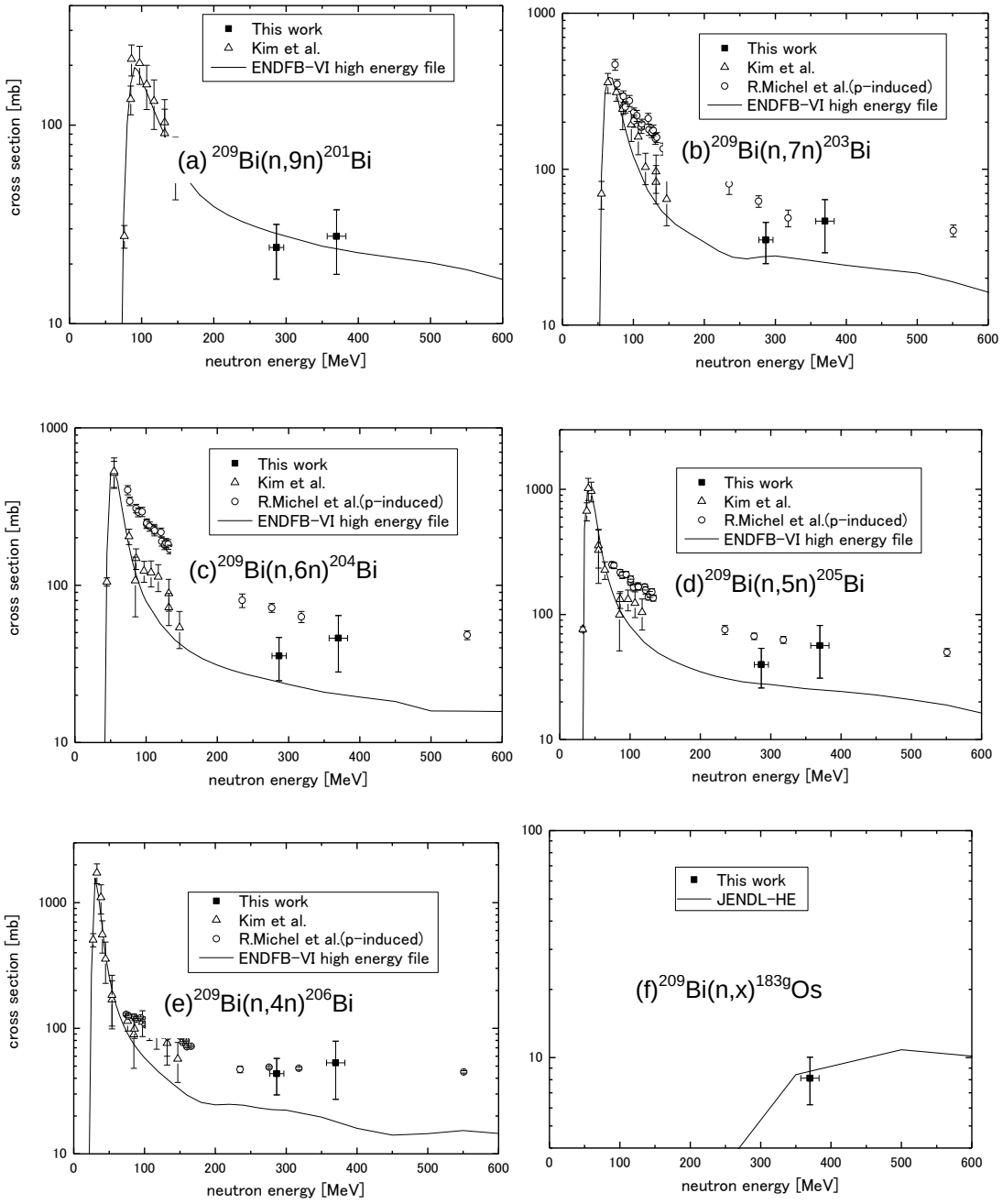

FIG. 5. Excitation function for nuclides produced from Bi.

3.2 NEUTRON ELASTIC SCATTERING CROSS SECTION

Angular differential neutron elastic scattering cross sections have been measured by using a ^{7}Li(p,n) quasi-monoenergetic neutron beam as shown in *Fig. 6* [8,9]. Neutron beams are extracted into the 100 m tunnel through a collimator. An additional collimator, which consists of iron 100 cm long and 5.5 cm in diameter at the exit side, was placed in front of a

preinstalled collimator for more aggressive beam collimation. A cylindrical sample of natural carbon (5 cm ϕ × 5 cm) was set 10 m downstream from the lithium target, and bombarded with the 134 MeV neutron beam.

TABLE 2. EXPERIMENTAL DATA AT 287 AND 370 MEV NEUTRONS

Reaction	287 MeV neutrons		370 MeV neutrons	
	cross section[mb]	error[mb]	cross section[mb]	error[mb]
^{209}Bi(n,9n)^{201}Bi	28	10	24	7
^{209}Bi(n,7n)^{203}Bi	46	17	35	10
^{209}Bi(n,6n)^{204}Bi	46	18	36	11
^{209}Bi(n,5n)^{205}Bi	56	25	40	14
^{209}Bi(n,4n)^{206}Bi	53	26	44	14
^{209}Bi(n,x)^{183g}Os			8.1	1.9

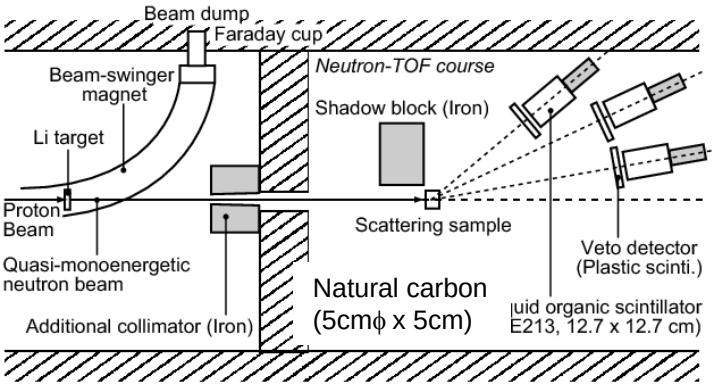

FIG. 6. Experimental setup for measurements of neutron elastic scattering cross sections at RCNP.

NE213 liquid organic scintillators (12.7 cm ϕ × 12.7 cm) were employed to detect the scattered neutrons. The flight-path length between a carbon sample and a detector was extended to 5.0 m to allow measurement at forward angles, while it was 2.5 m at larger angles to enhance the counting rate. Thin plastic scintillators were mounted in front of the NE213 scintillators as veto detectors to tag the charged particles emitted from the sample.

Figure 7 shows the neutron elastic scattering cross sections together with the UC Davis data [21], and the evaluated nuclear data from JENDL/HE-2007 [22] and ENDF/B-VII.0 [23]. It was concluded that experimental data gives good agreement with nuclear data from JENDL-HE-2007 and the UC Davis data measured by using a continuous energy neutron source and a recoil-proton telescope.

3.2. Ion-induced quasi-monoenergetic and white neutron beams

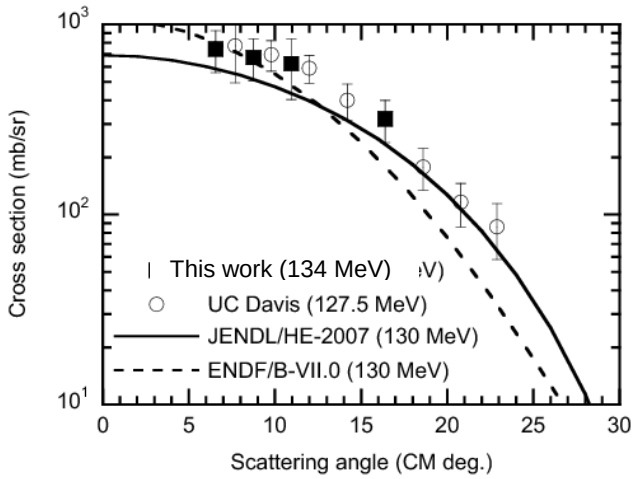

FIG. 7. Comparison of measurements of C(n,n') differential cross sections with the experimental data of UC Davis and the evaluated nuclear data, JENDL/HE-2007 and ENDF/B-VII.0.

3.3 NEUTRON SHIELDING EXPERIMENTS

Shielding benchmark experiments have been performed using a quasi-monoenergetic ^{7}Li(p,n) neutron source with 140, 246 and 389 MeV protons in order to investigate the accuracy of nuclear data libraries and calculation codes for hundreds of MeV neutrons [10-12]. Figure 8 illustrates the experimental setup.

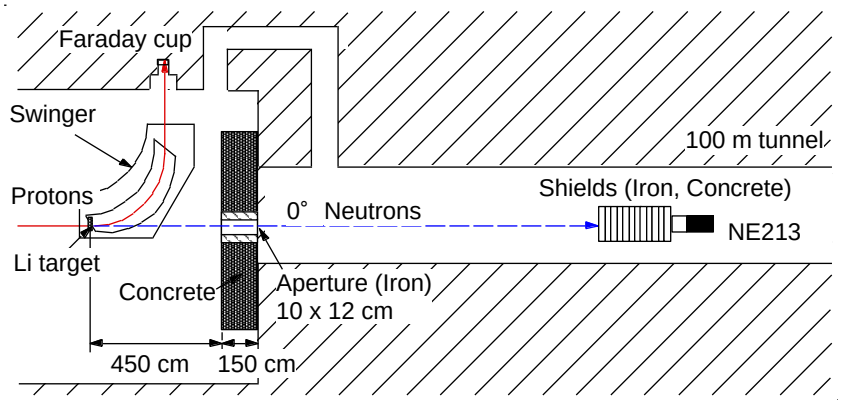

FIG. 8. Illustration of experimental setup for shielding experiment.

Shielding blocks, 118 × 118 × 10 cm-thick iron blocks and 120 × 120 × 25 cm-thick concrete blocks, were assembled with thickness from 10 to 100 cm for the iron shield, from 25 to 300 cm for the concrete shield. For the composite shield, 70 cm-thick iron were mounted in front of 200 cm-thick concrete. The shielding assemblies were placed ~18 m away from the Li target. The density of the iron and concrete used in this experiment was 7.87 and 2.33 g·cm^{-3}, respectively, and the atomic compositions of the concrete are listed in [10]. A large NE213 scintillator of 25.4 cm in diameter and 25.4 cm in thickness and He-3 detector with Bonner spheres were used for measurement of high-energy neutrons [11,12] and low-energy neutrons[10], respectively. The distance between the target and the detector were changed from 18 m to 21 m with increasing the thickness of the shields. The proton beam was used of intensity between 1 nA to 1 μA.

3.2. Ion-induced quasi-monoenergetic and white neutron beams

Figure 9 shows the measured energy spectra of neutrons transmitted through the iron, concrete and their composite shields with energies above 30 MeV, in comparison with the calculation results using the PHITS code coupled with the JENDL-HE data library. For 246 MeV, the experimental spectra are generally in good agreement with the calculated results. In the energy region below 150 MeV, however, the measured spectra are larger than the calculation results which show rather flat spectra comparing to the measured data. For 389 MeV, the measured data are generally several tens % higher than the calculation results in addition to the difference in the low energy region below 150 MeV. This difference might come from counting the charged hadrons (p, π±) produced in the shields. This effect will be checked in the future study and will be corrected.

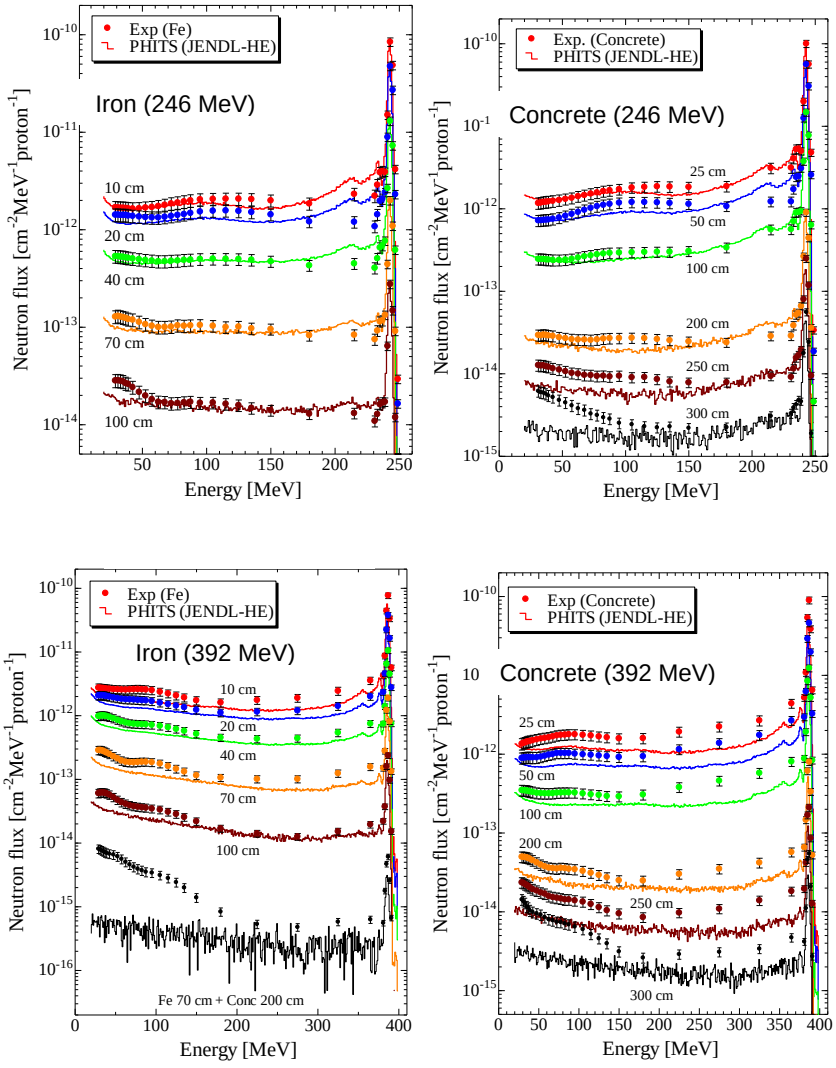

FIG. 9. Comparison of the neutron energy spectra transmitted through the iron, concrete and their composite shield with various thicknesses for the 246 and 389 MeV p-Li reactions.

Figure 10 shows the peak flux attenuation profiles in the iron and concrete shields, and the fitting results with single exponential curves are also given. These attenuation lengths of 244 and 387 MeV monoenergetic neutrons, which are produced by 246 and 389 MeV protons, respectively, give good agreement between experiment and calculation within 6%.

3.2. Ion-induced quasi-monoenergetic and white neutron beams

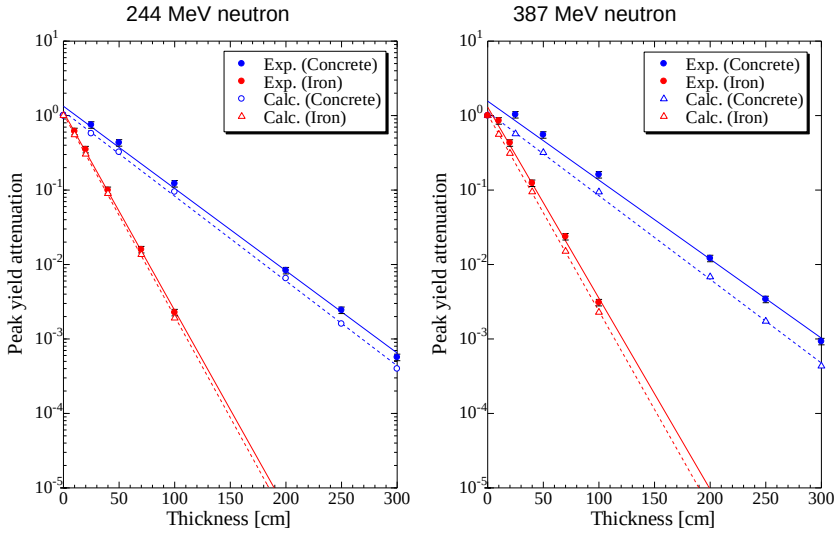

FIG. 10. Comparison of the measured and the calculated peak flux attenuation of 244 and 387 MeV neutrons transmitted through the iron and concrete shields as a function of the thickness.

3.4 MEASUREMENT OF THICK TARGET NEUTRON YIELDS FOR WHITE NEUTRON SOURCE

Neutron energy spectra at 0° produced from stopping-length graphite, aluminum, iron and lead targets bombarded with 140, 250 and 350 MeV protons were measured at the neutron TOF course [24]. Figure 11 shows the measured and calculated neutron energy spectra from thick targets bombarded with 140, 250 and 350 MeV protons for graphite and iron. The experimental data for 210 MeV proton incidence on the stopping-length iron target at RIKEN [25] is also plotted in the figure of 250 MeV proton incidence on iron. These experimental results with energy resolution of 12MeV at RIKEN and that of 4 MeV at RCNP agreed well with each other at energies below 200 MeV. Past our data of 350 MeV proton incidence on iron are higher than the present data due to the difference in the calculation code of the neutron detection efficiency of NE213. SCINFUL-QMD [15] which is used in the present data improved the agreement between the experimental data and the calculation because it describes more correct nuclear reaction in high-energy region than old detection efficiency model, CECIL [26].

Calculations of these spectra were carried out with the PHITS and MCNPX codes using the evaluated nuclear data files JENDL-HE and LA 150, and the theoretical models, ISOBAR in PHITS and LAHET in MCNPX. For 140MeV proton incidence, calculations with the evaluated nuclear data files generally reproduced the experimental data well. For 250 and 350MeV proton incidences, JENDL-HE values for C used in evaluation with JQMD/GEM underestimated the experimental data by a factor of two, and therefore it is better to use other models such as ISOBAR model in this nuclear data evaluation. Calculated results of ISOBAR and LAHET generally agree with the experimental results in the energy range above 20MeV except for graphite at 350 MeV.

Neutrons produced from a thick target have a potential to be new white neutron sources for measurement of nuclear data, shielding experiments and so on. These measurement data, therefore, will be useful to design the white neutron field for these purposes.

3.2. Ion-induced quasi-monoenergetic and white neutron beams

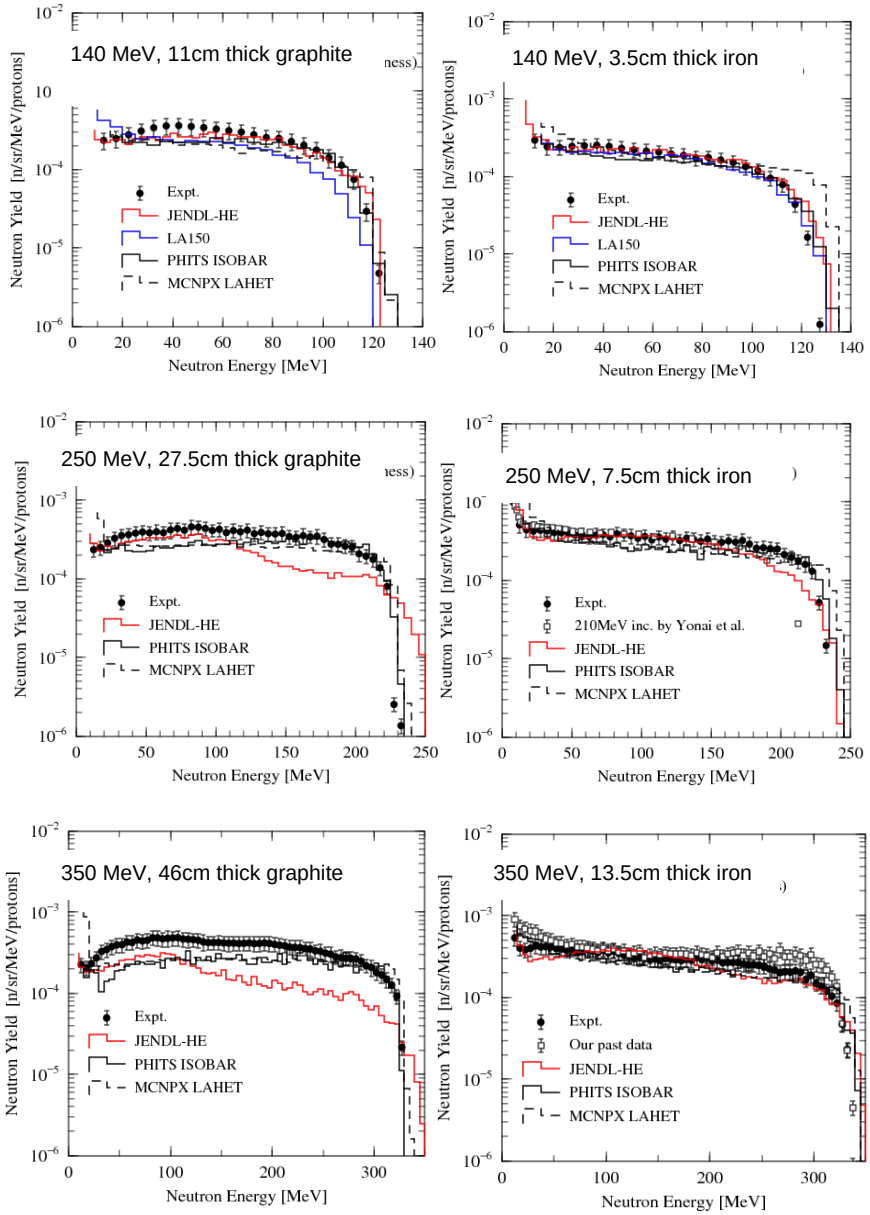

FIG. 11. Neutron energy spectra for 140, 250 and 350 MeV proton incidence on thick graphite, and iron targets. The experimental results are compared with the calculated results as given in the text.

4. SUMMARY

A quasi-monoenergetic neutron field using ^{7}Li(p,n) reaction for the higher energy range has been developed at the RCNP cyclotron facility of Osaka University. The neutron energy spectra at angles from 0° to 30° have been investigated for the proton beams with the energies of 140, 250, 350 and 392 MeV. The highest neutron fluence reaches 1.0×10^{10} n/sr /μC, and the contribution of peak intensity to the total intensity varied between 0.4 and 0.5. Using quasi monoenergetic neutron beams, measurement of neutron induced activation cross sections of Bi, elastic cross sections for neutron and shielding benchmark experiments have been carried out. Further systematic experimental studies will be performed for evaluation of neutron-induced cross sections. Other experiments, the calibration of neutron monitors [27-31], were also performed and will be reviewed elsewhere. Thus quasi-monoenergetic neutron

field at RCNP are suitable for measurement of nuclear data, shielding experiments and the calibration of monitors.

REFERENCES

[1] TANIGUCHI, S., et al., "Development of a quasi-monoenergetic neutron field using the ^{7}Li(p,n)^{7}Be reaction in the energy range from 250 to 390 MeV at RCNP," Rad. Prot. Dosim. **126** (1-4) (2007) 23.

[2] IWAMOTO, Y., et al., "Quasi-monoenergetic neutron energy spectra for 246 and 389 MeV ^{7}Li(p,n) reactions at angles from 0° to 30°", Nucl. Instr. and Meth. A 629 (2011) 43.

[3] IWAMOTO, Y., et al., "Characterization of quasi-monoenergetic neutron source using 137, 200, 246 and 389 MeV ^{7}Li(p,n) reactions", Proceedings of the 12th International Conference on Radiation Shielding (ICRS-12), Nara, Japan (2012), to be published.

[4] MIURA, T., et al., "Commissioning of the RCNP ring cyclotron", Proceedings of the 13th International Conference on Cyclotrons and their Applications, Vancouver, Canada, (1992), p. 3.

[5] SAITO, T., et al., "The flat-topping system for the RCNP ring cyclotron," in Proceedings of the 14th International Conference on Cyclotrons and their Applications, Cape Town, South Africa (1995) 169.

[6] NINOMIYA, S., et al., "Ultra high stabilization of the magnetic field of the RCNP cyclotron," in Proceedings of the 17th International Conference on Cyclotrons and their Applications, Tokyo, Japan (2004) 140.

[7] YASHIMA, H., et al., "Measurements of the neutron activation cross sections for Bi at 287 and 370 MeV", Proc. Radiochim. Acta 1 (2011) 135.

[8] SATOH, D., et al., "Experimental method for neutron elastic scattering cross-section measurement in intermediate energy region at RCNP", Progress in Nuclear Science and Technology **1** (2011) 20.

[9] SATOH, D., et al., "Measurement of neutron elastic scattering cross sections for carbon at 134 MeV", Radiation Measurements 45 (2010) 1159.

[10] YASHIMA, H., et al., "Benchmark experiment of neutron penetration through iron and concrete shields for hundreds-of-MeV quasi-monoenergetic neutrons - I: Measurements of neutron spectrum by a multimoderator spectrometer," Nuclear Technology 168 (2009) 298.

[11] HAGIWARA, M., et al., "Benchmark experiment of neutron penetration through iron and concrete shields for hundreds-of-MeV quasi-monoenergetic neutrons - II: Measurements of neutron spectrum by an organic liquid scintillator", Nuclear Technology **168** (2009) 304.

[12] HAGIWARA, M., et al., "Shielding benchmark experiment using hundreds of MeV quasi-monoenergetic neutron source by a large organic scintillator", Proceedings of the 12th International Conference on Radiation Shielding (ICRS-12), Nara, Japan (2012), to be published.

[13] IEEE, "IEEE Standard Modular Instrumentation and Digital Interface System (CAMAC) (Computer Automated Measurement and Control) IEEE Std 583-1975.

[14] YASU Y., et al., "Development of a Pipeline CAMAC Controller with PC/104 Plus Single Board Computer", International Conference on Computing in High Energy and Nuclear Physics CHEP03, La Jolla, California, USA, March 24-28, 2003 and http://www-online.kek.jp/~yasu/Parallel-CAMAC/.

[8] SATOH, D., et al., "SCINFUL-QMD: Monte Carlo based computer code to calculate response function and detection efficiency of a liquid organic scintillator for neutron energies up to 3GeV", JAEA-Data/Code, 2006-023.
[9] NIITA, K., et al., "PHITS: Particle and Heavy Ion Transport code System, Version 2.23, JAEA-Data/Code", 2010-022, Japan Atomic Energy Agency, (2010) and http://phits.jaea.go.jp/index.html.
[10] TADDEUCCI, T.N., et al., "Zero-degree cross sections for the ^{7}Li(p,n)^{7}Be(g.s.+0.43-MeV) reaction in the energy range 80 – 795 MeV", Phys. Rev. C **41** (1990) 2548.
[11] SEKIMOTO, S., et al., "Measurements of cross sections for production of light nuclides by 300 MeV-proton bombardment of Cu and Y", Nucl. Instr. and Meth. B **294** (2013) 475.
[12] SEKIMOTO, S., et al., "Measurement of High Energy Neutron Induced Cross Sections for Chromium", Journal of the Korean Physical Society **59** (2011) 1916.
[13] SEKIMOTO, S., et al., "Measurement of Neutron Cross Sections for Yttrium and Terbium at 287 MeV", Progress in Nuclear Science and Technology **1** (2011) 89.
[14] OSBORNE, J.H., et al., "Measurement of neutron elastic scattering cross sections for ^{12}C, ^{40}Ca, and ^{208}Pb at energies from 65 to 225 MeV" Phys. Rev. C **70** (2004) 054613.
[15] WATANABE, Y., et al., "Nuclear data evaluation for JENDL high-energy file", AIP Conf. Proc. **769** (2005) 326.
[16] CHADWICK, M.B., et al., "ENDF/B-VII.0: next generation evaluated nuclear data library for nuclear science and technology", Nucl. Data Sheets 107 (2006) 2931.
[17] IWAMOTO, Y., et al., "Measurement of thick target neutron yields at 0° bombarded with 140, 250 and 350 MeV protons", Nucl. Instr. and Meth. A **593** (2008) 298.
[18] YONAI, S., et al., "Measurement of neutrons from thick Fe target bombarded by 210 MeV protons", Kurosawa, H. Iwase, et al., Nucl. Instr. and Meth. A 515 (2003) 733.
[19] CECIL, R.A., et al., "Improved Predictions of Neutron Detection Efficiency for Hydrocarbon Scintillators from 1-Mev to about 300-MeV", Nucl. Instr. and Meth. 161 (1979) 439.
[20] MASUDA, A., et al., "Response measurement of a bonner sphere spectrometer for high-energy neutrons", IEEE transactions on nuclear science, **59** 1 (2012) 161.
[21] PIOCH, V., et al., "Calibration of a Bonner sphere spectrometer in quasi-monoenergetic neutron fields of 244 and 387 MeV", Journal of Instrumentation, **6** (2011) P10015.
[22] JÄGERHOFER, L., et al., "Characterization of the wendi-II rem counter for its application at medaustron", Progress in Nuclear Science and Technology **2** (2011) 258.
[23] VINCKE, H., et al., "Response of ionization chambers to high-energy mono-energetic neutrons", Nuclear Technology **168** (2009) 5.
[24] THEIS, C., et al., "Field calibration studies of the PMI ionization chambers in the UX85 cavern", CERN Technical Note CERN-SC-2008-053-RP-TN, (2008).

HIGH-ENERGY NEUTRON BEAM FACILITIES AND NUCLEAR DATA MEASUREMENTS AT THE SVEDBERG LABORATORY

A.V. PROKOFIEV[*], B. GÅLNANDER[*], O.I. BATENKOV[**], C. GUSTAVSSON[***], S. POMP[***], A.N. SMIRNOV[**], V. WAGNER[+], A. WALLNER[++, +++], D Y. WATANABE[§]

[*]The Svedberg Laboratory, Uppsala University, P.O. Box 533, 751 21 Uppsala, Sweden
[**]V.G. Khlopin Radium Institute, 2oi Murinskiy Prospect 28, Saint Petersburg 194021, Russia
[***]Dept. of Physics and Astronomy, Uppsala University, P.O. Box 516, 751 20, Sweden
[+] Nuclear Physics Institute, 250 68 Řež near Prague, Czech Republic
[++]Vienna Environmental Research Accelerator, Faculty of Physics, University of Vienna, Waehringer Strasse 17, A-1090 Wien, Austria
[+++]Department of Nuclear Physics, Research School of Physics and Engineering, The Australian National University ACT 0200, Australia
[§] Department of Advanced Energy Engineering Science, Kyushu University, Kasuga, Fukuoka, Japan
Email: alexander.prokofiev@tsl.uu.se

Abstract

The Svedberg Laboratory (TSL) belongs to Uppsala University and exploits the Gustaf Werner cyclotron that delivers beams of protons and heavy ions to different beam lines and irradiation facilities. The main activities at TSL comprise proton treatment of cancer patients, radiation testing services, detector development, and nuclear data measurements. Currently, two high-energy neutron beam facilities are in regular use at TSL: (1) The quasi-monoenergetic neutron facility (QMN), and (2) The ANITA facility (Atmospheric-like Neutrons from thIck TArget). Both the facilities are driven by the proton beam from the cyclotron, with energy selectable in the range 20 – 180 MeV. The beam is pulsed, which allows one to use time-of-flight techniques. In the present report, we describe the neutron beam facilities at TSL, with focus on the QMN facility, including beam monitors as well as quality assurance and user support routines. Furthermore, we give an overview of neutron nuclear data measurements performed at the QMN facility.

1. INTRODUCTION

The Svedberg Laboratory (TSL) is an accelerator facility belonging to Uppsala University. The laboratory operates the Gustaf Werner cyclotron for production of high-energy fields of protons, neutrons, and heavy ions. Available proton beams have variable energy (20-180 MeV) and intensity (from 10 μA down to single protons per second). 180-MeV proton beam is used for treatment of cancer patients during the major part of the year. During last years, the laboratory has developed routines for sharing of the proton beam between the therapy area and other irradiation facilities, which allows efficient use of the beam. In total, TSL is capable of offering at least 2000 hours beam time per year for users from industry and science, at the following irradiation facilities that make use of the proton beam from the cyclotron: (1) the Quasi-Monoenergetic Neutron (QMN) facility, (2) the ANITA facility (Atmospheric-like Neutrons from thIck TArget), (3) the PAULA facility (Proton fAcility in UppsaLA).

The QMN facility utilizes the ^{7}Li(p,n) reaction for neutron production. The peak energy of the resulting quasi-monoenergetic neutrons is selectable in the region from 20-175 MeV. The facility was rebuilt in 2003-2004, resulting in a factor of ~10 higher neutron beam flux and improved flexibility in the size of the neutron beam spot.

3.2. Ion-induced quasi-monoenergetic and white neutron beams

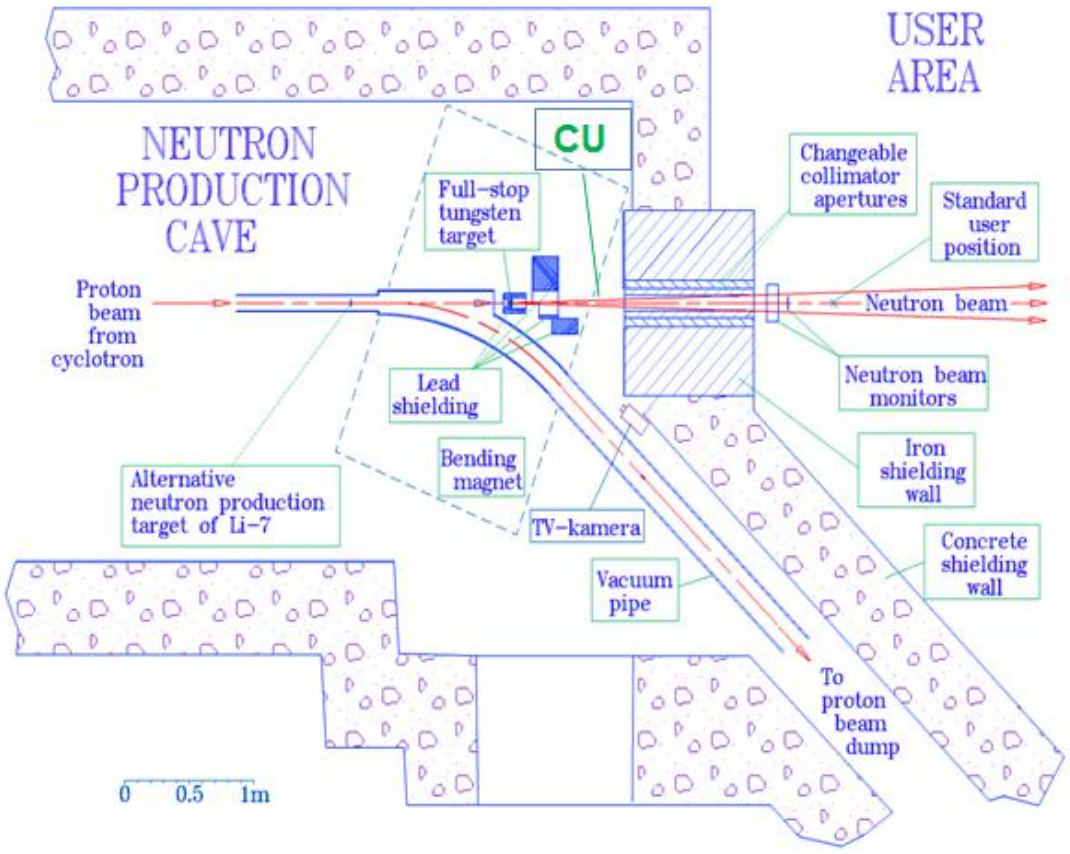

FIG.1. A schematic layout of the QMN and ANITA neutron facilities. A new high-flux irradiation position under development, the so-called Close User Position (CUP), is indicated.

Alternatively, neutrons can be produced at the ANITA facility, which was developed in 2007. At the ANITA facility, a continuous "white" spectrum is available, from thermal energies up to ~180 MeV with a flux density ~10^6 cm^{-2} s^{-1} for neutrons above 10 MeV and with the beam spot size controllable from 1 to 120 cm. The ANITA facility has been described in detail elsewhere [1].

Furthermore, the proton beam from the cyclotron can be delivered to the PAULA facility, constructed in 2011. The user can choose proton energy (20-180 MeV), flux (from single protons up to 10^{12} cm^{-2} s^{-1}), and beam spot size (up to 20 cm). Both scattered and unscattered beams can be delivered.

The ANITA and PAULA facilities are used primarily for industrial applications, which are dominated by radiation testing of electronic components and systems for spacecraft, avionics, telecommunication, IT (high-end servers and routers), solar energy applications, automotive, railway, medical devices, accelerators, and accelerator-driven systems.

The present article has a focus on the QMN facility, which is in use for both industrial applications and nuclear data measurements. The facility is described in Sect. 2, and an overview of the nuclear data programmes is given in Sect. 3.

2. THE QMN FACILITY

2.1. THE DESIGN

In Fig. 1, an overview of the neutron facilities is shown. The proton beam from the cyclotron, with the energy selectable in the range from 25 to 180 MeV, arrives at a target of ^{7}Li located in a heavily shielded neutron production cave. The lithium targets are available in thicknesses of 2, 4, 8.5 and 23.5 mm and consist of isotopically pure ^{7}Li to 99.9%. Proton energy loss in the target amounts to 2–6 MeV depending on the incident beam energy and target thickness. The targets are rectangular in shape, 20 × 32 mm^2, and are mounted in a remotely controlled water-cooled copper rig. An additional target position contains a fluorescent screen viewed by a TV camera, which is used for beam alignment and focusing. There is also a position with an empty target frame, intended for background measurements. In Fig. 2, a photograph of the neutron production area is presented.

Only a minor fraction of incident protons undergoes nuclear interactions in the lithium target. The remaining protons that pass through the target are deflected by a magnet into a 10-m long dumping line and guided onto a heavily shielded water-cooled graphite beam dump. The maximum proton beam current on the target is 0.2 - 5 μA, dependent on the incident energy. At the lowest energies, the current on target is limited by cooling efficiency, whereas at the highest energies the target is capable of receiving the maximum beam current that the cyclotron can deliver. The reduced neutron flux at high incident proton energies can be partly compensated by using thicker lithium targets, see Sect. 2.2.

In Fig. 1, the neutron production target of the ANITA facility is shown as well. The QMN and the ANITA facilities share the same neutron production cave, neutron beam path, the user area, and the Standard User Position (SUP), located at the distance of 3.73 m downstream of the lithium target position.

As seen in Fig. 1, the neutron production cave is shielded by concrete from all the sides except in the forward direction, where there is a 1-m thick iron frontal wall that separates the cave from the user area. The neutron beam is geometrically shaped by a collimator aperture in the iron wall, see Fig. 3. A modular design of the collimator allows the user to vary the size and the shape of the neutron beam at the user area by choosing different apertures. At present, the following apertures are available: (1) cylindrical: 2, 3, 5.5, 7.5, 10, 15, 20, and 30 cm in diameter; (2) conical, with an entrance diameter of 3.66 cm and an exit diameter of 5.4 cm; (3) with a quadratically shaped cross-section of 1 cm^2 area. Using the largest aperture, 30 cm in diameter, one can achieve a neutron beam size of at least 80 cm towards the end of the neutron beam path.

The user area extends from 3.73 m to ≈16 m downstream of the production target. The neutron beam propagates from the production target towards the beam dump as a cone or as a pyramid, for cylindrical and square apertures, respectively, with the beam axis going at the height of 1.5 m above the floor. Not less than 30 m^2 area is available for users' equipment, with the overall height of at least 2.5 m.

The highest neutron flux is currently available at the SUP (see Sect. 2.2). A new irradiation position, so-called Close User Position (CUP), is under development. The CUP is located between the bending magnet and the frontal wall (see Fig. 1), at the distance of ~2 m from the Li target. The CUP is expected to give a gain in the peak neutron flux by a factor of ~3.5 relative to the SUP.

2.2. CHARACTERIZATION OF QMN FIELDS

Using the Medley setup (see Sect. 3.2), neutron spectra at 0° were obtained in Ref. [2] by measuring elastic *np*-scattering. The scattered protons were detected at an angle of 20° relative to the neutron beam direction. The measured neutron spectra for the peak energies from 22 to 143 MeV are shown in Fig. 4 in comparison with model calculations [3, 4] folded with a function that describes the energy resolution in the experiment in Ref. [2]. The neutron spectrum for the peak energy of 175 MeV is presented in Ref. [5]. In all cases, the spectrum at 0° is dominated by a peak situated a few MeV below the energy of the primary protons and comprising about 40-50% of the total number of neutrons.

FIG. 2. The neutron production area at the QMN facility: the incoming beam line (to the left, in the foreground), the bending magnet (in the background), and the target elevator (upstream the magnet).

FIG. 3. The iron frontal wall and the largest collimator aperture (left panel); collimator inserts of different sizes (right panel).

In Table I, the main features of the measured spectra and the achieved neutron fluxes are summarized. The latter have been measured with a monitor based on a thin-film breakdown counter (TFBC), see Sect. 2.3.

Further details on the facility, including the temporal structure of the beam, neutron beam profiles, thermal neutron component in the beam, contamination of the neutron beam by γ rays and stray protons, etc. are described in Ref. [6].

3.2. Ion-induced quasi-monoenergetic and white neutron beams

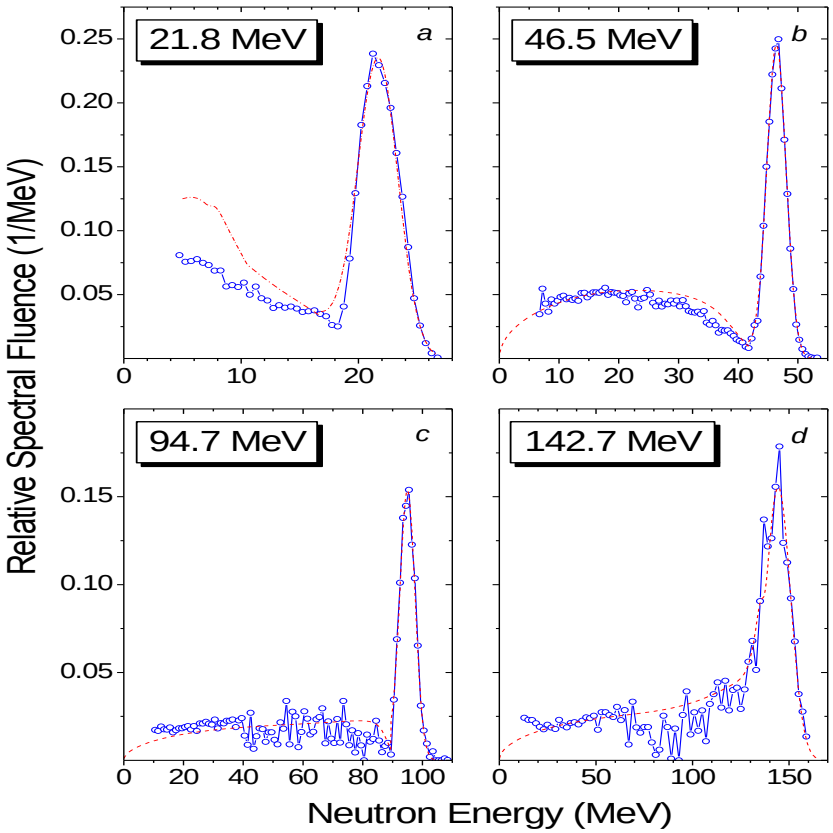

*FIG. 4. The neutron spectra at 0° for peak neutron energies of 21.8 MeV (**a**), 46.5 MeV (**b**), 94.7 MeV (**c**), and 142.7 MeV (**d**). The symbols represent experimental data [2]. The lines represent model calculations from Ref. [3] (panel **a**) and Ref. [4] (panels **b, c, d**).*

2.3. NEUTRON MONITORS

For most experiments, whether for nuclear data, detector development, or electronics testing, it is necessary to monitor the neutron flux versus time. A monitor device should be accurate, durable, reliable under radiation, non-perturbing for the beam, instantaneous (real-time), suitable for time-of-flight (TOF) techniques, and capable of delivering suitable event rate. These different criteria are often difficult to combine in one single device. Furthermore, for reliable monitoring, one should preferably use at least three independent monitors. This allows one to assure the quality of the monitoring data and to identify and troubleshoot a monitor that would operate improperly. More monitors can give "healthy redundancy", provided that they do not perturb the beam significantly.

At TSL, five or more non-perturbing monitors are routinely used. Most frequently, ionization chambers (IC) [7] and TFBC [8] are employed, see Fig. 5. Both the monitors utilize neutron-induced fission of ^{238}U with the cross section adopted as neutron flux standard [9]. Other neutron-induced fission reactions may be utilized as well. In addition, the neutron flux is indirectly monitored by a Faraday cup, which integrates the current of protons collected at the beam dump (see Sect. 2.1).

3.2. Ion-induced quasi-monoenergetic and white neutron beams

TABLE 1. PARAMETERS OF TYPICAL AVAILABLE NEUTRON BEAMS

Proton beam energy (MeV)	^{7}Li target thickness (mm)	Proton beam current (μA)	Average energy of peak neutrons (MeV)	Fraction of neutrons in the high-energy peak (%)		Peak neutron flux at the SUP (10^{5} $cm^{-2}s^{-1}$)
				Measured	Calculated	
24.68 ± 0.04	2	5	21.8	~50	-	0.34
49.5 ± 0.2	4	5	46.5	39	36	1.3
76.9 ± 0.2	8	5	73.4	-	40	3.1
97.9 ± 0.3	8.5	2	94.7	41	39	1.2
147.4 ± 0.6	23.5	0.4	142.7	-	40	0.69
179 ± 1	23.5	0.2	175	-	42	0.37

[1]At the neutron beam path at the distance of 8 m from the lithium target.

At TSL, five or more non-perturbing monitors are routinely used. Most frequently, ionization chambers (IC) [7] and TFBC [8] are employed, see Fig. 5. Both the monitors utilize neutron-induced fission of ^{238}U with the cross section adopted as neutron flux standard [9]. Other neutron-induced fission reactions may be utilized as well. In addition, the neutron flux is indirectly monitored by a Faraday cup, which integrates the current of protons collected at the beam dump (see Sect. 2.1).

2.4. QUALITY ASSURANCE AND USER SUPPORT

Irradiation facilities at TSL, including QMN, are run and supported by the Irradiation Facilities (IF) group consisting of three research scientists and three engineers. The group is responsible for setting up the neutron beams and the monitors, as well as for the quality assurance (QA) and for the external user support. Setting up the neutron beams and the monitors is performed according to traceable and reproducible procedures summarized in checklists. Prior to releasing the beam to the user, a number of quality checks is performed, including the ones for beam transport, temporal structure of the beam, backgrounds, linearity of the monitor count rates and their stability over time, reproducibility of count rates and their ratios from run to run, etc. Furthermore, as soon as the user's setup is ready-to-run, more checks are performed to reveal any possible influence of user's objects/equipment in the beam area on the performance of the monitors. Many of the checks are repeated daily, as well as with any event that may potentially influence the quality of the beam/monitoring.

3.2. Ion-induced quasi-monoenergetic and white neutron beams

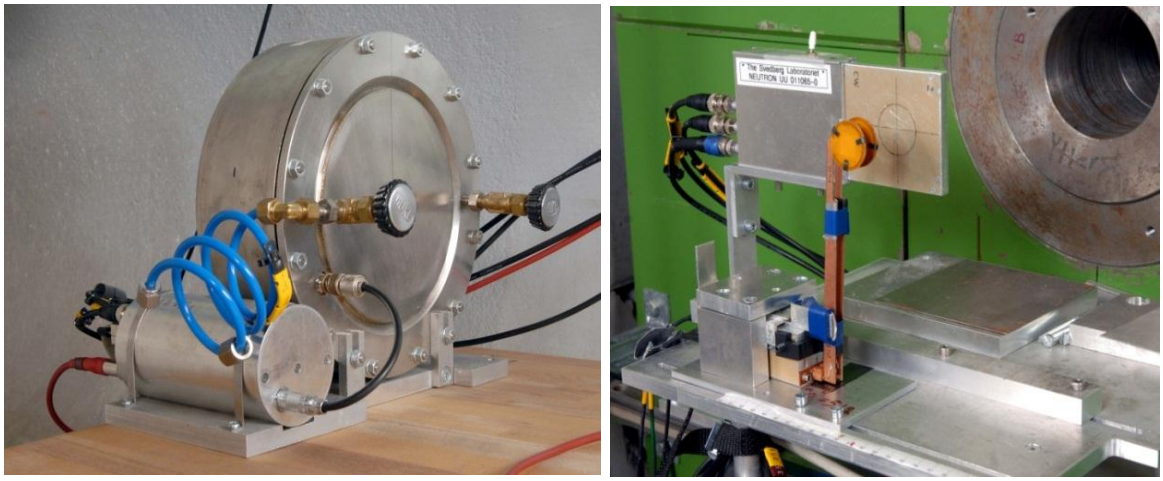

FIG. 5. The neutron flux monitors: an IC (left panel) and TFBCs (right panel).

A number of neutron monitors (see Sect. 2.3) operate continuously during the user beam time. During the experiment, all the monitor readings are continuously logged by the control system versus time, in order to detect variations in the neutron flux, e.g. due to fluctuations in the primary proton beam current. The data coming from the monitors can be inspected online as well as delivered to the user upon request. With a deviation of monitor count rates from the designated ranges, an alarm is activated, and automatic messages are sent to the responsible TSL personnel.

For user groups, Automated Workplaces (AWP) are developed for controlling the radiation protection (RP) status of the experimental area, turning the beam on and off, inspecting the intensity/flux plots, etc. A part of the AWP is the BORN system (Beam Off with pReset flueNce) that allows the user to pre-program the irradiation with the desired number of neutrons per unit area.

During the entire user beam time, the user may contact: (1) the cyclotron operator, available on-site, (2) a scientist or an engineer on duty in the IF-group, available on-site or on-call. Support to user groups is provided as well concerning RP training, handling and storage of irradiated objects, shipment/customs procedures, IT infrastructures, etc.

To facilitate networking with user groups as well as with other neutron facilities, TSL has created a discussion group “Neutron beam facilities and users” at LinkedIn [10].

3. NUCLEAR DATA PROGRAMMES AND EXPERIMENTS

Nuclear data for high-energy neutrons are important not only for basic physics research but also in a number of applications, e.g. in the fields of accelerator-driven systems, dose estimates in advanced particle therapy, and radiation effects in microelectronic devices. The QMN facility at TSL is one of the most useful instruments in the world for neutron nuclear data measurements at the energies in the region 20 – 200 MeV. During the last decade, QMN beams have been employed for studies of elastic and inelastic neutron scattering (Sect. 3.1), light-ion production (Sect. 3.2), fission (Sect. 3.3), and radionuclide production (Sect. 3.4).

3.1. ELASTIC AND INELASTIC NEUTRON SCATTERING CROSS SECTIONS

Measurements of neutron scattering cross sections were performed using the SCANDAL (SCAttered Nucleon Detection AssembLy) setup at the old QMN facility [11, 12]. The SCANDAL setup (see Fig. 6) was designed to detect neutrons scattered from a target under study. The detection of neutrons is based on conversion to protons in a thick plastic scintillator. The angular resolution of 1.4° (r.m.s.) was achieved [12]. Further details are available in Refs. [12, 13].

Data from elastic neutron scattering at 96 MeV have been published for the following scattering targets: ^{1}H, ^{2}H, C, O, Fe, ^{89}Y, ^{208}Pb, and U [13-19]. As examples of elastic scattering data from SCANDAL, angular-differential cross sections for three different targets, Fe, ^{89}Y, and ^{208}Pb [13] are shown in Fig. 7.

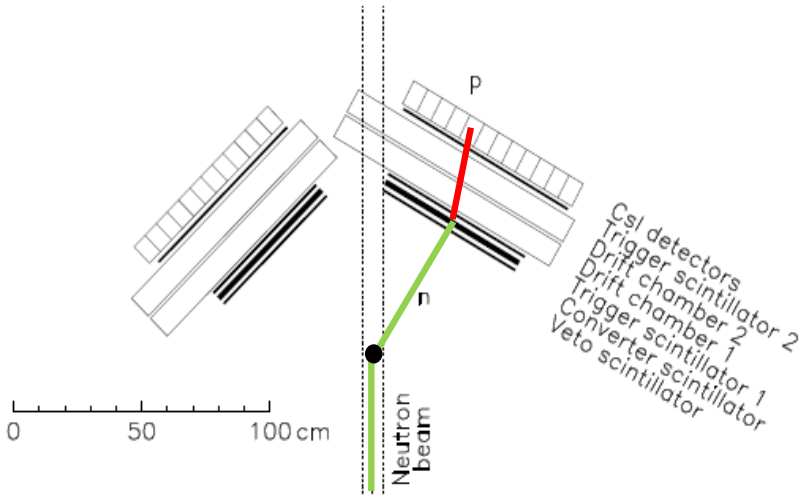

FIG. 6. Overview of the SCANDAL set-up. An idealized scattering event is indicated [13].

Initially, SCANDAL was designed for elastic scattering measurements. However, with an extended and refined data analysis, it has also been possible to extract inelastic (*n,n'x*) scattering data from the same data sets. Preliminary results for targets of Fe, ^{89}Y, and ^{208}Pb have recently been published [20].

An alternative approach to the measurements of (*n,n'x*) cross section data is presented in the recent work of Sagrado García et al. [21]. Emitted secondary neutrons were detected using two independent setups: DECOI-DEMON time-of-flight telescope for detection of neutrons with energies from a few MeV to 50 MeV, and CLODIA-SCANDAL, which covered neutron energies above 40 MeV and consisted of a combination of a SCANDAL arm and the CLODIA setup. The latter comprises seven plastic neutron-to-proton converters and eight multidrift chambers that make it possible to measure the recoil proton trajectories and to determine in which converter the interaction occurred. The data in Ref. [21] were obtained for Fe and ^{208}Pb targets at the primary neutron energy of 96 MeV.

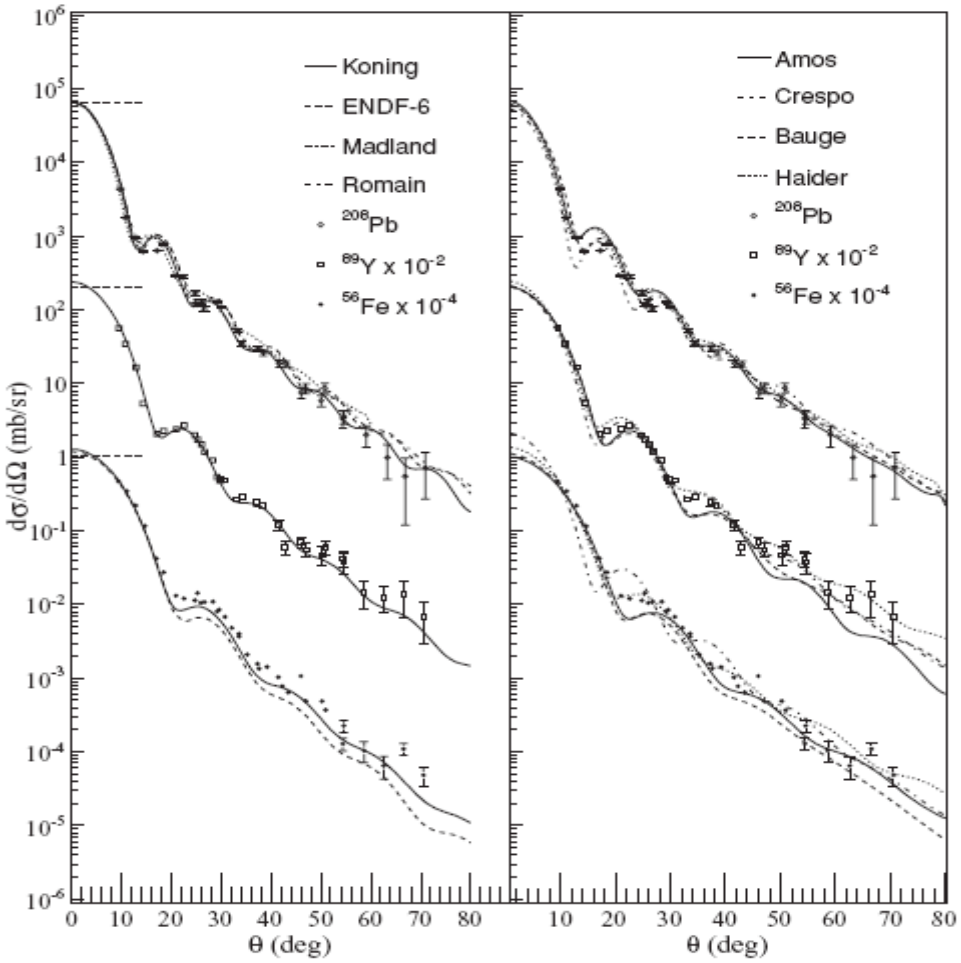

FIG. 7. Angular-differential cross sections of elastic neutron scattering from Fe, ^{89}Y, and ^{208}Pb nuclei, together with model predictions [13].

3.2. NEUTRON-INDUCED LIGHT-ION PRODUCTION CROSS SECTIONS

Neutron-induced production of light charged particles has been studied mostly with the Medley setup. Medley is designed to detect and identify light ions (*p*, *d*, *t*, ^{3}*He, α)* and heavier charged particles. The setup consists of eight telescope detectors, placed in a scattering chamber at angles between 20° and 160°, see Fig. 8. Each telescope consists of two fully depleted silicon surface-barrier detectors and a CsI(Tl) scintillator. Particle identification is achieved by means of the *ΔE-ΔE-E* technique, ensuring a large dynamic range over two orders of magnitude in the energy of the secondary particle. Thus, double differential cross sections, *σ(E,θ)*, can be measured for the produced light ions. The Medley setup has been described in detail in Refs. [22-24].

Neutron-induced cross section measurements with Medley at TSL began at the old QMN facility [10, 11]. The data for production of light ions, from protons to *α*-particles, were collected at the neutron energy of 96 MeV for the targets of ^{1}H, ^{2}H, C, O, Si, Fe, Pb, and U, see Refs. [16, 17, 23, 25, 26]. The measured data for Ca are still under analysis. From 2004, the measurements continued at the upgraded facility (see Sect. 2), and in 2007 the detectors and the neutron collimator system were upgraded, including installation of an

additional shielding wall for background suppression [24, 27]. The upgrades made it possible to collect data at the neutron energies up to 175 MeV. Light-ion production cross sections were measured at 175 MeV for the targets of C, O, Si, Fe, and ^{209}Bi, see Refs. [28-32]. The measured data for U are still under analysis.

As an example of results obtained with Medley, the double-differential cross section of the reaction Fe(*n,p*) at 175 MeV is shown in Fig. 9 [32]. Overviews of results at 96 MeV and 175 MeV are given in Refs. [32, 33]. A continuation of the measurement program with Medley is planned at the future NFS facility at GANIL [34].

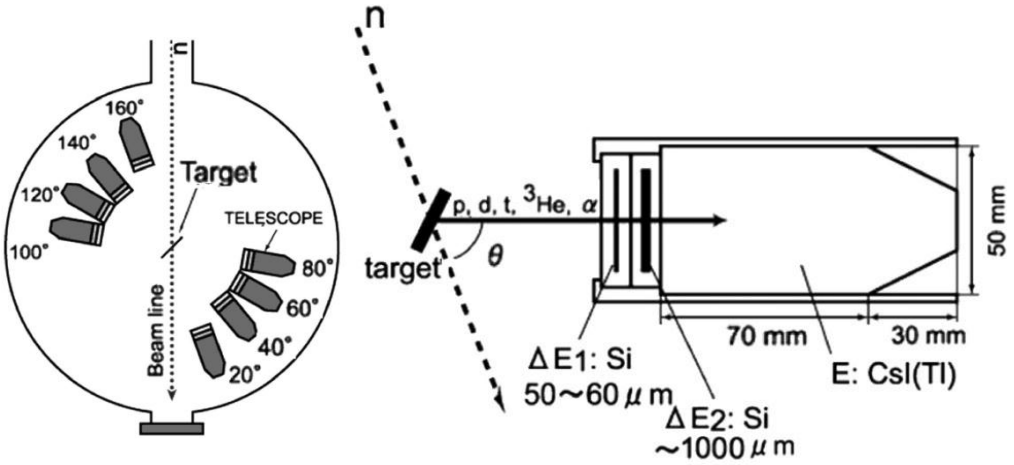

FIG. 8. Medley: Detector arrangement of the telescopes in the scattering chamber (left panel) and details of the detector telescope design (right panel).

In addition, the SCANDAL setup (see Sect. 3.1) was employed for measurements of double-differential cross sections for secondary proton production by 96-MeV neutrons [17]. The (*n,px*) data were taken for Fe, Pb, and U targets. In parallel, light-charged particle production data were taken by the Medley setup for the targets of the same materials, as described above. The results obtained with Medley and SCANDAL were individually normalized, allowing two independent determinations of the cross sections for all the studied targets. Over the energy range covered by both the setups, a very good agreement was observed [17].

3.3. NEUTRON-INDUCED FISSION

During the last decade, QMN beams have been employed for studies of integral neutron-induced fission (Sect. 3.3.1), as well as angular and mass distributions of fragments (Sect. 3.3.2 and 3.3.3, respectively).

3.2. Ion-induced quasi-monoenergetic and white neutron beams

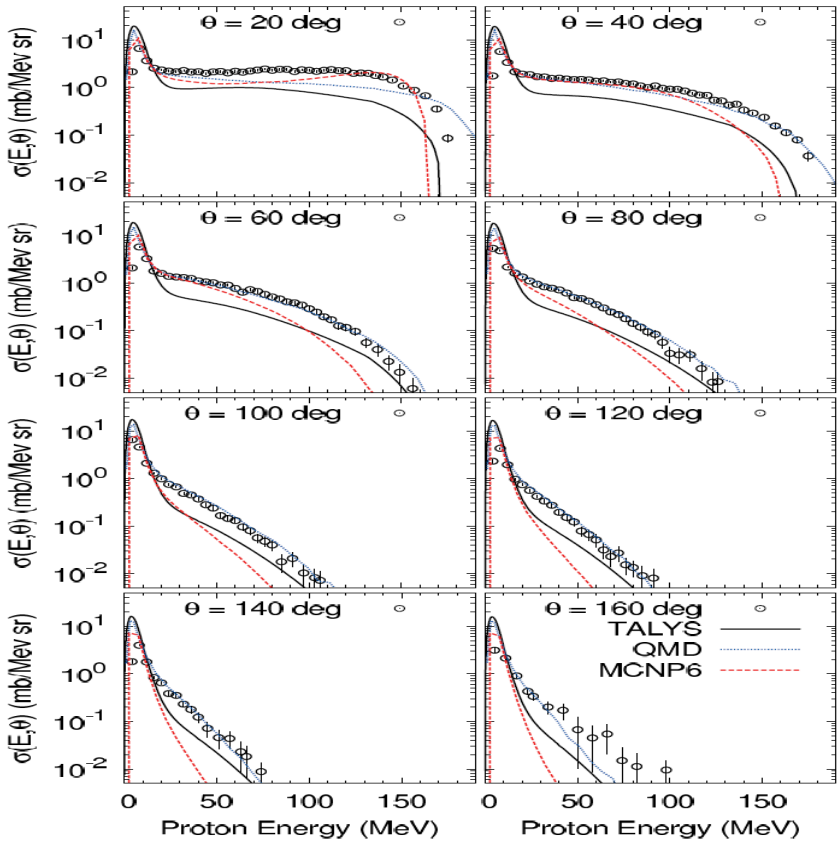

FIG. 9. The double-differential cross section of the reaction Fe(n,p) at 175 MeV. The symbols represent results of measurements with the Medley setup [32]. The lines represent model calculations. For further details, see Ref. [32].

3.3.1. Fission cross sections

Measurements of neutron-induced fission cross sections at TSL have a long tradition, covering the time periods both before and after the upgrade of the QMN facility in 2003-2004. Two measurement techniques have been employed: (1) Frisch-grid ionization chamber (FGIC) [35], and (2) TFBC [8, 36, 37]. Both the techniques utilize the time-of-flight (TOF) capability of the QMN facility for energy selection of fission events. As an example, the (*n,f*) cross sections for separated tungsten isotopes were measured in Ref. [37] for the first time in the world. The results are shown in Fig. 10 in comparison with predictions of the CEM03.01 event generator [38]. The work reported in Ref. [37] included as well (*p,f*) cross section measurements with the same targets and detectors at TSL proton beam facility, followed by the comparative analysis of the neutron- and proton-induced data. In particular, the CEM03.01 event generator was found to reproduce satisfactorily the (*p,f*) data, but not the (*n,f*) data.

3.3.2. Angular distributions of fragments

Measurements of fission fragment angular distributions (FFAD) were performed at the old QMN facility, before its upgrade in 2003-2004. Two experimental techniques were employed, FGIC (see Sect. 3.3.1) [39, 40] and semiconductor detectors in the Medley chamber [41]. The Medley chamber setup for FFAD measurements was basically the same as

for the light-ion production experiments (see Sect. 3.2), except that the target, the electronics and the data acquisition system were optimized for detection of fission fragments. Natural α-radioactivity of the studied target of uranium made it possible to perform ”embedded” calibration of the fission fragment detectors. The fragment angular distribution from the reaction U(*n,f*), obtained at the neutron energy 21 MeV, together with the deduced anisotropy factor, is shown in Fig. 11. Further details are available in Ref. [41].

3.3.3. Mass distributions of fragments

For measurements of mass distribution of fission fragments, the technique of position-sensitive semiconductor detectors was employed. The detectors were located at both sides of a multi-section fission target, ”transparent” for the fragments. Fragment energies E_1 and E_2, as well as the difference t_1-t_2 in the flight times for two fragments, were measured for every detected fission event. With that information as input, fragment masses A_1 and A_2 after neutron emission were deduced. The achieved mass resolution amounted to 5 a.m.u. In Fig. 12, the mass distribution of fragments from the reaction ^{237}Np(*n,f*) is shown, at the neutron energy of 175 MeV. Preliminary results are presented at Ref. [42].

3.4. RADIONUCLIDE PRODUCTION CROSS SECTIONS

Two distinct techniques have been used at the QMN facility for measurements of neutron-induced radionuclide production cross sections: γ ray spectrometric techniques, see Sect. 3.4.1 and accelerator mass spectrometry (AMS), see Sect. 3.4.2.

3.4.1. Measurements with γ ray spectrometric techniques

An early study of neutron-induced radionuclide production cross sections was performed at the old QMN facility by Michel et al, see Ref. [43] and references therein.

After the upgrade of the facility, which allowed one to achieve higher neutron fluxes, similar studies were performed by Wagner and co-authors, see Refs. [44, 45] and references therein. So far, the irradiations were performed at seven neutron energies in the range 22-94 MeV. Samples of Al, Au, Bi, Ta, In, and I (in the form of KIO_4) were studied at all the energies, whereas samples of Y, Co, Zn, Fe, Cu, Ni, and Mg were irradiated at certain energies only. γ rays from reaction products were measured using a spectrometer based on a high-purity Ge detector. In this way, (*n,xn*) threshold reactions have been studied up to x = 10, e.g. ^{209}Bi(*n,10n*)^{200}Bi and ^{197}Au(*n,10n*)^{188}Au [44]. Corrections had to be made for contributions to the reaction rates due to neutrons in the low-energy tail of the spectrum. The corrections were applied on the basis of results obtained by the same group at lower energies at the QMN facilities at TSL and Řež [44], together with the literature data from earlier studies at energies below 40 MeV, and also by means of calculations with the TALYS code [46]. An example of measurement results is presented in Fig. 13 for the reaction ^{197}Au(*n,4n*)^{194}Au, which is of importance for high-energy neutron dosimetry.

3.2. Ion-induced quasi-monoenergetic and white neutron beams

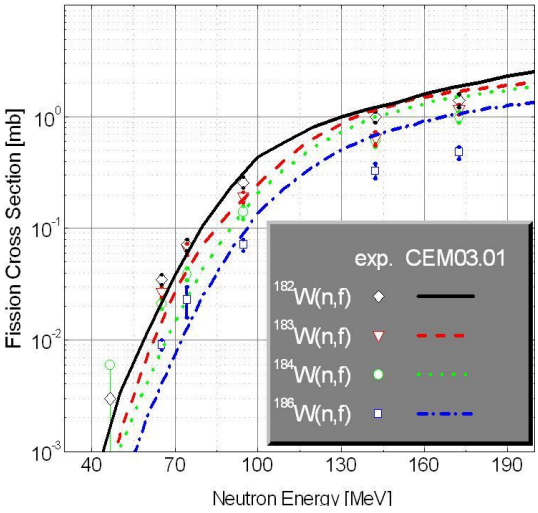

FIG. 10. Neutron-induced fission cross sections for W isotopes. The symbols represent the experimental results [37]. The lines show the predictions of the CEM03.01 model [38].

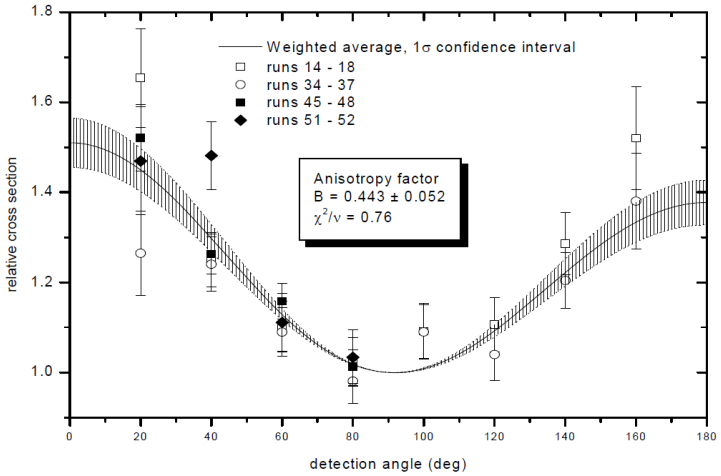

FIG. 11. Angular distribution of the reaction U(n,f), at neutron energy 21 MeV [41].

The same technique makes it possible to observe decay of reaction products in isomeric states, and thus to separate reactions that result in nuclei in ground and isomeric states. An example is the reaction ^{89}Y($n,3n$) that may lead to the production of the isomer ^{87m}Y. Preliminary cross-section data for ^{89}Y($n,3n$)^{87m}Y and ^{89}Y($n,3n$)^{87g}Y reactions, taken in Uppsala and Řež, have been recently published [45].

3.2. Ion-induced quasi-monoenergetic and white neutron beams

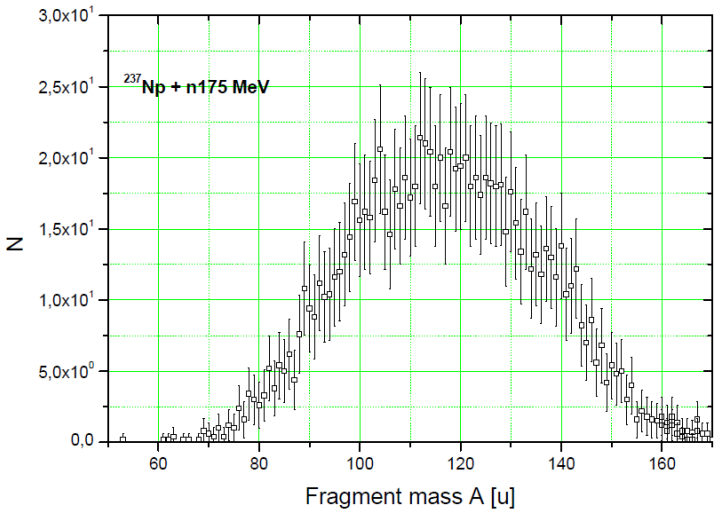

FIG. 12. The mass distribution of fragments from the reaction ^{237}Np(n,f) at the neutron energy of 175 MeV [42]. The horizontal axis shows the fragment mass after neutron emission and the vertical axis shows the number of detected fragments.

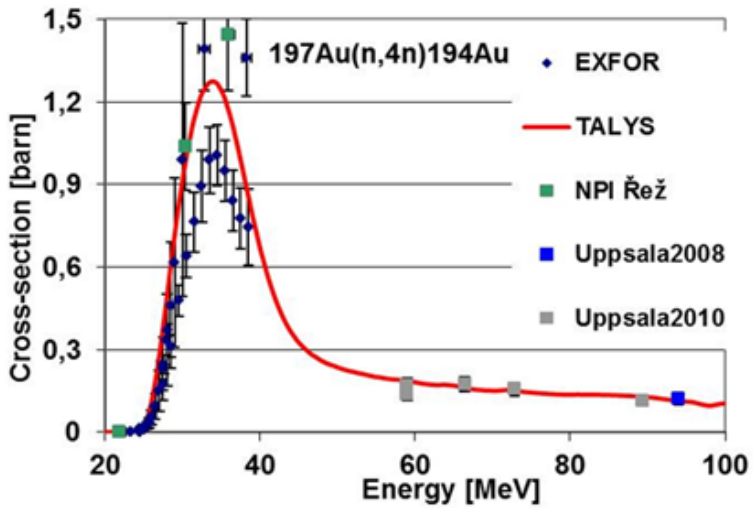

FIG. 13. Cross section of the ^{197}Au(n,4n)^{194}Au reaction [44]. The square symbols represent the results obtained by Wagner et al. at the QMN facilities in Uppsala (blue and grey squares) and in Řež (green squares). The diamond symbols come from literature data from the EXFOR database. The red line represents a model calculation with the TALYS code [46].

3.4.2. Measurements with AMS

Long-lived radionuclides are difficult to measure in standard activation experiments due to their low activities [43]. This disadvantage can be overcome by using mass-spectrometric techniques for measuring directly the number of atoms of the produced radionuclides rather than their decay. Such long-lived nuclides might either be the direct product of a reaction, or a decay product of a directly produced short-lived nuclide [47]. AMS can be applied for separation of atoms of long-lived radionuclides under study from the atoms of the primary material and for subsequent counting of the atoms.

3.2. Ion-induced quasi-monoenergetic and white neutron beams

There is an ongoing project at TSL [48], devoted to cross-section measurements for neutron-induced production of long-lived radionuclides in ^{nat}Fe, ^{54}Fe, and Th. The samples were irradiated at the QMN facility in December 2012, at the peak neutron energy of 46 MeV, at both SUP and CUP (see Sect. 2.1). The irradiated samples will be studied with AMS techniques at Vienna Environmental Research Accelerator and at the Australian National University.

4. SUMMARY AND CONCLUSIONS

Judging from the variety of successful nuclear data programmes performed (or being performed) at TSL, the efforts in construction and upgrades of the neutron facility were worthwhile. Currently, the QMN facility at TSL is the only one in EU that is capable of delivering quasi-monoenergetic neutrons above 40 MeV, and one of only three QMN facilities in the world being able to deliver beams with energies above 100 MeV.

During the last decade, funding for nuclear data measurements at TSL has been decreasing. Presently, there is no governmental support for beam time at TSL, which implies that all operational costs have to be covered by external funding or user fees. As a consequence, currently only ~10% of the beam time is allocated for nuclear data measurements. Significantly more beam time can potentially be scheduled, provided that appropriate funding is available. The facility is capable of increasing the beam time for nuclear data programmes by a factor of five at the energy of 175 MeV and by a factor of two at lower energies. In the future, after 2015, even more beam time can potentially be made available, due to the fact that the proton therapy treatments will move to a dedicated facility, the Skandion clinic. In addition, there will be no limitations for scheduling of irradiations with different particles and energies, whereas at present the facility is run with 180-MeV protons during 85% of the time. In order to be able to continue operating TSL, including the QMN facility with its unique properties, beyond 2015, it is mandatory that sufficient funding becomes available.

ACKNOWLEDGEMENTS

The authors are grateful to P. Andersson, A. Ataç, R. Bevilacqua, V. Blideanu, J. Blomgren, V. Corcalciuc, J.-C. David, S. Dangtip, V.P. Eismont, C. Ekström, N.P. Filatov, M. Hayashi, S. Hirayama, A. Hjalmarsson, O. Jonsson, J. Klug, A. Koning, F.-R. Lecolley, J.-F. Lecolley, X. Ledoux, S. Leray, Y. Maeda, M. Majerle, N. Marie, S.G. Mashnik, P. Mermod, R. Michel, P. Nadel-Turonski, Y. Naitou, S. Neumann, L. Nilsson, N. Olsson, D. Reistad, P.-U. Renberg, I.V. Ryzhov, I. Sagrado García, V. Simutkin, M. Suchopár, O. Svoboda, M. Tesinsky, U. Tippawan, G.A. Tutin, J. Vrzalová, A. Öhrn, M. Österlund, and the scientific and technical staff at TSL for contributions to the measurements, the analyses, and the facility upgrades. We acknowledge the financial support for the nuclear data measurements by the European Commission within FP5, FP6, and FP7 through the HINDAS, EFNUDAT, and ERINDA projects, Grant agreements no. FIKW-CT-2000-0031, 036434 and 269499, respectively.

REFERENCES

[1] PROKOFIEV, A., et al., "Characterization of the ANITA Neutron Source for Accelerated SEE Testing at The Svedberg Laboratory", Proc. IEEE Radiation Effects Data Workshop 2009, Quebec, Canada, 166 (2009), DOI:10.1109/REDW.2009.5336295 .

[2] POMP, S., "The New Uppsala Neutron Beam Facility". (Proc. Int. Conf. NDST, Santa Fe, NM, 2004), AIP Conf. Proc. **769**, 780 (2005).

[3] MASHNIK, S.G., et al., "^{7}Li(*p*,*n*) nuclear data library for incident proton energies to 150 MeV", LANL Report LA-UR-00-1067 (2000).

[4] PROKOFIEV, A.V., et al., "Development and Validation of the ^{7}Li(*p*,*n*) Nuclear Data Library and Its Application in Monitoring of Intermediate Energy Neutrons", (Proc. Int. Conf. NDST, Tsukuba, 2001), J. of Nucl. Sci. Tech., Suppl. 2, **1**, 112 (2002).

[5] WATANABE, Y., et al, "Characterization of ANITA and QMN Neutron Beams at TSL Using Proton Recoil Techniques", (Proc. ND 2010), J. Kor. Phys. Soc. **59**, 1439 (2011). DOI: 10.3938/jkps.59.1439

[6] PROKOFIEV, A.V., et al. "The TSL Neutron Beam Facility", (Proc. NEUDOS10, Uppsala, 2006), Rad. Prot. Dosim. **126**, 18 (2007); DOI: 10.1093/rpd/ncm006 .

[7] WENDER, S.A., et al., "A fission ionization detector for neutron flux measurements at a spallation source", Nucl. Instr. Meth. A **336**, 226 (1993).

[8] SMIRNOV, A.N., et al, "Measurements of Neutron-Induced Fission Cross-Sections for ^{209}Bi, ^{nat}Pb, ^{208}Pb, ^{197}Au, ^{nat}W, and ^{181}Ta in the Intermediate Energy Region", Phys. Rev. C **70**, 054603 (2004).

[9] CARLSON, A.D., et al. "Update to Nuclear Data Standards for Nuclear Measurements". Proc. Int. Conf. NDST, Trieste, 1997, Part II, pp 1223-1229, Italian Physical Society (1997).

[10] http://www.linkedin.com/groups?gid=1943399 .

[11] CONDÉ, H., et al., "A facility for studies of neutron-induced reactions in the 50-200 MeV range," Nucl. Instr. Meth. A **292**, 121 (1990).

[12] KLUG, J., et al., "SCANDAL—a facility for elastic neutron scattering studies in the 50–130 MeV range", Nucl. Instr. Meth. A **489**, 282 (2002).

[13] ÖHRN, A., et al. "Elastic scattering of 96 MeV neutrons from iron, yttrium, and lead", Phys. Rev. C **77,** 024605 (2008).

[14] MERMOD, P., et al., "Search for three-body force effects in neutron–deuteron scattering at 95 MeV" Phys. Lett. B **597**, 243 (2004).

[15] MERMOD, P., et al., "Evidence of three-body force effects in neutron-deuteron scattering at 95 MeV", Phys. Rev. C **72**, 061002(R) (2005).

[16] MERMOD, P., et al., "95 MeV neutron scattering on hydrogen, deuterium, carbon, and oxygen", Phys. Rev. C **74**, 054002 (2006).

[17] BLIDEANU, V., et al., "Nucleon-induced reactions at intermediate energies: New data at 96 MeV and theoretical status", Phys. Rev. C **70**, 014607 (2004).

[18] KLUG, J., et al. "Elastic neutron scattering at 96 MeV from ^{12}C and ^{208}Pb", Phys. Rev. C **67**, 031601(R) (2003).

[19] JOHANSSON, C., et al., "Forward-angle neutron-proton scattering at 96 MeV", Phys. Rev. C **71**, 024002 (2005).

[20] GUSTAVSSON, C., et al., "Inelastic neutron scattering from carbon, iron, yttrium and lead." (Proc. CNR*11, Prague, 2011), EPJ Web of Conferences **21**, 03004 (2012) DOI:10.1051/epjconf/20122103004 .

[21] SAGRADO GARCÍA, I.C., et al., "Neutron production in neutron-induced reactions at 96 MeV on ^{56}Fe and ^{208}Pb", Phys. Rev. C **84**, 044619 (2011)

[22] DANGTIP, S., et al., “A facility for measurements of nuclear cross sections for fast neutron cancer therapy”, Nucl. Instr. Meth. A **452**, 484 (2000).
[23] TIPPAWAN, U., et al., ”Light-ion production in the interaction of 96 MeV neutrons with silicon”, Phys. Rev. C 69, 064609 (2004).
[24] BEVILACQUA, R., et al., “Medley spectrometer for light ions in neutron-induced reactions at 175 MeV”, Nucl. Instr. Meth. A 646, 100 (2011).
[25] TIPPAWAN, U., et al., “Light-ion production in the interaction of 96 MeV neutrons with carbon”, Phys. Rev. C 79, 064611 (2009).
[26] TIPPAWAN, U., et al., “Light-ion production in the interaction of 96 MeV neutrons with oxygen“, Phys. Rev. C 73, 034611 (2006).
[27] BEVILACQUA, R., Neutron induced light-ion production from iron and bismuth at 175 MeV, Licentiate of Philosophy Thesis, Uppsala University, January 2010.
[28] HIRAYAMA, S.,et al., “Production of protons, deuterons, and tritons from carbon bombarded by 175 MeV quasi mono-energetic neutrons”, (Proc. ISORD-5), Progr. Nucl. Sci. Tech. 1 69 (2009).
[29] WATANABE, Y., et al., “Light ion production in 175 MeV quasi mono-energetic neutron induced reactions on carbon, oxygen, and silicon”, (Proc. ICRS-12, Sept 2-7 2012, Nara, Japan), accepted for publication in Progress in Nuclear Science and Technology (2013).
[30] TIPPAWAN, U., et al., “Light-Ion Production in 175 MeV Neutron-Induced Reactions on Oxygen” (Proc. ND 2010), J. Korean Phys. Soc. 59, 1979 (2011); DOI:10.3938/jkps.59.1979.
[31] HIRAYAMA, S., et al. “Production of protons and deuterons from silicon bombarded by 175 MeV quasi mono-energetic neutrons,” (Proc. ND 2009), JAEA-Conf. no. 005 (2010).
[32] POMP, S., et al., "Light-ion production in 175 MeV quasi-monoenergetic neutron-induced reactions on iron and bismuth and comparison with INCL4 calculations"; (Proc. ICRS-12, Sept 2-7 2012, Nara, Japan), accepted for publication in Progress in Nuclear Science and Technology; R. BEVILACQUA, Neutron-Induced Light-Ion Production from Iron and Bismuth at 175 MeV, Doctoral dissertation, Uppsala, 2011. Acta Universitatis Upsaliensis. http://urn.kb.se/resolve?urn=urn:nbn:se:uu:diva-149999 .
[33] POMP, S., et al., “A Medley with over ten years of (mostly) light-ion production measurements at The Svedberg Laboratory”, EPJ Web of Conferences **8,** 07013 (2010); DOI:10.1051/epjconf/20100807013 .
[34] GUSTAVSSON, C., et al., “Nuclear data measurements at the new NFS facility at GANIL”, Physica Scripta T150, 014017 (2012).
[35] RYZHOV, I.V., et al., “Measurements of neutron-induced fission cross-sections of ^{205}Tl, ^{204,206,207,208}Pb and ^{209}Bi with a multi-section Frisch-gridded ionization chamber”, Nucl. Inst. Meth. A 562, 439 (2006).
[36] EISMONT, V.P., et al. “Relative and Absolute Neutron Induced Fission Cross Sections of ^{208}Pb, ^{209}Bi and ^{238}U in the Intermediate Energy Region”, Phys. Rev. C 53, 2911 (1996).
[37] SMIRNOV, A.N., et al., “Nucleon-induced fission cross-sections of tantalum and separated tungsten isotopes and ”compound nucleus” effect in intermediate energy region”, Proc. Int. Conf. NDST, Nice, 2007, pp 1095-1098, DOI: 10.1051/ndata:07749 .
[38] MASHNIK, S.G., et al., “CEM03 and LAQGSM03—new modelling tools for nuclear applications”, J. Phys. Conf. Series 41, 340 (2006).
[39] TUTIN, G.A., et al, “An ionization chamber with Frisch grids for studies of high-energy neutron-induced fission” Nucl. Instr. Meth. A 457, 646 (2001).

[40] RYZHOV, I.V., et al, "Influence of multichance fission on fragment angular anisotropy in the ^{232}Th(*n,f*) and ^{238}U(*n,f*) reactions at intermediate energies", Nucl. Phys. A 760, 19 (2005).

[41] PROKOFIEV, A.V., et al, "A New Facility for High-Energy Neutron-Induced Fission Studies", (Proc. Int. Conf. NDST, Santa Fe, NM, 2004), AIP Conf. Proc. 769, 800 (2005).

[42] BATENKOV, O.I., "Developing the experimental database on fragment yield in fission of the main nuclear fuel isotopes and other minor actinides induced by intermediate energy neutrons", Final Technical Report of ISTC Project No. 3363 (2010).

[43] MICHEL, R., et al., "Residual nuclide production from iron, lead, and uranium by neutron-induced reactions up to 180 MeV", (Proc. Int. Conf. NDST 2004, Santa Fe), AIP Conf. Proc. 769, 861 (2005).

[44] VRZALOVA, J., et al, "Measurements of cross-sections of (*n,xn*) threshold reactions in various materials", EPJ Web of Conferences 21, 10007 (2012), DOI: 10.1051/epjconf/20122110007 .

[45] WAGNER, V., et al., "Studies of deuteron and neutron cross-sections important for ADS research", Proc. XXI International Baldin Seminar on High Energy Physics Problems, September 10-15, 2012, JINR, Dubna, Russia, http://pos.sissa.it/archive/conferences/173/090/Baldin%20ISHEPP%20XXI_090.pdf .

[46] KONING, A. J., et al., "TALYS-1.0.", Proc. of NDST 2007, 211 (2007) DOI: 10.1051/ndata:07767; http://www.talys.eu/home/ .

[47] WALLNER, A., et al., "Production of Long-lived Radionuclides ^{10}Be, ^{14}C, ^{53}Mn, ^{55}Fe, ^{59}Ni and ^{202g}Pb in a Fusion Environment" J. Korean Phys. Soc. 59, 1378 (2011) DOI: 10.3938/jkps.59.1378 .

[48] WALLNER, A., "Fe(*n,x*) and Th(*n,x*) reactions at energies up to 60 MeV measured with AMS", proposal at the ERINDA programme (2012).

3.2. Ion-induced quasi-monoenergetic and white neutron beams

FAST NEUTRON GENERATORS AT NUCLEAR PHYSICS INSTITUTE ŘEŽ

M. MAJERLE, P. BÉM, J. NOVÁK, E. ŠIMEČKOVÁ, M. ŠTEFÁNIK

Nuclear Physics Institute of ASCR PRI,
250 68 Řež near Prague,
Czech Republic
Email: majerle@ujf.cas.cz

Abstract

Nuclear reaction department of the NPI Řež operates two different fast neutron sources: neutrons with continuous neutron spectrum (fusion/IFMIF like) up to 37 MeV from p+D_2O (flowing target) reaction and quasi-monoenergetic neutrons with energies up to 37 MeV from p+Li (C backing) reaction. Isochronous cyclotron U120M provides protons of energies up to 38 MeV and currents up to 20 μA. The integral-benchmark tests and the measurements of activation cross-sections are the core of the experimental program. Gamma-spectrometry is used for the investigation of daughter nuclei. Besides, the electronic hardness tests are routinely performed on white-spectrum fast neutrons. The spectral flux at the positions of irradiated samples is determined by the MCNPX simulation, backed by the experimental data from dosimetry foils, scintillation, and proton recoil telescope techniques. In the first part of this paper recent studies of the neutron spectra from the Li(C) target are described, as well as subsequent evaluation of the uncertainties of the measured reaction rates and of the extracted cross-sections. The second part describes the neutron detection techniques being introduced to our laboratory, the scintillation detector together with 500 MHz 8-bit digitizer card, which have been successfully used to obtain neutron spectra from the scintillator response and to record the limited Time-Of-Flight spectrum.

1. INTRODUCTION

The cyclotron-based fast neutron sources at Nuclear Physics Institute Řež were mainly constructed for the integral- and differential benchmark tests of the neutron cross-section data in the energy range relevant to the IFMIF (International Fusion Material Irradiation Facility).

The IFMIF neutron source reaction d(40 MeV)+Li produces a white spectrum with a high energy tail up to 35 MeV (50 MeV at lower intensity). As deuterons up to only 20 MeV energy are available on the NPI cyclotron and two-fold energy could be reached for $H^{(-)}$ and $^{3,4}He^{(++)}$ beams, another reactions were deliberated to simulate the d+Li neutron source spectrum of IFMIF. An upgraded white-neutron spectrum source based on the thick Be target starts to be used routinely as well.

The Summary report from the last Consultants' meeting [1] describes the neutron generators for white neutron spectra on the basis of ^{3}He(40MeV)+D_2O and p(37MeV)+D_2O reactions, and the neutron generator for quasi-monoenergetic (QM) spectra based on p(20-37MeV)+^{7}Li(C) source reaction.

Our recent program mainly concerns the detailed studies of the validation of activation cross-sections with QM neutrons. For this purpose we review the characteristics of the present QM neutron generator in terms of extensive MCNPX simulations. Within this approach the sensitivity analysis of the extracted cross-sections is discussed with respect to evaluated experimental uncertainties. An attempt to validate experimentally the neutron spectra with the Time-Of-Flight (TOF) method using inherent time-structure of cyclotron beam is described as well.

2. THE EXPERIMENTAL VALIDATION OF ^{59}CO ACTIVATION CROSS-SECTIONS USING QUASI-MONO ENERGETIC NEUTRON SPECTRUM (<35 MEV)

This work was a part of the Fusion for Energy (F4E) task 4.2. In the frame of this task, the cross-sections from EAF-2010 in the neutron energy range 20-35 MeV were validated for the following elements: Al, Au, Bi, Co, and Nb [2,3]. A stripped down version of the final report [3] with the emphasis on the neutron spectrum and subsequent extracted cross-sections is presented here.

2.1. EXPERIMENT

The neutron irradiation of Co has been performed at the NPI cyclotron at 7 incident proton energies (19.8, 25.1, 27.6, 30.1, 32.6, 35.0, and 37.4 MeV). The resolution (FWHM) and uncertainty of the incident proton energy were measured to be 1.5%.

The foils made from pure metallic Co had a disc shape with diameter 15 mm and thickness of 0.25 mm. In every experimental run two foils were simultaneously irradiated at two distances (48-49 and 86-87 mm from the front of the Li target) to check the consistency of the measurements.

The samples were irradiated for the time period of about 20 hours. The irradiation time profile was recorded by measuring the proton current at the target assembly on pulse by pulse scale and the correction for beam instabilities was included in the calculation of the reaction rates.

Six radioactive products were detected in Co foils by the offline γ-spectroscopy employing calibrated HPGe detectors. The decay gamma ray spectra were measured during cooling period from minutes up to 100 days. The activities of the specific isotopes at the end of the irradiation were calculated using tabulated decay half-lives and gamma intensities from the LUND database.

The ratio of the specific activities measured at two distances varies as a function of the proton energy, it is lower than the ratio calculated on the basis of target-foil distances (inverse square law) and exhibits the increasing trend with the energy. This effect is well understood and is mainly due to the different shape of the neutron spectra at two distances (closer distance = larger spatial angle = softer spectrum).

2.2. MCNPX SIMULATION OF THE P-LI NEUTRON SOURCE AND VALIDATION AGAINST CYRIC EXPERIMENT

To overcome the effect of different neutron spectral shapes in two sample positions and to study its effect on measured activities, the detailed computational investigation of all relevant arrangement details and their influence on the shape of the spectra was carried out.

The Monte-Carlo particle transport code MCNPX with the Los-Alamos evaluations for proton induced cross-sections on ^{7}Li and ^{12}C (LA-150h), and FENDL 2.1 library for other nuclides and reactions were employed.

3.2. Ion-induced quasi-monoenergetic and white neutron beams

At first, the computational approach was validated against the neutron differential yields from p+Li reaction measured at the CYRIC laboratory (Tohoku university) with a 20-40 MeV proton beam (neutron spectra measured by TOF with NE213 scintillator 12 m from the target) [4]. The geometry of the CYRIC target setup was accurately modelled in MCNPX and the detailed study comparing the simulated and experimental values was done. The conclusions from previous similar studies were confirmed, and some new facts were discovered. The comparisons of the spectra for proton energies 20, 25, 30, 35, and 40 MeV as in Fig. 1.

MCNPX manages to describe the neutron spectrum to some extent and can be used as a prediction tool. It is also obvious that the detailed analysis of the uncertainties of the cross-sections based on the quality of the neutron field prediction has to be performed. In general the mentioned uncertainties depend on the studied cross-section curve and are between 10-50%. Special care should be put on the reaction rates which are in partly produced by the neutrons of energies below quasi-monoenergetic peak. The calculations show that in some cases up to 75% of the reaction rates can be produced by these neutrons. The resulting extracted cross-sections have in such cases higher uncertainties.

2.3 SIMULATION OF NEUTRON SPECTRA FOR NPI/ŘEŽ EXPERIMENTAL SETUP

In Monte Carlo calculations, the target setup at NPI/Řež was represented by the exact geometrical model. The proton beam was approximated with Gaussian profile (3 mm FWHM) and with well defined energy (0 MeV FWHM). The neutron spectra averaged at the places of the foils at 48 and 86 mm (grouped to 0.25 MeV) were calculated for all proton energies and are shown in Fig. 2.

The second set of spectra was obtained from the spectra measured at the CYRIC facility binned to 0.25 MeV bins and interpolated to the energies which were used at NPI irradiations of Nb and Co.

2.4 EXTRACTION OF ^{59}CO CROSS-SECTION CURVES WITH MODIFIED SAND-II CODE

The Li/C source neutron spectra calculated at the locations of the Co samples indicate that monoenergetic peaks account for 30-50% of the total flux, the rest being the low energy neutrons from the Li breakdown reaction and scattering on the target assembly. To derive the activation cross-sections curves in such complex neutron field a modified version of the SAND-II code [5] was used. Using this code and known neutron spectra, the cross-section curves for the ^{59}Co(n,*) reactions were adjusted to the measured reaction rates.

The EAF-2010 evaluated data grouped to 0.25 MeV bins were used (all according cross-sections channels were summed) as input cross-sections, and maximal number of SAND-II iterations was used. Several cross-section curves were obtained (for different positions and different spectra) with differences of up to 30%, see Fig. 3.

3.2. Ion-induced quasi-monoenergetic and white neutron beams

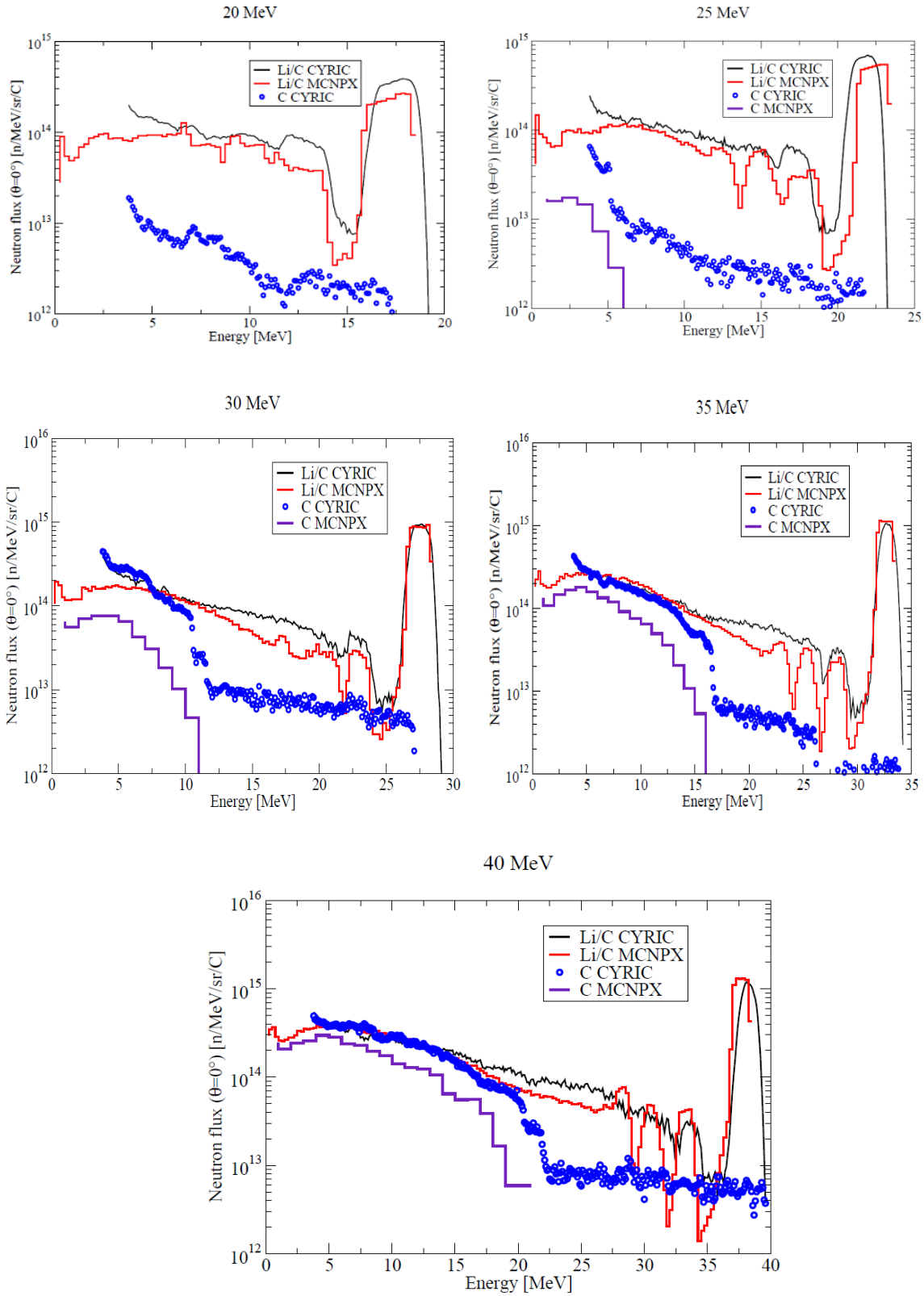

FIG. 1. Energy differential neutron yield: measured for Li/C and bare C targets and calculated by MCNPX/LA150h.

3.2. Ion-induced quasi-monoenergetic and white neutron beams

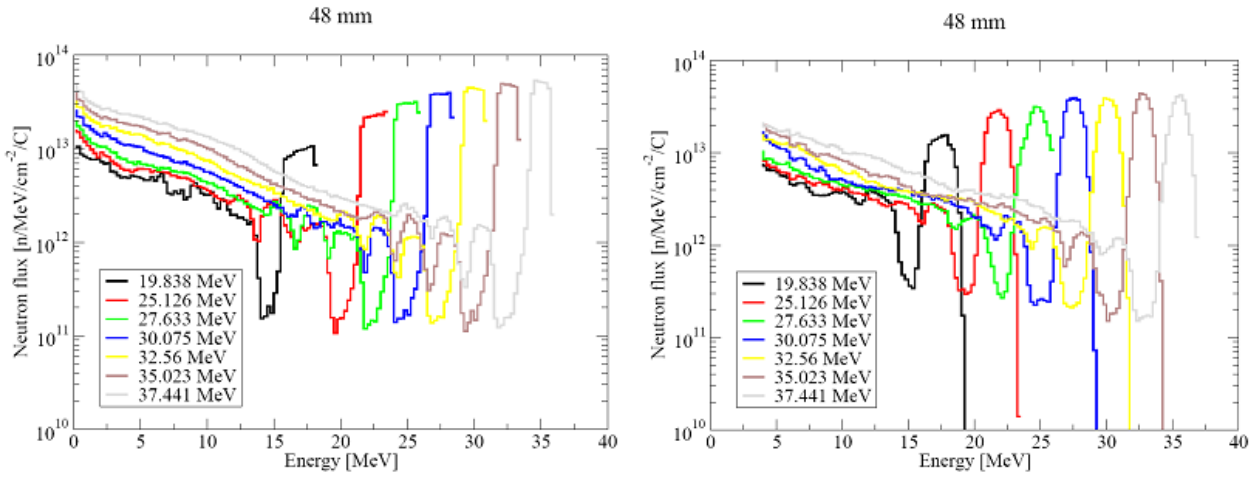

FIG. 2. Neutron spectra calculated with MCNPX (left) and obtained by the modification of the spectra from the CYRIC experimental facility (right) at the place of activation foils 48 mm from the target front.

The final experimental data for the measured cross-sections were obtained from the produced curves by averaging the curves in the regions determined by the quasi-monoenergetic peaks (Fig. 4). The uncertainties are discussed in the next section. Another analysis of the measured cross-sections is presented in [6,7], where another method of cross-section extraction and slightly different neutron spectra were used (Uwamino spectra normalized to foil positions with $1/r^2$ law), however the results of both methods are close to each other.

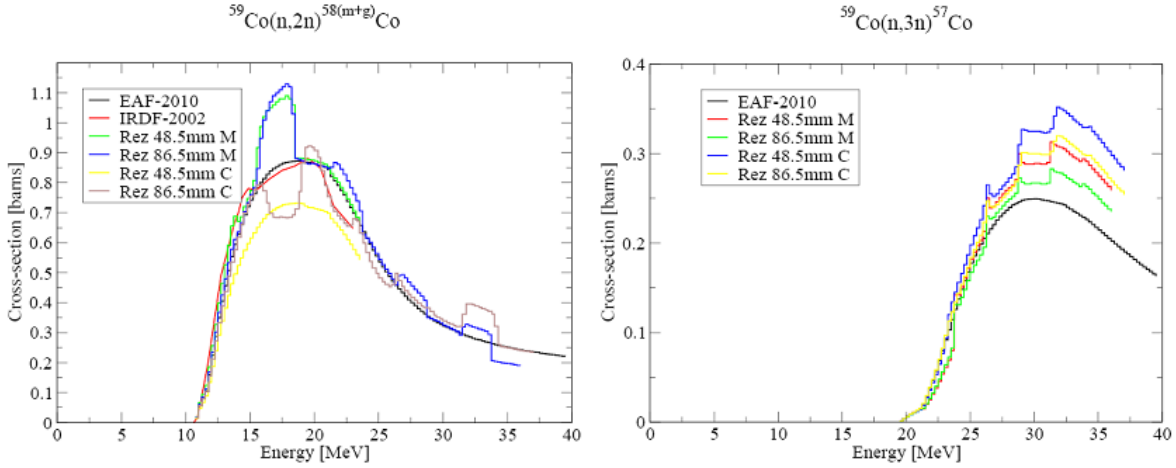

FIG. 3. The cross-section curves for ^{59}Co(n,2n)$^{58(m+g)}$Co and ^{59}Co(n,3n)^{57}Co reactions extracted with SAND-II and the comparison with evaluated data in EAF-2010 and IRDF-2002. Cross-sections marked with "M" are extracted with MCNPX spectra, these with "C" are extracted with CYRIC extrapolated spectra.

2.5 REACTION RATE AND CROSS-SECTION UNCERTAINTIES

Statistical uncertainties arise at the analysis of the gamma peaks and in Monte Carlo simulations (simulations are used in the extraction procedure). The uncertainties of the

gamma peak analysis are in range of 1-2% (in some cases higher). The number of histories used in Monte Carlo simulations was always sufficient to keep the statistical uncertainties of the results below 1-2% (production by low energy neutron background), usually below 0.5% (production by quasi monoenergetic neutrons). In most cases the statistical uncertainties are the smallest contribution to the total uncertainty.

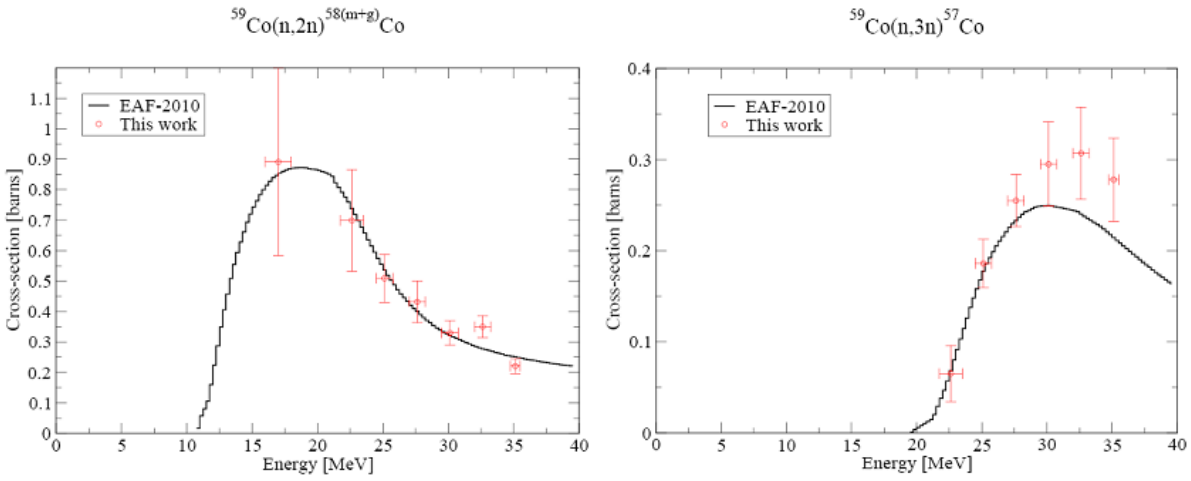

FIG. 4. The cross-sections extracted from NPI/Řež experimental data with evaluated data in EAF-2010 database.

Systematic uncertainties cover a broad range of inaccuracies which are always present in the experimental work. During the irradiation, these are the parameters of the proton beam (energetic distribution, profile, position), the measurement of the total proton flux, the exact location of the activation samples in relation to the target (accuracy 1 mm to target, <1 mm in relation to other activation samples),.. After the irradiation, the activity of the foils is measured by spectroscopy methods, where other uncertainties because of positioning (<1%), calibration (2%), etc. arise. To determine the effect of the setup parameters, the analysis with the MCNPX simulations was performed. The simulations of reaction rates with parameters varying within the parameter accuracy were compared. Summing up all important contributions of uncertainties – mainly: current measurement, Li target thickness, and positioning of the foils - the total uncertainty originating from the irradiation part is 10-15%.

At the extraction of cross-sections from reaction rates by SAND-II method, further uncertainties are added to existing ones. These are caused by not well known neutron spectrum and are reflected on cross-section as different curves in Fig. 3. As was mentioned the differences between these curves are up to 30% (reaction rate is mostly produced by neutrons below monoenergetic peak), but mostly below 10-15% (reaction rate produced mostly by monoenergetic neutrons).

In future experiments, we might obtain a significant decrease of uncertainties by direct monitoring of the neutron flux (avoiding systematic uncertainties from the Li target thickness + current measurement). The decrease of the uncertainties due to not well known neutron spectrum should be obtained by the parallel irradiation of the same foils out of the

beam axis (subtraction of the reaction rate produced by the neutrons below monoenergetic peak) [8] and by improving our spectrum knowledge.

3. THE MEASUREMENTS OF SPECTRA WITH THE BICRON SCINTILLATOR IN THE TIME-OF-FLIGHT MODE

In the past, online measurements of the neutron spectra were already performed using the scintillation detector technique with n/γ discrimination hardware and pulse-height deconvolution procedure for the spectrum from the ^{3}He+ thick D_2O source [9], and proton-recoil-telescope spectrometer for the neutron spectrum from the p+Li source [10]. Recently, we have started to perform tests with the BICRON scintillator. The pulse output from the scintillator was digitized during the irradiation. We have succeeded to obtain some information on the neutron spectra and scintillator response with such setup.

The pulses from the U120M cyclotron have macro- and micro-structure. 100-150 Hz repetition rate of the duty cycle (duty cycle is in the range of 5-80%) corresponds to the macro-structure – consisting of e.g. 1 ms irradiation of the target every 10 ms. The micro-structure of the pulse is determined by the frequency 20-25 MHz on the dipoles – the protons are repeatedly impinging on the target for ca. 5 ns (FWHM of our beam) every 50 ns.

The time window of 50 ns can therefore be used for the TOF, for longer times the frame overlap makes it impossible to determine from which bunch is the neutron (in the case of the scintillator detector). The detector was placed at 5 m distance from the neutron source target. 50 ns at 5 m is enough to determine the neutron spectrum from the maximal energy of 35 MeV down to ca. 15 MeV.

Our approach consists of sampling the signals from the scintillator with 500 MHz frequency for the duration of the whole macro-pulse (digitizer ZTEC ZT4211-01, 8 bit ADC, 500 MHz). Two channels can be sampled simultaneously, the second channel samples the signal from a small antenna placed in the cyclotron hall (which records the RF signal from dipoles to determine the phase of each macro-pulse). We are able to sample and record about 2-3 entire macro-pulses per second (out of 100-150).

The analysis of the sampled pulses is performed offline by the ROOT package. The pulses from the scintillator are fitted with the complex function which includes Gaussian form for the signal increase and exponential form for the decrease. Two different decay times are used for the fitting of the exponential decrease in order to enable the charge comparison method to discriminate neutrons and gammas.

This method was already tested at 5 experiments with the p+Li reaction and 3 experiments with the p+Be reaction. For several of these irradiations we obtained reasonable results, which agree well with the prediction of the TOF spectrum from the MCNPX simulated spectra.

3.1. N/γ DISCRIMINATION

The BICRON scintillator which we used in these measurements allows us to use n/γ discrimination methods based on the falling edge of the signal. We used charge comparison method. In the Fig. 5 are seen 2D plots of energy deposited in the scintillator against slow/fast component of the signal decrease ratio for two sources: PuBe neutron source with

neutrons up to 15 MeV, and p+Li with neutrons up to 27 MeV. While for PuBe neutron source, neutrons and gammas can be well discriminated, at higher neutron energies they start to mix. This is due to the digitization card – in order to have signal with higher amplitudes sampled (the case of p+Li@27MeV), it was necessary to set higher input range (and have worse resolution at lower energies of gammas). It seems that digitization with 12 or more bit ADC would solve such problems.

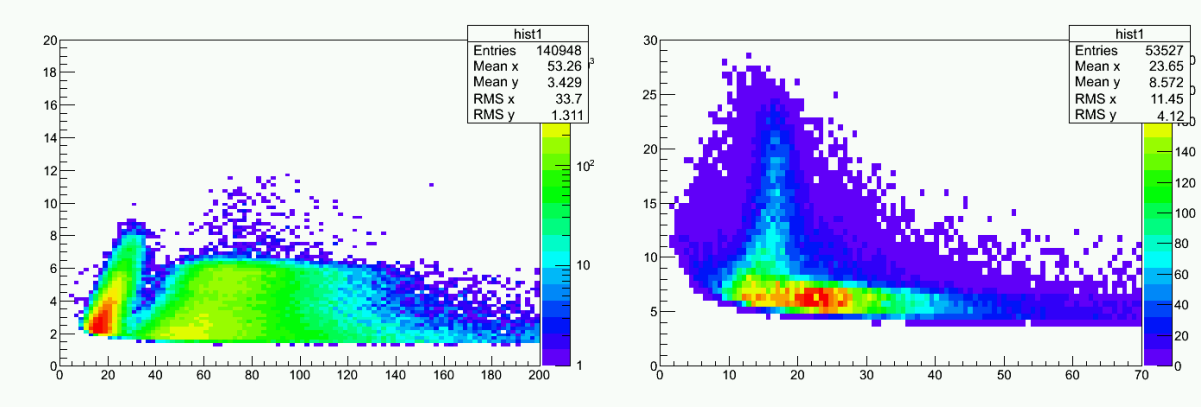

FIG. 5. n/γ separation plot for PuBe neutron source (left) and p+Li neutron source with proton energy of 27 MeV (right). Deposited energy is on the Y axis (in relative units), ratio between slow and fast component of the signal decrease is on the X axis.

3.2. SCINTILLATOR RESPONSE

Figure 6 shows the signals sampled 2 m from the target front during the irradiation of the thick Be target with 20 MeV protons. The response of the scintillator is on the Y axis, time within the duration of 1 frame (ca. 50 ns) is on X axis. The vertical extracts from such graph represent the scintillator response at given time/energy. Figure 7 shows the scintillator response to the monoenergetic peak (determined by the TOF time window) at the experiment p+Li (27 MeV). The scintillator response was normalized to MeV units using the gammas of 4.43 MeV originating in the C stopper hit by protons.

3.3. Measured TOF spectrum

The case of the white neutron spectrum on Fig. 6 does not provide much information about the time resolution. On the other hand, the p+Li neutron source provides a clear gamma line (prompt gamma from C excited by protons), which can be used to study the time characteristics of the proton beam. Figure 8 shows the TOF spectrum recorded 4.59 m from the target front. The gammas are seen at 15 ns (c×4.59 m). The FWHM of the gamma peak is around 4 ns, this is the combined time resolution of the proton beam and of our acquisition. Since 500 MHz acquisition should safely cover the exact reconstruction of each pulse [11], these 4 ns can be attributed to the FWHM of the proton beam.

3.2. Ion-induced quasi-monoenergetic and white neutron beams

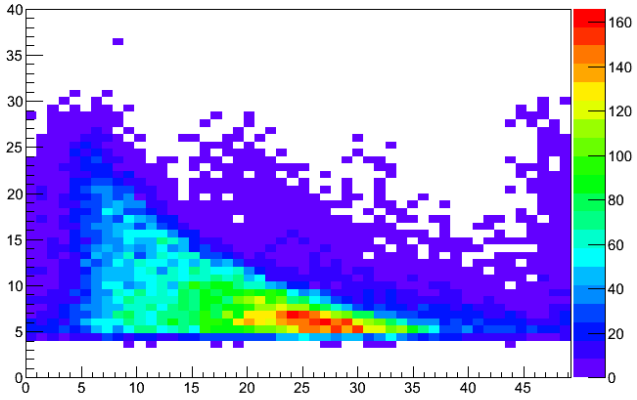

FIG. 6. Scintillator response vs. TOF for p+Be@20 MeV. Repetition rate was 20.297 MHz, ca. 50 ns per frame (X axis). The scintillator response (Y axis) is in relative units. The distance from the target front was 202 cm.

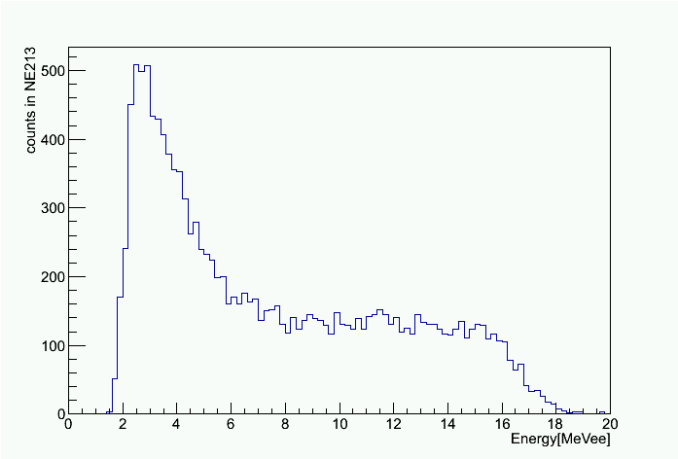

FIG. 7. Scintillator response to monoenergetic neutrons (ca. 25 MeV, determined by the TOF window) at the irradiation of the Li target with 27 MeV protons.

A smaller peak appears 3 ns before the gamma peak, a similar peak is also seen 3 ns before the neutron peak (with n/γ discrimination). These peaks were carefully studied, however they cannot be explained. Hopefully, they should disappear when a proper beam pickup system is installed (at the moment the signal from antenna is used to determine the phase). The peak from the monoenergetic neutrons is located around 23 ns. Figure 9 shows the neutron energy spectrum calculated from the TOF spectrum shown in Fig. 8. Due to frame overlap the neutron spectrum is available only down to 20 MeV at the distance of 4.59 m. The correction for scintillator efficiency was not applied to Fig. 9.

4. CONCLUSION

Current development of the present p+Li neutron source is focused on the improvement of the methodical uncertainties. The detailed study of uncertainties shown in Section 2 points out the biggest contributions to the total uncertainty and suggests how to remove some of them. It seems that online neutron monitor would significantly improve the situation with the systematic uncertainties originating from the Li target thickness and beam current measurements. The parallel irradiation at non zero angle could on the other hand help with the subtraction of contribution from neutrons below the monoenergetic peak.

3.2. Ion-induced quasi-monoenergetic and white neutron beams

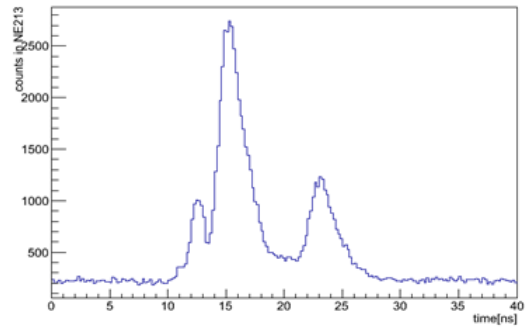

FIG. 8. TOF spectrum recorded 4.59 m from the target front. The energy of the protons directed to Li(C) target was 31 MeV. Gamma peak around 15 ns and neutron peak around 23 ns are seen.

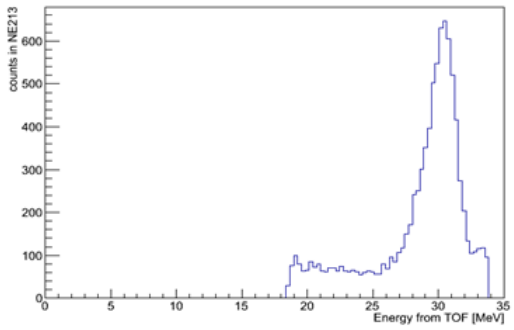

FIG. 9. Neutron energy spectrum calculated from the measured TOF spectrum. The energy of the protons directed to Li(C) target was 31 MeV. The correction for scintillator efficiency was not applied.

We are also continuing with the online measurements based on the digitization of the response from the scintillator detector. At several irradiations the responses were sampled using 500 MHz digitizer card. The studies of the feasibility of the TOF method showed that with relatively simple equipment we are able to experimentally determine the neutron spectrum to some extent.

ACKNOWLEDGMENTS

The work was supported in part by the contract F4E-2010-F4E-GRT-056(ES-AC) Action 2 and the grant of Ministry of Trade and Industry of Czech Republic 2A-1TP1/101. Authors are indebted to the staff of the NPI cyclotron laboratory for unfailing operation of the accelerator.

REFERENCES

[1] BÉM, P., Summary Report from the Consultants' Meeting on Neutron Spectra for EXFOR, INDC(NDS)-0590, 2011, p.31
[2] SIMAKOV,S.P., Final Report F4E-2008-GRT-014 Action2 D7
[3] MAJERLE, M. Final Report F4E-2010-GRT-056 Action2 Task 4.2
[4] UWAMINO, Y., et al. High-energy p-Li neutron field for activation experiment, NIM A389 (1997) 463-473, EXFOR E1826
[5] SIMAKOV, S,. et al., ISRD 13 (2008), 532-540, ISBN-13 978-981-4271-10-3
[6] HONUSEK, M., et al. Journal of the Korean Physical Society, Vol. 59, No. 2, August 2011, pp. 1374-1377
[7] ŠIMEČKOVÁ, E., et al. Journal of the Korean Physical Society, Vol. 59, No. 2, August 2011, pp. 1801-1804
[8] NOLTE, R., et al. NIM A 476 (2002) 369–373
[9] BÉM, P., et al. Report NPI ASCR Řež, EXP-EFDA-03/2003, Final report on EFDA task TW0-TTMI-003/D14a-b
[10] NOVÁK, J., et al. Journal of the Korean Physical Society, Vol. 59, No. 2, August 2011, pp. 1157-1580

3.2. Ion-induced quasi-monoenergetic and white neutron beams

[11] BELLI, F., et al. “A study on the pulse height resolution of organic scintillator digitized pulses” to be published in Fusion Engineering and Design

THE NEUTRONS FOR SCIENCE FACILITY AT SPIRAL-2

X. LEDOUX[1,14], M. AÏCHE[2], M. AVRIGEANU[3], V. AVRIGEANU[3], L. AUDOUIN[4], E. BALANZAT[5], B. BAN-D'ETAT[5], G. BAN[6], G. BARREAU[2], E. BAUGE[1], G. BÉLIER[1], P. BEM[7], V. BLIDEANU[8], J. BLOMGREN[9], C. BORCEA[3], S. BOUFFARD[5], T. CAILLAUD[1], A. CHATILLON[1], S. CZAJKOWSKI[2], P. DESSAGNE[10], D. DORÉ[11], M. FALLOT[12], U. FISCHER[13], L. GIOT[12], T. GRANIER[1],S. GUILLOUS[5], F. GUNSING[11], C. GUSTAVSSON[9], B. JACQUOT[14], K. JANSSON[9], B. JURADO[2], M. KERVENO[10], A. KLIX[13], O. LANDOAS[1], F. R. LECOLLEY[6], J. F. LECOLLEY[6], J. L. LECOUEY[6], M. MAJERLE[7], N. MARIE[6], J. MRAZEK[7], F. NEGOITA[3], J. NOVAK[7], S. OBERSTEDT[15], A. OBERSTEDT[16], S. PANEBIANCO[11], L. PERROT[4], M. PETRASCU[3], A. J. M. PLOMPEN[15], S. POMP[9], J. M. RAMILLON[5], F. FARGET[14], D. RIDIKAS[11], B. ROSSÉ[1], G. RUDOLF[10], O. SEROT[10], S. P. SIMAKOV[13], E. SIMECKOVA[7], A. G. SMITH[18], J.C. STECKMEYER[6], J. C. SUBLET[19], J. TAÏEB[1], L. TASSAN-GOT[4], A. TAKIBAYEV[11], I. THFOIN[1], I. TSEKHANOVICH[18] AND C. VARIGNON[1]

[1] CEA/DAM/DIF, F) 91297, Arpajon, France
[2] CENBG, Gradignan, France
[3] NIPNE, Bucharest, Romania
[4] IPNO, Orsay, France
[5] CIMAP, Caen, France
[6] LPC, Caen, France
[7] NPI, Řež, Czech Republic
[8] CEA/DSM/IRFU/ Senac, Saclay, France
[9] Uppsala university, Uppsala, Sweden
[10] IPHC, Strasbourg, France
[11] CEA/DSM/IRFU/ SPhN, Saclay, France
[12] Subatech, Nantes, France
[13] FZK, Karlsruhe, Germany
[14] GANIL, Caen, France
[15] JRC/IRMM, Geel, Belgium
[16] Orebro university, Orebro, Sweden
[17] CEA/DEN, Cadarache, France
[18] Department of Physics and Astronomy, University of Manchester, Manchester, UK
[19] Culham Centre for Fusion Energy, United Kingdom
Email: xavier.ledoux@ganil.fr

Abstract

The "Neutrons For Science" (NFS) facility will be a component of the SPIRAL-2 laboratory under construction at Caen (France). The SPIRAL-2 facility will be dedicated to the production of high intensity of Rare Ions Beams (RIB). Additionally to the RIB production, two Linag Experimental Areas (LEA) will be constructed in order to use stable beams (protons, deuterons as well as heavy ions) delivered by the accelerator: NFS is one of them. It will be composed of a pulsed neutron beam for in-flight measurements and irradiation stations for cross-section measurements and material studies. The beams delivered by the LINAG (linear accelerator of GANIL) will allow producing intense pulsed neutrons sources in the 100 keV to 40 MeV energy range. Continuous and quasi-monokinetic energy spectra will be produced by the interaction of deuteron beam on thick Be converter and by ^{7}Li(p,n) reaction on thin converter respectively. The flux at NFS will be up to 2 orders of magnitude higher than those of other existing time-of-flight facilities in the 1 MeV - 40 MeV range. Irradiation stations for neutron, proton and deuteron induced reactions up to 40MeV will also allow to perform cross-sections measurements by activation technique. NFS will be a very powerful tool for fundamental research as well as applications like the transmutation of nuclear waste, design of future fission and fusion reactors, nuclear medicine or test and development of new detectors. The facility and its characteristics are described, and several examples of the first potential experiments are presented.

1. INTRODUCTION

Neutron-induced reactions play an important role in a wide range of applications including nuclear power reactors, accelerator-driven systems (ADS), fusion technology, medical diagnostics and therapy, production of radio-elements, dosimetry concerning dose

effects and radiation damage and upsets in electronic devices, as well as basic science research. The data used in transport codes are embodied in evaluated data libraries, which are based on measurements and reaction models. As a matter of fact, the quality of the evaluated data depends on the accuracy of the measured data. Today there is still a large demand of data in neutron-induced reactions above, say, 14 MeV. In many cases (n,fission), (n,n'γ), (n,xn) and (n,Light Charged Particles) reaction cross sections are unknown or known with a very limited accuracy. The neutron energy range between 1 and 40 MeV is particularly well suited for the applications previously mentioned as well as for fundamental research.

NFS will be a very powerful tool dedicated to these studies. It will be a component of the future SPIRAL-2 facility [1][2], currently under construction at GANIL, Caen (France). SPIRAL-2 will produce very intense rare isotope beam (RIB) in the mass range from A=60 to A=140. These nuclei will be produced by the fission of ^{238}U induced by fast neutrons, which are generated by break-up reaction of the deuteron beam on a carbon converter. The LINAG (high-power superconducting driver LINAC of GANIL), delivering a high-intensity deuteron beam for RIB production, will also be used to produce neutrons in the NFS facility. NFS will deliver a well-collimated neutron beam in a long experimental area in order to perform measurements at neutron energies up to 40 MeV. In addition, neutron, proton and deuteron induced reaction cross-sections could be measured by means of activation technique.

2. DESCRIPTION OF THE NEUTRONS FOR SCIENCE FACILITY

2.1. INFRASTRUCTURES

The NFS facility is composed of two main areas, a converter cave and a time-of-flight (TOF) area. The converter cave contains the ion beam line, the converter to produce neutrons and the irradiation station for the study of ion-induced reactions. The TOF area is an experimental area of 6 m width and 30 m long allowing high-resolution energy measurements. The two rooms are separated by a 3 m thick concrete wall pierced of a hole to define the neutron beam in the TOF hall. This part is called the collimator, its design defines the neutron beam spatial extension and the neutron background in the TOF hall. The two rooms of NFS as well as the accelerator are undergrounded at a depth of -9.5 m.

2.2. NEUTRON PRODUCTION

The LINAG will deliver proton and deuteron beams with a maximum energy of 33 and 40 MeV respectively. These beams will be used to produce neutrons with continuous and quasi-mono-energetic energy spectra. A continuous spectrum is obtained in the interaction of the deuteron beam on a thick converter (≈8 mm) made of beryllium or carbon. Neutrons are produced up to 40 MeV at 0° with an average energy of 14 MeV (see Fig.2). The beam is stopped in the converter and the full power is deposited in the converter. Quasi-mono-energetic neutrons can be produced by using a proton beam and a thin converter of lithium or beryllium (see Fig.3). In this case the proton beam crosses the converter and is deflected by a clearing magnet to a proton beam dump. Since the primary beam frequency of the LINAG (88 MHz) is not adapted to the measurements by time-of-flight technique, a fast beam chopper will be used to reduce the frequency by a factor 100 to 10000. The maximum intensity will be then limited to 50 μA.

3.2. Ion-induced quasi-monoenergetic and white neutron beams

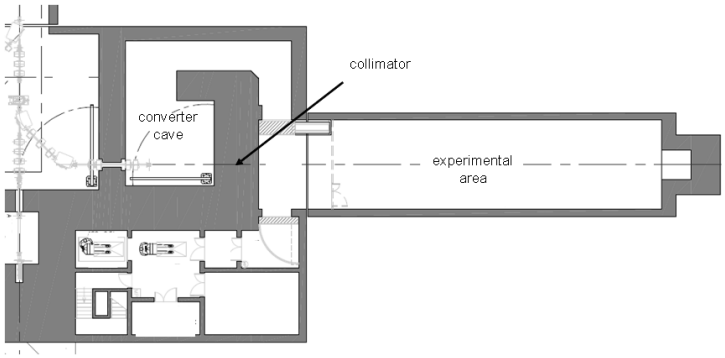

FIG.1. Scheme of the converter and TOF areas.

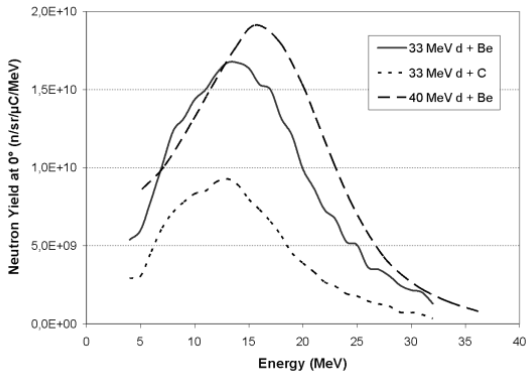

FIG.2. Neutron yield at 0° for reaction induced by deuteron on thick target [3][4].

The converter design must take into account the maximum power deposition and the handling procedure after activation. A rotating converter is required to sustain the maximum power of 2 kW (40 MeV × 50 µA). It will be composed of a disk of 170 mm in diameter and 8 mm thick rotating at a speed of 2000 tr/min. Thermal calculations show that the maximum temperature will not exceed 700°C well below the melting point. After irradiation the converter being highly activated, especially due to the production of ^{7}Be, it will be moved automatically into a lead shielding to be manipulated and replaced.

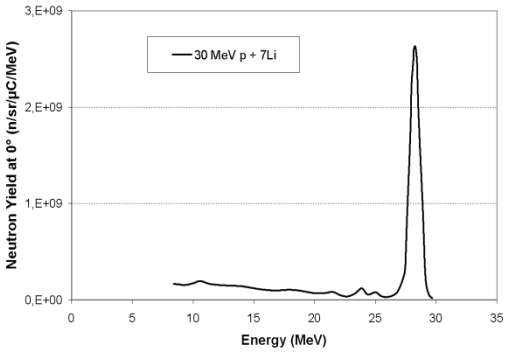

FIG.3. Neutron yield at 0° produced by Li(p,n) reaction at 30 MeV on thin converter [5].

2.3. THE COLLIMATOR

The collimator is placed in the thick concrete wall separating the converter and the TOF rooms. The role of the collimation system is to define a well-collimated neutron beam and, therefore, its design is of special importance to the beam characteristics. The collimator will be composed of several materials arranged in ring fashion [6]. The inner part, a cylinder of iron pierced in its centre by a conical channel to define the beam, will scatter away high-energy neutrons. The outer part (in concrete and borated polyethylene) will then absorb them. Its design was studied with simulations realized with the MCNPX code [7]. Several sets of inner cylinders with different inside channel are envisaged in order to adjust the neutron beam size to the physic request.

2.4. THE NEUTRON BEAM-DUMP

The neutron beam is "stopped" at the end of the TOF room in a beam dump whose design has been optimized in order to reduce the neutron backscattering to the TOF room and the gamma production. The beam dump is a hole of 4 m long and $1 \times 1 m^2$ of section centred on the beam axis in the concrete wall. A borated polyethylene sheet (15 cm thick) in the bottom of the hole reduces the backscattering of neutrons. A tube at the entrance of the hole (composed of borated polyethylene in the inner part and concrete in the outer part) with a diameter greater than the beam spot allows catching the neutrons and the photons.

2.5. THE SAMPLE TRANSFER SYSTEM

Cross-section measurements by activation technique will also be possible at NFS. The samples will be irradiated in the convertor room and their activity measured in the TOF area with a gamma spectroscopy set-up. A pneumatic system will ensure the movement of the samples between the two rooms, the time transfer will be of approximately 1 s. For neutron-induced reactions the sample will be placed in front of the converter. The very intense available flux (see Fig. 3) will permit to measure small cross-sections or to use small amount of material. For ion-induced reactions (mainly protons and deuterons), the sample will be placed under vacuum in the irradiation box placed in the beam line upstream of the converter.

3. BEAM CHARACTERISTICS

3.1. FLUX

The neutron flux is estimated considering the maximum ion intensity and the neutrons yield [3] and compared to existing neutron TOF facilities around the world namely n_TOF at CERN, WNR at Los Alamos (where neutrons are produced in a spallation reaction) and GELINA in Geel (where neutrons are produced by photo-reactions). The length of the TOF area allows either high-intensity flux (5 m) or high-resolution (20 m) measurements. In order to avoid the overlap of neutrons from successive bursts, the beam repetition rate is adapted to the flight path: 1 MHz and 250 kHz for 5 and 20 m respectively. The maximum deuteron beam intensity is then 4 times lower at 20 m than at 5 m. It can be seen in the Fig. 3 that NFS is very competitive in terms of average flux in comparison with n_TOF, GELINA or WNR between 1 and 35 MeV. This intense average flux is due to the high beam-repetition rate, the instantaneous flux is lower than the other facilities. Moreover, NFS presents some advantages due to the neutron production mechanism itself. In spallation sources the high energy neutrons (up to hundreds MeV), may imply challenges for both collimation and background.

Secondly, the gamma-flash, which is known to be very penalizing, especially because it induces dead time, will probably be strongly reduced at NFS.

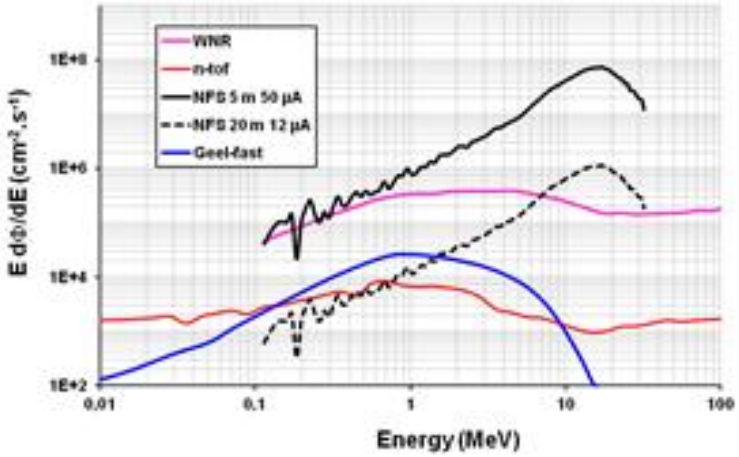

FIG. 4. Comparison of the neutron flux of NFS with three other TOF facilities, WNR, n-tof and GELINA. The fluxes for NFS are shown at 5 m and 20 m.

The neutron flux in the converter room very close to the converter is presented in Fig. 3. By using the thick beryllium converter a flux greater than 5.10^{11} n/cm^2/s can be reached. This very high flux can be used to measure reaction cross-sections by activation technique with small target.

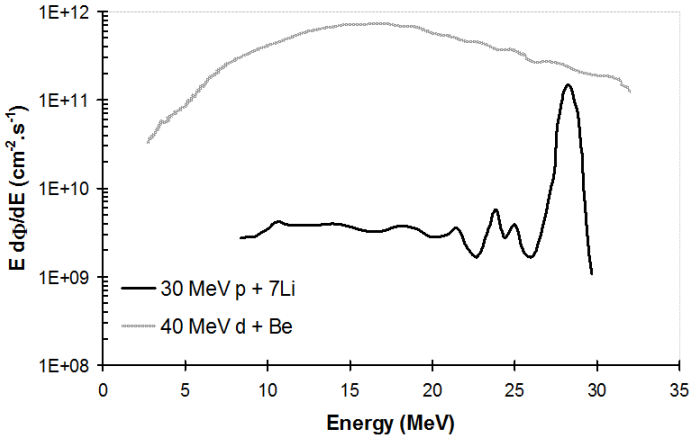

FIG. 3. Neutron flux at 5 cm in front of the converter.

3.2. ENERGY RESOLUTION

The time resolution of the ion-beam and the length of the experimental area allow the energy measurement of the incident neutrons by TOF technique with a rather good resolution. Actually the burst time spread at the converter point is estimated to be about 1 ns. The use of fast detectors (photomultipliers or silicon detectors for example with $\Delta t \approx 1$ ns) allows to measure the energy of neutrons with a resolution better than 1% (see Fig. 4). With slow detectors, like High Purity Germanium detector ($\Delta t \approx 8$ ns), the energy resolution at 40 MeV will not be worse than 5%.

3.2. Ion-induced quasi-monoenergetic and white neutron beams

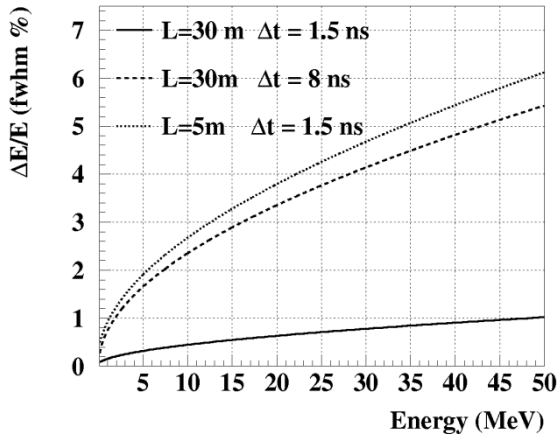

FIG.4. Energy resolution obtained with fast and slow detectors for flight path of 5 and 30 m.

3.3. BEAM SIZE AND BACKGROUND

The neutron beam characteristics and the background in the TOF area are key parameters of the NFS facility. Actually, the neutron beam must be very well collimated to interact only with the target and not hit the detection set-up surrounding the target. The background originates mainly from the collimator, the neutron beam dump and the building design. Neutron transport calculations have been realized to optimize the design of these components. All the simulations were performed with the MCNPX code version 2.5. The energy and angular distribution of the neutrons produced in the 40 MeV d + Be have been calculated using the model described in reference [7].

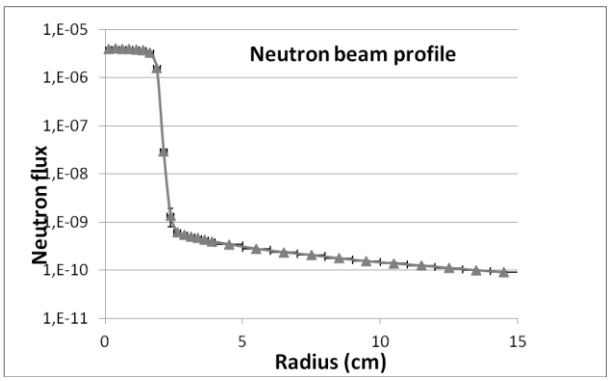

FIG.5. Neutron beam radius at 1 m from the exit of the collimator for several collimator designs.

Several designs of the collimator have been studied in order to determine the best compromise between efficiency and cost.

Figure 5 shows the result of MCNPX simulations with several configurations of collimator. It can be seen that at 1 m of the exit of the collimator (approximately 5 m from the converter point) the neutron beam has a radius of 2 cm and the ratio signal over noise is around 10^4.

3.2. Ion-induced quasi-monoenergetic and white neutron beams

The effect of the beam-dump design optimization is illustrated in Fig. 6. In the simulations the neutrons are emitted from an extended source (a disk whose diameter is equal to the diameter of the beam at the center of the beam dump). The number of neutrons backscattered to the TOF area is strongly reduced in the optimized design. The photons created by neutron interaction (n,n'),(n,γ)… have also been treated and the result is presented in Fig.7. The gamma produced in converter has not been taken into account.

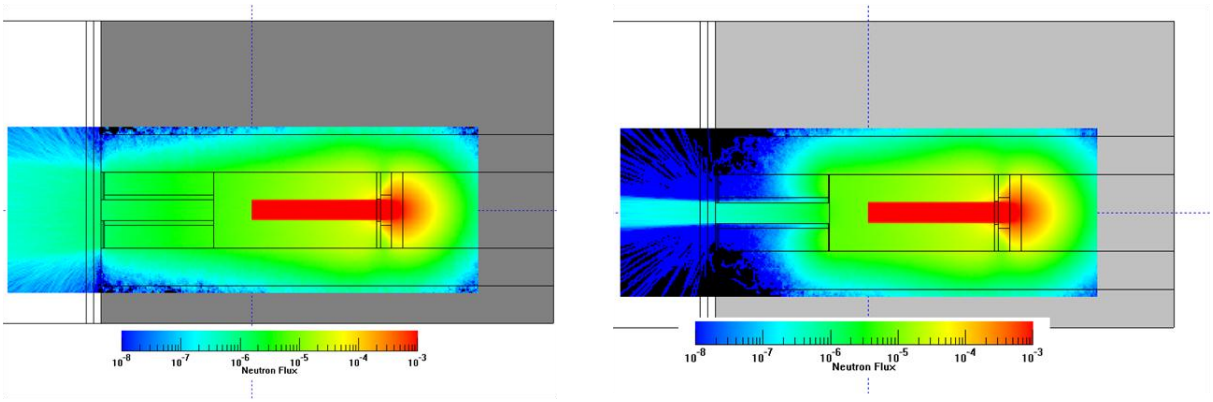

FIG. 6. Neutron flux simulations (arbitrary units) in the beam dump zone, with the raw design (left) and the optimized design (right).

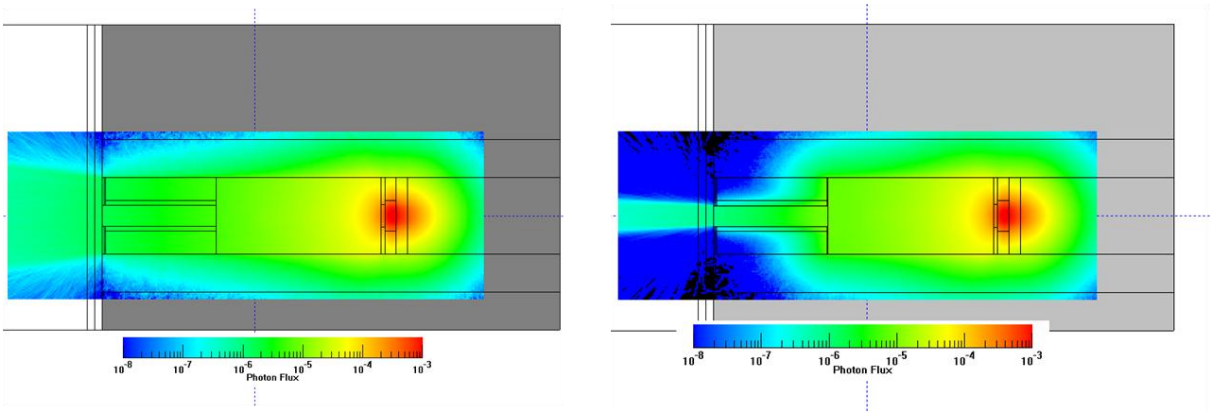

FIG. 7. Photon flux simulations (arbitrary units) in the beam dump zone, with the raw design (left) and the optimized design (right).

4. SAFETY

The safety study was of prime importance for the design of the biological protections, the maintenance operations and the evaluation of the waste production for future dismantling operations. The Fig.8 shows a bidimensionnal representation of the neutron dose equivalent in the NFS facility when the most intense neutron production mode is used (40 MeV d + Be at 50 µA). In this calculation the inner part of the collimator has been removed in order to maximize the neutron dose in the TOF area. It can be observed that the neutron doses in the rooms adjoining the TOF and converter areas are compatible with the safety rules and validating the biological protections.

3.2. Ion-induced quasi-monoenergetic and white neutron beams

The activation of the elements of the process as well as the concrete has been estimated by using the FISPACT code [8]. The results were used to estimate the waste production and the residual gamma dose. The highest activated element in the NFS facility will be the beryllium converter and a dedicated lead shielding has been designed to store the converter after use. For most of the elements of the beam line aluminum is preferred to steal because the produced radioactive species have shorter half-lives.

5. BUDGET AND PLANNING

The SPIRAL-2 project is split in two phases. The phase 1, today under construction, includes the accelerator, the Super Spectrometer Separator (S3)[9] and the NFS facility. The phase 2 will content the production building for RIB production and the Desir facility [10].

The infrastructure of NFS (building, equipment, radioprotection) is funded by the SPIRAL-2 project (CEA, CNRS and region Basse-Normandie) and the Upsalla University for a budget of approximately 3100 k€. The NFS process (beam line, converter, collimator, clearing magnet, irradiation box, pneumatic transfer system…) is funded by 8 French and European partners for a total amount of 3200 k€ including investment and manpower.

The permit of construction for the phase one was obtained in October 2010. The buildings will be finished in the beginning of 2013 and the accelerator will be installed in 2013. The components of the NFS process are under construction and will be installed in the beginning of 2014. The first beam is expected to be delivered mid-2014. The final safety file will be submitted to the French Nuclear Safety Authority by June 2013 for a starting authorization one year later.

6. PHYSICS CASE

Neutrons-induced reactions in the NFS energy-range play an important role in numerous applications like in reactors of the new generation, in nuclear medicine, for describing the so-called Single Event Upset (SEU) in electronics devices, for advancing the fusion technology or the development of nuclear model codes in general. Only very limited data exist for neutron induced reactions above 14 MeV and for many cases both fission and (n,xn) reaction cross sections are unknown. The NFS energy range corresponds also to the opening of new reaction channels like (n,p), (n,α), allowing the pre-equilibrium model studies, i.e. the transition between low (evaporation) and high energy models (intra-nuclear cascade). Among these topics, NFS is particularly well suited for the study of the neutron induced fission, the (n,xn) and (n,lcp) reactions and the proton and deuteron induced reactions.

Letters Of Intent (LOI) for “Day-one experiments in phase 1” were submitted to the Scientific Advisory Committee (SAC) of SPIRAL-2. It corresponds to experiments which could be performed just after the commissioning of NFS with a reduced intensity (≈10 µA).

6.1. FISSION

The probable development of innovative fast nuclear reactors being able to transmute long-lived nuclear wastes requires new high-quality data for a large set of fissioning systems (from thorium to curium) for an energy range going from thermal up to the fast (~2 MeV)

region. Complementary to reaction cross section data, the mass and charge distributions are needed with a high precision for burn-up calculations of the reactor fuel, because they are directly connected to the control and the safety of the reactor.

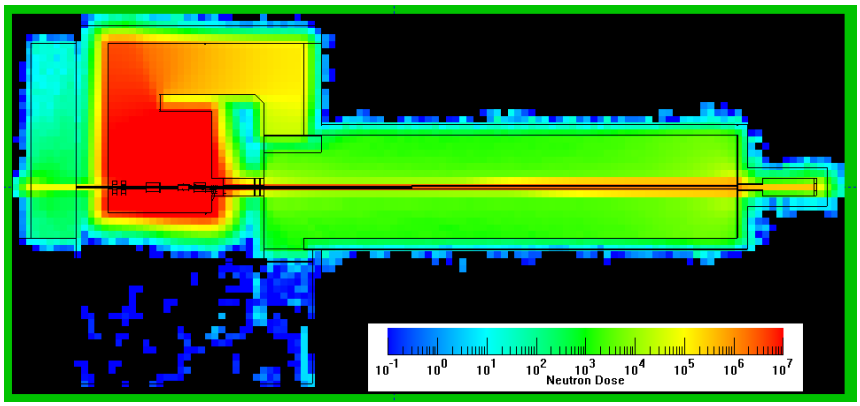

FIG.8. Prompt neutron dose equivalent in µSv/h in the NFS facility. Neutrons are produced by reaction 40 MeV d + Be at an intensity of 50 µA.

The TOF area is designed to receive actinides with an activity up to 1 GBq and 10 GBq for thin and thick samples respectively. The white intense pulsed neutron beam of NFS allows performing simultaneous measurements at several incoming neutron energies. The cross-section variations around fission threshold or at second chance fission energy range can be accurately described. The fission process can also be scanned over a wide range of excitation energy. In addition the collimated neutron beam and the low neutron background will allow using 4π neutron or gamma detectors.

The measurement of fission cross-sections and the corresponding fragment angular distributions with different experimental techniques is the subject of 2 Letters of Intent. In both cases the two fission fragments are detected in coincidence and their trajectory measured. In addition the simultaneous measurement of elastic np scattering events will allow for good determination of the fission cross section.

The high neutron flux allows performing measurement of fission fragment characteristics (mass, charge, kinetic energy) in the energy range between 500 keV and 20 MeV. In contrary to thermal neutron energies, only few data are available in the fast domain. For fundamental studies, it is important to perform measurements for even-even, even-odd and odd-odd systems. Fission modes, even-odd effects, deformation energy, etc, can be studied with such measurements. Thanks to the results of these measurements, models will be improved and more precise predictions will be done for nuclei difficult to access experimentally.

The neutron multiplicity distributions as well as the energy released by gamma emission can also be measured at NFS.

6.2. (n,xn) REACTIONS

In fast reactors, a new kind of reactions appears compared to the situation in thermal reactors. Among them, the (n,xn) reactions (with x>1) are then possible despite their high threshold and play a non-negligible role, since above 10 MeV they have cross sections

comparable to fission. They modify the neutron spectrum by converting fast neutrons (E_n>5 MeV) into slow neutrons (E_n<1 MeV) and especially they act upon the criticality of the reactor core. A good knowledge of the cross sections is necessary for assessing the neutron balance or to predict radioactive waste inventories. These reactions play also an important role in the Accelerator Driven Systems where neutrons in the energy range up to few 10^{th} of MeV represent a significant part of the total neutron flux. Three methods allowing (n,xn) cross sections measurements will be used at NFS; namely the direct detection of neutrons, prompt gamma ray spectroscopy or the activation technique.

In addition to cross-section measurements, the study of pre-equilibrium processes in (n,xn) reactions is of first importance to improve or constrain existing nuclear reaction models. The energy range of NFS is particularly well suited because the pre-equilibrium importance increases in the 20-50 MeV range.

6.3. LIGHT CHARGED PARTICLE PRODUCTION

In neutron therapy a large part of the dose is deposited by light-ion production, a precise knowledge of the double-differential cross-section is absolutely required to accurately evaluate the dose. These data are also essential for the estimation of radiation effects in electronics like Single Events Upset in chips and for various nuclei like oxygen and silicon. The energy region between 15 and 30 MeV is important for the following reason; while the neutron flux in this energy range decreases with roughly 1/E (e.g. secondary cosmic ray neutrons), the light-ion production channel opens up in the 10-20 MeV range. Thus, folding the neutron flux in an application with the cross section for light-ion production generally results in a peak in the 15 to 30 MeV range. Double-differential cross-sections measurement for neutron-induced light-ion production (p, d and alpha particles) will be performed at NFS.

6.4. PROTON AND DEUTERON INDUCED REACTION

Proton and deuteron induced activation reactions are of great interest for the assessment of induced radioactivity in accelerator components, targets and beam stoppers and are important for isotope production for medical purposes. The cross sections are needed in the energy range from the threshold of the activation reactions (2-10 MeV) up to 40 MeV for both incident ions: deuterons and protons. Present status of the measured and evaluated data needs urgent and strong improvement. The measurement of excitation functions can be performed at NFS in an energy domain (20-40 MeV) where data are not existing or known with poor accuracy. These cross-sections will be measured by activation technique.

7. SUMMARY

Neutrons For Science is a component of the SPIRAL-2 facility under construction in the GANIL site at Caen (France). The NFS characteristics in terms of flux or energy resolution make it a very attractive and powerful tool for physics with neutrons in the 100 keV-40 MeV range. The high neutron fluxes will allow measurements of small reaction cross-sections and/or with very small targets, which might be rare, expensive, and in some cases radioactive. The energy range and conditions offered by the SPIRAL-2/NFS time-of-flight facility is complementary to other such facilities in Europe, notably GELINA of the European Commission’s Joint Research Centre in Geel and the CERN based n_TOF facility.

3.2. Ion-induced quasi-monoenergetic and white neutron beams

The irradiation facility is particularly well adapted to cross-section measurements in neutron, proton or deuteron induced reactions which are needed for the fusion technology. Several experiments have been identified as potential Day-one experiments and presented to the Scientific Advisory Committee of SPIRAL-2. The facility is expected to be operational in 2014.

REFERENCES

[1] "Report of the SPIRAL 2 Detail Design Study", available on http://www.ganil.fr
[2] "The scientific objective of the SPIRAL-2 project", available on http://www.ganil.fr
[3] SALTMARSH, M., et al., NIMA145 (1977) p81-90
[4] MEULDERS, J., et al., Phys. Med. Biol. (1975)vol 20 n°2, p235
[5] BATTY, C., et al., NIM 68 (1969) p273-276
[6] TAKIBAYEV, A., CEA/Saclay, Internal Report Irfu 11-75 (2011)
[7] MAJERLE M. and SIMAKOV, S., Karlsruher Institut für Technologie, Internal report, INR-Nr. 15/10 FUSION Nr. 368 (2010)
[8] FISPACT-2007 user manual ("http://www.fusion.org.uk/techdocs/ukaea-fus-534.pdf")
[9] DROUART, A., et al., Nucl. Phys. A834, (2010) p747-751
[10] DESIR facility Letter of Intent, available on http://pro.ganil-spiral2.eu/

3.2. Ion-induced quasi-monoenergetic and white neutron beams

HIGH INTENSITY FAST NEUTRON BEAM FACILITY AT CYRIC

Y. SAKEMI, M. ITOH, T. WAKUI

Cyclotron and Radioisotope Center,
Tohoku University, Miyagi 980-8578,
Japan
Email: sakemi@cyric.tohoku.ac.jp

Abstract

A high intensity quasi-monoenergetic neutron beam from 14 to 80 MeV is available to be supplied at the Cyclotron and Radioisotope Center (CYRIC), Tohoku University, Sendai, Japan. The available neutron flux is about 10^6 n/cm^2/sec/uA at the experimental region where the irradiated sample is located. The experiments to study the mechanism of the radiation damage of many types of the integrated circuit system or the radiation hardness of the detector components for the particle and physics are performed with this neutron beam.

1. INTRODUCTION

A high-intensity fast neutron beam facility in CYRIC has been developed at the straight beam line (32 course) from the K = 110 MeV AVF cyclotron since 2004[1][2]. This course is used for the cross section measurement of the nuclear physics, testing of semiconductors for single-event effects, and dosimetry development. The AVF cyclotron can provide the proton beam with an energy range from 14 to 80 MeV at present. Figure 1 shows the schematic view of the neutron source. The quasi-monoenergetic neutron beam is produced by using the ^{7}Li(p,n)^{7}Be reaction. The primary proton beam is bombarded to the water-cooled production (Li) target. After penetrating the target, the proton beam is bent in the clearing magnet by 25° and stopped in the water-cooled beam dump which consists of a carbon block shielded by copper and iron blocks.

The typical neutron beam intensity is about 10^{10} n/sr/sec/uA with a beam spread of about 5 % for the beam energy and ± 2° for the horizontal and vertical directions. The neutron beam is collimated by iron blocks of 595 mm thick and sufficiently low background at the off-axis position. The available flux of the neutron beam is about 10^6 n/cm^2/sec/uA at the sample position which is located at about 1.2 m downstream of the production target. The thermal neutron flux at the sample position is about 2×10^4 n/cm^2/s, which was measured by a foil activation method combined with imaging plate.

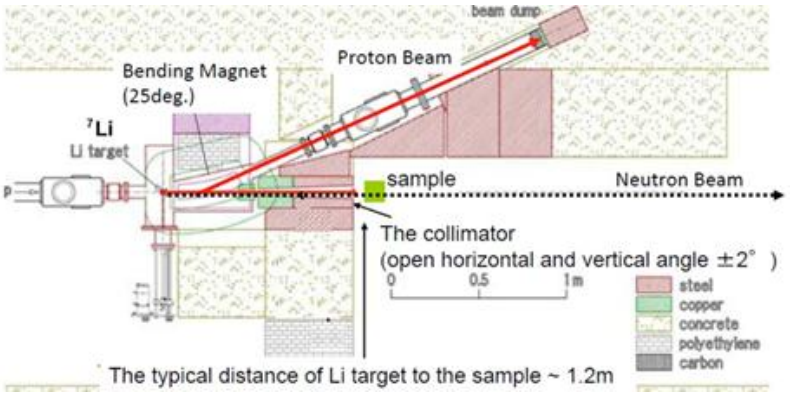

FIG.1. Schematic layout of the fast neutron beam facility

2. K 110 MEV AVF CYCLOTRON

In this section, the accelerator system to supply the primary proton beam to produce the neutron is described. The K110-MeV AVF cyclotron at CYRIC, which was installed in 2000, is an ion accelerator capable of accelerating ions from light ions such as hydrogen and helium to heavy ions up to krypton and xenon. The cyclotron itself has a bending limit of 130 MeV for ^{4}He particle and a focusing limit of 90 MeV for proton. The main magnet produces the maximum magnetic field of 1.96 T at hill. The cyclotron has four spiral sectors and two RF Dee electrodes. The frequency range is from 11 to 22 MHz with the maximum voltage of 50 kV. The extraction radius is 923 mm. Ions from external ion sources are axially injected into the cyclotron and led onto the median plane with a spiral inflector.

The cyclotron is equipped with three ECR ion sources of 2.45 GHz, 10 GHz and 14.5 GHz. The 2.45 GHz ECR ion source supplies hydrogen and the others heavy ions. The 1 GHz source supplies ions of gaseous elements as well as that from solid materials. The 14.5 GHz source consists of all permanent magnet. The power consumption is then quite small. Ions available with the sources are listed in Table I. The beam intensity depends strongly on the beam energy and the maximum values for elements are shown in the Table.

TABLE 1. AVAILABLE IONS

Elements	Energy range [MeV]	Beam intensity [eμA]
H	14 – 70	3
H	80	0.1
He	30 – 105	3
C	30 – 140	2
N	30 – 188	2
O	30 – 236	2
Ne	30 – 260	1
Ar	30 – 378	1
Kr	30 – 405	0.1
Xe	30 – 233	0.01

The cyclotron has two acceleration modes, positive and negative ion acceleration mode. In the negative ion acceleration mode, the magnetic field direction is turned over and a stripper foil is inserted on 650 mm position from the center of cyclotron. In the negative hydrogen acceleration, the maximum proton energy is 50 MeV according to the 650 mm extraction radius.

3.2. Ion-induced quasi-monoenergetic and white neutron beams

FIG.2. K110-MeV AVF Cyclotron.

3. ENERGY SPECTRUM OF THE NEUTRON BEAM

Figure 3 shows a typical energy spectrum of the neutron beam at 65 MeV which was produced by 70 MeV protons. The thickness of the Li target was 9.1 mm. The energy spectrum was measured by the time of flight (TOF) method at 7.37 m downstream of the Li target [3, 4]. The energy spread of the neutron beam was 4 MeV which was included the time spread of the primary beam of 1.6 ns, the energy loss difference due to the thick Li target, and so on. The ratio of peak area to the total fast-neutron flux is about 0.4.

The detection system of the fast neutron consists of a liquid scintillator of NE213 type with the size of 140Φ mm × L 100 mm, a 5 inch photomultiplier tube, HAMAMATSU H6527, which were assembled by OHYO-KOKEN cooperation, and a CAMAC data acquisition (DAQ) system [5, 6]. Figure 4 shows the CAMAC DAQ system. The signal of a liquid scintillator is divided to three. First is the full signal to obtain light output of NE213. Second is the tail signal in order to identify neutrons by the n-γ discrimination. Third is the signal for making a DAQ trigger.

4. EXPERIMENTAL ROOM AND USER INTERFACE

The irradiation room is a narrow room which size is 1.8 m (W) × 10 m (L) × 5 m (H). The irradiation sample can be placed at 1.2 m downstream of the Li target, as shown in fig. 1. The spot size of the neutron beam is about 84 mm (horizontal) × 84 mm (vertical) at that point. The flux of the neutron beam can be varied from about a few hundreds n/sec to 3×10^{10} n/sr/sec. The largest amount of the accumulated flux in one experiment was about 5 × 1011 n/cm2 for the practical irradiation time of 50 hours. The flux of the neutron beam is monitored by a primary beam current in the beam dump and a NE102A plastic scintillator with the size of 100 mm Φ× 1 mm (t) during the irradiation experiment. Users can control the beam on/off by the LabVIEW program.

3.2. Ion-induced quasi-monoenergetic and white neutron beams

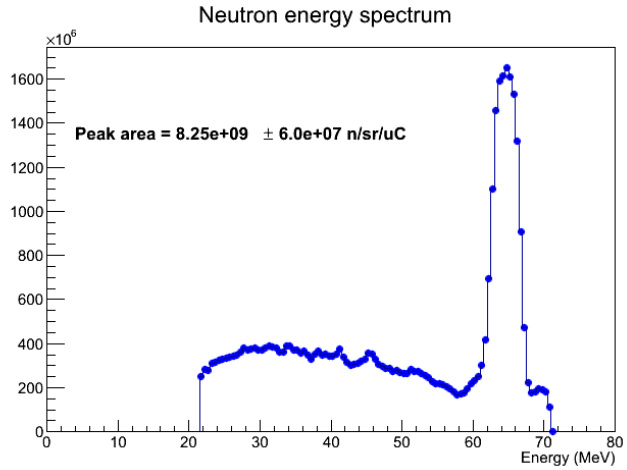

FIG. 3. A typical energy spectrum of the neutron beam at 65 MeV. The neutron flux of a peak area from 58 to 68 MeV is 8.25×109 neutrons/sr/μC. The ratio of the peak area to the total fast neutrons is about 0.4. The tail at around 70 MeV is attributed to the flame overlap due to the cyclotron RF cycle.

After recovering the CYRIC facility from the Great East Japan Earthquake on 11th March 2011, the performance of the neutron source also was recovered completely. Actually, the energy spectrum of the neutron beam in Fig. 3 was measured on December 2012 [5][6]. Now, we are preparing the further user friendly interfaces and developing the neutron source in order to supply higher intensity and higher quality neutron beam.

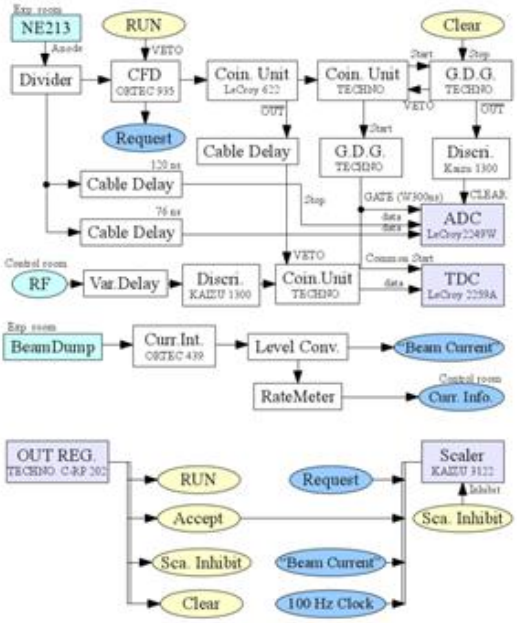

FIG. 4. The detection system of the fast neutron beam in CYRIC. Modules displayed by bule gray are those of CAMAC system. Data are accumulated into hard disks by the crate controller, TOYO CC7700, and Linux PC with kernel version 2.6.

3.2. Ion-induced quasi-monoenergetic and white neutron beams

5. FINAL REMARKS - CONCLUSIONS

The beam time for the neutron beam irradiation is allocated with 10 days typically at present in a year. The activity of the study on the neutron induced soft errors in the memory device is increased [7]. Now the upgrade plan of the AVF cyclotron to realize the high intensity proton beam for the BNCT and fundamental physics using low energy neutron beam is discussed.

REFERENCES

[1] OKAMURA, H., et al., CYRIC annual report (2004) 13.
[2] KAMATA, S., et al., CYRIC annual report (2004) 15.
[3] BABA, M., 'Quasi-monoenergetic neutron sources', Proceedings of Science; Proc. Int. Symposium on Fast Neutron Detectors and its Application, April 2006, Cape Town
[4] BABA, M., et al., 'Characterization of 40-90 MeV 7Li(p,n) Neutron Source at TIARA using a Proton Recoil Telescope and a TOF Method.', Nucl. Instrum. Methods, A428, (1999) 454-465
[5] YOSHIDA, H.P., ITOH, M., and SAKEMI, Y., CYRIC annual report (2009) 22.
[6] YOSHIDA, H.P., Itoh, M., and Sakemi, Y., CYRIC annual report (2010-2011) 33.
[7] TAKASHI, N., et al.,' Terrestrial Neutron-Induced Soft Errors in Advanced Memory Devices', World Scientific (2007), ISBN-13 978-981-277-881-9, ISBN-10 981-277-881-0

DESIGN OF A HIGH INTENSITY NEUTRON SOURCE FOR NEUTRON-INDUCED FISSION YIELD STUDIES

M. LANTZ[*], D. GORELOV[**], A. JOKINEN[**], V.S. KOLHINEN[**], A. MATTERA[*], H. PENTTILÄ[**], S. POMP[*], V. RAKOPOULOS[*], S. RINTA-ANTILA[**], A. SOLDERS[*]

[*]Physics and Astronomy, Applied Nuclear Physics division, Uppsala University, Box 516, SE-75120 Uppsala, Sweden
[**]Department of Physics, P.O. Box 35 (YFL), FI-40014 University of Jyväskylä, Finland
Email: Mattias.Lantz@physics.uu.se

Abstract

The upgraded IGISOL facility with JYFLTRAP, at the accelerator laboratory of the University of Jyväskylä, has been supplied with a new cyclotron which will provide protons of the order of 100 μA with up to 30 MeV energy, or deuterons with half the energy and intensity. This makes it an ideal place for measurements of neutron-induced fission products from various actinides, in view of proposed future nuclear fuel cycles. The groups at Uppsala University and University of Jyväskylä are working on the design of a neutron converter that will be used as neutron source in fission yield studies. The design is based on simulations with Monte Carlo codes and a benchmark measurement that was recently performed at The Svedberg Laboratory in Uppsala. In order to obtain a competitive count rate the fission targets will be placed very close to the neutron converter. The goal is to have a flexible design that will enable the use of neutron fields with different energy distributions. In the present paper, some considerations for the design of the neutron converter will be discussed, together with different scenarios for which fission targets and neutron energies to focus on.

1. INTRODUCTION

The Applied Nuclear Physics division at Uppsala University and the IGISOL group at the Department of Physics at University of Jyväskylä are collaborating, with the purpose of measuring neutron-induced independent fission yields of different actinides of relevance for partitioning and transmutation of spent fuel and for other aspects where information on nuclear fuel inventories are important. The project will use the upgraded IGISOL-JYFLTRAP facility at the accelerator laboratory of the University of Jyväskylä. The Jyväskylä group is on the forefront when it comes to accurate measurements of reaction products from nuclear interactions involving short lived nuclei. With the Ion Guide Isotope Separator On-Line (IGISOL) technique high yields of reaction products are selected and then accurately determined through mass measurement in the JYFLTRAP Penning trap. This method has proven to be very useful for the determination of independent fission yields, and experiments have been performed with 20-50 MeV protons on ^{232}Th and ^{238}U, and with 25 MeV deuterons on ^{238}U [1].

In order to measure neutron-induced independent fission yields some sort of neutron source is needed. The IGISOL facility was recently moved to a new experimental hall where it is supplied with a new cyclotron which provides proton beams of the order of 100 μA with 18-30 MeV energy, or deuterons of half that energy and intensity [2]. Therefore a neutron converter is designed, utilizing (p,xn) or (d,xn) reactions. Different options have been investigated, and our approach is to use protons on a water cooled Beryllium plate through the Be(p,xn) reaction. The design is based on simulations with Monte Carlo codes such as FLUKA [3, 4] and MCNPX [5], and deterministic codes such as COMSOL Multiphysics [6]. There will always be uncertainties in the predictions given by the Monte Carlo codes. Therefore a benchmark measurement was performed in June 2012 at The Svedberg Laboratory (TSL) in Uppsala, funded through the ERINDA EU framework programme [7].

3.2. Ion-induced quasi-monoenergetic and white neutron beams

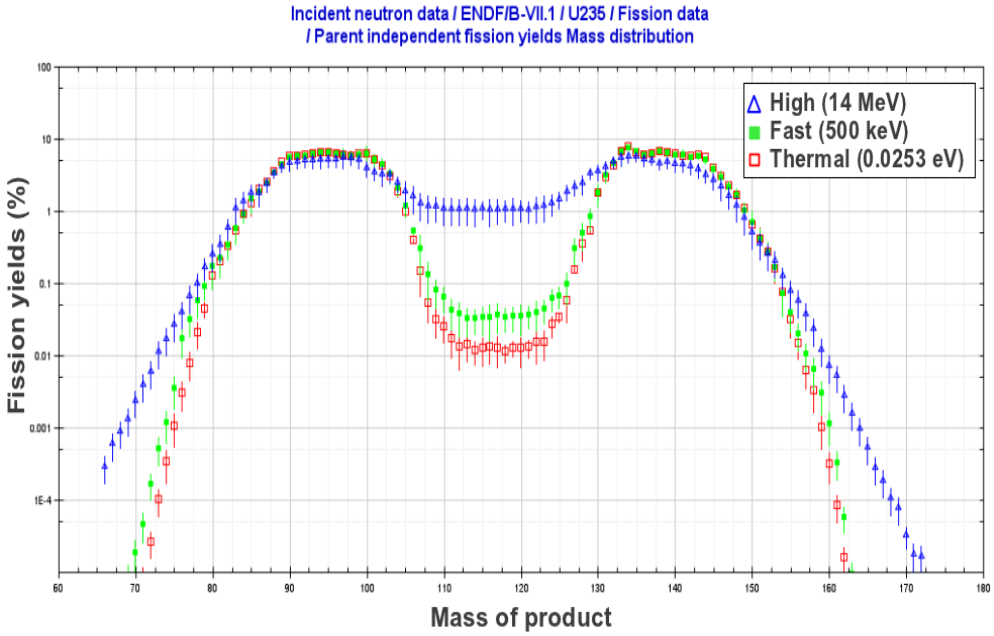

FIG. 1. Fission yield mass distributions for thermal (0.0253 eV), fast (500 keV) and high energy (14 MeV) neutrons on ^{235}U from the ENDF/B-VII.1 evaluation. The plot is produced with JANIS [11].

In order to obtain competitive count rates the fission targets will be placed very close to the neutron converter [8]. The goal is to have a flexible design that will enable the use of neutron fields with different energy distributions. Different fields can be obtained by varying the proton energy, inserting moderator materials, using deuterons instead of protons, or by varying the converter material and thickness. Challenges for the design include the need for cooling, how to avoid too much activation of the converter material and an intense background of low energy neutrons and high energy photons.

2. INDEPENDENT FISSION YIELDS

Accurate knowledge about fission yields distributions is of importance for a better theoretical understanding of the fission process itself. Besides theoretical development there are also a number of applications related to nuclear power generation where better knowledge is beneficial, for instance [9]:

- information about the composition of the resulting spent fuel (spent fuel repositories, partitioning and transmutation issues, Gen-IV reactor scenarios),
- various safety measures (decay heat, fission gas production, criticality, dosimetry, safeguards, delayed neutrons),
- information about neutron poisoning (significant discrepancies between different evaluations have been identified, especially for ^{135}Xe, ^{149}Sm and ^{157}Gd [10]), and
- improvement of burn-up predictions.

3.2. Ion-induced quasi-monoenergetic and white neutron beams

The well known shape of the fission yield mass distribution with two peaks around mass number A = 95 and A = 135 is characteristic for the thermal neutron field in a light water reactor (LWR) with ^{235}U. But as shown in Fig. 1 the mass distribution varies with neutron energy, and it also depends on the initial actinide. Therefore systematic measurements at different neutron energies and for different fission target nuclides are of importance. Furthermore, the mass distribution seen in Fig. 1 reflects the situation for many experiments where only the masses of the fission products are determined, though usually in combination with other observables such as kinetic energy [12]. Therefore it is valuable to obtain independent fission yields as complementary information to other data. It should be mentioned that independent fission yields are defined as the percentage of atoms of a specific nuclide produced directly in fission reactions, i.e., before radioactive decay has occurred [9].

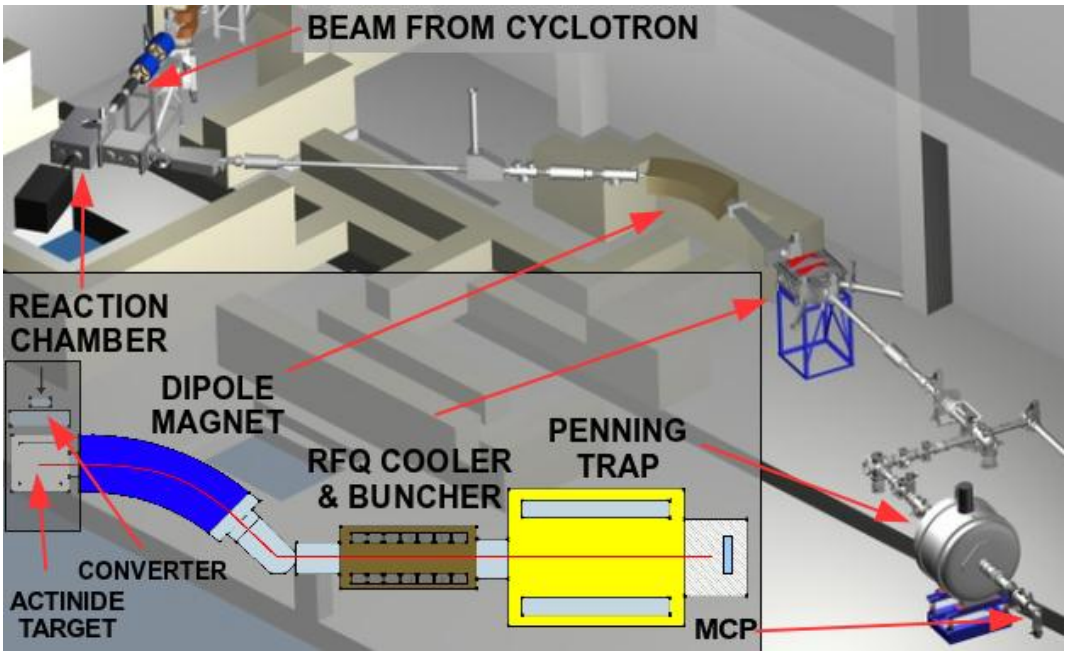

FIG. 2. Layout of the IGISOL-JYFLTRAP facility (schematic view in the inset). A particle beam enters from the top left impinging on a neutron converter, resulting in a neutron field causing fission in an actinide target. The fission products are accelerated and transported through a dipole magnet for mass selection, followed by an RFQ cooler and buncher for improvement of the beam properties. The cooled ions are injected into the Penning trap for accurate mass determination and finally the count rate is determined by sending the ions to an MCP detector. CAD drawing by Tommi Eronen.

3. THE EXPERIMENTAL TECHNIQUE

The description of the experimental technique applies both for charged particle beams and neutron beams, and the principles are the same irrespective of if it is fission products or other kinds of reaction products that are measured. The principle layout of the IGISOL-JYFLTRAP facility is shown in Fig. 2 for the case of using a neutron converter and moderator in order to measure independent fission yields with neutrons down to thermal energies. The considerations for a neutron converter are discussed in Section 4.

3.2. Ion-induced quasi-monoenergetic and white neutron beams

3.1. PARTICLE BEAMS

The recent move of the IGISOL facility to a new experimental area means a general upgrade of the facility. An important addition is a new MCC30/15 cyclotron [2] providing protons in the energy range 18-30 MeV and deuterons of 9-15 MeV. For protons a beam current of 100 μA or more is expected, making it possible to consider high intensity neutron beams. The new cyclotron will commence operation during 2013. Together with the existing K-130 cyclotron more than 4000 hours of beam time can be provided annually for the IGISOL facility.

3.2. REACTION (FISSION) CHAMBER AND ION GUIDE

The reaction chamber contains the beam target from which reaction products or fission products are ejected. The target has to be thin enough to allow the fission products to escape from it. Helium or other noble gases are used as buffer gas that flows through the reaction chamber and slows down all fission products with energies less than 2 MeV. The gas pressure in the chamber is about 200 mbar. Fission products with higher energies are lost as they will hit the chamber walls. The fission products are initially completely ionized, but rapidly change their charge state through interactions with the buffer gas. Due to the high ionization potential of noble gases, a large fraction of the products retain a 1^+ charge state. The gas flow transports the fission products out of the chamber into an ion guide that centers them on the axis and accelerates them in steps to about 30 kV [13].

3.3. MASS SELECTION, BEAM REFINEMENT, AND MASS DETERMINATION

The accelerated ions are sent through a 55° dipole magnet for a first mass selection, with mass resolving power up to 500. At this stage the ions have a relatively large transverse emittance and energy spread. Therefore they are refined in a gas-filled Radio Frequency Quadrupole (RFQ) buncher and cooler before being injected to the JYFLTRAP two stage Penning trap. The Penning trap can be used to determine the mass of an ion by finding its cyclotron frequency in a strong magnetic field. The cyclotron frequency of the oscillating ion can be probed by applying an alternating quadrupole potential to a set of segmented ring electrodes and the mass can be determined through the relation $f_c=(1/2\pi)(Bq/m)$. Here f_c is the cyclotron frequency of the ion with charge q and mass m, oscillating in an external magnetic field B.

The trap can also be used as a high resolution mass filter. By first subjecting the ions to a dipole oscillating field, followed by a mass selective quadrupole field combined with a buffer gas, only those ions for which the frequency of the applied field matches the cyclotron frequency are selected. Finally the selected ions are ejected from the trap through a narrow aperture and are detected at a Multichannel Plate Detector (MCP) where the count rate is measured as a function of the quadrupole frequency. This method selects ions with a mass resolving power of up to 10^5 which means that it is possible, through peak fitting, to resolve metastable states that are 0.5 MeV apart [14].

The total time from fission product emission in the reaction chamber to detection in the MCP is a few hundred milliseconds, enabling the determination of the independent fission yields for a large selection of nuclides.

3.2. Ion-induced quasi-monoenergetic and white neutron beams

3.4. POTENTIAL DIFFICULTIES WITH THE ION GUIDE TECHNIQUE

The experimental method has some potential limitations that need to be considered [1]:

- The low stopping power of the helium gas only stops 1-10% of all fission products. This could potentially lead to a bias in which fission products that are being studied.
- To a first approximation the ion guide technique is insensitive to chemical properties as ions of any element can be produced. But some elements rapidly form oxides, and there are several elements that tend to be extracted as 2^+ ions.
- It may be relevant to consider whether there is some sort of mass dependence in how well different fission products are transported by the ion guide.
- For fast neutrons there may be non-isotropic effects on the spatial distribution of fission products due to the fact that the incident particle brings high momentum into the fissioning system.

A dedicated investigation was performed by comparing the isotopic yields of Rb and Cs isotopes obtained in proton-induced fission of ^{238}U [13, 15] with high quality data from a different experimental method [16]. The results were found to be in good agreement. Further cross checks have been performed by comparing results with some experiments performed at Tohoku University [17]. The Tohoku experiments use a similar ion guide technique, but the different geometry compared with IGISOL allows useful inter-comparisons of several of the concerns, usually with reasonable agreement [1].

Also the Penning traps have chemical effects to consider. Several cross checks, including calibration with alpha recoil sources or fission sources placed inside the ion guide, have been performed or have been suggested. Other concerns are corrections for decaying isomers, the accumulation of decay products in the trap, and time dependent variations of the count rate. An important remedy for the latter uncertainty is that for all measurements there are data taken during the same run for known reference masses, enabling data renormalization [1].

4. THE NEUTRON SOURCE

Although most fission yield experiments at IGISOL were performed with protons, two attempts have been made with neutrons, showing that the ion guide technique is feasible also for such measurements [18, 19]. In those tests the ^{12}C(d,xn) and ^{13}C(p,xn) reactions were used, and the incident beam currents were a few μA. In the present project higher neutron yields are sought through proton- or deuteron-induced reactions on other target materials, and with the new MCC30/15 cyclotron that provides higher beam currents.

4.1. DESIGN CONSIDERATIONS

For the introduction of a neutron source to the IGISOL facility there are several issues to consider:

- Neutron yield: In order to be competitive in comparison with other experimental facilities, in studies of nuclides far from the stability line, the neutron converter should be able to deliver about 10^{12} fast neutrons (E_n > 1 MeV) on a ^{238}U target.
- Neutron energy spectra: For studies of independent fission yields of relevance for nuclear power applications the incident neutrons should have an energy distribution

resembling those in light water reactors (LWR) or fast reactors. Mono-energetic neutrons are also considered.

- Cooling issues: With 30 MeV protons of 100 μA beam intensity or more, at least 3 kW of heat is deposited into a very small volume of the neutron converter. Therefore sufficient cooling of the converter has to be provided, and the number of suitable converter materials becomes limited.
- Activation and structural integrity: The neutron converter will become activated through the reactions with protons or deuterons, and the produced neutrons will activate surrounding materials. This may reduce access to the facility after irradiation. Furthermore, the converter may suffer structural problems through hydrogen buildup if it is thick enough to fully stop protons or deuterons. For thinner targets the residual beam may activate other material.
- Flexible design: Several of the issues above can be handled by using different materials and thicknesses. This requires a design where the converter easily can be replaced with a new one, without complicated issues of breaking vacuum and risk of leakage of the cooling media. Furthermore, for toxic materials such as Be, a design is required that reduces the amount of handling and machining of the converter material.

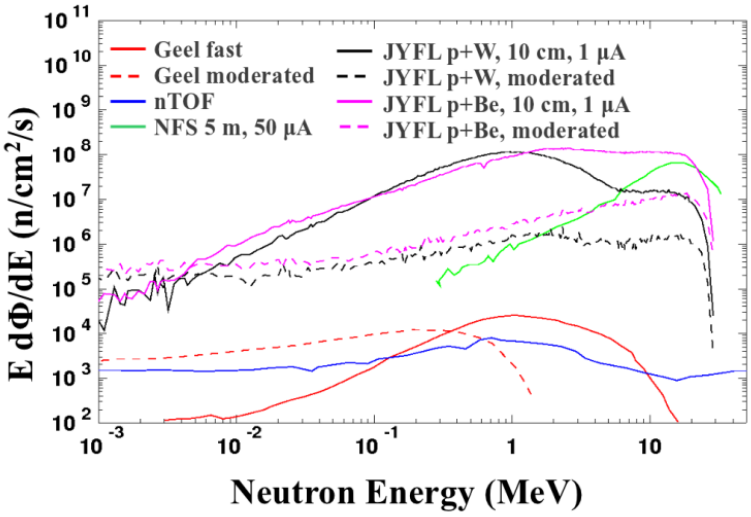

FIG. 3. Isolethargic neutron spectra calculated for thick Be and W targets considered for the Jyväskylä laboratory (JYFL), compared with other neutron beams. It should be noted that the calculations are shown for 1 μA protons, the actual neutron flux may thus be increased by two orders of magnitude. Calculations were made with FLUKA [3, 4].

With these issues in mind Be and W converters with different geometries have been considered [8]. Both materials have high melting points and heat transfer properties, and may be coupled mechanically to a cooling device. The requirement of high neutron intensity may be fulfilled by placing the converter very close, about 10 cm, to the fission target. Monte Carlo codes have been used in order to estimate the neutron flux for different options. Figure 3 shows neutron spectra for Be and W converters, with and without moderator material, compared with other neutron facilities. It is noteworthy that due to the close proximity of the fission target the overall neutron yield will be much higher than for any of the other facilities. Finally, a Be converter gives many more fast neutrons than W and therefore it was decided to use it for the converter.

4.2. SIMULATIONS

Monte Carlo simulations have been performed both with FLUKA [3, 4] and MCNPX [5]. As seen in Fig. 4 it is relatively easy to moderate neutrons in such a way that the low energy part resembles that of an LWR, while it is difficult to obtain fast neutron spectra similar to those in fast reactors. For the fast spectra the simulations also reveal a significant discrepancy in the low energy part between the two Monte Carlo codes, the reason for this has not been determined yet.

Studies of the need for cooling of the converter have been performed with COMSOL Multiphysics [6]. Both for Be and W it has been possible to identify geometries thick enough to fully stop 30 MeV protons that can be sufficiently cooled by a flow of water in a closed loop.

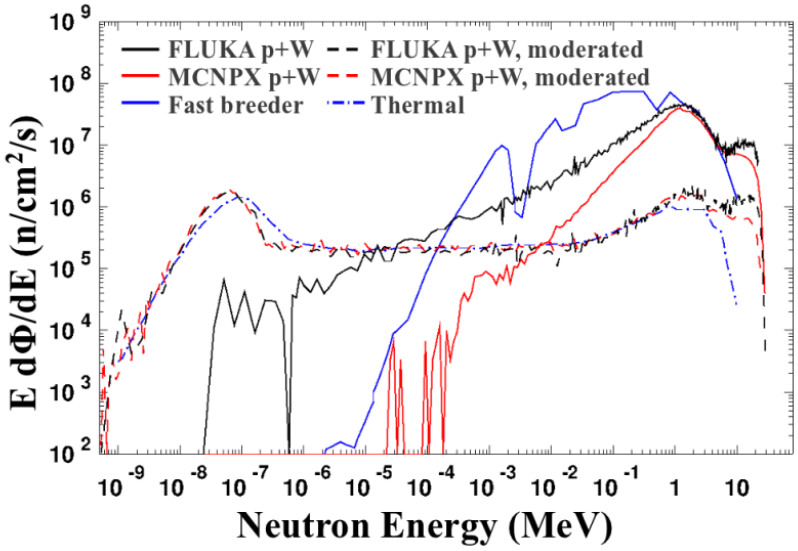

FIG. 4. Comparison of neutron spectra from 30 MeV protons on a thick W converter, with and without 10 cm water moderator, simulated with FLUKA (black) and MCNPX (red). Typical LWR (thermal) and fast breeder spectra (blue) are shown for comparison [20]. The reactor spectra have been arbitrarily scaled for the comparison.

4.3. APPROACHING A FINAL DESIGN

Taking into account all the initial criteria, and the results from the simulations, a preliminary design has been agreed on that fulfills most of the criteria. The design is inspired by the LENS target developed at Indiana University Cyclotron Facility (IUCF), where a Be target slightly thinner than the full proton stopping length is used [21]. The target is assembled in a holder and acts as a window between the evacuated beam pipe on the upstream side, with a 0.5 cm thick layer of cooling water on the downstream side. By not stopping the protons within the target itself the cooling requirement is drastically reduced, as is the risks of structural degradation from hydrogen buildup. The reduction in neutron yield is about 5%. The main drawback is that there may be chemical effects in the cooling water due to the stopping of protons in it. In order to avoid exposure to beryllium dust, target cylinders will be bought at standard dimensions from commercial utilities and be used without any

further machining. The holder uses O-rings on both sides of the plate in order to ensure an airtight assembly. Furthermore a second window, made of steel or havar, will be inserted in the beam pipe in order to reduce the effects in case of a water leak. A preliminary design is shown in Fig. 5.

4.3. BENCHMARK EXPERIMENT

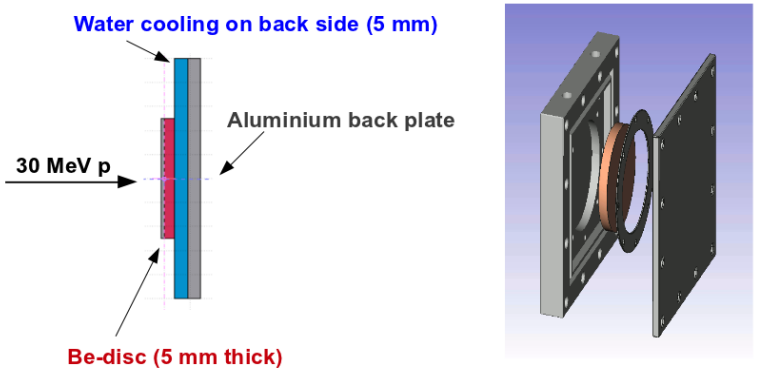

FIG. 5. Principle design of a beryllium neutron converter for the IGISOL setup.

Due to the discrepancies in predictions between FLUKA and MCNPX it was necessary to compare the simulations with experimental data. The few experiments performed in the relevant energy range all have some question marks of relevance, and none of them cover the full energy range. Therefore it was deemed necessary to perform a reference measurement that could provide some guidance on how to interpret the simulated results. Through the EU-funded ERINDA framework programme, beam time was obtained for a measurement of the neutron energy spectra from a Be converter resembling the preliminary design. The experiment was performed in 2012 at The Svedberg Laboratory, using 37 MeV protons degraded to 30 MeV. Outgoing neutrons were measured with Bonner Sphere Spectrometers, covering the range from thermal energies up to about 20 MeV, with a ^{6}Li(Eu) scintillator as thermal neutron detector [22]. In parallel a NE-213 liquid scintillator, allowing n-γ pulse shape discrimination, was used for a Time-of-Flight (ToF) measurement in the energy range 5-30 MeV, thus providing a good overlap region for intercomparisons between the two methods [7]. The ToF data were saved on two different data acquisition systems, one with pre-set thresholds, and one where the detector pulses were saved event by event for off-line analysis.

The experiment was performed with different settings, including background measurements with shadow cones and with slow neutrons moderated through polyethylene. For the ToF measurement it was also possible to vary the thickness of the Be converter [23]. It is important to stress that the background conditions at TSL will be very different from those at IGISOL due to different geometries around the converter. By having a controlled experiment to compare the simulations with it will be possible to make better predictions of the neutron spectrum that induces the fission yields measured at IGISOL.

Simulations showed that the low energy neutron background at TSL was significant. This will also be expected at IGISOL and has to be taken into account. For measurements on

actinides such as ^{238}U with a high energy threshold for fission the background is of no importance, while for actinides with high fission cross sections at thermal energies, such as ^{235}U, the effects may be significant. Furthermore, high energy photons may induce photofission. While having relatively low cross sections, the effect should be estimated from the measurements and from simulations. The analyses from the measurements will be finalized during the spring 2013 [7, 22, 23] helping in deciding the final design of the neutron converter to be used at IGISOL.

5. OUTLOOK

The first experiments at the upgraded IGISOL-JYFLTRAP facility are planned for the late spring of 2013, including a measurement of isomeric yield ratios from 25 MeV protons on ^{238}U. Thereafter the commissioning of the neutron converter will start. The plan is to begin with neutron-induced fission from a large ^{238}U foil with neutrons from a Be converter. Thereafter a number of parameters can be changed in order to obtain different neutron energy distributions; reduced proton energy, use of deuterons, use of thin target, and use of different converter material. For thin target measurements semi-monoenergetic neutron beams will provide reference points. None of the neutron fields will agree with those in a reactor, but from measurements with different fields the energy dependence of the independent fission yields can be obtained and used in unfolding.

Another parameter to change is the fission target. Although it is the most obvious thing to change, it may be very difficult to obtain different target actinides of interest. Besides the practical difficulty of obtaining and manufacturing targets from some fissile nuclides, there may be regulatory restrictions making transfer of the material between different countries difficult or even impossible. It may seem a bit ironic that research of relevance for the development of safer nuclear power and safer handling of used fuel may be hindered due to rules regulating the safe handling of the very same nuclides. A preliminary wish list includes the following actinides:

- Relatively easy to access and handle: ^{235}U, ^{238}U, ^{232}Th
- Somewhat more difficult to obtain: ^{237}Np, ^{239}Pu, ^{234}U
- Very difficult to manufacture or handle: ^{240}Pu, ^{243}Am

In spite of these challenges there will be plenty of experiments to be done starting with ^{238}U, both from an applications point of view and for fundamental research in nuclear structure. It is the ambition of the groups in Jyväskylä and Uppsala to make a long term commitment to this project. For a long term dedicated effort follows some challenges with respect to securing funding and to have continuity in manpower, not the least in order to attract talented students. It should be emphasized that the EU-funded programmes for transnational laboratory access are increasingly important in order to enable these kinds of projects, and for providing people with relevant expertise both for research and industry.

6. SUMMARY

The IGISOL-JYFLTRAP experimental programme at University of Jyväskylä has been successful in developing the method of combining the ion guide technique with proton-induced independent fission yields, enabling high accuracy mass determinations of the fission

products. The new high intensity cyclotron makes it feasible to initiate measurement campaigns of neutron-induced independent fission yields. A beryllium neutron converter is planned for the facility, and a flexible design enables measurements with many different neutron fields, providing nuclear data of importance for future nuclear power systems and for the safe handling of used nuclear fuel. In order to quantify the neutron energy distributions at IGISOL a reference measurement has been performed at The Svedberg Laboratory with an experimental setup that resembles the preliminary design. The reference measurement will help with interpretations of predictions from Monte Carlo codes and may help in further benchmarks of those codes. The described project is in its initial phase, but the involved groups view it as a long term commitment where nuclear data for society and fundamental research go hand in hand.

ACKNOWLEDGEMENTS

The work was supported by the European Commission within the Seventh Framework Programme through Fission-2010-ERINDA (project no. 269499), by the Swedish Radiation Safety Authority (SSM), and by the Swedish Nuclear Fuel and Waste Management Co. (SKB).

REFERENCES

[11] PENTTILÄ, H., et al., “Fission yield studies at the IGISOL facility”, Eur. Phys. J. A 48 (2012) 43.
[12] HEIKKINEN, P., “New MCC30/15 Cyclotron for the JYFL Accelerator Laboratory”, Cyclotrons and Their Applications (Proc. 18th Int. Conf. Giardini Naxos, 2007), (RIFUGGIATO, D., Ed.), INFN, Rome (2007) 128-130.
[13] BATTISTONI, G., et al., “***The FLUKA code: Description and benchmarking***”, AIP Conf. Proc. 896 (2007) 31.
[14] FASSÒ, A., et al., “FLUKA: A Multi-Particle Transport Code”, Reports CERN-2005-10, INFN/TC05/11, SLAC-R-773, (2005).
[15] McKINNEY, G.W., et al., “MCNPX features for 2006”, Proc. 2006 ANS Winter Meeting, Albuquerque, NM (2006).
[16] COMSOL Multiphysics ®, © 1997-2013 Comsol AB. Url: http://www.comsol.com.
[17] MATTERA, A., et al., “Characterization of a Be(p,xn) neutron source for fission yields measurements”, manuscript to be presented at the Nuclear Data for Science and Technology Conference, New York (2013).
[18] LANTZ, M., et al., “Design of a neutron converter for fission studies at the IGISOL facility”, Phys. Scr. T150 (2012) 014020.
[19] INTERNATIONAL ATOMIC ENERGY AGENCY, Compilation and evaluation of fission yield nuclear data – Final report of a co-ordinated research project 1991–1996, IAEA-TECDOC-1168, Vienna (2000).
[20] LOURDEL, B., “Research on fission yields evaluation and measurements within the ALFONS project”, M.Sc. Thesis, Chalmers University of Technology and Uppsala University (2010).
[21] OECD / NUCLEAR ENERGY AGENCY DATA BANK, Java-based Nuclear Information Software (JANIS) 3.4., Issy-les-Moulineaux (2012).
[22] SIMUTKIN, V., “Fragment Mass Distributions in Neutron-Induced Fission of ^{232}Th and ^{238}U from 10 to 60 MeV”, Ph.D. Thesis, Uppsala University (2010).

[23] PENTTILÄ, H., et al., "Determining isotopic distributions of fission products with a Penning trap", Eur. Phys. J. A 44 (2010) 147.
[24] ERONEN, T., et al., "Preparing isomerically pure beams of short-lived nuclei at JYFLTRAP", Nucl. Instrum. Meth. B 266 (2008) 4527.
[25] KARVONEN, P., "Fission yield studies with SPIG-equipped IGISOL: A novel method for nuclear data measurements", Ph.D. Thesis, Research Report No. 7/2010, Department of Physics, University of Jyväskylä (2010).
[26] TRACY, B.L., et al., "Rb and Cs Isotopic Cross Sections from 40-60-MeV-Proton Fission of ^{238}U, ^{232}Th, and ^{235}U", Phys. Rev. C 5 (1972) 222.
[27] KUDO, H., et al., "Most probable charge of fission products in 24 MeV proton induced fission of ^{238}U", Phys. Rev. C 57 (1998) 178.
[28] LHERSONNEAU, G., et al., "Production of neutron-rich isotopes in fission of uranium induced by neutrons of 20 MeV average energy", Eur. Phys. J. A 9 (2000) 385.
[29] STROE, L., et al., "Production of neutron-rich nuclei in fission induced by neutrons generated by the p + ^{13}C reaction at 55 MeV", Eur. Phys. J. A 17 (2003) 57.
[30] US DEPARTMENT OF ENERGY, DOE Fundamentals Handbook: Nuclear Physics and Reactor Theory, vol 1 (DOE-HDBK-1019/1-93, FSC-6910), Department of Energy, Washington, D.C. (1993).
[31] LAVELLE, C.M., "Neutronic design and measured performance of the Low Energy Neutron Source (LENS) target moderator reflector assembly", Nucl. Instrum. Meth. A 587 (2008) 324.
[32] BEDOGNI, R., et al., "Neutron energy spectra of the Be(p,n) reaction at 30 MeV", (in preparation).
[33] RAKOPOULOS, V., et al., "Target thickness dependence of the Be(p,n) neutron energy spectrum", (in preparation).

3. ACCELERATOR BASED NEUTRON BEAM FACILITIES

3.3. ELECTRON-INDUCED WHITE SPECTRUM NEUTRON BEAMS

3.3. Electron induced white spectrum neutron beams

NUCLEAR DATA MEASUREMENTS AT GELINA

W. MONDELAERS, F.-J. HAMBSCH, J. HEYSE, S. KOPECKY, S. OBERSTEDT, A. PLOMPEN, P. SCHILLEBEECKX, P. SIEGLER

European Commission,
DG Joint Research Centre IRMM,
Retieseweg 111, B-2440 Geel,
Belgium
Email: willy.mondelaers@ec.europa.eu

Abstract

Measurements of nuclear data in the interests of standards for safety, security and safeguards are a prime focus for the IRMM Geel electron linear accelerator laboratory GELINA. At GELINA a pulsed white neutron source is realised using a 1 ns FWHM electron bunch impinging on a rotary uranium target at a repetition rate of 800 Hz. Flight paths from 8 to 400 m length allow simultaneous measurements of a variety of cross sections and reaction parameters with dedicated equipment and high energy resolution for the incident neutrons through the use of the time-of-flight technique. The program of work addresses established measurement needs aiming at improved reliability of safety assessments for current and foreseen power plants and fuel cycles. This translates to the need for significantly reduced uncertainties for nuclear data and, therefore, improved accuracy and standardisation of measurements, their analysis and evaluation.

1. INTRODUCTION

Accurate neutron cross section data over a broad energy range are an essential to evaluate the safety and risks related to the operation of nuclear power plants and to nuclear waste management. They also play an important role in many other disciplines such as nuclear safeguards and security, astrophysics, and medicine.

In the energy interval from thermal neutron energies to a few MeV neutron cross sections reveal a resonance structure-type of energy dependence, which largely differs from nuclide to nuclide. The cross sections in the resonance region are parameterized by the R-matrix reaction theory [1]. Unfortunately the resonance parameters required to reproduce the cross sections cannot be predicted by theory. They can only be obtained from an adjustment to experimental data. To cover a broad energy range, resonance structured neutron induced reaction cross sections are best studied at a pulsed white neutron source that is optimized for time-of-flight (TOF) measurements [2].

More generally, neutron time-of-flight facilities allow mapping the energy dependence of cross sections over a wide range in one, or a few experiments with good to excellent resolution.

2. THE TOF-FACILITY GELINA

The TOF-facility GELINA of the EC-JRC-IRMM in Geel (B) has been especially designed and constructed for high-resolution cross section measurements in the resonance region. A detailed description of the accelerator and its neutron producing target can be found in [3]. The Geel Electron Linear Accelerator (GELINA) is a 150 MeV pulsed-beam electron accelerator in combination with a metallic uranium target, serving as a neutron source for TOF measurements. The facility is one of the most powerful white spectrum neutron sources available in the world, especially designed for high-resolution neutron cross-section measurements. The accelerator consists of three S-band accelerator sections operating at 3 GHz. The first section is a standing-wave buncher, while the two other sections are of the

travelling-wave type. The electron source is a Pierce-type thermionic gun. The RF power is produced with three pulsed klystrons, powered with pulse-line type modulators. The facility has been designed for maximum peak currents in very short pulses. The accelerator is usually operated at a pulse length of 10 ns with repetition rates between 50 Hz and 800 Hz. Using a unique post-acceleration pulse-compression system, the 10ns width electron pulses can be further reduced to about 1 ns (FWHM) with peak currents up to 100 A [4]. Accelerated electrons produce Bremsstrahlung in a uranium target which in turn, by photo-nuclear reactions, produces neutrons [5]. Within a 1 ns pulse a peak neutron production of up to 4.3 $\times 10^{10}$ neutrons is achieved (average flux of 3.4×10^{13} neutrons/s at 800 Hz). Two water filled beryllium containers mounted above and below the neutron producing target are used to moderate the neutrons. By applying different neutron beam collimation conditions, experiments can use either a fast or a thermalized neutron spectrum. Figure 1 compares the neutron flux as a function of neutron energy for the fast and the thermal beam. Experimental data are compared with results of Monte Carlo simulations reported in Ref. [6]. The neutron production rate is continuously monitored by BF_3 proportional counters placed at different locations around the target hall. The output of these counters together with some performance parameters of the accelerator, such as the operating frequency and current, are registered and used to monitor the stability of the accelerator. Since 2001 we started the refurbishment of the accelerator [6]. Various parts of the accelerator have been renewed or upgraded: the klystron pulse modulators, the injector, the electrical power distribution, the magnet and vacuum power supplies. In addition the whole control and interlock system has been fully automated. The facility is operated on a continuous 24 h shift from Monday morning to Friday.

GELINA is a multi-user facility, where measurements can be carried out simultaneously at 10 flight-paths with lengths between 8 m and 400 m. The measurement stations have special equipment, to perform transmission and reaction cross section measurements. The stations are equipped with air-conditioning to reduce electronic drifts in the detection chains due to temperature changes and to keep the sample at a constant temperature of about 20°C. The temperature at the sample position is continuously monitored.

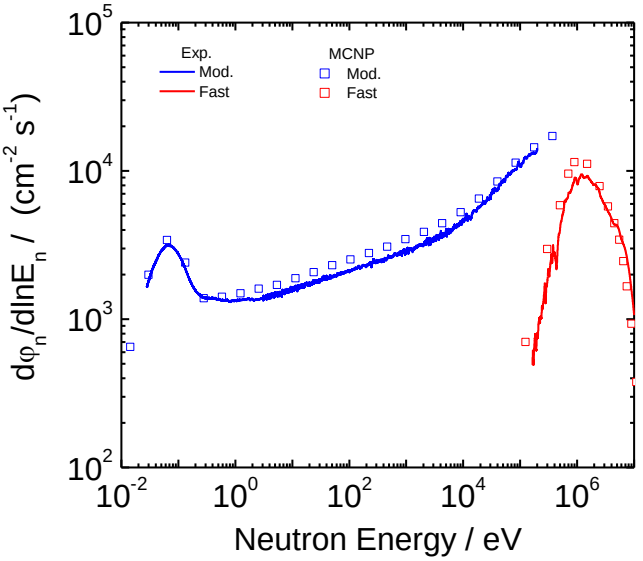

FIG. 1. Neutron flux of the moderated and the fast beam as function of neutron energy.

3.3. Electron induced white spectrum neutron beams

An important characteristic of a TOF-spectrometer for measurements of resonance structured cross section data is its response function R(t,E), i.e. the probability that a neutron with energy E is detected with a time-of-flight t. This response function can be considered as a convolution of different independent components. Flaska et al. [6] and Ene et al. [8] reported response functions for GELINA which have been calculated by Monte Carlo simulations and validated by experiment. The response at the fast neutron beam is dominated by the time structure of the pulsed electron beam and the time response of the detector and associated electronics. For measurements at the moderated neutron beam, the main component is the neutron transport in the target-moderator assembly. Hence, the response functions depend strongly on the type and size of the materials used in the assembly. This is illustrated in Fig. 2 which compares the experimental yield around the 34 keV resonance of ^{56}Fe obtained from measurements at GELINA and at the n_TOF facility at CERN using a similar detection system consisting of C_6D_6 detectors. Although the measurement station at the n_TOF facility is at a 180 m distance from the neutron producing target, the observed resonance profile for the 34 keV resonance is broader compared to the profile resulting from measurements at a 60 m station of GELINA. In addition, a more pronounced tail on the low energy side of the resonance profile is observed. This difference is mainly due to the difference in neutron producing target-moderator assembly, which is more compact for a neutron source based on photonuclear reactions, such as GELINA, compared to a spallation type of neutron sources as the one at n_TOF. Details about the basic principles of TOF-cross section measurements, the data reduction and analysis procedures are given in Ref. [2].

A comprehensive overview of the neutron and gamma output of GELINA in function of energy and angle of the outgoing particle and based on optimized MCNP calculations [6], is given in [8]. For actual experiments these source characteristics are modified in an experiment-dependent way by collimation and filters.

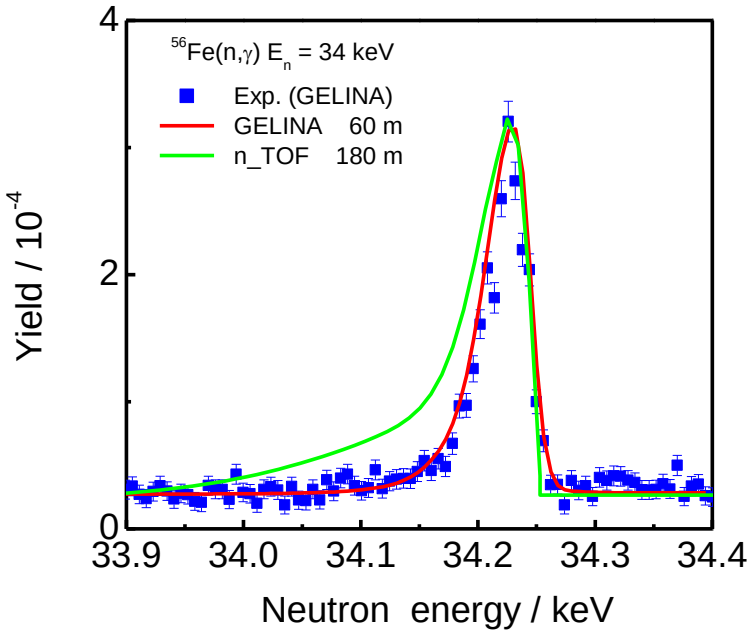

FIG. 2. Experimental yield at the 34 keV resonance of 56Fe resonance obtained at the 60m station of GELINA.

3.3. Electron induced white spectrum neutron beams

3. MEASUREMENT PROGRAM AT GELINA

The main part of the measurement program focuses on neutron transmission, capture, fission, and inelastic scattering cross-section measurements. The program also includes improvement of standard cross-section data, e.g. $^{10}B(n,\alpha)$, $^{6}Li(n,\alpha)$ and $^{197}Au(n,\gamma)$, with the goal to extend the range of validity as standard reaction. A second part aims at the investigation of fundamental aspects of nuclear reactions, e.g. study of the fission process (with a main emphasis on fission fragment yields and prompt-neutron emission), study of nuclear level statistical theories and spin-parity violation studies. In addition to the experimental activities, efforts are being made to improve the procedures for the analysis of time-of-flight cross section data [2], including the production of full covariance information [2], [9], and to contribute to the production of full ENDF-6 compatible [10] evaluated data files in the resolved and unresolved resonance region [11] - [15]. Most of the files are produced in support to the JEFF project [16].

The methods developed for high-resolution neutron cross section measurements in the resonance region generated also spin-off techniques, such as Neutron Resonance Transmission Analysis (NRTA) and Neutron Resonance Capture Analysis (NRCA) [17]. These techniques can be applied for the non-destructive determination of the elemental and isotopic composition of materials and objects. GELINA is also a very useful facility to test and calibrate neutron detectors.

3.1. TRANSMISSION EXPERIMENTS

Transmission measurements can be performed at several distances using Li-glass, plastic or liquid (NE213 type) scintillators. Li-glass scintillators are used for measurements below 1 MeV, while the plastic and organic scintillators are used at higher energies. The total cross section measurements on natural iron, which were carried out by Berthold et al. [18] at a 400 m station, illustrate the importance of a long flight in case high resolution data for light nuclei are required. To study the Doppler broadening one of the transmission stations is equipped with a cryostat, which is able to cool the samples down to 10K.

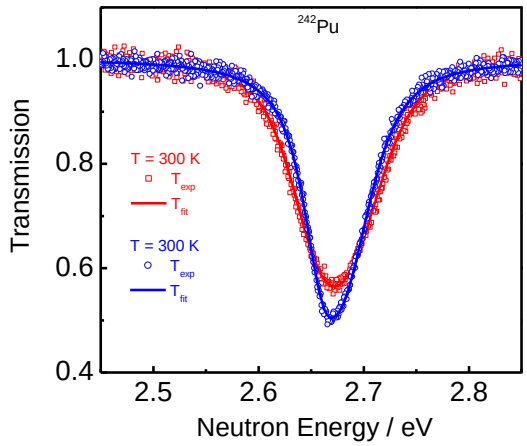

FIG. 3. Transmission for a 240PuO2 at sample temperatures of 77K and 300K compared to the resonance shape analysis including sample inhomogeneities.

3.3. Electron induced white spectrum neutron beams

Figure 3 compares the result of a transmission measurement around the 2.65 eV resonances of ^{242}Pu for a PuO_2 powder sample at 77 K and 300 K. The full line is the result of a resonance shape analysis which includes a model to account for sample inhomogeneities. This model has been developed at the EC-JRC-IRMM [2], [19].

Results of transmission measurements are essential to produce a consistent set of resonance parameters. In the resonance region transmission data are mostly combined with results of reaction cross section measurements. From transmission data the total cross section can be determined without a reference to another cross section. The total absorption cross section (2480 ± 40 b) for neutron induced reactions on ^{nat}Cd determined by Volev et al. [12] results from transmission experiments at GELINA. They also demonstrated the importance of transmission measurements on thick samples to adjust parameters of bound states and effective scattering radii. In Fig. 4 the result of a transmission measurement on a 25 mm thick ^{nat}Cd sample is compared with the calculated curve based on cross sections in evaluated data libraries. Transmission data can also be used to normalize reaction cross section data. Examples of a normalization of capture data using results of transmission measurements are given in [20] for ^{60}Ni(n,γ), [21] for ^{237}Np(n,γ) and [22] for ^{241}Am(n,γ). Finally, the total cross section and the neutron width of a resonance are needed to determine various corrections, such as corrections for self-shielding, multiple interaction events and the neutron sensitivity of the detection system, in the analysis of reaction cross section data [2].

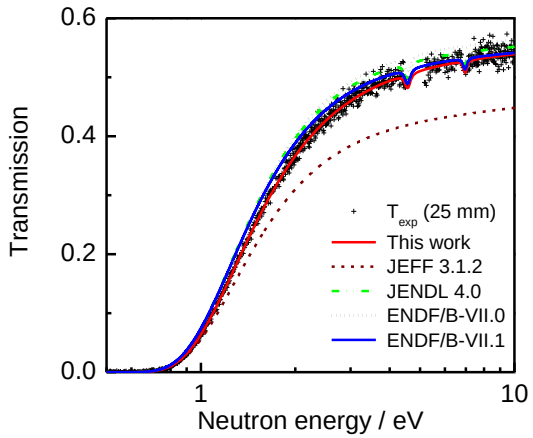

FIG. 4.Transmission of natCd as function of the neutron energy compared to calculations based on evaluated data libraries.

3.2. CAPTURE EXPERIMENTS

Experiments to study neutron induced capture reactions can be carried out at a 12.5 m, 30 m and 60 m station. For capture cross section measurements mostly the total energy detection principle is applied using a set of C_6D_6 detectors [23]. The pulse height weighting technique is applied to make the probability to detect a capture event directly proportional to the total γ ray energy that is released in the event [2], [23]. The detectors are positioned at an angle of 125^o with respect to the direction of the neutron beam. This geometry minimises systematic effects due to the anisotropy in the primary dipole γ ray emission from resonances which can be spin and orbital momentum dependent. The detection of scattered neutrons is minimised by coupling each scintillator to a boron-free quartz windowed PMT. The energy dependent neutron flux below 200 keV is based on the ^{10}B(n,α)^{7}Li reaction [24],[25]. A

double Frisch-gridded ionization chamber is used with a common cathode which is loaded two layers of ^{10}B. The ^{10}B layers with an area density of about 40 μg/cm^2 are evaporated back-to-back on a 30-μm thick aluminium backing. The chamber is almost transparent for the neutron beam. The bias on the amplitude spectra, taken from the anode, is set low enough to accept the signals from both the ^{7}Li and α-particles. This choice, together with the back-to-back configuration, rules out a systematic bias effect related to the forward-to-backward emission ratio. For energies between 150 keV and 1000 keV the neutron flux is derived from measurements with a parallel plate chamber loaded with ^{235}U layers using the ^{235}U(n,f) standard reaction cross section [24],[25].

Most of the capture cross section measurements have been carried out in the interest of nuclear technology, more in particular nuclear energy production. The low uncertainty on the capture cross section for ^{232}Th in the unresolved resonance region (about 1.5%) in the latest ENDF/B-VII. evaluated data library [26] is primarily due to the accurate data of Borella et al. [27] resulting from capture cross section measurements at a 12.5 m station of GELINA. This data has been included in a full ENDF-compatible evaluation performed by Sirakov et al. [11], which was part of Coordinated Research Project organized by the IAEA [28]. In response to the high priority request list (HPRL) [29] to improve the accuracy of the capture cross section for ^{241}Am, transmission and capture cross section measurements were carried out a GELINA [22]. From the combined analysis of both data sets a thermal capture cross section of $\sigma(n_{th},\gamma) = 745 \pm 45$ b was derived [22], meeting the requested 5% uncertainty of the HPRL. The resulting resonance parameter is also fully consistent with results of integral experiments and experimentally determined resonance integrals [22]. Figure 5 illustrates the result of a combined analysis of transmission and capture data.

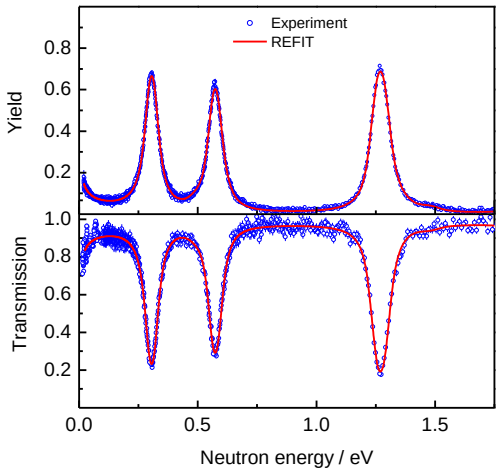

FIG. 5. Illustration of a combined resonance shape analysis of neutron capture and transmission data for 241Am.

Capture cross section experiments have also been carried out in support to nuclear astrophysics, more in particular to studies of the s-process nucleosynthesis. Examples of such data are the Maxwellian averaged cross sections for ^{206}Pb determined by Borella et al. [30] and work performed by Corvi and collaborators [20],[31]. For special applications, such as spin and parity assignments [32],[33], determination of branching ratios [34] and study of photon strength functions, HPGe-detectors can be installed. In some cases the capture and

total cross section data are complemented by results of self-indication measurements to determine the spin of the resonances [35].

3.3. NEUTRON INELASTIC SCATTERING EXPERIMENTS

In-elastic scattering reactions are studied at a 30 m and 200 m station using the (n,xng)-technique with high purity germanium (HPGe) detectors. The neutron flux at both stations is determined by measurements with parallel plate ionization chambers loaded with ^{235}U, in the form of evaporated layers of UF_4 enriched to more than 99% in ^{235}U. These deposits were prepared and characterized at IRMM [36] and the flux measurement procedure was validated through inter-comparison at PTB [37]. The GRAPHEME setup at 30 m was constructed by IPHC, CNRS Strasbourg and consists of four planar detectors for the study of the low energy gamma rays typical of actinides. So far, ^{235}U, ^{232}Th and ^{238}U were measured along with the tungsten isotopes[38],[39]. The GAINS setup at 200 m [40],[41] is optimized for neutron-energy resolution. It has 12 coaxial HPGe detectors of 8 cm diameter and length (see Fig. 6). At this flight path high resolution data were obtained for ^{28}Si, ^{52}Cr, ^{206,207,208}Pb, ^{209}Bi, ^{56}Fe, and ^{23}Na [39] - [46].

FIG. 6. The GAINS array for (n,xng)-measurements at GELINA.

3.4. FISSION AND CHARGED PARTICLE REACTION EXPERIMENTS

Experiments studying neutron induced fission and charged particle reactions can be performed at 8 m, 10 m and 30 m flight paths. At GELINA a double Frisch gridded ionization chamber filled with ultrapure methane is typically used, with the sample being investigated mounted back-to-back with a sample to monitor the neutron flux [47]. In some cases a separate experiment was done with the sample for the reaction cross section measurement being replaced by a well characterized sample for which the cross section is well known [48]. Due to the working principle of an ionization chamber [49] the intrinsic detection efficiency is close to 100% and the solid angle is close to 2π, both for the reaction and the flux measurement.

Through the use of thin samples, the escape probability of the reaction products is close to 1. However, even for thin layers one still has to take into account absorption in the sample itself for reaction products emitted nearly parallel to the sample. Reaction products that loose a significant part of their energy before escaping from the sample will show up as a low energy tail in the pulse height spectrum of the detector.

3.3. Electron induced white spectrum neutron beams

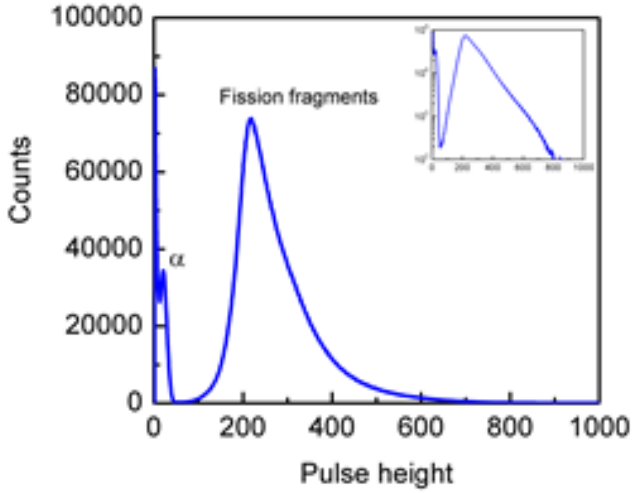

FIG. 7. An amplitude spectrum obtained with a parallel plate ionization chamber for fission cross section measurements on 235U.

In the case of (n,f) cross section measurements on a material with a significant alpha activity, the low energy tail of the fission fragments is very likely to overlap with the signals produced by the alpha particles. In this case, a lower threshold is applied to the pulse height spectrum in order to avoid contributions of alpha particles. The loss of fission fragments due to this threshold can be estimated by extrapolation of the shape of the fission fragment spectrum or by energy loss calculations in combination with MC simulations. The separation between alpha particles and fission fragments depends on the characteristics of the detector that is being used, the alpha activity and the thickness of the sample. Figure 7 shows a pulse height spectrum for a multi-layer parallel plate chamber loaded with ^{235}U, where fission fragments and alpha particles are well separated.

Due to the high energy of fission fragments, background contributions from low energy particles can be reduced significantly. For other charged particle reactions this might be more problematic. In the case of very active samples limited detection geometry can be used in order to avoid strong overlap between fission fragments and alpha pile-up. Typically a vacuum chamber in combination with a Si surface barrier detector is used, with the sample mounted at 45 degrees relative to the incoming beam and with the detector mounted out of the collimated beam [47].

Special care should be taken during the sample preparation and a good characterization of the samples used is essential [50]. For a measurement of (n,f) cross sections, a small presence of other fissile material can give a large contribution to the observed response. Another important aspect is the variation of sample characteristics with time due to physical and chemical instability of the material or due to radioactive decay. When determining e.g. the ^{243}Am(n,f) cross section, the in-growth of ^{239}Pu due to successive decay processes following the alpha decay of ^{243}Am has to be accounted for [51]. These contributions can be corrected for, provided that the nuclear data necessary are known. Both the uncertainties on the amount of parasitic nuclei and on the nuclear data will contribute to the uncertainty of the final result of the reaction cross section measurement. In summary, when homogeneous, well

characterized samples are used for both the reaction under study and the one for the flux measurement, uncertainties of 2% can be reached.

In recent years neutron induced fission cross sections have been studied for a number of nuclei in order to improve the prediction of heavy actinide concentrations in reactor fuel elements and in support of reduction scenarios of the long-term nuclear waste radio-toxicity by using transmutation. Measurements have been performed for ^{234}U [47], ^{236}U [52] and ^{245}Cm in the resonance region [53] and for ^{245}Cm in the thermal neutron energy region [54]. Charged particle reactions - more specifically (n,p) and (n,α) reactions which are of astrophysical interest - have been studied for ^{26}Al [54], ^{36}Cl [48] and ^{41}Ca [56].

3.5. Standard cross-sections

The ^{10}B(n,α)^{7}Li reaction is widely used in nuclear applications. The large reaction cross section with smooth energy dependence and the simple detection of the reaction products make this reaction very convenient for a number of applications. In addition, this reaction is also a nuclear-cross-section standard. Despite all the effort that has been devoted to the measurement of this reaction cross section, it is considered as a standard for neutron energies E_n only up to around 200 keV [52]. Above this energy discrepant experimental results made the analysis within nuclear reaction theory very difficult. A new standards evaluation was completed in 2006 by an International Atomic Energy Agency (IAEA) Coordinated Research

Project, to which the work at IRMM has largely contributed to improve the ^{10}B(n,$\alpha_1\gamma$)^{7}Li standard up to 1 MeV [24],[25]. The present accuracy of the ^{10}B(n,α) standard cross section is dependent on the energy region between 0.2% and 5%. The present work is dedicated to extend the range of incident neutron energy to E_n > 2 MeV.

The level structure of the compound nucleus ^{11}B is rather complicated above an excitation energy of 11.456 MeV, which corresponds to the neutron binding energy. However, in the interaction of ^{10}B with neutrons with kinetic energies up to 1 MeV, the two most important reaction channels are the decay to the ground state (α_0 channel) and the decay to the first excited state (α_1 channel). The probability for each of these reaction channels is quite different: At thermal incident neutron energy, the (n,α_1) channel is dominant with a cross section of ~ 3600 b; the (n,α_0)-channel cross section is ~ 240 b [58]. The influence of the other possible reaction channels like ^{10}B(n, n), ^{10}B(n,γ), ^{10}B(n, p), and ^{11}B disintegration are negligible because of their relatively small cross sections in this energy region. The very low Q-value of the reaction channels (~ 2-3 MeV) makes it quite difficult to measure the characteristics of the reaction products.

Many measurements have been performed using different detection techniques and methods, but mainly for the reactions induced by neutrons with energies below E_n < 100-200 keV. In the E_n < 100 keV incident neutron energy region, both cross sections are smooth and obey nearly $1/E_n^{1/2}$ behaviour. In this region, the calculated branching ratio [(^{10}B(n,α_0)/^{10}B(n,$\alpha_1\gamma$)] is practically constant, and the angular distributions are isotropic in both the laboratory (LAB) and centre-of-mass (c.m.) systems. At higher neutron kinetic energies, experimental difficulties lead to disagreements between the results from different measurements. These difficulties are related on one side to the low cross-section values in this region. On the other side they are connected with the strongly changing probability for the different reaction channels and the non-isotropic behaviour of the angular distributions. In

3.3. Electron induced white spectrum neutron beams

addition, reaction kinematic effects make the interpretation of the laboratory results not an easy and straightforward task.

The behaviour of alpha-particle angular distributions is predicted in [59] but so far, the distributions were measured at only a few angles (in the LAB system) and with rather thick ^{10}B targets, making the separation of the two observed alpha peaks difficult [60]. However, to perform a global fit to all the available reaction cross sections, leading to the same compound system, a multichannel, multilevel R-matrix theory is needed. High-quality angular distribution data covering a large solid angle can help to reduce the ambiguity of these fits. Also, the anisotropy of the angular distribution can affect the response of the detector system. Not accounting for kinematical effects, which take place at higher incident neutron energies, will lead to wrongly determined reaction cross sections.

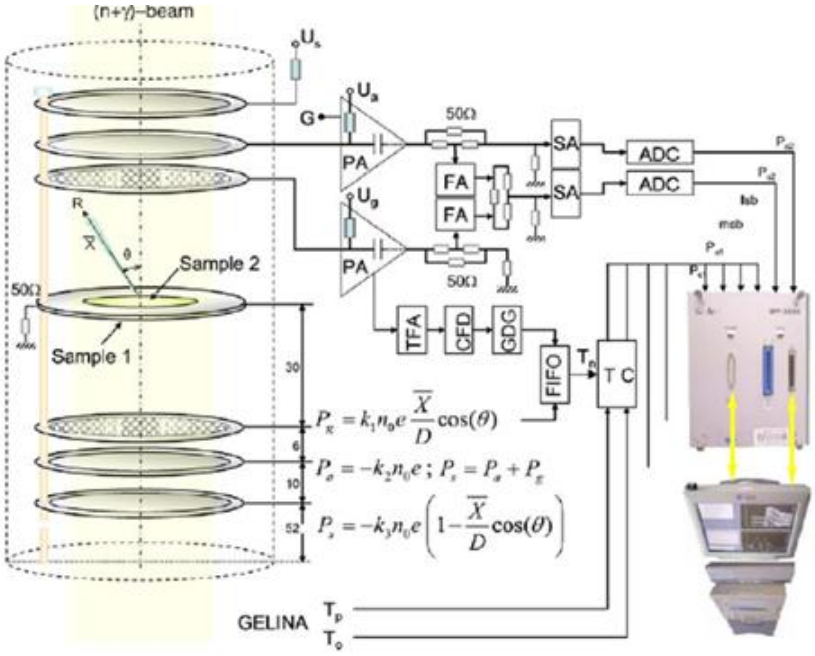

FIG. 8. The chamber electrode configuration and a basic layout of the electronics; PA: charge sensitive preamplifiers; grid: U_g = 700 V; anode: U_a = 1130 V; shield electrode: U_s = 1200 V; MPI 8000 multipurpose data acquisition interface.

The chamber electrode configuration and a basic layout of the electronics; PA: charge sensitive preamplifiers; grid: *Ug* = 700 V; anode: Ua = 1130 V; shield electrode: *Us* = 1200 V; MPI 8000 multipurpose data acquisition interface.

At the IRMM, traditionally, twin Frisch-grid gas ionization chambers (TFGIC) are used for studying fission fragment mass, energy, and angular distribution properties [49] covering nearly a 2×2π angular range. The TFGIC was loaded with very thin ^{10}B samples in back-to-back geometry, to determine simultaneously the alpha-particle angular distributions from both reaction channels in forward and backward direction in the incident neutron energy range from 0.1 keV to 1 MeV. Both samples were enriched to 94% of ^{10}B and had a thickness of (14.5 0.8) μg/cm^2 and (15.7 0.8) μg/cm^2, respectively. Figure 8 gives an overview of the electrode configuration and the basic layout of the electronics in use. The complete experimental setup is described in [61],[62]. As counting gas a mixture of 95% Ar (N50) + 5% CO_2 (N45) was used.

3.3. Electron induced white spectrum neutron beams

The measurements were performed at two different flight-path distances from the GELINA neutron-producing target: L1 = 28.24 m (moderated beam) and L2 = 57.41 m (non-moderated beam). A B_4C filter was placed in the beam, which effectively removed neutrons with thermal and epithermal energies. A neutron collimating system consisting of paraffin, B_4C, Cu, and Pb collimators reshaped the neutron beam from a 100×40 mm^2 rectangular profile to a circular profile with 90 mm diameter, at the position of the ionization chamber.

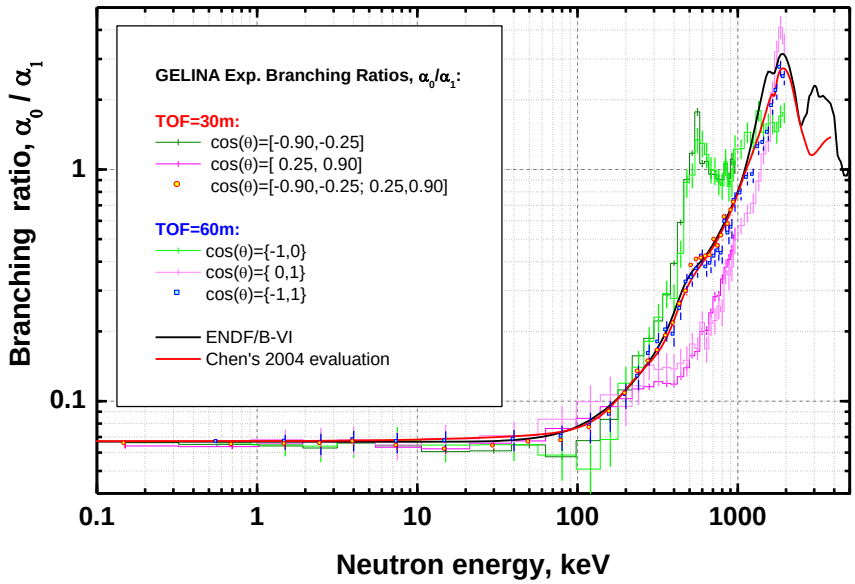

FIG. 9. Branching ratios (forward, backward and total) as a function of the neutron energy obtained from the two measurements at L = 30 m and L = 60 m.

At the longer flight path, looking at the non-moderated beam, a depleted uranium filter (212 mm diameter, 4 mm thickness) of 3.203 kg was used to suppress the gamma-flash accompanying the neutron production. Additional filters from Bi (34 mm thick) and Pb (40 mm thick) were placed in front of the charged-particle spectrometer. The neutron capture and scattering resonance positions in the latter materials allowed a TOF-to-energy calibration of the collected spectra. Details of the data analysis are given in [61], [62]. Here only the final result of the branching ratio as a function of incident neutron energy is shown (Fig. 9). As it is evident, the branching ratio strongly varies with energy and emission angle, which demonstrates the necessity of measuring the complete angular distribution. The results obtained at the GELINA facility confirm the ENDF/B-VI evaluation up to about 1 MeV and show increasing deviation for higher incident neutron energies. Chen's evaluation from 2004 is able to well describing the experimental data up to 2 MeV.

In a next step the set-up was modified to a double TFGIC to accommodate also two samples of ^{235}U. This configuration is used to measure the branching ratio simultaneously with the (n,α) cross-section relative to ^{235}U.

As a follow-up the modified TFGIC will be used for the investigation of the reaction $^{6}Li(n,\alpha)t$, which is presently considered as a reaction standard for neutron energies up to E_n = 1 MeV. Here, the goal of the measurement campaign is to verify or disprove the existence of a resonance around E_n = 2 MeV. This requires measurements well above 2 MeV and, therefore, will contribute to extend the range as standard cross-section also to E_n = 3 MeV.

3.3. Electron induced white spectrum neutron beams

The neutron capture cross section of ^{197}Au is used as a standard for neutron induced reaction cross section measurements at 0.0253 eV and in the energy range between 200 keV and 2.5 MeV. The use of the ^{197}Au(n,γ) reaction as a reference has several advantages. This is due to the mono-isotopic nature and chemical purity of gold, the relatively large thermal neutron capture cross section and the simple decay scheme of the product nucleus formed by neutron capture. The ^{197}Au(n,γ) cross section is often used as a reference cross section for astrophysical calculations in the energy region below 200 keV [63]. However, the results of the standards evaluations is approximately 6% to 8% above the reference cross section adopted for astrophysics applications. The latter results from the energy dependent data of Macklin et al. [64] normalized to the results of activation measurements performed by Ratynski and Käppeler [63]. On the other hand, results of ^{197}Au(n,γ) measurements from 5 keV to 120 keV reported by Borella et al. [27], which were not included in the evaluation process of Ref. [24],[25], are within 2% to 3% consistent with the standards evaluation [24],[25]. To clarify these inconsistencies capture measurements have been performed at the GELINA. An effort has been made to avoid as much as possible systematic bias effects due to dead time, background, weighting function, neutron flux and normalization [65]. In addition, transmission measurements [66] have been carried out to improve the accuracy on the total cross section and to allow for an evaluation in terms of average resonance parameters similar to the one of ^{232}Th [11]. A preliminary analysis of the data indicates that the capture cross section between 4 keV and 90 keV, which is determined with an accuracy of 1.5%, confirms the standard cross section [24],[25], as shown in Fig. 10.

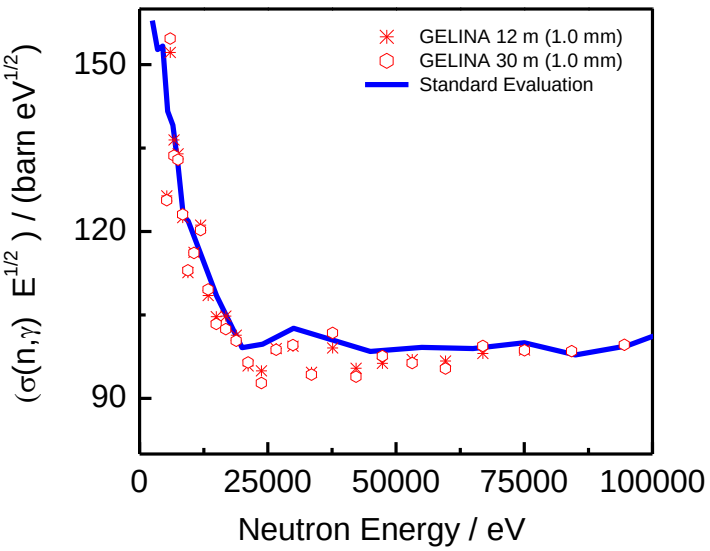

FIG. 10. Comparison of the measured capture cross section of 197Au with the standard evaluation.

3.6. NRTA AND NRCA

The resonance structure in neutron induced reaction cross sections can be used to determine the elemental compositions of materials or objects. The occurrence of resonances are the basis of neutron resonance capture analysis (NRCA) and neutron resonance transmission analysis (NRTA) [17],[67]. NRCA and NRTA are fully non-destructive

methods to determine the bulk elemental composition without the need of any sample preparation and resulting in a negligible residual activity. They have been applied to determine the elemental composition of archaeological objects [68]-[72] and to characterize reference materials used for cross section measurements [73],[74]. For imaging applications a position sensitive neutron detector has been developed within the ANCIENT CHARM project. The detector is based on a 10 × 10 array of ^{6}Li-glas scintillators mounted on a pitch of 2.5 mm, resulting in a 25 × 25 mm^2 active area. The detector has been tested at the time-of-flight facility GELINA and was used at the ISIS spallation source to study cultural heritage objects [75]. A combination of NRTA and NRCA referred to as Neutron Resonance Densitometry (NRD) is being investigated as a non-destructive method to quantify nuclear material, in particular the amount of Pu, in particle-like debris of melted fuel that is formed in severe nuclear accidents.

4. CONCLUSIONS AND OUTLOOK

The multi-user facility GELINA of the EC-Joint Research Centre has been proven to be an ideal research tool addressing a wide range of open questions and measurement needs related to nuclear safety, security and safeguards interests. This is explicitly demonstrated by the variety and the quality of the research program currently under execution. The combination of a high resolution neutron TOF-facility with different experimental measurement capabilities allows for detailed as well as complementary studies of different neutron interaction processes. Results of those experiments play an essential role in applications as divers as the safe operation of nuclear power plants, the nuclear fuel cycle and waste management, nuclear safeguards until astrophysics and nuclear medicine. The aim for an improved accuracy and thus ultimately the improvement of the quality of nuclear data is interlinked with the need for a standardization of the whole process ranging from the measurements, their analysis until the final evaluation.

Beside this, at GELINA, a continuous adaptation to the need of the scientific community is ongoing and reflected in the following developments.

In the near future, a new neutron-detector array SCINTIA will be installed at a 10 m flight path to investigate prompt neutron emission spectrum and multiplicity as a function of incident neutron energy in the resolved resonance region of ^{235}U and ^{239}Pu. Dedicated studies on the population of fission isomers by means of neutron capture will be taken up again with a set of high-purity germanium detectors to obtain information about fission barriers relevant for modeling the fission process.

The capabilities for the application of NRTA and NRCA will be improved especially in view of the development of NRD. One of the measurement stations is being refurbished as a calibration facility of neutron and γ ray detectors used in nuclear safeguards and security applications. This laboratory will also be used for training.

Finally, the capabilities at GELINA will be expanded with high resolution transmission measurements up to 10 MeV and with a new setup for elastic scattering angular distribution measurements.

ACKNOWLEDGMENTS

Our special thanks to all colleagues and students who have contributed to the information that was used in this paper. We are also grateful to the Nuclear Data Section of the IAEA and the Nuclear Energy Agency of the OECD for their support and interest in our work. A substantial part of the work is supported by the European Commission through the projects NUDAME (FP6-516487) and EUFRAT (FP7-211499).

REFERENCES

[1] Lane, A.M., and Thomas, R.G., "R-matrix theory of nuclear reactions", Rev. Mod. Phys. 30, 257 - 353 (1958).
[2] Schillebeeckx, P., et al., "Determination of resonance parameters and their covariances from neutron induced reaction cross section data", Nuclear Data Sheets 113, 3054 – 3100 (2012).
[3] Mondelaers, W., and Schillebeeckx, P., "GELINA, a neutron time-of-flight facility for high-resolution neutron data measurements", Notiziario Neutroni e Luce di Sincrotrone, 11, 19 - 25 (2006).
[4] Tronc, D., et al., "A new pulse compression system for intense relativistic electron beams", Nucl. Instr. Meth. 228, 217 – 227 (1985).
[5] Salome, J.M., and cools, R., "Neutron producing targets at GELINA", Nucl. Instr. Meth. 179, 13 – 19 (1981).
[6] Flaska, M., et al., "Modelling of the GELINA neutron target using coupled electron-photon-neutron transport with the MCNP4C3 code," Nucl. Instr. Meth. A 531, 394 – 406 (2004).
[7] Schillebeeckx, P., et al.,"Neutron resonance spectroscipy at GELINA", Proceedings of the Final Scientific EFNUDAT workshop, 30 August – 2 September, 2010, CERN, Zurich (CH).
[8] Ene, D., et al., "Global characterization of the GELINA facility for high-resolution neutron time-of-flight measurements by Monte Carlo simulations", Nucl. Instr. Meth. A 618, 54 – 68 (2010).
[9] Becker, B., et al., "Data reduction and uncertainty propagation of time-of-flight spectra with AGS", J. of Instrumentation, **7**, P11002 – 19 (2012).
[10] CSEWG, "ENDF-6 Formats Manual. Data Formats and Procedures for the Evaluated Nuclear Data file ENDF/B-VI and ENDF/B-VII", BNL-90365-2009, June 2009, (2009).
[11] Sirakov, I., et al., "An ENDF-6 compatible evaluation for neutron induced reactions of ^{232}Th in the unresolved resonance region", Ann. Nucl. En. 35, 1223 -1231 (2008).
[12] Volev, K., et al., "Evaluation of resonance parameters for neutron induced reactions in cadmium", accepted for publication in Nucl. Instr. Meth. B.
[13] Sirakov, I., et al., "Evaluation of neutron induced reaction cross sections on gold", JRC Scientific and Policy Report, EUR 25803 EN, ISBN 978-92-79-28319-2 , (2013)
[14] Sirakov, I., et al., "ENDF-6 compatible evaluation of neutron induced reaction cross sections for ^{182,183,184,186}W", JRC Scientific and Policy Report, EUR 25808 EN, ISBN 978-92-79-28539-4, (2013)
[15] Sirakov, I., et al., "ENDF-6 compatible evaluation of neutron induced reaction cross sections for ^{106,108,110,111,112,114,116}Cd", JRC Scientific and Policy Report, EUR 25800 EN, ISBN 978-92-79-28421-2, (2013)

[16] Koning, A.J., et al., "Status of the JEFF Nuclear Data Library", J. of the Korean Physical Society, 59, 1057 – 1062 (2011).
[17] Postma, H., and Schillebeeckx, P., "Neutron Resonance Capture and Transmission Analysis", Encyclopedia of Analytical Chemistry, R.A. meyers ed., John Wiley & Sons Ltd. (2009).
[18] Berthold, K., et al., "Very high resolution measurements of the total cross section of natural Iron", in Proc. Intern. Conf. on Nuclear Data for Science and Technology, Gatlinburg, Tennessee, May 9-13, pp. 218 -220 (1994).
[19] Kopecky, S., Pet al., "Low energy transmission measurements of ^{240,242}Pu at GELINA and their impact on the capture width", Proc. Int. Conf. Nuclear Data for Science and Techn., Nice, France, April, 2007, pp. 623 -626 (2007).
[20] Corvi, F., et al., "Resonance neutron capture in ^{60}Ni below 450 keV", Nucl. Phys. A 697, 581 - 610 (2002).
[21] Guerrero, C., and the n_TOF Collaboration, "Measurement and resonance analysis of the ^{237}Np neutron capture cross section", Phys. Rev. C 85, 044616 - 15 (2012).
[22] Lampoudis, C., et al., "Neutron transmisson and capture cross section measurements for ^{241}Am at the GELINA facility", to be published
[23] Borella, A., et al., "The use of C_6D_6 detectors for neutron induced capture cross-section measurements in the resonance region", Nucl. Instr. Meth. A 577, 626 - 640 (2007).
[24] Carlson, A.D., et al., "International evaluation of neutron cross section standards", Nuclear Data Sheets 110, 3215 - 3324 (2009).
[25] Badikov, S.A., et al., "International evaluation of neutron cross-section standards", IAEA Report, STI/PUB/1291, (2007)
[26] Chadwick, M.B., et al., "ENDF/B-VII.1 Nuclear Data for Science and Technology: Cross Sections, Covariances, Fission Product Yields and Decay Data", Nuclear Data Sheets 112, (2011) 2887 – 2996.
[27] Borella, A., et al., "Determination of the ^{232}Th(n,γ) cross section from 4 to 140 keV at GELINA", Nucl. Sci. Eng. 152, 1 - 14 (2006).
[28] Capote, R., et al., "Evaluated nuclear data for nuclides within the thorium-uranium fuel cycle", IAEA Report, STI/PUB/1435, (2010).
[29] OECD/NEA/WPEC-26, Technical Report (2008)
[30] Borella, A., et al., "High-resolution neutron transmission and capture measurements of the nucleus ^{206}Pb", Phys. Rev. C 76, 014605 - 18 (2007).
[31] Beer, H., et al., "Neutron capture of the bottleneck isotopes ^{138}Ba and ^{208}Pb, s-process studies, and the r-process abundance distribution", Ap. J. 474, 843 - 861 (1997)
[32] Gunsing, F., et al., "Spins of resonances in reactions of neutrons with ^{238}U and ^{113}Cd", Phys. Rev. C 56 , 1266 – 1275 (1997)
[33] Zanini, L., et al., "Dependence of the populations of low-energy levels in ^{108,110}Ag on the resonance spin and parity", Phys. Rev. C 61, 054616 -11 (2000)
[34] Gunsing, F., et al., "Neutron capture on ^{209}Bi: determination of the production ratio of ^{210m}Bi/^{210g}Bi", J. Korean Phys. Soc. 59, 1670 – 1675 (2011).
[35] Massimi, C., et al., ``Neutron resonance parameters of ^{197}Au from transmission, capture and self-indication measurements", J. Korean Phys. Soc. 59, 1689 - 1692 (2011).
[36] Plompen, A., et al., "Method developing and testing for inelastic scattering measurements at the GELINA facility," J. Korean Physical Society, vol. 59, p. 1581, 2011.
[37] Mosconi, M., et al., "Characterisation of fission ionisation chambers using monoenergetic neutrons." Proc. of the Final scientific EFNUDAT Workshop, p.99, 30

August - 2 September 2010, Ed. E. Chiaveri, ISBN 978-92-9083-365-9, CERN, Geneva, Switzerland, 2010.

[38] Bacquias, A., et al., "Study of (n,xn) reactions on $^{235;238}$U." Proceedings of the Varenna conference, 2012.

[39] Thiry, J., et al., "Measurement of (n; xn) reactions of interest for the new nuclear reactors," J. Korean Physical Society, vol. 59, p. 1880, 2011.

[40] Negret, A., et al., "A new setup for neutron inelastic cross section measurements." Proc. Int. Conf. on Nuclear Data for Science and Technology - ND2007, Apr. 22 - Apr. 27, 2007, Nice, France, EDP Sciences, ISBN 978-2-7598-0091-9, 2008.

[41] Deleanu, D., et al., "The gamma efficiency of the GAINS spectrometer," Nucl. Instrum. Methods Phys. Res. A, vol. 624, p. 130, 2010.

[42] Mihailescu, L., et al., "High resolution measurement of neutron inelastic scattering and (n,2n) cross-sections for ^{52}Cr," Nucl. Phys. A, vol. 786, p. 1, 2007.

[43] Mihailescu, L. C., et al., "High resolution measurement of neutron inelastic scattering and (n,2n) cross-sections for ^{209}Bi," Nucl. Phys. A, vol. 799, pp. 1–29, 2008.

[44] Mihailescu, L. C., et al., "A measurement of (n, xng) cross sections for ^{208}Pb from threshold up to 20 MeV," Nucl. Phys. A, vol. 811, pp. 1–27, 2008.

[45] Negret, A., et al., "Cross sections for neutron inelastic scattering on ^{28}Si," J. Korean Physical Society, vol. 59, p. 1765, 2011.

[46] Rouki, C., et al., "High resolution measurement of neutron inelastic scattering cross-sections for ^{23}Na," Nucl. Instrum. Methods Phys. Res. A, vol. 672, p. 82, 2012.

[47] Heyse, J., et al., "High resolution measurement of the ^{234}U(n,f) cross section in the neutron energy range from 0.5 eV to 100 keV", Nucl. Sci. Eng. 156, 211 - 218 (2007).

[48] De Smet, L., et al., "Experimental determination of the ^{36}Cl(n,p)^{36}S and ^{36}Cl(n,α)^{33}P reaction cross section and the consequence on the origin of ^{36}S", Phys. Rev. C 75, 034617 - 8 (2007).

[49] Budtz-Jørgensen, C., et al., "A twin ionization chamber for fission fragment detection", Nucl. Instr. Meth. A 258, 209 - 220 (1987).

[50] Schillebeeckx, P., et al., "Target requirements for neutron-induced cross-section measurements in the resonance region", Nucl. Instr. Meth. A 613, 378 - 385 (2010).

[51] Wagemans, C., et al., "Measurement of the Thermal Neutron Induced Fission Cross Section of ^{243}Am", Nucl. Sci. Eng. 101, 293 - 297 (1989).

[52] Wagemans, C., et al., "Measurement of the ^{236}U(n, f) Cross Section in the Neutron Energy Range from 0.5 eV up to 25 keV", Nucl. Sci. Eng. 160, 200 - 206 (2008).

[53] Serot, O., et al., "Measurement of the Neutron Induced Fission of ^{245}Cm in the Resolved Resonance Region and Its Resonance Analysis", J. of the Korean Physical Society, 59, 1896 – 1899 (2011).

[54] Serot, O., et al., "^{245}Cm fission cross sections measurement in the thermal energy region", Proc. Seminar on Fission, Gent, Belgium, May 17-20, 247 – 253 (2010).

[55] De Smet, L., et al., "Experimental determination of the ^{26}Al(n,α)^{23}Na reaction cross section and calculation of the Maxwellian averaged cross section at stellar temperatures", Phys. Rev. C, 76, 045804 - 8 (2007).

[56] Vermote, S., et al., "Experimental determination of the ^{41}Ca(n,α)^{38}Ar reaction cross section up to 80 keV, and calculation of the Maxwellian averaged cross section at stellar temperatures", Phys. Rev. C, 85, 015803 - 8 (2012).

[57] "Nuclear Data Standards for Nuclear Measurements—1991", NEANDC/INDC Nuclear Standards File, NEANDC-311 "U", INDC(SEC)-101, Nuclear Energy Agency Nuclear Data Committee (1992).

3.3. Electron induced white spectrum neutron beams

[58] Carlson, A. D., et al., "The ENDF0B-VI Neutron Cross-Section Measurement Standards", NISTIR-5177, National Institute of Standards and Technology, and ENDF-351, Brookhaven National Laboratory (1993); see also "Data T-2 Nuclear Information Services": http://t2.lanl.gov/data/.

[59] Hausladen, S. L., and Lane, R. O., "Predictions of Differential Cross-Section for the Reactions $^{10}B(n,\alpha_0)^7Li$ and $^{10}B(n,\alpha_1)^7Li^*(0.48MeV)$", Phys. Rev. C, 5, 277 (1972).

[60] Sealock, R. M., and Overlay, J. C., "$^{10}B(n,\alpha)^7Li,^7Li^*$ Differential Cross-Section Measurement between 0.2 and 1.25 MeV", Phys. Rev. C, 13, 2149 (1976)

[61] Hambsch F.-J., and Ruskov, I., "The $^{10}B(n,\alpha_0)/^{10}B(n,\alpha_1\gamma)$ Branching Ratio", Nucl. Sci. Eng., 156, 103 (2007).

[62] Hambsch, F.-J., and Ruskov, I., "The $^{10}B(n,\alpha_0)^7Li$ and $^{10}B(n,\alpha_1\gamma)^7Li$ Alpha-Particle Angular Distributions for $E_n < 1$ MeV", Nucl. Sci. Eng. 163, 1-16 (2009).

[63] Ratynski, W., and Käppeler, F., "Neutron capture cross section of ^{197}Au: A standard for stellar nucleosynthesis", Phys. Rev. C. 37 (1988) 595 – 604.

[64] Macklin, R.L., "Gold Neutron Capture Cross Section from 100 to 2000 keV", Nucl. Sci. Eng, 79, 265, 1981.

[65] Massimi, C., et al., "Neutron capture cross section measurements for ^{197}Au from 4 keV to 80 keV at GELINA", to be published.

[66] Sirakov, I., et al., "Results of total cross section measurements for ^{197}Au in the energy region from 4 keV to 100 keV at GELINA", to be published

[67] Schillebeeckx, P., et al., N.J. Rhodes, E.M. Schooneveldd and C. Van Beveren, "Neutron resonance spectroscopy for the characterization of materials and objects", J. of Instrumentation, 7, C03009 -18 (2012).

[68] Postma, H., et al., "Neutron resonance capture analysis of some genuine and fake Etruscan copper alloy statuettes", Archaeometry 46, 635 – 646 (2004).

[69] Postma, H., and Schillebeeckx, P., "Non-destructive analysis of objects using neutron resonance capture", J. Radioanal. Nucl. Chem. 265, 297 – 302 (2005).

[70] Schut, P.A.C., et al., "Neutron resonance capture and neutron diffraction analysis of Roman bronze water taps", J. Radioanal. Nucl. Chem. 278, 151 – 164 (2008).

[71] Postma, H., et al., "Non-destructive bulk analysis of the Buggenum sword by neutron resonance capture analysis and neutron diffraction", J. Radioanal. Nucl. Chem. 283, 641 - 652 (2010).

[72] Postma, H., et al., "The metal compositions of a series of Geistingen-type socketed axes", J. Archaeological Sci. 38, 1810 – 1817 (2011).

[73] Schillebeeckx, P., et al., "Target requirements for neutron-induced cross-section measurements in the resonance region", Nucl. Instr. Meth. A 613, 378 - 385(2010).

[74] Noguere, G., et al., "Non-destructive analysis of materials by neutron resonance transmission", Nucl. Instr. Meth. A 575, 476 (2007) 476.

[75] Perelli Cippo, E.,et al., "Imaging of cultural heritage objects using neutron resonances", J. Anal. At. Spectrom. 26, 992 - 999 (2011).

3.3. Electron induced white spectrum neutron beams

THE N_ELBE NEUTRON TIME-OF-FLIGHT FACILITY

A. R. JUNGHANS[*], A. WAGNER[*] , D. BEMMERER[*], R. BEYER[*], E. BIRGERSSON[*, **], A. FERRARI[*], E. GROSSE[**], R. HANNASKE[*, **], A. R. JUNGHANS[*], M. KEMPE[*,**], T. KÖGLER[*,**], R. MASSARCZYK[*], A. MATIC[*,**], R. NOLTE[***], R. SCHWENGNER[*]

[*]Institute of Radiation Physics, Helmholtz-Zentrum Dresden-Rossendorf
Bautzner Landstr. 400, D-01328 Dresden, Germany
[**]Institute of Nuclear and Particle Physics, Technische Universität Dresden
D-01062 Dresden, Germany
[***]Physikalisch-Technische Bundesanstalt
Bundesallee 100, D-38116 Braunschweig, Germany
Email: a.junghans@hzdr.de; a.wagner@hzdr.de

Abstract

The compact neutron-time-of-flight facility nELBE at the superconducting electron accelerator ELBE of Helmholtz-Zentrum Dresden-Rossendorf is currently being rebuilt. As the neutron radiator consists of a liquid-lead circuit no moderated neutrons are produced and also the background from capture gamma rays is very small. The useful neutron spectrum extends from some tens of keV to about 10 MeV. nELBE is intended to deliver cross section data of fast neutron nuclear interactions e.g. for the transmutation of nuclear waste and an improvement of neutron physical simulations of innovative nuclear systems. The new experimental hall will allow measurements of angular distributions in neutron scattering. Inelastic neutron scattering, e.g. on ^{56}Fe, has been studied with a double time-of-flight setup and with photon detectors to measure the gamma rays produced in the process. The neutron total cross sections of Au and Ta were determined in a transmission experiment.

1. 1. INTRODUCTION

The radiation source ELBE (Electron Linear Accelerator with High Brilliance and Low Emittance) at Helmholtz-Zentrum Dresden-Rossendorf (HZDR) makes use of a superconducting continuous-wave electron linear accelerator delivering beams with energies up to 40 MeV. The high-intensity beam with average beam currents of up to 1.6 mA at pulse repetition rates up to 26 MHz serves as a driver for the production of various secondary beams. Figure 1 shows the layout of the accelerator facility and the beam lines for secondary radiations. Table 1 lists the available secondary beams and their primary applications.

ELBE is operated as a user facility. Experiment proposals from international groups are welcome. For details see the website https://www.hzdr.de/db/Cms?pNid=1732.

As one of the secondary beams, an intense neutron beam is being produced by bremsstrahlung photons via the (γ,n)-process inside a liquid-lead circuit. The lead acts threefold as the electron-to-bremsstrahlung converter, as the source of evaporation neutrons, as well as an efficient method for the heat dissipation of the electron beam.

The neutron and photon intensities as well as time and energy distributions, the neutron transport and the shielding of the experimental setup have been optimized by Monte Carlo particle transport simulations with MCNP, GEANT4 and FLUKA. The neutron source strength at the nominal beam current has been calculated to be 10^{13} neutrons/s [1].

3.3. Electron induced white spectrum neutron beams

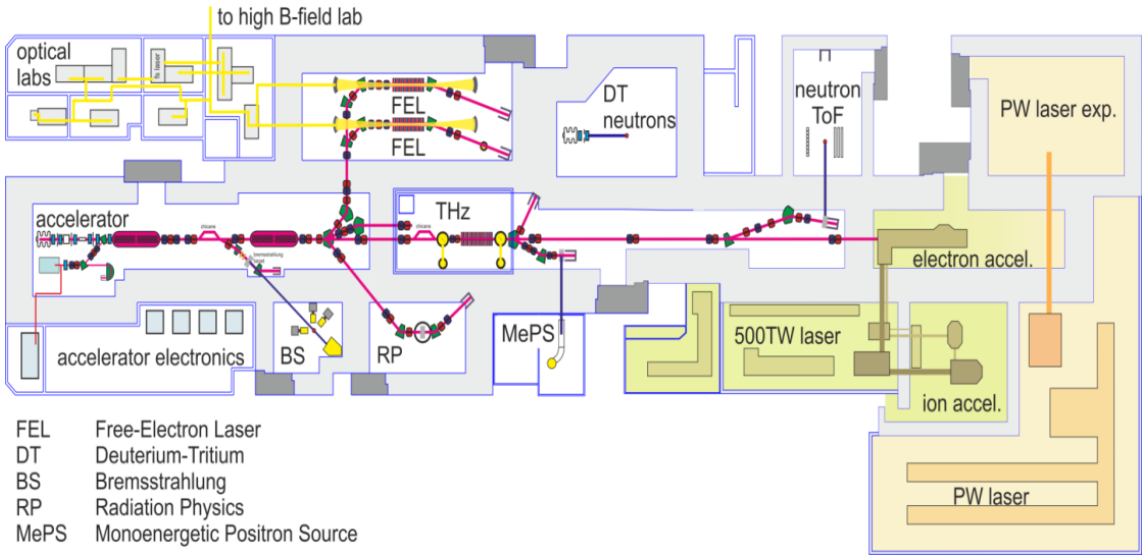

FIG.9. Layout of the accelerator facility ELBE. Two superconducting accelerator structures are located inside the accelerator hall. In the years 2012-2013, the facility has been extended in order to house several high-intensity laser systems and the new neutron time-of-flight facility is situated at the upper right side.

The design of the liquid-lead loop is shown in Fig.2. To achieve a good time-of-flight resolution using a short flight path for high neutron beam intensity a small active volume of neutron production with a correspondingly high local heat load of about 5 kW / g was chosen. A liquid-lead loop operated at a temperature of about 700 K has been built (Altstadt, et al.) which is also favourable with respect to induced radioactivity caused by various (γ,xn)- and (γ,p)-reactions as compared to e.g. liquid mercury. While using lead as material for efficient neutron production the beam dump is made from pure aluminium (>99.9%) resulting in low induced activities and little neutron generation (neutron separation energy of ^{27}Al: S_n=13.1 MeV).

The short beam pulses (about 5 ps FWHM) delivered by the superconducting electron accelerator provide the basis for an excellent time resolution for neutron time-of-flight experiments while the pulse repetition rates can be varied between 102 kHz and 26 MHz according to the demands of the experiments. The typical rates are 102 and 203 kHz, resulting in a neutron pulse repetition period of about 5 – 10 µs. With the existing electronically pulsed thermionic electron source electron pulse charges of up to 80 pC are realized allowing a moderate average electron beam current of 16 µA at a repetition rate of 200 kHz. The corresponding neutron source strength has been measured to be 10^{11} neutrons/s.

The electron beam passes through a beryllium window mounted on a stainless-steel vacuum chamber and hits the radiator, consisting of a molybdenum channel confining the liquid lead. The channel has a rhombic cross section with 11 mm side length. The electrons generate bremsstrahlung photons which release neutrons in secondary (γ,n) reactions on lead. These leave the radiator almost isotropically, whereas the electrons and photons are strongly forward-peaked. A neutron beam collimator of 2.6 m length is mounted at an angle of 110° w.r.t. the beam. The collimator contains three replaceable elements of lead and borated polyethylene that are mounted inside a precision steel tube [1]. The new neutron production

target has the same dimensions as the old photo-neutron source, as has the collimator. Therefore, a very similar neutron spectrum and spatial beam profile is expected.

A cross section of the neutron production target and of the collimator is shown in the insets of Fig.3.

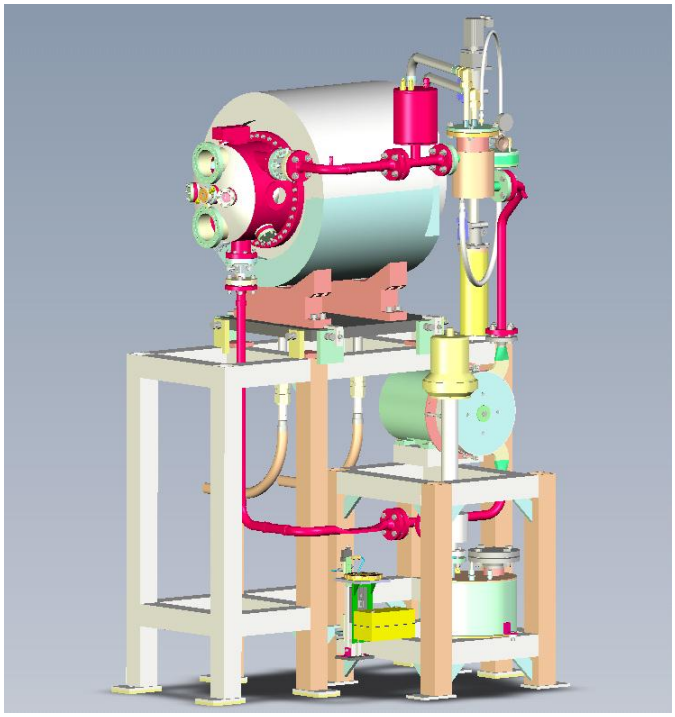

FIG. 10 Three-dimensional rendering of the liquid-lead loop installed at the ELBE facility. The intense electron beam impinges from the front left. The beam transport system is not shown here. The lead flow is driven by means of a magneto-hydrodynamic pump avoiding mechanical contact with the fluid and avoiding mechanical feedthroughs. Thermal insulation, heating units, and support systems are not shown. The beam dump is made from aluminium surrounded by lead in backward and radial directions.

A new experimental hall with a size of 6×6×9 m^3 with the neutron scattering target being located close to the centre (see Fig. 3) has been built. The room-return background of neutrons scattered from the walls will thus be reduced. An evacuated beam tube is planned to reduce the scattering of neutrons on air.

A new superconducting radio-frequency injector is already installed which in the near future will allow increase of the electron bunch charge by a factor of 10 at a repetition rate of 100 kHz [3].

The insets in Fig. 3 also show the double time-of-flight setup. Around the target, an array of 16 BaF_2 scintillation detectors for the detection of secondary photons has been installed. Each detector consists of two 190 mm long prisms with hexagonal bases of 53 mm inner radius glued together and read out on both ends using fast photomultiplier tubes[1] (PMT). The double-sided readout helps to reduce background signals stemming from anode dark-currents, it improves the energy resolution and it permits the determination of the

[1] Hamamatsu Photonics K.K., http://www.hamamatsu.com, PMT: R2059-01 selected with quartz windows.

longitudinal hit position. The signals from the PMTs are processed in dedicated VME-based readout units allowing pulse-shape discrimination of charged particles and photons.

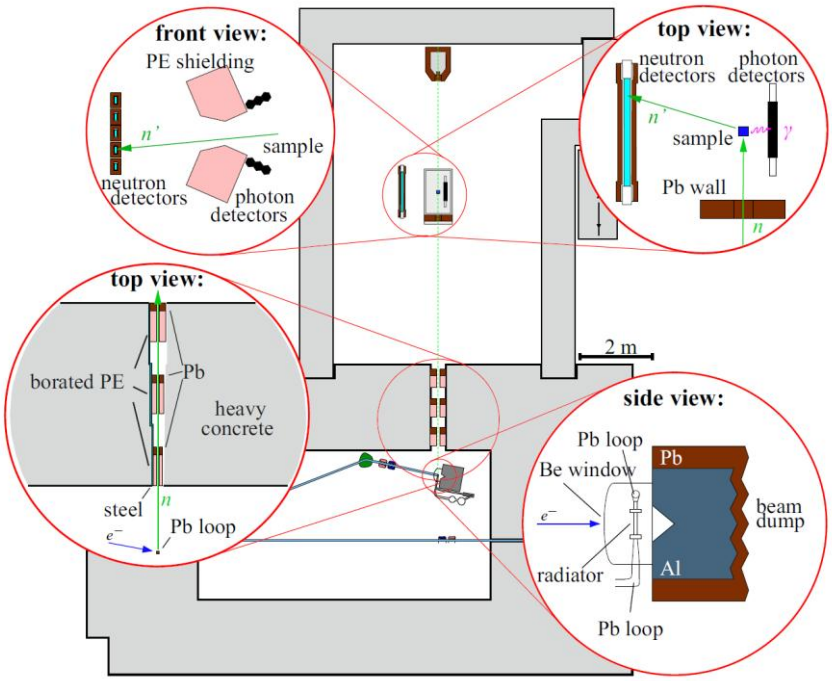

FIG. 11. Sketch of the setup in preparation for inelastic neutron scattering experiments. Details of the neutron source, the collimator, and the target area are shown enlarged.

Scattered neutrons are detected using proton-recoil plastic scintillation detectors at a distance of about 1 m from the target. The plastic scintillation detectors[4] are strips of 1000 mm length and 42 mm x 11 mm cross section read-out double-sided using the same PMTs as described above. The trigger threshold is selected to detect single photo-electrons permitting detection limits for neutrons as low as 30 keV for detection efficiencies above 10%. The design, operation, and calibration of these detectors are described in a previous publication. The system is optimized for high time resolution of the time-of-flight detectors reaching about 600 ps FWHM for the BaF_2-detectors and about 860 ps FWHM for the plastic scintillation detectors in order to allow a compact setup ensuring high beam repetition rates with no pulse-to-pulse overlap. Scattered neutrons and photons originating from the BaF_2-array are suppressed by borated polyethylene absorbers in the direction of the neutron detectors. The distribution of random background has been determined in measurements without target.

The neutron spectral rate has been measured using the ^{235}U fission chamber from PTB [5]. The data-acquisition system is controlled by a VME-based computer[2] running the real-time operating system LynxOS and the versatile data acquisition system MBS[3]. The readout of the double-sided BaF_2-detectors is done using CAEN[4] V874B QDC providing the energy information, while the plastic-scintillation neutron-detector information is processed by in-house made constant-fraction

[2] Creative Electronics Systems, http://www.ces.ch, RIO VME single board computer.
[3] GSI Multi-Branch System, http://daq.gsi.de.
[4] CAEN s.p.A., http://www.caen.it.

discriminators. CAEN V1190a time-to-digital converters provide the timing information for both the BaF_2 and the plastic scintillator detectors. For measurements of photon energies with a higher precision 8 (3) cylindrical $LaBr_3$ detectors[5] with dimensions of 2 (3) inch diameter × 2 (3) inch length have been acquired.

2. NEUTRON BEAM PROPERTIES

The spatial profile of the neutron beam has been determined at different flight path lengths using an 11 mm wide plastic scintillator bar that was moved through the beam in horizontal and vertical directions [6]. The bar was moved continuously with a typical speed of 12.5 mm/min and a time-of-flight spectrum analysed in 5 s intervals. By gating on the time-of-flight interval of neutrons the spatial profile of the neutron beam was determined.

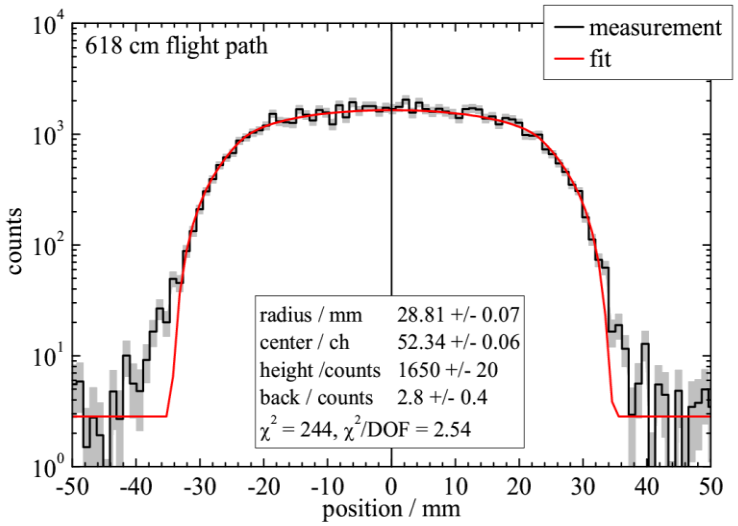

FIG. 12. Measured spatial profile of the neutron beam at a flight path of 618 cm.

The measured profiles were fitted assuming a uniform neutron beam profile with a sharp edge as shown in Fig. 4. Only a small beam halo is found experimentally. The beam radius follows from the conical geometry of the collimator: Length 2.6 m, diameter increasing from 2 cm at the entrance to 3 cm at the exit.

The neutron spectral rate was determined with the transfer instrument (a ^{235}U parallel-plate fission chamber) H19 from PTB Braunschweig [5]. Figure 5 shows the measured spectral rate at a flight path of 618 cm with electron energy of 30 MeV and an electron beam current of 15 µA.

The time resolution of the fission chamber was estimated from the width of the photo-fission peak due to bremsstrahlung to be 3.8 ns (FWHM). The spectrum has the typical shape of an evaporation spectrum of photo-neutrons from a heavy nucleus. The usable energy range extends about two orders of magnitude from above 50 keV to 7 MeV. Some absorption dips at 78, 117, 355, 528, 722, 820 keV due to scattering from resonances in ^{208}Pb can be seen. Emission peaks at 40, 89, 179, 254, 314, 605 keV are due to near threshold photo-neutron emission from ^{208}Pb.

[5] Saint-Gobain Crystals Inc., http://www.detectors.saint-gobain.com/

3.3. Electron induced white spectrum neutron beams

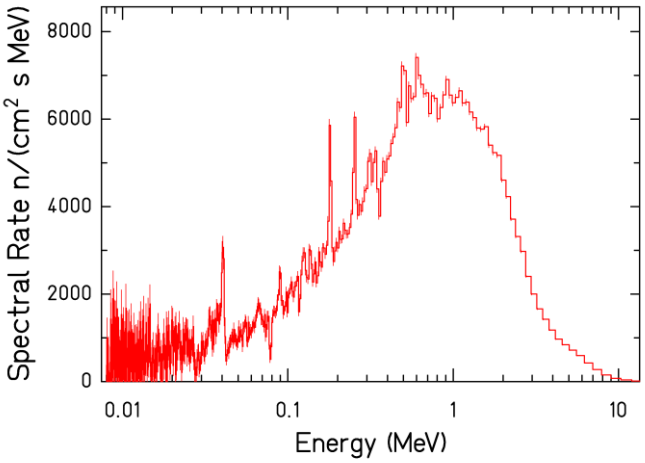

FIG. 13. Neutron spectral rate measured with a ^{235}U fission chamber (H19 from PTB) at a flight path of 618 cm.

The stability of the neutron beam is very good, as the ELBE electron beam hitting the neutron producing target is very stable. The stability has been investigated at very reduced electron beam current used in neutron transmission measurements.

A typical time-of-flight spectrum was measured with a plastic scintillator in the beam, see FIG. 14. The electron beam current was reduced to the sub-µA range and a 3 cm thick absorber made of the technical lead alloy PbSb4 was moved into the beam in addition to a 1 cm PbSb4 shield that surrounded the detector to reduce the count rate. In this configuration the peak from bremsstrahlung has only about a factor 60 higher than the neutron intensities that start to arrive at about 100 ns later. The width of the bremsstrahlung peak of 1.0 ns (FWHM) is typical for the time resolution that is dominated by the detection system. Due to the rather low instantaneous flux and high repetition rate the signals from the bremsstrahlung have decayed to the random background level already after 50 ns.

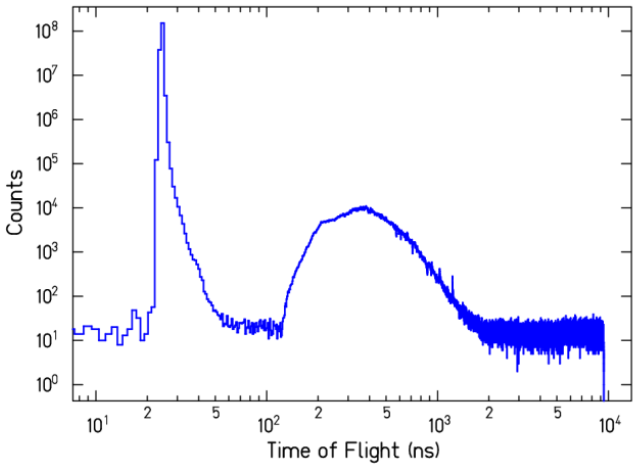

FIG. 14. Time-of-flight spectrum measured with reduced electron beam intensity at a flight path of 718 cm with additional shielding of 3 cm PbSb4 in the beam to reduce the detector count rate.

3.3. Electron induced white spectrum neutron beams

The energy resolution of the experiment was simulated with MCNP5 for a flight path of 700 cm including the plastic scintillator and its Pb shield. The neutron energy to time-of-flight correlation can be changed by scattering of neutrons in the neutron-producing target and all materials in the beam line including the collimator. Figure 7 shows that the energy resolution is dominated by the detection system. At energies above 1 MeV the scattering of neutrons in the Pb shield close to the detector dominates the energy resolution. The simulated energy resolution was verified by the measurement of two broad resonances in the transmission of ^{208}Pb at 355 keV and 527 keV [7].

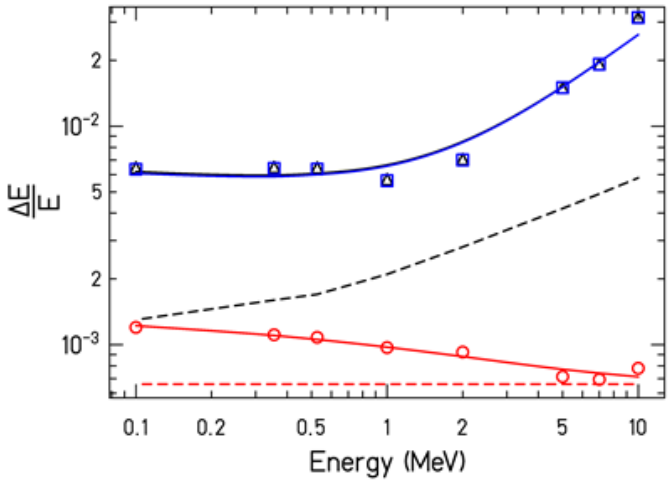

FIG. 15. Simulated energy resolution (1σ) of a transmission measurement at nELBE. The resolution of the neutron source including the collimator is shown as circles with a full line in red. In the simulation all layers of matter in the neutron beam line are taken into account. The resolution coming only from the geometrical size of the neutron radiator is shown as a dashed red line. The energy resolution from a 1.1 cm thick plastic scintillator including a 1 cm Pb shield on all sides is shown as a blue line (square data symbols). The quadratic sum of source and detector resolution is shown as a blue line (triangles). The dashed black line corresponds to the total resolution taking into account the source and detector dimension and the time-of-flight resolution of the detector only, without inclusion of scattering.

3. EXPERIMENTS

3.1. NEUTRON INELASTIC SCATTERING

The inelastic scattering reaction on ^{56}Fe(n,n'γ) was studied by measuring the gamma rays emitted as a function of time-of-flight. The target was a cylinder of iron with a diameter of 20 mm and thickness of 8 mm of natural isotopic composition.

An HPGe detector (60% relative efficiency) located at 125 degrees to the neutron beam and a distance of 20 cm from the target was used to measure the gamma ray energy spectrum. In coincidence the time-of-flight was determined from the HPGe detector and the accelerator RF signals. The background was subtracted with the help of gamma-spectra that were taken with the target out of the beam. A time resolution of 10 ns (FWHM) was determined from the width of the bremsstrahlung peak.

3.3. Electron induced white spectrum neutron beams

In total, sixteen gamma ray lines from excited states in ^{56}Fe were detected. To determine the inelastic scattering yield for the first few excited states the feeding from higher-lying states has been subtracted according to the known level scheme.

The cross section was determined using the neutron spectral rate as shown in Fig. 4 including corrections for the absorption and scattering of neutrons in air and the materials between the fission chamber and the target position, for details see [6].

From the photon production cross section measured at 125 degree the angle-integrated scattering cross section can be determined by Gaussian quadrature [8].

The inelastic scattering cross section for ^{56}Fe(n,n'γ) to the first 2^+,4^+,6^+ states is shown in Fig. 8.

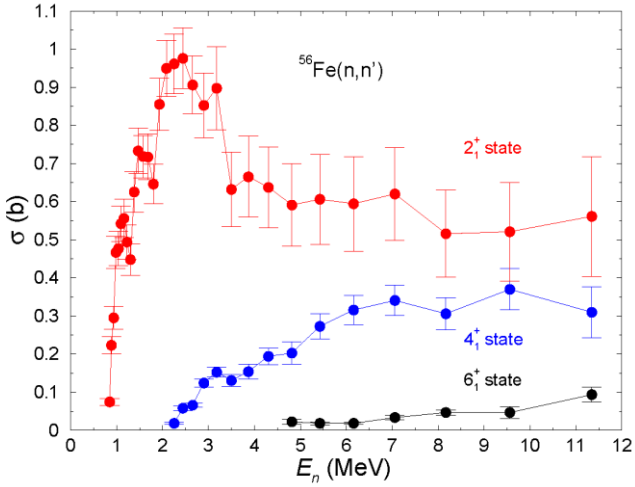

FIG. 16. Inelastic scattering cross sections for the first 2^+,4^+ and 6^+ states in ^{56}Fe.

In the double time-of-flight experiment list-mode data are taken for coincident signals in the BaF_2-array and the neutron-detector array selecting primarily reactions with at least one photon and one neutron in the exit channel. Time-of-flight calibration is done using the photon flash stemming from scattered bremsstrahlung inside the radiator. The target consisted of a cylindrical slab of natural iron (isotopic composition: 5.85% ^{54}Fe, 91.75% ^{56}Fe, 2.12% ^{57}Fe, 0.28% ^{58}Fe) with a mass of 19.82 g. The average neutron intensity on target amounts to about $4 \cdot 10^4$ $s^{-1}cm^{-2}$.

Figure 9 shows the correlation of the time-of-flight of the incoming neutron and the time-of-flight of the scattered neutron. The time-of-flights are measured using the timing signals of the BaF_2-detectors, plastic neutron detectors, and the reference signal of the accelerator radio-frequency. Path length variations have been accounted for. One advantage of the double time-of-flight method is that with sufficient resolution scatterings to excited states could be measured even when the level scheme of the nucleus is not known completely. Scattering to higher lying excited states in ^{56}Fe is significant as can be seen qualitatively from Fig. 9. The normalization of the inelastic scattering cross section in the double time-of-flight experiment has not yet been completed. The absolute efficiencies of all detectors enter in this calculation. The deduced cross sections in Fig. 10 do not agree with the results from other experiments. In measurements, where both neutron and gamma rays are detected correlations of their angular distribution, could play a significant role. By gating on

the neutron energy loss corresponding to a given excited state, the cross section for this particular channel can be extracted.

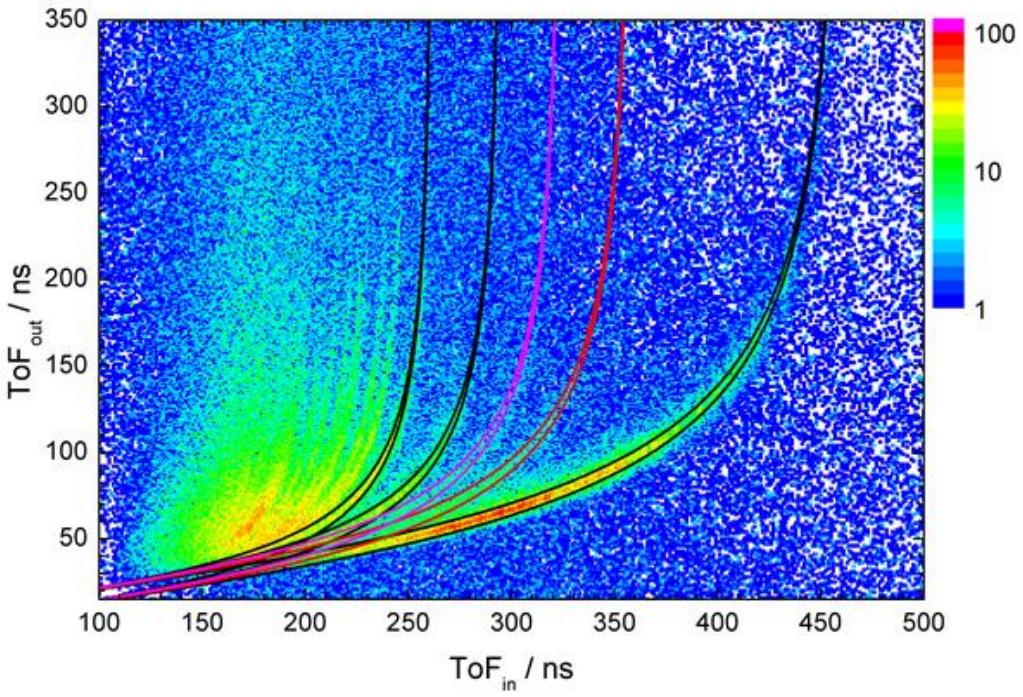

FIG. 17. Velocity correlations for neutron inelastic scattering from iron of natural isotopic abundance. The black lines surround inelastic scattering events from the 1st, 2nd, and 3rd excited states of ^{56}Fe, the red lines surround events from ^{54}Fe, which is contained in the natural isotopic composition, the purple lines surround events where a neutron scattered twice inside the target.

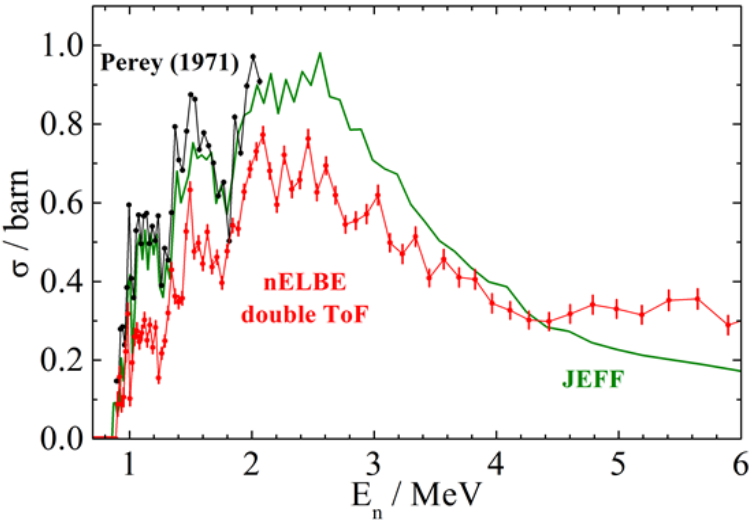

FIG. 18. Preliminary results (Beyer, Bemmerer, Grosse, & al.) for the cross section for the direct excitation of the 847 keV level in ^{56}Fe in kinematically-complete inelastic neutron scattering (red data points). The green line shows the estimate from the JEFF library. Black data points below an energy of 2.1 MeV show data taken in scattering experiments where only the outgoing photon is detected (Perey, Kinney, & Macklin) .

3.3. Electron induced white spectrum neutron beams

3.2 TRANSMISSION EXPERIMENTS

The neutron total cross sections of Au and Ta were measured in a transmission experiment. The high-purity target samples of Au (areal density: 0.0945(6) atoms/barn) and Ta (0.1413(6) atoms/barn) together with bremsstrahlung absorbers made from PbSb4 alloy were cycled in and out of the beam by a pneumatically driven computer-controlled target ladder directly in front of the collimator entrance. The data taking time per cycle for the empty sample (3 cm thick PbSb4 bremsstrahlung absorber only) was 600s, for the Au and Ta samples it was 900 s. The total measurement time was about 78 hours.

TABLE 2. AVAILABLE BEAMS AT THE SUPERCONDUCTING ELECTRON ACCELERATOR ELBE, THE TYPE OF RADIATION, AND THE PRIMARY APPLICATION

Secondary beam	Radiation	Application
Free-Electron Laser	Coherent infrared light, wavelength range from 3-230 μm	IR spectroscopy in semiconductors, quantum systems, soft matter, biological systems
THz radiation	Coherent light from 100 μm to 1 mm wavelength	THz spectroscopy in seminconductors and quantum systems
(Polarized) Bremsstrahlung	Broad-band high-energy photons, 0 – 16 MeV	Nuclear astrophysics and transmutation-related (γ, γ)- (γ,n)-, (γ,p)-, (γ,α)-reactions, materials research with positrons
Positrons	Pulsed and mono-energetic positrons, 0 – 50 keV kinetic energy	materials research with positrons, defect studies in thin films and bulk materials
Neutrons	Evaporation neutrons produced in (γ,n)-processes, 100 keV – 10 MeV	Nuclear data measurements of neutron-induced reactions
Electrons	Direct beams of 6 MeV – 35 MeV	Detector tests with < 10 ps timing resolution and intensities from single electrons to 10^5 s^{-1} cm^{-2}

The transmitted neutrons were detected using a 1000 x 42 x 11 mm^3 plastic scintillator[6] that was read out on both ends using high-gain Hamamatsu R2059-01 photomultiplier tubes (PMT). The scintillator was surrounded by a 1 cm thick lead shield to reduce the background count rate. The detection threshold for neutrons through recoiling protons in this detector is in the 1-10 keV range [4]. The electron beam intensity was reduced to the sub-μA range with a micropulse repetition rate of 102 kHz to have a detector count rate of 10 kHz (empty sample beam). This corresponds to a neutron count rate of ca. 250 neutrons/s. Thus, only about every tenth accelerator pulse is measured in the scintillator.

[6] Eljen Technology Inc., EJ200, http://www.eljentechnology.com/

3.3. Electron induced white spectrum neutron beams

The dead time at a pulsed neutron source is the most important correction to be made in this type of measurement, as the count rate is very different with the target sample in and out of the beam. The data acquisition dead time was measured for each event of the list-mode data acquisition system. The most probable dead time is 15 μs due to the readout times of the QDC and TDC used. The measured dead time per event was used to construct a time-of-flight dependent correction factor, see [11]. With the target out of the beam the live time factor was approx. 0.575. In addition, a dead time of 2.7 μs was included in the single signals of the two photomultiplier's constant fraction modules which results in an additional live time factor of approx. 0.96. The total systematic uncertainty including the transmission normalization (due to fluctuations of the neutron source intensity), areal density of the target samples, and the dead time correction factor amounts to less than 2%. The statistical uncertainty is shown in the error bars of Figs. 11 and 12. Our data are about 2% systematically higher than the previous measurements of Poenitz and Abfalterer (Abfalterer, Bateman, Dietrich, Finlay, Haight, & Morgan) (Poenitz & Whalen, Neutron Total Cross Section Measurements in the energy region from 47 keV to 20 MeV, 1983 ANL/NDM-80) (Poenitz, Whalen, & Smith, Nucl. Sci. Eng. 78 (1981) 333).

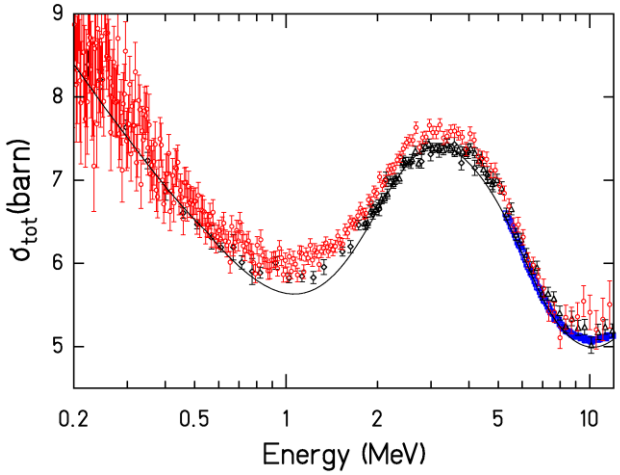

FIG. 19. Neutron total cross section of ^{197}Au measured at nELBE (red). The blue data points were measured by Abfalterer et al. (Abfalterer, Bateman, Dietrich, Finlay, Haight, & Morgan) The black data symbols are from Poenitz et al. (Poenitz & Whalen, Neutron Total Cross Section Measurements in the energy region from 47 keV to 20 MeV, 1983 ANL/NDM-80) (Poenitz, Whalen, & Smith, Nucl. Sci. Eng. 78 (1981) 333). The full line was calculated using Talys 1.4 [15].

4. OUTLOOK

Starting in June 2013, the new neutron time-of-flight facility will be commissioned for routine operation. Experiments will start in the second half of 2013. Measurements of neutron total cross sections and neutron induced fission are planned. A new setup consisting of 11 $LaBr_3$ scintillators is in preparation for neutron scattering studies including angular distribution measurements and measurements of prompt fission γ-spectra.

3.3. Electron induced white spectrum neutron beams

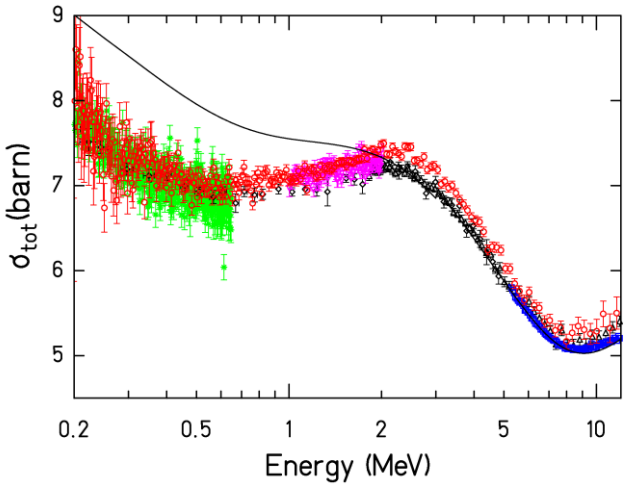

FIG.12. Neutron total cross section of ^{nat}Ta measured at nELBE. The symbols are the same as in Fig. 11. The purple and green data points are from (Islam, Hussain, Ameen, Enayetullah, & Islam) (Smith, Guenther, & Whalen). The full line was calculated using Talys 1.4 (Koning).

ACKNOWLEDGMENTS

The project is supported by the European Commission in the FP7 project ERINDA (269499), and the German Federal Ministry of Education and Research (02NUK13).

REFERENCES

[1] KLUG, J., et al. Nucl. Inst. Meth. A 577 (2007) 641.
[2] ALTSTADT, E. et al. Ann. Nucl. Ene. 34 (2007) 36.
[3] ARNOLD, A., TEICHERT, J. Phys. Rev. Spec. Top. - Accel Beams 14 (2011) 024801.
[4] BEYER, R., et al. Nucl. Inst. Meth. A575 (2007) 449–455.
[5] GAYTHER, D. B., Metrologia 27 (1990) 221.
[6] BEYER, R., Nucl. Inst. Meth. A, submitted.
[7] SCHILLEBEECKX, P., et al. Nuclear Data Sheets 113(2012), 3054-3100.
[8] MIHAILESCU, L. C., et al. Nucl. Inst. Meth. A 531 (2004) 375.
[9] BEYER, R. et al., Jour. of Instr. 7 (2012) C02020.
[10] PEREY, F. G.; KINNEY, W. E.; MACKLIN, R. L. Proc. 3rd Int. Conf. Neutron Cross Sections and Tech. (1971) 191.
[11] MOORE, M. S., Nucl. Inst. Meth. 169 (1980) 245-247.
[12] ABFALTERER, W. P., et al. Phys. Rev. C 63 (2001) 044608.
[13] POENITZ, W. P., WHALEN, J. F. Neutron Total Cross Section Measurements in the energy region from 47 keV to 20 MeV. Argonne, U.S.A. 1983 ANL/NDM-80.
[14] POENITZ, W. P., WHALEN, J. F., SMITH, A. B. Nucl. Sci. Eng. 78 (1981) 333.
[15] KONING, A. J., H. S. D. M. C. TALYS-1.0. Proc. Int. Conf. Nucl. Data for Science and Tech., EDP Sciences (2008) 211-214.
[16] ISLAM, E., et al. Nucl. Phys. A209 (1973) 189.
[17] SMITH, A. B., GUENTHER, P. T., WHALEN, J. F., Phys. Rev. 168 (1968) 1344.

3.3. Electron induced white spectrum neutron beams

ACTIVITIES FOR NUCLEAR DATA MEASUREMENTS USING POHANG NEUTRON FACILITY

G. N. KIM[*], K. S. KIM[*], K. KIM[*], S. YANG[*], S. G. SHIN[**], M. H. CHO[**], M. W. LEE[***], Y. R. KANG[***], T. I. RO[+]

[*]Department of Physics, Kyungpook National University, 80 Daehak-ro, Buk-gu, Daegu 702- 701, Korea
[**]Division of Advanced Nuclear Engineering, Pohang University of Science and Technology, San 31, Hyoja-dong, Nam-gu, Pohang 790-784, Korea
[***]Research Center, Dongnam Institute of Radiological and Medical Science, Busan 619-953, Korea
[+]Department of Physics, Dong-A University, Busan 604-714, Korea
Email: gnkim@knu.ac.kr

Abstract

We report on activities for nuclear data measurements using a pulsed neutron facility consisting of an electron linear accelerator, a water-cooled Ta target with a water moderator, and a 12 m time-of-flight path. It is possible to measure neutron total cross sections in the neutron energy range from 0.01 eV to a few hundred eV by using the neutron time-of-flight method; photo-neutron cross sections can also measure by using the bremsstrahlung from the electron linac. A ^{6}LiZnS(Ag) glass scintillator was used as a neutron detector. The neutron flight path from the water-cooled Ta target to the neutron detector was 12.1 m. In this paper, we report the total cross-section measurement for Nb by the time-of-flight method and the thermal neutron capture cross-sections and the resonance integrals for the ^{165}Ho(n,γ)^{166g}Ho reaction by the neutron activation method. We also report on the isomeric-yield ratios for the ^{120m,g}Sb and ^{122m,g}Sb isomeric pairs produced by ^{nat}Sb(γ,xn)^{120m,g,122m,g}Sb photonuclear reactions in the bremsstrahlung energy region from 40 to 60 MeV with a step size of ΔE = 5 MeV by the activation method, and the mass-yield distribution of fission products from ^{nat}Pb, ^{209}Bi, and ^{232}Th with bremsstrahlung beams using a recoil catcher and an off-line γ ray spectrometric technique.

1. INTRODUCTION

Electron linear accelerators (linac) are being used throughout the world in a variety of important applications. The pulsed neutron facility based on an electron linac is effective for measuring energy dependent cross sections with high resolution by the time-of-flight (TOF) technique covering the energy range from thermal neutrons to a few tens of MeV. The measurement of neutron cross sections gives basic information about the internal structure of atomic nuclei and their constituents. Precise measurements of neutron cross sections are of great importance for the safety design of nuclear reactors and for the evaluation of the neutron flux density and the energy spectrum around a reactor.

The pulsed neutron facility based on a 100-MeV electron linac was proposed in 1997 and construction was completed at the Pohang Accelerator Laboratory in 1999 [1]. Its main goal is to provide the infrastructure for nuclear data measurements in Korea.

2. POHANG NEUTRON FACILITY BASED ON ELECTRON LINAC

The pulsed neutron facility consists of an electron linac, a water-cooled Ta target, and a ~12-m-long TOF path. The characteristics of the facility are described elsewhere [2]. The beam energy of the 100-MeV electron linac is varied from 80 MeV to 40 MeV, and the beam currents at the end of linac are in between 100 mA and 30 mA. The length of electron beam pulse is 1-2 μs, and the pulse repetition rate is 10 Hz. Pulsed neutrons were produced via the ^{181}Ta (γ,*x*n) reaction by bombarding a metallic Ta-target with the pulsed electron beam. The estimated neutron yield per kW of beam power is 1.9×10^{12} n/s for electron energies above 50 MeV at the Ta-target based on the MCNP code [3]. To maximize the thermal neutrons in this

3.3. Electron induced white spectrum neutron beams

facility, we used a cylindrical water moderator contained in an aluminum cylinder with a wall thickness of 0.5 cm, a diameter of 30 cm, and a height of 30 cm. The water level in this experiment was 3 cm above the target surface. The pulsed neutron beam was collimated to 5 cm diameter in the middle position of the collimation system where the sample changer was located. The sample changer consisted of a disc with 4 holes; each hole was 8 cm in diameter, which matched the hole in the collimator in the neutron beam line. The sample changer was controlled remotely by using a CAMAC module.

The neutron guide tubes were constructed of stainless steel with two different diameters, 15 cm and 20 cm, and were placed perpendicularly to the electron beam. The neutron collimation system was mainly composed of H_3BO_3, Pb, and Fe collimators, which were symmetrically tapered from a 10 cm diameter at the beginning to a 5 cm in the middle position where the sample was located, to an 8 m diameter at the end of guide tube where the neutron detector was placed. There was a 1.8 m thick concrete wall between the target and the detector room.

2.1. MEASUREMENT OF NEUTRON TOTAL CROSS-SECTIONS BY THE TIME-OF-FLIGHT METHOD

Since the experimental procedure has been published previously [4-6], only a general description is given here. The experimental arrangement for the transmission measurements is shown in Fig. 1.

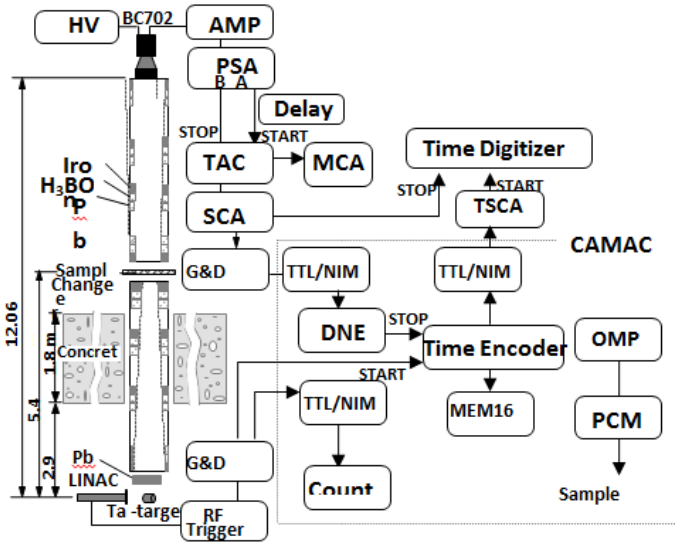

FIG. 1. Configuration of experimental setup and data acquisition system

The neutron detector was located at a distance of 12.1 m from the photo-neutron target. A ^{6}Li-ZnS (Ag) scintillator (BC702) with a diameter of 12.5 cm and a thickness of 1.6 cm mounted on an EMI-93090 photomultiplier was used as a neutron detector. During the transmission measurement, the electron linac was operated with a repetition rate of 15 Hz, a pulse width of 1.1 μs, and the electron energy of 65 MeV. The peak current in the beam current monitor located at the end of the second accelerator section was greater than 50 mA, which was almost the same as that in the target.

3.3. Electron induced white spectrum neutron beams

As an example of neutron total cross section measurements, we present the results of total cross sections for natural niobium. A high purity (99.99%) natural niobium (^{93}Nb 100% abundance in nature) metal plate with a diameter of 80.11±0.01 mm and thickness of 15.04±0.03 mm was used as a transmission sample. The main impurities of this sample were Ta (<0.1%), O (<0.06%), N (<0.04%), and C (<0.02%). A set of notch filters of Co, In, and Cd plates was used for the background measurement and the energy calibration. The configuration of the experimental arrangement and the data acquisition system used in this measurement is described elsewhere [4].

The neutron total cross section is determined by measuring the transmitted neutrons through a known amount of sample and comparing this with the transmitted neutrons without sample. The accumulated neutron TOF spectrum for the open beam operation and for the transmission spectra of the natural Nb sample are shown in Fig. 2, together with the estimated background level, which is indicated by a solid line.

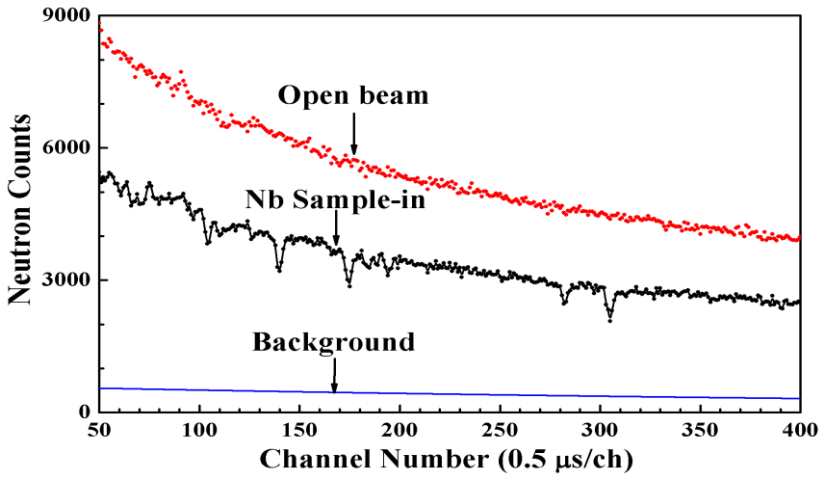

FIG. 2. Neutron TOF spectra for the sample-in and for the sample out of 15-mm Nb, together with the estimated background level indicated as a solid line.

The total neutron cross sections for natural Nb were obtained in the neutron energy range from 0.05 to 300 eV assuming that numbers of count in each energy group are uniformly distributed. The overall statistical errors for the measured total cross sections ranged from 5% to 25%, depending on the neutron energy. The systematic uncertainties came from the following sources: uncertainties from the flight-path measurements (2.0%), the background estimation (0.04%), the sample thickness (2.6%), and the dead time, the normalization, etc. (2.0%). Thus, the total systematic error of the present measurement is about 3.8%.

The measured total cross sections are generally in good agreement with other existing data [7-10] and with ENDF/B-VII.0 [11] and JENDL 3.3 [12] evaluated data assuming 300 K for Doppler broadening, as shown in Fig. 3. The data measured by M. Adib et al. [7] in the energy region from 0.00232 to 2.2461 eV are lower than present results. The data from M. R. Serpa [8] are almost similar to that of the present values in the energy region from 0.14 to 2.1 eV, but his results in the neutron energy below 0.14 eV are different from the present results and other measurements. The data measured by V. E. Pilcher at al. [9] are higher than the present results at energies from 3.03-9.47eV and 29.2-299.7 eV, respectively.

3.3. Electron induced white spectrum neutron beams

K. K. Seth et al. [10] measured the total cross sections from 47.1-166.9 eV and their results are in general good agreement with the present results. The present results are in general good agreement with the evaluated data from ENDF/B-VII.0 [11] but slightly lower than those of JENDL 3.3 [12].

We fitted the transmission of the natural Nb sample with the SAMMY code [13] to obtain resonance parameters of each resonance peak in the neutron energy region from 10-280 eV, as shown in the Fig. 4.

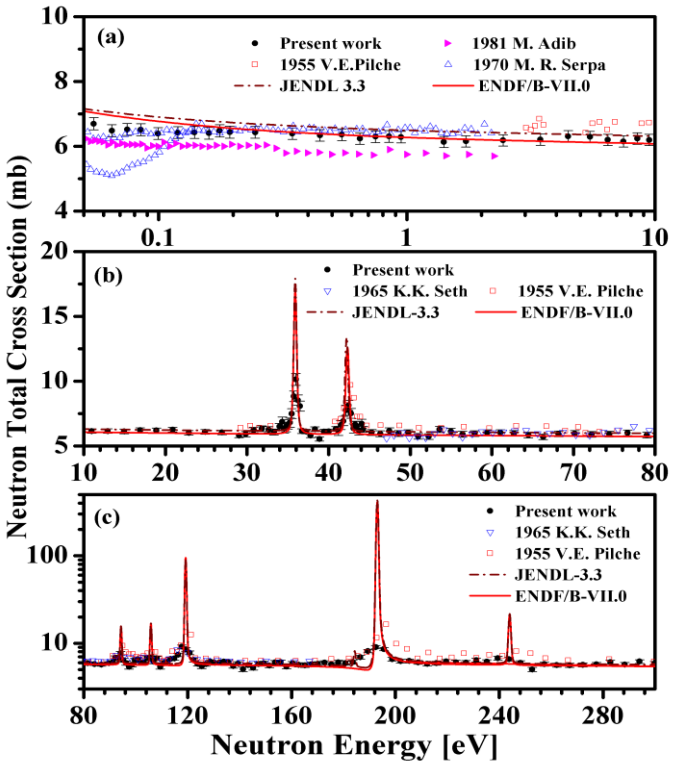

FIG.3. Measured total neutron cross-sections for ^{nat}Nb compared with previous experimental and evaluated data.

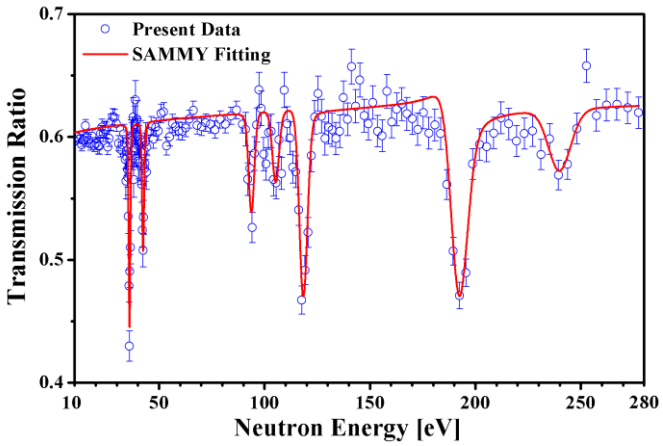

FIG.4. Measured transmission of Nb was fitted with the SAMMY code.

3.3. Electron induced white spectrum neutron beams

2.2. MEASUREMENT OF THERMAL NEUTRON CROSS-SECTIONS AND RESONANCE INTEGRALS BY THE NEUTRON ACTIVATION METHOD

We could measure the thermal neutron cross-sections and the resonance integrals for various reactions by the neutron activation method. We present one of examples measured in this facility [14]: the thermal neutron cross-section and the resonance integral for the ^{165}Ho(n,γ)^{166g}Ho reaction using a ^{197}Au(n,γ)^{198}Au monitor reaction as a single comparator [15]. The high-purity natural Ho and Au foils with and without a cadmium shield case of 0.5 mm thickness were irradiated in a neutron beam. The neutron fluxes exposed to each sample during the irradiation were determined from activities of In monitors stacked alternatively between Ho and Au foils. The Ho, Au, and In foils were stacked on the sample holder, and the sample holder was placed on the upper surface of the water moderator as shown in Fig. 5, where Ho(Cd) and Au(Cd) denote the activation foil covered with a 0.5-mm thick Cd. The neutron flux exposed to each sample was extrapolated from the measured activities of In foils irradiated simultaneously with the foil samples. The cadmium ratio is defined by $CR=(R/R_{cd})$, where R and R_{cd} are reaction rates per atom for bare and Cd-covered isotope irradiation, respectively. The measured cadmium ratio for ^{197}Au was 2.76±0.04, and that for ^{165}Ho was 2.18±0.03, respectively.

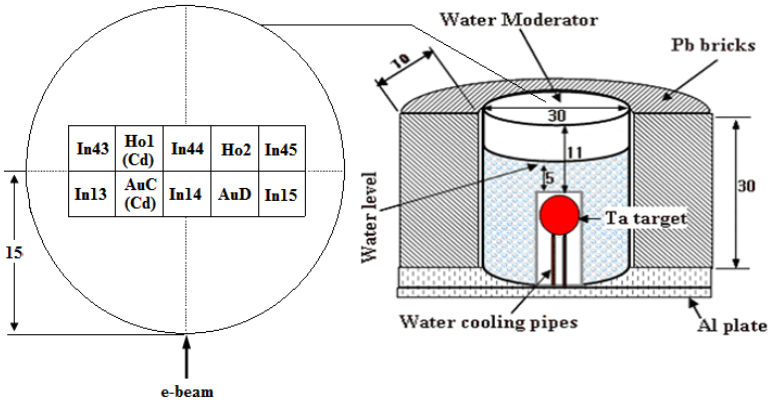

FIG. 5. Configuration of the neutron source based on the Ta target and water moderator system and the experimental arrangement of the activation samples. The numbers in this figure refer to dimension in cm.

In this study, the irradiation time was 180 min. The main nuclear data for the ^{165}Ho(n,γ)^{166g}Ho, ^{197}Au(n,γ)^{198}Au, and ^{115}In(n,γ)^{116m}In reactions are based on the table of isotopes [16].

The induced activities in the activated foils were measured with a calibrated p-type high-purity Ge detector. To measure the activities of the reaction products formed via the ^{165}Ho(n,γ)^{166g}Ho, ^{197}Au(n,γ)^{198}Au and ^{115}In(n,γ)^{116m}In reactions, we have chosen the γ ray peaks with high intensity, well separated, and relatively low background. The activity of the ^{166g}Ho was determined by using the γ ray of 80.576 keV (6.56%). The activity of the ^{198}Au was determined by using the 411.80 keV (95.58%) γ ray peak. In case of the ^{116m}In, the activity was measured using the 1293.54 keV (84.4%) γ ray peak. The measuring times were varied from several ten minutes to several hours depending on the statistics of the γ ray peaks.

3.3. Electron induced white spectrum neutron beams

The thermal neutron cross-section and the resonance integral for the $^{165}Ho(n,\gamma)^{166g}Ho$ reaction have been measured relative to the reference values of σ_0=98.65±0.09 barn and I_0=1550±28 barn for the $^{197}Au(n,\gamma)^{198}Au$ reaction [17]. The measured thermal neutron cross-section of the $^{165}Ho(n,\gamma)^{166g}Ho$ reaction is 59.7±2.5 barn which is consistent with the existing experimental [18] and evaluated data [11,19]. The present resonance integral for the $^{165}Ho(n,\gamma)^{166}Ho$ reaction is 671±47 barn by assuming the cadmium cut-off energy of 0.55 eV and is consistent with the existing experimental [18] and evaluated data [11,19].

3. EXPERIMENTS WITH BREMSSTRAHLUNG-INDUCED REACTIONS

3.1. MEASUREMENT OF ISOMERIC-YIELD RATIOS FOR BREMSSTRAHLUNG-INDUCED REACTIONS

The relative population of metastable- and ground-states of a residual nuclide formed in a nuclear reaction, which is called the isomeric cross-section ratio ($IR=\sigma_m/\sigma_g$), becomes an important source of information on the structure and properties of the excited states of the atomic nuclei. Because the metastable-state and the ground-state have significantly different spin values, the isomeric ratio can be represented as the ratio of the cross-sections for the production of high- and low-spin states; specifically, IR = σ (high-spin)/ σ (low-spin). In our case, the activation was performed by non-monoenergetic bremsstrahlung photons, and the isomeric ratio is expressed through the yields of the two states instead of the two cross-sections, $IR=Y_{high\text{-}spin}/Y_{low\text{-}spin}$.

We present one of the isomeric-yield ratios measured in this facility [20], the isomeric-yield ratios for the $^{120m,g}Sb$ and $^{122m,g}Sb$ isomeric pairs produced by $^{nat}Sb(\gamma,xn)^{120m,g,122m,g}Sb$ photonuclear reactions in the bremsstrahlung energy region from 40 to 60 MeV with a step size of ΔE = 5 MeV by the activation method [21].

Bremsstrahlung photons were produced when pulsed electrons of 40, 45, 50, 55, and 60 MeV from the 100-MeV electron linac hit a thin W target with a size of 100 mm ×100 mm and a thickness of 0.1 mm [3]. The experimental samples were prepared from high-purity (99.999%) natural antimony in powder form (200 mesh), made by the Alfa Aesar, a Johnson Mathey Company (Ward Hill, MA, USA). The antimony powders were encapsulated into identical polyethylene capsules with diameters of 12 mm. The irradiation sample was placed in air at a distance of 12 cm from the thin W target, and it was positioned at 0^o to the direction of the electron beam.

The induced activities of the activated samples were measured by a γ spectrometer without any chemical purification. The γ spectrometer consisted of a coaxial high purity germanium (HPGe) detector (ORTEC) with an energy resolution of 1.75 keV and a relative efficiency of 10% at the 1332.5 keV γ peak of ^{60}Co. The detector was coupled to a computer-based multichannel analyzer card system, which could determine the photopeak area of the γ spectrum with the Gamma Vision software, version 5.10, EG&G ORTEC. The detector efficiency was determined experimentally using a set of standard gamma sources. After measurement and analysis of the γ spectra, the radioactive isotopes under consideration were identified based on their characteristic γ ray energies and half-lives [16].

The experimental results at bremsstrahlung energies of 40, 45, 50, 55, and 60 MeV were 0.045 ± 0.003, 0.046 ± 0.003, 0.048 ± 0.003, 0.050 ± 0.003, and 0.049 ± 0.003 for the $^{120m,g}Sb$ isomeric pair, and 0.341±0.022, 0.362±0.020, 0.374±0.021, 0.371±0.021, and

0.358±0.022 for the ^{122m,g}Sb isomeric pair, respectively. We observed that the isomeric-yield ratios for the ^{nat}Sb(γ,xn)^{120m,g}Sb and ^{123}Sb(γ,n)^{122m,g}Sb reactions increased gradually as the incident bremsstrahlung energies increased from the reaction threshold to approximately 60 MeV. In addition, the effect of reaction channels on the production of the ^{120m,g}Sb and ^{122m,g}Sb isomeric pairs was also observed. The values provided by the experimental data for the photonuclear reactions [22] are relatively small compared with those measured by other reaction channels, such as (n,2n) [23], (p,n) [24], and (α,pn) reactions [25].

3.2. MEASUREMENT OF MASS-YIELD DISTRIBUTIONS FOR BREMSSTRAHLUNG-INDUCED FISSION OF ^{NAT}PB AND ^{209}BI

The mass-yield distribution of fission products in the 45–70 MeV and 2.5-GeV bremsstrahlung-induced fission of ^{nat}Pb and ^{209}Bi have been measured by using a recoil catcher and an off-line γ ray spectrometric technique.

The bremsstrahlung was produced when a pulsed electron beam from the 100-MeV electron linac hit a thin W target with a size of 10 cm × 10 cm and a thickness of 0.1 mm [3]. The W target is located at 18.0 cm from the beam exit window. A know amount (12.417 g) of ^{nat}Pb metal foil of 2 mm thick and a ^{209}Bi metal foil (74.417 g) of 3 mm thick and 25 cm^2 area was wrapped with 0.025 mm thick aluminum foil with purity more than 99.99%, respectively and was fixed on a stand in air at 12 cm from the tungsten metal foil. The target assembly was irradiated for 5-7 hours with the 45-70 MeV bremsstrahlung. The irradiated target assembly was cooled for half an hour or two hours.

The 2.5-GeV bremsstrahlung was produced when a pulsed electron beam from the main electron linac of PAL hit a tungsten (W) target with a size of 5 cm × 5 cm and a thickness of 1 mm. The W target was located 38.5 cm from the electron exit window. The details on the experiment are given elsewhere [26, 27]. The ^{nat}Pb metal foil of 0.5 mm thick and 25 cm^2 area (12.417 g) and the ^{209}Bi metal foil of 3 mm thick and 25 cm^2 area (74.417 g) were wrapped with 0.025 mm thick aluminum foil with purity more than 99.99%. Each sample was fixed on a stand in air 24 cm from the W target and positioned at 0^o with respect to the direction of the electron beam. Each sample was irradiated for 4-7 hours with the end point energy of 2.5 GeV bremsstrahlung. The irradiated target assembly was cooled for 2 hours.

The aluminum catcher and the lead or the bismuth foil were taken out from the irradiated assembly and were mounted separately on two different Perspex (acrylic glass, 1.5 mm thick) plates. The Perspex plate with an Al catcher contains primarily fission products together with reaction products from the Al catcher itself. The other Perspex plate with an irradiated Pb (Bi) metal foil contains fission products and significant (γ,*x*n) reaction products from the lead (bismuth) foil with high γ ray intensity.

The γ ray activities from fission and reaction products were measured using an energy- and efficiency-calibrated HPGe detector coupled to a PC-based 4K-channel analyzer. The HPGe detector with 20% efficiency was a p-type coaxial CANBERRA detector of 7.62 cm diameter × 7.62 cm length. The γ ray spectrum was obtained by using a program Gamma Vision 5.0 (EG&G Ortec).

The data analysis was done primarily from the γ ray spectrum of the fission products of the Al catcher to avoid difficulties of efficiency calibration for low energy g rays in the thick

lead or bismuth foil. The details on the data analysis are given elsewhere [26, 27]. The absolute cumulative yields of the various fission products as a function of the mass number for the 2.5-GeV bremsstrahlung-induced fission of ^{nat}Pb and ^{209}Bi are plotted in Fig. 6. We do not consider the charge distribution corrections on the cumulative yields because of the closeness of the fission products to the beta stability line. The yields of fission products are fitted with a Gaussian curve to obtain the mean mass and the FWHM of the mass-yield distribution. The mean mass and the FWHM of the mass-yield distribution for the photo-fission of ^{nat}Pb and ^{209}Bi at 2.5-GeV bremsstrahlung are 94±0.5 and 55.0±2.0 mass units, and 95.0±0.5 and 51.0±2.0 mass units, respectively. It can be seen from Fig. 6 that for both ^{nat}Pb and ^{209}Bi, the FWHM of the mass-yield distribution increases with increasing bremsstrahlung energy. On the other hand, the mean mass of the mass-yield distribution decreases with increasing bremsstrahlung energy. These phenomena are due to the increase of the multi-nucleon emission and due to the increase of the multi-nucleon emission and the multi-chance of fission probability with incre asing excitation energy.

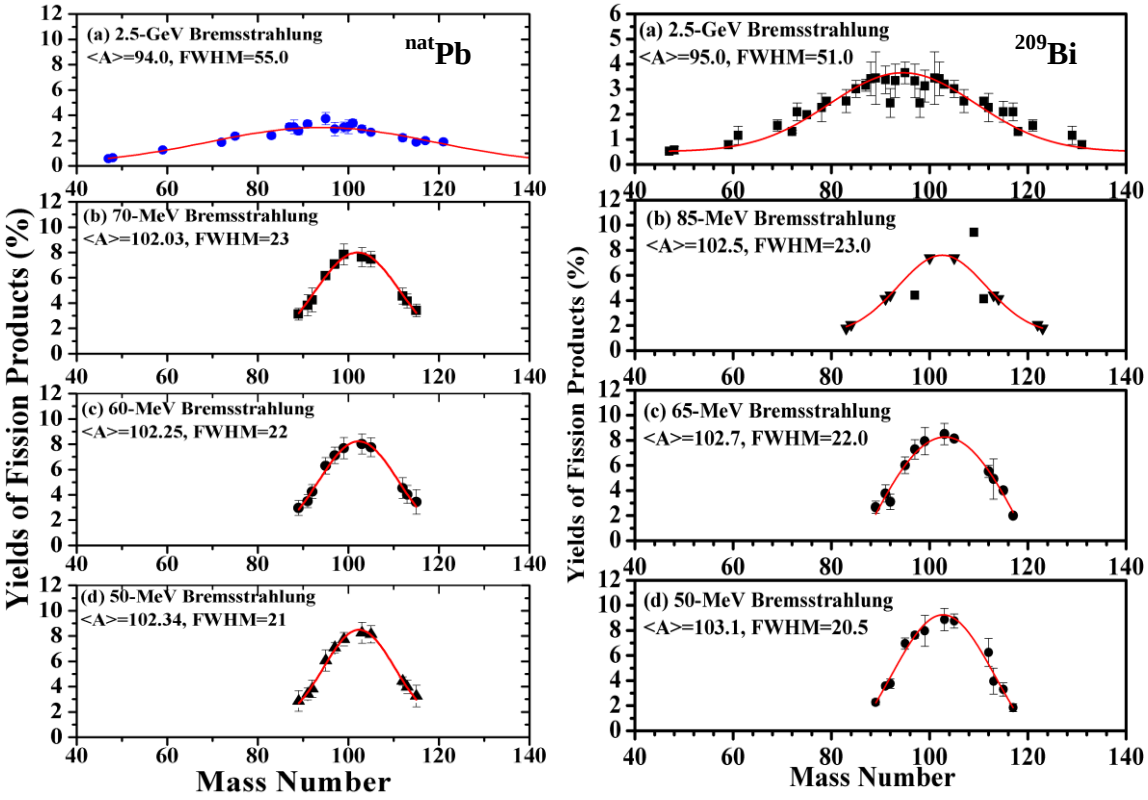

FIG. 6. Measured yields of fission products (%) from the photo-fission of ^{nat}Pb and ^{209}Bi as a function of the mass number. The line indicates the fitting for the measured data points <A> and FWHM are the mean mass number and the full-width at half-maximum of the mass-yield distribution.

3.3. MASS-YIELD DISTRIBUTIONS IN THE 50-80 MEV BREMSSTRAHLUNG-INDUCED FISSION OF ^{232}TH

The mass-yield distribution of fission products for 45-, 50-, -60-, 70-, and 80-MeV bremsstrahlung-induced fission of ^{232}Th are plotted in Fig. 7. There is a well-known third peak around the symmetric mass region in the mass-yield distribution of 10-80 MeV bremsstrahlung-induced fission of ^{232}Th as shown in Fig. 7, which is similar to ^{232}Th(n,f) [28-36]. It can be also seen from Fig. 7 that the yields of fission products for A= 133-134, 138-

3.3. Electron induced white spectrum neutron beams

139, and 143-144, and their complementary products are higher than those of the other fission products. A similar observation was shown by us in the neutron-induced fission of various actinides [37, 38], in the 10-MeV bremsstrahlung-induced fission of ^{232}Th, ^{238}U, and ^{240}Pu [39], and in the 50-70 MeV bremsstrahlung-induced fission of ^{232}Th [40]. Piessens *et al*. [41] and Pommé *et al*. [42] also observed the similar tendency in the bremsstrahlung-induced fission of ^{232}Th and ^{238}U in the energy region of 6.1-13.1 MeV. The higher yields of fission products for A=133-134, 138-139, and 143-144 and their complementary products are due to the corresponding even numbers of Z of 52, 54, and 56, respectively [39-41].

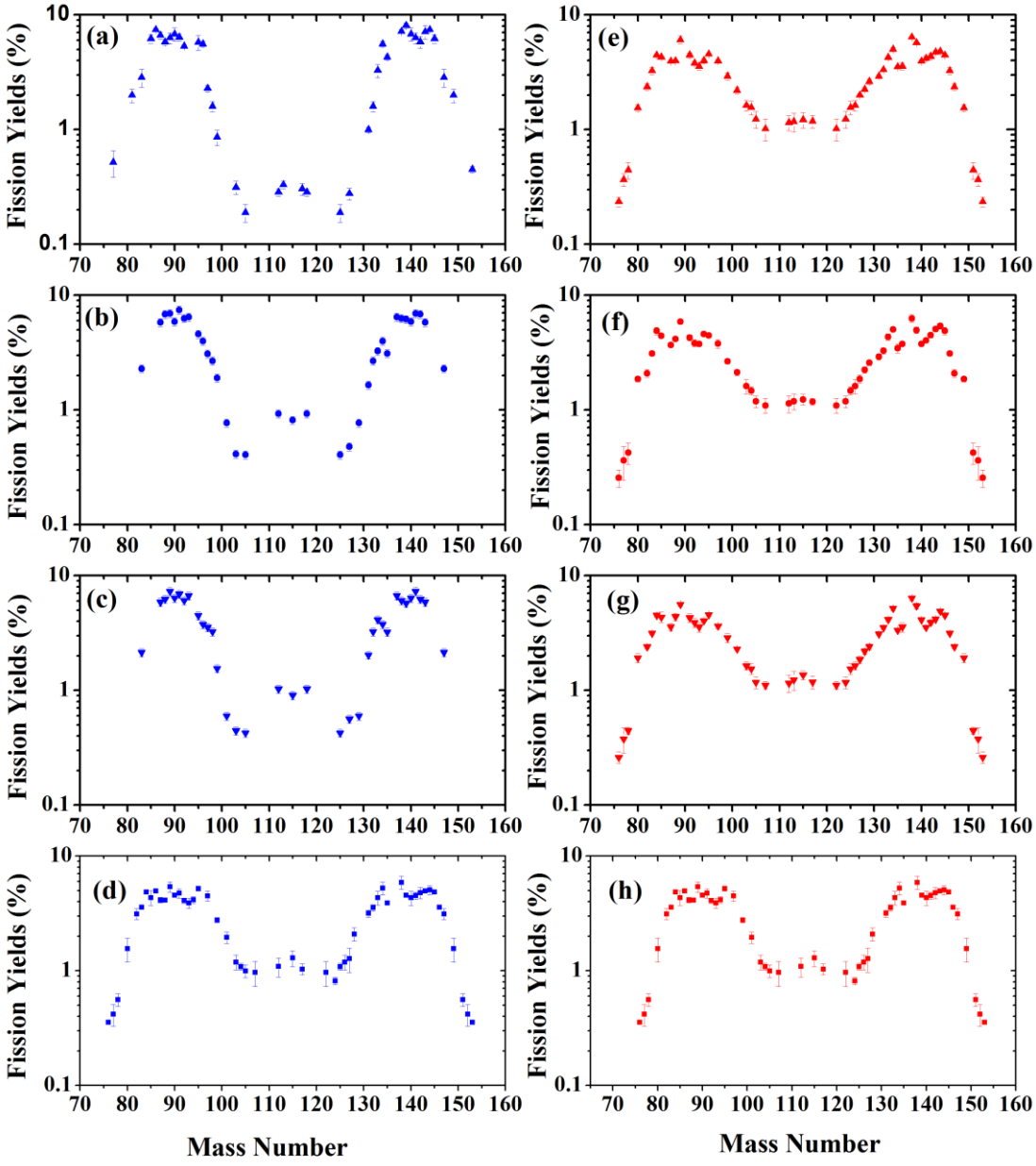

FIG. 7. The yields of fission products (%) as a function of mass number in (a) 10-, (b) 25-, (c) 40-, (d) 45-, (e) 50-, (f) 60-, (g) 70-, and (h) 80-MeV bremsstrahlung-induced fission of ^{232}Th.

3.3. Electron induced white spectrum neutron beams

4. DISCUSSION AND SUMMARY

The Pohang neutron facility based on an electron linac was constructed for nuclear data measurements in Korea. We presented the total cross-section measurement for Nb by the time-of-flight method and the thermal neutron capture cross-sections and the resonance integrals for the ^{165}Ho(n,γ)^{166g}Ho reaction by the neutron activation method. The isomeric-yield ratios for the ^{120m,g}Sb and ^{122m,g}Sb isomeric pairs produced by ^{nat}Sb(γ,xn)^{120m,g,122m,g}Sb photonuclear reactions in the bremsstrahlung energy region from 40 to 60 MeV with a step size of ΔE = 5 MeV by the activation method were presented. The mass-yield distribution of fission products from ^{nat}Pb, ^{209}Bi, and ^{232}Th with bremsstrahlung endpoint energies with 45-, 50-, 60-, 70-, 80-MeV, and 2.5-GeV using a recoil catcher and an off-line γ ray spectrometric technique were also presented.

ACKNOWLEDGMENTS

The authors would like to express their sincere thanks to the staff of the Pohang Accelerator Laboratory for the excellent operation of the electron linac and their strong support. This work was partly supported by Kyungpook National University Research Fund, 2012, by the National Research Foundation of Korea (NRF) through a grant provided by the Korean Ministry of Education, Science and Technology (MEST) in 2012 (Project No. 2010-0021375), by the World Class University (WCU) program (R31-30005), and by the Institutional Activity Program of Korea Atomic Research Institute.

REFERENCES

[1] KIM, G., N, et al., J. Korean Phys. Soc. 38 (1), 14-18 (2001).
[2] KIM, G., N. et al., Nucl. Instr. Meth. A 485, 458-467 (2002).
[3] NGUYEN, V. D., et al., J. Korean Phys. Soc. 48 (3), 382-389 (2006)
[4] SKOY, V.et al., J. Korean Phys. Soc. 41 (3), 314-321 (2002).
[5] MEAZE, A., et al., J. Korean Phys. Soc. 46 (2), 401-407 (2005).
[6] WANG, T.,et al., Nucl. Instr. Meth. B 268 (2), 106-113 (2010).
[7] ADIB, M., et al., <http://www.nndc.bnl.gov/exfor7/exfor00.htm>, EXFOR No. 30591.005 (1981).
[8] SERPA, M. R., <http://www.nndc.bnl.gov/exfor7/exfor00.htm>, EXFOR No. 10404.006 (1970).
[9] PILCHER, V. E., and Zimmerman, R. L., < http://www.nndc.bnl.gov/exfor7/exfor00.htm>, EXFOR No. 11909.002 (1955).
[10] SETH, K. K., et al, Phys. Rev. 110 (3), 692-700 (1958).
[11] CHADWICK, M. B., et al. NuclearData Sheets 107 (12), 2931-3060 (2006).
[12] SHIBATA, K., et al., J. Nucl. Sci. Technol. 39 (11), 1125-1136 (2002).
[13] LARSON, N. M., ORNL/TM-9179/R5, Oak Ridge National Laboratory (2000).
[14] NGUYEN, V. D., et al., Nucl. Instr. Meth. B 266, 863-871 (2008); V. D. Nguyen et al., Nucl. Instr. Meth. B 266, 21-29 (2008); V. D. Nguyen et al., Nucl. Instr. Meth. B 267, 462-468 (2009).
[15] NGUYEN, V. D., et al., Nucl. Instr. Meth. *B* 269, 159-166 (2011).
[16] FIRESTONE, R.B., et al., Table of Isotopes, eighth ed., Wiley, New York (update on CD-ROM), (1998).
[17] MUGHABGHAB, S.F., Neutron Cross Section, vol. 1. Academic Press, Inc., Sandiego, New York, Boston, London, Sydny, Tokyo, Toronto, 1984.

[18] RAJPUT, M.U., et al., *Radiochim. Acta* 97, 63 (2009); YUCEL, H., KARADAG, M., *Ann. Nucl. Energy* 32, 1 (2005); Kafala, S.I., *J. Radioanal. Nucl. Chem.* 215, 193 (1997); CORTE, F., SIMONITS, De A., *J. Radioanal. Nucl. Chem.* 133, 43 (1989); A. Simonits et al., *J. Radioanal. Nucl. Chem.* 81, 369 (1984).
[19] MUGHABGHAB, S.F., Thermal Neutron Capture Cross Section, Resonance Integrals and g Factor, INDC(NDS)-440, IAEA (2003); JFF Report 14, Table of Simple Integral Neutron Cross Section Data from JEFF-2.2, ENDF/B-VI, JENDL-3.2, BROND-2 and CENDL-2, OECD, (1994).
[20] RAHMAN Md. S., et al. *Nucl. Instr. Meth. B* 276, 44-50 (2012); Md. S. Rahman et al. *Nucl. Instr. Meth. B* 268, 13-19 (2010); Nguyen, V.D., et al., *J. Radianal Nucl. Chem.* 283, 683-690 (2010); Rahman Md. S., et al. *Nucl. Instr. Meth. B* 267, 3511-3518 (2009); V.D. Nguyen et al., *Nucl. Instr. Meth. B* 266, 5080-5086 (2008).
[21] NGUYEN, V.D., et al., *Nucl. Instr. Meth. B* 283, 40-45 (2012).
[22] DAVYDOV, M.G., et al., *At. Energ.* 84, 66 (1998); O.A. Bezshejko et al., *Akademii Nauk, Ser. Fiz.* 69, 663 (2005); T.D. Thiep et al., Commun. Phys. 4, 97 (1994) ; T.D. Thiep et al., *Sci. Bull., NCSR* 2, 25 (1987).
[23] KANDA, Y., *J. Phys. Soc. Japan* 24, 17 (1968); J.L. Casanova, M.L. Sanchez, *Anales de Fisica y Quimica* 71, 123 (1975); B. Minetti, A. Pasquarelli, *Z. Phys.* 217, 83 (1968); E. Rurarz et al., Acta Phys. Pol. B1, 415 (1970); S.K. Mangal, P.S. Gill, *Nucl. Phys.* 49, 510 (1963).
[24] SKAKUN, E.A., Batij, V.G., *Z. Phys. A* 344, 13 (1992); V.G. Batij et al., *Yad. Fiz.* 47, 978 (1988).
[25] BASKOVA K.A., et al., Proceedings of the 36th Annual Conference Nuclear Spectroscopic Structure At. Nuclei, Kharkov, 83 (1986); M.G. Davydov et al., *At. Energ.* 84, 66 (1998).
[26] NAIK, H., et al., *Eur. Phys. J.* A **47**(3), 37- 46 (2011).
[27] NAIK, H., et al., *Nucl. Instr. Meth.* B **267**(11), 1891-1898 (2009).
[28] BROOM, K. M., Phys. Rev. 133, B874 (1964).
[29] GANAPATHY, R., and KURODA, P. K., J. Inorg. Nucl. Chem. 28, 2017 (1966).
[30] MO, T., and RAO, M. N., J. Inorg. Nucl. Chem. 30, 345 (1968).
[31] THEIN, M. et al., J. Inorg. Nucl. Chem. 30, 1145 (1968).
[32] GEVAERT, L. H., et al., J. Chem. 48, 641 (1970).
[33] SWINDLE, D. L., et al., J. Inorg. Nucl. Chem. 33, 3643 (1971).
[34] TROCHON, J., et al., Nucl. Phys. A 318, 63 (1979).
[35] Glendenin, L. E., et al., Phys. Rev. C 22, 152 (1980).
[36] Lam, S. T., et al., Phys. Rev. C 28, 1212 (1983).
[37] Naik, H., et al., Radiochimica Acta 75, 69 (1996).
[38] IYER, R. H., et al., Nucl. Sci. Eng. 135, 227 (2000).
[39] NAIK, H.V., et al., Nucl Phys. A 853, 1 (2011).
[40] NAIK, H., et al., Phys. Rev. C 85, 024623 (2012).
[41] PIESSENS, M., et al., Nucl Phys. A 556, 88 (1993).
[42] POMMÉ, S., et al., Nucl. Phys. A 572, 237 (1994).

3.3. Electron induced white spectrum neutron beams

NUCLEAR DATA MEASUREMENT AT KURRI-LINAC

J. HORI

Research Reactor Institute, Kyoto University, Kumatori-cho, Sennan-gun, Osaka 590-0494, Japan

Email:hori@rri.kyoto-u.ac.jp

Abstract

The electron linear accelerator (KURRI-LINAC) has been used for nuclear data measurement as a pulsed white neutron source since 1965. Recently, the systematic study of neutron cross sections of minor actinides (MAs) and long-lived fission products (LLFPs) has been performed for nuclear transmutation of nuclear waste. The KURRI-LINAC consists of a 46-MeV electron linear accelerator and a water-cooled Ta target with a light water moderator. Maximum beam power is 6 kW and the pulse width is ranged from 2 ns to 4 μs. There are three flight paths of 10, 12 and 22 m for neutron capture cross section measurements with the time-of-flight technique. There is also a lead slowing-down spectrometer for fission cross section measurements. In this paper the outline of the experimental arrangement is overviewed.

1. INTRODUCTION

The electron linear accelerator at the Research Reactor Institute, Kyoto University (KURRI-LINAC) was originally established in 1965 by the High Voltage Engineering Co., USA and started as a 23 MeV machine. In 1971, the machine power was increased to 46 MeV. The KURRI-LINAC has been used as intense electron, neutron and photon sources in various research subjects of nuclear data measurement, isotope production by photo-reactions, photon activation analysis, low-temperature electron irradiation, and spectroscopy with coherent THz radiation. About one third of operation time was spent for the nuclear data measurement with the neutron time-of-flight (TOF) method and a lead slowing-down spectrometer. Most of recent nuclear data researches were carried out as collaborative works with Tokyo Institute of Technology, Hokkaido University, Japan Atomic Energy Agency and Tohoku University. Those works were financial supported from the Innovative Nuclear Research and Development Projects such as titled “Fundamental R&D on Neutron Cross Sections for Innovative Reactors using Advanced Radiation Measurement Technology” (fiscal year 2002 to 2006) and “Study on Nuclear Data by using a High Intensity Pulsed Neutron Source for Advanced Nuclear System” (fiscal year 2005 to 2009) of the Ministry of Education, Culture, Sports, Science and Technology of Japan [1, 2]. Moreover, the next project titled “Systematic Study on Neutron Capture Reaction Cross Sections for the Technological Development of Nuclear Transmutation of Long-Lived Nuclear Wastes” was started in 2010 with financial support from the Grants-in-Aid for Scientific Research (KAKENHI) of the Japan Society for the Promotion of Science [3]. A part of the projects was performed using the KURRI-LINAC. The results of those projects have been described in detail elsewhere [4-8], so the outline of the experimental arrangement such as characteristics of the accelerator, neutron source and measurement equipments of the KURRI-LINAC is overviewed in this paper.

2. THE KURRI-LINAC FACILITY

The KURRI-LINAC facility is an L-band electron linear accelerator which produces a maximum power of 6 kW electron beam with an energy of 30 MeV. Maximum energy is 46 MeV with no-load. It consists of an electric gun, a RF source, a pre-buncher, 2.000 and 1.845 m-long two accelerator tubes and a beam transport system. Two different operation modes are selectable. One is a long mode with a maximum repetition rate of 120 Hz, a pulse width of 0.1-4.0 μs, a peak current of about 0.5 A. Another is a short mode with a maximum repetition rate of 300 Hz, a pulse width of 2-100 ns, a peak current of about 5 A. In the short

3.3. Electron induced white spectrum neutron beams

mode, the electron gun can produce short bursts of electrons with 100 keV and 10 A. The frequency of RF is 1300.8 MHz. Two klystrons produce electromagnetic waves, which are injected into the accelerator tubes.

The layout of the KURRI-LINAC is shown in Fig. 1. A picture of the accelerator room is shown in Fig. 2. A water-cooled photo-neutron target was set at the target room. The target assembly [9] is composed of twelve sheets of Ta plate with the total thickness of 29 mm in a cylindrical titanium case 5 cm in diameter and 6 cm long. To enhance the neutron flux in thermal and epi-thermal regions, a light water moderator in an aluminum canning was placed around the target assembly. There are two kinds of light water moderators. One is a water tank, 30 cm in diameter and 35 cm height. Another is an octagonal shape moderator in a 10 cm thick and 30 cm diameter as shown in Fig. 3. Two flight paths are in the direction of 90° and 135° to the linac electron beam. Two measuring stations at 10 and 22 m from the target on the 90° beam line and a measuring station at 12 m from the target on the 135° beam line are located, respectively. A lead shadow bar, 5 cm in diameter and 10 cm long, was placed on the neutron beam axis in front of Ta target to reduce intense gamma-flash from the target effectively. The neutron beam was collimated from about 12 cm in diameter at the entrance of the flight tube to about 2 cm in diameter at the measuring positions with the collimators composed of B_4C, Li_2CO_3, Pb and borated paraffin. At those stations, neutron capture cross section measurements are performed.

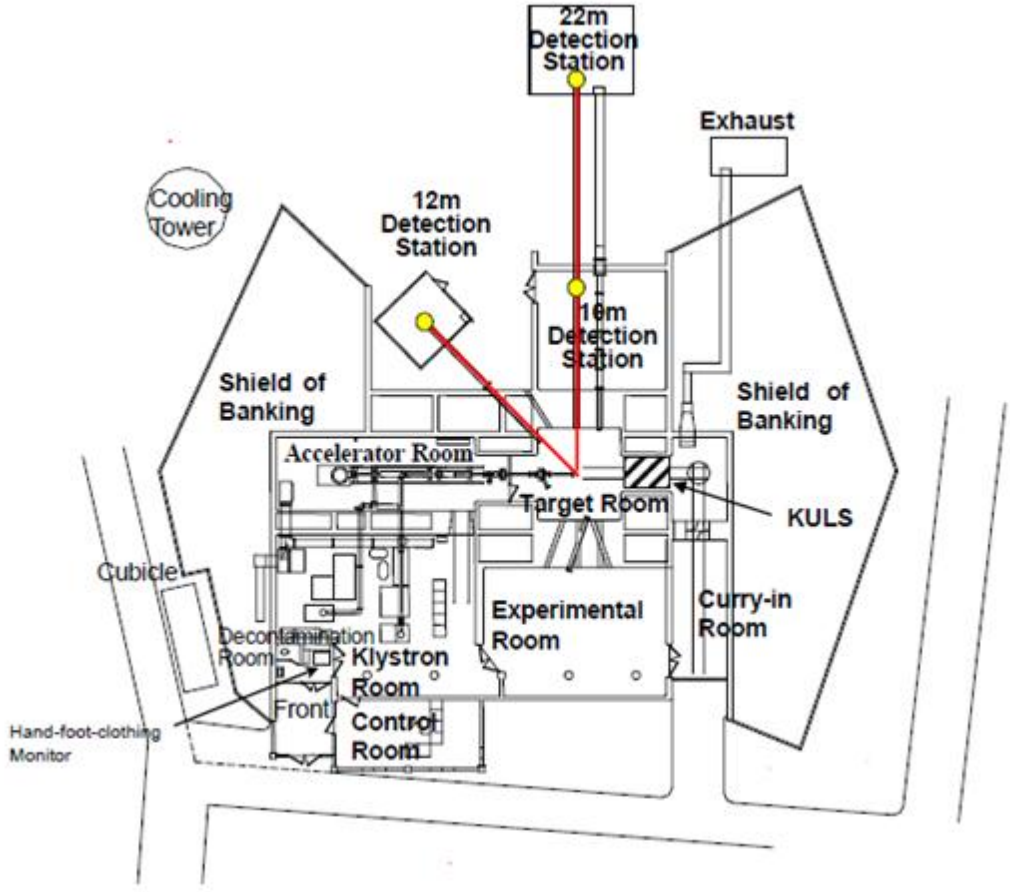

FIG. 1. Layout of the KURRI-LINAC

3.3. Electron induced white spectrum neutron beams

Though almost beam path was evacuated, there is a gap between two evacuated flight tubes. A BF_3 proportional counter was set in the gap as a neutron intensity monitor. The edge of the last flight tube was not evacuated. The Kyoto University Lead slowing-down Spectrometer (KULS) was installed in the target room for neutron fission cross section measurements.

FIG. 2. Picture of the accelerator room.

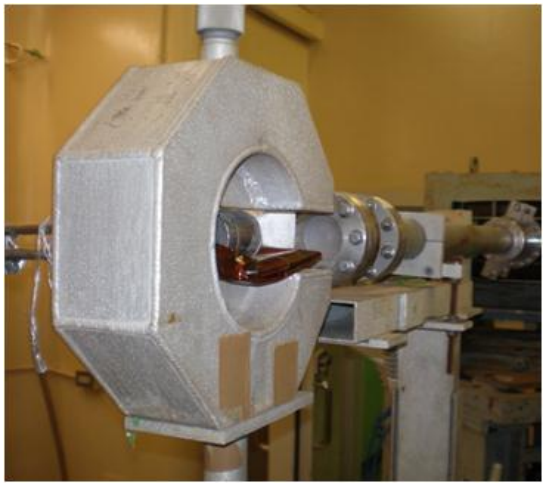

FIG. 3. Picture of the neutron target and moderator.

3. MEASUREMENT EQUIPMENT

3.1. DETECTORS FOR NEUTRON CAPTURE CROSS SECTION MEASUREMENT

Two kinds of detectors were installed for the detection of neutron capture γ rays from the sample. One is a pair of C_6D_6 liquid scintillators which are 11 cm in diameter and 5 cm thick. Since the detector has a low sensitivity to scattered neutrons, it is useful to measure the capture γ rays with a large amount of sample. The neutron capture cross section of ^{237}Np was measured with a pair of C_6D_6 liquid scintillators [10]. The detector should be used as a total energy detector in combination with the Pulse Height Weighting Technique [11]. Recently, the weighting function was obtained using the response function that were calculated with a Monte-Carlo simulation code EGS5 [12] and applied to the neutron capture cross section measurements of $^{151, 153}$Eu [13]. The neutron capture cross section measurement on ^{243}Am is ongoing with the detector.

Another is a detection assembly of $Bi_4Ge_3O_{12}$ (BGO) scintillators, which consists of twelve scintillation bricks of each $5\times5\times7.5$ cm^3 [14]. The total volume of the BGO scintillators is about 2.25 liters. Figure 4 shows the experimental arrangement with the BGO assembly. A through-hole of 1.8×1.8 cm^2 is made in the BGO assembly and a collimated neutron beam is led through the hole to the sample. The sample position is fixed at 12.7 ± 0.02 m from the neutron target. The assembly was shielded with lead blocks of 5 to 10 cm in thickness against background radiation from the surroundings. The inside of the through-hole was covered with ^{6}LiF tiles of 3 mm in thickness to absorb neutrons scattered by the sample as shown in Fig. 5. As the BGO assembly has a large efficiency for γ rays and 4π geometry around the sample, the detection efficiency of a capture event is sufficiently high to be considered as a constant independent of neutron energy. Therefore, the detector was used as a total absorption detector.

3.3. Electron induced white spectrum neutron beams

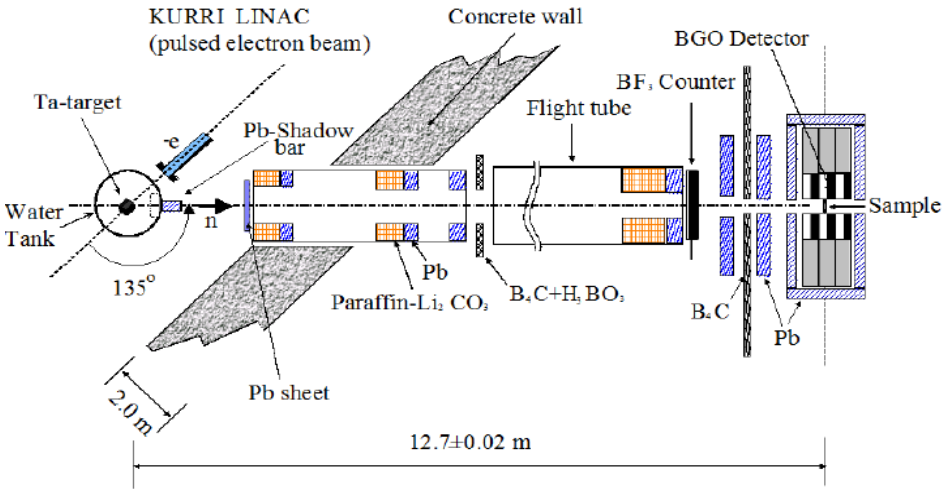

FIG. 4. Experimental arrangement for the TOF measurement with the BGO assembly.

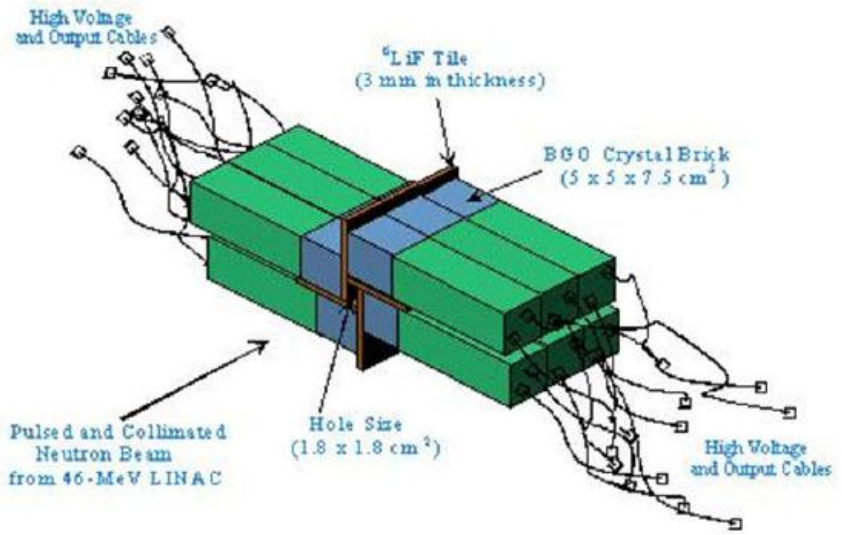

FIG. 5. BGO assemble for neutron capture cross section measurement.

Since the BGO assembly has a high sensitivity to scattered neutrons, it is useful to measure the capture γ rays with a small amount of sample which has not a large value of scattering-to-capture ratio.

Neutron capture cross section has been measured relative to the $^{10}B(n,\alpha\gamma)$ standard cross section. It is worth noting that the $^{10}B(n,\alpha\gamma)$ reaction emits a single γ ray of 478 keV independent of neutron energy. Therefore, the detection efficiency can be determined at any neutron energy. In the measurement with the BGO assembly, the detection efficiency was experimentally determined to be 0.82 at thermal energy as described before [14] and absolute neutron flux measurement is available. Typical results of absolute neutron flux measurements in short and long operation modes at the sample position of the BGO assembly are shown in Fig. 6. The long mode operation with a pulse width of 4 μs, a repetition rate of 50 Hz and a peak current of 0.5 A was used for the measurement at low energies below 10 eV.

3.3. Electron induced white spectrum neutron beams

The short mode operation with a pulse width of 100 ns, a repetition rate of 300 Hz and a peak current of 5 A was used for the measurement at high energies above 1 eV. In the short mode operation, a cadmium sheet of 0.5 mm in thickness was inserted into the TOF neutron beam to avoid overlap of neutrons from the previous pulses due to the high frequency. A Maxwellian peak can be observed around thermal energy region in the only long mode. In the epi-thermal neutron region, the neutron flux in the short mode is approximately equals to that in the long mode. Neutron capture cross sections of LLFP and its stable isotopes with the BGO assembly have been measured. Some of the results have been already been published [15, 16].

3.2. KULS FOR NEUTRON FISSION CROSS SECTION MEASUREMENT

The lead slowing-down spectrometer originally installed at University of Tokyo [17] was transferred to KURRI in 1991. The spectrometer was coupled to the KURRI-LINAC and called as Kyoto University Lead Slowing-down Spectrometer (KULS) [18]. A picture of the KULS is shown in Fig. 6. The KULS is a 1.5 meter-cube and about 40 tons in weight, which consists of about 1600 lead blocks (each size: $10\times10\times20$ cm^3, and purity 99.9%). The KULS is set on a platform car in the target room so that it can be removed behind the target room when TOF experiment is carried out as shown in Fig. 1.

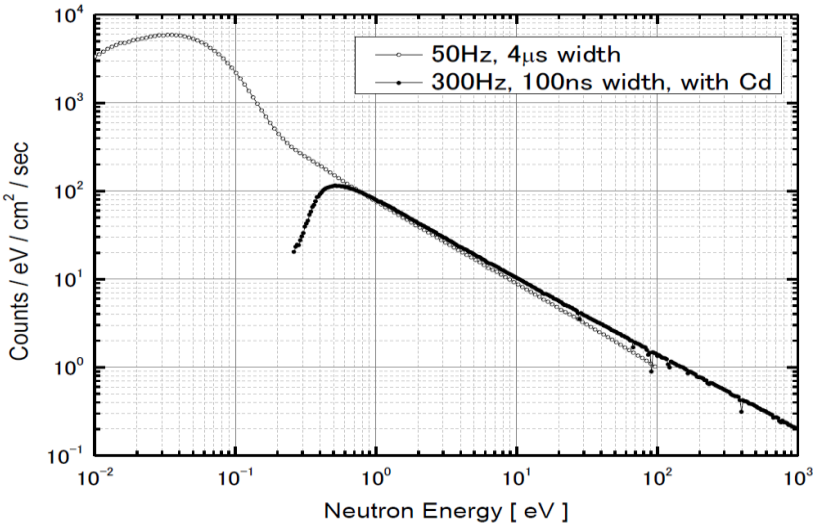

FIG. 6. Neutron fluxes at 12.7 m flight path with short and long operation modes.

A photo-neutron Ta target assembly cooled by compressed air flow as described above was set in the center of KLUS through a beam hole. There are eight experimental holes (10×10 cm^2, 55 or 45 cm in depth) to the spectrometer. One of the lead holes was covered by a bismuth layer of 10 to 15 cm (neutron source side of the hole) in thickness to shield high energy γ rays (6 to 7 MeV) by the Pb(n, γ) reaction in the spectrometer. For the fission event measurement, the bismuth layers can reduce background due to photo-fission events. All sides of the KULS, except for the experimental holes, were covered with cadmium sheet of 0.5 mm in thickness to shield low energy neutrons scattered from the surroundings. Lead is one of the heavy mass elements which has the neutron total cross section mainly consists of elastic scattering cross section. Therefore, the neutrons are slowed down by repeating many elastic scattering processes when pulsed neutrons are generated in the center of assemble and the slowing-down time corresponds to the neutron energy. The detail characteristics of KULS

were reported [18]. An advantage of the KULS is that neutron flux is three or more orders higher than that in the TOF experiment because the distance between photo-neutron source and sample can be close to about 12 cm. However, the neutron energy resolution of the KULS was not so good, which was obtained to be around 40% [18].

In order to obtain the neutron-induced fission cross sections, a back-to-back (BTB) type of double fission chamber was used as a fission fragment detector. The ionization chamber has two parallel electrodes so that two different deposited samples of a standard and a measuring object can be irradiated with the same condition. Making use of the BTB chamber and the KULS, the neutron-induced fission cross sections of a few MAs and nuclear fuel materials were measured relative to that of the ^{235}U(n,f) reaction. The results have already been published [10, 19-23]. Recently, a multi-layered plate ionization chamber (MLPPIC) was developed to obtain higher performance in particle discrimination [24]. Some results using the MLPPIC and the KULS can be found in the following references [24-26].

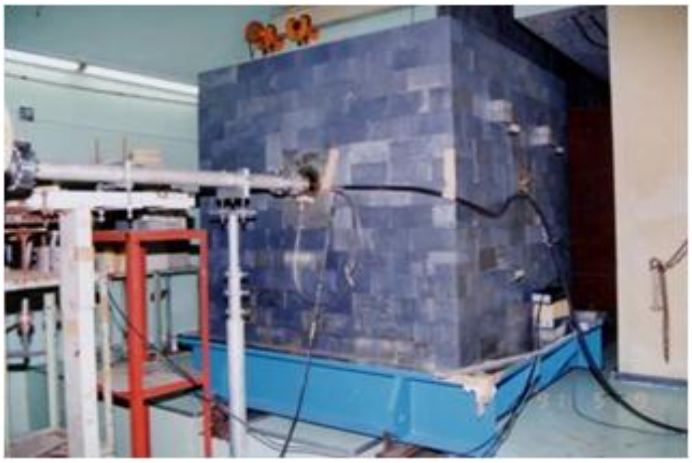

FIG. 7. Picture of the Kyoto University Lead Spectrometer

3.3. DATA ACQUISITION SYSTEM

Three types of data acquisition systems are available for measuring neutron capture rays as a two-dimensional list data of TOF and pulse-height (P.H.) in the KURRI-LINAC. The first system is the FAST ComTec's MPA-3 (PC-board Multiparameter Multichannel Analyzer System). Coincident events can be defined as almost any combination of external ADCs and time-of-flight units. The second item is the Yokogawa's WE7562 multi channel analyzer. In the module, the PH value was obtained with a digital sampling method and the timing of detection was stored as a time stamp. In the case of neutron capture cross section measurement, two input signals of the trigger from the linac and the neutron capture events from the detector were digitalized independently. The program searches the trigger signal corresponding to each capture γ ray signal and makes a set of TOF and PH values. The method is applicable to measurement on a wide energy range because there is no upper limit of TOF measurement. The third item is the Acqiris's DP235 Dual-Channel PCI Digitizer Card which is a fast waveform recorder. Every signal from the γ ray detector was stored as a waveform with the Acqiris DP235 for each shot. The peak search and undershoot correction are able to be performed in offline analysis. The intense γ ray flash distorts the pulse height of the detector at the initial TOF. Therefore, the method is appreciable to measurement in fast neutron energy region.

4. SUMMARY

The KURRI-LINAC has been used for the nuclear data measurement as a pulsed white neutron source. Recently, the systematic study of neutron cross sections of MAs and LLFPs has been performed for nuclear transmutation of nuclear waste. There are three flight paths of 10, 12 and 22 m for neutron capture cross section measurements with the TOF method and a lead slowing-down spectrometer for neutron-induced fission cross section measurements. This paper overviewed the outline of the experimental arrangement such as characteristics of the accelerator, neutron source and measurement equipments and the current status of nuclear data measurement in the KURRI-LINAC.

ACKNOWLEDGEMENTS

I would like to express my thanks to many collaborators in KURRI (Drs. K. Nakajima, H. Yashima, J. H. Lee, H. Yamana, T. Fujii and S. Fukutani), TIT (Drs. M. Igashira, M. Mizumoto, and T. Katabuchi), Hokkaido University (Drs. Y. Kiyanagi and K. Kino), JAEA (Drs. M. Oshima, H. Harada, K. Furutaka, S. Goko, A. Kimura, T. Kin, F. Kitatani, M. Koizumi and S. Nakamura) for neutron capture cross section measurements in KURRI-LINAC, and also collaborators in KURRI (Drs. K. Takamiya and S. Sekimoto), Tohoku University (Drs. T. Ohtsuki, Y.Shibasaki and N. Iwasa) and JAEA (Drs. K. Hirose and K. Nishio) for neutron-induced fission cross section measurements in KULS. I am much indebted to the linac staff for operation and support and Drs. K. Kobayashi, S. Yamamoto and S. Lee for their encouragement and invaluable suggestions. This study includes the results of "Fundamental R&D on Neutron Cross Section for Innovative Reactors using Advanced Radiation Measurement Technology" entrusted to Tokyo Institute of Technology and "Study on Nuclear Data by using a High Intensity Pulsed Neutron Source for Advanced Nuclear System" entrusted to Hokkaido University by the Ministry of Education, Culture, Sports, Scientific and Technology of Japan (MEXT). This work is supported by JSPS KAKENHI Grand Number 22226016.

REFERENCES

[1] IGASHIRA, M., et al., "A nuclear data project in Japan", Proc. of Int. Conf. on Nuclear Data for Science and Technology 2004 (ND2004), Santa Fe, Sep. 26- Oct. 1, 2004, 1-2 (2005).

[2] KIYANAGI, Y., et al., "The 'Study on Nuclear Data by Using a High Intensity Pulsed Neutron Source for Advanced Nuclear System' Nuclear Data Project and the Characteristics of the Neutron Beam Line for the Capture Cross Section Experiments at J-PARC", Journal of Korean Physics Society, 59 (2011) 1791-1784.

[3] IGASHIRA, M., "Systematic Study on Neutron Capture Reaction Cross Sections for the Technological Development of Nuclear Transmutation of Long-Lived Nuclear Wastes", http://www.jsps.go.jp/j-grandsinaid/12_kiban/ichiran_22/edata/e66_igashira.pdf

[4] KOIZUMI, M., et al., "Minor actinide neutron capture cross-section measurements with a 4π Ge spectrometer", Nucl. Instrum. and Methods, A 562 (2006) 767-770.

[5] MIZUMOTO, M., et al, "Neutron capture cross section measurements on ^{237}Np with a 4π Ge spectrometer", Proc. of Int. Conf. on Nuclear Data for Science and Technology 2007 (ND2007), Nice, France, Apr. 22-27, 2007, 591-594 (2008).

[6] OSHIMA, M., et al., "Performance of 4p Ge spectrometer for neutron capture cross section measurements", Proc. of Int. Conf. on Nuclear Data for Science and Technology 2007 (ND2007), Nice, France, Apr. 22-27, 2007, 603-606 (2008).
[7] HORI, J., et al., "Neutron Capture Cross Section Measurement on ^{243}Am with a 4π Ge spectrometer", Proc. the 2008 Symposium on Nuclear Data, JAEA-Conf-2009-004, 123-128 (2009).
[8] HARADA, H., et al., "Study of Neutron Capture Reactions Using the 4π Ge Spectrometer", Journal of Korean Physics Society, 59 (2011) 1547-1552.
[9] KOBAYASHI, K., et al., "KURRI-Linac as a Neutron Source for Irradiation", Annu. Rep. Res. Reactor Inst. Kyoto Univ., 22 (1987) 142-153.
[10] KOBAYASHI, K., et al., "Measurement of Neutron Capture Cross Section of ^{237}Np by Linac Time-of-Flight Method and with Linac-driven Lead Slowing-down Spectrometer", J. Nucl. Sci. Technol., 39 (2002) 111-119.
[11] MACKLIN, R. L. and GIBBONS, J. H., "Capture-Cross-Section Studies for 30-220-keV Neutrons Using a New Technique", Phys. Rev., 159, (1967) 1007-1012.
[12] HIRAYAMA, H., et al., "The EGS5 Code System", Stanford Linear Accelerator Center Report SLAC-R-730 (2005).
[13] LEE, J. H., et al., "Measurement of $^{151, 153}$Eu Neutron Capture Cross Sections using a pair of C_6D_6 Detectors", Proc. the 2010 Symposium on Nuclear Data, JAEA-Conf-2011-002, 101-106 (2011).
[14] YAMAMOTO, S., et al., "Application of BGO Scintillators to Absolute Measurement of Neutron Capture Cross Sections between 0.01 eV and 10 eV", J. Nucl. Sci. Technol., 33 (1996) 815-820.
[15] KOBAYASHI, K., et al., "Neutron Capture Cross-Section Measurement of ^{99}Tc by Linac Time-of-Flight Method and the Resonance Analysis", Nucl. Sci. Engin., 146 (2004) 209-220.
[16] KOBAYASHI, K., et al., "Neutron Capture Cross Section Measurements of I-129, Cs-133 and Pr-141 with linac time-of-flight method", Proc. of 11th Int. Symp. On Reactor Dosimetry, Brussels, Belgium, Aug. 18-23, 2002, 588-596 (2003).
[17] WAKABAYASHI, H., et al., "Some New Applications of Neutron Slowing Down Time Spectrometry", J. Nucl. Sci. Technol., 7 (1970) 487-499.
[18] KOBAYASHI, K. et al., "Characteristics of the Kyoto University Lead Slowing-down Spectrometer (KULS) coupled to an electron linac", Nucl. Instrum. Methods, A 385 (1997) 145-156.
[19] YAMAMOTO, S., et al., "Fission cross-section meausurements of Am-241 between 0.1 eV to 10 keV with lead slowing-down spectrometer and at thermal neutron energy", Nucl. Sci. Engin., 126 (1997) 201-212.
[20] KOBAYASHi, K., et al., "Measurements of neutron-induced fission cross section of americium-243 from thermal neutron energy to 15 keV using lead spectrometer and thermal neutron facility", J. Nucl. Sci. Technol., 36 (1999) 20-28.
[21] KOBAYASHI, K., et al., "Measurements of neutron-induced fission cross section of protactinium-231 from 0.1 eV to 10 keV with lead slowing-down spectrometer and at 0.0253 eV with thermal neutron facility", J. Nucl. Sci. Technol., 36 (1999) 549-551.
[22] KOBAYASHI, K., et al., "Measurement of Neutron-Induced Fission Cross Sections of ^{229}Th and ^{231}Pa Using Linac-Driven Lead Slowing-Down Spectrometer", Nucl. Sci. Engin., 139 (2001) 273-281.
[23] KAI, T., et al., "Measurements of neutron induced fission cross-section for Am-242m from 0.003 eV to 10 keV using lead slowing-down spectrometer, thermal neutron facility and time-of-flight method", Annals of Nuclear Energy, 28 (2001) 723-739.

3.3. Electron induced white spectrum neutron beams

[24] HIROSE, K., et al., "Multi-layered parallel plate ionization chamber for cross-section measurements of minor actinides", Nucl. Instrum. Meth., A 621 (2010) 379-382.
[25] HIROSE, K., et al., "Cross-section Measurements for Neutron-induced Fission of Minor Actinides with Lead Slowing-down Spectrometer at KURRI", Journal of Korean Physics Society, 59 (2011) 1733-1736.
[26] HIROSE, K., et al., "Fission cross-section measurements of ^{237}Np, ^{242m}Am, and ^{245}Cm with lead slowing-down neutron spectrometer", J. Nucl. Sci. Technol., 49 (2012) 1057-1066.

3. ACCELERATOR BASED NEUTRON BEAM FACILITIES

3.4. SPALLATION PROTON-INDUCED (>200MeV) WHITE SPECTRUM NEUTRON BEAMS

3.4. Spallation proton-induced (>200MeV) white spectrum neutron beams

STUDY OF BACK-STREAMING WHITE NEUTRONS AT CSNS FOR NUCLEAR DATA MEASUREMENT

X.C. Ruan[*], H.T. Jing[**], J.Y. Tang[**], H.Q. Tang[*], J. Ren[*]

[*]China Institute of Atomic Energy, Beijing 102413, China
[**]Institute of High Energy Physics, CAS, Beijing 100049, China
Email: ntof@ciae.ac.cn

Abstract

The characteristics of the back-streaming neutrons through the incoming proton channel at the spallation target station of China Spallation Neutron Source (CSNS) were studied for nuclear data measurement. The neutron yields and energy spectrum as well as the time structures of the neutrons from a tungsten target impinged by a proton beam of 1.6 GeV in energy and 63 μA in average current were simulated. Based on this study, two experimental halls for nuclear data measurement have were proposed and the civil construction is undergoing. Some neutron cross section measurement programs are considered.

1. INSTRUCTION

China Spallation Neutron Source (CSNS) is a large scientific facility dedicated mainly to multidisciplinary research on material characterization using the neutron scattering techniques [1, 2]. This project was officially approved by the Chinese central government in 2008, and will be in operation in 2018 for the 1st stage. In the first phase (CSNS-I), the machine will deliver 1.6 GeV protons on a tungsten target (TS1 [3,4]) with 100 kW beam power and a pulse repetition rate of 25 Hz. It is planned to build 18 neutron beam lines for neutron scattering at TS1. Applications other than using neutron scattering techniques such as muon source and white neutron source were proposed to be exploited in the second phase (CSNS-II)[5,6]. However, the CSNS-II is far away from now, therefore study of the applications based on muon source and white neutrons with CSNS-I is important at this stage. In this report, the characteristics of the back-streaming neutrons through the incoming proton channel at the spallation target station of CSNS-I were studied for nuclear data measurement. The back-streaming neutrons are harmful to the proton beam line and should be dealt with carefully. But on the other hand, those back-streaming neutrons may be useful for other applications, such as nuclear data measurement, neutron induced SEE study, neutron radiography, and so on.

THE NEUTRON BEAM CHARACTERISTICS

Detailed study of the characteristics for the back-streaming neutrons at CSNS is described in ref. [7]. Here only a brief description is given.

Figure 1 shows the neutron intensity as a function of neutron energy of CSNS compared with those of LANSCE and CERN_ntof. One can see that the CSNS can provide intensive neutrons over the neutron energy from eV to GeV. This is essentially important for nuclear data measurement, low reaction cross section measurement can be performed or small samples (especially for radioactive isotopes) can be used.

Another key characteristic for a pulsed white neutron source is time resolution. This is important for cross section measurement using the Time-Of-Flight (TOF) technique, especially at the resonance region. The CSNS accelerator is designed to operate in 3 modes:

double bunch mode, single bunch mode and a special mode with 3.7 ns FWHM beam width. Normally the machine will be operated in double bunch mode with a repetition rate of 25 Hz. In this mode each proton pulse has two bunches with a discrepancy of less than 1% in intensity between them. The width of the bunch is about 50 ns and the time interval between the two bunches is 400 ns, respectively. It is also possible to operate the CSNS accelerator in 2 special modes where the accelerator provides only one bunch in each proton pulse.

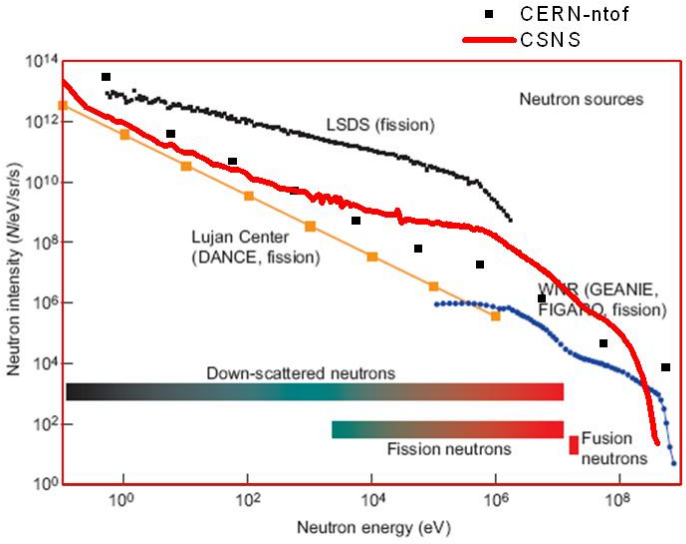

FIG.1. The neutron intensity of CSNS compared with those of LANSCE and CERN_ntof.

The width of the bunch can be 50 ns as usual and also can be adjusted to about 3.7 ns. The beam power for these two modes will be 50% and 30% as usual. Based on this design, Fig. 2 shows the time resolution of CSNS compared with that of CERN_ntof. The results shown in the figure were obtained with 80 meters away from the spallation target. The resolution of CSNS is not very good, but it is acceptable. One can see that the resolution is always better than 1% from eV to 100 MeV if the machine deliver the proton beam on the target with 3.7 ns width. For low energy neutrons (< 1 keV), the neutron transportation in the target will mainly contribute to the time resolution, since we have a 60 cm long target. While at higher energy, the proton beam pulse width will play a significant role. It should be noted that in reality, the resolution may be better because in this study, the energy bin width taken in the simulation is about 0.5%. It will play a main role in the results.

NEUTRON CROSS SECTION MEASUREMENT USING CSNS BACK-STREAMING NEUTRON BEAM

High precision neutron cross-section data are very important for a wide variety of research fields in basic and applied nuclear physics. In particular, neutron data on neutron-nucleus reactions are essential in Nuclear Astrophysics for understanding the production rate of heavy elements in the Universe, which occurs mainly through slow and rapid neutron capture processes during the various phases of stellar evolution [8, 9]. In the field of nuclear technology, more and more interests on new generation nuclear energy systems such as fast breeder reactors or accelerator driven system have aroused. Many studies aimed at developing these new systems that would address major safety, proliferation and waste concerns have been carried out. For these applications the available nuclear data for many nuclides is of insufficient accuracy and sometimes even lacking [10-13].

3.4. Spallation proton-induced (>200MeV) white spectrum neutron beams

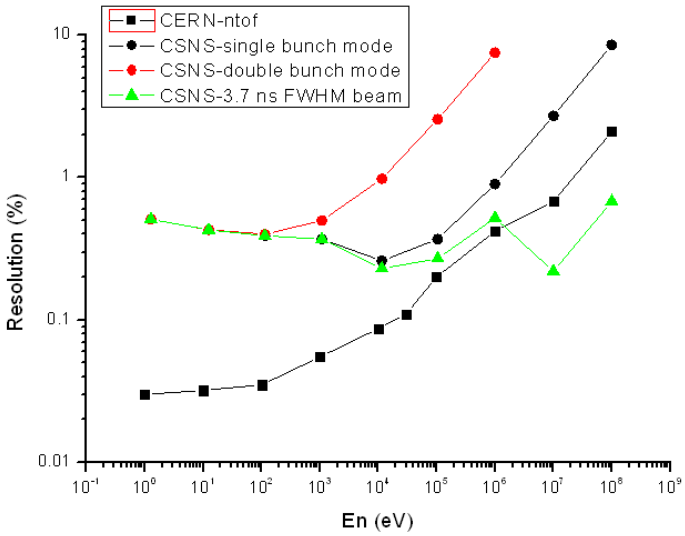

FIG.2. Time resolution obtained at 80 meters away from the target.

Based on the neutron beam characteristics study, a nuclear data measurement program using the CSNS back-streaming neutron beam was proposed. The layout of the neutron beam tunnel and the experimental halls are shown in Fig.3. Two end stations are under construction, with ~50 meters flight path for end station 1 and ~80 meters for end station 2, respectively. The maximum flight path is limited by the space, for the left side of the end station 2 shown in Fig.3 is occupied by a building. The end station 1 will be used for higher neutron flux required experiment while the end station 2 for better time resolution required experiment.

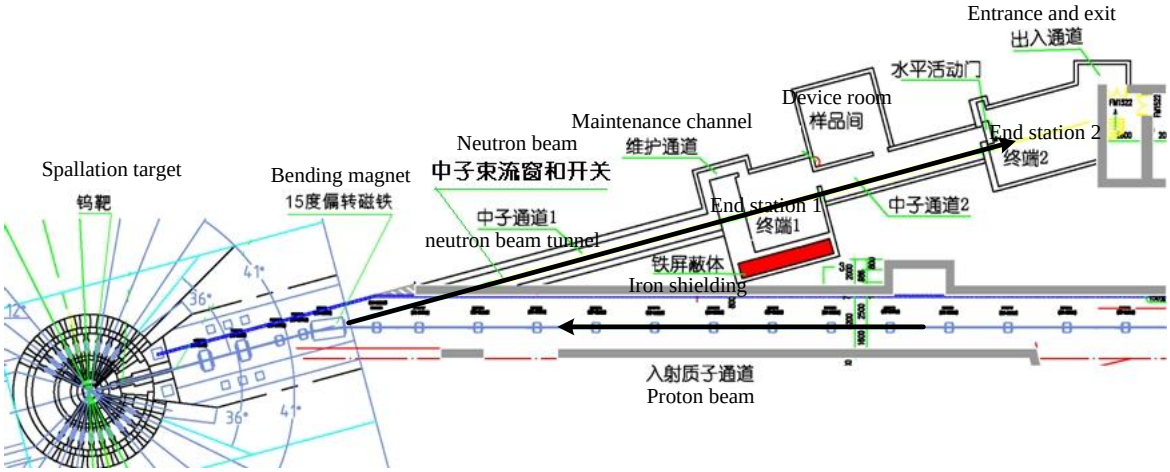

FIG.3. Layout of the CSNS back-streaming neutron beam tunnel and the experimental halls.

In the first stage, the neutron total cross section, capture cross section, fission cross section and prompt fission neutron spectrum (PFNS) measurements are planed with this back-streaming neutron beam. More details about capture cross section and PFNS measurement are described in the following.

3.4. Spallation proton-induced (>200MeV) white spectrum neutron beams

CAPTURE CROSS SECTION MEASUREMENT

To measure the (n,γ) cross section precisely, a 4π Gamma Total Absorption Facility (GTAF) [14] with more than 95% event detection efficiency has been built at China Institute of Atomic Energy (CIAE). A picture of the GTAF is shown in Fig.4. The facility consists of 40 BaF_2 crystals. And the signals are read out by 40 channels 1 GS/s Flash-ADC (Acquiris-DC271A). The expected key performances are that neutron capture event detection efficiency is more than 95% and time resolution is less than 1 ns. Construction of the facility has been finished and test measurement using the CIAE neutron source will be carried out.

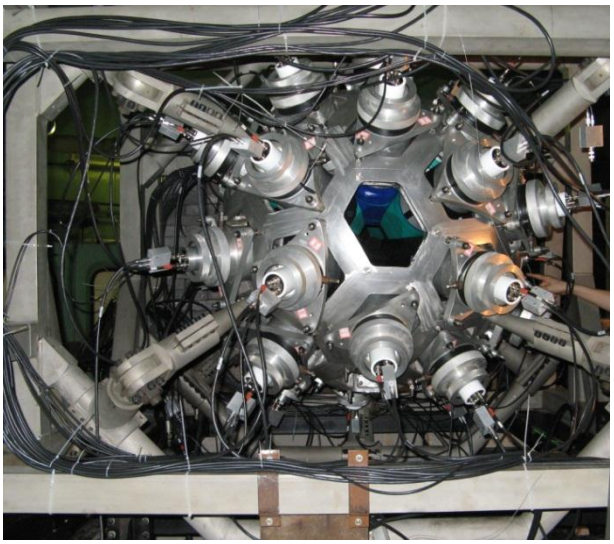

FIG.4. The GTAF at CIAE.

PROMPT FISSION NEUTRON SPECTRUM MEASUREMENT

A neutron detector array consists of 64 neutron detectors (BC501A or EJ301) is considered for measuring the PFNS from fissile nuclei. A schematic view of this system is shown in Fig.5. A multi-layer fission chamber will be used for tagging the fission event and increasing the amount of fissile sample. Such a neutron detection array is useful not only for PFNS measurement, but also for neutron inelastic scattering cross section measurement and neutron induced deuteron breakup reaction study. For neutron inelastic cross section measurement, a γ detector will be needed. While for neutron induced deuteron breakup reaction study, the fission chamber will be replaced by a deuterated liquid scintillator.

SUMMARY

The CSNS back-streaming neutron beam will be the first intensive pulsed white neutron beam in China. It will greatly improve the capability for nuclear data measurement and other related studies in China. The advantages for this neutron beam line are: 1) about 5000 hours beam time is available every year. The beam time is always available during the accelerator operation, without interference with other applications. Of course, if the special mode beam time is needed to do good resolution measurements above 1 keV, then the special beam time will need to be applied. 2) Compare to build a new machine or spallation target station, the investment is quite small.

3.4. Spallation proton-induced (>200MeV) white spectrum neutron beams

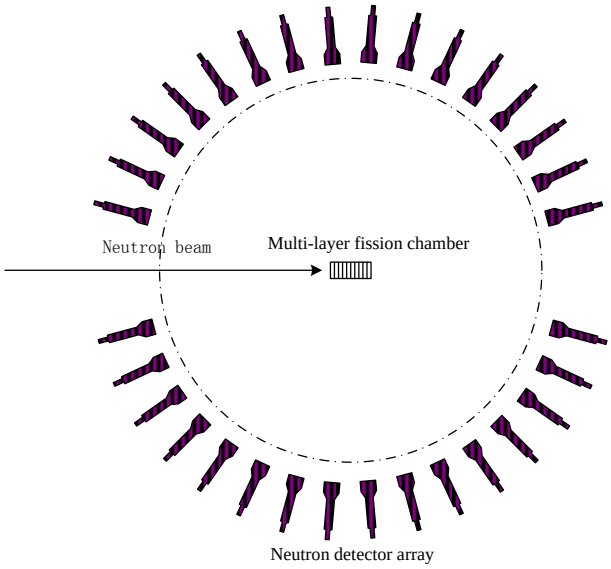

FIG. 5. Schematic view of the PFNS measurement system.

REFERENCES

[1] FANG, S., et al., J. Kor. Phys. Soc. 48 (2006) 697.
[2] WEI, J., et al., J. Kor. Phys. Soc. 50 (2007) 1377.
[3] WANG, F., et al., Nucl. Tech. 28 (2005) 593 (in Chinese).
[4] WANG, F., et al., Physics 37 (2008) 449 (in Chinese).
[5] TANG, J., et al., J. Kor. Phys. Soc. 52 (2008) 710.
[6] TANG, J., et al., Chin. Phys. C 34 (2010) 121.
[7] JING, H., et al., Nucl. Instr. and Meth. A (2010), doi:10.1016/j.nima.2010.06.097.
[8] KAEPPELER, F., Prog. Part. Nucl. Phys. 43, 419 (1999).
[9] WALLERSTEIN, G., et al., Rev. Mod. Phys. 69, 995 (1997).
[10] Nuclear Energy Agency, Nuclear Data High Priority Request List, http://www.nea.fr/dbdata/hprl/
[11] PALMIOTTI, G., et al., Nuclear Data for innovative Fast Reactors: Impact of Uncertainties and New Requirements. International Conference on Fast Reactors and Related Fuel Cycles (FR09) - Challenges and Opportunities. INL/CON-09-17363, 2009.
[12] SALVATORES, M., et al. UNCERTAINTY AND TARGET ACCURACY ASSESSMENT FOR INNOVATIVE SYSTEMS USING RECENT COVARIANCE DATA EVALUATIONS. A report by the Working Party on International Evaluation Co-operation of the NEA Nuclear Science Committee. Vol.26, OECD 2008.
[13] ALIBERTI, G., et al., Target Accuracy Assessment for an ADS Design. 4th Workshop on Neutron Measurements, Evaluations and Applications -- Nuclear Data Needs for Generation IV and Accelerator-Driven Systems. INL/CON-07-13353, 2007.
[14] ZHONG Qi-Ping et al. Chinese Physics C (HEP & NP), Vol. 32, Suppl.II, Oct., 2008.

3.4. Spallation proton-induced (>200MeV) white spectrum neutron beams

NUCLEAR DATA EXPERIMENTAL PROGRAM AT CERN FOR REACTOR PHYSICS

C. GUERRERO[1], S. ALTSTADT[2], S. ANDRIAMONJE[1], J. ANDRZEJEWSKI[3], L. AUDOUIN[4], M. BARBAGALLO[5], V. BECARES[6], F. BECVAR[7], F. BELLONI[8], E. BERTHOUMIEUX[8,1], J. BILLOWES[9], V. BOCCONE[1], D. BOSNAR[10], M. BRUGGER[1], M. CALVIANI[1], F. CALVINO[11], D. CANO-OTT[6], C. CARRAPIÇO[12], F. CERUTTI[1], E. CHIAVERI[8,1], M. CHIN[1], N. COLONNA[5], G. CORTES[11], M.A. CORTES-GIRALDO[13], M. DIAKAKI[14], C. DOMINGO-PARDO[15], I. DURAN[16], R. DRESSLER[17], N. DZYSIUK[18], C. ELEFTHERIADIS[19], A. FERRARI[1], K. FRAVAL[8], S. GANESAN[20], A.R. GARCIA[6], G. GIUBRONE[15], K. GOBEL[2], M.B. GOMEZ-HORNILLOS[11], I.F. GONCALVES[12], E. GONZALEZ-ROMERO[6], E. GRIESMAYER[21], F. GUNSING[8], P. GURUSAMY[20], A. HERNANDEZ-PRIETO[1,11], P. GURUSAMY[20], D.G. JENKINS[22], E. JERICHA[21], Y. KADI[1], F. KAPPELER[23], D. KARADIMOS[14], N. KIVEL[17], P. KOEHLER[24], M. KOKKORIS[14], M. KRTICKA[7], J. KROLL[3], C. LAMPOUDIS[8], C. LANGER[2], E. LEAL-CIDONCHA[16], C. LEDERER[2,25], H. LEEB[21], L.S. LEONG[4], R. LOSITO[1], A. MANOUSOS[19], J. MARGANIEC[9], T. MARTINEZ[6], C. MASSIMI[26], P.F. MASTINU[18], M. MASTROMARCO[5], M. MEAZE[5], E. MENDOZA[6], A. MENGONI[27], P.M. MILAZZO[28], F. MINGRONE[26], M. MIREA[29], W. MONDALAERS[30], R. PALOMO[13], T. PAPAEVANGELOU[8], C. PARADELA[16], A. PAVLIK[25], J. PERKOWSKI[3], A. PLOMPEN[30], J. PRAENA[13], J.M. QUESADA[13], T. RAUSCHER[31], R. REIFARTH[2], A. RIEGO[11], F. ROMAN[1,29], C. RUBBIA[1,32], M. SABATE-GILARTE[11], R. SARMENTO[12], A. SAXENA[20], P. SCHILLEBEECKX[30], S. SCHMIDT[2], D. SCHUMANN[17], P. STEINEGGER[17], G. TAGLIENTE[5], J.L. TAIN[13], D. TARRIO[15], L. TASSAN-GOT[5], A. TSINGANIS[1,12], S. VALENTA[3], G. VANNINI[26], V. VARIALE[21], P. VAZ[12], A. VENTURA[27], R. VERSACI[1], M.J. VERMEULEN[22], V. VLACHOUDIS[1], R. VLASTOU[14], A. WALLNER[25], T. WARE[9], M. WEIGAND[2], C. WEIß[1,21], T. WRIGHT[9], P. ZUGEC[10]

[1] European Organization for Nuclear Research (CERN), Geneva, Switzerland
[2] Johann-Wolfgang-Goethe Universität, Frankfurt, Germany
[3] Uniwersytet Lodzki, Lodz, Poland
[4] Centre National de la Recherche Scientifique/IN2P3 - IPN, Orsay, France
[5] Istituto Nazionale di Fisica Nucleare, Bari, Italy
[6] Centro de Investigaciones Energeticas Medioambientales y Tecnologicas (CIEMAT), Madrid, Spain
[7] Charles University, Prague, Czech Republic
[8] Commissariat a l'Energie Atomique (CEA) Saclay - Irfu, Gif-sur-Yvette, France
[9] University of Manchester, Oxford Road, Manchester, UK
[10] Department of Physics, Faculty of Science, University of Zagreb, Croatia
[11] Universitat Politecnica de Catalunya, Barcelona, Spain
[12] IST/ITN, Instituto Superior Técnico, Universidade Técnica de Lisboa, Lisboa, Portugal
[13] Departamento de Física Atómica, Molecular y Nuclear, Universidad of Sevilla, Spain
[14] National Technical University of Athens (NTUA), Greece
[15] Instituto de Fisica Corpuscular, CSIC-Universidad de Valencia, Spain
[16] Universidade de Santiago de Compostela, Spain
[17] Paul Scherrer Institut, Villigen PSI, Switzerland
[18] Istituto Nazionale di Fisica Nucleare, Laboratori Nazionali di Legnaro, Italy
[19] Aristotle University of Thessaloniki, Thessaloniki, Greece
[20] Bhabha Atomic Research Centre (BARC), Mumbai, India
[21] Atominstitut, Technische Universität Wien, Austria
[22] University of York, Heslington, York, UK
[23] Karlsruhe Institute of Technology, Institut für Kernphysik, Karlsruhe, Germany
[24] Oak Ridge National Laboratory (ORNL), Oak Ridge, TN 37831, USA
[25] University of Vienna, Faculty of Physics, Austria
[26] Dipartimento di Fisica, Universita di Bologna, and Sezione INFN di Bologna, Italy
[27] Agenzia nazionale per le nuove tecnologie, l'energia e lo sviluppo economico sostenibile (ENEA), Bologna, Italy
[28] Istituto Nazionale di Fisica Nucleare, Trieste, Italy
[29] Horia Hulubei National Institute of Physics and Nuclear Engineering - IFIN HH, Bucharest - Magurele, Romania
[30] European Commission JRC, Institute for Reference Materials and Measurements, Retieseweg 111, B2440 Geel, Belgium

3.4. Spallation proton-induced (>200MeV) white spectrum neutron beams

[31]Department of Physics and Astronomy - University of Basel, Basel, Switzerland
[32]Laboratori Nazionali del Gran Sasso dell'INFN, Assergi (AQ), Italy Email: carlos.guerrero@cern.ch

Abstract

The neutron time-of-flight facility n_TOF, operating at CERN since 2001, features a neutron beam that covers the energy range from thermal to 1 GeV. Its most outstanding characteristics are its long flight path (185 m) and the high instantaneous intensity ($0.5\text{-}12\cdot10^6$ neutrons/pulse depending on the collimator configuration). The ambitious program carried out in the last decade includes a large number of experiments in the fields of nuclear energy technologies, astrophysics, basic physics, detector development and medical applications. Within the field of nuclear energy technologies most measurements are focused on determining, for the first time and/or with unprecedented accuracies, the capture and fission cross sections of actinides, both at low (resolved resonance region) and high (keV-GeV) neutron energies. This paper present a summary of all the measurements carried out since 2001 at n_TOF, including some details for several of these experiments.

1. INTRODUCTION

The research for nuclear reactor applications comprises a wide range of fields, being essential the collaboration between the communities characterizing the reactions that take place in the reactors, simulating experimental and full size reactors, and working on integral experiments and benchmarks in research reactors. The n_TOF Collaboration makes use of the high intensity neutron beam at CERN to measure with high accuracy the reaction cross sections of relevance for the design and operation of current and future nuclear reactors [1-3].

At the neutron time-of-flight n_TOF facility [4] at CERN, neutrons produced by spallation of 20 GeV/c protons on a lead target travel through an evacuated beam line of 185 meters before reaching the experimental area. The cross section measurements consist then in measuring, as function of the time-of-flight of the neutrons, the reactions occurring in a sample intersecting the beam. The corresponding neutron energy of the reaction is determined from kinematics using the measured time-of-flight. Full details of the facility and the neutron beam characteristics are given in Ref. [4].

Since its construction in 2001, the n_TOF facility has provided the nuclear technology and astrophysics communities with a large set of new experimental data. Regarding nuclear technology, most measurements have been focused on the capture and fission cross sections of minor and major actinides. In the following sections we describe the detectors used for such measurements and present some of the most recent and/or challenging measurements performed at n_TOF. Finally, the new neutron beam facility n_TOF-EAR2 (shorter flight path and higher intensity) is presented.

2. MEASUREMENTS ON NUCLEAR DATA FOR NUCLEAR TECHNOLOGIES PERFORMED AT N_TOF

The measurement carried out at the n_TOF facility are proposed by n_TOF Collaboration members and reviewed by an international panel of experts, the CERN *Isolde and n_TOF Technical Committee* INTC. The table below is a summary of the experiments related to nuclear technologies proposed since the start of n_TOF in 2001. The measured reactions, the detection systems and the data of the corresponding data taken period are also given. The different detection systems available at n_TOF are summarized and described in the next section, while section 4 contains a detailed summary of some selected experiments of capture and fission reactions.

3.4. Spallation proton-induced (>200MeV) white spectrum neutron beams

TABLE. 1. SUMMARY OF THE NUCLEAR TECHNOLOGIES EXPERIMENTS PROPOSED AND PERFORMED AT N_TOF SINCE 2001. THE MEASURED REACTIONS, THE DETECTION SYSTEMS AND THE DATA OF THE CORRESPONDING DATA TAKEN PERIOD ARE ALSO GIVEN

Reactions measured	Proposal	Detect.	Date
^{232}Th, ^{234}U (n,f)	Measurements of fission cross Sections for the isotopes relevant to the Thorium Fuel Cycle	PPAC	2002/03
^{232}Th, ^{234}U (n,γ)	Measurement of the neutron capture cross sections of ^{232}Th, ^{231}Pa, ^{234}U and ^{236}U	C6D6 TAC	2002/04
^{233,236}U, ^{237}Np, ^{245}Cm (n,f)	Measurements of fission cross sections of actinides	FIC	2003/04
^{nat}Pb, ^{209}Bi, ^{237}Np (n,f)	Measurements of fission cross sections of actinides	PPAC	2003
^{233}U, ^{237}Np, ^{240}Pu, ^{243}Am (n,γ)	Measurement of the (n,γ) cross sections of ^{233}U, ^{237}Np, ^{240,242}Pu, ^{241,243}Am and ^{245}Cm with a Total Absorption Calorimeter at n_TOF	TAC	2004
^{241}Am, ^{238}U (n,γ)	Neutron capture cross section measurements of ^{238}U, ^{241}Am and ^{243}Am at n_TOF	C6D6 TAC	2010/12
^{235}U(n,γ/f)	Validation of simultaneous (n,γ/f) measurement of capture and fission reactions at n_TOF	TAC MGAS	2010
^{232}Th(n,f), ^{235,238}U(n,f)	Angular distributions in the neutron-induced fission of actinides	PPAC	2010/11
^{236}U(n,γ)	Measurement of the neutron capture cross-section of ^{236}U	TAC C6D6	2011
^{240,242}Pu(n,f)	Measurement of the fission cross-section of ^{240}Pu and ^{242}Pu at CERN's nTOF Facility	MGAS	2011/12
^{93}Zr(n,γ)	Neutron capture cross section of ^{93}Zr	C6D6	2012
^{234,236}U(n,f)	Fission fragment angular distributions in the ^{234}U(n,f) and ^{236}U(n,f) reactions	PPAC	2012
^{235}U(n,γ/f)	Measurements of neutron-induced capture and fission reactions on ^{235}U	TAC MGAS	2012

3. DETECTORS FOR NEUTRON INDUCED-REACTIONS

Several types of detection systems are available at n_TOF; a significant effort has been devoted to improve both the actual detectors and the associated techniques with respect to previously existing ones.

1. The neutron beam monitors used at present are based on an array of silicon detectors (SiMon [5]) looking to a ^{6}Li foil and MicroMegas (MGAS [6]) detectors measuring ^{10}B(n,α) and ^{235}U(n,f) reactions.
2. The measurements of capture reactions on isotopes where the neutron scattering dominates over the capture channels are performed with specially built low neutron

sensitivity C_6D_6 detectors [7], basing the data analysis on the improved accuracy Pulse Height Weighting Technique [8].

3. A higher performance in terms of efficiency, multiplicity and background rejection in neutron capture reactions is provided by the Total Absorption Calorimeter (TAC [9]), a 4π array made of 40 BaF_2 crystals.
4. The low noise, radiation hard MicroMegas (MGAS [6]) detector is used for fission cross section measurements.
5. The use of a set of parallel plate avalanche counters (PPAC [10]) allows to study, in addition to fission cross sections, the angular distribution of the emitted fission fragments using the coincidence method.

Using these detection systems, some of which are shown in Fig. 1, a large number of experiments have been performed at n_TOF in the two experimental campaigns (2001-2004 and 2009-2012).

FIG.1. Photographs of the detectors mentioned in section 2. Top-left: C_6D_6. Top-rightt:TAC. Bottom-left: MGAS. Bottom-right: PPAC.

3.4. Spallation proton-induced (>200MeV) white spectrum neutron beams

4. MEASUREMENTS OF RELEVANCE TO NUCLEAR REACTORS

Many different reactions, most of them induced by neutrons, play a key role in the design and operation of nuclear reactors. Their cross sections are however not as well known as needed and therefore there are ambitious research programs devoted to improve the accuracy of the nuclear data of interest for reactor applications. The nuclear data needs have been assessed by the WPEC-26 Group of the NEA [11], which also provides an updated High Priority Request List (HPRL [3]) of measurements.

4.1. FISSION CROSS SECTIONS OF ACTINIDES

According to the NEA HPRL, the fission cross section measurements deserving priority are ^{238,239,240,241,242}Pu, ^{241,242}Am and ^{244,245}Cm. Out of these, ^{240,242}Pu [12], ^{241}Am [13] and ^{245}Cm [14] have been already measured at n_TOF.

In particular, the neutron-induced fission cross section of ^{245}Cm was measured from 30 meV to 1 MeV by Calviani et al. [14] with 5% accuracy relative to the ^{235}U(*n,f*) cross section, normalizing the absolute value at thermal energy to recent measurements performed at ILL and BR1. As seen in Fig. 2, the results are in fair agreement with some previous measurements and confirm, on average, the evaluated cross section in the ENDF/B-VII.0 database, although sizable differences are observed for some important resonances below 20 eV. A similar behavior is observed relative to JENDL/AC-2008, a reactor-oriented database for actinides. The new results contribute to the overall improvement of the databases needed for the design of advanced reactor systems and may lead to refinements of fission models for the actinides.

3.4. Spallation proton-induced (>200MeV) white spectrum neutron beams

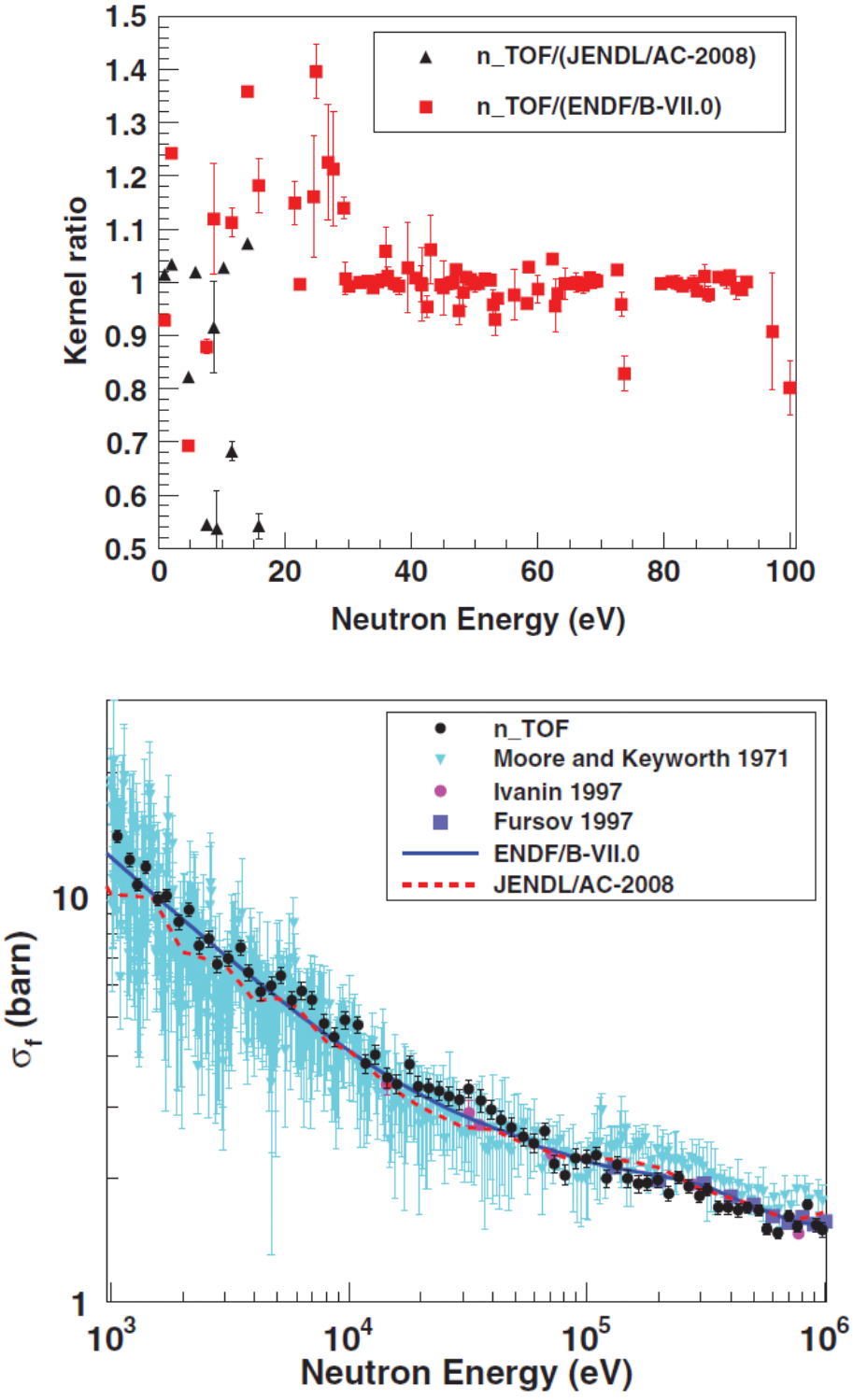

FIG. 2. The ^{245}Cm(n,f) cross section in the resolved (top) unresolved (bottom) resonance regions compared with the previous data and with the evaluated data sets of ENDF/B-VII.0 and JENDL/AC-2008.

3.4. Spallation proton-induced (>200MeV) white spectrum neutron beams

The fission cross section of ^{241}Am was measured up to 20 MeV also using the FIC detector. The details of the measurement and analysis have been recently published by Belloni et al. [13]. The comparison with previous data shows good agreement with some works and large differences (between -10% and +20%) with others. However, when compared to the evaluations a very good agreement is found, thus indicating that the evaluations are based on the correct choice f experimental data.

Using a PPAC fission detector n_TOF has provided the only measurements to date all the way up to 1 GeV. With this technique, the fission cross sections of ^{234}U and ^{237}Np were measured in 2003 by Paradela et al. [10], while ^{232}Th and ^{236}U have been measured in 2010/12.

As for the results on ^{237}Np, the cross section shape was found to agree with ENDF/B-VII.0, but the cross-section values are systematically higher by about 3% below and 6% above 1 MeV. Even larger differences of 8% are found above 6 MeV with respect to JENDL-3.3, significantly beyond the 3% to 4% systematic uncertainty of the n_TOF data. When compared to the large body of experimental results, these data are in agreement with most of the experiments performed with monoenergetic sources around 14 MeV. These important results are illustrated in Fig. 4 and further details are given in Ref. [10].

3.4. Spallation proton-induced (>200MeV) white spectrum neutron beams

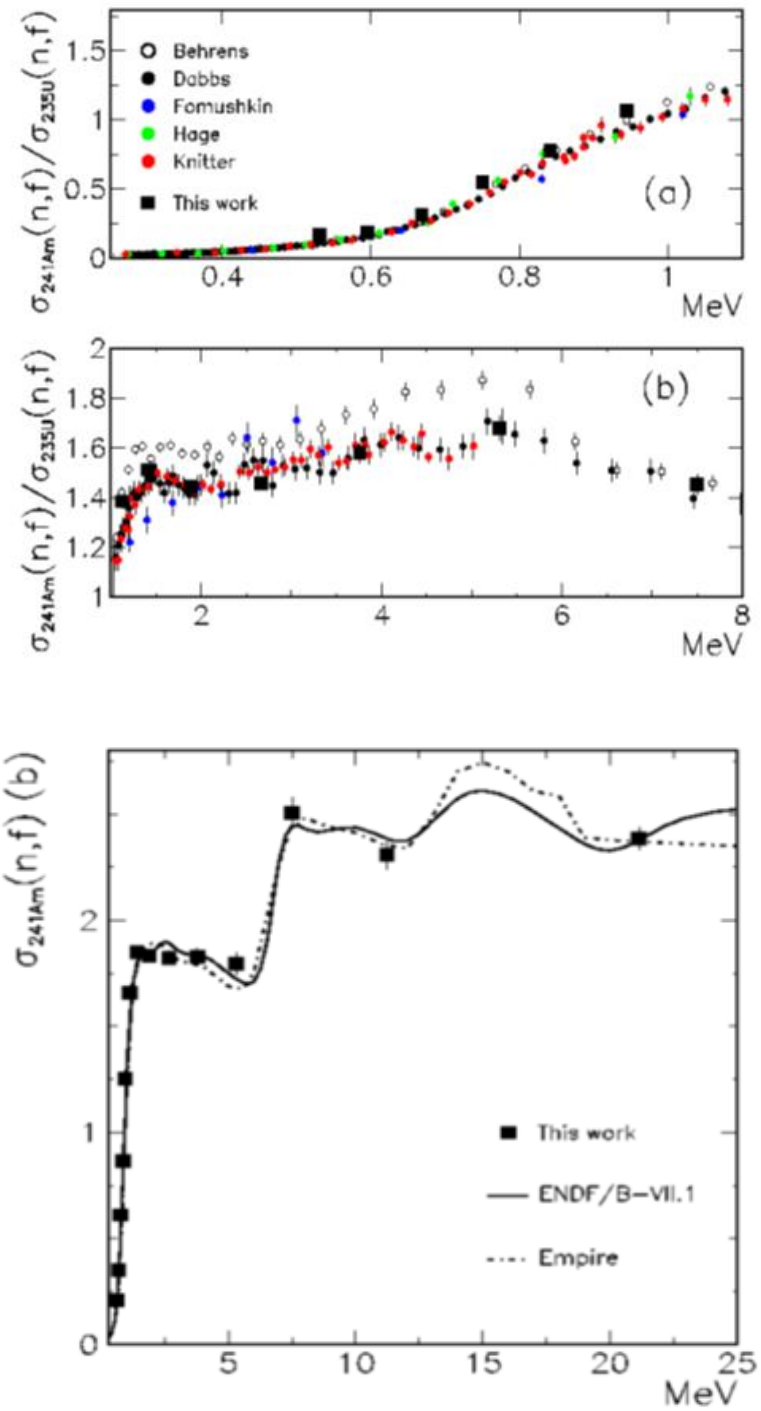

FIG. 3. Top: The ^{241}Am(n,f) cross section measured at n_TOF, from the threshold up to 8 MeV, compared to previous data. Bottom: comparison of the n_TOF cross section with ENDF/B-VII.1 and to a calculation with EMPIRE.

Another interesting measurement was performed on neutron-induced fission of ^{232}Th with the PPAC detectors by Tarrio et al. [15]. This detector provides the means for studying

the emission angle of the fission fragments, which varies rapidly as higher chance fission channels open. This is illustrated in Fig. 5, which shows the cross section measured at n_TOF (left) together with the associated anisotropy in the emission of fission fragments (right).

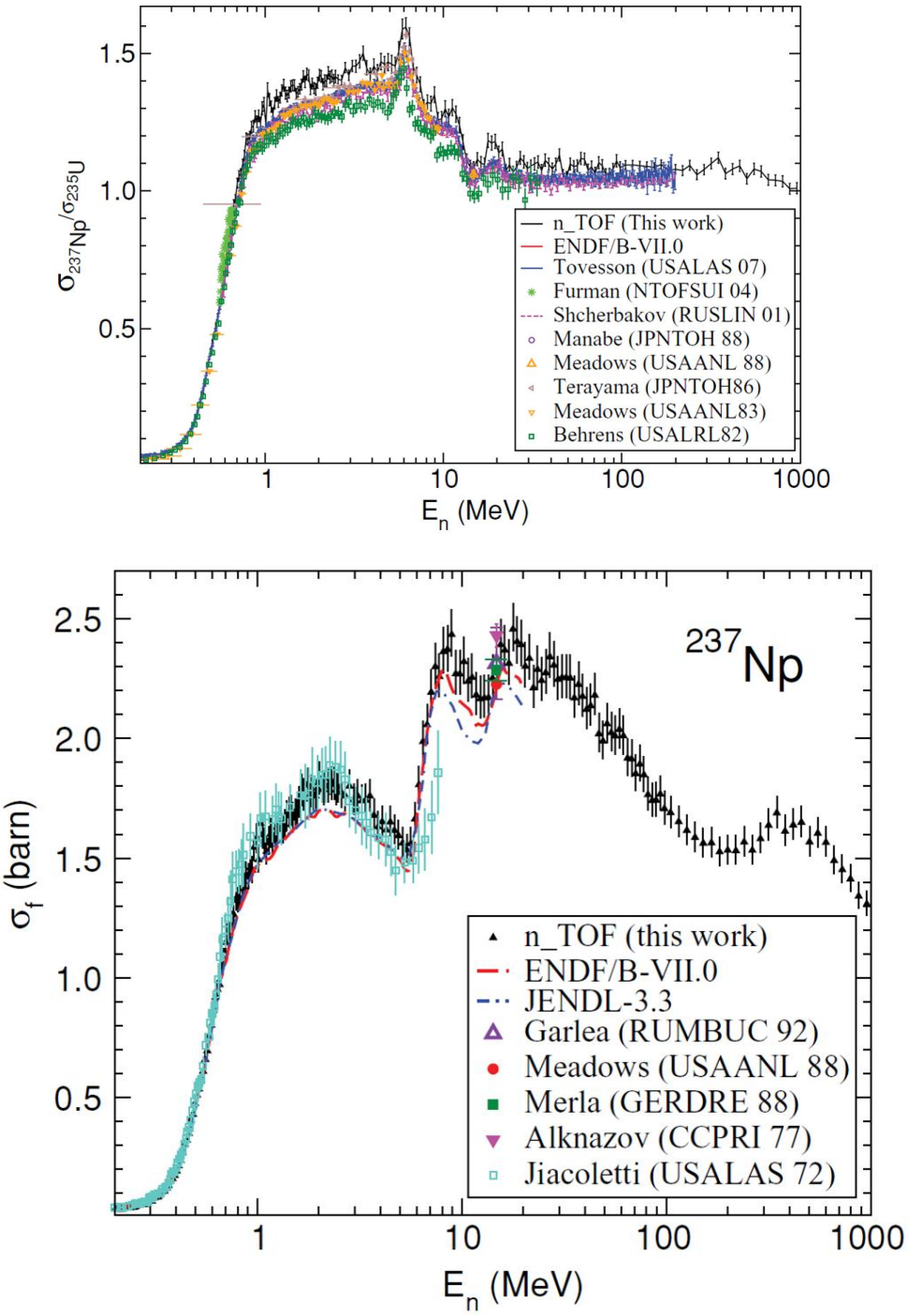

FIG. 4. The ^{237}Np(n,f) cross section measured at n_TOF, from the threshold up to 1 GeV, compared to previous data and to the available evaluations.

4.2. CAPTURE CROSS SECTIONS OF ACTINIDES

Most of the experimental program at n_TOF is devoted to neutron capture cross section measurements of interest in nuclear technology as well as for stellar nucleosynthesis. In this case the NEA HPRL includes as priority ^{233,235,238}U, ^{239,241,242}Pu, ^{241}Am, out of which ^{233,235,238}U [16-18] and ^{241}Am [18] have been measured recently at n_TOF.

As part of the program for nuclear data for the Thorium fuel cycle, the ^{232}Th(n,γ) cross section was measured in 2002 with a pair of low neutron sensitivity C_6D_6 detectors between 1 eV and 1 MeV, the highest energy reached in a capture measurement at n_TOF to date (Fig. 6). The results from both the resolved (Gunsing et al. [19]) and unresolved (Aerts et al. [20]) resonance regions are now included in the ENDF-B/VII.0 library (2005).

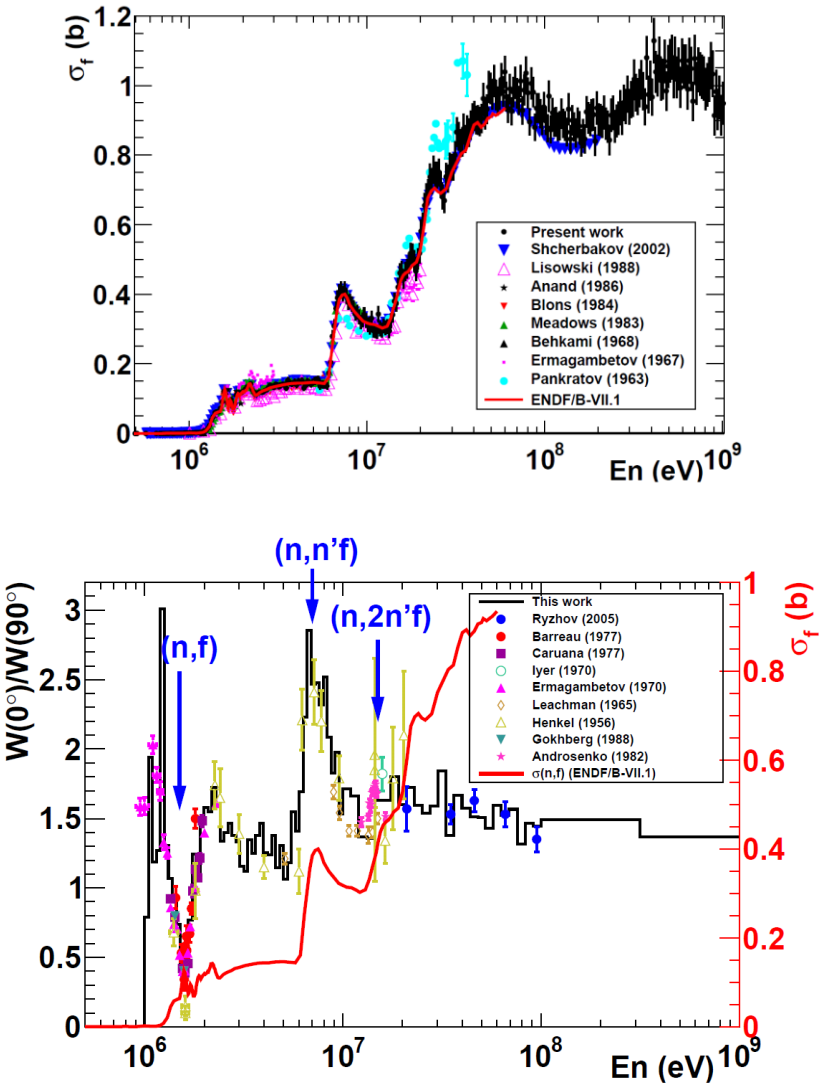

FIG. 5. Top: The ^{232}Th(n,f) cross section measured at n_TOF (preliminary) compared to previous measurements and evaluations. Bottom:measured anisotropy (preliminary) compared to the other available experiments.

3.4. Spallation proton-induced (>200MeV) white spectrum neutron beams

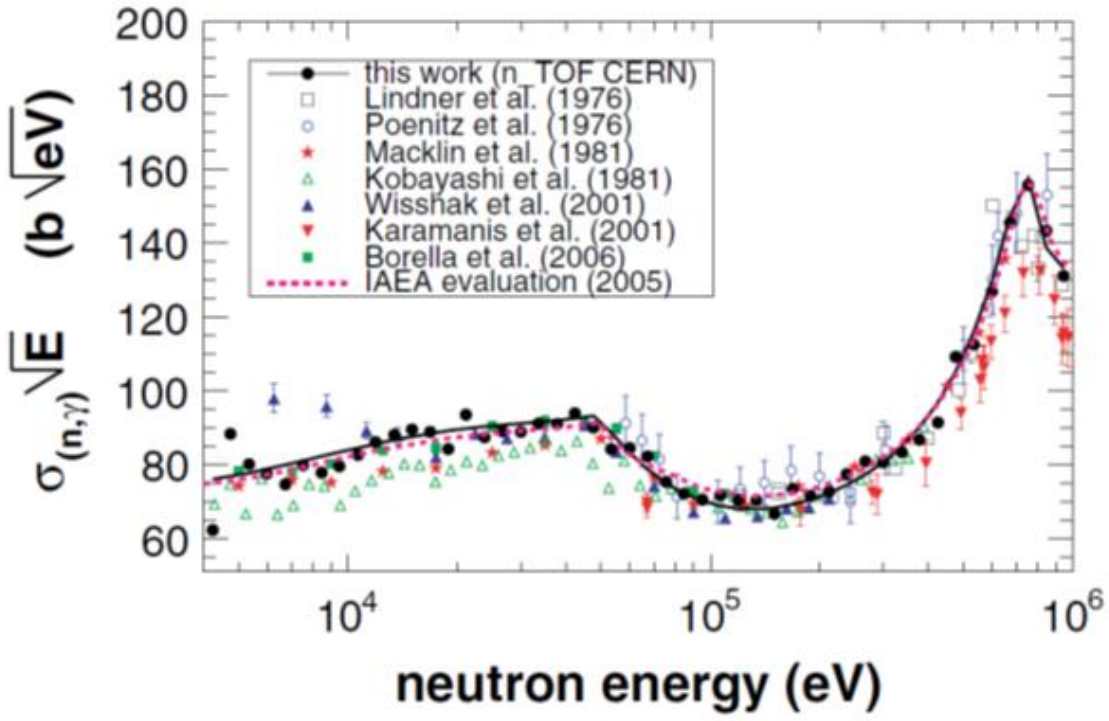

FIG. 6. Neutron capture cross section of ^{232}Th(n,γ) measured at n_TOF multiplied by the square root of the neutron energy, showing the measured data and an average parameter fit, compared to several other experimental data sets.

The main challenge of measuring the ^{241}Am capture reactions is related to its very high intrinsic activity, in our case 4 GBq (dominated by the emission of 60 keV γ rays) for a 40 mg sample 12 mm in diameter. The two available capture detection systems, C_6D_6 and TAC, were employed in order to reduce systematic uncertainties. In the case of the C_6D_6 measurement, the full energy range from thermal to 1 MeV was covered, as illustrated in Fig. 7. The data analysis, which includes the extension of the resolved resonance region beyond 150 eV, is now in progress and final results will be published in 2013 by Fraval et al. [21].

In addition to ^{241}Am, the capture cross section of ^{243}Am has also been measured at n_TOF, in this case with a sample of 6.2 mg and using the TAC detector. In the resolved resonance region, below 250 eV, the results from n_TOF by Mendoza et al. [22] indicate that the recent evaluated cross sections underestimate the capture cross section between 2% and 10%, in the case of ENDF/B-VII.0 and VII.1, and between 3 and 25% in the case of JEFF-3.1 and JENDL-4.0. In the unresolved resonance region and up to a few keV, the underestimation of the cross section by the evaluations ranges between 8% and 20%, which was also suggested by one of the two measurements of Weston, which is the one not included in the existing evaluations (Fig. 8).

3.4. Spallation proton-induced (>200MeV) white spectrum neutron beams

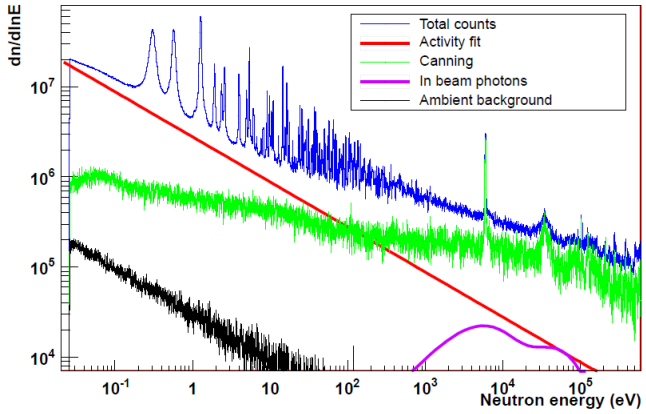

FIG. 7. Neutron energy distribution corresponding to the measurement with C_6D_6 detector of a 40 mg ^{241}Am sample with an activity of 4 GBq.

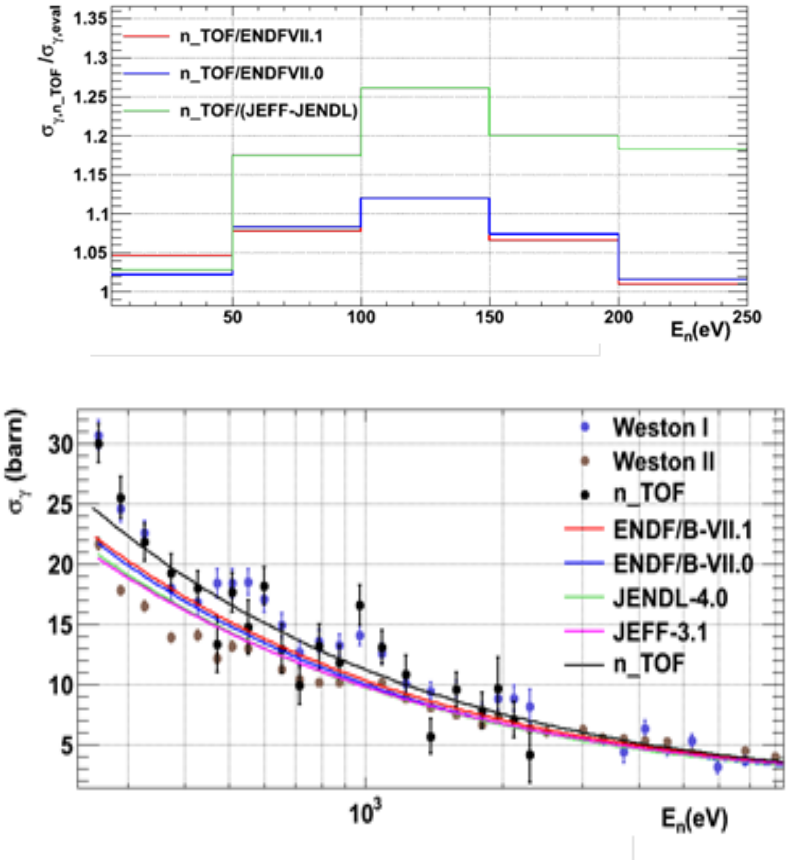

FIG. 8. Comparison of the n_TOF measured capture cross section of ^{243}Am with the available evaluations in the resolved and unresolved resonance regions.

Neutron capture measurements at n_TOF have provided a high level of resolution and statistics compared to previous experiments. With the data taken for ^{241}Am and ^{243}Am, the resolved resonance region will be significantly extended to higher energies. In the case of ^{237}Np, the full resolved resonance region had never been studied before in the capture channel, only transmission data had been available so far. The n_TOF results of Guerrero et al. [23] have allowed analyzing a combination of transmission and capture data all the way up to 500 eV, as illustrated in Fig. 9.

3.4. Spallation proton-induced (>200MeV) white spectrum neutron beams

The measurement of capture in fissile isotopes requires distinguishing between the γ rays emitted in fission and those from capture. In the case of ^{233}U this was done by relying in the differences in energy and multiplicity of the γ rays cascades from the two different reactions [16].

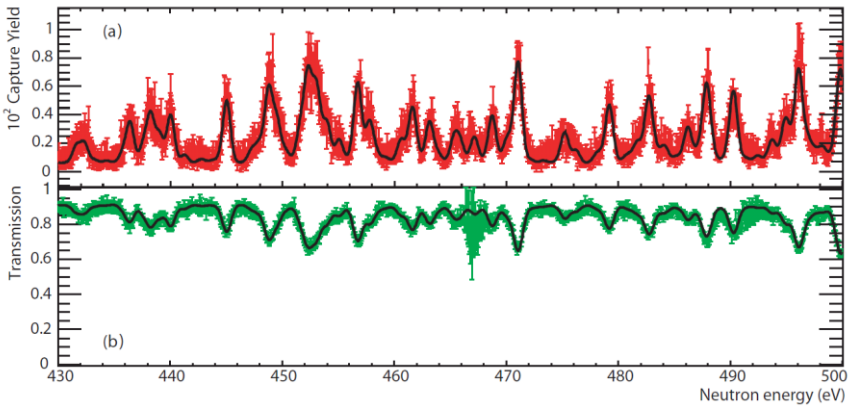

FIG. 9. Capture yield (n_TOF) and transmission (GELINA) of ^{237}Np in the higher limit of the resolved resonance region. The solid lines correspond to the resonance parameterization obtained from SAMMY fits.

In the case of ^{235}U this distinction was obtained by combining the TAC with a MGAS fission detector that provided the necessary fission tagging capabilities. The results from a test experiment on ^{235}U made in 2010 [24] are shown in Fig. 10. A new experiment covering the full range of interest between thermal and 10 keV has been performed in 2012. The data analysis is now ongoing but some more details can be found in ref. [17].

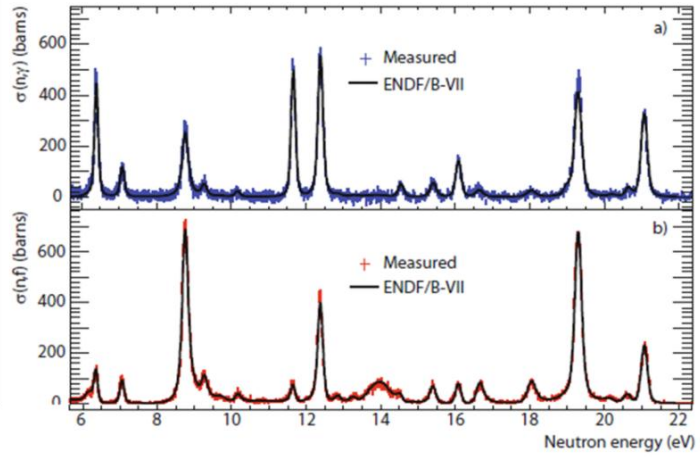

FIG. 10. Capture and fission cross section of ^{235}U measured at n_TOF in a test experiment in 2010. A new measurement covering the full range between thermal and 10 keV has been performed in 2012.

5. CONCLUSIONS AND OUTLOOK

The measurement of nuclear data of importance for the development of innovative nuclear reactors is one of the main objectives of the n_TOF facility, which operates at CERN since 2001. During these years many measurements have been performed, in particular for capture and fission cross section of actinides. A summary has been presented in this paper, which includes also some details on the most interesting results to date.

3.4. Spallation proton-induced (>200MeV) white spectrum neutron beams

The n_TOF Collaboration keeps increasing and as of 2012 brings together 101 scientists from 32 institutions. The future looks even brighter ahead; a new complementary neutron beam line, with a short 20 meters flight path and a 25 times higher intensity beam, will be constructed in 2013 and shall become operative by the end of 2014. This will open the door to new challenging measurements with sub-milligram samples [25]. More information is given in the corresponding chapter of this IAEA document.

REFERENCES

[1] SALVATORES, M., and JACQMIN, R., Uncertainty and target accuracy assessment for innovative system using recent covariance data evaluations, ISBN 978-92-64-99053-1, NEA/WPEC-26 (2008).

[2] COLONNA, N., et al, Advanced nuclear energy systems and the need of accurate nuclear data: the n_TOF project at CERN , Energy Environ. Sci. 3 (2010) 1910-1917.

[3] The NEA Nuclear Data High Priority Request List (HPRL) www.oecd-nea.org/dbdata/hprl

[4] GUERRERO, C., et al., Performance of the neutron Time-of-Flight facility n TOF at CERN, submitted to Eur. Phys. J. A (2012).

[5] MARRONE, S., et al., A low background neutron flux monitor for the n_TOF facility at CERN, Nucl. Inst. Meth. A 517 (2004) 389-398.

[6] ANDRIAMONJE, S., et al., J. of the Korean Phys. Soc. 59 (2011) 1597-1600.

[7] PLAG, R., et al., An optimized C6D6 detector for studies of resonance-dominated (n,γ) cross-sections, Nucl. Instr. Meth. A 496 (2003) 425-436.

[8] ABBONDANNO, U., et al., New experimental validation of the pulse height weighting technique for capture cross-section measurements, http://www.sciencedirect.com/science/article/pii/S0168900203029425 Nucl. Instr. Meth. A 521 (2004) 545-467.

[9] GUERRERO, C., et al., The n_TOF Total Absorption Calorimeter for neutron capture measurements at CERN, Nucl. Instr. Meth. A 608 (2009) 424-433.

[10] PARADELA, C., et al, Neutron-induced fission cross section of ^{234}U and ^{237}Np measured at the CERN Neutron Time-of-Flight (n_TOF) facility, Phys. Rev. C 82, 034601 (2010).

[11] NEA-WPEC26, Uncertainty and target accuracy assessment for innovative systems using recent covariance data evaluations, ISBN 978-92-64-99053-1.

[12] TSINGANIS, A., et al., Measurement of the ^{240,242}Pu(n,f) cross section at the CERN n_TOF facility, Proc. Int. Conf. Nuclear Data for Sc. and Tech., New York, USA (March 2013).

[13] BELLONI, F.,et al., Measurement of the neutron induced fission cross section of ^{241}Am at the time-of-flight facility n_TOF, accepted for publication in Eur. Phys. J. A (2012).

[14] CALVIANI, M., et al., The neutron-induced fission cross-section of 245Cm: new results from n_TOF, Phys. Rev. C 85, 034616 (2012).

[15] TARRIO, D.,et al., Neutron-induced fission fragment angular distribution at CERN: the ^{232}Th case, PhD Thesis at Universidad de Santiago de Compostela, Spain, (April 2012).

[16] CARRAPIÇO, C., et al., Neutron induced capture and fission discrimination using Calorimetric Shape Decomposition, Nucl. Instr. Meth. A (2012) (In press http://dx.doi.org/10.1016/j.nima.2012.11.082).

[17] GUERRERO, C., et al., Neutron capture and fission reactions on ^{235}U : cross sections, a-ratios and prompt g ray emission from fission, EPJ Web of Conferences (WONDER 2012).

3.4. Spallation proton-induced (>200MeV) white spectrum neutron beams

[18] CANO-OTT, D., et al., Neutron capture cross section measurements of ^{238}U, ^{241}Am and ^{243}Am at n_TOF, CERN-INTC-2009-025.

[19] GUNSING, F., et al., Measurement of resolved resonances of ^{232}Th(n,γ) at the n_TOF facility at CERN, Phys. Rev. C 85, 064601 (2012).

[20] AERTS, G.,et al., Neutron capture cross section of ^{232}Th measured at the n TOF facility at CERN in the unresolved resonance region up to 1 MeV, Phys. Rev. C 73, 054610 (2006).

[21] FRAVAL, K.,et al., Analysis of ^{241}Am(n,g) cross section with C6D6 detectors, Proc. Int. Conf. Nuclear Data for Sc. and Tech. 2013, New York, USA (2013).

[22] MENDOZA, E., et al., Measurement of the ^{241}Am and the ^{243}Am neutron capture cross sections at the n_TOF facility at CERN, Proc. Int. Conf. Nuclear Data for Sc. and Tech. 2013, New York, USA (2013).

[23] GUERRERO, C., et al., Measurement and resonance analysis of the ^{237}Np neutron capture cross section, Phys. Rev. C 85, 044616 (2012).

[24] GUERRERO, C.,et al., Simultaneous measurement of neutron-induced capture and fission reactions at CERN, Eur. Phys. J. A 48, 29 (2012).

[25] CHIAVERI, E., et al., Proposal for n_TOF Experimental Area 2 (EAR-2), CERN-INTC-2012-029.

3.4. Spallation proton-induced (>200MeV) white spectrum neutron beams

THE N_TOF FACILITY AT CERN: STATUS AND PERSPECTIVES

E. CHIAVERI[1], S. ALTSTADT[2], J. ANDRZEJEWSKI[3], L. AUDOUIN[4], M. BARBAGALLO[5], V. B´ECARES[6], F. BEˇCV´AˇR[7], F. BELLONI[8], E. BERTHOUMIEUX[8], J. BILLOWES[9], V. BOCCONE[1], D. BOSNAR[10], M. BRUGGER[1], M. CALVIANI[1], F. CALVIˇNO[11], D. CANO-OTT[6], C. CARRAPI¸CO[12], F. CERUTTI[1], , M. CHIN[1], N. COLONNA[5], G. CORT´ES[11], M.A. CORT´ES-GIRALDO[13], M. DIAKAKI[14], C. DOMINGO-PARDO[15], I. DURAN[16], R. DRESSLER[17], N. DZYSIUK[18], C. ELEFTHERIADIS[19], A. FERRARI[1], K. FRAVAL[8], S. GANESAN[20], A.R. GARC´IA[6], G. GIUBRONE[15], M.B. G´OMEZ-HORNILLOS[11], I.F. GON¸CALVES[12], E. GONZ´ALEZ-ROMERO[6], E. GRIESMAYER[21], C. GUERRERO[1], F. GUNSING[8], P. GURUSAMY[20], D.G. JENKINS[22], E. JERICHA[21], Y. KADI[1], F. K¨APPELER[23], D. KARADIMOS[14], N. KIVEL[17], P. KOEHLER[24], M. KOKKORIS[14], G. KORSCHINEK[25], M. KRTIˇCKA[7], J. KROLL[7], C. LANGER[2], C. LEDERER[26], 2 H. LEEB[21], L.S. LEONG[4], R. LOSITO[1], A. MANOUSOS[19], J. MARGANIEC[3], T. MART´INEZ[6], P.F. MASTINU[18], M. MASTROMARCO[5], C. MASSIMI[27], M. MEAZE[5], E. MENDOZA[6], A. MENGONI[28], P.M. MILAZZO[29], F. MINGRONE[27], M. MIREA[30], W. MONDELAERS[31], C. PARADELA[16], A. PAVLIK[26], J. PERKOWSKI[3], M. PIGNATARI[32], A. PLOMPEN[31], J. PRAENA[13], J.M. QUESADA[13], T. RAUSCHER[32], R. REIFARTH[2], A. RIEGO[11], F. ROMAN[1, 30,] C. RUBBIA[1, 33], R. SARMENTO[12], P. SCHILLEBEECKX[31], S. SCHMIDT[2], D. SCHUMANN[17], G. TAGLIENTE[5], J.L. TAIN[15], D. TARRIO[16] ,L. TASSAN-GOT[4], A. TSINGANIS[1,14], S. VALENTA[7], G. VANNINI[27], V. VARIALE[5], P. VAZ[12], A. VENTURA[28], R. VERSACI[1], M.J. VERMEULEN[22], V. VLACHOUDIS[1], R. VLASTOU[14], A. WALLNER[26], T. WARE[9], M. WEIGAND[2], C. WEIß[21], T.J. WRIGHT[9], AND P. ˇZUGEC[10]

[1] European Organization for Nuclear Research (CERN), Geneva, Switzerland
[2] Johann-Wolfgang-Goethe Universit¨at, Frankfurt, Germany
[3] Uniwersytet L´odzki, Lodz, Poland
[4] Centre National de la Recherche Scientifique/IN2P3 - IPN, Orsay, France
[5] Istituto Nazionale di Fisica Nucleare, Bari, Italy
[6] Centro de Investigaciones Energeticas Medioambientales y Tecnol´ogicas (CIEMAT), Madrid, Spain
[7] Charles University, Prague, Czech Republic
[8] Commissariat `a l'´ Energie Atomique (CEA) Saclay - Irfu, Gif-sur-Yvette, France
[9] University of Manchester, Oxford Road, Manchester, UK
[10] Department of Physics, Faculty of Science, University of Zagreb, Croatia
[11] Universitat Politecnica de Catalunya, Barcelona, Spain
[12] Instituto Tecnol´ogico e Nuclear, Instituto Superior T´ecnico, Universidade T´ecnica de Lisboa, Lisboa, Portugal
[13] Universidad de Sevilla, Spain
[14] National Technical University of Athens (NTUA), Greece
[15] Instituto de F´ısica Corpuscular, CSIC-Universidad de Valencia, Spain
[16] Universidade de Santiago de Compostela, Spain
[17] Paul Scherrer Institut, Villigen PSI, Switzerland
[18] Istituto Nazionale di Fisica Nucleare, Laboratori Nazionali di Legnaro, Italy
[19] Aristotle University of Thessaloniki, Thessaloniki, Greece
[20] Bhabha Atomic Research Centre (BARC), Mumbai, India
[21] Atominstitut, Technische Universit¨at Wien, Austria
[22] University of York, Heslington, York, UK
[23] Karlsruhe Institute of Technology, Campus Nord, Institut f¨ur Kernphysik, Karlsruhe, Germany
[24] Department of Physics, University of Oslo, N-0316 Oslo, Norway
[25] Technical University of Munich, Munich, Germany
[26] University of Vienna, Faculty of Physics, Vienna, Austria
[27] Dipartimento di Fisica, Universit`a di Bologna, and Sezione INFN di Bologna, Italy
[28] Agenzia nazionale per le nuove tecnologie, l'energia e lo sviluppo economico sostenibile (ENEA), Bologna, Italy
[29] Istituto Nazionale di Fisica Nucleare, Trieste, Italy
[30] Horia Hulubei National Institute of Physics and Nuclear Engineering - IFIN HH, Bucharest - Romania
[31] European Commission JRC, Institute for Reference Materials and Measurements, Retieseweg 111, B-2440 Geel, Belgium
[32] Department of Physics and Astronomy - University of Basel, Basel, Switzerland
[33] Laboratori Nazionali del Gran Sasso dell'INFN, Assergi (AQ), Italy Email:enrico.chiaveri@cern.ch

3.4. Spallation proton-induced (>200MeV) white spectrum neutron beams

Abstract

The outstanding features of the existing CERN n_TOF neutron beam are the very high instantaneous neutron flux, excellent n_TOF resolution, low intrinsic backgrounds and coverage of a wide range of neutron energies, from thermal to a few GeV. These characteristics provide a unique possibility to perform neutron-induced cross-section and angular distribution measurements for applications such as nuclear astrophysics, nuclear reactor technology and basic nuclear physics. This paper presents in detail all the characteristics of the present neutron beam in the different available configurations, which correspond to two different collimation systems and two choices of neutron moderator. The features include shape and intensity of the neutron flux, beam spatial profile, in-beam background components and the energy resolution broadening. The description of these features is based upon both dedicated measurements as well as Monte Carlo simulations, and includes an estimation of the systematic uncertainties in the mentioned quantities. The overall efficiency of the experimental program and the range of possible measurements will be expanded in the near future with the construction of a second experimental area (EAR-2), vertically located 20 m on top of the present n_TOF spallation target. This upgrade, which will benefit from a neutron flux 25 times higher than the existing one, will provide a substantial improvement in measurement sensitivities and will open the possibility to measure neutron cross-section of isotopes with very short half-lives or available in very small quantities. The technical study for the construction of this new neutron beam will be presented, highlighting the main advantages compared to the presently existing Experimental Area (EAR-1).

1. INTRODUCTION

High precision neutron cross-section data are of major importance for a wide variety of research fields in basic and applied nuclear physics [1]. In particular, neutron data on neutron-nucleus reactions are essential in Nuclear Astrophysics for understanding the production rate of heavy elements in the Universe, which occurs mainly through slow and rapid neutron capture processes during the various phases of stellar evolution [2, 3]. In the field of nuclear technology new studies aimed at developing future generation nuclear system which would address major safety, proliferation and waste concerns are requiring more accurate data in neutron-induced fission and capture cross-section on radioactive isotopes. Based on these motivations the neutron time-of-flight facility n_TOF has been constructed at CERN, Geneva in 2001.

2. N_TOF FACILITY

The idea of a new neutron time-of-flight facility at CERN was proposed by C. Rubbia in 1998 [4], as a follow up of the TARC experiment, also conducted at CERN.

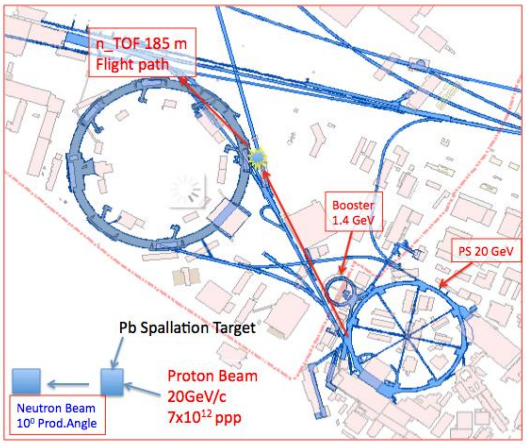

Main features of the n_TOF:
- Proton intensity ..... $8x10^{12}$ p/pulse
- Proton beam momentum ..... 20 GeV/c
- Proton pulse width ..... 6 ns (rms)
- high instantaneous n flux 10^5 n/cm^2/pulse
- wide energy spectrum ..... 25 meV<E_n<1GeV
- low repetition rate → < 0.8 Hz
- good energy resolution $\Delta E/E = 10^{-4}$

FIG.1. The figure show the configuration of the installation as well as the main parameters of the installation.

3.4. Spallation proton-induced (>200MeV) white spectrum neutron beams

The concept of the n_TOF neutron beam [5] makes use of both the specifically high flux of neutrons attainable using the spallation process of 20 GeV/c protons on a massive lead target (see Fig. 1.), able to contain practically the whole spallation shower as well as the remarkable beam density of the CERN Proton Synchrotron (PS) [6]. The CERN n_TOF facility has been set in operation and commissioned in 2001 with performances matching the expectations. The PS machine of CERN can generate high intensities up to 7x1012 ppp (protons per pulse) - high enough to produce the vast number of 2x1015 neutrons per pulse - in the form of short (6 ns width) pulses with a repetition time varying from 1.2s to 16.7s and a prompt "flash" considerably smaller compared to electron machines. The high neutron flux, the low repetition rates and the excellent energy resolution of 5.5x10-4 (1KeV) have opened new possibilities for high precision cross section measurements in the energy range from thermal to GeV, for stable and, in particular, for radioactive targets.

3. N_TOF FACILITY FROM 2008

After three years long stop due to cooling water activation by spallation products diluted in the water, a new lead target was constructed, and new systems developed in order to meet safety requirements for the restart of the facility. In particular, a ventilation system was installed in the primary target area, while a new optimized cooling system was developed, which allows to control and balance the chemical parameters of the water (in particular the oxygen content and conductivity) and to properly filter activation products eventually present in the water circuit. An extensive study of target corrosion mechanism had been performed as well, in order to improve the long-term stability of the system. A new cylindrical shape lead block of 40 cm radius and 60 cm length, developed in order to optimize cooling and neutron production was designed and built. The new target assembly consists of a separated cooling and moderator circuit, which enables the use of different moderator materials, thus allowing a greater flexibility on the characteristics of the neutron beam.

After the commissioning which started in November 2008 and continue during mid-2009 two other changes have been implemented; the first one consists in the implementation of a different moderator material other than light water. In particular, the program has envisaged the use of water enriched in ^{10}B, which has greatly enhanced the measuring capabilities of neutron-induced capture cross-section, by reducing significantly the presence of the in-beam photon component, and in particular the 2.2 MeV γ rays, produced both by neutron capture in hydrogen. Since this photon contribution is delayed, i.e. emitted after about 1 microsecond from the proton interaction (due to the fact that it is produced by thermalized neutrons), it results in a background component in the 1-100 keV neutron energy range, which is problematic for capture reaction measurements performed with C6D6 detectors. The realized system has reduced the 2.2 MeV photon components by a factor of about 10, leaving the neutron fluence unchanged above 1eV.

Another upgrade performed during the 2010 run has been the transformation of the n_TOF experimental area into a Work Sector Type A, which has allowed the possibility to perform measurements of capture and fission cross-section of "unsealed" samples of highly radioactive isotopes, such as actinides like ^{241}Am, ^{243}Am and $^{240-2}$Pu, taking full advantage of the facility's high instantaneous neutron flux. This has required a complete revision of the experimental area and of the related technical services. Table1 summarizes the list of

performed measurements up to now. The results are displayed with a 100 bins-per-decade in the upper panel of Fig. 2, where the wide range of neutron energies provided by the n_TOF neutron beam is clearly visible.

TABLE.1. LIST OF PERFORMED MEASUREMENTS OF CAPTURE AND FISSION CROSS-SECTIONS AT N_TOF PHASE1/PHASE2. IN THE FIRST COLUMN ON THE LEFT SIDE THE BLUE MARKED ISOTOPES ARE STABLE WHILE THE RED ONE IS RADIOACTIVE

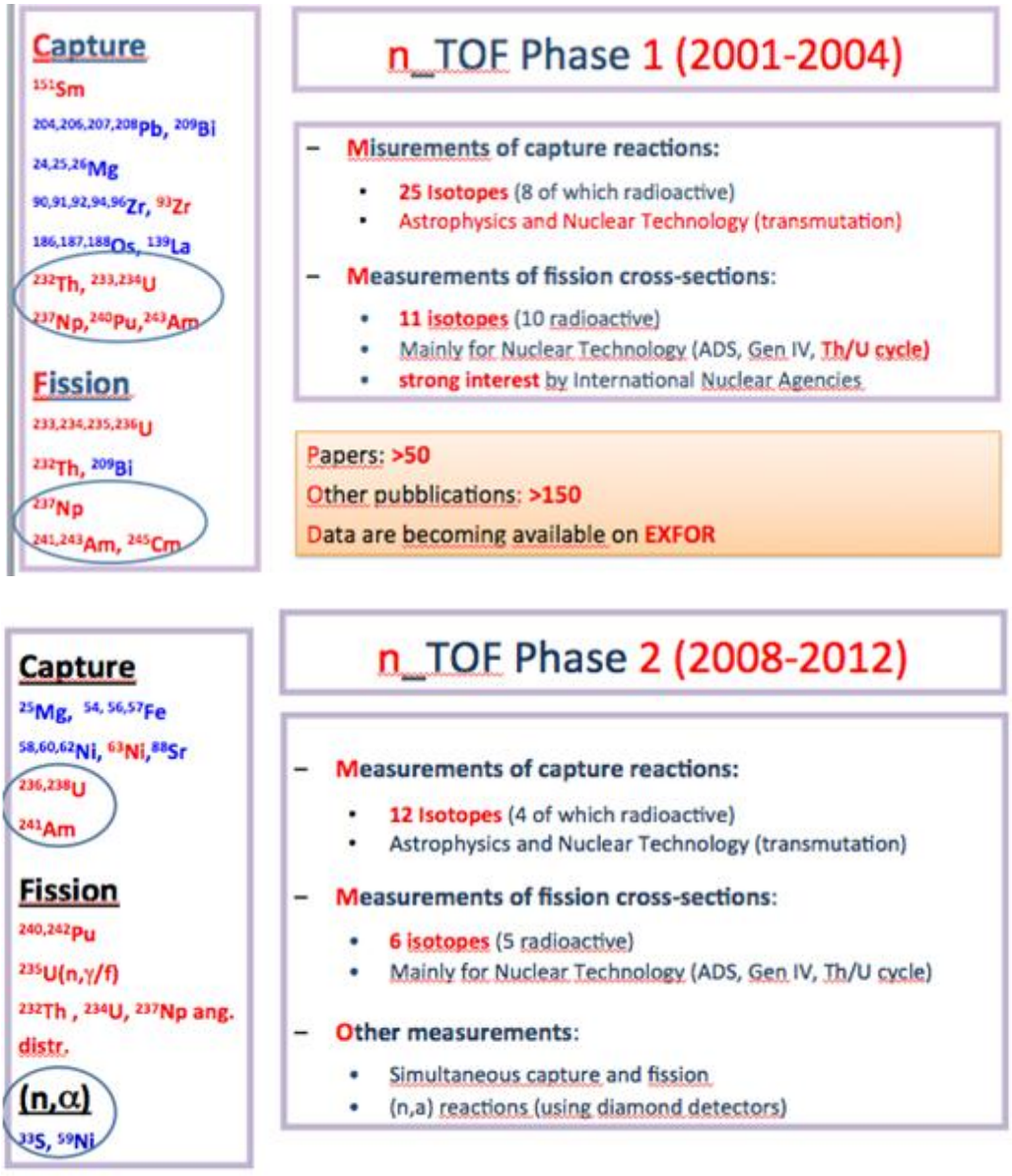

3.4. Spallation proton-induced (>200MeV) white spectrum neutron beams

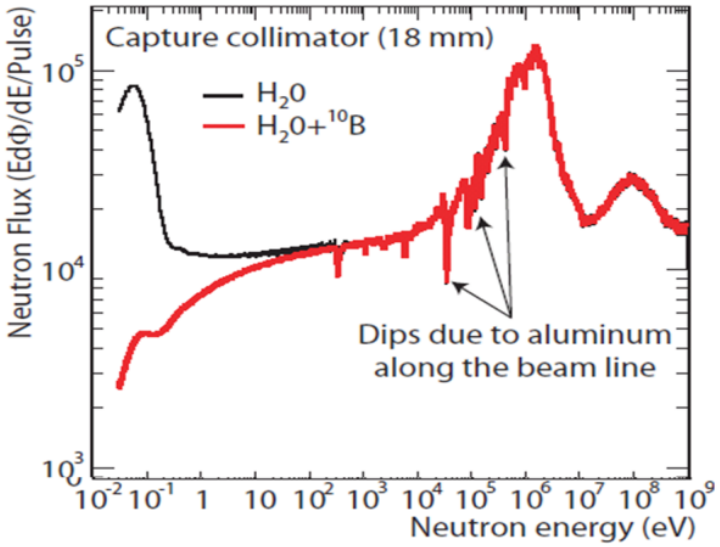

FIG. 2. Evaluated neutron flux in the configuration with the capture collimator (18 mm diameter) with water and borated water as moderator.

TABLE.2. NUMBER OF NEUTRONS PER PULSE, ASSUMING A NOMINAL PULSE INTENSITY OF 7X1012 PROTONS PER PULSE, IN DIFFERENT NEUTRON ENERGY RANGES IN THE CAPTURE AND FISSION COLLIMATOR MODES USING WATER AND BORATED WATER AS MODERATOR

Neutron energy	Neutrons/pulse		
	Capture mode		Fission mode
	H_2O	$H_2O+^{10}B$	$H_2O+^{10}B$
10-100 meV	1.0×10^5	1.5×10^4	3.3×10^5
0.1-1 eV	4.3×10^4	1.3×10^4	2.9×10^5
1-10 eV	2.7×10^4	2.0×10^4	4.3×10^5
10-100 eV	2.8×10^4	2.5×10^4	5.3×10^5
0.1-1 keV	2.9×10^4	2.9×10^4	6.2×10^5
1-10 keV	3.2×10^4	3.2×10^4	6.8×10^5
10-100 keV	4.4×10^4	4.4×10^4	9.4×10^5
0.1-1 MeV	1.3×10^5	1.3×10^5	2.7×10^6
1-10 MeV	1.5×10^5	1.5×10^5	3.1×10^6
10-100 MeV	5.0×10^4	5.0×10^4	1.0×10^6
0.1-1 GeV	4.7×10^4	4.7×10^4	9.5×10^5
Total	$\mathbf{6.8\times10^5}$	$\mathbf{5.5\times10^5}$	$\mathbf{1.2\times10^7}$

4.2. SPATIAL BEAM PROFILE

The spatial profile of the neutron beam and its energy dependence in the capture collimator configuration were already investigated in detail in n_TOF Phase1 by means of a 1D-stripped MicroMegas detector [8]. The results were found to be in agreement with simulations available at the time. In the current t n_TOF Phase2, a new 2D pixelated MicroMegas (pixel-MGAS) detector has been developed [9]. This new detector, with a 5 cm

diameter active area including 308 square pixels of 2.5 mm side read out by 4 Gassiplex cards, has provided in 2012 results compatible with those measured in 2001 with the stripped-MicroMegas detector. An illustration of the n_TOF beam profile at 183.2 m flight path is given in Fig. 3, where the beam projection in the vertical direction for neutron energies between 0.1 and 1eV is shown for both capture and fission collimator modes.

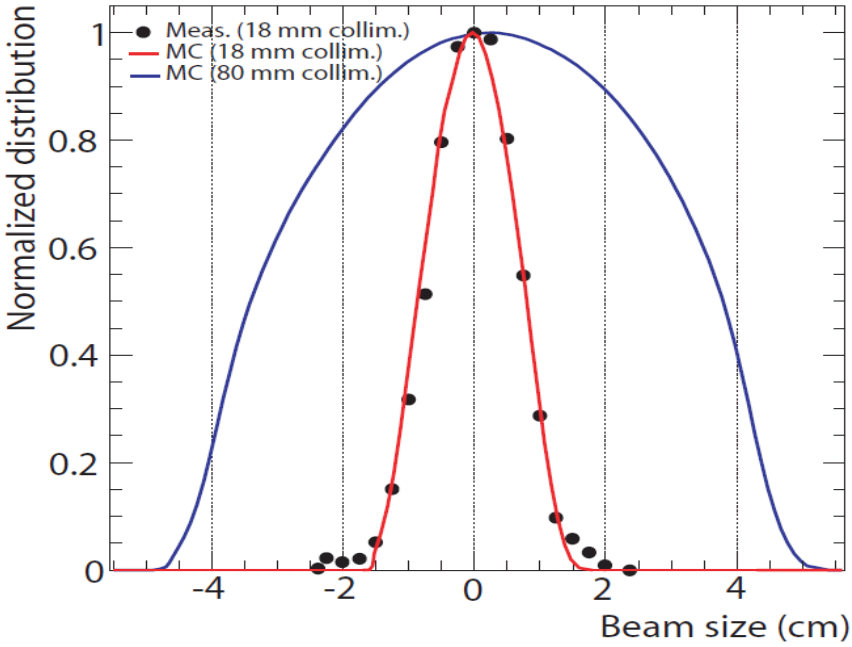

FIG.8. Neutron beam profile at 183.2 m in the vertical direction as measured with the pixel-MGAS detector between 0.1eV and 1eV.

4.3. THE N_TOF RESOLUTION FUNCTION

The resolution function describes the distribution of the measured time-of-flight for neutrons with a given kinetic energy. Several experimental conditions like the primary beam pulse duration (7 ns RMS in the case of n_TOF), the moderation time in the target-moderator assembly, and the detector response, contribute to the fact that the time-of-flight *t* and the flight length *L* for a neutron of energy *En* are not fixed values but merely distributions. The resolution function of the n_TOF facility has been simulated in the start-up phase by two different codes, including FLUKA [10] and CAMOT [11], yelding similar results within the available statistics.

5. N_TOF EXPERIMENTAL APPARATUS

The n_TOF Collaboration has setup all the necessary infrastructure for neutron cross section measurements in the present n_TOF experimental area. These include neutron flux monitors, capture γ ray detectors, fission detectors and a high-performance data acquisition system based on fast FADC (flash analogue-to-digital converters).

3.4. Spallation proton-induced (>200MeV) white spectrum neutron beams

TABLE.3. VALUES OF THE RESOLUTION FUNCTION WIDTHS AND CORRESPONDING ENERGY RESOLUTION AS FUNCTION OF NEUTRON ENERGY FOR THE CONFIGURATION WITH BORATED WATER AS MODERATOR

E_n (eV)	$\Delta E_n/E_n$
1	$4.3{\cdot}10^{-4}$
10	$4.3{\cdot}10^{-4}$
10^2	$4.3{\cdot}10^{-4}$
10^3	$7.5{\cdot}10^{-4}$
10^4	$1.7{\cdot}10^{-3}$
10^5	$5.4{\cdot}10^{-3}$
10^6	$2.8{\cdot}10^{-3}$

5.1. THE INNOVATIVE DATA ACQUISITION SYSTEM AT N_TOF

Due to the specific experimental conditions present at the n_TOF facility, namely the high instantaneous neutron flux, a critical element of the setup is the data acquisition and the associated processing system. In fact, in the presence of high count rates - which are a direct consequence of the intense neutron flux - the density of signals in the detectors is very high. Therefore, a high probability of signal pile-up exists. In such experimental context the use of standard Data Acquisition Systems (DAQ) would be inadequate, since they would be affected by a large dead-time. Additionally, pile-up events would not be identified and reconstructed, with the consequence of large systematic uncertainties on the final cross-section data.

According to these requirements, the n_TOF DAQ has been designed based on Flash Analogue to Digital Converters (flash-ADCs or FADC). Their main benefit is the possibility to sample and record the full analogue waveform of the detector signals for each neutron pulse, which can be later processed off-line in order to extract the required information, such as time-of-flight, amplitude, charge, baseline and others signal characteristics. The use of FADCs allows keeping under control systematic uncertainties associated with the detectors performances, during the off-line analysis [12]. The sampling is performed by means of fast Flash Analogue to Digital Converter (FADC), with sampling rates up to 1 Giga Samples/s.

5.2. DETECTORS

For neutron capture cross section measurements at a neutron time-of-flight facility such as n_TOF, the detection of γ ray following a capture or fission event can be done with different techniques (see Fig. 4.).

A technique in which one γ ray per capture event is detected has been used at n_TOF and it is based on C6D6 liquid scintillator detectors. A different approach is to use a detection system in which the full γ ray cascade is detected for each capture event. In this case it is fundamental to record the γ rays with high detection efficiency, ideally 100% [13].

3.4. Spallation proton-induced (>200MeV) white spectrum neutron beams

The n_TOF TAC is based on BaF2 crystals. It is an array of 40 modules which covers 95% of the 4πsolid angle the detection efficiency (when used in calorimeter mode) is of the order of 99%. With the high efficiency of the n_TOF TAC it has been possible to measure samples with low mass (hence, with relatively low intrinsic activity for radioactive species) [14].

For neutron-induced charged particle (n,cp) reaction cross-section measurements, the Diamond Mosaic-Detector has been developed at n_TOF. The detector consists of 9 single-crystal chemical vapour deposition (sCVD) diamond diodes, of 0.15 mm thickness. The detector is designed to be positioned in the n_TOF neutron beam, downstream of the isotope of interest, covering 2π of the solid angle. The high-resolution spectroscopic detector allows the discrimination of background from physics events via the recorded amplitude spectrum [15].

For fission reaction, one employed detector is the Parallel Plate Avalanche Chamber (PPAC) consisting of two twin parallel stretched foils with a very low gas pressure in between, operating with the same principles as a multi-wire proportional chamber. The targets are deposited on 2 μm aluminium foils, which are thin enough to allow the coincident detection of the fission fragments. On both sides of each target two 20x20 cm^2 PPACs are used for detecting the fission fragments and to measure their position of origin [16].

Simirlarly, MicroMegas is a gaseous detector based on a relatively simple detection principle and adapted to (n,cp) and (n,f) measurements. The gas volume is separated in two regions by a "Micromesh" which is a thin metallic foil (several μm) composed on all usable surface of holes having a 35 μm of diameter and spaced on 100 μm. A low electric field (~1 kV/cm) is applied to the first region where the conversion (by using for instance a ^{6}Li or ^{10}B foil to convert incident neutron into charged particles) and drift of the ionization electrons occur. In the second region a high electric field (> 10 kV/cm) is applied where the multiplication and amplification take place. Ionization electrons are created by the energy deposition of an incident charged particle in the conversion gap. In the amplification region, a high field (40 to 70 kV/cm) is created by applying a voltage of a few hundred volts between the micromesh and the anode plane, which collects the charge produced by the avalanche process [8].

6. EXPERIMENTAL AREA 2 (EAR-2)

The overall efficiency of the experimental program and the range of possible measurements will be significantly improved with the construction of a 2nd Experimental Area (EAR2), vertically located 20 m on top of the n_TOF spallation target (see Fig. 5) [17]. The configuration of the foreseen n_TOF Experimental Area 2 allows to measure neutron-induced reactions with the following advantages:

6.1. HIGHER NEUTRON FLUX

Being closer to the spallation target (flight path of 20 m) the configuration provides a higher instantaneous neutron flux with respect to the present neutron fluence in EAR1 (flight path of 185m from the spallation target); this is a clear advantage for the measurement of reactions on samples with very small masses or reactions with very small cross sections. The reduced energy resolution – which is an important aspect for the resolved resonances region -

due to the smaller distance between the new experimental area and the target does not affect the measurements at high neutron energies.

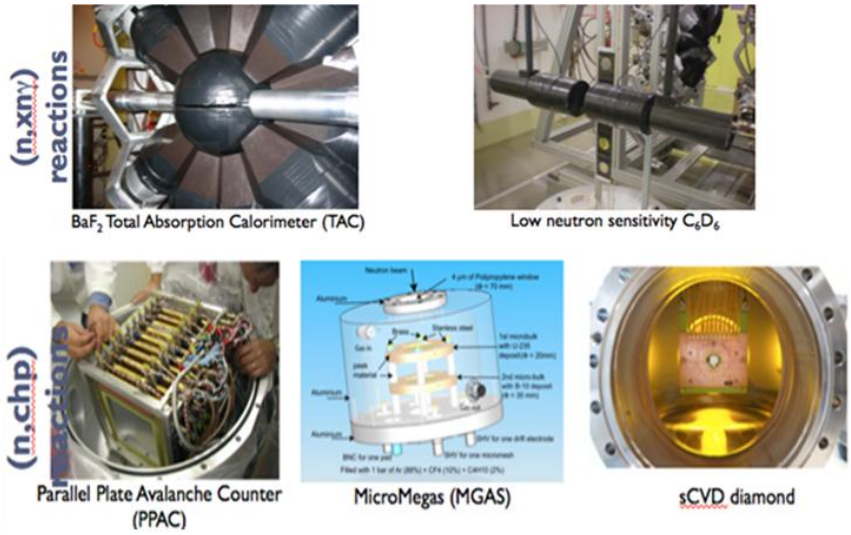

FIG.4. Different Detectors set-ups used at n_TOF.

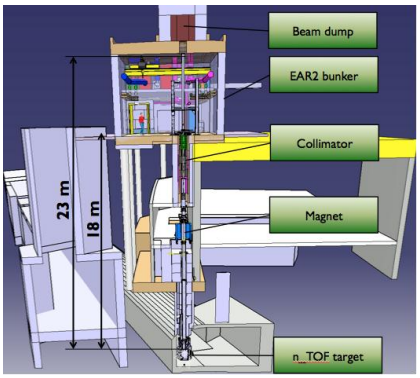

FIG.5. Schematic view of the EAR2.

The neutron fluence, energy resolution and background are the basic parameters that describe the performances of each facility. Typically each facility made a great effort to reduce the background by introducing appropriate shielding, collimation system etc. However, when short lived radioactive targets are to be measured (as it is the majority of most of the recent n_TOF proposals) the background due to the natural radioactivity can be decreased by decreasing the sample mass, with direct consequence a proportional decrease on the reaction rate $dN_{reaction}/dt$. The reaction rate is also directly proportional to the neutron fluence , which in the case of EAR2 is ~25 times larger than what is available in EAR1 (see Fig. 6). This means that lower mass samples can be used or that an improved signal-to-background ratio can be obtained.

3.4. Spallation proton-induced (>200MeV) white spectrum neutron beams

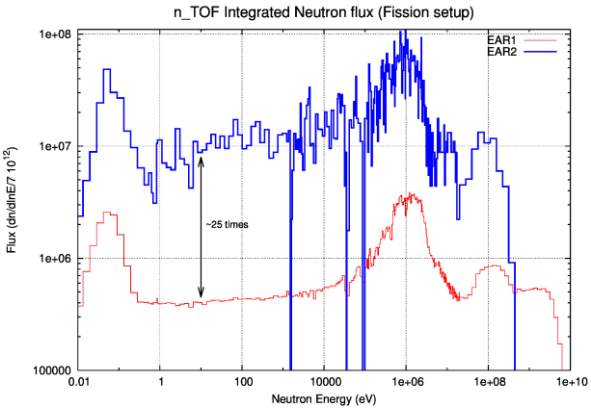

FIG. 6. Comparison between the neutron fluence of the proposed EAR2 and the existing EAR1. The significant absorption dips in the EAR2 fluence are due to the large amount of structural Al between the spallation target and the vertical vacuum tube leading to EAR2.

6.2. Higher signal to background ratio for radioactive samples

In the case of time-of-flight measurements on radioactive samples, the background induced by the radioactive decay of the sample is directly proportional to the time needed for the measurement. A range of neutron energy ΔE corresponds to a window in time-of-flight ΔT, and the signal-to-noise ratio is therefore proportional to the ratio $\Delta E/\Delta T$. From the classical relation between time-of-flight and neutron energy, it follows that $\Delta E/\Delta T$ is inversely proportional to the flight length L. Therefore the new short flight path will result in a more favorable signal to radioactive background ratio by a factor 185/19 which equals nearly a factor 10 *(see FIG.7.)* [18].

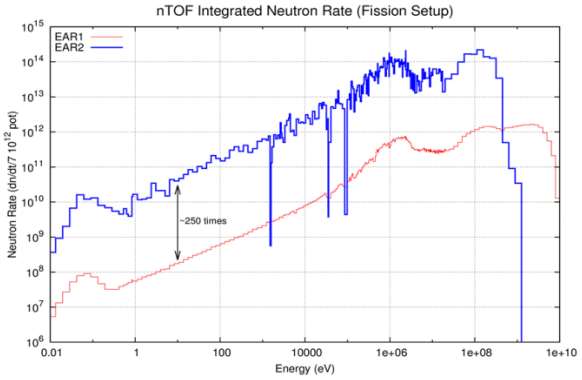

FIG. 7. Neutron rate (dN/dt) for the two experimental areas EAR1 and EAR2.

7. SCIENTIFIC CASE

The realization of the 2nd Experimental Area, with its short flight path, will contribute to a substantial improvement in experimental sensitivities and will open a new window to stellar nucleosynthesis, technological issues (such as transmutation or design of safety of future nuclear energy systems) and basic nuclear physics by allowing to measure neutron-induced reactions which are not accessible so far at any other installation. The main advantages of the 2nd Experimental Area are the following:

3.4. Spallation proton-induced (>200MeV) white spectrum neutron beams

- Neutron-induced reaction measurements can be performed on very small mass samples. This feature is crucial to reduce the activity of unstable samples and in cases where the available sample material is limited. (ex. ^{238}Pu, ^{241}Pu ^{243}Cm, ^{244}Cm, ^{245}Cm, ^{242}mAm, ^{231}Pa, ^{233}Pa).
- Measurement can be performed on isotopes with very small cross sections for which the optimization of the signal/background ratio is an essential prerequisite.(ex. ^{86}Kr, ^{138}Ba, ^{140}Ce, ^{208}Pb).
- Measurement can be performed on much shorter time scales. Repeated runs with modified conditions are essential to check corrections and to reduce systematic uncertainties.

8. CONCLUSION

CERN n_TOF has proven to be a unique facility in the world for its performance. Since 2001 with its rich scientific program, the n_TOF experiment is contributing to the world efforts aimed at collecting high quality data, mostly on capture and fission neutron-induced reactions.

The transformation of the Experimental Area into Work Sector of Type A has allowed performing measurement of capture and fission cross section of "unsealed" samples of highly radioactive isotopes.

With the construction of the Experimental Area 2, the n_TOF installation is going to open new perspectives in the measurements of fission and capture cross-section with lower samples masses and/or with improved signal-to-background ratio for radioactive species.

REFERENCES

[1] CHIAVERI, E., et al. Past,Present and future of the n_TOF facility, Journal of the Korean Physical Society, Vol. 59, No. 2, August 2011, pp. 1620_1623.

[2] KAEPPELER, F., Progr.Particles Nucl. Phys. 43(1999) 439.

[3] WALLESTEIN, G., et al. Rev.Mod.Phys. 69(1997) 995.

[4] RUBBIA, C., et al., A high Resolution Spallation Driven Facility at the CERN-PS to measure Neutron Cross Sections in the Interval from 1eV to 250MeV, CERN/LHC/98-02(EET)+Add1.

[5] ABRAMOVICH, S., et al. (the n_TOF Collaboration) European Collaboration for High Resolution Measurements of Neutron Cross Sections between 1eV and 250MeV, CERN/SPSC 99-8, 1999.

[6] BILLINGE, R., the CERN PS Complex: A multipurpose Particle Source, Proc.Of XIIth Int. Conf. on High Energy Acc., 1983.

[7] GUERRERO, C., et al., Performance of the neutron Time-of-Flight facility n TOF at CERN, submitted to Eur. Phys. J. A (2012).

[8] GIOMATARIS, Ph., et al., "MICROMEGAS: a high-granularity position-sensitive gaseous detector for high particle-flux environments," Nucl. Instr. and Methods, A 376, 29 (1996).

[9] BELLONI, F., et al., A micromegas detector for neutron beam imaging at the n TOF facility at CERN, Procc. Int Conf. Nuclear Data for Sc. and Tech., NY, USA (2013).

[10] The n TOF Collaboration, CERN n TOF Facility: Performance Report, CERN/INTC-O-011, INTC-2002-037 CERN-SL-2002-053 ECT (2006).
[11] COCEVA, C., et al., on the figure of merit in neutron time-of-flight measurements Nucl. Instrum. Meth. A 489 (2002) 346-356.
[12] ABBONDANNO, U., et al. The data acquisition system of the neutron time-of-flight facility n_TOF at CERN. Nucl. Instr. And Methods in Physics research A 538 (2005) 692-702.
[13] PLAG, R., et al., An optimized C6D6 detector for studies of resonance-dominated (n,γ) cross-sections, Nucl. Instr. and Meth. A 496 (2003) 425-436.
[14] GUERRERO, C., et al., The n_TOF Total Absorption Calorimeter for neutron capture measurements at CERN, Nucl. Instr. and Meth. A 608 (2009) 424-433.
[15] PERNEGGER, H., et al., Charge-carrier properties in synthetic single-crystal diamond measured with the transient-current technique, J. Appl. Phys. 97, 073704 (2005).
[16] PARADELA, C., et al, Neutron-induced fission cross section of ^{234}U and ^{237}Np measured at the CERN Neutron Time-of-Flight (n_TOF) facility, Phys. Rev. C 82, 034601 (2010).
[17] CHIAVERI, E., et al., Proposal for n_TOF Experimental Area 2 (EAR-2), CERN-INTC-2012-029.
[18] CHIAVERI, E., et al. Present Status and future programs of the n_TOF experiment EPJ Web of Conferences 21, 03001(2012).

3.4. Spallation proton-induced (>200MeV) white spectrum neutron beams

SPALLATION NEUTRON SOURCE OF THE TOF-FACILITY GNEIS IN GATCHINA

O.A. SHCHERBAKOV, A.S. VOROBYEV

Petersburg Nuclear Physics Institute,
188300, Gatchina, Leningrad district,
Russia
Email: shcherba@pnpi.spb.ru

The neutron spectrometer GNEIS [1,2] is based on the 1000 MeV proton synchrocyclotron of PNPI and intended for neutron-nucleus interaction studies utilizing the TOF-technique over a wide range of neutron energy from ~ 10^{-2} eV up to ~ 800 MeV. The diagram of the experimental complex of the SC-1000 synchrocyclotron (including the hangar of the GNEIS TOF-spectrometer) at the PNPI is shown in Fig.1. The main parameters of the accelerator and GNEIS facility are given in Tables 1, 2.

The general layout of the GNEIS is given in Fig.2. The water-cooled lead target situated inside the vacuum chamber of the accelerator is used as a pulsed spallation neutron source with maximal average intensity $3 \cdot 10^{14}$ n/s (in 4π solid angle), the burst duration of ~10 ns and repetition rate up to 50 Hz. The neutron source is equipped with the polyethylene moderator. The mutual disposition of the target and moderator slabs is shown if the insert of Fig.2. The target and moderator can be moved remotely in the vertical and radial directions for optimum position. There are 5 holes for the neutron beams coming through 6 m thick heavy concrete shielding wall of the SC-1000 central machine room. The flight paths of the GNEIS are arranged so that only neutron beam N5 looks at the bare lead target being used for measurements in the fast and intermediate neutron energy range 100 keV to 800 MeV. The other paths used for measurements with neutron resonance energies of 1 eV-100 KeV are collimated so that their axes come through the moderator surface. This reduces the overloading effect induced in the detectors by γ-flash and fast neutrons.

The flight paths are evacuated aluminium and steel tubes sealed with 0.25 mm thick Al-windows. The collimation system of the spectrometer consists of the brass collimator K1, cast-iron collimator K2, and a number of brass, lead, and borated polyethylene collimator jaws located inside the evacuated tubes. Each flight path is equipped with the cast-iron baffle and steel-concrete beam-stop. The measurement stations at flight path distances of 35-50 m are situated in the experimental area of the GNEIS building. If necessary, measurements at the flight path N5 are carried out with the use of "clearing" magnet placed at 30 m from the neutron producing target. This magnet removes charged particles produced in the collimators and filters of the neutron beam.

In the inserts of Fig.2 are shown the titles of some experiments [3-8] carried out at the GNEIS facility which are associated with the nuclear data measurements. The experimental capabilities of the GNEIS in this field could be demonstrated by the results of two following works. The highest accuracy has been achieved in the measurements of neutron total cross sections of lead isotopes Pb-204, Pb-206, Pb-207 and Pb-208 [5] in the energy range 1 eV – 10 KeV. The unique set of the measurements of neutron fission cross sections of U-233, U-238, Th-232, Np-237, Pu-239, Pu-240, Am-243, Bi-209, Pb-nat and W-nat [7,8] has been carried out in the intermediate energy range 1 MeV – 200 MeV under support of the ISTC Projects 609 and 1971. The neutron flux and energy resolution at the flight path 48.5 m, used in these measurements, are shown in Fig.3 and 4, respectively.

3.4. Spallation proton-induced (>200MeV) white spectrum neutron beams

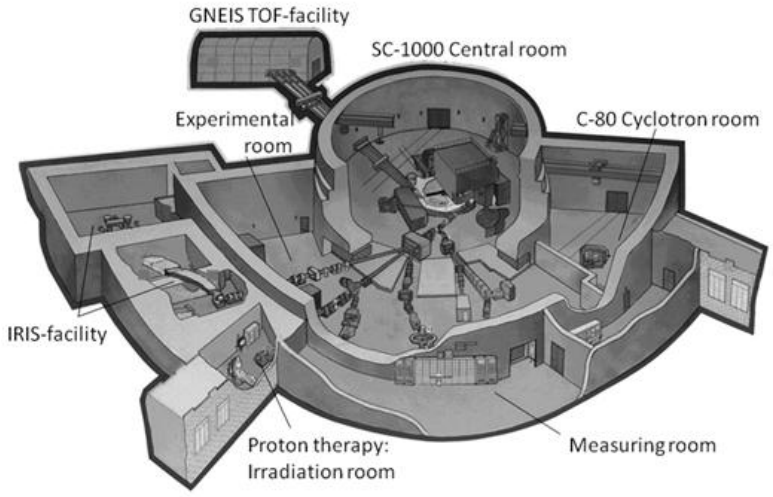

FIG.1. General view of the PNPI accelerator complex rooms.

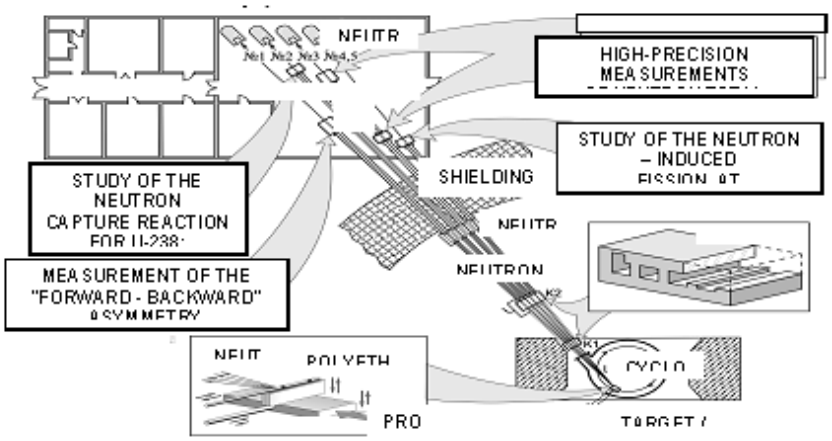

FIG.2. General view of the GNEIS time-of-flight facility.

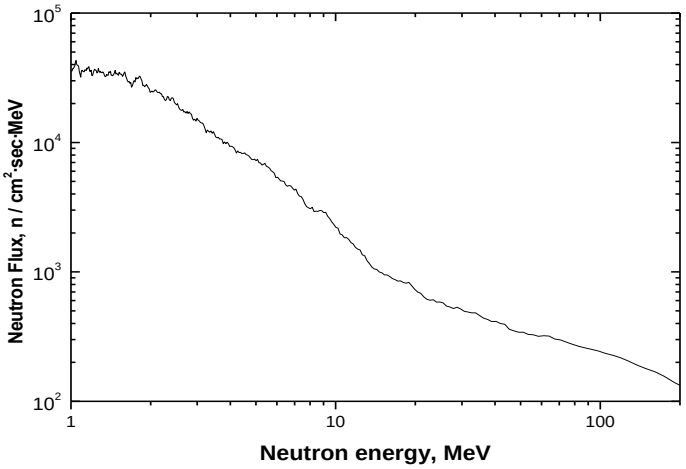

FIG.3. The neutron flux at the 48.5 m- flight path normalized to a value of 1μA of the proton beam on the neutron source target.

3.4. Spallation proton-induced (>200MeV) white spectrum neutron beams

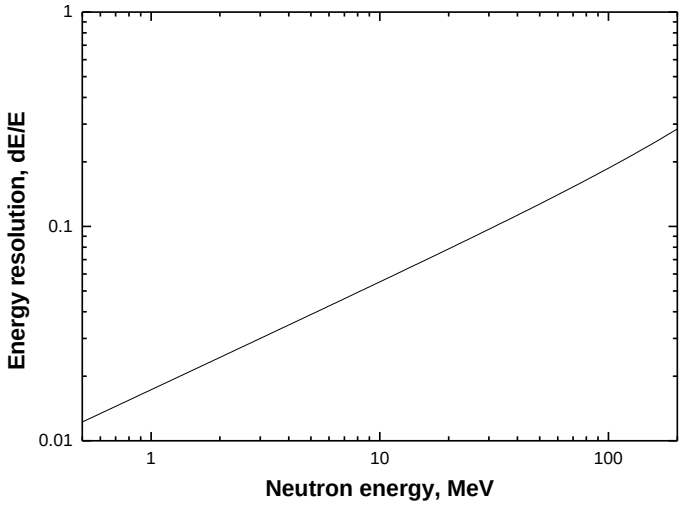

FIG.4. Neutron energy resolution for the flight path length 48.5 m.

The shape of the neutron spectrum of beam N5 resembles that of atmospheric neutron radiation in the energy range 1 MeV- 1000 MeV and meets the requirements of the JEDEC international standard. Recently, testing of the neutron radiation resistance of electronics has been started at the GNEIS facility [2].

TABLE 1. PARAMETERS OF THE PNPI SYNCHROCYCLOTRON

Proton energy	1000 MeV
Internal proton beam current	≤ 3 μA
Repetition rate	40–60 Hz
Extraction coefficient	30 %
Duty cycle coefficient	50 %
Accelerating voltage	10 kV
Frequency range	30-13 MHz
Electric power supplied	1 MW
Diameter of the magnet pole pieces	685 cm
Width of the gap between poles	50 cm
Magnet weight	8,000 t

3.4. Spallation proton-induced (>200MeV) white spectrum neutron beams

TABLE 2. PARAMETERS OF THE NEUTRON TIME-OF-FLIGHT SPECTROMETER GNEIS

Pulsed neutron source	
Average fast neutron intensity	$\leq 3 \cdot 10^{14}$ n/s
Duration of the fast neutron pulse	~ 10 ns
Repetition rate	≤ 50 Hz
Dimensions of internal water-cooled rectangular lead target	40 cm x 20 cm x 5 cm
Dimensions of rectangular polyethylene moderator	1 m x 10 cm x 5 cm
Spectrometer	
Number of evacuated flight paths	5
Length of flight paths	35-50 m
Experimental area (GNEIS Building)	15 m x 30 m

REFERENCES

[1] ABROSIMOV., N.K., et al., Neutron Time-of-Flight Spectrometer GNEIS at the Gatchina 1 GeV Proton Synchrocyclotron. Nucl. Instrum. Methods A242, N1, 1985, p.121-133.

[2] ABROSIMOV., N.K., et al.,. Development and experimental study of the neutron beam at the synchrocyclotron of the Petersburg Nuclear Physics Institute for radiation tests of electronic components. Instruments and experimental techniques, v.53, N4, 2010, p.469-476.

[3] SHCHERBAKOV., O.A., Experimental investigations of the (n,γf)-reaction. Soviet Journal of Particles and Nuclei, 21(2), March-April, 1990, p.177-198.

[4] SHCHERBAKOV., O.A., Laptev, A.B., Prefission and Capture Gamma rays in Neutron Resonances of 235U, 238U and 239Pu. In book "Capture Gamma ray Spectroscopy and Related Topics: 10th International Symposium, Santa Fe, New Mexico, 30 August – 3 September 1999". Ed. S.Wender. Melville, New York, American Institute of Physics, 2000, v.529, p.710-712.

[5] LAPTEV., A.B., et al., Neutron Total Cross Sections of ^{204}Pb, ^{206}Pb, ^{207}Pb and ^{208}Pb and the Neutron Electric Polarizability. Proceedings of the International Conference on Nuclear Data for Science and Technology, October 7-12, 2001, Tsukuba, Ibaraki, Japan. J.Nucl.Sci. and Tech., Suppl.2, v.1, 2002, p.327-330.

[6] GAGARSKII., A.M., et al., Properties of *p* resonances in the fission of ^{235}U by neutrons with energies of 1-136 eV. JETP Lett., v.54, No.1, 1991, p.7-10.

[7] SHCHERBAKOV., O.A.,et al., Neutron-Induced Fission of ^{233}U, ^{238}U, ^{232}Th, ^{239}Pu, ^{237}Np, ^{nat}Pb and ^{209}Bi Relative to ^{235}U in the Energy Range 1-200 MeV. Proceedings of the International Conference on Nuclear Data for Science and Technology, October 7-12, 2001, Tsukuba, Ibaraki, Japan. J.Nucl.Sci. and Tech., Suppl.2, v.1, 2002, p.230-233.

[8] LAPTEV., A.B., et al., Neutron-induced fission cross sections of ^{240}Pu, ^{243}Am and ^{Nat}W in the energy range 1-200 MeV. In book "The International Conference on Nuclear Data for Science and Technology, September 26-October 1, 2004, Santa Fe, New Mexico, USA. Editors: Haight R., Chadwick M. , Kawano T., Talou P. AIP Conference Proceedings, Vol.769, Melville, New York, 2005, Part 1, p.865-869.

3.4. Spallation proton-induced (>200MeV) white spectrum neutron beams

NUCLEAR DATA MEASUREMENT USING THE ACCURATE NEUTRON-NUCLEUS REACTION MEASUREMENT INSTRUMENT (ANNRI) IN THE JAPAN PROTON ACCELERATOR RESEARCH COMPLEX (J-PARC)

T. KATABUCHI[*], K. FURUTAKA[**], T. FUJII[***], S. GOKO[**], K. Y. HARA[**], H. HARADA[**], K. HIROSE[**], J. HORI[***], M. IGASHIRA[*], T. KAMIYAMA[+], A. KIMURA[**], T. KIN[**], K. KINO[+], F. KITATANI[**], Y. KIYANAGI[+], M. KOIZUMI[**], T. MATSUHASHI[*], M. MIZUMOTO[*], S. NAKAMURA[**], M. OHTA[**], M. OSHIMA[**], K. TERADA[*], Y. TOH[**]

[*]Research Laboratory for Nuclear Reactors, Tokyo Institute of Technology,
2-12-1 Ookayama, Meguro-ku, Tokyo 152-8550, Japan
[**]Nuclear Science and Engineering Directorate, Japan Atomic Energy Agency,
2-4 Shirakata Shirane, Naka, Ibaraki 319-1195, Japan
[***]Research Reactor Institute, Kyoto University, Kumatori, Sennan, Osaka 590-0494, Japan
[+]Graduate School of Engineering, Hokkaido University,
Kita 13 Nishi 8, Kita-ku, Sapporo, Hokkaido 060-8628, Japan
Email:buchi@nr.titech.ac.jp

Abstract

A nuclear data measurement project using a spallation neutron source is ongoing at the Japan Proton Accelerator Research Complex (J-PARC). The Accurate Neutron-Nucleus Reaction Measurement Instrument (ANNRI) was built as a beam line for measurement of neutron capture cross sections in J-PARC. The project is aimed to measure the neutron capture cross sections of minor actinides (MA) and long-lived fission products (LLFP) for design of innovative nuclear reactors and study of nuclear transmutation of nuclear waste. The ongoing ANNRI project is overviewed.

1. PROJECT OVERVIEW

Prior to the present ongoing project, we executed a project on comprehensive nuclear data research from Japanese fiscal year 2005 to 2009, titled “Study on nuclear data by using a high intensity pulsed neutron source for advanced nuclear system,” as a collaborative work of eight organizations [1,2]. This project was carried out with financial support from the Innovative Nuclear Research and Development Program of the Ministry of Education, Culture, Sports, Science and Technology of Japan. We were motivated to start the project by demand for accurate nuclear data of MAs and LLFPs, required to estimate the production and the transmutation rates for the design of advanced nuclear reactors or accelerator driven systems. In the main part of the project, we designed and built a neutron beam line for neutron capture cross section measurements using the emerging new Japanese Spallation Neutron Source (JSNS) in J-PARC. A large Ge detector array was built and installed in the beam line. This is the first large-scale use of Ge detectors for time-of-flight (TOF) experiments with a spallation neutron source. We also prepared radioactive samples of MA and LLFP for the measurements. In addition, this project covered not only activities in J-PARC but also research activities in other facilities, for example, capture experiments in the Kyoto University Research Reactor Institute (KURRI) and the Tokyo Institute of Technology (Tokyo Tech) as well as fission cross section measurements in KURRI and (γ, n) cross section measurements in the National Institute of Advanced Industrial Science and Technology.

Following the end of the project in March, 2010 (Japanese fiscal year 2009), we started the next project in 2010, titled “Systematic Study on Neutron Capture Reaction Cross Sections for the Technological Development of Nuclear Transmutation of Long-Lived Nuclear Wastes,” with financial support from the Grants-in-Aid for Scientific Research

(KAKENHI) of the Japan Society for the Promotion of Science [3]. The purpose of this project is systematic study of neutron capture cross sections of MAs and LLFPs for nuclear transmutation of nuclear waste. The highlight of this project is measurement in J-PARC, taking full advantages of the intense pulsed neutron beam of J-PARC and the high energy resolution of the Ge spectrometer. In addition, the project includes measurements in the keV energy region in Tokyo Tech, and in the energy region from thermal to eV in KURRI. We intend to reduce systematic uncertainties by overlapping the measurements of the three facilities. A nuclear theorist of the Nuclear Data Center of the Japan Atomic Energy Agency (JAEA) also participates in the project to analyze the experimental results, to elucidate the reaction mechanism and to provide reliable calculated cross sections. This overview focuses on J-PARC and ANNRI. Facilities and research activities at KURRI and Tokyo Tech are described in other pages in this report.

2. J-PARC

J-PARC is a research complex utilizing a high intensity proton beam to produce secondary particle beams such as neutrons, muons, kaons and neutrinos. Providing the secondary particle beams, J-PARC serves a wide range of scientific fields. J-PARC consists of a series of accelerators: a 180 MeV linear accelerator (planned to upgrade to 400 MeV in 2013), a 3 GeV synchrotron and a 50 GeV synchrotron. For neutron production, a proton beam from the 3 GeV synchrotron is used. JSNS in the Materials and Life Science Facility (MLF) provides neutron beams for users.

2.1. JAPANESE SPALLATION NEUTRON SOURCE (JSNS)

The 3 GeV proton beam from the rapid cycling synchrotron is injected into a mercury target at MLF at a repetition rate of 25 Hz. Mercury is chosen as the target material, because it can remove the high density heat generated by the proton beam efficiently. Mercury is liquid metal at room temperature, thus allowing for heat removal by circulating mercury between the target vessel and a heat exchanger. Mercury is also good from the viewpoint of neutron production. Its high weight density and large atomic number yield large neutron production. One 3 GeV proton produces about 75 neutrons in the spallation reaction in the mercury target [4].

The spallation neutrons generated in JSNS are moderated with liquid hydrogen moderators. The liquid hydrogen in the moderators is maintained at a temperature below 20K. There were three types of moderators installed: Coupled, Decoupled and Poisoned Decoupled. Each of them has a different time structure of moderated neutron beam. The moderators were located under or above the mercury spallation target. JSNS has 23 beam ports to extract neutrons from the moderators.

The proton beam power deposited into the spallation target has been increased in stages since it was commissioned. The facilities in J-PARC were severely damaged by the 2011 East Japan earthquake. However, after only a ten month shutdown, thanks to efforts of the accelerator and technical staff, J-PARC started to provide beams for users. The current beam power at JSNS reaches about 300 kW (December, 2012). The upgrade of the linear accelerator is planned to increase beam power in 2013. The final goal of the beam power at JSNS is set to be 1 MW.

3.4. Spallation proton-induced (>200MeV) white spectrum neutron beams

2.2. ANNRI

ANNRI was built as an instrument for measuring neutron capture cross sections at the No. 4 beam port that extracts neutrons from the Coupled Moderator. The details of ANNRI were described in Ref. 1-3. Figure 1 illustrates ANNRI. The neutron beam from the spallation neutron source is collimated with collimators to form a beam spot at the sample positions with a desired beam diameter. ANNRI has two experimental areas as shown in Fig. 1. The upstream experimental area (Experimental Area 1) is for experiments using the Ge spectrometer, which is a large Ge detector array. The high energy resolution of Ge detectors allows for high resolution γ ray spectroscopy, leading to a more detailed study of the neutron capture reaction. The downstream experimental area (Experimental Area 2) is for an NaI(Tl) spectrometer. NaI (Tl) detectors have been used for capture cross section measurements for decades. The pulse-height weighting technique with NaI (Tl) detector is an established, reliable method. The combination of these two different detector systems (Ge and NaI(Tl)) aims to reduce systematic uncertainties by utilizing independent and complementary measurements of both new and traditional techniques. The NaI(Tl) detectors are also intended for use for neutron energies above 1 keV, where a Ge detector cannot work well due to its slow recovery time from saturation by strong γ ray bursts called “gamma flash” occurring when the proton beam impacts the spallation target.

There were installed the three instruments, a T0 chopper, a double disk chopper and a neutron filter system, in the upstream area between L=13 m and L=15 m. The T0 chopper is used for cutting neutron bursts with energies higher than about 10 eV. The double disk chopper is a band filter to transmit neutrons in a selected energy window in the eV region. The double disk chopper can be also used for cutting low energy neutrons overlapping the next TOF frame. The neutron filter system consists of Pb, Mn, Co, In, Ag, Cd and Al filters. The Pb filter is two thick Pb plates for shielding against the gamma flash. The Mn, Co, In, Ag and Al filters are notch filters for the neutron beam. The Cd filter is for cutting the low energy frame-overlapping neutrons.

The collimator system of ANNRI was designed carefully to minimize background in capture experiments using the Ge spectrometer and the NaI(Tl) spectrometer [5]. The collimator design is based on the results of Monte Carlo simulation using the PHITS code. There are five collimators from the moderator to the sample position of the Ge spectrometer (L = 21.5 m). The most downstream collimator called the "rotary collimator" defines the spatial distribution at the L = 21.5 m position. Using the rotary collimator, the beam size can be selected from four sizes by rotating a cylinder having four differently sized holes. The cylinder is 400 mm diameter x 1700 mm long, mainly made of iron except for the 100 mm downstream part which is made of borated polyethylene. The designed diameters of the beam spot sizes are 3, 7 and 22 mm. One hole is currently not in use. These diameters are the sizes of the umbra region of the beam spot that has penumbra caused by the distance between the rotary collimator and the sample position. The penumbra sizes are 18.5, 22 and 37 mm for 3, 7 and 22 mm umbra sizes, respectively.

3.4. Spallation proton-induced (>200MeV) white spectrum neutron beams

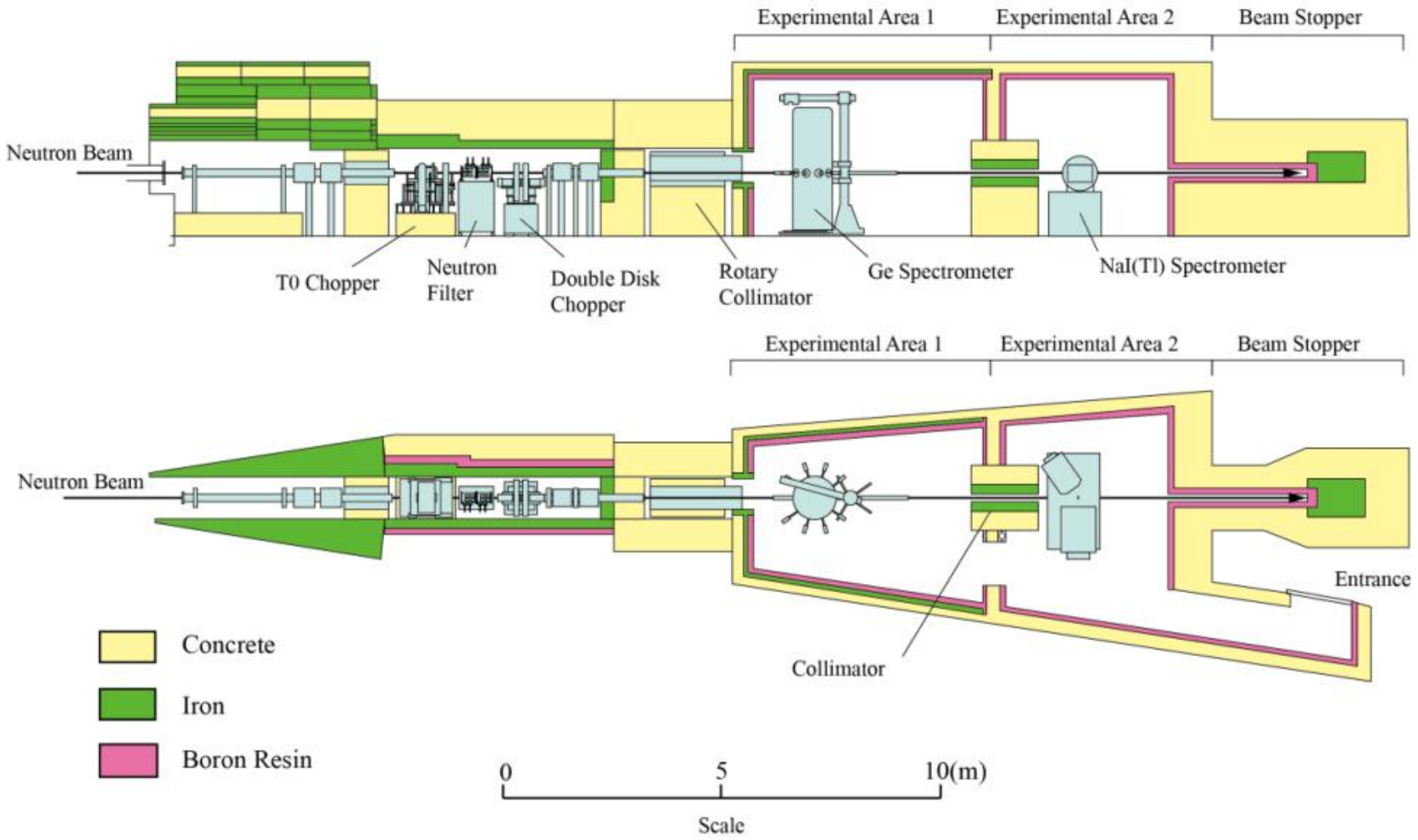

FIG. 1. Accurate Neutron-Nucleus Reaction Measurement Instrument (ANNRI).

3.4. Spallation proton-induced (>200MeV) white spectrum neutron beams

Beam collimation for Experimental Area 2 is done by a collimator system in between Experimental Areas 1 and 2. The in-between collimator is a series of iron and borated polyethylene parts inserted into a beam duct. The beam duct is located in a thick shielding made of iron and concrete to suppress background caused by the collimator. In typical experiments in Experimental Area 2, the beam size defined by the in-between collimator is 13 mm at the NaI(Tl) spectrometer sample position (L = 28 m).

The neutron intensity at the L = 21.5 m sample position of ANNRI was compared with those of other spallation neutron facilities in Fig. 8 of Ref. 5. There are two other spallation facilities serving for neutron-induced nuclear data measurements in the world. One is DANCE at LANSCE, the other is n_TOF at CERN. The comparison was made at the proton beam powers of 17.5 kW, 120 kW and 1 MW. The comparison showed that the neutron intensity of ANNRI is the most intense among these facilities for both the time-averaged flux and the spontaneous flux. The J-PARC currently operates at 200-300 kW and is planned to upgrade for 1 MW at operation. Calculation shows that 1 MW operation will provide the neutron intensity at ANNRI that is 60 times higher than that of DANCE.

In the typical operation mode, a double bunched proton beam is accelerated in the 3GeV synchrotron at a repetition rate of 25 Hz. At each neutron burst, two 100 nsec proton pulses with a 600 nsec delay between the first and the second pulses are injected into the spallation target. This mode was chosen to increase the flux of thermal neutrons, which are used by most of the users in MLF. The time structure of the proton beam disappear in the neutron TOF spectrum due to the neutron moderation time at low energies such as the thermal region. The Doppler broadening effect in samples also wipes out the time structure. However it is very problematic in ANNRI experiments at neutron energies above around 100eV, which depends on sample material and temperature. Resonance peaks in TOF spectra of detected capture events become doublet in the high energy region. Single bunch proton beam or a resonance shape analysis algorithm including the double pulse structure is necessary to resolve this issue.

Another aspect of J-PARC beam operation is that a few proton pulses are delivered to the 50GeV synchrotron (Main Ring) typically every 3 seconds. While the beam direction is switched to the Main Ring, the proton pulse does not come to the spallation target for a long period of time. This is very useful for the capture experiments. Background caused by frame-overlap neutrons (TOF > 40 msec) can be estimated from measurements in the long pulse-absent period.

2.3. GE SPECTROMETER

The Ge spectrometer is an array of Ge detectors composed of two cluster Ge detectors, eight coaxial Ge detectors and BGO anti-coincidence detectors suppressing the Compton scattering events in the Ge crystals [6, 7]. Figure 2 illustrates the Ge spectrometer. Each cluster Ge detector consists of seven Ge crystals. The BGO detectors are placed around the Ge detectors. In order to cut down the number of scattered neutrons coming into the Ge crystals, borated silicon rubber sheets and ^{6}LiH disks canned in Al containers are placed in front of the Ge detectors. In addition, the entire spectrometer is enclosed in shielding made of borated polyethylene, iron and lead. The peak efficiency of the Ge spectrometer is 2.3% for 1.33 MeV γ rays. The typical energy resolution for 1.33 MeV γ rays is 2.4 keV in full-width at half-maximum (FWHM). However we have had noise deteriorating the energy resolution

to 5.5 keV during operation at MLF [8]. The source of the noise is under investigation. It is not yet clear whether the origin is ANNRI itself or from the outside.

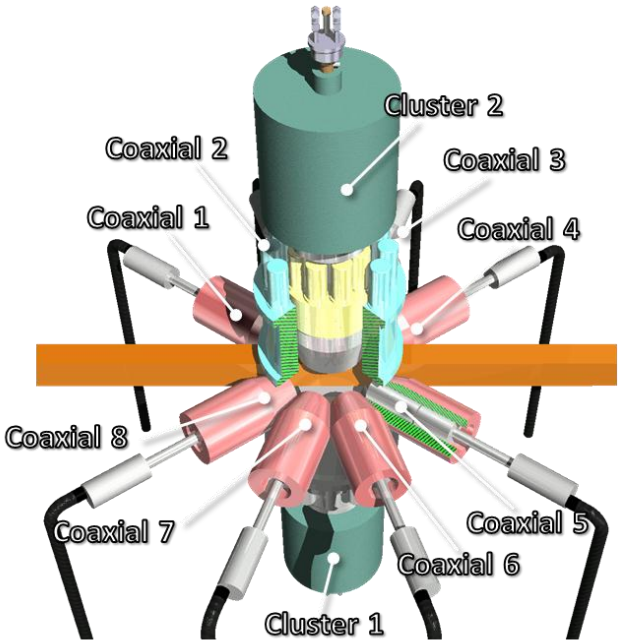

FIG. 2. Ge Spectrometer of ANNRI.

The data acquisition (DAQ) system of the Ge spectrometer utilized digital signal processing technology [9,10]. This DAQ system is very compact, fast and low cost in comparison with conventional Nuclear Instrumentation Module (NIM) systems. The DAQ system analyzes the digitized signal to calculate the pulse height. Finally, the pulse height, TOF and detector ID are sent to a PC and recorded sequentially in a list-data format.

2.3. NAI(TL) SPECTROMETER

The NaI(Tl) spectrometer is illustrated in Fig. 3. The NaI(Tl) spectrometer consists of two differently sized detectors placed at angles of 90° and 125° with respect to the beam axis. The NaI(Tl) crystal size of the 90° detector is 330 mm diameter x 203 mm long. The 125° detector crystal is 203 mm diameter x 203 mm long. The 90° detector was designed to provide larger detection efficiency than the 125° detector, by setting the larger detector at closer distance from the sample position. On the other hand, the 125° detector is for measurement at the special angle of 125°, where the angular dependent term of the E1 and M1 γ ray transitions vanishes. Both the 90° and 125° detectors are surrounded with annular plastic scintillation detectors to suppress cosmic ray background by anti-coincidence detection. Shielding of the detectors was made with lead, cadmium, borated polyethylene and borated rubber. In addition, ^{6}LiH is used in front of the detectors as a neutron absorber.

3.4. Spallation proton-induced (>200MeV) white spectrum neutron beams

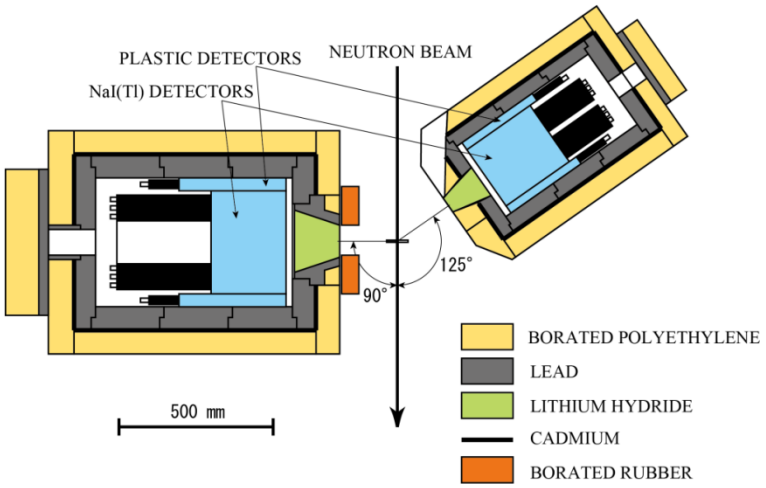

FIG. 3. NaI(Tl) Spectrometer of ANNRI.

2.4. RADIOACTIVE SAMPLES

Radioactive samples of MAs and LLFPs were prepared. The MA samples are ^{237}Np (5.2 MBq, 1 MBq), ^{241}Am (0.95 GBq), ^{244}Cm (1.8 GBq) and ^{246}Cm (1.8 GBq). The LLFP samples are ^{93}Zr (47 MBq), ^{99}Tc (50 MBq), ^{107}Pd (380 kBq) and ^{129}I (3 MBq). The samples were enclosed in aluminium or titanium containers. The samples of ^{244}Cm, ^{246}Cm, ^{93}Zr and ^{107}Pd were newly fabricated for the J-PARC project. The other samples already existed in other facilities and were transported to J-PARC. Isotopic analysis has been performed for the ^{244}Cm, ^{246}Cm and ^{107}Pd samples. A small amount of each sample material prepared from the same manufacturer's batch was analyzed by thermal ionization mass spectroscopy. The isotopic compositions of ^{244}Cm and ^{246}Cm sample were double-checked by γ ray spectrometry. The isotopic compositions were determined consistently.

2.5. EXAMPLES OF MEASUREMENTS

The neutron capture cross sections of ^{244}Cm and ^{246}Cm have been measured with the Ge spectrometer of ANNRI [8, 11]. This measurement was a long-desired update of the cross section data of these isotopes 40 years after the first and only measurement done by a nuclear explosion experiment. The capture cross sections were determined in the energy region from 1 eV to 300 eV. The uncertainties were 5.8% (^{244}Cm) and 6.6% (^{246}Cm) at the top of the first resonance. The high specific activity of ^{244}Cm ($T_{1/2}$ = 18 years), which is contained in the ^{246}Cm sample as impurity, limits the amount of samples (0.6 mg for ^{244}Cm and 2.1 mg for ^{246}Cm) for measurements. The intense pulsed neutron beam of J-PARC allowed us to measure the cross sections of such a sub-milligram sample.

The capture cross section of ^{237}Np has been measured with the NaI(Tl) spectrometer of ANNRI [12]. The cross section was determined in the energy range from 10 meV to 1 keV. The determined thermal capture cross section was in good agreement with those of the Japanese Evaluated Nuclear Data Library (JENDL-4.0), recommendation by Mughabghab and a recent TOF measurement by LANL. The deduced Westcott's g-factor supports results of previous activation measurements but disagreed with the LANL TOF measurement. Resonance analysis of the experimental data in the resolved resonance region is ongoing.

3.4. Spallation proton-induced (>200MeV) white spectrum neutron beams

Measurements and data analysis of other MAs and LLFPs are in progress. Preliminary results of some of the measurements can be found in Ref. 13 and 14.

3. SUMMARY

To measure neutron capture cross sections, the nuclear data measurement instrument ANNRI was built in J-PARC. The most intense pulsed neutron beam in the world is available in ANNRI. The beam collimation and shielding were carefully designed using Monte Carlo simulation and experimental results. The Ge spectrometer and the NaI(Tl) spectrometer were installed for capture experiments. Using these spectrometers, cross section measurements are ongoing. Some of the results have already been published.

This overview focused on only the projects to measure the capture cross section of MA and LLFP for nuclear engineering. Capture experiments for other fields, for example, astrophysics have started. Prompt γ ray analysis using the Ge spectrometer of ANNRI also started. J-PARC is open to the international researchers. We openly welcome new users to join or start experiments using ANNRI.

ACKNOWLEDGEMENTS

The authors would like to thank the accelerator and technical staff of J-PARC for operation and support. This study includes the results of, "Study on nuclear data by using a high intensity pulsed neutron source for advanced nuclear system," entrusted to Hokkaido University by the Ministry of Education, Culture, Sports, Scientific and Technology of Japan (MEXT). This work is supported by JSPS KAKENHI Grant Number 22226016.

REFERENCES

[1] IGASHIRA et al., Nuclear Data Study at J-PARC BL04, Nuclear Instruments and Methods in Physics Research A 600 (2009) 332-334.

[2] KIYANAGI, Y., et al., The 'Study on Nuclear Data by Using a High Intensity Pulsed Neutron Source for Advanced Nuclear System' Nuclear Data Project and the Characteristics of the Neutron Beam Line for the Capture Cross Section Experiments at J-PARC, Journal of Korean Physical Society, 59 (2011) 1781-1784.

[3] IGASHIRA, M., Systematic Study on Neutron Capture Reaction Cross Sections for the Technological Development of Nuclear Transmutation of Long-Lived Nuclear Wastes, http://www.jsps.go.jp/j-grantsinaid/12_kiban/ichiran_22/e-data/e66_igashira.pdf

[4] MAEKAWA, F., et al., First Neutron Production Utilizing J-PARC Pulsed Spallation Neutron Source JSNS and Neutron Performance Demonstrated, Nuclear Instruments and Methods in Physics Research A 620 (2010) 159-165.

[5] KINO, K., et al., Measurement of Energy Spectra and Spatial Distributions of Neutron Beams Provided by the ANNRI Beamline for Capture Cross-Section Measurements at the J-PARC/MLF, Nuclear Instruments and Methods in Physics Research A 626-627 (2011) 58-66.

[6] HARADA, H., et al., Study of Neutron Capture Reactions Using the 4γ Ge Spectrometer, Journal of the Korean Physical Society, 59 (2011) 1547-1552.

[7] KIN, T., et al., The "4π Ge Spectrometer" for Measurements of Neutron Capture Cross Section by the TOF Method at the J-PARC/MLF/ANNRI, Journal of the Korean Physical Society, 59 (2011) 1769-1772.

[8] KIMURA, A., et al., Neutron-Capture Cross-Sections of ^{244}Cm and ^{246}Cm Measured with an Array of Large Germanium Detectors in the ANNRI at J-PARC/MLF, Journal of Nuclear Science and Technology 49 (2012) 708-724.

[9] KIMURA, A., et al., Development of a Data Acquisition System for a Multiple Gamma ray Detection Method, International Conference on ND2004, Santa Fe, USA, 27 September -1 October, 2004, AIP Conference Proceedings 769, (2009) 792-795.

[10] KIMURA, A., et al., Performance of a High Speed and High Density Data Acquisition System for Multiple Gamma ray Detection, NSS-MIC 2008, Dresden, Germany, 19-25 October, 2008, pp. 2107-2111, 2009.

[11] GOKO, S., et al., Measurement of Neutron Capture Cross Section Ratios of ^{244}Cm Resonances Using NNRI, Journal of Nuclear Science and Technology 47 (2010) 1097-1100.

[12] HIROSE, K., et al., Cross-Section Measurement of ^{237}Np(n,γ) from 10 meV to 1 keV at Japan Proton Accelerator Research Complex, Journal of Nuclear Science and Technology 50 (2013) 188-200.

[13] NAKAMURA, S., et al., Measurements of Neutron-Capture Cross Section of Palladium Isotopes at the J-PARC/MLF/ANNRI, Journal of the Korean Physical Society, 59 (2011) 1773-1776.

[14] HORI, J. et al., Measurements of Neutron Capture Gamma Rays from the Resonances of ^{91}Zr and ^{96}Zr at the J-PARC/MLF/ANNRI, Journal of the Korean Physical Society, 59 (2011) 1777-1780.

3. ACCELERATOR BASED NEUTRON BEAM FACILITIES

3.5 NEUTRON BEAMS FROM INVERSE KINEMATIC REACTIONS

3.5. Neutron beams from inverse kinematic reactions

NUCLEAR RESEARCH WITH QUASI MONO-ENERGETIC NEUTRONS AT THE IPNO LICORNE FACILITY

S. OBERSTEDT[*], J.N. WILSON[**], R. BILLNERT[*,***], G. GEORGIEV[+], P. HALIPRE[**], M. LEBOIS[**], B. LENIAU[**], J. LJUNGVALL[+], I. MATEA[**], A. OBERSTEDT[***], D. VERNEY[**]

[*]European Commission, DG Joint Research Centre IRMM, Retieseweg 111, B-2440 Geel
[**]Fundamental Fysik, Chalmers Tekniska Högskola, S-41296 Göteborg
[***]Institut de Physique Nucléaire Orsay, F- 91406 Orsay
[+]CSNSM Orsay, F-91405 Orsay

Email:stephan.oberstedt@ec.europa.eu

Abstract

LICORNE is a new neutron source recently installed at the *Institut de Physique Nucléaire* in Orsay, where a Li-beam is used to bombard a hydrogen-containing target to produce an intense forward-directed neutron beam. The directionality of the beam, which is the unique characteristic of LICORNE, will permit the installation of γ ray detectors dedicated to the investigation of fission fragment de-excitation and unimpeded by neutrons from the source. A first experimental program will focus on the measurement of prompt γ ray emission in the neutron-induced fission of fertile and fissile isotopes at incident neutron energies relevant for the core design of Generation-IV nuclear reactors.

1. INTRODUCTION

LICORNE is a new facility for neutron production recently installed at the IPN Orsay. The ability of the 15 MV tandem accelerator at the IPN to produce intense beams of ^{7}Li (up to 200 nA continuous or 50 nA pulsed) is exploited to run the p(^{7}Li,^{7}Be)n reaction in inverse kinematics. LICORNE is a unique facility in that it combines the best aspects of white neutrons sources (directional/collimated neutron beams) with the best aspects of quasi mono-energetic neutron facilities (ability to get very close to the neutron source). The natural directionality of the LICORNE source will allow placement of gamma detectors at angles outside the neutron cone to allow study of fast neutron induced fission via measurements of gamma rays from the fission fragment de-excitation process. Available neutron energies range from 500 keV to 4 MeV with neutron cone opening angles ranging from 5 – 25 degrees depending on the ^{7}Li bombarding energy.

The use of inverse reactions with ^{7}Li (or ^{11}B) beams to produce kinematically focused, mono-energetic neutrons to bombard actinide targets offers some distinct advantages:

1. Neutrons from the p(^{7}Li,n)^{7}Be reaction can be focused into a forward cone of between 5 and 25 degrees, allowing the possibility to cleanly detect prompt fission gamma rays from the target at all other angles. Thus no thick shielding is needed to protect gamma detectors from the neutron source background of up to 10^{7} neutrons per second (n/s) that occurs with mostly isotropic reactions such as ^{7}Li(p,n).
2. The kinematic focusing increases the available neutron flux over the non-inverse reaction by a factor of typically 30.
3. The background from neutron scattering in the room should be decreased by a similar factor. Only objects (e.g. concrete walls) in the path of the forward-focused cone will scatter neutrons.
4. The kinematically focused cone is much better adapted to radiation shielding from source neutrons than an isotropic neutron source.

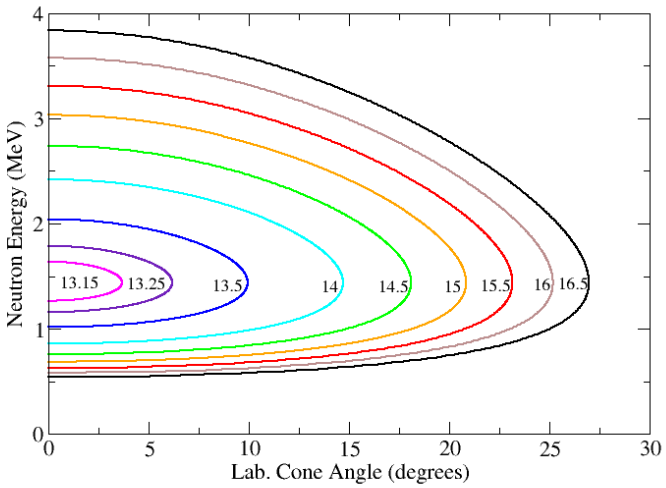

FIG. 1. Neutron energies produced as a function of laboratory angle for ^{7}Li bombarding energies between 13.15 and 16.5 MeV calculated with relativistic 2-body kinematics for the p(^{7}Li,^{7}Be)n inverse reaction.

LICORNE is initially intended to facilitate measurement of the prompt gamma decay from the fission process, a series of experiments that are at the top of the high priority list of the OECD/NEA for nuclear data needs [1]. However, it is clear that it could be used for other purposes such as fundamental physics, cross section measurements, activation studies or perhaps even irradiation for the aerospace industry.

2. LICORNE – DESIGN AND NEUTRON BEAM CHARACTERISTICS

2.1. BEAM CHARACTERISTICS

The kinematic curves for the p(^{7}Li,n)^{7}Be reaction are shown in Fig.1 where the emitted neutron energy is plotted as a function of the angle of emission in the laboratory. Each curve represents a different ^{7}Li bombarding energy and is associated with neutron cones of various opening angles. The reaction threshold for neutron production corresponds to a ^{7}Li bombarding energy of 13.09 MeV above which the beams are very narrow and highly focused leading to enhancement factors over the isotropic reaction of tens of thousands. Unfortunately, the cross section for neutron production is very low for these highly focused cones.

Above ^{7}Li energies of 16.53 MeV the possibility of exciting the first excited state at 429 keV of the ^{7}Be recoil becomes energetically feasible and, thus, the neutrons cease to be mono-energetic. A typical measured neutron time of flight spectrum from a liquid-scintillator neutron detector with a bombarding energy of 15 MeV is given in Fig. 2. Due to the possibility of backwards emission of neutrons in the centre-of-mass frame which are subsequently focused forwards, there exists a satellite peak in the spectrum at much lower energy.

3.5. Neutron beams from inverse kinematic reactions

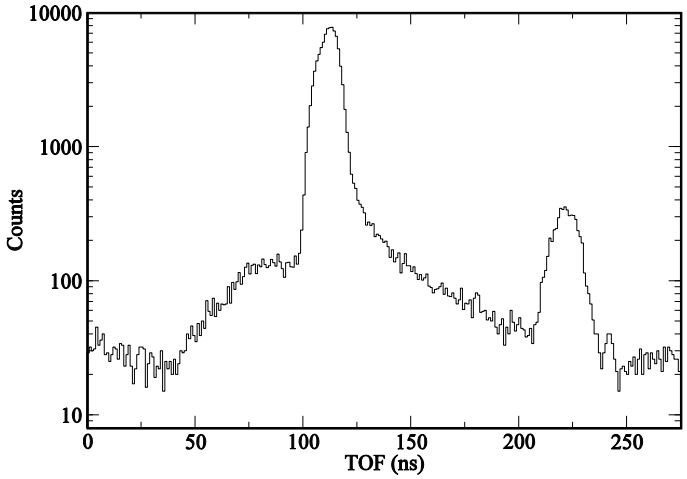

FIG.2. Neutron TOF spectrum produced by 7Li bombarding a 4 μm polypropylene target at 15 MeV. Neutrons were detected by placing a 20 cm diameter, 5 cm thick NE213 detector at 3 m from the neutron source at an angle of 0 degrees to the beam axis. At 15 MeV bombarding energy, the main neutron peak is at 3.03 MeV and its satellite at 0.58 MeV.

The satellite peak exists at all ^{7}Li beam energies but its relative size is highly dependent on the angular distribution in the centre of mass frame. At energies above 16 MeV the satellite peak actually becomes the dominant peak in the neutron spectrum. Since the satellite peak is always at low energy (500 – 800 keV) for most fertile samples it will be below the fission threshold so its existence will, therefore, be unimportant. However, for fissile samples the two peaks will need to be separated by the time of flight technique at short distances. There should be a few nanoseconds of separation in most cases, so this should not present a problem. In total seven different ^{7}Li bombarding energies of 13.5, 14, 14.5, 15, 15.5, 16 and 16.5 MeV are envisaged for LICORNE, corresponding to seven different average neutron energies between 1.5 and 4 MeV for the principal peak and 500 keV to 800 keV for the satellite peak.

2.2. NEUTRON CONVERTER DESIGN

The LICORNE neutron converter is designed with a rotating polypropylene target of 4 μm thickness and a diameter of 8 cm (see Fig. 3). The key limit on target thickness is the loss of energy of the beam across the target. This energy loss of ^{7}Li in a 4μm target is around 500 keV, but varies slightly depending upon the ^{7}Li energy. The polypropylene is a plastic with high melting point (160 degrees Celsius) and high hydrogen content (CH_2). The neutron background from fusion-evaporation reactions on the ^{12}C nuclei in the polypropylene is quite low. Polypropylene also has the advantage over a gaseous H_2 target that the neutron source has a very small, precisely defined spatial position. In addition gaseous H_2 targets require a thin window of Molybdenum (1-2 μm thick) to hold the vacuum. This would slow down and straggle the ^{7}Li beam and generate unwanted neutrons from parasitic fusion-evaporation reactions on the window material.

Monte Carlo calculations validated by the experimental data from a first test experiment have been used to calculate available neutron fluxes for extended targets (3-5 cm diameter) placed at short distances (5 - 20 cm) from the neutron source. Currently, LICORNE can produce up to 10^{7} n/s/steradian assuming a ^{7}Li beam current of 100 nA which is similar

to other facilities such as the 4 MV tandem at Bruyères-le-Châtel and the AFIRA accelerator at CENBG Bordeaux. If several rotating polypropylene discs are stacked together (permitted by design) then fluxes of around 5×10^7 n/s/steradian ought to be achievable but at the expense of producing a continuous neutron spectrum between 500 keV and 4 MeV. Again, the time of flight technique at short distances could be used to measure more precisely the neutron energy for the thick-target LICORNE configuration.

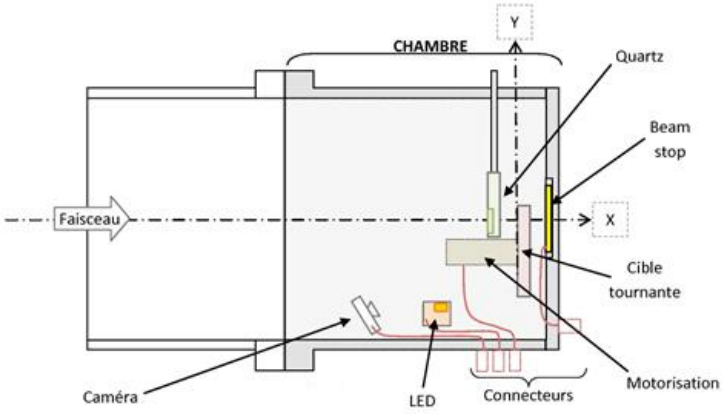

FIG. 3. The LICORNE chamber design with key components consisting of the rotating polypropylene target wheel, the 50 μm thick gold beam stop used to measure beam current and provide timing signals and a removable quartz foil and miniature camera for beam tuning. The source distance from the front face of the chamber is 2 cm.

The highest thin-target neutron fluxes are only available near the reaction threshold for the narrowest neutrons cones where the enhancement factors over the non-inverse/isotropic reaction are the greatest. For example, at a ^{7}Li bombarding energy of 13.5 MeV the opening angle of the neutron cone in the laboratory frame is 10 degrees and the principal and satellite neutron peaks are merged together into a broad peak centered at 1.53 MeV with a FWHM of approximately 0.3 MeV (see Fig. 4). For a 50 g sample of ^{238}U placed in such a beam we can thus expect a fission rate of around 10 kHz.

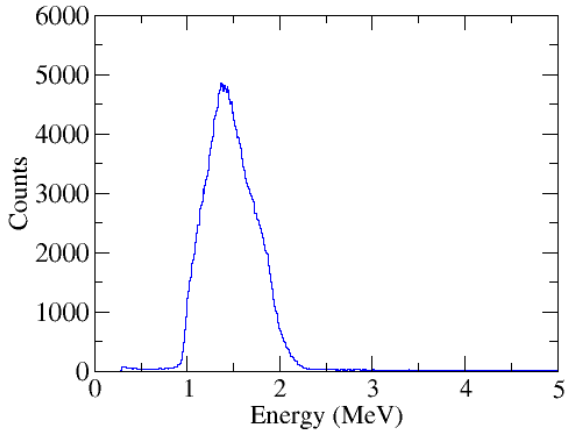

FIG. 4. Measured LICORNE spectrum at a 7Li bombarding energy of 13.5 MeV where the kinematic focusing is maximized and available neutron fluxes are the greatest.

3. OUTLOOK

In mid-2013 the first planned experiment with the LICORNE facility will be performed. This experiment will measure the average multiplicity, energy and spectral shape of prompt fission gamma rays from fission of ^{238}U by fast neutrons. It has been approved by the ERINDA (European Research Infrastructures for Nuclear Data Applications) [2] program advisory committee and will involve ten days of beam time. It is foreseen to induce fissions in a massive sample (30 – 50 g) with a pulsed beam so that the evolution of the prompt fission gamma ray spectral shape as a function of energy can be measured. In addition, an ionization chamber with a thin target will be used to produce a fission-fragment gated spectrum and to test the feasibility to perform time-of-flight discrimination at short distances to separate the principal and satellite neutron peaks. In theory this should allow measurements at two different neutron energies can be made simultaneously for fissile samples.

At some point in the second half of 2013, a new ion source will be installed at the IPN tandem. It is the sputter source that was originally built for the Vivitron accelerator in Strasbourg. The Vivitron is no longer operational; however, its ion source should be capable of producing a factor 5 times more beam current than the present tandem ion source. In the most favorable case, ^{7}Li beam currents of up to 1 μA may be available from 2014 onwards. This would take maximum neutron fluxes available at LICORNE close to the 10^{8} n/s/steradian range.

REFERENCES

[1] NEA nuclear data high priority request list, http://www.oecd-nea.org/dbdata/hprl
[2] ERINDA, http://www.erinda.org/